THE JOURNAL OF

PHYSICAL
CHEMISTRY

THE JOURNAL OF
PHYSICAL CHEMISTRY

Notice to Authors last printed in the issue of December 6, 1973

COMMUNICATIONS TO THE EDITOR

■ Supplementary material for this paper is available separately, in photocopy or microfiche form. Ordering information is given in the paper.

* In papers with more than one author, the asterisk indicates the name of the author to whom inquiries about the paper should be addressed.

NOTICE

Readers may have noticed recent changes in the grades of paper on which this and the other ACS basic journals are printed. The changes are a result of the general paper shortage and ACS regrets any possible inconvenience. The journals will continue to be printed on the best quality paper available in sufficient quantity for press runs.

AUTHOR INDEX

Alchalel, A., 336
Allaert, J., 462

Balcerski, J. S., 444
Baughman, E. H., 421
Bent, D. V., 446, 451
Bergmann, E., 405
Boettcher, J. W., 429

Chambers, R. W., 380
Christian, S. D., 432
Claes, P., 462

Davis, D. D., 463
de Pena, R. G., 325
Donnay, R. H., 440
Drago, R. S., 429, 454

Fee, D. C., 347, 354
Feng, D.-F., 393
Fueki, K., 393

Gangwer, T. E., 375
Garnier, F., 440
Giulianelli, J. L., 372
Guidry, R. M., 454
Gutman, D., 311

Hanrahan, R. J., 360, 366
Hayashi, K., 341
Heicklen, J., 325
Herring, F. G., 316

Irie, M., 341

Janauer, G. E., 411

Kajiwara, T., 380
Kanofsky, J. R., 311
Kearns, D. R., 380
Keenan, B. M., 432
Keil, M., 436
Kennedy, G. A., 360, 366

Kevan, L., 393
Kreevoy, M. M., 421

Lewis, D. K., 436
Lucas, D., 311
Luria, M., 325

Markowitz, S. S., 347, 354
Masuhara, H., 341
Mataga, N., 341

Nichol, L. W., 460

Olszyna, K. J., 325
Osterhoudt. H. W., 408
Ottolenghi, M., 336

Pollock, T. L., 398
Pruss, F., 311
Pysh, E. S., 444

Rampazzo, L., 417

Reidler, J., 424
Rosenfeld, T., 336

Safarik, I., 398
Sarr, M., 436
Schellman, J. A., 387
Schiff, R., 463
Schulte-Frohlinde, D., 446, 451
Sharma, H. D., 402
Silber, H. B., 424
Snir, J., 387
Sood, S. P., 402
Strausz, O. P., 398

Tapping, R. L., 316
Tilquin, B., 462

Van Wart, H. E., 411

Willard, J. E., 372
Winzor, D. J., 460
Wong, W., 463

Direct Identification of the Reactive Channels in the Reactions of Oxygen Atoms and Hydroxyl Radicals with Acetylene and Methylacetylene

Jeffrey R. Kanofsky,[1a] Donald Lucas, Frank Pruss,[1b] and David Gutman*

Department of Chemistry, Illinois Institute of Technology, Chicago, Illinois 60616   (Received August 10, 1973)

The reactions of O atoms and OH radicals with acetylene and methylacetylene were studied in high-intensity room temperature crossed molecular beams. Products were detected using photoionization mass spectrometry. Major and minor observed reactive channels were assigned on the basis of the identity of the products observed and the magnitudes of the product ion signals. The numbers of major observed reactive channels are two for $O + C_2H_2$, one for $OH + C_2H_2$, seven for $O + C_3H_4$, and four for $OH + C_3H_4$. Details on reaction dynamics were obtained using deuterated compounds, and are discussed in detail. Evidence is presented for several types of mechanisms including abstraction, displacement, and addition followed by decomposition.

Introduction

There has been considerable interest in the reactions of O atoms and OH radicals with alkynes because of their importance in thermal and photochemical oxidation cycles. Although rate constants for some of these reactions have now been determined,[2-9] the free-radical products produced by these processes have not been directly observed. Plausible assignments of reaction products have generally been inferred from the identity of the stable products produced,[2,5,9] the quasistable intermediates which have been observed,[2a,3,5,6,9] and the stoichiometric relationships between the amounts of reactants consumed and the amounts of products produced.[2,3,5,6,9]

Since successful quantitative modeling of thermal and photochemical oxidation systems involving these reactions will require, among other things, the establishment of the intermediates they produce, we have undertaken to identify these products directly by studying the reactions in high-intensity cross molecular beams. We report here the results of the study of the reactions of O and OH with C_2H_2 and C_3H_4 at room temperature. For both molecules studied deuterated compounds were also used to provide details of the reaction dynamics.

For three of the four reactions studied, there is little or no information in the literature which may be used to obtain a reasonably complete identification of the important reactive channels. That which is available on these four reactions is briefly reviewed here.

$O + C_2H_2$. The $O + C_2H_2$ reaction has been extensively studied and two major reactive channels have been proposed for which there is supporting evidence

$$O + C_2H_2 \longrightarrow C_2HO + H \tag{1a}$$

and

$$\longrightarrow CH_2 + CO \tag{1b}$$
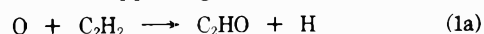
The evidence cited in support of channel 1a is as follows. (1) Considerable amounts of HD are produced when $O + C_2D_2$ reacts in the presence of H_2 which is cited as evidence that D is a primary product of the $O + C_2D_2$ reaction.[10] (2) The radical C_2HO has been observed to grow to a steady-state concentration in a flow reactor study of the $O + C_2H_2$ reaction which suggests it is a primary product.[11] The evidence reported to support channel 1b is as follows. (1) Reaction 1b, followed by the fast reaction $O + CH_2 \rightarrow CO + 2H$, accounts for the observed products formed and the reaction stoichiometry observed in the flow reactor studies of this reaction.[2,3,5,6] (2) Substantial amounts of C_3H_4 are formed when this reaction is studied at very low O atom concentrations presumably due to the reaction of CH_2 produced by (1b) with C_2H_2.[2a,5,12] (3) The CH_2 radical was detected in steady-state concentration in a flow reactor study of the $O + C_2H_2$ reaction.[11]

$OH + C_2H_2$. In a flow reactor study of the $OH + C_2H_2$ reaction, the reaction stoichiometry was felt to be most consistent with the reactive channel[9]

$$OH + C_2H_2 \longrightarrow C_2HO + H_2 \tag{2a}$$

but was also consistent with the route[9]

$$OH + C_2H_2 \longrightarrow C_2H + H_2O \qquad (2b)$$

The absence of CH_4 as an end product in this same study was cited as evidence that the channel

$$OH + C_2H_2 \longrightarrow CH_3 + CO \qquad (2c)$$

is not a significant one at room temperature.[9] However, in a crossed molecular beam study of this reaction CH_3 and CO were reported to have been detected supporting channel 2c as the principal one for this reaction.[13]

O + CH₃CCH. The reaction of O atoms with methylacelytene has been studied in flow reactors. The reactive channel

$$O + CH_3CCH \longrightarrow CH_3CH + CO \qquad (3a)$$

chosen because of its analogy with channel 1b, was found to account for the reaction stoichiometry when plausible fast secondary reactions were included in the mechanism.[3] The observation that acetylene is ultimately produced by this reaction was accounted for by an isomerization and decomposition reaction of the ethylidiene radical[2a,3]

$$CH_3CH \longrightarrow CH_2CH_2{}^* \longrightarrow C_2H_2 + H_2$$
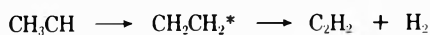
OH + CH₃CCH. There have been no prior investigations to determine the products produced by this reaction.

Experimental Section

The crossed-beam reactor used in this study is shown in Figure 1. It is based on the design of a similar reactor used by Foner and Hudson.[14] A carrier gas containing about 2% O atoms (produced by passing O_2 through a microwave discharge) or about 0.2% OH (produced by passing 7% H_2 in He through a microwave discharge followed by titration of the H atoms produced with NO_2 to produce OH and NO) flows through a pin hole (0.033 cm diameter, 0.025 cm length) in the Teflon end wall of the flow system. The resulting molecular beam intersects a beam of hydrocarbon molecules which emerges from a short section of stainless-steel tubing (0.060 cm i.d.). The insersection of the two beams acts as a diffuse-beam source from which the products of the reaction emerge in all directions. Those moving in the direction of the flow system beam pass through the 2.4 mm diameter skimmer and enter the mass spectrometer chamber. A two-tooth chopping wheel modulates the beam of molecules entering the skimmer at 143 Hz. Ion signals from the quadrupole mass spectrometer are monitored using either phase-sensitive detection or synchronous ion counting.

The only major difference between this apparatus and the one used by Foner and Hudson is that in this study photoionization is used to produce the ions in the mass analyzer. Photoionization was used to provide the selectivity necessary to detect free radicals in the presence of large amounts of gases (beam and background) capable of producing ions at the mass numbers of the free radicals of interest. In order to obtain the sensitivity necessary to detect the free-radical products produced in the molecular beam reaction, intense atomic resonance lamps such as those described by Gorden, Rebbert, and Ausloos[15] as well as by Davis and Braun[16] were used. Gases were chosen whose resonance radiation provides sufficient energy to ionize the free-radical products of interest without simultaneous production of the same ion by dissociative ionization of other molecules. A list of the gases used in the lamps, the energy of their resonance lines, and the corresponding window materials used appears as Table I.
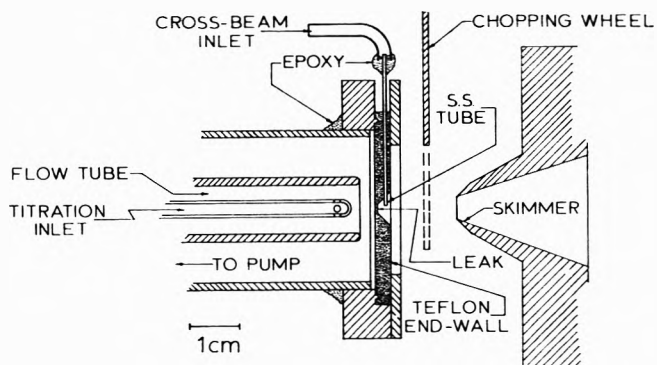
Figure 1. Drawing of crossed-beam reactor. Leak size not to scale.

The total gas pressures in the two gas beams were chosen to maximize the yield of primary products from the reactions studied without producing detectable amounts of secondary products. The gas pressure in the flow reactor was always about 2 Torr and the hydrocarbon gas beam flux used was always that which was sufficient to attenuate the O or OH beam by 50%.

In each reaction studied, three complete mass scans were performed with each lamp listed in Table I; the first scan with the olefin and O atom (or OH) containing beams on, the second with just the olefin beam on, and the last with only the O or OH beam on. To obtain the spectrum with the O or OH beam off, the microwave discharge was simply turned off. This left an unreactive beam from the reactor with almost identical scattering properties as the O or OH containing beam.

The criterion used to establish the presence of a reaction product was the presence of its ion signal with both reactant beams on and the absence of this signal with only one reactant beam on. After each set of three mass scans was taken, the ion signal from each apparent or suspected reaction product P_{net} was more precisely determined using ion counting and the relationship

$$P_{net} = P_{O+H} - P_H - 0.5P_O$$

where P_{O+H} is the ion count with both beams on, P_H is the ion count with the microwave discharge turned off, and P_O is the ion count with only the O atom beam on. Only $0.5P_O$ is subtracted because the alkyne beam scatters one-half the O atom beam and presumably other molecules in this beam as well. Mass 15 is a constant impurity in the OH beam and its signal is attenuated by 50% by the olefin beam (see Figure 2) which supports this presumption. Impurities like the one at mass 15 were at concentrations below 10^{-4} that of the O or OH. Reactions involving these impurities with the alkynes would not produce sufficient amounts of products to be detected in our experiments, even if the impurity were highly reactive.

The reaction products were identified not only by the mass number of the corresponding ion, but also by the isotopic shift observed when the deuterated olefins were used and on crude appearance potentials of the product molecules (*i.e.,* consistency of the lowest energy resonance radiation capable of producing the ion and the ionization potential of the corresponding free radical).

The observed products from each reaction are arbitrarily divided into two categories: major observable products (whose net ion signals are greater than 15% of the largest one), and minor observable products (whose net ion signals are less than 15% of the largest one yet are estab-

TABLE I: Atomic Resonance Lamps Used in Present Study

Emitting atom	Lamp gas composition and pressure	Photon energy, eV	Lamp window	Estimated intensity, photons/sec
Xe	1% Xe in He 1 Torr	8.44	Sapphire	6×10^{12}
O	1% O_2 in He 700 Torr	9.5	CaF_2	2×10^{13}
Kr[a]	1% Kr in He 1 Torr	10.03, 10.64	MgF_2	2×10^{13}
H	8.5% H_2 in He 1 Torr	10.2	MgF_2	4×10^{12}
Ar	Pure Ar 0.3 Torr	11.62, 11.83	LiF	2×10^{12}
Ne[b]	Pure Ne 0.1 Torr	16.67, 16.85	Collimated hole structure	8×10^{11}

[a] Used only in experiment to detect C_2H.[11] [b] Used only to monitor O and OH.

TABLE II: Products Observed from Reactions of O and OH with Acetylene and Methylacetylene[a]

Mass	Product	O + C_2H_2 Major	O + C_2H_2 Minor	OH + C_2H_2 Major	OH + C_2H_2 Minor	O + C_3H_4 Major	O + C_3H_4 Minor	OH + C_3H_4 Major	OH + C_3H_4 Minor
14	CH_2	Ar				Ar			
15	CH_3					H			H
26	C_2H_2						H[d]		
27	C_2H_3					O			O
28	C_2H_4					H[b]			
29	CHO					O			
39	C_3H_3						O	O	
41	C_2HO	H							
42	C_2H_2O			H		H		H	
55	C_3H_3O					O[c]			
56	C_3H_4O								H

[a] Symbol used to designate an observed product in this table identifies the rare gas resonance lamp of minimum energy capable of ionizing the product. [b] Identified as major product with Ar lamp. Detectable as minor product below its ionization potential (i.e., at 10.2 eV with H lamp). [c] Ion signal too small to determine presence with less energetic lamp. [d] Not detectable with Ar lamp due to cracking of parent. Detected as minor product below its ionization potential (i.e., at 10.2 eV; H lamp).

lished to be present with 99% confidence). Special efforts were made to compare ion signals from possible minor products with major observable ones of similar mass and structure. Such comparisons minimize detection sensitivity differences caused by differences in photoionization cross section, mass discrimination by the quadrupole mass filter, and differences in the laboratory velocities of the reaction products.

The major and minor products observed from the reactions studied are listed in Table II together with the least energetic resonance radiation used which was capable of ionizing the species. Table II is not a complete listing of all products produced by these reactions since several products (such as H, H_2, CO) are not detectable due to high background signals, and others are obscured by ion signals from impurities, the alkynes, and their cracking patterns.

Discussion

Assignment of Reactive Channels. Major and minor reactive channels have been assigned for the four reactions studied based on the major and minor products which were observed in the studies of each reaction. A listing of these assigned reaction paths is given in Table III.

O + C_2H_2. Major ion signals were observed from both CH_2 and C_2HO which establishes both previously proposed major channels for this reaction (1a and 1b) as being significant at room temperature. This observation is in agreement with the indirect evidence that there are two
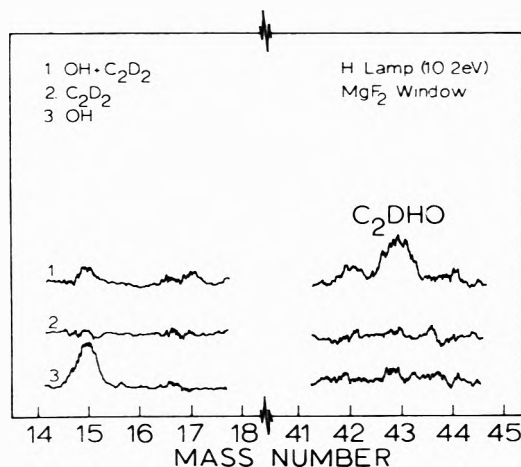
Figure 2. Mass scans of OH + C_2D_2 reaction using H lamp (10.2 eV). Actual presence or absence of net ion signal established by ion counting (see text). There is no net product ion signal at masses 15, 17, and 42.

major routes for this reaction. From measurements of CO and C_3H_4 production at low O atom concentrations Williamson and Bayes conclude channel 1b accounts for at least 12% and probably 25% of the reaction rate at room temperature.[12] Under similar experimental conditions Williamson estimates 42 ± 10% of the O + C_2H_2 reaction proceeds by channel 1a.[10]

The stoichometric arguments invoked by those who

TABLE III: Reaction Routes Observed for the Reactions of O and OH with Acetylene and Propyne[a]

Reaction	Product channel
	Major observable routes
O + C_2H_2	C_2HO + H
	CH_2 + CO
	Major observable routes
OH + C_2H_2	C_2H_2O + H
	Major observable routes
O + C_3H_4	C_3H_3O + H
	C_2H_2O + CH_2
	C_2H_4 + CO
	C_2HO + CH_3
	C_2H_3 + CHO
	Major or minor observable route[b]
	C_2H_2 + (CO + H_2)
	Minor observable route
	C_3H_3 + OH
	Major observable routes
OH + C_3H_4	C_2H_2O + CH_3
	C_3H_3 + H_2O
	Minor observable routes
	C_3H_4O + H
	C_2H_3 + CH_2O

[a] Products actually observed are italicized. Compounds not italicized were not capable of being observed under the experimental conditions used. [b] Since C_2H_2 was detected below the ionization potential of this molecule, peak height was not used to classify this channel as either major or minor.

studied this reaction in flow reactors in support of channel 1b are actually also applicable to channel 1a. If C_2HO produced by the O + C_2H_2 reaction is rapidly consumed by the reaction

$$O + C_2HO \longrightarrow H + 2CO$$
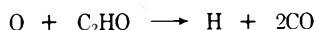
then two H atoms are produced and two O atoms are consumed for each C_2H_2 molecule which reacts, exactly as in the case of the pair of reactions beginning with (1b).

OH + C_2H_2. The only product detected for this reaction was C_2H_2O (see Figure 2) which establishes

$$OH + C_2H_2 \longrightarrow C_2H_2O + H \qquad (2d)$$

as a major reactive channel for this reaction. The H atom which leaves comes from the acetylene. This was established by using C_2D_2 instead of C_2H_2. The relative ion signals from the two possible isotopically different products are given above the arrows designating the respective routes[17]

$$OH + C_2D_2 \underset{-0.1 \pm 0.13}{\overset{1.0 \pm 0.14}{\rightleftarrows}} \begin{cases} C_2HDO + D & (2d') \\ C_2D_2O + H & (2d'') \end{cases}$$
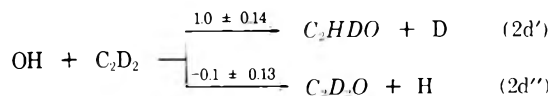
Since three other reactive channels have been suggested for the OH + C_2H_2 reaction at room temperature, major efforts were made to detect the products they would produce. No significant ion signal was observed from C_2HO ($C_2HO^+/C_2H_2O^+$ = (0.0 ± 0.1)/(1.0 ± 0.47) with the H lamp[18]). Thus channel 2a is not a major path for this reaction. Similarly C_2H was not detected ($C_2H^+/C_2H_2O^+$ = (0.0 ± 0.2)/(1.0 ± 0.47) with the Kr lamp[18,19]) which means channel 2b could be at best only of minor importance. Finally no net ion signal was detected from CHD_2 from the reaction of OH + C_2D_2 (CHD_2^+/C_2HDO^+ = (0.0 ± 0.07)/(1.0 ± 0.14) with the H lamp[18]) which also makes channel 2c of minor importance if present at all. Gehring, *et al.*, report observing CH_3^+ and CO^+ from a similar crossed-beam study of the OH + C_2H_2 reaction as we report here.[13] We also observe a mass peak from CH_3^+

when we studied this reaction (see Figure 2), but it originates from a CH_3 impurity in the OH radical source which could not be removed. For this reason C_2D_2 was used in our study to attempt to observe methyl radicals produced by the beam reaction. Gehring, *et al.*, report few details of their study so it is not possible to establish the origin of their CH_3^+ and CO^+ ion signals.

O + $CH_3C{\equiv}CH$. In the reaction of O atoms with propyne, products from seven reactive channels were observed. Two major routes

$$O + CH_3C{\equiv}CH \longrightarrow C_3H_3O + H \qquad (3b)$$

and

$$O + CH_3C{\equiv}CH \longrightarrow C_2HO + CH_3 \qquad (3c)$$
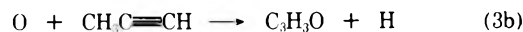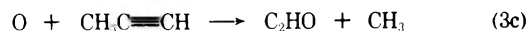
are apparent displacement reactions and are analogous to channel 1a in the O + C_2H_2 reaction.[20] In experiments with CH_3CCD and CD_3CCH, it was found that ejection of the acetylenic hydrogen predominated, but a methyl hydrogen left in about 10% of the reactive collisions in which a hydrogen was displaced. The H atom displacement routes observed were

$$O + CD_3C{\equiv}CH \begin{cases} \overset{1.0 \pm 0.09}{\longrightarrow} C_3D_3O + H & (3b')^{17} \\ \overset{0.10 \pm 0.06}{\longrightarrow} C_3D_2HO + D & (3b'') \end{cases}$$

$$O + CH_3C{\equiv}CD \begin{cases} \overset{1.0 \pm 0.15}{\longrightarrow} C_3H_3O + D & (3b')^{17} \\ \overset{0.11 \pm 0.05}{\longrightarrow} C_3H_2DO + H & (3b'') \end{cases}$$
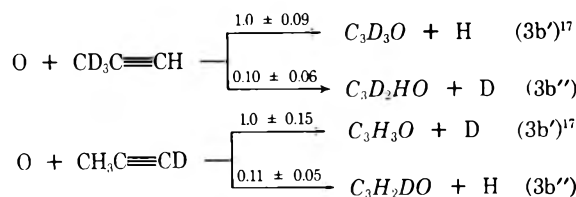
In the reactive channel in which a methyl group is displaced, the methyl group leaves intact. There was no significant evidence for hydrogen exchange when $CD_3C{\equiv}CH$ was used as the reactant. The relative amounts of the different methyls which are formed are

$$O + CD_3C{\equiv}CH \begin{cases} \overset{1.0 \pm 0.18}{\longrightarrow} CD_3 + HC_2O & (3c')^{17} \\ \overset{0.05 \pm 0.17}{\longrightarrow} CD_2H + DC_2O & (3c'') \end{cases}$$
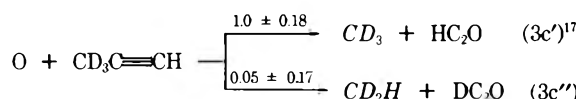
The observation of the products C_2H_4 and C_2H_2 are evidence of a route analogous to channel 1b in the O + C_2H_2 reaction which may be pictured as the O atom adding to the carbon on the least-substituted side of the triple bond, the H atom on this carbon migrating to the other side of the triple bond, and the triple bond breaking. The ethylidene radical thus formed could rearrange to yield ethylene or decompose to yield acetylene and H_2[2a,3]

$$O + CH_3C{\equiv}CH \longrightarrow CO + \begin{cases} CH_3\ddot{C}H \overset{C_2H_4^*}{\underset{C_2H_2^* + H_2}{\rightleftarrows}} \end{cases} \qquad (3a)$$
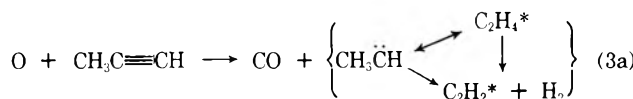
The fact that C_2H_4 was detected below its ionization potential means that either the ethylidene radical or internally excited ethylene was detected. The product C_2H_2 was detected at 1.2 eV below the ionization potential of acetylene indicating it is partially produced with at least this amount of internal energy. Acetylene has been observed as an intermediate in the O + propyne reaction in a flow reactor study of this reaction.[2a] This observation, together with the reaction stoichiometry, were cited as evidence that channel 3a is the principal one for this reaction.[3]

The remaining two major reactive channels have no observed analog in the O + C_2H_2 reaction. The first

$$O + C_3H_4 \longrightarrow C_2H_3 + HCO \qquad (3d)$$
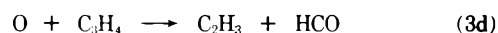
has the appearance of the O atom again adding to the car-

bon atom on the least-substituted side of the triple bond followed by the triple bond breaking. If this is the mechanism for this route, the experiments done with $CH_3C{\equiv}CD$ indicate the adduct lives long enough for hydrogen atoms to intramolecularly exchange, since both C_2H_3 and C_2H_2D are formed (see Figure 3)

$$O + CH_3C{\equiv}CD \begin{array}{c} \xrightarrow{1.0\ \pm\ 0.08} C_2H_3 + DCO \quad (3d')^{17} \\ \xrightarrow{0.25\ \pm\ 0.06} C_2H_2D + HCO \quad (3d'') \end{array}$$
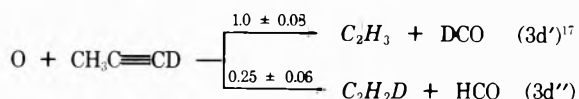
No information on the dynamics of the last major reactive channel observed

$$O + CH_3C{\equiv}CH \longrightarrow C_2H_2O + CH_2 \quad (3e)$$

were obtained since experiments using the deuterated propynes did not yield additional useful information. A possible mechanism here is the O atom adds to the more-substituted carbon adjacent to the triple bond, a hydrogen on the methyl group migrates to the terminal carbon on the other side of the triple bond, and then the triple bond breaks. Such a migration might involve a hot enol intermediate similar to one suggested for the reaction of O with 2-butyne,[21] i.e.

$$O + CH_3{-}C{\equiv}CH \longrightarrow$$

$$\begin{array}{ccc} O & OH & .O \\ \| & \| & \| \\ CH_3{-}C{-}CH & \rightleftharpoons CH_2{-}C{=}CH & \rightleftharpoons CH_2{-}C{=}CH_2 \\ & & \downarrow \\ & & :CH_2 + O{=}C{=}CH_2 \end{array}$$
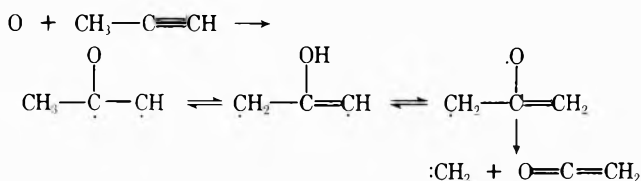
An apparent abstraction reaction

$$O + C_3H_4 \longrightarrow C_3H_3 + OH \quad (3f)$$
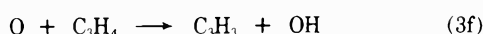
is the last observable route a is minor one. Only the propargyl hydrogen is lost

$$OH + CH_3C{\equiv}CD \begin{array}{c} \xrightarrow{1.0\ \pm\ 0.08} C_3H_2D + OH \quad (3f')^{17} \\ \xrightarrow{0.04\ \pm\ 0.04} C_3H_3 + OD \quad (3f'') \end{array}$$
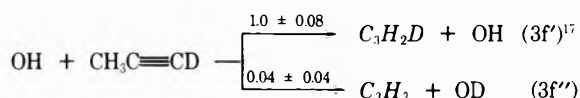
OH + CH₃CCH. In this reaction there are again analogies with the comparable reaction with acetylene. The only observed route in the $OH + C_2H_2$ reaction was an apparent displacement reaction and in this reaction both possible apparent displacement reactions

$$OH + C_3H_4 \longrightarrow C_2H_2O + CH_3 \quad (4a)$$

and

$$OH + C_3H_4 \longrightarrow C_3H_4O + H \quad (4b)$$
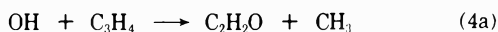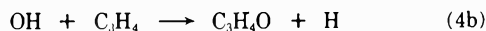
are observed. The methyl group leaves intact

$$OH + CD_3C{\equiv}CH \begin{array}{c} \xrightarrow{1.0\ \pm\ 0.18} CD_3 + C_2H_2O \quad (4b')^{17} \\ \xrightarrow{0.04\ \pm\ 0.20} CD_2H + C_2HDO \quad (4b'') \\ \xrightarrow{0.02\ \pm\ 0.15} CH_2D + CD_2O \quad (4b''') \end{array}$$
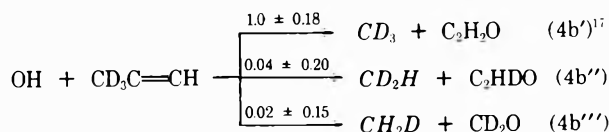
An apparent abstraction of H atoms by OH is a major route. The propargyl hydrogens are those abstracted

$$OH + CH_3C{\equiv}CD \begin{array}{c} \xrightarrow{0.04\ \pm\ 0.05} C_3H_3 + HDO \quad (4c')^{17} \\ \xrightarrow{1.0\ \pm\ 0.04} C_3H_2D + H_2O \quad (4c'') \end{array}$$

The channel

$$OH + CH_3C{\equiv}CH \longrightarrow C_2H_3 + CH_2O \quad (4d)$$
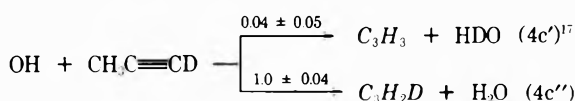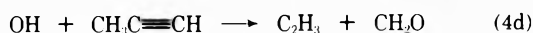
is of minor importance. It must proceed through a rather long-lived complex since the hydrogens internally migrate before decomposition of the $OH{\cdot}C_3H_4$ adduct
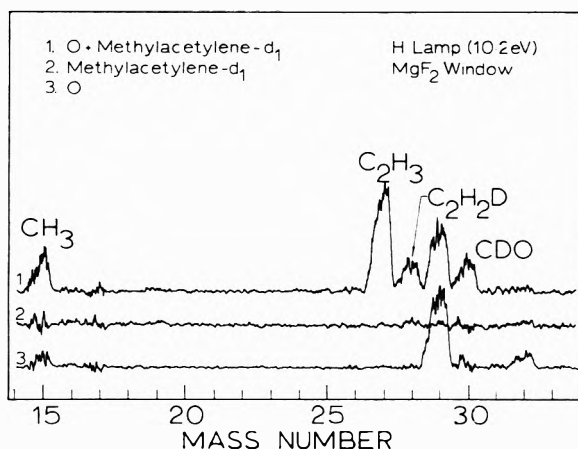
Figure 3. Mass scans up to $M = 35$ of O + methylacetylene-d_1 reaction using H lamp (10.2 eV). Mass 29 is an impurity in the O atom source.

$$OH + CH_3C{\equiv}CD \begin{array}{c} \xrightarrow{1.0\ \pm\ 0.11} C_2H_3 + H_2CO \quad (4d')^{17} \\ \xrightarrow{0.78\ \pm\ 0.35} C_2H_2D + HDCO \quad (4d'') \end{array}$$
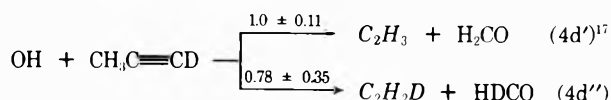
Final Remarks

The results of this study reveal the large number of reactive channels which are accessible to O + alkyne and OH + alkyne reactions at room temperature, the number increasing markedly with the complexity of the alkyne. There is also evidence that several different dynamics mechanisms may be occurring including (a) abstraction, (b) displacement, (c) addition followed by rupture of the triple bond, and (d) addition followed by major or minor rearrangements and then by rupture of the multiple bond. In mechanism c intramolecular isotope mixing of hydrogen atoms prior to bond rupture of the excited O or OH + alkyne adduct has been observed.

In none of the reactions studied here was the O (or OH) + alkyne adduct observed as a product. The lifetimes are expected to be extremely short. Avery has studied the O + methylacetylene reaction as a function of pressure and finds that at atmospheric pressure less than 10% of the reaction proceeds to stabilized adduct (acrolein).[22] Thus in modeling complex reactive systems at atmospheric pressure which include the elementary reactions studied here, all the major reactive channels identified here should be considered.

Studies are in progress of the reactions of O and OH with 1-butyne and 2-butyne. It is hoped that the results of these studies will make it possible to generalize more specifically on what reactive channels one could expect to occur in other O and OH reactions with alkynes.

References and Notes

(1) (a) NSF Fellow 1969–1971, U.S. Steel Fellow 1971–1972. (b) NSF Undergraduate Research Participant, 1972.
(2) (a) C. A. Arrington, W. Brennan, G. P. Glass, J. V. Michael, and H. Niki, *J. Chem. Phys.*, **43**, 525 (1965); (b) J. O. Sullivan and P. Warneck, *J. Phys. Chem.*, **69**, 1749 (1965).
(3) J. M. Brown and B. A. Thrush, *Trans. Faraday Soc.*, **63**, 630 (1967).

(4) G. S. James and G. P. Glass, *J. Chem. Phys.*, **50**, 2268 (1969).
(5) K. Hoyermann, H. Gg. Wagner, and J. Wolfrum, *Z. Phys. Chem.*, **63**, 193 (1969).
(6) A. A. Westenberg and N. DeHaas, *J. Phys. Chem.*, **73**, 1181 (1969).
(7) D. Saunders and J. Heicklen, *J. Phys. Chem.*, **70**, 1950 (1966).
(8) W. E. Wilson and A. A. Westenberg, *Symp. (Int.) Combust., [Proc.] 11th, 1966*, 914 (1967).
(9) J. E. Breen and G. P. Glass, *Int. J. Chem. Kinet.*, **3**, 145 (1970).
(10) D. G. Williamson, *J. Phys. Chem.*, **75**, 4053 (1971).
(11) I. T. N. Jones and K. D. Bayes, *Symp. (Int.) Combust., [Proc.] 14th, 1972*, in press.
(12) D. G. Williamson and K. D. Bayes, *J. Phys. Chem.*, **73**, 1232 (1969).
(13) M. Gehring, K. Hoyermann, H. Gg. Wagner, and J. Wolfrum, *Z. Naturforsch. A*, **25**, 675 (1970).
(14) S. N. Foner and R. L. Hudson, *J. Chem. Phys.*, **49**, 3724 (1968); **53**, 4377 (1970).
(15) R. Gordon, Jr., R. E. Rebbert, and P. Ausloos, *Nat. Bur. Stand. U. S., Tech. Note, No. 496* (1969).
(16) D. Davis and W. Braun, *Appl. Opt.*, **7**, 2071 (1968).
(17) In this equation and in similar ones to follow in which different isotopic variants of a product were detected, the actual product de-

(18) tected is italicized, and the net ion counts for each isotopic composition of interest is given (normalized so that the most abundant species is 1) above the arrow designating the reaction producing it. The 99% confidence limits of the net ion count (three standard deviations) is also given (*e.g.*, 1 ± 0.14). The relative ion counts should be close to the relative rate constants for the respective routes. Accurate relative rate constants could only come from crossed molecular beam experiments in which the intersection of the beams are more precisely defined and angular distributions of products are measured.
(18) The numbers in parentheses are the net ion counts for each isotopic composition designated normalized to one for the most abundant one. The error limits are the 99% confidence limits of the net ion count (three standard deviations).
(19) A krypton lamp was used to detect C_2H since Jones and Bayes[11] report it is ionized with this lamp.
(20) In this discussion the term "displacement reaction" is used when the experimental evidence for a reactive channel is consistent with the dynamic model of the attacking free radical displacing an atom or functional group from the alkyne.
(21) H. E. Avery and S. J. Heath, *J. Chem. Soc., Faraday Trans. 1*, **68**, 512 (1972).
(22) H. E. Avery, private communication.

A Study of Structural and Solvent Effects on the Rate of Reaction between Heterocyclic Bases and Copper(II) Bis(diethyldithiocarbamate)[1]

F. G. Herring* and R. L. Tapping

Department of Chemistry, University of British Columbia, Vancouver, British Columbia, Canada V6T-1W5

(Received September 14, 1973)

The reaction between copper(II) bis(diethyldithiocarbamate) and heterocyclic bases has been studied as a function of structural (methyl substitution) and solvent effects (benzene, toluene, and chloroform) using epr. The equilibrium constants are in the range 0.3–0.9 with $\Delta H°$ and $\Delta S°$ of the order −5 kcal/mol and −18.5 eu, respectively, at 298°K. The specific rate constants for adduct dissociation for the bases pyridine, 3-picoline, and 4-picoline exhibit an isokinetic relationship whereas 3,4-lutidine and 2-picoline do not conform; explanations for this are offered. The enthalpies of activation for adduct dissociation are all positive whereas those for adduct formation are negative. The specific rate constants for adduct formation ($\sim 10^8$ M^{-1} sec^{-1}) all, except 2-picoline, conform to an isokinetic model in the absence of a linear free-energy relationship. These results are explained in terms of a diffusion mechanism and a probability of reaction that decreases with increasing temperature.

The first observation of the modulation of the line width of an electron paramagnetic resonance line of a transition metal ion by ligand exchange appears to have been observed by McGarvey.[2a] Subsequently Pearson and Buch[2b] measured the rate of formation of ion pairs between the nitrosyldisulfonate ion and various transition metal ions. The specific rate constants for association were found to be within a factor of 2 of the diffusion-controlled limit. The only other epr kinetic studies of complex ion formation between ions are those carried out by McCain and Myers[3] and Lynds, Crawford, Lynden-Bell, and Chan.[4]

The first epr investigation of the kinetics of adduct formation between a neutral complex possessing a vacant coordination site and various bases is that of Walker, Carlin, and Rieger[5] who studied the adduct formation between vanadylacetylacetonate and various bases. The problems associated with the analysis of the Bloch equations[6] modified to include chemical exchange[7] were indi-

cated in this work. The other Lewis acid–base reaction to have been studied by epr is that represented by

$$Cu(DADC)_2 + base \rightleftharpoons Cu(DADC)_2 \cdot base \qquad (1)$$
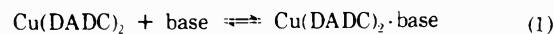
where $Cu(DADC)_2$ is a copper(II) bis(dialkyldithiocarbamate) complex. Reaction 1 was first studied by Corden and Rieger[8] and Shklyaev and Anufrienko[9] and subsequently by Farmer, Herring, and Tapping.[10] Corden and Rieger dealt in some detail with the problem of extracting formation and rate constants from the observed line position and line width data, respectively; this question will be discussed later.

The application of the epr technique in the fast exchange region to the study of an equilibrium such as that represented by eq 1 requires that the formation constant be approximately unity and the forward and reverse rates comparable to the reciprocal of the difference in Larmor frequencies between the free complex and the adduct. Both of these conditions are met in the present and previ-

ous studies so that the analysis of epr line position data can lead to formation constants in a way that is strictly analogous to the methods employed in nuclear magnetic resonance.[8-11] The previous studies[8-10] have all argued, on very sound chemical evidence, that only one molecule of base forms an adduct with the $Cu(DADC)_2$; it has since been demonstrated that the stoichiometry of adduct formation is in fact 1:1[11] over the entire range of base concentration.

The measurement of line width variation, provided that all the necessary requirements of fast or near-fast exchange are met, can lead to estimates of adduct lifetimes. Therefore, it is of great advantage that the parent Lewis acid have narrow epr lines so that line width variation can be readily observed as the concentration of the Lewis base is varied. The epr spectra of $Cu(DADC)_2$ species exhibit very narrow lines and it is for this reason that all previous successful studies on Lewis acid–base reactions have been carried out on molecules of this type. Consequently the epr technique may not have general applicability[8] but nonetheless these studies provide for the first time reliable data on fast reactions between neutral non-free-radical species in solution.

The specific rate constants and thermodynamic data obtained from experiments in which a fair temperature range is covered can be used to test current theories of solvent and base variation effects on the rate of fast reactions. Previous work has already shown that the temperature coefficient of an Arrhenius plot for the forward rate constant can be near zero[8] or even negative.[10] These results cannot be explained by a simple diffusion-controlled mechanism or by a simple preequilibrium encounter model.

The observation of an apparent "negative activation energy" in our previous study[10] of the rate of adduct formation between copper(II) bis(diethyldithiocarbamate) [Cu(DEDC)_2] and pyridine in benzene prompted us to extend the investigation to other bases and solvents. It is the results and conclusions that can be reached from these experiments, using methyl-substituted pyridines as bases in benzene and toluene and chloroform as solvents with pyridine as the base, that we wish to report here.

Experimental Section

Epr measurements and methods of analysis of data have been described previously.[10] The solvents (benzene, toluene, and chloroform) were of Spectrograde quality obtained from Fisher Scientific. The bases (pyridine, 2-, 3-, and 4-picoline, and 2,6- and 3,4-lutidine) were obtained from either Fisher or Kodak and were of the highest available purity. Gas chromatographic analysis failed to show any impurities. It must be noted that these isomers are difficult to resolve amongst themselves, consequently the gas chromatographic separation may not reveal isomeric impurities. The presence of an appreciable amount of impurity that might interfere in the exchange process should be detectable in epr spectra taken of $Cu(DEDC)_2$ in the neat bases. In all cases high-gain epr spectra failed to reveal any sign of impurity, although they did show sulfur-33 (0.7% natural abundance) hyperfine splitting.[12] As with the solvents, the bases were kept cool and dry before use, after which they were resealed under nitrogen with an appropriate drying agent.[13a] The $Cu(DEDC)_2$ employed was prepared from isotopically pure ^{63}Cu as previously described.[10] The maximum errors in the measurement of hyperfine coupling constant, g tensor, line positions, and

line widths were ± 0.05 G, ± 0.0002, $\pm 0.0005 \times 10^9$ sec^{-1}, and ± 0.2 G, respectively. These errors lead to uncertainties in the equilibrium constant, enthalpies, entropies, and lifetime of adducts of ± 0.02 M^{-1}, ± 0.2 kcal mol^{-1}, ± 1.2 eu, and 0.2×10^{-9} sec, respectively. The corresponding error in the rate constant is approximately $\pm 0.02 \times 10^8$ sec^{-1}. All measurements were corrected for temperature induced volume changes of the liquids.

Results

The least-squares analysis, described in detail previously, of the line position data allows for the free variation of the Larmor frequencies of the unbound complex (ω_{CuL_2}) and the adduct (ω_{CuL_2B}) in the determination of the stability constant, K, from the equation

$$\langle \omega \rangle = (\omega_{CuL_2} + \omega_{CuL_2B} K[B_0])/(1 + K[B_0]) \quad (2)$$

where $\langle \omega \rangle$ is the average line position for the $m_I = +\frac{3}{2}$ used in this work and $[B_0]$ is the concentration of added heterocyclic base. We note here that the concentration of $Cu(DEDC)_2$ is ca. 10^{-4} M and that $[B_0]$ varies from 10^{-2} to 10 M so that the approximation that $[Cu(DDC)_2B] \ll$ [free base] used in deriving[10] eq 2 is always valid. Table I contains the results of measurements carried out over the temperature range 270–330°K in the system of Cu(DEDC)_2 and pyridine in benzene,[10] toluene, and chloroform. The quantity $\Delta\omega(= \omega_{CuL_2} - \omega_{CuL_2B})$ is required in the determination of the adduct lifetime; it will be seen from the results contained in Table I that this quantity is temperature dependent (see below). Table II contains stability constants and $\Delta\omega$ values obtained from measurements on the reaction between Cu(DEDC)_2 and 2-, 3-, and 4-picoline and 3,4-lutidine in benzene over the temperature range 270–330°K. The epr technique employed here failed to detect any adduct formed between 2,6-lutidine and Cu(DEDC)_2; presumably the two methyl groups sterically prevent the formation of the copper–nitrogen bond. The formation of adduct between 2-picoline also became undetectable above 310°K and, in fact, the formation constant above this temperature can only be estimated using Scatchard plots[11] and not the least-squares analysis.

The values of $\Delta\omega$ contained in Table II also show a substantial temperature dependence. The inclusion of this variation has important consequences with regard to the determination of the lifetime of the adduct (τ_B).

The following expression for the line width of an epr line can be used.[8,13b,14]

$$T_2^{-1} = T_2^{-1}(ex) + T_2^{-1}(correction) + T_2^{-1}(nonsec) \quad (3a)$$

$$T_2^{-1}(ex) = P_A T_{2A}^{-1} + P_B T_{2B}^{-1} + P_A^2 P_B \tau_B (\omega_A - \omega_B)^2 \quad (3b)$$

$$T_2^{-1}(correction) = (P_B/\tau_B)\{(P_A - P_B)\delta(3\Delta^2 - \delta^2) + (5P_A P_B - 1)(\Delta^4 - 6\delta^2\Delta^2 + \delta^4)\} \quad (3c)$$

$$T_2^{-1}(nonsec) = (P_A^2 P_B \tau_B/2) \times \{[I(I+1) - m^2 I]/(1 + \omega_0^2 \tau_B^2 P_A^2)\}(a_A - a_B)^2 \quad (3d)$$

where A and B represent CuL_2 and CuL_2B, respectively, T_{2A} and T_{2B} are the line widths for the individual species A and B. P_A and P_B are the fractions of A and B and a_A and a_B are the hyperfine splitting constants for A and B.

The first term in eq 3a, i.e., $T_2^{-1}(ex)$ is the usual modified Bloch equation solution for fast exchange with lifetime broadening.[13b] The conditions that are imposed by the fast-exchange approximation are

TABLE I: Results for Cu(DEDC)$_2$ and Pyridines in Various Solvents[a]

Temp, °K	Benzene			Toluene			Chloroform		
	$\Delta\omega$, sec^{-1} $\times$ 10^{-9}	K, M^{-1}	k_r, sec^{-1} $\times$ 10^{-8}	$\Delta\omega$, sec^{-1} $\times$ 10^{-9}	K, M^{-1}	k_r, sec^{-1} $\times$ 10^{-8}	$\Delta\omega$, sec^{-1} $\times$ 10^{-9}	K, M^{-1}	k_r, sec^{-1} $\times$ 10^{-8}
270	0.480	0.73	3.28	0.502	0.92	2.17	0.554	0.60	1.96
280	0.479	0.60	4.13	0.465	0.66	2.70	0.539	0.41	2.56
290	0.445	0.53	5.24	0.447	0.47	4.18	0.525	0.30	4.15
300	0.431	0.38	5.85	0.434	0.36	5.08	0.504	0.24	6.02
310	0.419	0.30	6.62	0.424	0.30	6.06	0.490	0.19	7.63
320	0.409	0.24	7.52	0.417	0.22	7.41	0.471	0.15	10.10
330	0.395	0.17	8.28	0.414	0.18	9.61	0.459	0.12	12.50

[a] Data for ω_{CuL_2}, ω_{CuL_2B}, $T_1^{-1}CuL_2$, and $T_2^{-1}CuL_2B$ are available upon request.

TABLE II: Results for Cu(DEDC)$_2$ and Various Bases in Benzene[a]

Temp, °K	2-Picoline			3-Picoline			4-Picoline			3,4-Lutidine		
	$\Delta\omega$, sec^{-1} $\times$ 10^{-9}	K, M^{-1}	k_r, sec^{-1} $\times$ 10^{-8}	$\Delta\omega$, sec^{-1} $\times$ 10^{-9}	K, M^{-1}	k_r, sec^{-1} $\times$ 10^{-8}	$\Delta\omega$, sec^{-1} $\times$ 10^{-9}	K, M^{-1}	k_r, sec^{-1} $\times$ 10^{-8}	$\Delta\omega$, sec^{-1} $\times$ 10^{-9}	K, M^{-1}	k_r, sec^{-1} $\times$ 10^{-8}
275	0.400	0.082	2.34	0.495	1.10	2.75	0.515	1.47	1.79	0.632	2.02	1.73
285	0.399	0.060	4.00	0.445	0.79	3.08	0.463	1.05	2.26	0.531	1.55	2.03
295	0.396	0.054	6.89	0.406	0.57	4.05	0.425	0.74	3.00	0.455	1.14	2.35
300	0.331	0.050	9.35	0.393	0.49	4.55	0.411	0.62	3.28	0.426	0.97	2.48
310	0.323	0.038		0.374	0.37	5.60	0.390	0.46	4.13	0.381	0.71	3.01
320	0.320	0.032		0.356	0.29	6.67	0.374	0.34	5.35	0.344	0.56	3.33
335[b]	0.302	0.023		0.342	0.20	7.58	0.361	0.27	6.76	0.327	0.38	3.82

[a] Data for ω_{CuL_2}, ω_{CuL_2B}, and $T_2^{-1}CuL_2B$ are available upon request. [b] 330 for 4-picoline.

TABLE III: Comparison of Various Terms in Eq 3 for Benzene–Pyridine Data at 300°K

Base concn, M	Ordinary Bloch term (eq 3b), sec^{-1}	Extended Bloch term (eq 3c), sec^{-1}	Nonsecular term (eq 3d), sec^{-1}	T_2^{-1} (obsd), sec^{-1}
1.03	1.198 $\times$ 10^8	0.418 $\times$ 10^6	0.171 $\times$ 10^4	1.202 $\times$ 10^8
1.38	1.156 $\times$ 10^8	3.046 $\times$ 10^6	0.233 $\times$ 10^4	1.187 $\times$ 10^8
2.77	1.036 $\times$ 10^8	2.060 $\times$ 10^6	0.364 $\times$ 10^4	1.056 $\times$ 10^8
3.55	0.887 $\times$ 10^8	0.457 $\times$ 10^6	0.588 $\times$ 10^4	0.891 $\times$ 10^8
6.20	0.762 $\times$ 10^8	0.012 $\times$ 10^6	0.950 $\times$ 10^4	0.762 $\times$ 10^8
7.79	0.736 $\times$ 10^8	−0.006 $\times$ 10^6	1.086 $\times$ 10^4	0.736 $\times$ 10^8
12.41	0.717 $\times$ 10^8	−0.011 $\times$ 10^6	1.067 $\times$ 10^4	0.717 $\times$ 10^8

$$\tau|\omega_A - \omega_B| = \Delta \ll 1$$

$$\tau|T_{2A}^{-1} - T_{2B}^{-1}| = \delta \ll 1$$

$$\tau|P_A T_{2A}^{-1} + P_B T_{2B}^{-1}| = r \ll 1$$

where $\tau = \tau_A \tau_B/(\tau_A + \tau_B)$.

If any one of these conditions is not fulfilled then correction terms of the form eq 3c must be applied.[8] The most serious difficulty in the present study is that Δ can approach 0.8, in this case Corden and Rieger[8] have shown that corrections of the form in eq 3c are appropriate. Equation 3d is the nonsecular contribution to the line width which Atherton and Luckhurst[14] proposed should be included.

The analysis of line width was restricted, in this work, to the +3/2 line ($a_0 < 0$) since it was found that this line most closely satisfies the fast-exchange conditions outlined above. The lifetime of the adduct can be extracted from eq 3 by carrying out a least-squares analysis of eq 3 using the values of K, ω_{CuL_2}, and ω_{CuL_2B} previously determined. To do this it is necessary to decide which of the terms in eq 3 is the most important; this decision can be affected greatly by the chosen experimental conditions. Corden and Rieger, for example, constrained the base concentration in their work to be less than 3 M

with the bulk of their experimental determinations being carried out below 1 M. This choice is unfortunate since below about 1 M base concentration, for the types of system being considered here, T_2^{-1}(ex) and T_2^{-1}(correction) become comparable but above that concentration T_2^{-1}(ex) always dominates eq 3. The various terms in eq 3 are compared in Table III and the above statement is seen to be true. Presumably Corden and Rieger[8] kept the base concentration below 3 M to avoid any possible complications due to the formation of a second adduct, e.g., Cu(DEDC)$_2$·(pyridine)$_2$. The complete range of base concentration (0.5–12 M) can be used since a separate study[11] has shown that only a 1:1 adduct is formed over the entire base concentration range and in all solvents used. The line widths were analyzed in the present work by a least-squares fitting of eq 3a for the parameters $T_2^{-1}CuL_2$ measured in pure solvent at the appropriate temperature. The values of $T_2^{-1}CuL_2B$ obtained were found to be slightly less than the value measured in neat base solution. This is not unexpected since Cu(DEDC)$_2$ in pure pyridine, for example, corresponds to only 80% adduct formation and the fitted $T_2^{-1}CuL_2B$ should correspond to the experimentally unattainable situation of 100% adduct formation. The measured lifetime is simply the reciprocal of the first-order specific rate constant (k_r). The forward rate constant (k_f) is estimated from the rela-

TABLE IV: Thermodynamic Results in Previous[a-c] and Present Work for 298°K

Acid	Base	Solvent	K, M^{-1}	$\Delta H°$, kcal/ mol	$\Delta S°$, eu	k_r, sec^{-1} × 10^{-8}	ΔH_r^*, kcal/ mol	ΔS_r^*, eu	ΔH_f^*, kcal/ mol	ΔS_f^*, eu
Cu(Dn-BuDC)$_2$	C$_5$H$_5$N	C$_6$H$_{11}$CH$_3$[a]	0.40	−5	−19	20	5	−1	∼0	−18
Cu(DEDC)$_2$	C$_5$H$_5$N	C$_6$H$_5$CH$_3$[b]	0.49	−4.9		3.4	8.6		3.7	
Cu(DEDC)$_2$	C$_5$H$_5$N	C$_6$H$_6$[c]	0.38	−4.3	−16	5.8	2.1	−12	−2.2	−28
Cu(DEDC)$_2$	C$_5$H$_5$N	C$_6$H$_5$CH$_3$	0.36	−4.8	−18	5.1	3.8	−6	−1.0	−24
Cu(DEDC)$_2$	C$_5$H$_5$N	CHCl$_3$	0.24	−4.6	−18	6.0	5.1	−2	0.5	−20
Cu(DEDC)$_2$	2-CH$_3$C$_5$H$_4$N	C$_6$H$_6$	0.05	−3.1	−17	9.4	8.4	11	5.3	−6
Cu(DEDC)$_2$	3-CH$_3$C$_5$H$_4$N	C$_6$H$_6$	0.49	−5.2	−19	4.6	2.8	−10	−2.4	−29
Cu(DEDC)$_2$	4-CH$_3$C$_5$H$_4$N	C$_6$H$_6$	0.62	−5.7	−20	3.3	3.8	−7	−1.9	−27
Cu(DEDC)$_2$	3,4-(CH$_3$)$_2$C$_2$H$_5$N	C$_6$H$_6$	0.97	−5.2	−17	2.5	1.9	−14	−3.3	−31

[a] Reference 8. [b] Reference 9. [c] Reference 10.
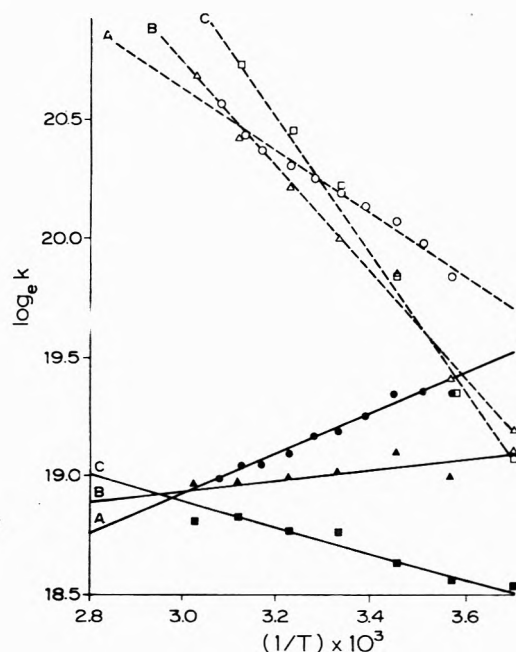
Figure 1. Arrhenius plots for forward (solid symbols) and reverse (open) reactions between Cu(DEDC)$_2$ and pyridine in benzene (circles), toluene (triangles), and chloroform (squares).

Figure 2. Arrhenius plots for forward (solids) and reverse (open) reactions between Cu(DEDC)$_2$ and pyridine (circles), 3-picoline (diamonds), 4-picoline (squares), and 3,4-lutidine (triangles) in benzene.

tion $k_f = Kk_r$ which assumes that the formation of the adduct is simply governed by the reaction given in eq 1, i.e., there is no preequilibrium. The results for the systems studied are collected in Tables I and II. It will be noticed in Table II that data for 2-picoline and Cu-(DEDC)$_2$ is not presented for temperatures in excess of 310°K, this is because the stability constant is so small above that temperature that exchange line width variations could not be detected.

The line width measurements were carried out over the temperature range 270–330°K. This temperature range being compatible with the systems studied still exhibiting fast or near-fast chemical exchange. The thermodynamic data so obtained are presented in Table IV. Figures 1 and 2 show Arrhenius plots for the forward and reverse rates as the solvent (Figure 1) or as the base (Figure 2) is varied. The results of previous studies[8-10] are also included in Table IV for the purpose of comparison.

It is perhaps appropriate at this point to compare our results with those of other workers. The basis of the method employed here is that the ω_{CuL_2}, ω_{CuL_2B}, and K be obtained from a least-squares analysis of eq 2 using the results of a set of experiments designed so that the so-called saturation factor, $S = P_B$, falls in the range 0.2–0.8. The

reason for this has been discussed by Deranleau[15] and has been used in a study[11] that demonstrates that only 1:1 adducts are formed in the present case. The least-squares analysis of the line position data obtained over the prescribed temperature range then provides the temperature dependence of the parameters ω_{CuL_2}, ω_{CuL_2B}, and K. The analysis of the line width data obtained over the same temperature range requires the temperature variation of ω_{CuL_2}, ω_{CuL_2B}, and K. Previous workers[8,9] have not allowed ω_{CuL_2} and ω_{CuL_2B} to vary but have constrained them to be temperature independent; this will lead to large errors in the estimated lifetimes.[16] The lifetimes obtained in such a way will be too high when $\omega_{CuL_2} - \omega_{CuL_2B}$ is less than the "temperature-independent" value and too low otherwise. This in turn will lead to errors in the measured activation energy.

Corden and Rieger[8] studied the system copper(II) bis(di-n-butyldithiocarbamate) with pyridine, piperidine, and n-hexylamine in methylcyclohexane, analyzing the results in a fashion similar to that employed here. In the present case we are most interested in the results obtained for pyridine so that a comparison, as to structural and solvent effects, with our results can be made. Unfortunately these authors found it necessary to both (i) constrain $\omega_A - \omega_B$ to be independent of temperature, leading

to the errors previously mentioned and (ii) to use the piperidine value of $\omega_A - \omega_B$, which leads to smaller values of τ_B since $\omega_A - \omega_B$ for pyridine is 30% less than that for piperidine. We also note that the saturation fraction covered in their experiments is only 0 to 0.4 which is insufficient to obtain reliable values of K. The results of these approximations render the results of Corden and Rieger somewhat uncertain and as a consequence comparison with our results are not very useful.

The more recent study by Shklyaev and Anufrienko[9] involved reaction between CuDDC and pyridine in toluene. Values of K obtained are in reasonable agreement with those obtained here, but discrepancies exist in the evaluations of ΔH^*. Once again, these authors make the assumption that a_0 and g_0 are temperature independent. Tables of data given by these authors indicate that this is not so, and as stressed here earlier to make use of this assumption invites large errors.[16] Examination of their data (not all the necessary data are provided so exact reconstruction of their results is not possible) shows that $\omega_A - \omega_B$ should change by 30% over the temperature range they consider. Appropriate corrections to τ_B and hence k_r then indicate that ΔH_r^* should be ~ 5 kcal/mol, rather than the value 8.6 kcal/mol obtained. This would be in agreement with that obtained here, and would yield a similar value of ΔH_f^* to that quoted in this work.

The method used by Shklyaev and Anufrienko is that of Dye and Dalton,[17] and is based on determining the m_1-dependent coefficients of the line widths. This is equivalent to the procedure used here, with one caution; to extract the line width coefficients from only a four-line epr spectrum, as is the case with copper(II) complexes in solution, is a difficult task at low or moderately low temperatures ($T \leq 280°K$). At such temperatures the two low-field lines become quite broad, often broad enough to overlap. Line width measurements on such lines are subject to large errors, and extraction of m_1-independent coefficients is likely to be subject to equally large uncertainty.

A final point with respect to the study of Shklyaev and Anufrienko is that the equilibrium constants were measured over a wide pyridine concentration range, but rate constants were evaluated only at 0.475 M pyridine in toluene. This may not cause any increase in error in the results, but it is clear that this region is not the most sensitive to the effects of exchange. The maximum exchange effects occur at pyridine concentrations ≥ 1 M for the temperature range 0–60°, and it would be expected that in order to minimize any possible errors, measurements of the exchange rate should be made over a reasonable concentration range, including very carefully the region of maximum exchange. Regions not in a sensitive part of the concentration range will be relatively insensitive to small changes in τ_B. These qualitative considerations, coupled with those of Deranleau,[15] for instance, suggest that all rate processes should be studied not only over a reasonable range of temperature, but also over a range of concentration sufficient to include all effects of exchange.

Discussion

(a) *Formation Constants.* The formation constants of the adducts of $Cu(DEDC)_2$ with the heterocyclic bases used here are uniformly smaller than those of the corresponding adducts formed with copper(II) bis(β-diketonates).[18] The greater Lewis acid properties of the β-diketonates presumably is a reflexion of the greater net posi-

tive charge on the copper atom. In other words, the greater ligand-field affect of the DADC relative to the β-diketonates leads to a greater transfer of negative charge to the metal from the ligand, thereby decreasing the ability for further coordination.

Relatively few studies of solvent effects on the stability constants of adducts fromed by the Lewis acid–base reaction of square-planer copper(II) complexes with bases have been carried out.[18,19] The results in Table IV indicate that the formation constants for the adduct formed between $Cu(DEDC)_2$ and pyridine decrease in the solvent order benzene $\geq$ toluene > chloroform, which is in accord with the previous findings.[18,19] The heats of solvation of pyridine in benzene (-0.01 kcal/mol) and chloroform (-1.82 kcal/mol), measured by Libutti, *et al.*,[19] suggest that chloroform interacts very strongly with pyridine; presumably *via* hydrogen bonding. It has been suggested that it is this strong solvation of pyridine in chloroform that causes the decrease in stability constant. An alternative suggestion, which probably amounts to the same thing, revolves around the observation that as the base strength is increased the formation constant increases (see below), consequently it is tempting to suggest that the base strength of pyridine decreases on going from benzene to chloroform; further evidence stems from the fact that there is an inverse correlation with dielectric constant. Such conclusions must be viewed critically since in this and other work the variation of activity coefficients has been neglected. The thermodynamic formation constant (K_{Th}) is given by

$$K_{Th} = [CuL_2B]\gamma_{CuL_2B}/[B][CuL_2]\gamma_B\gamma_{CuL_2} \approx K_c\gamma_B^{-1} \quad (4)$$

since the concentrations of free complex and adduc. are very small ($\sim 10^{-4}$ M). The value of γ_B, the activity coefficient of the base, depends directly upon the heat of mixing (solvation) of the base in the chosen solvent,[20] so that we expect γ_B(benzene) > γ_B(toluene) > γ_B(chloroform) whence K_c(benzene) > K_c(toluene) > K_c(chloroform). It may be noted that the work of Jannelli and Orsini[32] shows that the activity coefficient of pyridine in benzene varies only slightly from unity, the maximum deviation being 9% at 50 mol %.

Graddon and coworkers[18] have found that the stability constants of a series of adducts formed by methyl-substituted pyridines and copper(II) bis(β-diketonates) vary with basicity and steric factor. The order of the stability constants found in this work are in accorc with this finding. The stability constants increase as follows: 3,4-lutidine > 4-picoline > 3-picoline > pyridine > 2-picoline, which is the order of increasing base strength, except for the position of 2-picoline where the presence of the 2-methyl group sterically hinders adduct formation.

An inspection of Table IV reveals that the overall enthalpy ($\Delta H°$) and entropy ($\Delta S°$) changes for pyridine and 3- and 4-picoline correlate with base strength whereas in the case of the other bases and solvent variation no obvious correlations are apparent. In fact, $\Delta H°$ and $\Delta S°$ are fairly independent of solvent and base strength variation which serves to indicate that the temperature dependence of static (equilibrium) constants are not very sensitive indicators of structural or solvent effects for a series of closely related systems. The average value of -5.0 ± 0.7 kcal/mol for $\Delta H°$ is in the range of that expected for the formation of a copper–nitrogen bond in the type of system studied here.[18] The entropy change (-18.5 ± 1.5 eu) is also typical for the loss of entropy accompanying adduct

formation. The formation of the adduct between Cu-$(DEDC)_2$ and 2-picoline is accompanied by a $\Delta H° = -3.1$ somewhat lower than the other systems, the reason for this is the detailed balance between $\Delta H_f{}^*$ and $\Delta H_r{}^*$ (see below).

(b) *Adduct Dissociation.* The Arrhenius plot for the specific rate constants for adduct dissociation shown in Figure 1 indicates that the adducts formed between $Cu(DEDC)_2$ and pyridine and 3- and 4-methylpyridine conform to an isokinetic relationship. This is demonstrated by the fact that the lines in Figure 1 for these systems intersect at $520 \pm 20°K$. The lines for 2-picoline and 3,4-lutidine do not conform to this isokinetic relationship. The generally held view[21,22] is that those reactions which possess an isokinetic temperature proceed by the same mechanism and a different mechanism must be sought for those not possessing the same isokinetic temperature.

The presence of an isokinetic temperature indicates that the dissociation of the adducts formed between pyridine, 3-picoline, and 4-picoline and $Cu(DEDC)_2$ in benzene proceed by very similar mechanisms. The possible mechanism can be described in two ways, the first is a microscopic model involving the dissociation of the molecule and subsequent escape of the partners that formed the molecule from the solvent cage[21,23] and the second is a macroscopic model describing the variation of the enthalpy of activation in terms of a structural model of the solvent.[24]

The expression for the rate of diffusion away from an encounter between A and B is given by[25]

$$k_d = 3(D_A + D_B)/\sigma^2 \qquad (5)$$

where D_A and D_B are the translational diffusion coefficients (cm^2/sec) of the species A and B, and σ is a collision diameter. The translational diffusion coefficients can be estimated from the relation[26,27]

$$D_A = k_B T /[18(V_m{}^A/\sigma_A{}^2)\eta f_T{}^A] \qquad (6)$$

where η is the viscosity of the solvent, $V_m{}^A$ is the volume of the molecule in question, k_B is the Boltzmann constant, σ_A in the diameter of molecule A ($V_m{}^A = \pi\sigma_A{}^2/3$), and $f_T{}^A$ in the translational microviscosity factor.

$$f_T{}^A = (3r_S/2r_A) + 1/(1 + r_S/r_A)$$

where r_S and r_A are the radii of solvent and solute, respectively. Employing the molar volumes of pyridine and $Cu(DEDC)_2$, calculated from their respective densities,[28] we obtain diffusion constants of pyridine and $Cu(DEDC)_2$ in benzene of 0.63×10^{-5} and 0.55×10^{-5} cm^2/sec, respectively. The microviscosity theory employed here has also been used to estimate the rotational correlation time of $Cu(DEDC)_2$ as being between 1 and 2×10^{-11} sec, which is in good agreement with the measured value of *ca.* 1.5×10^{-11} sec.[29]

The substitution of the estimated diffusion coefficients into eq 5 lead to a rate of diffusion from an encounter of 3×10^9 sec^{-1} for a value $\sigma = 10$ Å. The observed rate constants of dissociation are between one and two orders of magnitude smaller than this; we conclude therefore that the dissociative rate constants depend upon an energy of activation of breaking the Cu–N bond as well as diffusion away from the cage containing the adduct. The necessary activation energy would only need to be about 2 kcal/mol. We therefore write

$$k_{obsd} = k_d e^{-E^*/RT} = \frac{k_B T}{6b}\left[\frac{\sigma_A{}^2}{V_m{}^A f_T{}^A} + \frac{\sigma_B{}^2}{V_m{}^B f_T{}^B}\right]\frac{e^{-(B + E^*)/RT}}{\sigma^2} \qquad (7)$$

where we have used the relationship $\eta = b e^{B/RT}$ which has been used to describe the temperature variation of viscosity.[30] The above equation can be used to estimate the preexponential factor for adduct dissociation in benzene ($b = 4.92 \times 10^{-5}$) by employing the various quantities mentioned above. The value obtained for A_1 is 3×10^{12} sec^{-1} which is to be compared with the observed value of 5×10^{10} sec^{-1}. The over estimate of the preexponential factor implies that it is not simply governed by diffusion and one must introduce the concept of an entropy of activation, which is small and negative. Nonetheless, the model provides a reasonable description of the observed trends in activation parameters.

The results in Table IV indicate that both $\Delta H_r{}^*$ and $\Delta S_r{}^*$ increase as the dipole moment of the base increases for the series pyridine, 3- and 4-picoline. Equation 7 above indicates that the enthalpy of activation is governed by both electronic factors (E^*) and solvent factors (B represents viscous enthalpy). We can expect both E^* and B to increase as the dipole moment increases for the following reasons: first, we expect the energy of the copper–nitrogen bond to increase as the electron donor properties of the base increases; second, the presence of a dipole in a solvent has a stiffening effect on the mixture which will lead to increase in B. The idea of a dipole being "relayed" through a solvent is quite well established[24,31] and has been used in a study of the activity coefficients of pyridine in benzene.[32] The existence of a small negative entropy of activation indicates that the activated state is formed by only very few motions other than those along the reaction coordinate.[21] The variation of $\Delta S_r{}^*$ is very difficult to interpret since the results for many solvents indicate[30] that as liquids become increasingly polar b (from $\eta = b e^{B/RT}$) decreases, which should mean that A_r decreases; however, the experimental results show an opposite trend. This indicates that the observed A_r is not simply a function of solvent stiffness but also of solvent openness. This observed variation of $\Delta S_r{}^*$ is that on going from pyridine to 4-picoline the entropy increases, this implies more ways of forming the transition state. Such a trend could be accomplished by an increased cage size and this is not an unreasonable explanation.

The above ideas can be translated into a model of the effects of solvent structure on the activation parameters of dissociation proposed by Bennetto and Caldin.[24] The model deals primarily with the enthalpy of activation which is divided into two parts

$$\Delta H_r{}^* = \Delta H_{ML} + \Delta H_{st}$$

where ΔH_{ML} is the enthalpy associated with the copper–nitrogen bond and ΔH_{st} is the contribution from the solvent structure. We can compare ΔH_{ML} and ΔH_{st} with E^* and B in eq 8. The essence of the theory of Bennetto and Caldin is that immediately around an ion, and between it and the bulk solvent, there is a disordered region which may be likened to the gas phase, and ΔH_{st} is made up of contributions from the passage of ligand or solvent molecules in or out of this region, and the ability of the bulk solvent to accommodate ligands or solvent molecules which leave this region during a dissociative interchange. The present study is not concerned with ligand replacement at ions but nonetheless a disordered region about the $Cu(DEDC)_2$ or its adduct can be envisaged, *i.e.*, similar to an encounter region.

Consider the dissociation of one of the adducts investigated here. The enthalpy of bond dissociation (ΔH_{ML}) will

vary with the electronic properties of the ligand; this is similar to the innersphere effect.[33] This is borne out by the correlation of ΔH_r^* with base strength for pyridine and 3- and 4-picoline. In addition to this important effect we have the effect of the base on the solvent which will, according to the theory of Bennetto and Caldin,[24] tend to reinforce the base strength effect since ΔH_{st} becomes more positive as the solvent structure stiffens. In summary, we may say that both theories have similar conclusions even though their origin is quite different.

The deviation of the dissociation of the adducts formed by 3,4-lutidine and 2-picoline from isokinetic behavior can now be interpreted on the basis of these two theories. The data in Table IV show that both ΔH_r^* and ΔS_r^* correlate with dipole moment for the series pyridine, 3- and 4-picoline. When 3,4-lutidine is added to the correlation ΔS_r^* still smoothly correlates but ΔH_r^* does not; in fact, the observed ΔH_r^* is too high relative to what might be expected on the basis of electronic and solvent stiffening effects. The lifetime of an encounter is essentially the same as that of rotational correlation so that when the adduct formed by 3,4-lutidine dissociates it will not have time to rotate before the base vacates the solvent cage. The increased ΔH_r^* may possibly be due to the repulsive interaction of the two methyl groups with the bulk solvent molecules as the molecule leaves the cage. In terms of the Bennetto–Caldin model more work must be done on the bulk solvent relative to the dissociation of the pyridine adduct.

The anomalously high ΔH_r^* for 2-picoline appears to be a manifestation of the effect of the increased activation in the forward direction due to steric repulsion and the fact that the adduct once formed has a $\Delta H°$ only ~ 1 kcal/mol less than the pyridine adduct. The other interesting aspect of the dissociation of the 2-picoline adduct is the very high frequency factor (3.4×10^{15} sec^{-1}). This can be explained using the ideas of Steel and Laidler[34] who suggest that high entropies of activation arise from the looseness of certain vibrations in the activated state due to a greater elongation of the bond to be broken, *i.e.*, the greater A_r for 2-picoline arises from a greater copper–nitrogen bond length in the activated state due to steric repulsion.

The variation of solvent from benzene to chloroform through toluene also shows deviations from isokinetic behavior. The results indicate that as the solvent is able to interact more strongly with the pyridine either by a weak dipole–dipole interaction (toluene) or a hydrogen bond (chloroform) the ΔH_r^* and ΔS_r^* increase. The increase in ΔH_r^* reflects the greater stiffening of the pyridine–solvent mixture due to greater base–solvent interactions. The fact that there is no isokinetic behavior suggests that there is minimal compensation between ΔH_r^* and ΔS_r^* and, in fact, ΔH_r^* is affected more than ΔS_r^*.

(c) *Adduct Formation.* The above discussion provides a reasonable, if somewhat speculative, interpretation of the specific rate constants of adduct dissociation and their concomitant temperature dependencies. The results for the forward rate constants, computed from $k_f = K k_r$, are even more interesting in that k_f is found to increase as the temperature decreases; see Figures 1 and 2. It is appropriate to consider first whether or not this unusual temperature dependence is artifactual in any way. The experimental details, presented earlier, indicate that all possible care has been taken to ensure that the measured K and k_r are free from as much uncertainty as possible. The only other factor that has been neglected, but mentioned ear-

lier, is that of activity coefficients. The measured value of K corresponds to K_c and k_f should be given by $K_{Th} k_r = K_c k_r / \gamma_B$ but we have employed $k_f = K_c k_r = K_{Th} k_r \gamma_B$. It is well known that as the temperature increases γ_B decreases whence k_f measured in this study would appear to increase more slowly than the true value. An apparent negative activation could result if the temperature dependence of γ_B were greater than $K_{Th} k_r$. The temperature dependence of γ_B is proportional to the heat of solvation[20] which is essentially zero for pyridine in benzene so that the result in benzene (and perhaps toluene) may be regarded as reliable. The result in chloroform is perhaps more suspect as the heat of solution is about -2 kcal/mol so that the activation parameter for k_f in this case may be underestimated. The results for the other bases are presumably reliable as we do not expect their heats of solvation to differ substantially from that of pyridine. It may be concluded then that it is safe to interpret the results for k_f as they stand.

The forward bimolecular rate constants are, with the exception of the 2-picoline, all approximately 2×10^8 M^{-1} sec^{-1}. The results in Tables I and II indicate that the forward rate constant is essentially independent of base variation but depends to some degree on solvent in that it decreases in the order benzene > toluene > chloroform. It can be noted that this is the order of increasing base–solvent interactions. The Arrhenius plots in Figures 1 and 2 for k_f show well-defined isokinetic points, 330 ± 7 and $323 \pm 5°$K, respectively. The direct measurement of rate constants on either side of the isokinetic temperature, has, to our knowledge, not been made previously. Since the k_f values are largely independent of the nature of the base no Hammett-type LFER exists for the forward direction, and we have therefore an example of an isokinetic behavior in the absence of a LFER. We conclude therefore, except for 2-picoline, that the mechanism of adduct formation is the same irrespective of solvent or base variation for the systems studied here. The existence of an isokinetic temperature implies compensation between ΔH_f^* and ΔS_f^* (*i.e.*, a linear relationship[21] which is in turn evocative of substantial solvent participation in the formation of the transition state.

A mechanism that is likely to be dominated by solvent characteristics is that of diffusion control. The simple Smoluchowski[35] relationship for a diffusion controlled mechanism is

$$k_f = 4\pi\sigma(D_A + D_B)N_0/1000 (M^{-1} \text{ sec}^{-1})$$
$$= 4\pi\sigma D_{AB}(N_0/1000)$$

which in the present case leads to a value of 2×10^{11} which is greater by three orders of magnitude than the observed rate constants. The Smoluchowski equation was derived on the premise that at the critical distance σ the concentration of diffusing species is zero. Subsequently, Noyes[36] modified the theory to include a finite concentration at the boundary. However, it was found necessary to implement Noyes' suggestion more rigorously in order to obtain the correct expression for a diffusion-controlled reaction rate. Logan[37] showed that the correct expression is

$$k_2 = 4\pi\sigma D_{AB}Zp/[1 + 4\pi\sigma D_{AB}(1 - p/2)] \qquad (8)$$

then

$$\frac{Z}{k_2} = \frac{Z}{4\pi\sigma D_{AB}} + \frac{1}{p} - \frac{1}{2} \qquad (9)$$

where Z is the collision number, and p is the probability

that reaction occurs on a collision. It may be noted here that $4\pi\sigma D_{AB}$ is the encounter number and that usually the ratio $Z/4\pi\sigma D_{AB}$ is between 10 and 100, i.e., molecules undergo between 10 and 100 collisions in every encounter.[21]

Logan investigated the behavior of eq 9 with respect to temperature for various choices of p and using

$$\left(\frac{Z}{4\pi\sigma D_{AB}}\right)_T = \left(\frac{Z}{4\pi\sigma D_{AB}}\right)_{25°} \exp\left\{\frac{(B + \frac{1}{2}RT)}{R}\left(\frac{1}{T} - \frac{1}{298}\right)\right\} \quad (10)$$

where B is the viscous enthalpy in $\eta = be^{B/RT}$ (see above). It was found for the form $p = \exp(-E^*/RT)$ that the activation energy of eq 9 (E_{obsd}) approached E^* for high values of E^* and approached B when $E^* \to 0$. When p was set to be temperature independent low values of p caused substantial changes in the E_{obsd}. In no cases, as expected, did E_{obsd} become negative for these choices. Typically, using $Z = 10^{12}$ and $B = 2.850$ kcal/mol, the p for pyridine in benzene has to be of the order 2.5×10^{-4} which corresponds to $E^* = 4.9$ kcal/mol (assuming $p = \exp(-E^*/RT)$). Consequently the intrinsic activation energy has a reasonable value, but in order to describe the observed temperature dependence of k_f the probability of reaction (p) must decrease with increasing temperature. Before attempting to offer possible explanations for this behavior in terms of the above and other models we shall discuss the observed trends in the activation parameters.

It was noted earlier that both ΔH_f^* and ΔS_f^* increase in the order of increasing solvent-base interaction as the solvents are changed; furthermore as the base is varied ΔH_f^* and ΔS_f^* increase as the dipole moment of the base increases. These observations, coupled with the discussion of the dissociation specific rate constants, are evocative of solvent structure playing a dominant role. Such a conclusion is further supported by the existence of a compensation effect between ΔH_f^* and ΔS_f^* in the absence of a LFER. It is interesting to note that the formation of the adduct of 3,4-lutidine also conforms to the isokinetic behavior, and possesses the most negative Arrhenius temperature coefficient.

The observation of an apparent negative "activation energy" (it is of course illogical to speak of a negative activation energy, a preferable term is a negative Arrhenius temperature coefficient) can either imply the existence of a preequilibrium[38] situation or a probability of reaction that indeed decreases with increasing temperature. The preequilibrium model has an intrinsic appeal in that it requires no new concept. One model consists of the postulate that both base and $Cu(DEDC)_2$ are rapidly solvated at a diffusion-controlled rate (10^{10} M^{-1} sec^{-1}) and that the overall energetics of adduct formation are a balance of heats of formation, solvation, and activation for the dissociation, thus

$$B + nS \rightleftharpoons BS_n \qquad \Delta H_1$$

$$Cu(DEDC)_2 + mS \rightleftharpoons Cu(DEDC)_2S_m \qquad \Delta H_2$$

$$Cu(DEDC)_2S_m + BS_n \rightleftharpoons Cu(DEDC)_2BS_{m-1} + (n + 1)S \qquad \Delta H_3$$
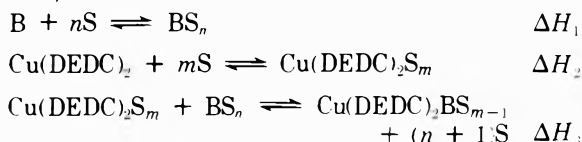
then

$$H_f^* = \Delta H_0 - \Delta H_1 - \Delta H_2 + \Delta H_r^* \quad (11)$$

where $\Delta H_3 = \Delta H_f^* - \Delta H_r^*$ and $\Delta H_0 = \Delta H_1 + \Delta H_2 + \Delta H_3$. The enthalpy of activation in the forward direction will be negative if the solvation of base and complex are sufficiently endothermic to outweigh ΔH_r^* and ΔH_0. In fact, the heat of solution of pyridine in benzene is essen-

tially zero and is about -2 kcal/mol in chloroform, so that although eq 11 predicts ΔH_f^*(benzene) $< \Delta H_f^*$(chloroform), all other things being equal, the exothermicity of the heat of solution will tend to lead to $\Delta H_f^* > 0$. The heat of solution of $Cu(DEDC)_2$ is unknown for the solvents employed here but it might be expected that ΔH_2 is less than zero. Clearly this model is inadequate from the point of view of providing an adequate molecular model. The heats of solution are related to the energy required for the respective molecules to leave their solvent cages. The solvents are noncoordinating so that adduct formation can be excluded, thus it is better to describe the present reaction in terms of diffusion of the reactive molecules from one cage to another until an encounter is reached. This idea leads to a second mechanism which suggests that $Cu(DEDC)_2$ and the base diffuse rapidly to an encounter complex which is established with respect to the average energy of the solvated individual molecules. The rate-controlling step is then reorientation of the molecules in the encounter complex so that the copper-nitrogen bond is formed. The addition of the base to the square-planar complex will no doubt require an expansion of the solvent cage and work will have to be done on the bulk solvent. Consequently the stiffer the solvent structure the more work that must be done. Thus, if the work done is less than the difference in stabilization energy of the encounter complex relative to the parent molecules the apparent activation energy will be negative, and if it is greater the observed activation energy will be positive. The idea of an encounter complex will therefore account for the observed results since ΔH_f^* increases as the base-solvent interactions increase, i.e., change of solvent from benzene to chloroform. Furthermore, if we assume that the dipole moment of the base induces dipoles in the benzene solvent molecules which then tend to stiffen the solvent this accounts for the observed trend that ΔH_f^* correlates with dipole moment of the base. The unsatisfactory nature of this model is the vagueness of the concept of an encounter complex. The energetics of the present system require that this encounter complex be stabilized by about 5 kcal/mol, which is quite substantial for neutral molecules.

The Bennetto-Caldin model can also provide an explanation for the negative temperature coefficients. The enthalpy of activation in their model will be given by $\Delta H_f^* = \Delta H_{MS} + \Delta H_{st}$ where ΔH_{MS} is the enthalpy associated with a solvent molecule leaving the encounter region to make way for the incoming base and ΔH_{st} corresponds to the energy of reorganization required to accept the outgoing solvent molecule and give up the ingoing base. Since we are dealing with noncoordinating solvents it is reasonable to expect that ΔH_{MS} will be small so that ΔH_f^* will be dominated by ΔH_{st}^*. The structural term will be negative if the process of the solvent molecule going from the encounter region dominates all other solvent reorganizational processes. The exothermicity arises from the fact that this process is similar to condensation. The structural term will become more positive as the solvent is stiffened. Thus, if ΔH_{MS} is small and ΔH_{st} is negative it is likely that ΔH_f^* will be negative. The unsatisfactory feature of this model is that there is no explanation as to why the condensation process dominates except to say that the solvents studied here are essentially uncooperative in the sense defined by Bennetto and Caldin.

The most satisfactory model is that embodied in the equation of Logan (eq 9) since it includes diffusion to the encounter as exemplified by the $4\pi\sigma D_{AB}$ term, the num-

ber of collisions in an encounter ($Z/4\pi\sigma D_{AB}$) and a probability of reaction (p). Logan has shown that when E^* is small, using $p = \exp(-E^*/RT)$, the observed activation energy tends to be affected most by the enthalpy of viscosity (B), i.e., structural features of the bulk solvent. To illustrate this, if we employ the rate constants of adduct formation between pyridine in benzene ($B = 2.850$ kcal/mol) $Z = 10^{12}$ and ($Z/4\pi\sigma D_{AB}$) ca. 10 at 298°K, the apparent activation of p is only -1.0 kcal/mol from a plot of $\log p$ vs. $1/T$, i.e., only a small and negative temperature coefficient. Changing the number of collision per encounter to 100 does not overly affect this result, and changing Z to 10^{13} will of course have a dramatic effect on the actual value of p but not its temperature variation. The origin of this small negative temperature coefficient is worth speculating upon.

The observation that the temperature coefficient of the forward rate constant is more negative the weaker the dipole moment of the base, or the weaker the solvent–solute interactions, leads to a possible explanation of this unusual effect. It is reasonable to conceive of a site on the Cu-$(DEDC)_2$ at the copper atom which is positive and attracts the negative end of the dipole moment of the base. Thus as dipole moment of the base increases, the interaction between base and $Cu(DEDC)_2$ becomes stronger, then as the molecules approach each other through the solvent the centers of reaction will be well corrleated; i.e., the donor and acceptor sites will be directed toward one another to facilitate reaction. Therefore the molecules on collision will tend to react, i.e., collide inelastically. The weaker the dipole moment the poorer the correlation between the appropriate centers, thus when the molecules collide they will do so elastically. The second manifestation of this dipole-moment-dependent "cross section" will be that the greater the translational motion of the molecules the more likely they are to collide elastically due to the poorly correlated reactive centers, hence the decreasing probability of reaction as the temperature increases. The implication of these qualitative ideas is that p is not the usual Arrhenius probability of reaction ($p = \exp(-E^*/RT)$) but rather an energy dependent cross section.

The effect of modification of the bulk solvent will be manifested in changes in B (eq 10), thus if B is large and E^* is about the same for all solvents then the apparent activation energy will be positive. The hydrogen bonding in the pyridine–chloroform mixture no doubt increases B so that the observed activation energy is positive. It is interesting to note that this model gives a qualitative reason for why the condensation process in the Bennetto–Caldin model is so important.

The exceptional behavior of the adduct formation between 2-picoline and Cu(DEDC)$_2$ is accounted for in the present model by stating that the presence of the 2-methyl group causes repulsions between the two molecules which serve to increase the E^* so that, as found by Logan, the intrinsic energy of activation dominates. Thus the observed activation energy in this case almost reflects the activation requirements for adduct formation, i.e., E_{obsd} approaches E^*.

Very recently Firestone and Christensen[39] have suggested that the requirement for a chemical reaction is that activation takes place through vibrational modes and that the molecules must be together long enough that several vibrations take place. The consequence of this is that if the molecules possess too much translational energy they will collide elastically so that insufficient time will be

available for the necessary vibronic coupling. The suggestion is that enzymes derive their catalytic power by immobilizing the reactants until they attain the required activation energy and sufficient vibration coupling. The present results offer some support for these ideas. We have suggested earlier that the molecules studied here are likely to undergo elastic collision unless the acceptor and donor sites are well correlated but in addition, or instead, it is equally reasonable that the collisions become progressively harder as the temperature (whence the translational energy is increased) is raised, thus the probability of reaction decreases, i.e., E^* is inherently negative because of this collisional effect. The true situation in the present work is likely to be a combination of both effects.

References and Notes

(1) Presented in part at the XIVth International Coordination Chemistry Conference, Toronto, Canada, 1972.
(2) (a) B. R. McGarvey, *J. Phys. Chem.*, **61**, 1232 (1957); (b) R. G. Pearson and T. Buch, *J. Chem. Phys.*, **36**, 1277 (1962).
(3) D. C. McCain and R. J. Myers, *J. Phys. Chem.*, **72**, 4115 (1968).
(4) L. Lynds, J. E. Crawford, R. M. Lynden-Bell, and S. I. Chan, *J. Chem. Phys.*, **57**, 5216 (1972).
(5) F. A. Walker, R. L. Carlin, and P. H. Rieger, *J. Chem. Phys.*, **45**, 4181 (1966).
(6) F. Bloch, *Phys. Rev.*, **102**, 104 (1956).
(7) H. M. McConnell, *J. Chem. Phys.*, **28**, 430 (1958).
(8) B. J. Corden and P. H. Rieger, *Inorg. Chem.*, **10**, 263 (1971).
(9) A. A. Shklyaev and V. F. Anufrienko, *J. Struct. Chem.*, **12**, 548 (1971).
(10) J. B. Farmer, F. G. Herring, and R. L. Tapping, *Can. J. Chem.*, **50**, 2079 (1972).
(11) J. B. Farmer, F. G. Herring, and R. L. Tapping, *Can. J. Chem.*, **51**, 1530 (1973).
(12) The magnitude of the ^{33}S isotropic splitting, measured from both $m_1 = \frac{1}{2}$ and $m_1 = \frac{3}{2}$ lines, is estimated to be 9.4 G.
(13) (a) See, e.g., L. E. Tenebaum, "The Chemistry of Heterocyclic Compounds," Interscience, New York, N. Y., 1961, Chapter 14; (b) S. Meiboom, Z. Luz, and D. Gill, *J. Chem. Phys.*, **27**, 1411 (1957).
(14) N. M. Atherton and G. R. Luckhurst, *Mol. Phys.*, **8**, 145 (1967).
(15) D. A. Deranleau, *J. Amer. Chem. Soc.*, **91**, 4044, 4050 (1969).
(16) R. R. Shoup, E. D. Becker, and M. L. McNeel, *J. Phys. Chem.*, **76**, 71 (1972).
(17) J. D. Dye and L. R. Dalton, *J. Phys. Chem.*, **71**, 184 (1967).
(18) D. P. Graddon, *Coord. Chem. Rev.*, **4**, 1 (1969).
(19) B. L. Libutti, B. B. Wayland, and A. F. Garito, *Inorg. Chem.*, **8**, 1510 (1969).
(20) E. F. Caldin, "An Introduction to Chemical Thermodynamics," Oxford University Press, London, 1958.
(21) J. E. Leffler and E. Grunwald, "Rates and Equilibria of Organic Reaction," Wiley, New York, N. Y., 1963.
(22) O. Exner, *Collect. Czech. Chem. Commun.*, **29**, 1094 (1964).
(23) E. A. Moelwyn-Hughes, "The Chemical Statics and Kinetics of Solutions," Academic Press, New York, N. Y., 1971.
(24) H. P. Bennetto and E. F. Caldin, *J. Chem. Soc. A*, 2191, 2207 (1971).
(25) F. Grunwald, *Progr. Phys. Org. Chem.*, **3**, 317 (1965).
(26) A. Gierer and K. Wirtz, *Z. Naturforsch A.* **8**, 532 (1953).
(27) J. H. Noggle and R. E. Schirmer, "The Nuclear Overhauser Effect," Academic Press, New York, N. Y., 1971, p 31.
(28) M. Bonamico, A. Dessy, A. Mugnoli, A. Vaciago, and L. Zambonelli, *Acta Crystallogr.*, **19**, 886 (1965).
(29) F. G. Herring and R. L. Tapping, unpublished work.
(30) E. A. Moelwyn-Hughes, "Physical Chemistry," Pergamon Press, Elmsford, N. Y., 1964.
(31) L. Onsager, *J. Amer. Chem. Soc.*, **58**, 1486 (1936).
(32) L. Jannelli and P. G. Orsini, *Gazz. Chim. Ital.*, **86**, 1104 (1956); **87**, 159 (1957).
(33) F. R. Shu and D. B. Rorabacher, *Inorg. Chem.*, **11**, 1496 (1972).
(34) C. Steel and K. J. Laidler, *J. Chem. Phys.*, **34**, 1827 (1961).
(35) M. von Smoluchowski, *Z. Phys. Chem.*, **92**, 129 (1913).
(36) R. M. Noyes, *Progr. React. Kinet.*, **1**, 129 (1961).
(37) S. R. Logan, *Trans. Faraday Soc.*, **63**, 1713 (1967).
(38) P. J. Zandstra and S. I. Weissman, *J. Amer. Chem. Soc.*, **84**, 4408 (1962).
(39) R. A. Firestone and B. G. Christensen, *Tetrahedron Lett.*, 389 (1973).

Kinetics of Particle Growth. III. Particle Formation in the Photolysis of Sulfur Dioxide–Acetylene Mixtures

Menachem Luria, Rosa G. de Pena, Kenneth J. Olszyna, and Julian Heicklen*

Departments of Chemistry and Meteorology and Center for Air Environment Studies, The Pennsylvania State University, University Park, Pennsylvania 16802 (Received June 21, 1973)

The photolysis of SO_2 with radiation >3000 Å in the presence of C_2H_2 was studied at 29°. The reaction is unaffected by the absence or presence of 1 atm of N_2 or CO_2. The sole reaction products are CO and a solid compound of the trimer of $C_3H_4S_2O_3$. The rate of CO production, $R(CO)$, is proportional to the SO_2 pressure at constant $[C_2H_2]/[SO_2]$ and increases slightly with an increase in C_2H_2 pressure. Initially as the reaction mixture is irradiated there is an induction period of about 45 sec, before which particles are not produced, though CO is. Then suddenly nucleation occurs, particles are produced for a few seconds, and then particle production ceases. The particles grow rapidly by condensation of the $C_3H_4S_2O_3$ trimer, which is continually produced during the radiation. The particle density drops slowly because of coagulation. Ordinary diffusional loss of particles to the wall is negligible, but many of the particles are lost, probably because of convective diffusion and gravitational settling. In some experiments, after about 1-hr radiation, second nucleation occurs and the particle density rises rapidly. The reactions of importance in the system are $T \rightarrow$ wall removal (6), $rT \rightarrow T_r$ (9), $T + T_n \rightarrow T_{n+1}$, (8), and $T_n + T_m \rightarrow T_{n+m}$ (7), where T is the $C_3H_4S_2O_3$ trimer, r is the average number of trimers needed to produce a nucleus capable of growth, and n and m are integers $>r$. The value found for r was 3.6 and the critical trimer concentration needed for particle nucleation was 4.9×10^{10} per cc. The values of the rate coefficients were $k_6 = 3.0 \times 10^{-3}$ sec^{-1}, $k_9 = 1.2 \times 10^{-34}$ cc$^{2.6}$/sec, and $k_7 = 1.5 \times 10^{-7}$ cm^3/sec for particles between 100 and 1000 Å in diameter. For larger particles, k_7 is smaller, as expected from theory. The value of 1.5×10^{-7} cm^3/sec for k_7 corresponds to coagulation on every collision for particles with diameters between 100 and 1000 Å. The value for k_8 increased with the size of T_n, and about as expected if every collision were effective. For particles <200 Å diameter, every collision is effective, and k_8 has collision efficiencies of >0.3–0.5 for particle diameters of ~3000 Å.

Introduction

Particle formation from gas-phase reactions is often important in the atmosphere as well as in laboratory studies. In our laboratory we have a program to examine the kinetics of particle formation, *i.e.*, both the size distribution and growth rates, as a function of time for particles produced from isothermal gas-phase chemical reactions. In previous publications, studies of NH_4NO_3 formation from the NH_3–O_3 reaction[1] and NH_4Cl formation from the NH_3–HCl reaction[2] have been discussed.

In this paper, particle production is examined under conditions in which the gas-phase reactions are photochemically induced. In particular, the system studied is the photolysis of SO_2 in the presence of C_2H_2. Reactions of photoexcited SO_2 studied previously include the reactions with O_2,[3-6] with CO,[7-11] with C_2F_4,[9] with thiophene,[12] and with hydrocarbons.[7,8,13-16] In particular, Dainton and Ivin[13,14] found that photoexcited SO_2 reacted with both paraffins and olefins to produce sulfinic acids. However, as far as we know, the reaction of photoexcited SO_2 with C_2H_2 has not been reported.

Experimental Section

The reaction was carried out in a 2.9-l. cylindrical cell about 115 cm long and 6.0 cm in diameter with 2-mm thick Pyrex walls. The light sources for irradiation were one-to-six General Electric Dark Light 40-W fluorescent lamps, each 120 cm long which surrounded the cell. The light which entered the cell was restricted to wavelengths >3000 Å since both the lamps and the cell wall were

Pyrex. During irradiation cold air was circulated around the cell to keep the temperature at 29 ± 2°.

The gases used were from the Matheson Co. These included SO_2, C_2H_2, CO_2, and N_2. C_2D_2 of 99% atom purity was obtained from ICN Chemical and Drug Isotope Division. Before use, the N_2 was passed through a trap at −196° packed with glass wool. The SO_2 was twice purified by distillation from −98 to −196° and the C_2H_2 was distilled twice from −130 to −196°. The gases were handled in a grease-free vacuum line containing Teflon stopcocks with Viton "O" rings. The vacuum line was connected to the reaction cell and could reduce the pressure in the cell to 0.1 mTorr.

The gases were introduced into the reaction cell as follows. Mixtures of SO_2 and C_2H_2 were made using pressures that could be measured on a Wallace and Tiernan absolute pressure indicator. The mixtures were then expanded by a factor of 10 or 100 into the reaction cell. N_2 (or CO_2) was then added to the reaction cell to raise the pressure to 750–780 Torr. To ensure thorough mixing, the N_2 was added through a thin tube which was in the reaction vessel and ran parallel to its axis. The tube contained 10 orifices along its length spaced at 10-cm intervals so that the N_2 would enter the reaction cell at several points along the cell length.

The reaction cell was connected through a stopcock to a gas chromatographic sample tube with a volume of 350 cc. The chromatograph utilized a Gow Mac power supply and thermistor detector at 0°. Two columns were used. One was 8 ft long containing 5A molecular sieves used for CO

analysis. The other was 30 ft long and contained dimethylsulfolane; and it was used to measure C_2H_4, CO_2, and OCS. All gaseous products could be detected at pressure of 0.3 mTorr. He with a flow rate of 100 cc/sec was the carrier gas in both columns.

Samples for particle analysis were withdrawn (up to 15 samples) during a run by expanding the reaction mixture into a small sample tube (1.1% of the reaction volume) under vacuum. The sample was then transferred to a syringe of 1-l. volume by diluting with N_2. Immediately the syringe was emptied into a particle counting device. The whole sampling and analytical procedure could be accomplished in 30 sec.

To measure the number of particles larger than 25 Å in diameter, a portable condensation nuclei counter Model No. 1012E-001 made by Environment One was used. This counter operates at a supersaturation of ~300% and was calibrated by the manufacturer against a Pollack counter.

To detect particles of larger minimum diameters, we used the thermal diffusion chamber built at Penn State.[17] It operates on the same principle as the Environment One condensation nuclei counter, but at supersaturations of only 0–5%. The relationship between per cent supersaturation and minimum particle can be computed[1,18] and is

$$S = 2500/\sigma \text{ for particles insoluble in } H_2O$$

$$S = 5000/\sigma^{3/2} \text{ for } NH_4NO_3$$

where S is the per cent supersaturation and σ is the particle diameter in Å. The first equation is for particles insoluble in H_2O, and the second is for NH_4NO_3 which is highly soluble in H_2O. Since the solid formed in this study is nearly insoluble in water, the "insoluble" curve was used to determine minimum particle diameter. Actually, diameters computed this way are somewhat large, the discrepancy becoming more pronounced the larger the minimum particle diameter.

More complete size distributions as well as information on the shape of particles were obtained by electron microscopy. For this purpose particles were collected by passing the entire contents of the cell through 0.4-μm diameter nucleopore filters. The filters with the samples were covered with a layer of SiO and Cr, placed on an electron microscope copper grid and the filter dissolved in chloroform according to Frank, et al.[19] If the particles to be observed are soluble in chloroform, the replicas on the filters remain.

The efficiencies of collection of the filters for different particle size were calculated according to Spurny, et al.[20] As the specific gravity of the particle is only known to be greater than 1, the calculations were performed for three different values: 1, 1.5, and 2.2, respectively, and for the velocity employed, i.e., 50 cm/sec. The results are shown in Figure 1. From this figure it can be seen that for particles larger than 3000 Å diameter and smaller than 30 Å, the efficiency is always 1. In the former case, the particles are too large to pass through the holes, and in the latter case, the likelihood that the particles strike a hole is negligible. For intermediate particle diameters, the efficiencies are smaller and depend on specific gravity, but the ratio between the efficiencies at sp gr = 2.2 and at 1.0 is always smaller than a factor of 2. The number obtained from direct countings on the electron microscope photographs were corrected according to the efficiencies calculated with a sp gr of 1.5. The maximum magnification for
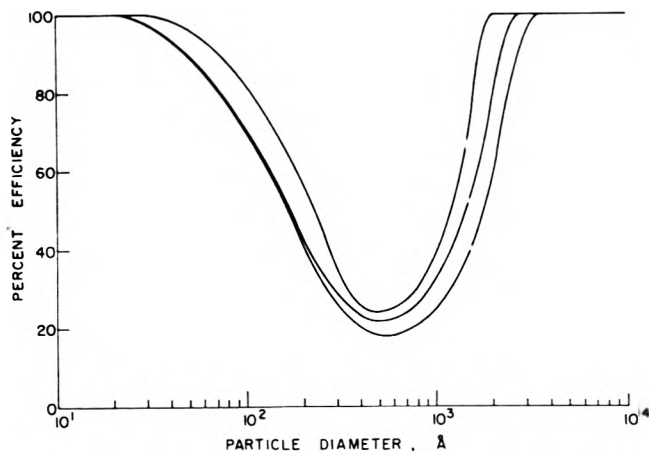
Figure 1. Semilog plot of filter collection efficiency vs. particle diameter for a flow speed of 50 cm/sec. The upper curve is for particles of density 2.2 g/cm³; the middle curve, for density 1.5 g/cm³; and the lower curve, for density 1.0 g/cm³.

which good contrast was observed was 43,200; consequently the smallest particle observed was 100 Å in diameter.

In some runs, the entire contents of the reaction cell were collected on electron microscope grids covered with carbon or formvar placed in an electrostatic precipitator made by T.S.I., Model 3100. This method gave less precision than the filter method, due to the fact that the sample was distributed on a surface 60 times larger than in the filter.

In some experiments the total particle mass was obtained. The entire contents of the cell were pumped at a rate of 1 l. min⁻¹ through a T.S.I. particle mass monitor Model 3200A. The mass monitor precipitates the particles which are bigger than 100 Å in diameter in one of two identical crystals. Using a Hewlett-Packard frequency reader Model 5326B, the frequency difference between the two crystals was followed. This difference is proportional to the particle sample weight.

Large amounts of the solid were collected for chemical analysis by radiating mixtures of 100 Torr of SO_2, 100 Torr of C_2H_2, and 550 Torr of N_2 for 30 min. The reacted mixture was then compressed by N_2 and forced through a sinterglass filter containing 2-μ diameter holes. In this way about 2 mg of solid was collected on the filter. The procedure was repeated several times to collect as much solid as desired. The solid was then subjected to mass spectral analysis, differential thermal analysis, elemental analysis, and a molecular weight determination. It was also tested for solubility in various solvents and its photodecomposition products were obtained. Samples were also prepared for infrared and nmr analysis by irradiating mixtures of 100 Torr of SO_2 and 100 Torr of C_2H_2 with radiation from a Hanovia medium-pressure U-shaped Type SH mercury arc.

Results

When mixtures of SO_2 and C_2H_2 were irradiated with radiation >3000 Å, particles were produced which ultimately settled as a yellow-brown solid. Gas chromatographic analysis gave CO as the only initial gas-phase product, though small amounts of CO_2 were also produced for extended conversions. There was no evidence for the formation of C_2H_4 or other gas-phase hydrocarbons. With the exception of CO_2, mass spectral analysis confirmed
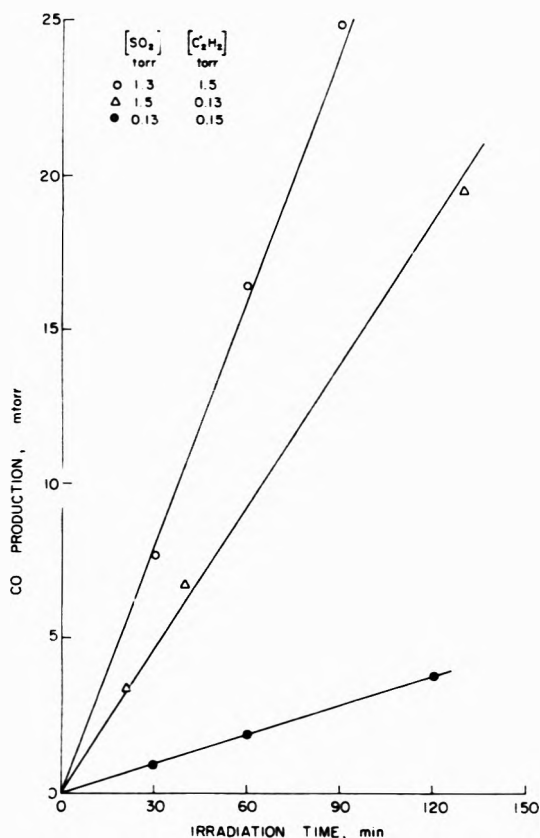
Figure 2. Plot of the CO production vs. irradiation time in the photolysis of SO₂-C₂H₂ mixtures at 29° with six lamps.

Figure 3. Log-log plot of the rate of CO formation vs. SO₂ pressure in the photolysis of SO₂-C₂H₂ mixtures at 29° with six lamps.

Figure 4. Plot of the rate of CO formation vs. light intensity in the photolysis of SO₂-C₂H₂ mixtures for an SO₂ pressure of 0.13 Torr at 29°.

the absence of any gas-phase compounds with molecular weight ≥36.

Monitoring the Reaction. The production of CO offered an easy internal means of monitoring the reaction. To study particle production more easily, it was essential to study the reaction in the presence of a large excess of an inert diluent gas to minimize wall losses by diffusion. The diluent gas of primary interest to us is N_2 since it is the major atmospheric constituent. Unfortunately in the presence of a large excess of N_2, it is difficult to measure small amounts of CO. However, a few runs in the presence of an atmosphere of CO_2 gave as much CO as in the absence of CO_2. It was also found that the particle number density and growth curves were essentially the same with either CO_2 or N_2 as the diluent. Thus we assumed the photochemistry is the same in the absence or presence of an atmosphere of N_2 (or CO_2). This is in keeping with other photochemical studies in our laboratory in which the chemistry of photoexcited SO_2 was not altered by the presence of N_2.[9]

Every experiment done in the presence of excess N_2 to measure particle growth was repeated in the absence of N_2 to monitor CO. Experiments were done at SO_2 and C_2H_2 pressures from 0.0015 to 1.5 Torr. The experiments with 0.0015 Torr of reactants followed the same trends expected from the results at higher pressures, but were quantitatively difficult to assess because of the large experimental uncertainty resulting from the small amounts of products formed. The production of CO from the other experiments (in the absence of N_2) is shown graphically in Figures 2–4.

Figure 2 shows that CO production is linear with irradiation time. The rate of CO production is enhanced by increasing either reactant pressure, the enhancement by SO_2 being more pronounced than that by C_2H_2.

The effect of reactant pressure is seen more clearly in Figure 3 which shows the rate of CO production, $R(CO)$, as a function of the SO_2 pressure for two $[C_2H_2]/[SO_2]$ ratios. The log-log plots are fitted by lines of slope one, indicating a proportional dependence of $R(CO)$ on the SO_2 pressure. The proportionality constants are 1.6×10^{11} and 1.3×10^{11} mol/cc sec Torr for $[C_2H_2]/[SO_2]$ ratios of 14 and 1.2, respectively. From the data in Figure 2, the proportionality constant can be computed to be 0.55×10^{11}

molecule/cc sec Torr for $[C_2H_2]/[SO_2] = 0.087$. Thus $R(CO)$ is relatively insensitive to the ratio $[C_2H_2]/[SO_2]$, changing only by a factor of 3 as the ratio changes by a factor of 160.

The fact that $R(CO)$ is proportional to the SO_2 pressure is attributed to the fact that the absorbed light intensity, I_a, is proportional to the SO_2 pressure. Thus, $R(CO)$ is proportional to I_a, as can be seen directly from Figure 4. This figure plots $R(CO)$ vs. the number of lamps used, i.e., the relative intensity. The plots are linear and pass through the origin.

Identification of the Solid. The yellow-brown solid had very low solubility in H_2O, acetone, CCl_4, CS_2, and chloroform, but is soluble in dimethyl sulfoxide. A differential thermal analysis showed no melting point as the temperature was raised from 35 to 250°. The solid started to decompose at 100°, and at the end of the run the residue appeared to be carbon. There was no evidence from the differential thermal analysis for phase transitions including those which might correspond to free water or elemental sulfur.

An elemental analysis was made by Midwest Microlab of Indianapolis, and the results are shown in Table I. In the same table is shown the analysis expected for $C_3H_4S_2O_3$. This empirical formula, which has a molecular weight of 152, fits the experimental results reasonably well. Midwest Microlab also attempted a molecular weight determination, using acetone as a solvent. Since the solid was only slightly soluble, only an approximate molecular weight of 450 could be obtained. This molecular weight is close to that of 456 for the trimer of $C_3H_4S_2O_3$.

In order to obtain information about the structure of the solid, infrared, mass, and nmr spectra were obtained. The solid was prepared for infrared analysis by irradiating a mixture of 100 Torr of SO_2 and 100 Torr of C_2H_2 for 3 hr with a Hanovia medium-pressure U-shaped Type SH mercury arc in a 10-cm Pyrex cell with KBr windows. The solid product from the reaction formed a thin coat on the windows. The infrared spectrum was taken immediately after the irradiation, then with the gases removed but before admitting air, again after air was admitted, and finally 6 days later. The solid spectra were essentially all the same. The spectrum taken after the gas-phase products were removed is shown in Figure 5 (available on microfilm, see paragraph at end of paper regarding supplementary material). The band at 5.80 μ indicates the presence of a carbonyl group. The two bands at 7.60 and 8.85 μ can be associated with an SO_2 group, and the band at 9.65 μ might be associated with an SO_2 group conjugated with a CO group.

The mass spectral data for the solid obtained from both SO_2–C_2H_2 and SO_2–C_2D_2 mixtures are given in Table II (available on microfilm). It was necessary to heat the solid beyond its decomposition temperature ($\sim100°$) in order to obtain the spectra. The lowest temperature at which significant peak heights were obtained was 150°. Prominent peaks were seen only to m/e ratios of 256, the parent peak for S_8, and sulfur surely must be a decomposition product. The other peaks could be associated with sulfur fragments, CO, CO_2, OCS, SO_2, and CH_2 (or CD_2) groups attached to the sulfur fragments. High-resolution spectra showed no oxygen in any peaks at $m/e > 64$. However, there were two high-resolution peaks at m/e 64, so that both S_2 and SO_2 ions were present.

A weak nmr spectrum was obtained for the solid dis-

TABLE I: Elementary Analysis of Solid Produced in the Photolysis of SO_2–C_2H_2 Mixtures

Element	Wt % (expt)	Wt % (for $C_3H_4S_2O_3$)
H	2.75	2.63
C	21.06	23.6
O	33.68	31.9
S	42.64	42.0
Total	100.13	100.13

solved in CCl_4, because of the low solubility of the solid. Only one unresolved band appeared at 2.15 ppm downfield from tetramethylsilane. This peak is consistent with the presence of CH_2 groups.

A thick layer of the solid was photodecomposed and the gas-phase products identified. They were CO, CO_2, OCS, and probably a small amount of C_2H_4. The gas chromatographic column used for the analysis was not suitable for determining SO_2, and no measurement for that compound was attempted.

Particle Formation. When mixtures of SO_2 and C_2H_2 are irradiated, there is an induction period before particles appear, but then about 10^5 particles per cc appear very quickly, essentially in a step function. Further irradiation does not markedly increase the particle density and, in fact, the particle density slowly drops as the run continues.

A typical plot is shown in Figure 6 for irradiation of a mixture of 0.13 Torr of SO_2 and 1.9 Torr of C_2H_2 in 1 atm of N_2. In these experiments the number of particles per cc with diameters exceeding 1000 Å (assuming complete insolubility of the particles in H_2O) were measured as a function of reaction time. With no radiation or for irradiation times less than 30 sec, when $R(CO) = 2.14 \times 10^{10}$ molecule/cc sec, the particle density was always below 800 per cc. Sometimes even for irradiations as long as 45 sec, the particle density remained this low. After about 1-min irradiation, the particle density increased by over two orders of magnitude in several seconds. Further irradiation, or even discontinuation of the radiation after 60 sec had little further effect on the particle number density. In either case the number density of particles rose slowly to a peak at about 10 min and then fell slowly for the duration of the experiment which was 60 min.

The very sharp rise at about 1-min irradiation indicates that particles of diameter <1000 Å suddenly pass 1000 Å in size. The relative flatness of the curves at larger times indicates that only a few additional particles reach this size at a later time. Thus only very slight deviations in the experimental parameters such as sampling time, $R(CO)$, or supersaturation in the thermal diffusion chamber should change the experimental findings so that either none or nearly all of the particles are detected at 60 sec. This is reflected in Figure 6 where the three points on the three upper curves at 1 min are replicates; yet the particle density differs by a factor of 26. For later times the two duplicate runs agree to within 60%.

There are two possible reasons why the number of particles does not change much after 60 sec under continuous radiation. Either no more particles are formed, or the production rate is essentially offset by a removal process. Thus experiments were done with the radiation discontinued after 60 sec so that particle production would cease. The data in Figure 6 show that the curves behave exactly as with continuous irradiation. In fact, the particle densi-
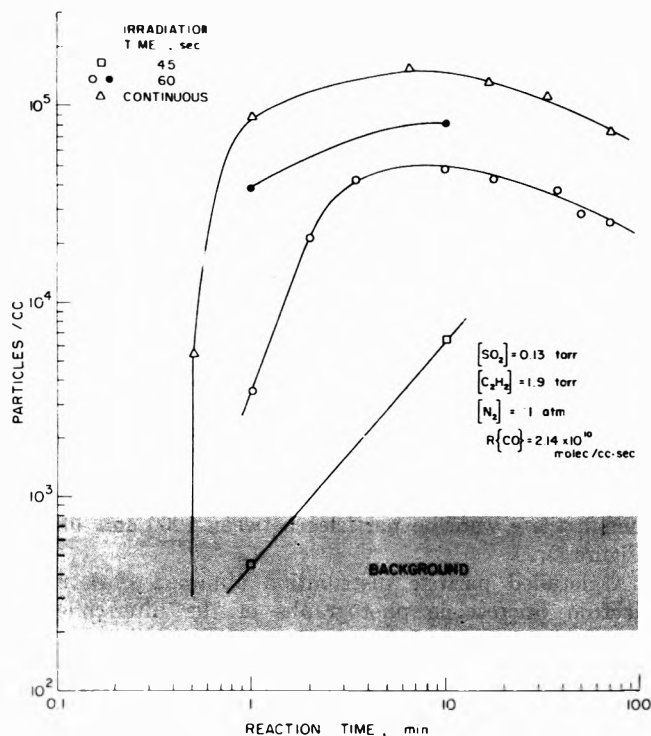
Figure 6. Log–log plots of the particle density for particles >1000 Å diameter vs. reaction time in the irradiation of mixtures containing 0.13 Torr of SO₂, 1.9 Torr of C₂H₂, and 1 atm of N₂ at 29° with six lamps. The particle density was measured with the thermal diffusion chamber assuming complete insolubility of the particles in H₂O. Experiments were done for continuous irradiation and for radiation terminated after 45 or 60 sec.

ties are within a factor of 3 of each other for times between 4 and 60 min in spite of the factor of 26 discrepancy at 1 min. Clearly these results indicate that particle production is a sudden process, occurring only over a very short time interval.

Runs were done for exposure times less than 60 sec. One run with a 45-sec exposure time is shown in Figure 6. After 1 min the particle density still corresponds to background because the growth of smaller particles has been slowed by stopping the radiation at 45 sec. However, after 10 min a measurably significant number of particles with diameters >1000 Å were seen.

When the irradiation time was reduced to 30 sec or less, usually no particles above background levels were seen even after 60 min (the one exception was for the run with continuous radiation shown in Figure 6).

A similar set of experiments was done for particles of diameters >25 Å with reaction conditions of [SO₂] = 0.13 Torr, [C₂H₂] = 1.9 Torr, [N₂] = 1 atm, and R(CO) = 3.5 × 10⁹ molecule/cc sec. Under these conditions for several experiments with continuous radiation, particle formation started at 45 ± 5 sec. For 30-sec radiations particle levels above background (150–300 particles/cc) were not seen even after 60 min. A series of experiments was done in which two 30-sec radiations were separated by a dark period of between 1 and 10 min. If the intervening dark period was ≤4 min, the particle density rose above background after the second radiation. However, if the intervening dark period was >4 min, the particle density did not rise above background levels.

The size distribution of the particles as a function of reaction time for continuous radiation was monitored for a
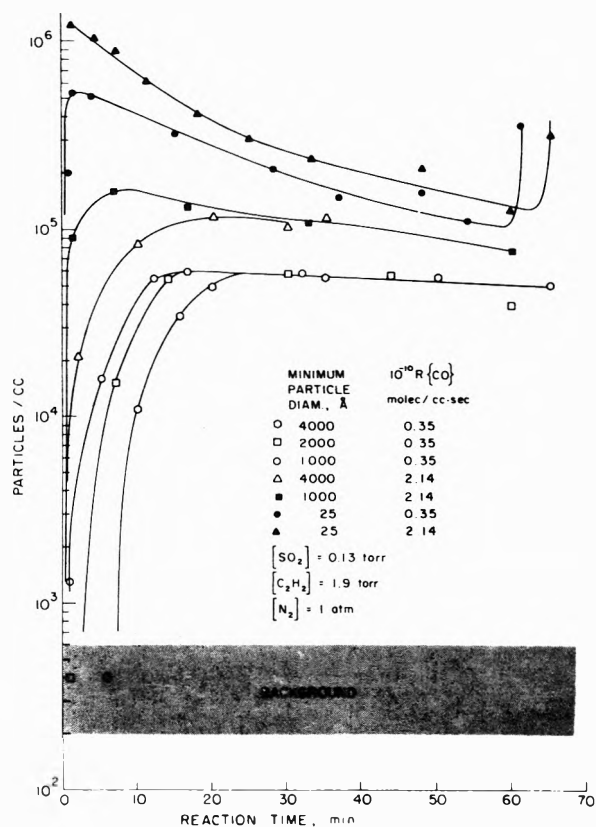
Figure 7. Semilog plots of the particle density for particles greater than a specified minimum diameter vs. reaction time for continuous radiation of mixtures containing 0.13 Torr of SO₂, 1.9 Torr of C₂H₂, and 1 atm of N₂ at 29°. The high and low intensities were obtained by using six lamps and one lamp, respectively. For measurement of particles >1000 Å, the thermal diffusion chamber was used. For measurement of particles >25 Å, the Environment One condensation nuclei counter was used.

mixture containing 0.13 Torr of SO₂, 1.9 Torr of C₂H₂ and 1 atm of N₂ for two different light intensities. The particle density for particles with diameters exceeding 25, 1000, 2000, and 4000 Å were measured, and the results are summarized in Figure 7.

Initially, there is an induction period which is followed by a very rapid rise in particle density, the smaller particles appearing before the larger ones. At the higher intensity, the induction period is shorter for a given particle size, and the peak particle density is higher. Of particular interest is the fact that at each intensity after 30-min irradiation, the number of particles exceeding 1000 Å diameter is the same as that exceeding 4000 Å, i.e., there are no particles between 1000 and 4000 Å diameter. This confirms the results in Figure 6 that particles are produced in a burst and then grow with no (or few) new particles being formed. Even for all particles >25 Å in diameter, there is less than a factor of 2 difference between them and those greater than 4000 Å for times between 30 and 60 min. Even this difference may be an artifact since the analysis of particles >25 Å in diameter is done on different equipment than for the large particles. A factor of 2 discrepancy between two particle counters is not out of the question.

An interesting feature of the data in Figure 7 is the increase in the number density of small particles (>25 Å) after 60 min. A period of second nucleation of particles is evident and the particle density rises rapidly. This was
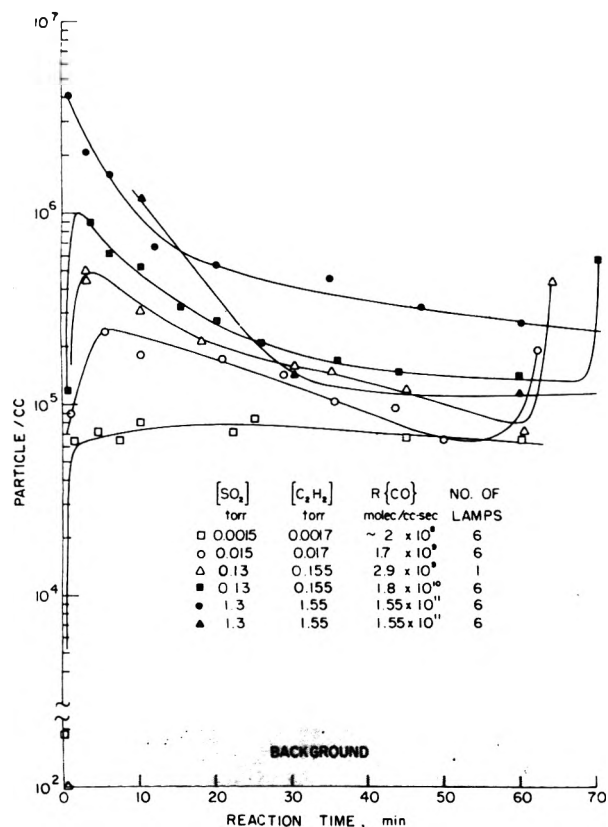
Figure 8. Semilog plots of the particle density for particles greater than 25 Å vs. reaction time for continuous radiation of SO_2–C_2H_2 mixtures (at a ratio of 0.9) in 1 atm of N_2 at 29°. (Note break in the ordinate.) The particle densities were measured with the Environment One condensation nuclei counter except for the data designated by filled triangles. For this curve the particles were collected on filter paper, photographed through the electron microscope, and counted by inspection; the minimum particle size was 100 Å.

TABLE III: Per Cent of Particles in Various Size Ranges at Different Radiation Times [a]

Radiation time, min	Diameter range, Å				
	100–500	500–1000	1000–2000	2000–4000	>4000
10	48	37	13	1	1
30	0	48	24.5	12.5	15
60	0	22	54	9	15
90	0	0	22	8	70

[a] $[SO_2]$ = 1.3 Torr, $[C_2H_2]$ = 1.55 Torr, $[N_2]$ = 1 atm, T = 29°, $R(CO)$ = 1.55 × 10^{11} molecule/cc sec.

cles between 25 and 100 Å diameter at later times, and the difference in the two measurements is a count of these small particles. In this regard it is interesting to note that for a reaction mixture of 0.13 Torr of SO_2, 1.9 Torr of C_2H_2, and 1 atm of N_2, the particle density for particles >25 Å was about twice that for particles >4000 Å, even though there were no particles between 1000 and 4000 Å (Figure 7).

A detailed particle distribution obtained from many electron microscope photographs of the filter-collected samples is shown in Figure 9. Four plots are shown corresponding to four different reaction times. The total particle density drops as the reaction time is lengthened, but the relative percentage of larger particles increases. A summary of the results is given in Table III. For a 10-min radiation, 48% of the particles are between 100 and 500 Å in diameter and 85% are smaller than 1000 Å in diameter. After 30 min there are no particles between 100 and 500 Å in diameter and 48% are between 500 and 1000 Å in diameter. At 60 min 54% of the particles are between 1000 and 2000 Å, and at 90 min 70% of the particles are >4000 Å in diameter and there are no particles between 100 and 1000 Å in diameter.

Usually, second nucleation starts between 60 and 120 min of radiation for the conditions depicted in Figure 9. For runs shown in Figure 9, there is no indication of second nucleation even for 90-min exposure. However, for another run at exactly the same conditions, second nucleation was seen at 85 min. The electron microscope photograph of this run is shown in Figure 10. For 85-min radiation, two distinct sizes of particles are seen with diameters of about 1000 and 8000 Å. Also it can be seen that there are, to within a factor of 2 or 3 after correcting for the filter collection efficiencies, about the same number of each size.

Theoretically for 60-min irradiation, the run depicted in Figure 9 should give a mass average diameter of 10,000 Å, if there was no mass loss. Actually it gives a mass average diameter of 4200 Å (4.5% recovery) and a number average diameter of 1600 Å for 60-min irradiation. To check the mass recovery, additional experiments were done under essentially the same conditions and the total particle mass measured as a function of reaction time. These results are shown in Figure 11, and it can be seen that as reaction proceeds the mass recovered in the particles drops, becoming 5% at 60 min in good agreement with the filter experiments. At 30 min there is 9.7% recovery, but this value drops to 5.6% at the same reaction time for lower $R(CO)$, i.e., for $[SO_2]$ = 0.13 Torr, $[C_2H_2]$ = 0.13 Torr, and $R(CO)$ = 1.82 × 10^{10} molecule/cc sec.

As a final check of the experimental methods, particles were collected in an electrostatic precipitator and electron microscope photographs taken. Such a picture is shown in Figure 12 (available on microfilm). Even though there are

observed in many (not all) experiments, though the time of second nucleation was not very reproducible; it occurred between 60 and 120 min.

The effect of reaction conditions is shown in Figure 8 for particles >25 Å diameter formed during continuous radiation. Five runs at $[SO_2]/[C_2H_2]$ ratios of 0.9 but in which the reactant pressures, and thus $R(CO)$, were varied by a factor of 870 are shown. The peak particle density rises with $R(CO)$, but less than proportionately. Likewise, the induction period may be somewhat lengthened as $R(CO)$ drops, but the effect is not very dramatic. The second nucleation after 60 min is apparent in three of the runs.

In order to check the accuracy of the particle counting method by nuclei condensation techniques, particle samples were collected on filter paper and electron microscope photographs taken. The particle density was then computed from the pictures using the filter collection efficiency curve in Figure 1 for an assumed density of 1.5 g/cc.

The results for a mixture of 1.3 Torr of SO_2, 1.55 Torr of C_2H_2, and 1 atm of N_2 are shown in Figure 9 for all particles with diameters >100 Å, the minimum size that could be seen. After 10-min irradiation, the results are essentially the same as from the measurement by the Environment One condensation nuclei counter for particles >25 Å diameter. However, at 30 and 60 min, the filter technique gives results 2–3 times lower. This discrepancy probably reflects the uncertainties in the two measurements. However, it is possible that there are many parti-

Figure 9. Semilog plots of the particle density vs. minimum particle diameter for continuous irradiation of a mixture of 1.3 Torr of SO_2 and 1.55 Torr of C_2H_2 in 1 atm of N_2 for various radiation times at 29°. Irradiation was from six lamps and $R(CO)$ = 1.55 × 10^{11} molecule/cc sec. The particle densities were computed from electron microscope photographs of samples collected on filter paper.
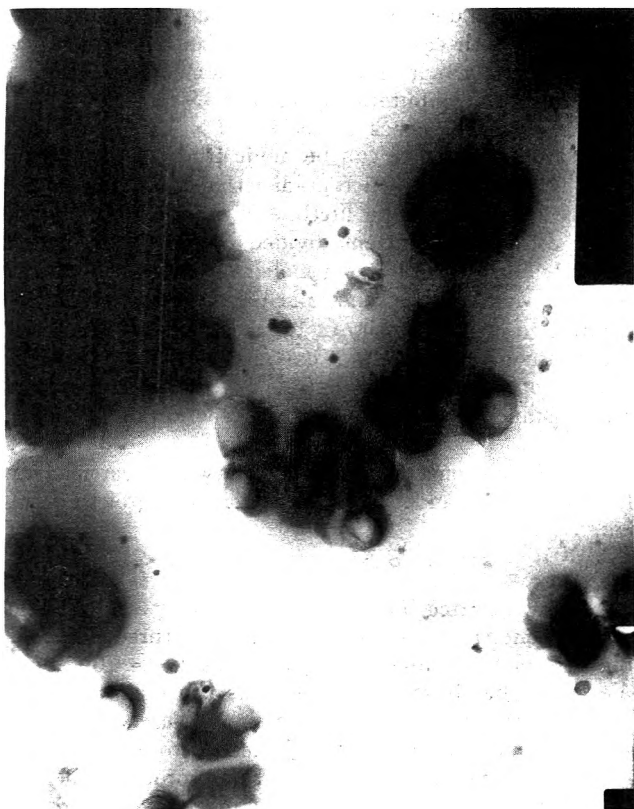
Figure 10. Electron microscope photograph of the particles collected on the filter paper for continuous radiation of a mixture of 1.3 Torr of SO_2 and 1.55 Torr of C_2H_2 in 1 atm of N_2 at 29° and $R(CO)$ = 1.55 × 10^{11} molecule/cc sec. The picture is for 85-min radiation. The large particles are about 8000 Å in diameter and the small particles are about 1000 Å in diameter. The white spots in the pictures are the holes in the filter paper.
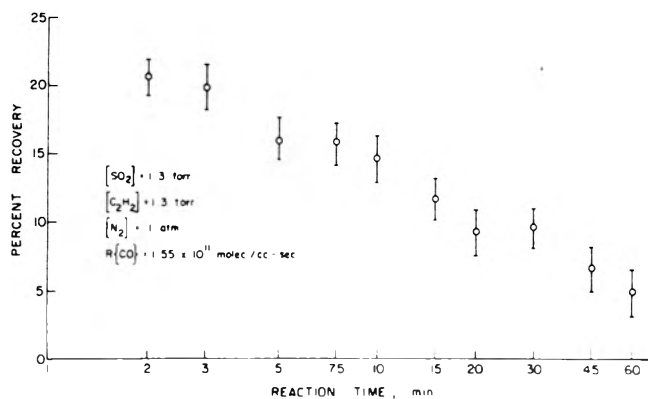
Figure 11. Semilog plot of per cent mass in the particles vs. reaction time for continuous radiation of mixtures containing 1.3 Torr of SO_2, 1.3 Torr of C_2H_2, and 1 atm of N_2 at 29° and $R(CO)$ = 1.55 × 10^{11} molecule/cc sec. The per cent recovery is based on the particles having a composition corresponding to $C_3H_4S_2O_3$.

only four particles, they are all the same size, i.e., 5600 Å in diameter. It should also be noticed that they are spherically shaped indicating an amorphous, noncrystalline solid.

Discussion

The results can be summarized as follows. Irradiation of SO_2–C_2H_2 mixtures produces CO and an amorphous solid as exclusive products. The amorphous solid is the trimer of $C_3H_4S_2O_3$. The solid particles are formed, after an induction period, in a very short time period. After that the particles already formed continue to grow and maintain a fairly uniform size. The particle number density slowly decreases until, after 1 or 2 hr of irradiation, a second nucleation occurs producing additional small particles. Ex-

cept for second nucleation, the time history of particle growth is exactly that obtained in our laboratory for NH_4NO_3 in a completely different system.[1] Similar time histories have been observed by others[21-23] in atmospheric systems. It is convenient to discuss the results in terms of the four stages: induction period, particle nucleation, particle growth, and particle removal.

Induction Period. The initial photochemical process is the absorption of radiation by SO_2 followed by the reaction of photoexcited SO_2 with C_2H_2

$$SO_2 + h\nu \rightarrow SO_2^* \tag{1}$$

$$SO_2^* + C_2H_2 \rightarrow CO + CH_2SO \tag{2}$$
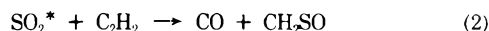
where SO_2^* represents electronically excited SO_2. The states involved are not those which emit radiation, since those states are removed by adding an atmosphere of N_2,[24] but the photochemical reaction is not. The states involved must be the nonemitting chemically reactive states and may include both the singlet and triplet states.[9]

One of the products of reaction 2 is CO. The other product is almost certainly CH_2SO rather than the fragments CH_2 and SO. If these fragments were formed, one would expect to see elemental sulfur, C_2H_4, C_3H_4 compounds, and possibly polymers of acetylene. The absence of all of these compounds rules out the diradical fragments.

Since the solid has the empirical formula $C_3H_4S_2O_3$, this compound is presumably produced in the gas phase *via* the overall reaction

$$CH_2SO + SO_2 + C_2H_2 \rightarrow C_3H_4S_2O_3 \tag{3}$$
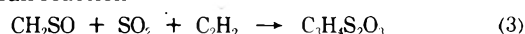
We suspect that the structure of the product molecule is
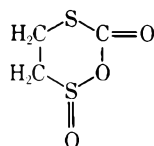
and that it is formed *via* the following steps. First CH_2SO reacts with C_2H_2
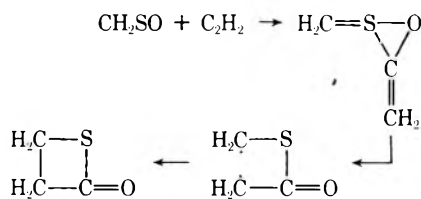
The C_3H_4SO intermediate could then add to SO_2 to form the final product
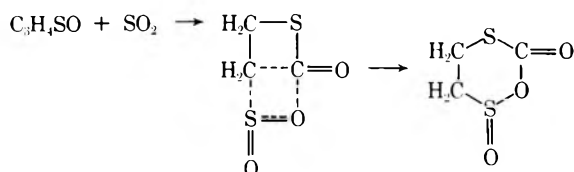
The structure of the final product is consistent with all the spectroscopic and photochemical evidence. Both the nmr and mass spectra show the presence of CH_2 groups. The infrared spectrum clearly indicates the presence of a carbonyl group and suggests bound SO_2. The observed photodecomposition products of the solid which are OCS, CO, CO_2, and possibly C_2H_4, can easily be rationlized from the above structure.

The solid is composed of the trimer of the $C_3H_4S_2O_3$ molecule. Is that trimer formed in the gas phase prior to

condensation, or does the monomer condense and form the trimer in the solid? At our lowest photolysis rates, *i.e.*, $R(CO) \sim 2 \times 10^8$ molecule/cc sec, particles are seen in < 100 sec radiation time. Consequently the monomer concentration cannot exceed 2×10^{10} molecule/cc when nucleation begins. It is difficult to believe that monomeric $C_3H_4S_2O_3$ could have such a low vapor pressure for sublimation when compounds of comparable complexity have vapor pressures at least 1000 times larger.

Presumably the trimer is formed in the vapor phase *via* the successive reactions

$$2C_3H_4S_2O_3 \rightarrow (C_3H_4S_2O_3)_2 \tag{4}$$

$$C_3H_4S_2O_3 + (C_3H_4S_2O_3)_2 \rightarrow (C_3H_4S_2O_3)_3 \tag{5}$$
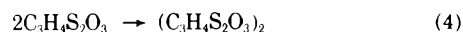
If reactions 4 and 5 have rate coefficients of $\sim 10^{-10}$ cm^3/sec, which is reasonable, and if the monomer concentration $\sim 10^{10}$ molecule/cc, the time to convert monomer to trimer is about 1 sec, a time short compared to the times of our experiment. Thus, except possibly for the experiments at lowest $R(CO)$, we can assume that the trimer is formed instantaneously in the gas phase.

The only reaction of importance for the trimer, before particle nucleation occurs, is diffusional loss to the wall

$$T \rightarrow \text{wall removal} \tag{6}$$
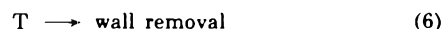
where T represents the trimer of $C_3H_4S_2O_3$. The diffusion constant k_6 can be computed from the experiment in which 0.13 Torr of SO_2 and 1.9 Torr of C_2H_2 in 1 atm of N_2 were irradiated at $R(CO) = 3.5 \times 10^9$ molecule/cc sec. For these conditions particle formation started after 45 ± 5 sec continuous radiation or after 60-sec radiation interrupted at the midway point by a 240-sec dark period. Presumably in both cases the trimer concentration was the same when particle nucleation commenced. Thus a straightforward computation gives $k_6 = 3.0 \times 10^{-3}$ sec^{-1}.

An approximate check to see if 3.0×10^{-3} sec^{-1} is a reasonable value for k_6 can be made from simple kinetic theory considerations which predict that the square of the distance of travel in one lifetime is approximately given by the diffusion coefficient divided by the diffusion rate constant. For T, which has a molecular weight of 456 and for which we assume a molecular diameter of 10 Å, corresponding to a solid density of 1.5 g/cc, the diffusion coefficient becomes 5.3×10^{-2} cm^2/sec.[1] Thus the average distance of travel in one lifetime is computed to be 4.2 cm, a distance comparable with the reaction cell radius of 3 cm.

The critical concentration of T at which particle nucleation begins can be computed from the growth equation

$$[T] = (R(CO)/3k_6)(1 - e^{-k_6 t}) \tag{a}$$

where t is the time, *i.e.*, 45 sec. The factor 3 reflects the fact that one trimer is produced for every three CO molecules. From this equation, [T] becomes 4.9×10^{10} molecule/cc for the above conditions. This value should not be confused with the equilibrium vapor pressure which must be lower, since supersaturation is needed to initiate particle growth. The critical concentration is probably at least a factor of 3 greater than the equilibrium vapor pressure.

Particle Removal. Though sequentially, particle nucleation must precede particle removal, the information obtained from a consideration of the removal process is necessary to interpret the nucleation process. Therefore, a discussion of nucleation will be preceded by discussions of the removal and growth processes.

Particle removal can be either by diffusion to the wall

$$T_n \longrightarrow \text{wall removal} \qquad (6')$$

or by coagulation

$$T_n + T_m \longrightarrow T_{n+m} \qquad (7)$$
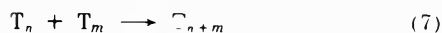
The diffusion rate constants k_6, are inversely proportional to the square of the particle diameter. Since T has a diameter of ~ 10 Å and a diffusion loss coefficient of $k_6 = 3.0 \times 10^{-3}$ sec^{-1}, then 25- and 100-Å diameter particles have diffusion loss coefficients of 4.8×10^{-4} and 3.0×10^{-5} sec^{-1}, respectively. Larger particles have even smaller diffusion loss coefficients. Since the particles grow to >100 Å in just a few minutes, particle loss by diffusion to the wall is negligible. Experimental verification of this conclusion comes from Figures 7 and 8. For particle densities $<10^5$/cc, where coagulation is also negligible, the particle density remains constant, once particle production is terminated.

Since particle removal is by coagulation, the particle density should obey the law

$$N^{-1} - N_0^{-1} = k_7 t \qquad (b)$$

where N is the particle density, N_0 is the particle density extrapolated to $t = 0$, and k_7 is some average coagulation constant. Actually, eq b is only valid if k_7 has the same value for coagulation by any T_n and T_m, i.e., for all values of n and m.

Plots of N^{-1} vs. t for the runs which show measureable decay are given in Figure 13. The data can be fitted reasonably by straight lines except for the one run at highest intensity. Except for the run at highest intensity (i.e., highest $R(CO)$), the coagulation constants are essentially all the same, i.e., $k_7 = (1.5 \pm 0.2) = 10^{-7}$ cm^3/min.

The question one may ask is why are six of the plots in Figure 13 linear, and why are their slopes the same? The experimental results indicate that the particles are nearly monodisperse, i.e., that they are grouped around a single diameter, though that diameter grows. Computations of coagulation constants for monodisperse particles[25] give rate constants, assuming every collision is effective, which increase from 3.6×10^{-8} cm^3/min at 40 Å to a maximum of 7.2×10^{-8} cm^3/min at 200 Å and then drop to 3.1×10^{-8} cm^3/min at 2000 Å. These diameters correspond to those covered in most of the experiments; the coagulation coefficient only varies by a factor of 2.3 over the whole range, i.e., it is more or less constant within the large experimental uncertainty. The experimental value of 1.5×10^{-7} cm^3/min is about a factor of 3 larger than theoretically possible for a monodisperse system. This can be explained if some dispersion exists among the particle diameters. For example, the experimental value of 1.5×10^{-7} cm^3/min corresponds exactly to the collision frequency between particles of 400 and 2000 Å diameters or between particles of 150 and 400 Å diameters. From the experimental results, the dispersity is certainly not more than this. Therefore, it can be concluded that coagulation occurs on every collision, at least for particles with diameters <2000 Å.

Particle Growth. Particles can grow either by coagulation or by condensation of the vapor. Since in every experiment, the particle density dropped less than a factor of 14 from the maximum value, coagulation could account for an increase of average diameter of less than a factor of 2.4. Since the particles grow from diameters of ~ 25 to
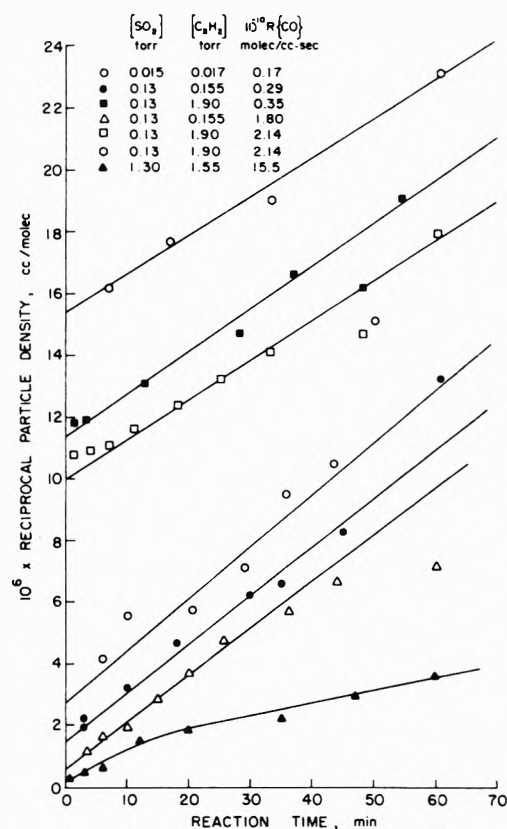
Figure 13. Plots of the reciprocal particle density vs. reaction time for continuous radiation of mixtures of SO$_2$ and C$_2$H$_2$ in 1 atm of N$_2$ at 29°. The particle densities include all particles with diameters >25 Å except for the plot with hexagons which is for particles with diameters >1000 Å. The upper three plots have been raised 10 units for clarity.

~ 5000 Å, it is clear that coagulation is negligible in terms of growth.

The predominant growth process is condensation

$$T + T_n \longrightarrow T_{n+1} \qquad (8)$$

where n is an integer. Values of k_8, which is a function of particle diameter, can be estimated for large particles from the onset of second nucleation. For the five runs which show second nucleation, the experimental parameters are listed in Table IV. Also listed is the time at the onset of second nucleation, τ, and the corresponding particle density, N_τ, at this time. If we assume that, except for the induction period (i.e., the first minute) when the C$_3$H$_4$S$_2$O$_3$ trimers condense on the particles, then the average diameter, σ_τ, at τ can be computed. The computed values of σ_τ are also listed in Table IV.

The experimental values of k_8 can be estimated from steady-state considerations on T. Since T is produced in the photochemical reaction and removed principally by condensation, then

$$k_8 = R(CO)/3N_\tau[T] \qquad (c)$$

Now $R(CO)$ and N_τ are known. Presumably at the onset of second nucleation, [T] is the same as at the onset of first nucleation, i.e., [T] $\sim 4.9 \times 10^{10}$ molecule/cc. Values for k_8 can then be estimated from eq c and they are listed in Table IV.

Theoretical values for k_8 can also be estimated as a function of particle diameter if every collision results in reaction. The appropriate rate coefficient is given by ei-

TABLE IV: Condensation Rate Coefficients at 29°

$10^{-10}R(CO)$, molecule/cc sec	[SO$_2$], Torr	[C$_2$H$_2$], Torr	τ, min	$10^{-5}N_\tau$, molecule/cc	$\sigma_\tau, \text{Å}^a$	$10^7 k_8$, cm^3/sec	
						Expt	Theory[b]
0.17	0.015	0.017	56	0.65	3060	1.8	51
0.29	0.13	0.155	62	0.8	3540	2.5	60
0.35	0.13	1.9	59	1.0	3430	2.4	58
1.8	0.13	0.155	69	1.4	5600	8.8	95
2.14	0.13	1.9	63	1.3	5900	11.2	98

[a] Assuming no mass loss. [b] Computed from diffusion-controlled collision theory.
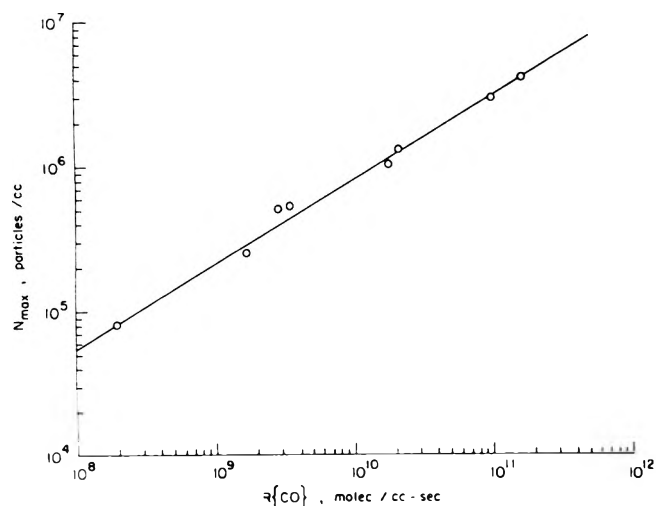
Figure 14. Log–log plot of the maximum particle density vs. the CO production rate for continuous radiation of mixtures of SO$_2$ and C$_2$H$_2$ in 1 atm of N$_2$ at 29°.

ther kinetic collision theory or diffusion-controlled collision theory, whichever gives the smaller rate coefficient. In our system, kinetic theory applies for $\sigma < 2000$ Å and diffusion theory for $\sigma > 2000$ Å. The appropriate expressions are

$$k_8(\sigma < 2000 \text{ Å}) = 2 \times 10^{-11}(\sigma_T + \sigma_n)^2/\mu^{1/2} \qquad (d)$$

$$k_8(\sigma > 2000 \text{ Å}) = \pi \times 10^{-8}(\sigma_T + \sigma_n)(D_T + D_n) \qquad (e)$$

where k_8 has the units of cm^3/sec, σ_T and σ_n are the diameters in Å of the C$_3$H$_4$S$_2$O$_3$ trimer, T, and the particle of n trimer units, T$_n$, respectively, μ is the reduced molecular weight for T and T$_n$, and D_T and D_n are the diffusion coefficients in cm^2/sec for T and T$_n$, respectively. The values for σ_T and D_T are 10 Å and 0.053 cm^2/sec, respectively.

The theoretical values for k_8 are given in Table V for each value of σ_r. These values are 9–28 times larger than the experimental values.

This discrepancy can be explained by the fact that all the mass is not recovered in the particles. The data in Figure 9 give a mass average diameter of 4200 Å and a number average diameter of 1600 Å for 60-min irradiation, even though the mass average diameter should be 10,000 Å if all the mass were recovered. Thus, if the observed number average diameter is used to compute the theoretical value for k_8, it is reduced by a factor of 6. For lower values of $R(CO)$ than used in Figure 9, the mass recovery is even less, so that the reduction in k_8 is correspondingly more. Thus the computed values of k_8 are close to the theoretical values, and the accommodation coefficients are at least 0.3–0.5.

It is not clear why the mass loss is so great. Presumably

TABLE V: Values of Condensation Rate Coefficients Computed from Kinetic Collision Theory at 29°[a]

σ, Å	$10^8 k_8$, cm^3/sec	σ, Å	$10^8 k_8$, cm^3/sec
10	0.053	200	4.14
25	0.12	400	15.8
100	1.14	1000	95
		2000	380

[a] For C$_3$H$_4$S$_2$O$_3$ trimer with $\sigma = 10$Å, molecular weight = 456.

this reflects losses by gravitational settling and convective diffusion in the reaction chamber.

Particle Nucleation. When, during the induction period, the concentration of T becomes sufficiently large, then particle production can occur

$$rT \longrightarrow T_r \qquad (9)$$

where r is the number of C$_3$H$_4$S$_2$O$_3$ trimers needed to produce a stable nucleus, i.e., one that will grow rather than sublime. Of course, some sublimation will occur, and for the critical size nucleus, condensation is equal to sublimation. However, for simplicity, we shall assume that T$_r$ always grows. It should be realized that reaction 9 is not a fundamental reaction but a composite of several equilibria consisting of species with fewer than r trimers, viz.

$$T + T_n \rightleftharpoons T_{n+1} \qquad (10)$$

Particle nucleation starts suddenly after an induction period, τ', the particle density builds up extremely rapidly reaching near its maximum value, N_{max}, very quickly, and then particle production suddenly stops. This whole process occurs over a period of just a few seconds. During this period of time, the critical concentration of T must be reached, [T] must pass through a maximum, and then fall. Since [T] passes through a maximum its net rate of production in the absence of particles, given by the time derivative of eq a, must be equal to its rate of removal due to the presence of particles.

Removal of T by particle production is negligible since $<10^8$ particles/cc are produced, and these particles contain only a few trimers of C$_3$H$_4$S$_2$O$_3$ when initially formed (later it will be shown that the average nuclei contains 3.6 trimers). Consequently $<10^8$ trimers/cc are removed in this way, even though the critical concentration of T is 4.9 $\times 10^{10}$ per cc. Clearly particle nucleation is a negligible removal process for T.

The important removal step is condensation, reaction 8. At the maximum in [T], the rate of this reaction, i.e., $k_8[T]N_{max}$ must equal the time derivative of eq a. Thus

$$k_a = k_6/N_{max}(e^{k_8\tau'} - 1) \qquad (f)$$

For the experiment in which τ' was carefully measured to be 45 ± 5 sec, (i.e., with $R(CO) = 0.35 \times 10^{10}$ molecule/cc sec, [SO$_2$] = 0.13 Torr, and [C$_2$H$_2$] = 1.9 Torr) $N_{max} = 5.4 \times 10^6$ particles/cc. With $k_6 = 3.0 \times 10^{-3}$ sec^{-1}, k_8 can

be computed to be 3.8×10^{-3} cm³/sec. Values of k_8 computed from kinetic collision theory, eq d, are listed in Table V for various diameter particles. It can be seen that the particles that are removing the trimer have already grown to at least almost 200 Å in a few seconds. In fact, with an average condensation rate coefficient of 2×10^{-8} cm³/sec and $[T] = 5 \times 10^{10}$ per cm³, the lifetime for growth to 200 Å would be about 3 sec. Since growth cannot be more rapid than this, it can be concluded that every collision between T and a small particle (i.e., <200 Å diameter) must lead to reaction.

When the particle density is at its maximum, then the rate of particle production must equal the rate of particle loss, i.e.

$$k_9[T]_{max}{}^r = k_7 N_{max}{}^2 \qquad (g)$$

where $[T]_{max}$ is $[T]$ when N is a maximum. Also, $[T]_{max}$ can be computed by assuming the steady-state hypothesis, i.e.

$$[T]_{max} = R(CO)/3(k_6 + k_8 N_{max}) \qquad (h)$$

Since $k_6 \ll k_8 N_{max}$, then eq g and h can be combined to give

$$\log N_{max} = \frac{r}{r+2} \log (R(CO)/3) - \frac{\log (k_7 k_8{}^r / k_9)}{r+2} \qquad (i)$$

Figure 14 is a log-log plot of N_{max} vs. $R(CO)$. The plot is linear and has a slope of 0.63. Thus, r becomes 3.6. From the intercept of the plot $k_7 k_8{}^r / k_9$ is found to be 17.8 cc. Now $k_7 = 1.5 \times 10^{-7}$ cm³/sec and $k_8 \sim 8 \times 10^{-8}$ cm³/sec. Thus, $k_9 \sim 1.2 \times 10^{-34}$ cc²·⁶/sec, which is a very large rate coefficient.

Supplementary Material Available. Table II and Figures 5 and 12 will appear following these pages in the microfilm edition of this volume of the journal. Photocopies of the supplementary material from this paper only or microfiche (105 × 148 mm, 24× reduction, negatives) containing all of the supplementary material for the papers in this issue may be obtained from the Journals Department, American Chemical Society, 1155 16th St., N.W., Washington, D. C. 20036. Remit check or money order for $3.00 for photocopy or $2.00 for microfiche, referring to code number JPC-74-325.

References and Notes

(1) R. G. dePena, K. Olszyna, and J. Heicklen, *J. Phys. Chem.*, **77**, 438 (1973).
(2) R. J. Countess and J. Heicklen, *J. Phys. Chem.*, **77**, 444 (1973).
(3) D. S. Sethi, *J. Air Pollut. Contr. Ass.*, **21**, 418 (1971).
(4) E. R. Allen, R. D. McQuigg, and R. D. Cadle, *Chemosphere*, **1**, 25 (1972).
(5) H. W. Sidebottom, C. C. Badcock, G. E. Jackson, J. G. Calvert, G. W. Reinhardt, and E. K. Damon, *Environ. Sci. Technol.*, **6**, 72 (1972).
(6) R. A. Cox, *J. Phys. Chem.*, **76**, 814 (1972).
(7) R. B. Timmons, *Photochem. Photobiol.*, **72**, 219 (1970).
(8) R. B. Timmons, H. F. LeFevre, and G. A. Hollinden, "Chemical Reactions in Urban Atmospheres," C. S. Tuesday, Ed., American Elsevier, New York, N. Y., 1971, p 159.
(9) E. Cehelnik, C. W. Spicer, and J. Heicklen, *J. Amer. Chem. Soc.*, **93**, 5371 (1971).
(10) G. E. Jackson and J. G. Calvert, *J. Amer. Chem. Soc.*, **93**, 2593 (1971).
(11) F. B. Wampler, A. Horowitz, and J. G. Calvert, *J. Amer. Chem. Soc.*, **94**, 5523 (1972).
(12) S. E. Braslavsky and J. Heicklen, *J. Amer. Chem. Soc.*, **94**, 4864 (1972).
(13) F. S. Dainton and K. J. Ivin, *Trans. Faraday Soc.*, **46**, 374 (1950).
(14) F. S. Dainton and K. J. Ivin, *Trans. Faraday Soc.*, **46**, 382 (1950).
(15) C. C. Badcock, H. W. Sidebottom, J. G. Calvert, G. W. Reinhardt, and E. K. Daman, *J. Amer. Chem. Soc.*, **93**, 3115 (1971).
(16) H. W. Sidebottom, C. C. Badcock, J. G. Calvert, B. R. Rabe, and E. K. Damon, *J. Amer. Chem. Soc.*, **93**, 3121 (1971).
(17) R. L. Ruth, "A Cloud Nucleus Sampler for Aircraft Use," M.S. Thesis, Penn State University, University Park, Pa., 1968.
(18) J. B. Mason, "Physics of Clouds," Clarendon Press, New York, N. Y., 1972.
(19) E. R. Frank, K. R. Spurny, D. C. Sheesley, and J. P. Lodge, Jr., *J. Microsc. (Paris)*, **9**, 735 (1970).
(20) K. R. Spurny, J. P. Lodge, Jr., E. R. Frank, and D. C. Sheesley, *Environ. Sci. Technol.*, **3**, 453 (1969).
(21) A. Goetz and R. Pueschel, *Atmos. Environ.*, **1**, 287 (1967).
(22) J. Bricard, F. Billard, and G. Madelaine, *J. Geophys. Res.*, **73**, 4487 (1968).
(23) R. B. Husar and K. T. Whitby, *Environ. Sci. Technol.*, **7**, 241 (1973).
(24) L. Stockburger, III, S. Braslavsky, and J. Heicklen, *J. Photochem.*, **2**, 15 (1973).
(25) N. A. Fuchs, "Mechanics of Aerosols," Pergamon Press, New York, N. Y., 1964, p 294.

On the Role of the Triplet State in the Photoisomerization of Retinal Isomers

Tchiya Rosenfeld, Aharon Alchalel, and Michael Ottolenghi*

Department of Physical Chemistry. The Hebrew University. Jerusalem. Israel (*Received July 23. 1973*)

The photoisomerization of 11-*cis*- and *all-trans*-retinals is investigated in aerated and deaerated solutions using direct singlet excitation as well as *via* sensitization from the triplet states of biacetyl and biphenyl. Triplet quantum yields are established for *all-trans*- and 11-*cis*-retinal using N_2-laser photolysis and pulse radiolysis. It is concluded that triplet energy transfer to 11-*cis*-retinal leads to isomerization with an efficiency of 15–17%, while no detectable isomerization can be induced by triplet transfer to the all-trans isomer. An analysis of the oxygen effects indicates that photosensitized isomerization precedes the formation of the fully thermalized retinal triplet. A mechanism in which isomerization is taking place from nonrelaxed vibronic triplet levels in competition with thermal deactivation is proposed. The new data are compared with available theoretical calculations and their relevance to the mechanism of isomerization induced by direct excitation is discussed.

Introduction

Vision is associated with light absorption by pigments such as rhodopsin in which a polyene aldehyde (retinal) is bound to a protein (opsin), most probably through a Schiff base with a lysine residue.[1] It also appears to be well established that the primary photochemical event involves isomerization of the 11-cis polyene chromophore to its all-trans configuration.[2] It is therefore likely that a clarification of the primary processes in the excited states of molecules such as retinal, its corresponding Schiff bases and alcohol (retinol or Vitamin A), retinyl acetate, etc., may be of primary importance in understanding the early photochemical events in vision. In this respect, the question has been repeatedly asked as to the role of the lowest triplet state in photoisomerization.[1b,3,4] This point has recently gained importance in view of evidence suggesting that the retinyllysine chromophore may actually exist as a charge-transfer complex with an appropriate protein residue,[5] and that charge-transfer interactions may strongly enhance intersystem crossing.[6]

The feasibility of triplet-state isomerization pathways in retinals has been considered theoretically.[7] Experimentally, the photoisomerization of retinal isomers has been studied by direct singlet excitation[8] as well as by triplet sensitization.[4] The latter experiments provided the first evidence indicating that isomerization can actually be induced by selective population of the triplet state. However, using the new value of $\phi_T = 0.6 \pm 0.1$ recently obtained[3] for the yield of intersystem crossing in retinal, the photosensitization data of Raubach and Guzzo[4] predict, in the case of direct excitation of the 11-cis isomer, a triplet contribution of ~0.5 to the photoisomerization yield, which is well above the overall value of 0.2 reported by Kropf and Hubbard.[8b] Thus, with the purpose of obtaining a better understanding of the role played by the triplet state in the photoisomerization of 11-*cis*- and *all-trans*-retinals, we have carried out a set of comparative experiments recording triplet and isomerization yields in systems excited directly and *via* triplet–triplet energy transfer. Seeking a direct experimental evidence for the occurrence of triplet energy transfer, we have carried out the experiments in a system where we could directly observe by laser photolysis the decay of the donor triplet as well as the matching growing-in of the acceptor triplet.

Special precautions were taken to discriminate between isomerization due to triplet energy transfer and that due to other photochemical pathways in the excited sensitizer such as radical formation.

Experimental Section

all-trans-Retinal (Sigma Chemicals or Eastman Kodak) and 11-*cis*-retinal (a gift of Hoffman LaRoche) were used without further purification. N,N,N',N'-tetramethyl-*p*-phenylenediamine (TMPD) and biphenyl, both Eastman Kodak, were zone refined. Biacetyl (BDH), *cis*-piperylene (Fluka), and spectrograde CCl_4 and *n*-hexane (Fluka) were used without further purification.

Absorption and emission spectra were recorded using a Cary-14 spectrophotometer and a Turner Model 210 fluorimeter. Continuous irradiations around 313 nm were carried out using the emission of a medium-pressure Hg arc filtered by a $NiSO_4$, $CoSO_4$, and potassium biphthalate solution and a 7-54 Corning glass filter. The 438-nm line was isolated combining a GG-15 Jena glass with a 7-59 Corning glass filter. Actinometry was carried out using uranyl oxalate solutions.

The pulsed photolysis technique using the 337.1-nm (10 nsec, 0.5 mJ) pulse of an Avco-Everett laser,[9] and the pulse-radiolysis apparatus,[10] have both been previously described. Solutions were deaerated by bubbling with nitrogen or argon and were oxygen saturated by bubbling with oxygen. All experiments were carried out under deep red light using freshly prepared solutions.

Results

I. Triplet Spectra and Quantum Yields. Figure 1 shows transient spectra attributable to the triplet intermediates[11] produced by N_2 laser excitation of 11-*cis*- and *all-trans*-retinal in *n*-hexane. The spectra of the two intermediates are very similar, exhibiting also the same ($1.2 \pm 0.1 \times 10^5$ sec^{-1}) decay rate constant. In aerated solutions the triplet lifetime is shortened to 100 nsec. However, aeration is not associated with any detectable change in either spectrum or yield (in contrast with the case of retinol[12]) of the triplet intermediate. The last observation is consistent with our failure to observe optically any form of ground-state interaction between retinal and oxygen as

well as with the lack of fluorescence[7c] or excited singlet-singlet absorption[12] in retinal solutions.

The triplet extinction coefficient and quantum yield were redetermined by the method recently described by Bensasson, et al.,[3] involving energy transfer to all-trans-retinal (R) from the triplet of biphenyl ($^3B^*$). To assure total quenching of $^3B^*$ by R, we determined the reaction rate constant by analyzing the effect of [R] on the lifetime of $^3B^*$ produced by laser photolysis in a TMPD-biphenyl system,[12] in which we observed the retinal triplet growing-in (450 nm) at a rate matching the decay of $^3B^*$ (at 370 nm). The essentially diffusion-controlled value obtained ($k_q = 3 \pm 1 \times 10^{10}$ sec^{-1} M^{-1}) guarantees complete triplet energy transfer in the 0.1 M biphenyl, 10^{-3} M trans-retinal solution in argon-saturated n-hexane which was submitted to pulse radiolysis excitation.[13] Using 4.28×10^4 M^{-1} cm^{-1} for the molar extinction coefficient of $^3B^*$ at 365 nm,[3] we obtained the value $\epsilon_T^R = 7.5 \times 10^4$ M^{-1} cm^{-1} for the extinction of retinal triplet at 450 nm, which is very close to the values reported by Dawson and Abrahamson[11b] and by Bensasson, et al.[3a,c]

In these two cases, the [TMPD] + [B] + [R] submitted to the laser photolysis and the [B] + [R] system irradiated by pulse radiolysis, we have recorded similar T-T absorption spectra (λ_{max} 450 nm) as compared with that obtained previously in the direct N$_2$-laser photolysis experiment of a system containing [R] alone. Moreover in all the three systems described above the decay rate constant of the triplet state of [R] measured at 450 nm is $(1.2 \pm 0.1) \times 10^5$ sec^{-1}. This procedure for the determination of ϵ_T^R assumes that triplet energy transfer from $^3B^*$ is the only route leading to $^3R^*$. The fact that the value obtained for ϵ_T^R is independent (within 5%) of the retinal concentration (varied from 10^{-3} to 5×10^{-4} M in the present work, and from 10^{-6} to 10^{-4} in the work of Bensasson, et al.[3a,c]) indicates that energy transfer from excited biphenyl singlets[3d] is not important in the present system. Other arguments, ruling out any substantial contribution of singlet energy transfer, have been discussed by Bensasson, et al.[3b]

The above value of ϵ_T^R was used for the evaluation of the yield of intersystem (ϕ_{ISC}) in all-trans-retinal by comparing the triplet absorbance formed by direct N$_2$-laser excitation of $\sim 5 \times 10^{-5}$ M retinal in n-hexane with those of the triplets of pyrene and anthracene produced under identical experimental conditions. Using the known anthracene[3a,b] and pyrene[14] triplet yields and extinction coefficients we obtained the value of $\phi_{ISC} = 0.7 \pm 0.1$ which is very close to that of Bensasson, et al.,[3] ($\phi_{ISC} = 0.6 \pm 0.1$) correcting the early estimate ($\phi_{ISC} = 0.11$) of Dawson and Abrahamson.[11b]

Using the pulse-radiolysis method we have also determined the extinction coefficient of the 11-cis triplet state, finding it identical with that of the all-trans isomer. From the laser photolysis data of Figure 1 we thus obtain for the yield of ISC in the cis isomer the value $\phi_{ISC} = 0.6 \pm 0.1$. We should finally point out that the above values of ϕ_{ISC} are derived assuming that in the pulse radiolysis experiments the observed triplets are those corresponding to the original ground-state isomers. The photosensitized isomerization data presented below show that this assumption is probably strictly valid in the case of the all-trans isomer and accurate to a degree of $\sim 15\%$ in the case of 11-cis-retinal.

II. Photoisomerization. a 11-cis-Retinal. Photoisomerizations of 11-cis-retinal were carried out using both direct
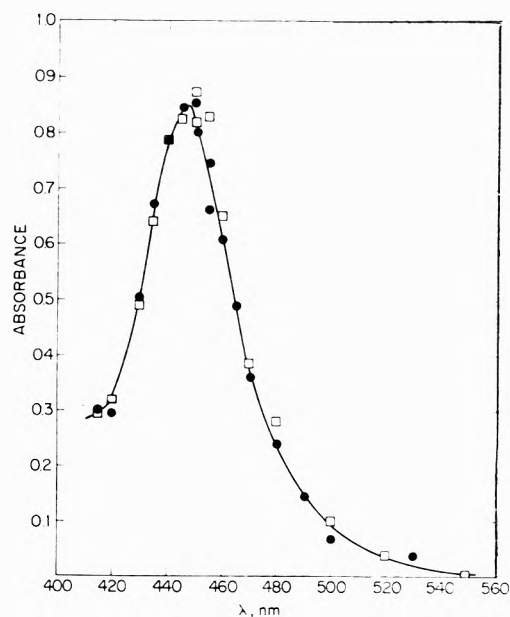
Figure 1. Transient triplet spectra obtained (100 nsec after pulsing) in the N$_2$-laser photolysis of $\sim 2 \times 10^{-4}$ M 11-cis- ($\square$) and 1×10^{-4} M all-trans- ($\bullet$) retinal in deaerated n-hexane at room temperature. With the purpose of matching the two spectra the 11-cis absorbance values have been normalized by a factor of 1.16.

and photosensitized excitation. In the direct-excitation experiments (irradiation at 313 nm) the 11-cis → all-trans conversion was monitored in 8×10^{-5} M hexane solutions by following the absorbance drops at 254 and 280 nm, as well as the accompanying rise at 365 nm.[8] The quantum yield obtained for this process (0.12) was found to be identical in both aerated and deaerated solutions.

Photosensitized isomerization experiments were carried out for 11-cis-retinal using as sensitizer $^3B^*$ produced in a TMPD-biphenyl (B) system excited at 313 nm. The present technique produces $^3B^*$ indirectly, via ^{1}(TMPD)* + B → ^{1}(TMPD·B)* → TMPD + $^3B^*$, where ^{1}(TMPD·B)* denotes a fluorescent charge-transfer exciplex.[6,12] This indirect method was preferred to direct excitation of either TMPD or biphenyl (followed by ISC and triple energy transfer) since it avoids reabsorption of the donor's fluorescence by retinal. We have also established that the lifetime of the exciplex fluorescence is unaffected by the presence of $(5 \times 10^{-5}$ $M)$ retinal, thus ruling out any exciplex quenching by R which could contribute to the generation of $^3R^*$ via singlet energy transfer. The decay rate of the retinal triplet ($^3R^*$) as measured on the laser apparatus in the TMPD-biphenyl solution was found identical with that recorded in pure retinal solutions. This excludes any interaction between $^3R^*$ and TMPD or biphenyl. The rates of isomerization determined from the initial absorbance increments at 365 nm[4,8] in aerated and deaerated solutions are shown in Figure 2A. In such photosensitized experiments the presence of biphenyl prevented measurements at 254 and 280 nm where, in the case of direct excitation of 11-cis-retinal, isomerization (to all-trans) is associated with a drop in absorbance accompanying the growth at 365 nm.[8] However, the initial change in the band shape around 365 nm was identical for both biphenyl-sensitized and direct excitation, indicating that the same photoprocess (i.e., isomerization to the all-trans isomer) takes place.
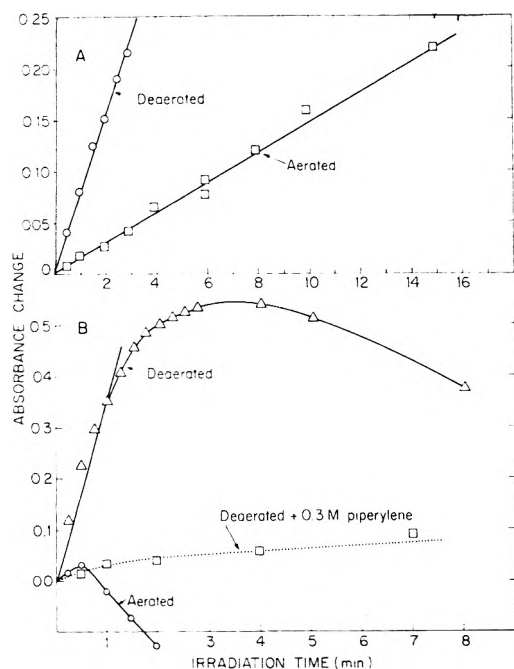
Figure 2. Absorbance changes induced by photosensitization at the maximum of the α (365 nm) band of 11-cis-retinal: (A) biphenyl sensitization, [TMPD] = 5 × 10⁻³ M, [biphenyl] = 0.1 M, [retinal] = 5.5 × 10⁻⁵ in n-hexane, excitation at 313 nm; (B) biacetyl sensitization, [biacetyl] = 7 × 10⁻² M, [retinal] = 5.5 × 10⁻⁵ M in CCl₄; excitation at 438 nm.

In order to determine the isomerization yield associated with energy transfer from ³B* ($\phi_{isom}{}^T$) we had to account for (a) the small light fraction absorbed directly by retinal, and (b) the fact that the quenching of ³B* was incomplete. (Higher [R] values required for total quenching lead to an excessively high optical density around 365 nm preventing reasonably accurate measurements of absorbance changes.)

The contribution of some direct excitation of retinal to isomerization in the deaerated photosensitized experiments of Figure 2A was estimated using the direct-excitation yield measured in the absence of TMPD and biphenyl, accounting for the relative amounts of light absorbed by retinal and TMPD in the mixed systems. It was found that ~10% of the isomerization rate is due to direct excitation of 11-cis-retinal.

The retinal triplet yield ($\phi_T{}^R$) formed by photosensitization was determined by measuring on the laser apparatus the retinal triplet absorbance in the TMPD-biphenyl-retinal system, relatively to the value obtained in pure retinal solutions (where ϕ_{ISC} = 0.6 ± 0.1). The value obtained (0.4 ± 0.04) is consistent with that calculated using the expression

$$\phi_T{}^R = \phi_T{}^B \phi_{ET}$$

where $\phi_T{}^B$ is the biphenyl quantum yield in the TMPD-biphenyl system and ϕ_{ET} is the yield of energy transfer. For $\phi_T{}^B$ a value of 0.5 was obtained by comparing the ³B* absorbance with that of the pyrene triplet produced on the laser apparatus in hexane solutions.[14b] ϕ_{ET} is given by $\phi_{ET} = k_q[R]/[k_q[R] + k_d]$ where k_d is the decay rate constant of ³B* in the absence of retinal. Using k_q = 3 × 10¹⁰ M⁻¹ sec⁻¹, k_d = 3 × 10⁵ sec⁻¹, and [R] = 6 × 10⁻⁵ M, we obtain ϕ_{ET} = 0.86, so that $\phi_T{}^R$ = 0.43. The photoisomerization yield obtained using the above corrections is presented in Table I along with the direct-excitation value.

TABLE I: Photoisomerization Yields Obtained for 11-cis- and all-trans-Retinal by Photosensitized and Direct Excitation[a]

	11-cis-Retinal	all-trans-Retinal
Biphenyl photosensitized[b]	0.17 ± 0.02	<0.002
Biacetyl photosensitized[c]	0.15 ± 0.02	<0.002
Direct excitation (313 nm)[d]	0.12 ± 0.01	0.10 ± 0.01

[a] Quantum yields were estimated from the initial changes in the absorbance at the α (370 nm) band using the known extinction coefficients of the retinal isomers.[4,8] The corresponding processes assumed were 11-cis → all-trans and (for an upper limit estimate[4,8]) all-trans → 13-cis. [b] 313-nm excitation. [TMPD] ≃ 5 × 10⁻³ M, [biphenyl] = 0.1 M, and [retinal] ≃ 6 × 10⁻⁵ M in deaerated n-hexane. The quantum yield represents the fraction of photoisomerized molecules produced for each triplet of retinal formed by energy transfer. The values have been corrected for some direct light absorption by retinal and for incomplete quenching of ³B* as described in the text. [c] 438-nm excitation. [Biacetyl] = 7.5 × 10⁻² M, [retinal] ≃ 6 × 10⁻⁵ M in deaerated CCl₄. Assuming ϕ_{ISC} = 0.9 for (³Ba*).[4] [d] ~6 × 10⁻⁵ M retinal in deaerated or aerated n-hexane.

Attention should now be paid to the oxygen effect on the photoisomerization of 11-cis-retinal in the sensitized experiments of Figure 2. In aerated solutions the quenching of the TMPD-biphenyl exciplex by oxygen is known to decrease the ³B* yield to 20% of the value measured in deaerated systems,[6b] leading to a corresponding drop in $\phi_T{}^R$. A further decrease in $\phi_T{}^R$ arises from the competition between O₂ and R on ³B* leading to an energy transfer yield in aerated solutions ($\phi_{ET}(O_2)$) which is smaller than the value (ϕ_{ET}) in deaerated systems. Since $\phi_{ET}(O_2)$ = $k_q{}^R[R]/[k_q{}^R[R] + k_d + k_q(O_2)[O_2]]$ we obtain, using $k_q(O_2)$ = 2 × 10⁹ M⁻¹ sec⁻¹ and [O₂] ≃ 2 × 10⁻³ M, $\phi_{ET}(O_2)$ ≃ 0.3 so that $\phi_T{}^R(O_2)$ = $\phi_T{}^B(O_2)$ $\phi_{ET}(O_2)$ = 0.03 where $\phi_T{}^R(O_2)$ and $\phi_T{}^B(O_2)$ = 0.1 are the retinal and biphenyl triplet yields in aerated solutions. Since $\phi_T{}^R(O_2)$ is around 10% of the value ($\phi_T{}^R$ = 0.4) in deaerated solutions, the triplet transfer mechanism will contribute 10% to the isomerization yield in the aerated system as compared to the deaerated solution. This assumption, obviously implying that the photosensitized isomerization of retinal is not affected by the quenching of ³R* by O₂ (see further arguments in the Discussion), leads to the conclusion that the residual (~20%) isomerization yield observed in the aerated solution of Figure 2A can be accounted for by an approximately equal (~10%) contribution of both direct-excitation and triplet-transfer mechanism. This agreement between observed and estimated values contribute a further indication to the conclusion that photosensitized retinal triplet formation is the major route leading to isomerization in the TMPD-biphenyl-11-cis-retinal system. It is furthermore consistent with the assumption that the quenching of ³R* by O₂ does not affect the isomerization proceeding via ³R*.

Photoisomerization experiments with the 11-cis isomer were also carried out using biacetyl (Ba) as sensitizer.[4] The corresponding data are presented in Figure 2B and Table I, showing that $\phi_{isom}{}^T$ is essentially identical with that measured in the biphenyl system. The photosensitized isomerization yield (using ³Ba* as a sensitizer) of this work (0.15) is in variance with the value of (0.75) reported by Raubach and Guzzo.[4] We would like to emphasize that the same value (0.17 ± 0.2, Table I) has been obtained in the present work using two different sensitizers. As shown in Figure 2B, 0.3 M piperylene essentially eliminates the

photoisomerization. Using a Stern–Volmer analysis on the phosphorescence of biacetyl (Ba) in CCl_4 at room temperature ($\tau = 0.8 \times 10^{-3}$ sec) we have determined a rate constant of 2.5×10^8 sec^{-1} M^{-1} for the reaction between the biacetyl triplet ($^3Ba^*$) and piperylene. We have also established that $^3R^*$ (35 kcal/mol)[4] is unreactive to 0.3 M piperylene (triplet energy 56.9 kcal/mol). Thus, the effect of piperylene on the biacetyl photosensitized isomerization is consistent with total quenching of $^3Ba^*$, preventing the formation of $^3R^*$. (For piperylene $k_q{}^P[P] = 7.5 \times 10^7$ sec^{-1}, while, for 11-cis-retinal $k_q{}^R[R] = 1.3 \times 10^5$ sec^{-1},[4] where $k_q{}^P$ and $k_q{}^R$ are the corresponding $^3Ba^*$ quenching rate constants and [P] and [R] are the quenchers concentrations.) In the case of molecular oxygen as a total quencher of $^3Ba^*$ (quenching rate constant 5.1×10^9 sec^{-1} M^{-1}[15]) the initial photoisomerization slope is similar to that with piperylene (Figure 2B). However, at longer irradiation time the change in absorbance changes sign probably indicating irreversible destruction of the retinal.[4]

b. all-trans-Retinal. The yield of the direct photoisomerization of all-trans-retinal irradiated at 313 nm in *n*-hexane solution is given in Table I and it is not affected by oxygen as was found in the case of 11-cis-retinal. Sensitization experiments with the all-trans isomer using as sensitizer $^3B^*$, produced in the deaerated TMPD–biphenyl system, did not lead to a detectable drop in the absorbance around 365 nm characterizing the (all-trans) → (cis isomers) isomerization.[8] Since the experimental conditions (including the amount of energy transfer as determined on the laser apparatus) were similar to those previously described for the 11-cis isomer, we conclude that triplet energy transfer to the all-trans isomer does not lead to isomerization. The estimated upper limit for this process is shown in Table I along with the upper limit for the direct photoisomerization quantum yield calculated assuming an *all-trans* → 13-cis process.[4,8]

The data concerning the diacetyl photosensitized isomerization are shown in Figure 3. The results in deaerated solutions show an absorbance drop around 380 nm indicating a substantial photoisomerization which apparently contradicts the previous conclusions derived for biphenyl sensitized system. However, one should note that oxygen, which quantitatively quenches $^3Ba^*$ preventing the formation of $^3R^*$, does not change the photoisomerization yield. A plausible explanation for this behavior is one attributing the photoisomerization in the presence and absence of O_2 to free radicals[16] formed in the photolysis of biacetyl.[17] In fact, the addition of 1.2×10^{-3} M piperylene to an oxygen saturated solution ([O_2] = 10^{-2} M) markedly decreases the isomerization yield although piperylene does not efficiently compete (less than 1%) with O_2 on the quenching of $^3Ba^*$. In view of the polyene character of piperylene this is consistent with a competition between piperylene and retinal on free radicals. In conclusion, we believe that the overall behavior with biacetyl as sensitizer does not contradict the conclusion derived in the biphenyl sensitized system, *i.e.*, that $^3R^*$ produced by energy transfer does not play a detectable role in the photoisomerization of *all-trans*-retinal. We should finally point out that at present we cannot account for the different sensitivity of the 11-cis and all-trans isomers toward radicals formed in the biacetyl photolysis. It is known however that the various retinal isomers show a different reactivity in the I_2-catalyzed[8a] and dye-catalyzed[16a] photoisomerization presumably involving free radicals.[16b]
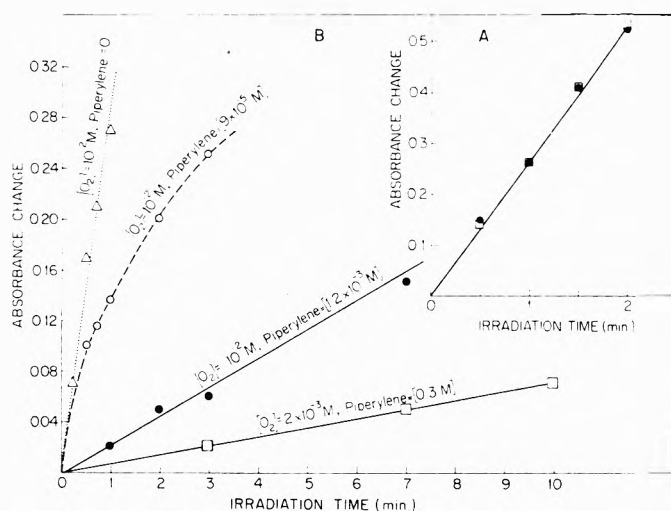
Figure 3. The effects of oxygen and piperylene in the biacetyl photosensitized isomerization of *all-trans*-retinal. ~5 × 10^{-5} M retinal and 7 × 10^{-2} M biacetyl in CCl_4 at room temperature excited at 438 nm: (A) (□) aerated, (●) deaerated; (B) (△) oxygen saturated, (○) oxygen saturated plus 9 × 10^{-5} M piperylene, (●) oxygen saturated plus 1.2 × 10^{-3} M piperylene, (□) aerated plus 0.3 M piperylene.

Discussion

a. The Mechanism of the Triplet-Sensitized Isomerization. The data of the present work indicate that triplet energy transfer to 11-cis-retinal leads to isomerization with an efficiency of 15–17%. In the case of the all-trans isomer, sensitized triplet population does not lead to detectable isomerization. Such observations are obviously inconsistent with an isomerization mechanism involving the establishment of thermal equilibrium between cis and trans forms during the lifetime of the triplet state. (Such a mechanism predicts a complementary (83–85%) yield for the reverse trans → cis triplet sensitized process which is in variance with the present data.) The experimental data are there explainable in terms of the following alternative mechanisms.

(a) Fast thermalization in the excited 11-cis T_1 state deactivates the system to a 0° (cis) T_1 trap from which a thermally activated rotation irreversibly leads to all-trans in competition with intersystem crossing to S_0 (11-cis). The reverse trans → cis process is prevented by a deeper potential well around the all-trans triplet configuration.

(b) Energy transfer from the triplet donor leads, in the case of 11-cis, to a nonrelaxed T_1 state where thermalization traps either cis (83–85%) or trans (15–17%) configurations. No subsequent thermal interconversion between isomers occurs during the triplet lifetime, meaning that the 0 (cis) and 180° (trans) traps in T_1 are considerably deep. It is possible that the nonthermalized T_1 states are reached *via* T_2 which being predicted around 53 kcal/mol[7] is still below the triplets of biphenyl (65 kcal/mol) and biacetyl (55 kcal/mol). However, the ~2 eV barrier calculated for both cis ⇌ trans rotations of T_2[7c] rules out any isomerization pathway directly involving this state.

It should be emphasized that, from a purely phenomenological point of view, isomerization from nonthermalized triplet level is equivalent to the "nonvertical" energy transfer suggested by Hammond and coworkers,[18] in which the acceptor is excited with significant change in geometry. Accordingly, triplet energy transfer to 11-*cis*-retinal may form directly the (thermalized) all-trans trip-

let, along with the 11-cis triplet, without requiring further interconversion between the two geometries during the lifetime of the thermalized triplet. Alternatively, a triplet of intermediate geometry ("phantom triplet") is formed following energy transfer which deactivates to either cis or trans ground states. In both cases the decisive change in geometry occurs before formation of the thermalized triplet following energy transfer and, in this respect, the "nonvertical" transfer process is analogous to the vibronic mechanism discussed above.

A discrimination between mechanisms a and b, favoring the second alternative, is provided by an analysis of the oxygen effects on both direct-excitation and photosensitized isomerization yields. Let us assume that isomerization to all-trans actually occurs according to a with 15% efficiency from the thermalized 11-cis triplet geometry. In view of the ISC yield (ϕ_{ISC} = 0.6) obtained for 11-cis-retinal, this assumption implies that most (~80%) of the isomerization yield (0.12) observed upon direct excitation of 11-cis-retinal is due to the (thermalized) triplet state. However, partition among ground-state isomers during the lifetime of the triplet is in variance with the complete lack of any oxygen effect on the direct-excitation isomerization under conditions of total quenching of $^3R^*$ by O_2. We therefore conclude that the thermalized 11-cis triplet state does not contribute substantially to the isomerization process. This conclusion is supported by our previous analysis of the oxygen effect on the biphenyl-sensitized isomerization of 11-cis-retinal (see above) which was found to be consistent with the assumption that the quenching of $^3R^*$ by O_2 does not affect the isomerization via $^3R^*$.

The question arises as to the inefficiency of the trans → cis conversion in the photosensitization experiments. Assuming the vibronic triplet mechanism, there should be no energetic reasons favouring the cis → trans over the trans → cis process. The experimental observations can be rationalized by assuming that isomerization from a nonrelaxed triplet can efficiently compete with thermalization in the case of 11-cis but not of all-trans. It is possible that, following triplet energy transfer to 11-cis-retinal, relatively more energy is accumulated in the isomerization-active tortional modes of the 11–12 bond, than in those of either 11–12, 9–10, or 13–14 bonds, following triplet excitation of the all-trans isomer.

b. On the Direct-Excitation Isomerization. When attempting to derive, from the triplet-sensitized experiments, conclusions relevant to the direct-excitation isomerization, it should be recalled that in photosensitization (of the retinal's systems) the decisive geometrical change occurs prior to the formation of the thermal T_1 state. Since we expect the initial energy distribution, and the consecutive changes with time, to depend on the particular way of excitation, it is difficult to infer from the triplet-sensitized yields on those expected in direct singlet excitation followed by ISC to T_1. All one can at present say is that here too no isomerization takes place from the thermalized 11-cis triplet configuration. However, a discrimination between isomerization paths proceeding via (thermalized or nonthermalized) S_1 and (nonthermalized) T_1 is still impossible. The wavelength dependence reported for the directly (singlet) excited photoisomerization of 11-cis-retinal[8b] indicates that vibronic effects have also to be considered for the direct (singlet or triplet) mechanism. The fact that directly excited all-trans-retinal undergoes isomerization with an efficiency comparable to

that of the 11-cis isomer, while being inactive upon triplet photosensitization (Table I), may in such a case favor S_1 over T_1 as the isomerizing intermediate following direct excitation. However, as long as additional evidence is not available, the mechanism of the direct-excitation isomerization remains an open question.

c. Comparison with Theoretical Energy Curves. It is interesting to consider the above conclusions in terms of the theoretical potential energy curves for twisting around the 11–12 bond.[7] The early calculations of Inuzaka and Becker[7a] and those of Wiesenfeld and Abrahamson[7b] predict essentially no barrier for the 11-cis → all-trans rotation in the lowest excited triplet state, T_1. A considerable energy barrier (higher than 0.5 eV) is however estimated for the reverse trans → cis rotation of T_1. Thus, although agreeing with the lack of thermalized triplet isomerization of all-trans to 11-cis, such estimates predict (assuming[16b] a normal frequency factor of 10^{13}–10^{14} sec^{-1}) a 100% cis → trans conversion in the thermalized 11-cis T_1 state and are therefore in variance with the results of the present work. The same applies to the more recent calculations of Becker, et al.,[7c] which include complete singly excited or complete singly plus partial doubly excited state configurational interaction, leading to three comparably shallow (of the order of 0.1 eV) potential energy minima around the 0 (cis), 90, and 180° (trans) configurations of T_1. This will seem to allow thermal isomerization within a totally relaxed 11-cis T_1 predicting a complementary (83–85%) yield for the reverse trans → cis triplet-sensitized process, which is not in keeping with the present data. In reference to the latter calculations, it should be noted that if the 90° minimum is sufficiently deep, part of the triplets observed after direct or photosensitized excitation may actually possess this partially twisted configuration. Also, the 90° triplet may be an intermediate in the 11-cis → all-trans isomerization (see above). However, in such a case the fact that we have ruled out mechanism a in favor of b means that such an intermediate cannot be formed from the thermal 11-cis triplet state.

The results of the present work, implying relatively deep energy minima at both 11-cis and all-trans geometries, appear to be in best agreement with the theoretical energy curves of Langlet, Pullman, and Berthod,[7d] predicting for T_1 a 1.4-eV trans → 11-cis barrier and ~1.0-eV barrier for the reverse 11-cis → trans rotation. Such potential wells essentially rule out any thermally activated isomerization within the lifetime (of the order of 6 μsec) of the triplet state, in keeping with the present observations.

References and Notes

(1) (a) R. A. Morton and G. Pitt, Biochem. J., **59**, 128 (1955); (b) E. W. Abrahamson and S. E. Ostroy, Progr. Biophys. Mol. Bio., **17**, 179 (1967); (c) "Handbook of Sensory Physiology," Vol. II, H. J. A. Dartnall, Ed., Springer, Berlin, 1972, Chapter 1.

(2) (a) R. Hubbard and A. Kropf, Proc. Nat. Acad. Sci. U. S., **44**, 130 (1958); (b) T. Yoshizawa and G. Wald, Nature (London), **197**, 1279 (1963).

(3) (a) R. Bensasson, E. J. Land, and T. J. Truscott, Photochem. Photobiol., **17**, 53 (1973); (b) R. Bensasson and E. J. Land, Trans. Faraday Soc., **67**, 1904 (1971); (c) J. H. Baxendale and P. Wardman, ibid., **67**, 2997 (1971).

(4) R. A. Raubach and A. V. Guzzo, J. Phys. Chem., **77**, 889 (1973).

(5) R. Mendelson, *Nature (London)*, **243**, 22 (1973).
(6) (a) M. Ottolenghi, *Accounts Chem. Res.*, **6**, 153 (1973); (b) N. Orbach, J. Novros, and M. Ottolenghi, *J. Phys. Chem.*, **77**, 2831 (1973).
(7) (a) K. Inuzaka and R. S. Becker, *Nature (London)*, **219**, 383 (1968); (b) J. R. Weisenfeld and E. W. Abrahamson, *Photochem. Photobiol.*, **8**, 487 (1968); (c) R. S. Becker, K. Inuzaka, J. King, and D. E. Balke, *J. Amer. Chem. Soc.*, **93**, 43 (1971); (d) J. Langlet, B. Pullman, and H. Berthod, *J. Chem. Phys.*, **66**, 55 (1969).
(8) (a) R. Hubbard, *J. Amer. Chem. Soc.*, **78**, 4662 (1956); (b) A. Kropf and R. Hubbard, *Photochem. Photobiol.*, **12**, 249 (1970).
(9) C. R. Goldschmidt, M. Ottolenghi, and G. Stein, *Isr. J. Chem.*, **8**, 29 (1970).
(10) D. Zehavi and J. Rabani, *J. Phys. Chem.*, **75**, 1738 (1971).
(11) (a) V. L. Wulff, R. Adams, H. Linschitz, and E. W. Abrahamson, *Ann. N. Y. Acad. Sci.*, **74**, 281 (1958); (b) W. Dawson and E. W. Abrahamson, *J. Phys. Chem.*, **66**, 2542 (1962); (c) K. H. Grellman, R. Nemming, and R. Livingston, *J. Amer. Chem. Soc.*, **84**, 546 (1962).
(12) T. Rosenfeld, A. Alchalal, and M. Ottolenghi, *Chem. Phys. Lett.*, **20**, 291 (1973).
(13) We have used pulse radiolysis to produce $^3B^*$ (where we measured decay rate constant of 6×10^4 sec^{-1}) rather than the laser excited TMPD–biphenyl system[12] since the biphenyl triplet decay constant in the latter case is considerably higher ($\sim 3 \times 10^5$ sec^{-1}). This requires a high $[R]$ value for total quenching of $^3B^*$, leading to direct excitation of R which efficiently competes with TMPD on the absorption of the 337.1-nm laser line.
(14) (a) T. Medinger and F. Wilkinson, *Trans. Faraday Soc.*, **61**, 620 (1965); (b) C. R. Goldschmidt, R. Potashnik, and M. Ottolenghi, *J. Phys. Chem.*, **75**, 1025 (1971).
(15) (a) H. L. J. Backstrom and K. Sandors, *Acta Chem. Scand.*, **16**, 958 (1962); (b) A. Lamola, private communication cited by P. S. Engel and B. M. Monroe, *Advan. Photochem.*, **8**, 29 (1971).
(16) (a) A. Knowles, *Nature (London)*, *New Biol.*, **236**, 202 (1972); (b) R. B. Cundall, *Progr. React. Kinet.*, **2**, 167 (1964).
(17) J. G. Calvert and J. N. Pitts, Jr., "Photochemistry," Wiley, New York, N. Y., 1966, p 421, and references therein.
(18) G. S. Hammond and J. Saltiel, *J. Amer. Chem. Soc.*, **85**, 2516 (1963); G. S. Hammond, J. Saltiel, A. A. Lamola, N. J. Turro, J. S. Bradshaw, D. O. Cowan, R. C. Counsell, V. Vogt, and C. Dalton, *ibid.*, **86**, 3197 (1964).

Laser Photolysis Studies on the Primary Processes of Photoinduced Ionic Polymerizations

Masahiro Irie,* [1a] **Hiroshi Masuhara,** [1b] **Koichiro Hayashi,** [1a] **and Noboru Mataga** [1b]

The Institute of Scientific and Industrial Research, Osaka University, Suita, Osaka, Japan and the Department of Chemistry, Faculty of Engineering Science, Osaka University, Toyonaka, Osaka, Japan (Received June 8, 1973)

Primary processes of photoinduced cationic polymerization of α-methylstyrene in the presence of tetracyanobenzene or pyromellitic dianhydride have been investigated by the nanosecond laser photolysis method. Ionic photodissociations in both charge-transfer singlet and triplet states are observed for the α-methylstyrene–tetracyanobenzene complex in methylene chloride. The contribution of these two states to the ion yield was found to depend on the temperature. In the case of the α-methylstyrene–pyromellitic dianhydride complex, however, ions are formed exclusively from the charge-transfer triplet state. The decay behavior of ion pairs depends on the states from which they are formed. Ions formed from the singlet state decay faster than those from the triplet state. The difference was interpreted by the concept of spin conservation in the reaction system. Initiation processes, *i.e.*, dimerization and trimerization, were also elucidated. The ions formed from the singlet state neither give a photocurrent nor do they initiate photopolymerization, while ions formed from the triplet state give a photocurrent and react with the monomer to form a dimer radical cation of α-methylstyrene. The dimerization rate constant was estimated to be $1 \times 10^5 M^{-1}$ sec^{-1}.

Introduction

Ionic photopolymerization is one of the most attractive photochemical reactions which are brought about by light absorption of charge-transfer (CT) systems. We reported in previous papers[2] that cationic polymerization of α-methylstyrene or styrene are induced by light in the presence of electron acceptor molecules such as tetracyanobenzene (TCNB) or pyromellitic dianhydride (PMDA). Although the ionization process is the essentially important step of the photopolymerization, the detailed study in the polymerization system has not yet been made because of experimental difficulties to detect the very fast reactions.

However, recently it has become possible to elucidate the behavior of excited electron donor acceptor (EDA) complexes with nanosecond time resolution by the application of the short-pulse laser excitation technique. The extensive studies in nonpolymerizable systems[3–9] have revealed that the excited complexes dissociate into ion pairs in polar solvents *via* three routes, CT singlet, CT triplet, and excited Frank-Condon states. The PMDA-mesitylene complex in ether-isopentane glass at $-156°$ was reported to dissociate in its CT triplet state[3] while it was proved that dissociation from the CT singlet state occurs in the case of TCNB-toluene complex in acetonitrile.[4a] Ionic dissociation in the excited Frank-Condon state was found for the TCNB-benzene complex in 1,2-dichloroethane.[5]

The phenomenological classification of the photodissociation mechanism described above is rather temporary and it has been pointed out that the mechanism markedly depends on several factors such as the combination of the donor and the acceptor, the nature of the solvent, and the

temperature of the system. Therefore, it is necessary to elucidate the primary processes of the polymerizing system under exactly the same condition as the polymerization.

The α-methylstyrene-TCNB complex was proved to dissociate into ions in the CT triplet state in amyl alcohol at low temperature,[6] though the dissociation was also observed to occur in its singlet state in 1,2-dichloroethane at room temperature.[4a] To clarify this solvent effect and to obtain further insight into the ionization mechanism as well as into the initiation process of the photopolymerization, we carried out a nanosecond laser photolysis study of the α-methylstyrene complex with TCNB or PMDA in methylene chloride under the same condition as the cationic polymerization study.[2]

The effects of temperature and solvents on the mechanism as well as the decay processes of ions are analyzed in detail. The dimerization and trimerization processes, which are the first steps of propagation, were also elucidated.

Experimental Procedure

α-Methylstyrene and methylene chloride were purified carefully and dried rigorously as described before.[2] TCNB and PMDA were purified by sublimation in vacuo. All samples were prepared in vacuo at less than 10^{-5} Torr pressure and special care was taken not to contaminate the samples with traces of moisture.

The Q-switched ruby laser photolysis apparatus has been described before.[4a] The second harmonics of the ruby laser of 347 nm was used as the exciting light pulse. The photocurrent induced by laser excitation was measured by the apparatus described before.[9] The time constant of the electronic circuit was less than 10 nsec. The intensity of the laser pulse was controlled with neutral filters composed of wire gauze.

Low-temperature experiments were carried out by placing the sample cell in a quartz Dewar vessel filled with cold ethanol and the temperature was measured by the use of a copper-constantan thermocouple and a microvolt meter.

Results

I. "Fast" Ionic Dissociation Process of α-Methylstyrene–TCNB Complex. The α-methylstyrene-TCNB complex gives a CT absorption band around 360 nm in methylene chloride at room temperature.[6] The exciting light pulse at 347 nm lies within the range of the CT band. Rigorously dried and degassed methylene chloride solutions containing 0.54 M α-methylstyrene and 1×10^{-3} M TCNB were exposed to the pulse laser excitation. The transient absorptions at 462 and 690 nm are followed and shown in Figure 1A and B, respectively. The absorption at 462 nm is due to a radical anion of TCNB[10] and that at 690 nm is of a radical cation of α-methylstyrene.[11] These radical anions and cations are formed immediately after the laser pulse and disappear in several hundred nanoseconds.

In order to examine the decaying behavior of the ions, the optical densities at 462 (Figure 2) and 690 nm were plotted as a function of time after the laser pulse. Both fit the first-order decay kinetics well and almost the same decay rates are obtained for both cations and anions. This good coincidence indicates a geminate recombination of ion pairs formed from an excited complex.
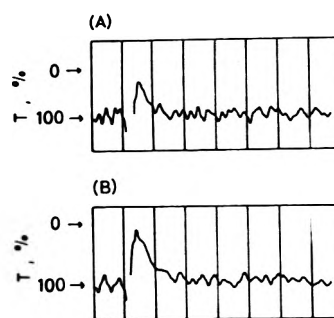
Figure 1. Oscillograms at (A) 462 nm and (B) 690 nm in the laser photolysis of methylene chloride solution containing 0.54 M α-methylstyrene and 6×10^{-3} M tetracyanobenzene at room temperature; 100 nsec/div.
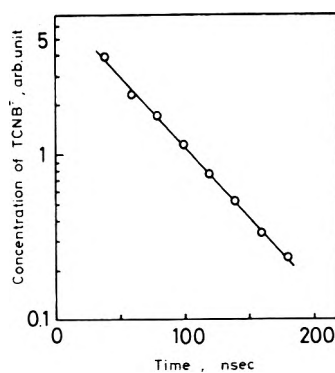
Figure 2. Decay of tetracyanobenzene radical anion formed immediately after the laser pulse in the solution containing 0.54 M α-methylstyrene and 6×10^{-3} M tetracyanobenzene at room temperature.
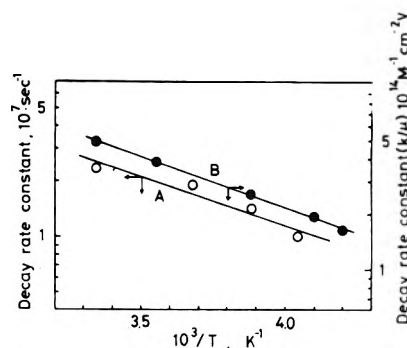
Figure 3. Arrhenius plots of (A) the first-order decay rates of α-methylstyrene radical cations formed in the solution containing 0.56 M α-methylstyrene and 6×10^{-3} M tetracyanobenzene immediately after laser pulse and (B) second-order decay rates of photocurrent observed in the solution containing 0.80 M α-methylstyrene and 4×10^{-3} M tetracyanobenzene.

The first-order decay rate and the yield of ions depended on the concentration of α-methylstyrene in methylene chloride. The rate increased drastically with increasing concentration of α-methylstyrene, while the yield decreased. For example, the lifetime of the ions is shortened to one-half when the concentration increased from 0.29 to 0.54 M. These dependences of the rate constant and the yield are summarized in Table I together with the dielectric constants of the systems estimated by Onsager's equation.[12] The activation energy of the decay of the ions was determined from the Arrhenius plots shown in Figure 3A to be 2.3 kcal/mol.

II. "Slow" Ionic Dissociation Process of α-Methylstyrene–TCNB Complex. Figure 4 shows the rise and decay
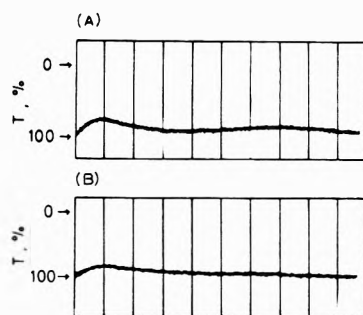
Figure 4. Oscillogram at (A) 462 nm and (B) 690 nm in the laser photolysis of the solution containing 0.29 M α-methylstyrene and 1 $\times$ 10^{-2} M tetracyanobenzene at room temperature; 10 μsec/div.

Figure 6. Transient absorption spectra at 10 μsec after pulse in the laser photolysis of the solution containing 0.56 M α-methylstyrene and 4 $\times$ 10^{-3} M pyromellitic dianhydride at room temperature.

Figure 5. Transient absorption spectra in the laser photolysis of the solution containing 0.29 M α-methylstyrene and 1 $\times$ 10^{-2} M tetracyanobenzene at room temperature; (A) O, 10 μsec after the pulse; (B) ●, 70 μsec after the pulse.

Figure 7. Temperature dependence of relative ion yields formed from CT singlet (●) and CT triplet (O) states in the solution containing 0.56 M α-methylstyrene and 6 $\times$ 10^{-3} M tetracyanobenzene.

TABLE I

| αMeSt, M | ϵ | Decay rate constant, sec^{-1} | | Φ_{ion}, relative | |
		TCNB·$^-$	αMeSt·$^+$	Singlet	Triplet
0.29	8.7	1.1 $\times$ 10^7	1.2 $\times$ 10^7	1	0.08
0.54	8.5	2.0 $\times$ 10^7	1.8 $\times$ 10^7	0.8	0.09
1.9	7.3	. . .	. . .	0.03	0.03

curves of the transient absorption at 690 and 462 nm in the microsecond region. The absorption at 462 nm builds up gradually in several microseconds and reaches a maximum at about 10 μsec. Another maximum is also observed at 70 μsec. To indentify these two intermediates the transient absorption spectra were recorded at 10 and 70 μsec after pulsing, shown in Figure 5A and B, respectively. Spectrum A consists of two superimposed bands attributable to TCNB radical anion and α-methylstyrene radical cation. The slow formation of these ion pairs suggests that these ions are formed from a metastable intermediate, presumably a CT triplet state.

The addition of air to the solution suppressed the "slow" formation of the sharp absorption peak at 462 nm due to the TCNB radical anion remarkably, though it affected the fast one slightly. This oxygen effect supports the dissociation of the CT triplet state.

The yield of the ions decreased with increasing concentration of α-methylstyrene though the concentration dependence is not so pronounced as in the case of the ions formed immediately after pulse.

III. "Slow" Ionic Dissociation Process of α-Methylstyrene-PMDA Complex. In the case of α-methylstyrene-PMDA complex, no fast formation of ions in the nanosecond region was detected. The transient absorption band, shown in Figure 6, grows-in slowly in several microseconds and the maximum is attained at 10 μsec after the pulse. The spectrum is composed of two bands due to PMDA radical anions[7] and α-methylstyrene radical cations. The slow formation of these ion pairs indicates that the excited EDA complex dissociates into ions not in the excited CT singlet state but exclusively in the CT triplet state.

IV. Effect of Temperature on the Yield of Ions. Upon lowering the temperature the yield of ions formed immediately after the pulse decreased, while that of the ions formed slowly increased. Figure 7 shows the effect of temperature on the yield of TCNB radical anions originating from these two states. The yields of the slowly produced ions were estimated from the absorption peak at 10 μsec after the pulse. A similar temperature effect on the yield was also observed for the α-methylstyrene radical cations.

V. Electrical Conductivity Measurement. The formation of free ions is directly evidenced by observing the transient photocurrent induced by the laser pulse. The typical photocurrent in the microsecond region is demonstrated in Figure 8. No photocurrent was detected in the nanosecond region.

The photocurrent increased slowly and reached its maximum at about 10 μsec. Considering the time constant in the electric circuit of less than 10 nsec, it is obvious that free ions are formed not immediately after the pulse but rather slowly. The matching of the growing-in curve of the photocurrent with that of the optical absorption suggests that the free ions originate from the ion pairs which dissociate in the CT triplet state.
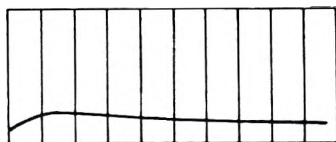
Figure 8. Transient photocurrent obtained in the solution containing 0.54 M α-methylstyrene and 6 × 10^{-3} M tetracyanobenzene at room temperature. The time constant of the electronic circuit is less than 10 nsec by the use of 50-Ω resistor; 10 μsec/div.
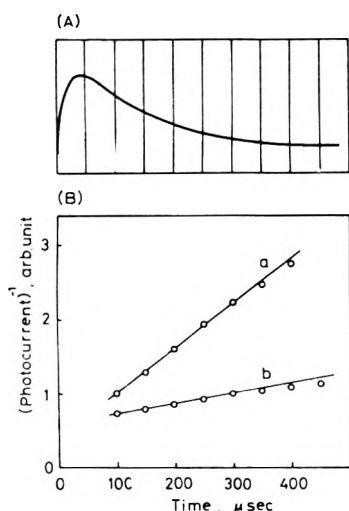
Figure 9. (A) Transient photocurrent obtained in the solution containing 0.40 M α-methylstyrene and 8 × 10^{-3} M tetracyanobenzene at room temperature; 10-kΩ resistor was used to analyze the decaying behavior precisely; 50 μsec/div. (B) Reciprocal plots of the photocurrents at a, 8° and b, −45° in the same solution as (A).

Figure 10. Absorption spectra of γ-irradiated n-butyl chloride–isopentane glasses (volume ratio of 1:1) containing (a) 0.077, (b) 0.39, (c) 0.77 M α-methylstyrene at 77°K. Irradiated dose is 1.3 × 10^{18} eV/g. Although the absorption spectrum longer than 800 nm is not shown because of difficulty to obtain precise spectra, a new band around 1500 nm was found to increase with increasing concentration of α-methylstyrene.

The first-order dependence of ion formation on the light intensity indicates that these ions are formed by a one-photon process. In order to analyze the decaying behavior of ions more precisely the photocurrents were remeasured by the use of a 10-kΩ resistor instead of a 50-Ω resistor, as shown in Figure 9A. Second-order plots of the two decay curves, measured at 8 and −45°, are represented in Figure 9B. These experimental results fit well to the second-order kinetics, though the decay rate becomes slower in the later period. The deviation from the second-order behavior is more evident at lower temperature. The decay rate $(k/\mu$, where k and μ are the recombination rate constant and the mobility of ions, respectively) was obtained to be 2.4 × 10^{-7} V cm at 25°, which is in good agreement with the theoretical value of 2.1 × 10^{-7} V cm obtained by the use of the Langevin's relation, $k/\mu = 4\pi e/\epsilon$,[13] where ϵ is the static dielectric constant.

The concentration of free ions at 10 μsec after the laser pulse was estimated to be about 10^{-8} M, assuming the mobility of 5 × 10^{-4} cm^2 V^{-1} sec^{-1}. On the other hand, one is capable of estimating the total concentration of ions from the absorption measurements, when the values of molar extinction coefficients ϵ of the ions are known. To obtain the ϵ values, the methods of sodium reduction and γ irradiation were adopted for TCNB radical anions and α-methylstyrene radical cations, respectively. The values obtained are 1.2 × 10^4 for the TCNB radical anion at 462 nm and 8.8 × 10^3 for the α-methylstyrene radical cation at 690 nm. By the use of these ϵ values, the total concen-

trations of the radical anion and cation are estimated to be 8 × 10^{-6} and 9 × 10^{-6} M, respectively. The good coincidence of these two concentrations represents another support of the mechanism that ion pairs are formed from excited complexes.

The difference in the concentration obtained by the two alternate experiments, conductivity and absorption measurements, indicates that most of the ions are in the paired state and only a very small fraction dissociates into free ions. The activation energy of the decay of free ions was determined to be 2.5 kcal/mol from the Arrhenius plot shown in Figure 3B.

VI. Dimerization Process. It is useful to investigate the chemical reaction in organic glass matrices at low temperature in order to make a qualitative interpretation of the rapid processes in the liquid state. Mixed organic glasses of n-butyl chloride and isopentane (volume ratio of 1:1) containing 0.077, 0.39, and 0.77 M α-methylstyrene were exposed to γ irradiation at 77°K. The absorption spectra obtained in the glasses are shown in Figure 10. According to the criterion proposed by Hamill, *et al.*,[14] the spectrum observed in the glass containing 0.077 M α-methylstyrene is attributable to radical cation of α-methylstyrene,[11] which indicates two absorption bands at 340 and 690 nm. Upon increasing the concentration of added α-methylstyrene these two bands disappeared and new bands at 485 nm and around 1500 nm growed up. Finally, at 0.77 M α-methylstyrene the monomer bands completely disappeared leaving only the new bands, which are attributable to α-methylstyrene dimer radical cations, on the basis of the assignments by Brochlehurst, *et al.*[15]

The spectrum obtained at 70 μsec after the laser pulse having an absorption maximum at 485 nm, shown in Figure 5B, agrees with that of the dimer radical cation. The formation of the 485-nm band at the rate matching the decay of the 690-nm band, which is produced slowly in 10 μsec, clearly exhibits the initial step of the polymerization. The time which the dimer radical cation needs to reach the maximum concentration depends on the concentration of α-methylstyrene, as shown in Figure 11A and B. Upon increasing the monomer concentration the maximum peak appeared after a shorter time. The formation of dimer radical cation together with the disappearing of the ions formed immediately after the laser pulse was not observed.
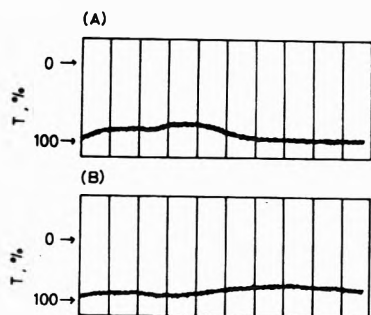
Figure 11. Oscillograms at 485 nm in the laser photolysis of the solutions containing (A) 0.54 M and (B) 0.29 M α-methylstyrene and (A) 6 $\times$ 10^{-3} M and (B) 1 $\times$ 10^{-2} M tetracyanobenzene at room temperature; 10 μsec/div.

Figure 12. Energy levels of excited CT states and ions.

Discussion

I. Two Ionic Dissociation Processes. The absorption bands around 460 nm due to TCNB radical anion and 690 nm due to α-methylstyrene radical cation appeared *once* immediately after laser pulse and *again* slowly at 10 μsec after the pulse as shown in Figure 4. The possibility that the fast growing-in absorption is due to $S_n \leftarrow S_1$ absorption of the EDA complex is excluded because the lifetime of the absorption, 50 nsec, is much longer than that of the fluorescence, which is less than 10 nsec. The twofold appearance of the absorption peaks due to ions indicates the existence of two ionic photodissociation processes in the α-methylstyrene-TCNB complex in methylene chloride.

The "fast" formation process of ions indicates that a fraction of the excited singlet EDA complexes dissociates into ion pairs, though the singlet state cannot be determined to be relaxed or not with present knowledge. The ions formed from the singlet state did not generate a photocurrent. This means that the ions exist in the paired state and recombine before the dissociation into free ions. The recombination rate is so fast that the ions can neither dissociate into free ions nor react with monomers to initiate the polymerization. It is interesting here to evaluate the rate constant for the diffusion controlled ion-pair dissociation by the use of Eigen's expression (eq 2 of ref 16b).[16] In the methylene chloride solution containing 0.5 M α-methylstyrene (ϵ 8.5), the rate constant is obtained to be 2 $\times$ 10^7 sec^{-1} at 25°, which suggests that the ions formed from the singlet state exist as undissociated ion pairs for $\sim$5 $\times$ 10^{-8} sec without dissociating.

The first-order decay of the ions, as shown in Figure 2, also proves the ion-pair formation. The activation energy of the decay obtained to be 2.3 kcal/mol is nearly equal to that of a diffusion process.

The "slow" formation process of ions and the oxygen effect on the process indicate that a part of ions are formed from a CT triplet state of the EDA complex. The ions formed from the triplet state have a longer lifetime than those formed from the CT singlet state and possibly give rise to an addition reaction with monomers to initiate the cationic polymerization. The growing-in curve of the photocurrent is similar to that of the ions formed from the CT triplet state, as shown in Figures 4 and 8. The similarity indicates that the ion pairs dissociate into free ions. The concentration of free ions estimated from the photoconductivity measurement is much less than the total concentration obtained from the absorption measurement. These results mean that only a small amount of ions formed from the triplet state dissociates into free ions.
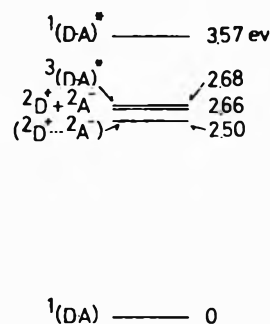
In the α-methylstyrene-PMDA complex, on the other hand, there exists only a "slow" ionic dissociation from the CT triplet state. The CT singlet state is presumably so unstable that the suitable orientation of solvents for ionic dissociation cannot be attained during its lifetime.

II. Kinetic Analysis of the Processes. The coexistence of the two ionic dissociation routes for the α-methylstyrene-TCNB complex and a single route for the α-methylstyrene-PMDA complex were observed in methylene chloride, as described above. The differences in behavior of the two complexes, of the ions formed through these two processes, and the temperature effect on the contribution of these processes are reasonably interpreted by the following reaction scheme including the energy levels of each states, as shown in Figure 12
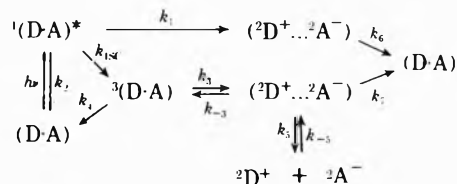
where k_1, k_{ISC}, k_3, and k_{-3} designate the rate constants of the dissociation from excited CT singlet state, of intersystem crossing, of dissociation from CT triplet state, and of association; k_5 and k_{-5} are the rate constants of dissociation of ion pairs to free ions and of association, respectively; k_2, k_4, k_6, and k_7 are the rate constants of deactivation from the excited CT singlet state to the ground state, of that from CT triplet state, of recombination of ions formed from the singlet state, and of ions from the triplet state.

In Figure 12, the excitation energy of the ruby laser lines and the O–O band of the CT triplet state of the EDA complex[6] are adopted as the energy levels of ^{1}(D·A)* and ^{3}(D·A), respectively. The energy levels of (^{2}D$^+$ ... ^{2}A$^-$) and (^{2}D$^+$ + ^{2}A$^-$) are estimated from the oxidation–reduction potentials.[9,17]

The ionic dissociation rate from the excited CT singlet state is much faster than that from CT triplet state. At 20°, for example, k_1 is larger than 10^8 sec^{-1} but k_3 is about 10^3 sec^{-1}. The former process is significantly exothermic, while the latter one is slightly exothermic, as indicated in Figure 12. Therefore, the dissociation from the triplet state is expected to be more difficult to occur than from the singlet state.

Figure 7 indicates a symmetric relation between the decrease in the yield of ions from the singlet state and the corresponding increase in that from the triplet state. The temperature effect on the two process is reasonably interpreted by the competition between ionic dissociation and intersystem crossing processes from the excited singlet

state.[18] The reaction scheme shown above leads to the equations

$$\Phi_{ion.S} = \frac{k_1}{k_1 + k_2 + k_{ISC}} \tag{1}$$

$$\Phi_{ion.T} = \frac{Ak_{ISC}}{k_1 + k_2 + k_{ISC}} ; A = \frac{k_3^2}{(k_3 + k_4)(k_3 + k_{-3})} \tag{2}$$

where $\Phi_{ion.S}$ and $\Phi_{ion.T}$ are the yields of ions formed from the singlet state and the triplet state, respectively.

The temperature dependence of $\Phi_{ion.S}$ and $\Phi_{ion.T}$ is reduced to the competition between k_1 and Ak_{ISC}. Upon lowering the temperature, k_1 and k_3 are expected to decrease due to the activation energy necessary to reorganize the solvent molecules, though k_{ISC} is presumed to be independent of the temperature.[18] k_{-3} and k_4 are also expected to decrease due to the increase of viscosity. Consequently, Ak_{ISC} becomes larger than k_1 at lower temperature.

The different behavior of the two complexes, α-methylstyrene-TCNB and -PMDA complexes, in ionic dissociation processes is also interpreted by the competition between k_{ISC} (and/or k_2) and k_1. The fact that ionization in CT singlet state was not detected in PMDA complex is due to either k_{ISC} is predominant because of large intersystem crossing probability or/and k_1 is small because of a less polar structure of the excited CT singlet state. At this moment the former is more probable, because the excited CT singlet state is considered to be in a quite polar structure.

The decay behavior depends on the processes, from which ions are formed, as shown in Figures 1 and 4. The decay rate of ions formed from the triplet state is much less than that from the singlet state. It is worthwhile to consider the spin conservations in the reaction system to account for the remarkable difference. At room temperature the spin–lattice relaxation time, T_1, is known to be in the range of 10^{-6} sec.[19] Therefore, the ion pairs formed from the singlet state recombine to form $^1(D \cdot A)^{\ddagger}$ before the inversion of the spins occurs, as follows

$$^1(D \cdot A)^* \xrightarrow{k_1} |^2D^+(\uparrow)...^2A^-(\downarrow)| \longrightarrow \;^1(D \cdot A)^{\ddagger}$$
$$\downarrow \tag{3}$$
$$(D \cdot A)$$
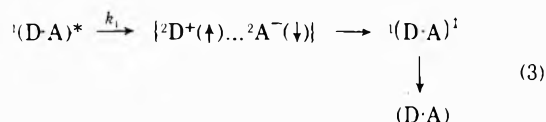
$^1(D \cdot A)^{\ddagger}$ formed by the recombination of the ion pair deactivates quickly to the ground-state complex, because the energy of $^1(D \cdot A)^{\ddagger}$ is much smaller than $^1(D \cdot A)^*$, as indicated in Figure 12.

On the other hand, the ion pairs formed from the CT triplet state, which are expected to have the total spin quantum number of 1 during the first 10^{-6} sec, recombine to reproduce the $^3(D \cdot A)$ complex, as follows

$$^3(D \cdot A) \rightleftharpoons |^2D^+(\uparrow)...^2A^-(\uparrow)| \tag{4}$$
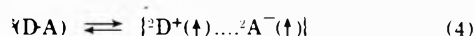
The above dissociation and association reactions will be successively repeated until either the triplet complex deactivates to the ground state, reaction 5, or the inversion of the spins of radical ions, reaction 6, occurs.

$$^3(D \cdot A)^* \xrightarrow{k_4} (D \cdot A) \tag{5}$$

$$|^2D^+(\uparrow)...^2A^-(\downarrow)| \longrightarrow |^2D^+(\uparrow)...^2A^-(\downarrow)| \tag{6}$$
$$\downarrow$$
$$(D \cdot A)$$
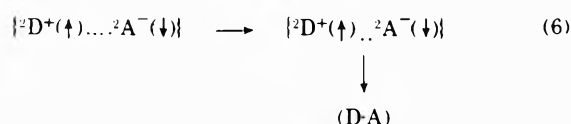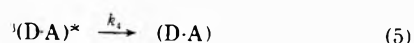
The rather slow rates of the processes 5 and 6 are considered to cause the slow decay of the ions formed from the triplet states.

III. Initiation Process of the Polymerization. The above discussions reveal the ionization processes in the polymerization system itself. The next problem that should be studied is the reaction mechanism of the early stage of the polymerization initiated by the ions formed from the excited complex. The methylene chloride system, which is dried rigorously, makes it possible to correlate the behavior of ions directly to the cationic polymerization reaction because we really obtained the polymer in this system.

The radical cations of α-methylstyrene formed from the triplet state react with α-methylstyrene to form dimer radical cations, as shown in Figures 5 and 10, though the ions from singlet state cannot.

$$^2D^+ + D \xrightarrow{k_{p_1}} \;^2D_2^+ \tag{7}$$
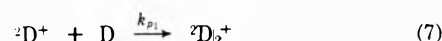
The decay of the radical cation may be described by the equation

$$-\frac{d[^2D^+]}{dt} = k_{p_1}[^2D^+][D] + k_r[^2D^+]^2 + \dots \tag{8}$$

The second term of eq 8, which denotes the decay process of D^+ by the ion recombination, can be ignored when the concentration of monomer is large enough as in this experiment. Then the lifetime of the monomer radical ion is expressed by eq 9.

$$\tau_{1/2} = \frac{0.693}{k_{p_1}[D]} \tag{9}$$

$\tau_{1/2}$ was obtained to be 2×10^{-5} sec at the monomer concentration of 0.29 M. This leads to $k_{p1} = 1 \times 10^5 \; M^{-1}$ sec^{-1}.

This dimerization rate is much slower than that obtained in the case of the dimerization reaction of radical cations of aromatic molecules, such as pyrene radical cations, where $1.9 \times 10^9 \; M^{-1}$ sec^{-1} has been reported.[20] However, this rate is faster when compared with the rate of dimerization of the 1,1-diphenylethylene radical anion, which was estimated to be $1 \times 10^4 \; M^{-1}$ sec^{-1}.[21] The slower rate of dimerization reaction of radical ions of aromatic molecules containing a vinyl group is probably due to the fact that it involves not only the formation of the sandwich structure but also the opening reaction of the double bond. The k_{p1} value of $1 \times 10^5 \; M^{-1}$ sec^{-1} is in good agreement with that obtained in styrene by pulse radiolysis.[22]

In addition to the dimerization reaction, the trimerization reaction is also an important step of the initiation process.

$$^2D_2^+ + D \xrightarrow{k_{p_2}} \;^2D_3^+ \tag{10}$$
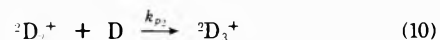
The decay of the dimer ions may be expressed by the equation

$$\frac{d[^2D_2^+]}{dt} = k_{p_1}[^2D^+][D] - k_{p_2}[^2D_2^+][D] \tag{11}$$

where the recombination reaction is also ignored. The time when the concentration of dimer ions reaches its maximum is derived from eq 11 as

$$t_{max} = \left(\ln \frac{k_{p_1}}{k_{p_2}}\right)\frac{1}{(k_{p_1} - k_{p_2})[D]} \tag{12}$$

t_{max} is in inverse relation with the monomer concentra-

tion. The experimental data in Figure 11 show that t_{max} is reduced to one-half, from 70 to 35 μsec, upon increasing the monomer concentration from 0.29 to 0.54 M, as predicted by eq 12. This result indicates that the decay of the dimer radical cation is due to the trimerization reaction, eq 10. These dimerization and trimerization reactions are considered to be the initial step of the photoinduced cationic polymerization.

Acknowledgment. The authors express their thanks to Dr. W. Schnabel for kindly reading the manuscript.

References and Notes

(1) (a) Institute of Scientific and Industrial Research, Osaka University; (b) Department of Chemistry, Faculty of Engineering Science, Osaka University.
(2) (a) M. Irie, S. Tomimoto, and K. Hayashi, J. Polym. Sci., **B8**, 585 (1970); (b) M. Irie, S. Tomimoto, and K. Hayashi, ibid., **A10**, 3235 (1972); (c) M. Irie, S. Tomimoto, and K. Hayashi, ibid., **A10**, 3243 (1972).
(3) R. Potashnik, C. R. Goldschmidt, and M. Ottolenghi, J. Phys. Chem., **73**, 3170 (1969).
(4) (a) H. Masuhara, M. Shimada, N. Tsujino, and N. Mataga, Bull. Chem. Soc. Jap., **44**, 3310 (1971); (b) H. Masuhara, N. Tsujino, and N. Mataga, Chem. Phys. Lett., **12**, 481 (1972).
(5) M. Shimada, H. Masuhara, and N. Mataga, Chem. Phys. Lett., **15**, 364 (1972).
(6) M. Irie, S. Tomimoto, and K. Hayashi, J. Phys. Chem., **76**, 363 (1972).
(7) Y. P. Pilette and K. Weiss, J. Phys. Chem., **75**, 3805 (1971).
(8) Y. Achika, S. Katsumata, and K. Kimura, Chem. Phys. Lett., **13**, 213 (1972).
(9) Y. Taniguchi, Y. Nishina, and N. Mataga, Bull. Chem. Soc. Jap., **45**, 764 (1972).
(10) M. Sofue and S. Nagakura, Bull. Chem. Soc. Jap., **38**, 1048 (1965).
(11) K. Tsuji, J. Lin, and F. Williams, Trans. Faraday Soc., **64**, 2896 (1968).
(12) T. Hanai, N. Koizumi, and Y. Goto, Nippon Kagaku Zasshi, **80**, 17 (1959).
(13) (a) P. Langevin, Ann. Chim. Phys., VII, **28**, 433 (1903); (b) A. O. Allen and A. Hummel, Discuss. Faraday Soc., **36**, 95 (1963).
(14) W. H. Hamill, "Radical Ions," E. T. Kaiser and L. Kevan, Ed., Interscience, New York, N. Y., 1968, p 321.
(15) B. Badger and B. Brochlehurst, Trans. Faraday Soc., **65**, 2582 (1969).
(16) (a) M. Eigen, Z. Phys. Chem., **1**, 176 (1954); (b) K. H. Grellmann, A. R. Watkins, and A. Weller J. Lumin. **1, 2**, 678 (1970).
(17) A. Weller, Nobel Symp., **5**, 413 (1967).
(18) N. Orbach, R. Potashnik, and M. Ottolenghi, J. Phys. Chem., **76**, 1133 (1972).
(19) P. B. Ayscough, "Electron Spin Resonance in Chemistry," Methuen, London, 1967, p 121.
(20) M. A. Rodgers, Chem. Phys. Lett., **9**, 107 (1971).
(21) T. L. Staples, J. Jaqur-Grodzinski, and M. Szwarc, J. Amer. Chem. Soc., **91**, 3721 (1969).
(22) H. Yoshida, M. Noda, and M. Irie, Polym. J., **2**, 359 (1971).

Recoil Tritium Reactions with Cyclohexene and Alkenes. Determination of Rate Parameters[1a]

Darrell C. Fee*[1b] and Samuel S. Markowitz

Department of Chemistry and Lawrence Berkeley Laboratory, University of California, Berkeley, California 94720
(Received July 2, 1973)

Kinetic rate parameters can be determined from recoil tritium reaction studies although the energy distribution of the reacting tritium atoms is not known. T is produced by ^{3}He(n,p)T. Recoil T-for-H substitution on cyclohexene gives excited cyclohexene-t molecules. The dependence of product yield on pressure (in the 300–1500 Torr pressure range) showed that the excited cyclohexene-t molecules decomposed unimolecularly to give ethylene-t and butadiene-t with an apparent rate constant (at 135°) of 5 × 10^6 sec^{-1}. The s parameter in the RRK (Rice, Ramsperger, and Kassel) treatment of the unimolecular decomposition of cyclohexene was determined as $s = 24$. Similarly, the pressure dependence of product yield showed that cyclohexyl-t radicals which are formed by recoil T atom addition to cyclohexene decomposed unimolecularly to give n-hexene-t, 1-butene-t, and methane-t with rate constant 8 × 10^3, 3 × 10^4, and 5 × 10^2 sec^{-1}, respectively. The relative rate of abstraction vs. addition of radicals in alkenes was determined from the scavenger dependence of the yields of products with a radical precursor.

Introduction

A Maxwell–Boltzmann distribution of the thermal energies of reactive species is a barrier to the study of high-energy bimolecular reactions. Of two competing reactions, the reaction with the lower energy threshold tends to predominate simply because of the larger number of molecules with sufficient energy for reaction. For many years, the role of translational energy in promoting virtually all reactions has been emphasized. This suggests that the energy barrier to the study of high-energy bimolecular reac-

tions may be circumvented. One (or both) of the reactants could be a translationally excited species whose energy is not given by a Maxwell–Boltzmann distribution. Translationally excited ("hot") atoms have been introduced into a system via nuclear reaction and resulting recoil.[2]

We are interested in the study of recoil tritium atoms. Recoil tritium studies are often limited by the lack of knowledge of the energy of the tritium atom when it reacts. The tritium atom is produced via nuclear recoil with an energy (192 keV, 1 eV = 23 kcal/mol) which is

virtually infinite on the chemical scale. The tritium ion (atom) undergoes a series of energy-losing collisions with its environment until it enters the energy region below 20 eV where reactions which produce stable tritium-labeled products are thought to occur. The tritiated product distribution which is experimentally measured is the summation of tritium atom reactions at all energies from 20 to 0.02 eV (thermal energies). Experimental determinations of the tritium atom energy distribution in the 20–0.02 eV range have not been made.[2] Attempts to calculate a theoretical tritium atom energy distribution that would explain the existing recoil tritium reaction data have not been too successful.[3-7] At most, the Wolfgang–Estrup kinetic theory of hot atom reactions would determine the "reactivity integral," the area under a plot of reaction cross section vs. the logarithm of the energy of the reacting tritium atom. To date, application of the Wolfgang–Estrup theory has been unable to determine convincingly even the relative average energy of the hydrogen atom abstraction vs. T-for-H substitution process.[8-11]

In recoil tritium reactions, the only well-known energy "bench mark" is that T-for-H substitution deposits an average excitation energy of 5 eV in the resultant tritiated molecule.[12,13] This relatively high energy of excitation, unless removed by collision, may cause the tritiated molecule to undergo unimolecular decomposition. In fact, analysis of the pressure dependence of the unimolecular decomposition of cyclobutane-t (following T-for-H substitution) with the RRKM theory (Rice, Ramsperger, Kassel, and Marcus) of unimolecular reactions[14,15] led to the 5 eV figure. The average energy of the reacting tritium atom is still not known. As Rowland[2a] points out, measurements have not been made of the kinetic energies of the replaced hydrogen atoms. Therefore there is no direct indication as to whether an excitation energy of 5 eV corresponds to a 10-eV T atom knocking out a 5-eV H atom or a 5.5-eV T atom giving rise to a 0.5-eV H atom.

Because of the lack of knowledge of the energy of the tritium atom when it reacts and because the average energy of excitation is not too useful in analyzing competing unimolecular reaction channels, kinetic parameters often cannot be extracted from recoil tritium reaction studies. Even the simplest concepts of rate processes include an explicit energy dependence (see ref 14 and 15 and references therein). In this paper we attempt to show that kinetic parameters can be determined from selected, carefully designed recoil tritium experiments, namely: (1) studying the pressure dependence of the unimolecular decomposition of excited tritiated molecules following T-for-H substitution, (2) studying the pressure dependence of the unimolecular decomposition of an excited tritiated alkyl radical following T atom addition to an alkene, (3) studying the scavenger dependence of alkyl-t radicals formed in a T + alkene system.

Experimental Section

The samples were prepared in 1720 Pyrex capsules (14-ml internal volume) using vacuum line techniques similar to those previously described.[16] More details of sample preparation are given elsewhere.[17] The ³He (Mound Laboratories) was certified as 99.7 mol % ³He with a tritium content of 1.0×10^{-11} mol %. A standard radio gas chromatographic analysis[18] of an unirradiated aliquot of He containing at least twice the moles normally sealed in the 1720 Pyrex capsules showed no measurable tritiated contaminant. The ³He was used directly from the Mound

Laboratories' container without further purification. All other materials used were research grade. All irradiations were made in the Berkeley Campus Nuclear Reactor. Irradiations at 25° were made in the Lazy Susan facility for 10 min at a flux of 3.8×10^{11} n cm^{-2} sec^{-1}. Irradiations at $135 \pm 0.5°$ were made in the Hohlraum in a specially designed irradiation container described elsewhere.[19] The irradiations at 135° were for 8.0 hr at a flux of 3.9×10^8 n cm^{-2} sec^{-1}. Radiation damage due to the recoils following the ³He(n,p)T reaction was less than 1%.

The samples were analyzed with a radio gas chromatographic technique detailed elsewhere.[18] Good resolution was obtained for all major product peaks in an analysis time of 10 hr (for cyclohexene samples) or less (C$_2$ to C$_4$ parent hydrocarbons). "Polymer-t" is defined as tritiated material not eluted in the normal radio gas chromatographic analysis. "Polymer-t" was recovered and monitored by procedures similar to those previously described.[20] All data reported represent the average of the yields from two identical samples. Unless otherwise stated, the yields of major products from identical samples agreed to within 3%.

Results and Discussion

Determination of the s Parameter in the RRK Treatment of Cyclohexene Unimolecular Decomposition. The unimolecular decomposition of cyclohexene to give primarily ethylene and butadiene has been well established in pyrolysis,[21-25] shock tube,[26-28] photolysis,[29,30] and mercury-sensitized photolysis[31] studies. Of the total unimolecular decompositions, 96% occur giving ethylene and butadiene, 3% occur by H$_2$ elimination to give cyclohexadienes and benzene, and the remaining 1% give C$_5$ and smaller hydrocarbons presumably through a free-radical mechanism.[23,24,30] A possible radical contribution to the ethylene and butadiene yield has been proposed from cyclohexyl radicals via H-atom addition to cyclohexene.[26,27] However, addition of scavenger does not affect the ethylene and butadiene yield.[23,30,31] The unimolecular rate constant for cyclohexene decomposition

$$k_{.1} = 10^{15.3} \exp(-66,900 \text{ cal}/kT) = A \exp(-E_0/kT) \quad (1)$$

has been so well determined that cyclohexene is used as an internal standard in shock tube studies.[27,28]

Strong evidence for the retro-Diels–Alder cleavage of cyclohexene comes from the photolysis of cyclohexene-3, 3,6,6,-d$_4$. The photolysis of cyclohexene-3,3,6,6-d$_4$ occurred as shown to give C$_2$H$_4$ and C$_4$H$_2$D$_4$ in 98% of the decomposition at 4.9-eV photolysis energy and 86% of the decompositions at 8.4-eV photolysis energy. At 8.4 eV the remaining 14% of the decompositions gave C$_2$H$_2$D$_2$ and C$_4$H$_4$D$_2$.[30]

Scavenger studies of recoil tritium reactions with cyclohexene at 25°[32,33] show that ethylene-t (C$_2$H$_3$T) and butadiene-t (C$_4$H$_5$T) are chiefly "hot" reaction products: (a) the ethylene-t yield is reduced by less than 10% with oxygen scavenging; (b) the "hot" butadiene-t yield could *only*

be determined with oxygen or butadiene-d_6 scavenging. Survival in the presence of oxygen scavenging is consistent with ethylene-t and butadiene-t resulting from unimolecular decomposition of cyclohexene-t formed via a T-for-H substitution reaction

$$
\begin{array}{c}
T + (c\text{-}C_6H_{10}) \longrightarrow [c\text{-}C_6H_9T]^* \xrightarrow[k_s]{\omega} \begin{array}{l} C_6H_9T\ (S) \\ (C_2H_3T + C_4H_6)\ \text{or} \\ (C_2H_4 + C_4H_5T) \end{array} \quad (3) \\
(D) = C_2H_3T + C_4H_5T
\end{array}
$$

where $\omega = ZP$ = collision frequency, P = cyclohexene pressure in Torr, Z = collision number,[34] S = collisional stabilization product, and D = unimolecular decomposition product.

The apparent rate constant of unimolecular decomposition, k_a, is given by[35]

$$k_a = \omega(D/S) = Z(D/S)P \qquad (4)$$

The S/D ratio should vary linearly with pressure for a unimolecular process. The collision frequency at the pressure where $S/D = 1$ is k_a.

The unimolecular formation of ethylene-t and butadiene-t as shown in eq 3 was confirmed by the linear pressure dependence of the stabilization (S)/decomposition (D) ratio shown in Figure 1. Experiments at elevated temperature were required to obtain a larger pressure range than the (zero to) 7 cm cyclohexene vapor pressure available at 25°. In Figure 1, the pressure represents the total effective collisional deactivation pressure in the sample capsule. Each sample contained 98 Torr of ^{3}He at 135° and a variable pressure of cyclohexene. Relative collisional deactivation efficiencies estimated from published sources[36] show that on a pressure-for-pressure basis ^{3}He is only 20% as effective as cyclohexene (C_6H_{10}) in deactivating excited cyclohexene molecules. Hence the "effective" collisional deactivation pressure of cyclohexene in the capsule is defined as

$$P_{eff} = P_{C_6H_{10}} + 0.2P_{^3He} \qquad (5)$$

The use of the effective pressure for the P in eq 4 is an attempt to correct for the effect of a weak collider in the system, ^{3}He. Otherwise, it is assumed that only a single collision between an activated cyclohexene-t molecule and an unlabeled cyclohexene molecule is necessary for complete deactivation of the excited cyclohexene-t species. We point out that this "strong collision"[14,15] assumption may not be valid at the high energies of excitation encountered in recoil tritium experiments. No correction was made for the effect of changing the mole fraction of ^{3}He moderator from 0.25 in the lowest pressure samples to 0.06 in the highest pressure samples. Changes in the tritium atom energy distribution with added moderator are usually observed only with the moderator in great excess of the parent hydrocarbon.[2]

The least-squares fitted line of the S/D ratio vs. pressure (actually log S/D vs. log (pressure)) was extrapolated to $S/D = 1.0$. The pressure at which S/D was 1.0 was 0.50 Torr. Extrapolation over the large pressure range is a standard hot atom technique.[12] Nevertheless, a large uncertainty $(-0.4, +1.1$ Torr) results from this extrapolation. This uncertainty is inherent in hot atom chemistry where low-pressure regions (below 20 Torr) are not experimentally accessible.[2] A previous determination by Weeks and Garland of the pressure at which the S/D ratio from

Figure 1. The unimolecular decomposition of cyclohexene-t to give ethylene-t or butadiene-t; unscavenged data at 135°. Activated cyclohexene-t molecules are formed by recoil T-for-H substitution. The abscissa is the effective collisional deactivation pressure (in the sample capsule) defined as effective pressure = cyclohexene pressure + 0.2 (helium-3 pressure).

the recoil tritium initiated unimolecular decomposition of cyclohexene equalled 1.0 gave a pressure of 0.2 Torr. However, in these previous experiments, the temperature ranged from 25° from the lowest pressure unscavenged sample to 135° for the highest pressure unscavenged sample.[37]

The data shown in Figure 1 are for unscavenged samples at 135°. For both O_2 and SO_2 scavenger, a (scavenger)/(scavenger + cyclohexene) ratio of 0.08 was insufficient to intercept the cyclohexyl-t radical intermediate to the cyclohexane-t yield. At 25°, this concentration of scavenger was sufficient to intercept cyclohexyl-t radicals.[32,33] The failure of both SO_2 and O_2 scavenger at 135° may be due to macroscopic reactions between cyclohexene and the scavenger. The reaction of cyclohexene with oxygen scavenger has been discussed.[32] For oxygen scavenging, a (scavenger)/(scavenger + cyclohexene) ratio of 0.14 was sufficient to intercept the cyclohexyl-t radicals. At this scavenger concentration and with 300 Torr of cyclohexene pressure the ethylene-t yield relative to the sum of yields from excited cyclohexene-t molecules $(C_2H_3T + C_4H_5T + c\text{-}C_6H_9T)$ was decreased by 9% with O_2 scavenging. This indicates that at 135° (as at 25°) ethylene-t results largely from "hot" tritium atom reactions. The unscavenged data were "corrected" by subtracting a 9% radical contribution to the ethylene-t yield at all pressures. The resultant "scavenged" plot of S/D vs. effective pressure extrapolated to $S/D = 1$ at 0.33 Torr. Because this value lies within the uncertainty of the unscavenged value and the assumption of a constant radical contribution may not be valid; we chose to use the unscavenged data in further calculations.

Another interesting scavenger effect was noted. At 135°, unlike 25°,[32,33] the butadiene-t yield is the same in O_2 scavenged, butadiene-d_6 scavenged, and unscavenged samples. Apparently the butadiene-t yield was not selec-

tively depleted by radiolysis-produced H atoms in unscavenged samples at 135° (unlike 25°). The butadiene-t is selectively depleted because butadiene is extremely reactive with H atoms (see Table I). The total radiolysis damage in the samples at 135° was similar to samples at 25°. The temperature effect on the individual rate constants for H-atom addition to cyclohexene and for H-atom addition to butadiene is not known. The temperature effect on the competitive rates of H-atom addition to cyclohexene vs. butadiene is probably slight. In unscavenged T + cyclohexene reactions at 25°, the butadiene-t yield was increased to within 10% of the oxygen scavenged value when the irradiation period was increased from 10 min to 8 hr (with total dose similar to that previously reported[32,33]). Apparently the butadiene-t yield is not selectively depleted by reactions with radiolysis produced H atoms when the irradiation period is 8 hr. This trend is consistent with a decreased steady-state concentration of H atoms with the lower tritium atom production rate that existed in 8 hr (vs. 10 min) irradiations.

The apparent rate constant, k_a, for the unscavenged unimolecular decomposition of cyclohexene-t to ethylene-t or butadiene-t was calculated from eq 4 as 5.1 × 10^6 sec^{-1}. The calculation of Z was made with an estimated[36] collision diameter for cyclohexene of 5.47 × 10^{-8} cm. Using this value of k_a and an average excitation energy (following T-for-H substitution) of 5 eV for the E in eq 6,[s] the s parameter in the RRK treatment[38-41] of the unimolecular decomposition of cyclohexene was determined as s = 24. The A and E_0 used were from eq 1.

$$k_a = A[(E - E_0)/E]^{s-1} \tag{6}$$

For a fixed s = ($\frac{1}{2}$)($3N$ − 6) = 24, E was 4.6 eV. For s = ($\frac{2}{3}$)($3N$ − 6) = 28, E was 5.6 eV. For a fixed s = 32 ≈ ($\frac{3}{4}$)($3N$ − 6), E was 6.2 eV.

Determination of the Apparent Rate Constants of the Unimolecular Decomposition/Isomerization of Cyclohexyl Radicals. The cyclohexene-t yield in T + cyclohexene reactions at 25° appears to have a radical precursor.[32,33] The cyclohexane-t yield (a) decreases to nearly zero with O$_2$ or SO$_2$ scavenging; (b) decreases with butadiene-d_6 scavenging; (c) increases with H$_2$S scavenging. All of these trends indicate a radical precursor. The proposed mechanism of cyclohexane-t formation was tritium atom addition to the double bond of cyclohexene to form a cyclohexyl-t radical. The cyclohexyl-t radical could then abstract a hydrogen atom from the bulk system to form cyclohexane-t. Hydrogen atom abstraction by cyclohexyl radicals to form cyclohexane has been observed in other systems.[42] Addition of a moderator should increase the number of tritium atoms which survive collisions in the 20-0.02-eV energy range and ultimately react as thermal tritium atoms. The lowest activation energy process for thermal tritium atoms is addition to the double bond. The monotonic increase in the cyclohexane-t yield (from T + cyclohexene reactions at 25°) with increasing amounts of added moderator that was observed with helium,[43] krypton,[43] and nitrogen[44] as moderators was reproduced in this laboratory with neon as a moderator.

Cyclohexyl radicals have also been observed to add to the double bond of cyclohexene to initiate a radical chain.[45,46] The radical chain initiated by a cyclohexyl-t radical would eventually undergo termination and be monitored as polymer-t. The yield of polymer-t also increased with increasing amounts of added moderator. All this indicates the presence of relatively large amount of

TABLE I: Hydrogen Atom Reaction Rate Constants at 25°[a]

Reactant	Addition, 10^9 cm^3 mol^{-1} sec^{-1}	Abstraction, 10^9 cm^3 mol^{-1} sec^{-1}
Butadiene	1500[b]	22[b]
Isobutene	770[b]	25[b]
Cyclohexene	600[c]	nd[g]
1-Butene	320[b]	30[b]
Propylene	300[b]	25[b]
O$_2$	300[d]	h
Ethylene	200[b]	13[b]
H$_2$S	h	160[b]
SO$_2$	6[e]	h
n-Butane	h	0.6[f]

[a] Addition by H-atoms forms a radical; abstraction by H atoms forms H$_2$. [b] References 55 and 56. [c] Reference 57. [d] References 58 and 59. [e] Reference 60. [f] Reference 61. [g] Not determined. [h] Not applicable.

cyclohexyl-t radicals in the T + cyclohexene system. Cyclohexane-t alone is a major product.

Cyclohexyl radicals have also been observed to undergo decomposition or isomerization.[47-49] The isomerization of cyclohexyl radicals to straight-chain alkenyl radicals has been postulated as the first step of a unimolecular decomposition process which leads to a complex series of products including methane, ethane, ethylene, propane, propylene, butenes, and methylcyclopentane.[47-49] The formation of n-hexenyl radicals without a cyclohexyl radical precursor results in (a) n-hexene via H-atom abstraction, (b) methylcyclopentane via an isomerization reaction.[50] The decomposition (isomerization) of cyclohexyl-t radicals from T + cyclohexene reactions may result in any or all of the aforementioned products from cyclohexyl radicals being tritium labeled.

Many of the species which may result from the decomposition/isomerization of cyclohexyl-t radical are observed as tritiated products in T + cyclohexene reactions. This list includes methane-t, ethane-t, ethylene-t, propane-t, propylene-t, 1-butene-t, trans-2-butene-t, cis-2-butene-t, and n-hexene-t/methylcyclopentane-t.[51] These products are observed in small yields. Both at 135°, and 135 and 25° roughly 85% of unscavenged T + cyclohexene reactions which gave gas-phase products resulted from abstraction to form HT, addition to form cyclohexyl-t radicals (a portion of which were monitored as cyclohexane-t), and T-for-H substitution to form cyclohexene-t. Some of these small-yield tritiated products show the same scavenger dependence as the cyclohexane-t yield. At 25° the yields of methane-t, ethane-t, 1-butene-t, and n-hexene-t decrease to nearly zero with O$_2$ or SO$_2$ scavenging and increase with H$_2$S scavenging, indicating a radical precursor. Therefore we propose the reaction scheme shown in eq 7 for excited cyclohexyl-t radicals formed by the addi-

tion of a tritium atom to cyclohexene. The site of the tritium label in the n-hexenyl-t radical and the 1-butenyl-t radical shown in eq 7 is purely arbitrary and is shown only
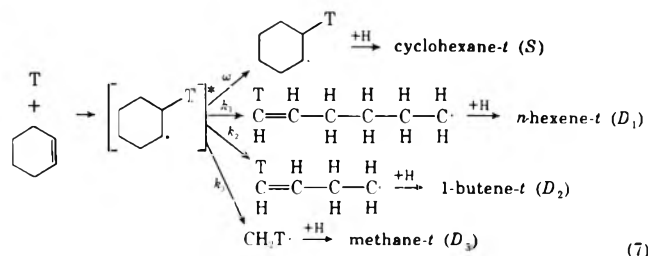
for the sake of material balance along the reaction path. The +H over the arrow in eq 7 indicates abstraction of a hydrogen atom. For collisionally stabilized tritiated radicals in unscavenged T + cyclohexene systems, the alternative to abstraction is addition to cyclohexene.

With H_2S scavenging,[33] all the radicals react rapidly with H_2S to abstract a hydrogen atom before they add to cyclohexane to eventually form polymer-t. (See Table II for a comparison of the rate constants of reaction of alkyl radicals with H_2S vs. alkenes at 25°. Similarly, at 135°, the rate constant of the reaction of alkyl radicals with H_2S is larger than with alkenes by several orders of magnitude.) For example, all n-hexenyl radicals formed by channel 1 (with rate constant k_1) are monitored as n-hexene-t when H_2S is employed as a scavenger. The pressure dependence of the S/D ratio for reaction channel 1, 2, and 3 (with rate constants k_1, k_2, and k_3) are shown in Figure 2.

The pressure dependence of the S/D_1 and S/D_2 ratio may be well represented by a line for the unimolecular decomposition/isomerization of cyclohexyl-t radicals to give n-hexenyl-t and 1-butenyl-t radicals, respectively. The increase scatter in the pressure dependence of the S/D_3 ratio for the unimolecular decomposition of cyclohexyl-t radicals to give methyl-t radicals results from the small yield of methane-t. A small uncertainty in the methane-t yield is reflected in a large uncertainty in the S/D_3 ratio. In this respect the yield of ethane-t is so small that the resultant uncertainty in the S/D ratio for $D =$ ethane-t makes observation of a pressure-dependence impossible.

The rate constants k_1 and k_2 were determined from extrapolation of S/D vs. effective pressure to $S/D = 1$. The calculation of Z was made with an estimated collision diameter of 5.67×10^{-8} cm for cyclohexyl-t radicals.[36] The values of the calculated rate constants at 135° and the pressure at which $S/D = 1$ were $k_1 = 8.4 \times 10^3$ sec^{-1} (7.9 $\times 10^{-4}$ Torr), $k_2 = 3.4 \times 10^4$ sec^{-1} (3.2 $\times 10^{-3}$ Torr). Using eq 4 to determine k_3 at each effective pressure and comparing k_3 with k_1 and k_2 values similarly derived allowed k_3 to be estimated as 5×10^2 sec^{-1}. The large uncertainty in the cyclohexane-t/methane-t ratio, as indicated by the large error bars in Figure 2, prevented meaningful extrapolation over a large pressure range to the pressure at which $S/D = 1$.

A previous determination by Weeks and Garland of k_1 in a recoil tritium–cyclohexene system showed that S/D_1 = 1.0 at 26 Torr. As discussed before, the temperature control employed by Weeks and Garland was inadequate.[37] It is interesting to note that the effect of inadequate temperature control in determining the pressure at which $S/D = 1.0$ was larger for cyclohexyl-t radical unimolecular decomposition/isomerization than for the unimolecular decomposition of cyclohexene-t. This is consistent with cyclohexene-t decomposition being a higher energy process.

Determination of the Relative Rate of Abstraction Vs. Addition of Radicals in Alkenes. Collisionally stabilized alkyl-t radicals which are formed from T + alkene reactions can react only by abstraction of a hydrogen atom to form an alkane-t species or by addition to the double bond (provided, of course, that the concentration of radicals from radioylsis damage is kept low enough to make radical–radical reactions negligible). The addition of a tritiated alkyl radical to the alkene may sufficiently energize the newly formed alkyl-t radical to cause it to undergo unimolecular decomposition/isomerization. The newly
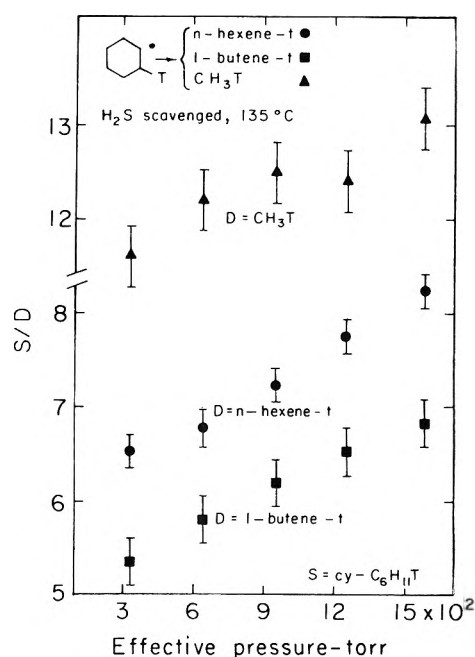
Figure 2. The unimolecular decomposition of cyclohexyl-t radicals to n-hexene-t, 1-butene-t, or methane-t; H_2S scavenged data at 135°. Activated cyclohexyl-t radicals are formed by recoil T atom addition to cyclohexene. The abscissa is the effective collisional deactivation pressure (in the sample capsule) defined as effective pressure = cyclohexene pressure + 0.2 (helium-3 pressure) + 0.5 (hydrogen sulfide pressure).

formed alkyl-t radical, once collisionally stabilized, may also abstract a hydrogen atom to form a tritiated alkene or add to the alkene to lengthen the tritiated radical chain. Tritiated dimers from recoil tritium reactions with alkenes have been monitored by radio gas chromatography.[52,53]

Methylcyclohexane-t has been observed in unscavenged T + cyclohexene systems. Methylcyclohexane-t presumably arises from the addition of CH_2T radicals to cyclohexene. In O_2 and SO_2 scavenged systems, the yield of methylcyclohexane-t was zero. Either the CH_2T radical or the methylcyclohexyl-t radical precursor to the methylcyclohexane-t yield could be scavenged by O_2 or SO_2. In neon moderated systems, the yield of methylcyclohexane-t increased with increasing amounts of added moderator. This is consistent with increased stabilization of the methylcyclohexyl-t radical formed from CH_2T addition to cyclohexene.

In H_2S scavenged T + cyclohexene systems, the yield of methylcyclohexane-t was also zero. A precursor to the methylcyclohexyl-t radical was being intercepted by H_2S. If methylcyclohexyl-t radicals were formed directly from T + cyclohexene reactions, H_2S would readily donate a hydrogen atom to the methylcyclohexyl-t radical and the yield of methylcyclohexane-t would increase with H_2S scavenging. As shown by the data in Table II, H_2S would intercept the CH_2T radical (to form methane-t) before the CH_3T radical could add to the parent alkene, cyclohexene. The yield of methane-t increased with H_2S scavenging.

We propose that (a) the increase in the methane-t yield with H_2S scavenging represents that portion of the total CH_2T radicals formed by T + alkene reactions that add to the parent alkene in unscavenged systems; (b) the decrease in the methane-t yield with O_2 or SO_2 scavenging represents that portion of the total CH_2T radicals formed

TABLE II: Radical Reaction Rate Constants at 25°

Reactants		k_9,[a] 10^6 cm³ mol⁻¹ sec⁻¹	k_8/k_9,[b] lit.	k_8/k_9, this work
Radical	Double bond			
Methyl	O₂	300,000[g]	na[c]	d
	SO₂	5,000[h]	na	d
	H₂S	3,000[e,i]	na	d
	Butadiene	160[j]	d	0.0019[f]
	Ethylene	1.2[j]	0.015[j]	0.0028
	Propylene	1.2[j]	0.096[j]	0.060
	1-Butene	1.0[j]	0.37[j]	0.075
	Isobutene	4.0[j]	0.040[j]	0.086
	Cyclohexene	d	d	0.36
Ethyl	Ethylene	d	d	0.091
	Cyclohexene	d	d	0.37
Propyl	Propylene	d	d	0.15
n-Butyl	1-Butene	d	d	0.16
Ethyl	Cyclohexene	d	d	0.35
Cyclohexyl	Cyclohexene	d	d	0.29
n-Hexenyl	Cyclohexene	d	d	0.32

[a] k_9 = rate constant of radical addition to the double bond. [b] k_8/k_9 = ratio of abstraction/addition rate constants of radicals with alkenes. [c] Not applicable. [d] Not determined. [e] For H-atom abstraction. [f] The typical sample contained 110 Torr of parent hydrocarbon (55 Torr in the case of cyclohexene), 16 Torr of ³He and ∼10 mol % scavenger when used. [g] Reference 62. [h] Reference 63. [i] Reference 64. [j] Reference 65.

from T + alkene reactions that abstract a hydrogen atom from the parent alkene in unscavenged systems. This allows the determination of the relative rate constants of addition vs. abstraction by alkyl radicals in alkenes. The method is shown in eq 8–13 for the specific methyl-t radical + cyclohexene case, but is readily generalized. The argument is analogous to previous determinations of the rates of methyl radical addition to alkenes by "methane deficiency" type experiments.[54] Both reactions 8 and 9

$$\cdot CH_2T + \bigcirc \xrightarrow{k_8} CH_3T + R\cdot \qquad (8)$$

$$\cdot CH_2T + \bigcirc \xrightarrow{k_9} \bigcirc^{CH_2T} \quad (C_7H_{12}T) \qquad (9)$$
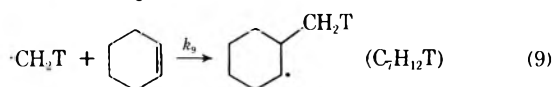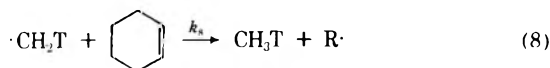
$$d[CH_3T]/dt = k_8[\cdot CH_2T][C_6H_{10}] \qquad (10)$$

$$d[C_7H_{12}T]/dt = k_9[\cdot CH_2T][C_6H_{10}] \qquad (11)$$

$$CH_3T(H_2S) - CH_3T \text{ (unscavenged)} \approx \Delta[C_7H_{12}T] \qquad (12)$$

$$CH_3T \text{ (unscavenged)} - CH_3T(O_2) \approx \Delta[CH_3T] \qquad (13)$$

occurred in the same sample capsule. The concentrations of methyl-t radicals and cyclohexene are identical in eq 10 and 11, hence

$$\frac{CH_3T\text{(unscavenged)} - CH_3T(O_2)}{CH_3T(H_2S) - CH_3T\text{(unscavenged)}} = \frac{k_8}{k_9} \qquad (14)$$

The substraction of the O₂ scavenged methane-t yield value removes that portion of the methane-t yield which is formed by an unscavengeable, nonradical reaction path. This nonscavengeable methane-t yield may result from a direct T-for-alkyl substitution process on the terminal carbon in the carbon chain.[2]

The implicit assumption in this determination of the abstraction/addition ratio of CH₂T radicals (or other tritiated radicals) in T + alkene systems is that the added scavenger does not affect the production of CH₂T radicals. The added scavenger has two effects.

(a) *Increased Pressure.* Increasing the pressure of the system may increase the stabilization of the alkyl-t radical (cyclohexyl-t radical) formed from tritium atom addition to the alkene (cyclohexene). With increased stabilization there is less unimolecular decomposition of the alkyl-

t radical to form CH₂T radicals. The increase in the effective collisional deactivation pressure is small, however. The scavenger pressure is usually only 5–10% of the hydrocarbon pressure. In addition, the scavenger is usually less efficient as a collisional deactivator than the parent alkene. The effect of increased effective pressure on CH₂T radical production is very probably less than the experimental error.

(b) *Removal of Thermal Tritium Atoms.* Scavenging of the thermal tritium atoms (which constitutes the majority of tritium atoms which undergo addition[52]) before they add to the alkene reduces the number of excited alkyl-t radical precursors to the CH₂T yield. From the data in Table I, oxygen is obviously capable of removing all thermalized tritium atoms. This does not affect the proposed determination of the abstraction/addition ratio. Oxygen scavenging of thermalized tritium atoms means that oxygen has two changes (thermal T atom and CH₂T radical) to eliminate a radical contribution to the methane-t yield. The methane-t yield which remains with oxygen scavenging is truly the result of a high-energy, non-scavengeable process.

The data in Table I also show that H₂S is not too efficient in removing H atoms. In fact, the rate constant of tritium atom addition to the alkene may be slightly larger than the rate constant for the tritium atom to abstract a hydrogen atom from H₂S to form HT.

$$T + \text{alkene} \xrightarrow{k_{15}} \text{alkyl-}t \text{ radical}\cdot \qquad (15)$$

$$T + H_2S \xrightarrow{k_{16}} HT + HS\cdot \qquad (16)$$
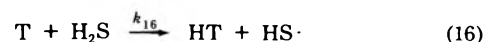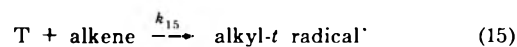
$$-d[T]/dt = k_{15}[T][\text{alkene}] + k_{16}[T][H_2S] \qquad (17)$$

fraction of thermalized tritium atoms scavenged by H₂S $= \dfrac{k_{16}[H_2S]}{k_{15}[\text{alkene}] + k_{16}[H_2S]}$ (18)

The fraction of thermalized tritium atoms scavenged by H₂S may be (a) lessened by using the minimum mole per cent scavenger required for complete scavenging of alkyl-t radicals, or (b) corrected for if k_{15} and k_{16} are known. When corrections are made for the reaction of thermal tritium atoms with H₂S, the denominator of eq 14 becomes (to first order)

$CH_3T(H_2S) - CH_3T(\text{unscavenged}) +$

$$\frac{k_{16}[H_2S]}{k_{15}[\text{alkene}] + k_{16}[H_2S]}[CH_3T(H_2S) - CH_3T(O_2)] \quad (19)$$

The quantity $[CH_3T(H_2S) - CH_3T(O_2)]$ represents the total CH_3T yield from a radical precursor formed by the addition of a tritium atom to the alkene parent. Without the correction factor the abstraction/addition ratio (k_8/k_9 from eq 14) would be overestimated.

The results in Table II are for uncorrected k_8/k_9 values. The comparison to literature values of abstraction/addition ratios is made on the assumption of a negligible small secondary isotope effect in the reactions of the alkyl-t ($vs.$ fully protonated) radicals. The differences between the k_8/k_9 values for methyl-t radicals from recoil tritium reactions (this work) and for methyl radicals from photolytic methods (ref 65) may indicate differences in the energy spectra of the methyl-t $vs.$ methyl radicals. "Hot" methyl-t radicals may comprise a significant portion of the methyl-t radicals produced by recoil tritium reactions.

The determination of relative rate constants may be extended to a system with two alkenes in the same sample. The relative rate constants for the addition of CH_2T radicals to the two alkenes may be determined with two sets of yield and pressure (of each parent alkene) values substituted into two equations with two unknowns. If for one of the alkenes $k_8/k_9 \approx 0$ (as is the case for butadiene) the simpler set of equations does not require simultaneous solution. For the butadiene-d_6–cyclohexene system, k_9(butadiene-d_6)/k_9(cyclohexene) was determined as 7.5 and 5.0 for two sets of yield and pressure values. Although there is a large spread in the data, the determination that k_9 for butadiene is larger than k_9 for cyclohexene is consistent with the trend of rate constants in Table II. Similarly for the butadiene-1-butene system, k_9(butadiene)/k_9(1-butene) was determined as 76 and 309 for two sets of yield and pressure values. The literature value of k_8/k_9 for 1-butene of 0.37 (Table II) was used. The reported value of k_9(butadiene)/k_9(1-butene) from Table II is 160. Once again the determination that k_9 for butadiene is larger than k_9 for 1-butene is qualitatively correct. The large spread in the values is inherent in the extension of the determination of relative rate constants to a system with two alkenes in the same sample. Determination of relative k_9 values depends on taking the difference of two yield values which are nearly equal. This small difference between two large numbers is often only a factor of 2 or 3 larger than the uncertainty of each of the large yield values. The resultant spread in the data is obvious. This effect is also inherent in the determining k_8/k_9 but is not as serious.

Summary and Conclusions

Recoil tritium studies often are limited by the lack of knowledge of the energy of the tritium atom when it reacts. This often precludes determining kinetic parameters from hot atom studies. More frequently kinetic parameters from other chemical methods are used with recoil tritium reaction yields to further the study of recoil tritium reactions. In this paper we have tried to use recoil tritium reactions to determine kinetic parameters. First, the pressure dependence (in the 300–1500 Torr range) of the unimolecular decomposition of cyclohexene-t to ethylene-t and butadiene or ethylene and butadiene-t was determined. The apparent rate constant of cyclohexene unimolecular decomposition at $135°$ (5.1×10^6 sec^{-1}) and the

s parameter in RRK treatment of the unimolecular decomposition of cyclohexene ($s = 24$) were calculated from these data. Second, the unimolecular decomposition/isomerization of cyclohexyl-t radicals to give n-hexene-t, 1-butene-t, and methane-t was established and the individual rate constants for these processes were determined as 8.4×10^3, 3.4×10^4, and 5×10^2 sec^{-1}, respectively. Finally, the scavenger dependence of yields with an obvious radical precursor was used to determine the relative rate constants of abstraction $vs.$ addition of that radical in the alkene parent compound. This area looks promising. Further comparisons of abstraction/addition ratios from recoil tritium experiments with conventional kinetic determinations are necessary.

We conclude that rate parameters can be determined in carefully designed recoil tritium experiments.

References and Notes

(1) (a) Work done under the auspices of the U. S. Atomic Energy Commission. (b) Submitted in partial fulfillment of Ph.D. requirements, University of California, Berkeley, Ph.D. Thesis LBL-1687, June 1973.
(2) (a) F. S. Rowland, MTP Int. Rev. Sci., Phys. Chem. Ser., 9, 109 (1972); (b) D. S. Urch, MTP Int. Rev. Sci., Inorg. Chem. Ser., 8, 149 (1972).
(3) P. J. Estrup and R. W. Wolfgang, J. Amer. Chem. Soc., 82, 2665 (1960).
(4) R. Wolfgang, J. Chem. Phys., 39, 2983 (1963).
(5) A. H. Rosenberg and R. Wolfgang, J. Chem. Phys., 41, 2159 (1964).
(6) V. Phillips, T. Thomas, and M. B. Hostin, J. Chem. Phys., 53, 4436 (1970).
(7) J. Keizer, J. Chem. Phys., 56, 5958 (1972).
(8) J. W. Root and F. S. Rowland, J. Phys. Chem., 74, 451 (1970).
(9) R. T. K. Baker, M. Silbert, and R. Wolfgang, J. Chem. Phys., 52, 1120 (1970).
(10) F. S. Rowland, J. Phys. Chem., 74, 4603 (1970).
(11) R. Wolfgang, J. Phys. Chem., 74, 4601 (1970).
(12) E. K. C. Lee and F. S. Rowland, J. Amer. Chem. Soc., 85, 897 (1963).
(13) A. Hosaka and F. S. Rowland, J. Phys. Chem., 75, 3781 (1971).
(14) R. A. Marcus and O. K. Rice, J. Phys. Colloid. Chem., 55, 894 (1951).
(15) R. A. Marcus, J. Chem. Phys., 20, 359 (1952). See also ref 38-41.
(16) C. T. Ting and F. S. Rowland, J. Phys. Chem., 74, 445 (1970).
(17) D. C. Fee, Ph.D. Thesis, University of California, Berkeley. LBL-1687, 1973.
(18) D. C. Fee and S. S. Markowitz, Anal. Chem., 45, 1827 (1973).
(19) D. C. Fee and S. S. Markowitz, Nucl. Instrum. Methods, 109, 445 (1973).
(20) J. K. Garland, Anal. Lett., 1, 273 (1969).
(21) N. D. Zelinski, B. M. Mikhailov, and Y. A. Arbuzov, J. Gen. Chem. (USSR), 4, 856 (1934).
(22) L. Kuchler, Trans. Faraday Soc., 35, 874 (1939).
(23) S. R. Smith amd A. S. Gordon, J. Phys. Chem., 65, 1124 (1961).
(24) M. Uchiyama, T. Tomioka, and A. Amano, J. Phys. Chem., 68, 1178 (1964).
(25) T. Sakai, T. Nakatani, T. Takahashi, and T. Kungi, Ind. Eng. Chem., Fundam., 11, 529 (1972).
(26) W. Tsang, J. Chem. Phys., 42, 1805 (1965).
(27) W. Tsang, Int. J. Chem. Kinet., 2, 311 (1970).
(28) W. Tsang, J. Phys. Chem., 76, 143 (1972).
(29) R. D. Doepker and P. Ausloos, J. Chem. Phys., 42, 3746 (1965).
(30) R. Lesclaus, S. Searles, L. W. Sieck, and P. Ausloos, J. Chem Phys., 53, 336 (1970).
(31) G. R. DeMare, O. P. Strausz, and H. E. Gunning, Can. J. Chem., 43, 1329 (1965).
(32) D. C. Fee, J. K. Garland, and S. S. Markowitz, Radiochim. Acta, 17, 135 (1972).
(33) D. C. Fee and S. S. Markowitz, J. Inorg. Nucl. Chem., 35, 2153 (1973).
(34) P. J. Robinson and K. A. Holbrook, "Unimolecular Reactions, Wiley-Interscience, New York, N. Y., 1972, p 164.
(35) J. D. Rynbrandt and B. S. Rabinovitch, J. Phys. Chem., 75, 2164 (1971).
(36) S. C. Chan, B. S. Rabinovitch, J. T. Bryant, L. D. Spicer, T. Fujimoto, Y. N. Lin, and S. P. Pavlon, J. Phys. Chem., 74, 3160 (1970).
(37) R. W. Weeks and J. K. Garland, J. Amer. Chem. Soc., 93, 2380 (1971).
(38) O. K. Rice and H. C. Ramsperger, J. Amer. Chem. Soc., 49, 1617 (1927).
(39) O. K. Rice and H. C. Ramsperger, J. Amer. Chem. Soc., 50, 617 (1928).
(40) L. S. Kassel, J. Phys. Chem., 32, 225 (1928).

(41) L. S. Kassel, *J. Phys. Chem.*, **32**, 1065 (1928).
(42) M. Cher, C. S. Hollingsworth, and B. Browning, *J. Chem. Phys.*, **41**, 2270 (1964).
(43) R. W. Weeks and J. K. Garland, *J. Phys. Chem.*, **73**, 2508 (1969).
(44) D. C. Fee and J. K. Garland, *Trans. Mo. Acad. Sci.*, **3**, 46 (1969).
(45) S. K. Ho and G. R. Freeman, *J. Phys. Chem.*, **68**, 2189 (1964).
(46) W. A. Cramer, *J. Phys. Chem.*, **71**, 1112 (1967).
(47) S. Aria, S. Sato, and S. Shida, *J. Chem. Phys.*, **33**, 1277 (1960).
(48) A. S. Gordon and S. R. Smith, *J. Phys. Chem.*, **66**, 521 (1962).
(49) A. S. Gordon, *Pure Appl. Chem.*, **5**, 441 (1962).
(50) R. A. Sheldon and J. K. Kochi, *J. Amer. Chem. Soc.*, **92**, 4395 (1970).
(51) The *n*-hexene-*t* radio gas chromatographic peak was neither resolved into 1-, 2-, 3-hexene-*t* components nor resolved from methylcyclopentane-*t*. Only the sum of these tritiated yields was monitored. This sum of products is referred to as *n*-hexene-*t*. The major component of cyclohexyl-*t* radical decomposition/isomerization is probably 1-hexeneyl-*t* radicals. A strong preference for C–C cleavage β to the radical site has been observed in other studies. See H. M. Frey and R. Walsh, *Chem. Rev.*, **69**, 103 (1969); E. K. C. Lee and F. S. Rowland, *J. Phys. Chem.*, **74**, 439 (1970).

(52) R. Kushner and F. S. Rowland, *J. Phys. Chem.*, **75**, 3771 (1971).
(53) K. I. Mahan and J. K. Garland, *J. Phys. Chem.*, **75**, 1031 (1971).
(54) See R. J. Cvetanovic and R. S. Irwin, *J. Chem. Phys.*, **46**, 1694 (1967), and references therein.
(55) G. R. Wolley and R. J. Cvetanovic, *J. Chem. Phys.*, **50**, 4697 (1969).
(56) R. J. Cvetanovic and L. C. Doyle, *J. Chem. Phys.*, **50**, 4705 (1969).
(57) H. Melville and J. C. Robb, *Proc. Roy. Soc., Ser. A*, **202**, 181 (1950).
(58) R. W. Getzinger and G. L. Schott, *J. Chem. Phys.*, **43**, 3237 (1965).
(59) P. Riesz and E. J. Hart, *J. Phys. Chem.*, **63**, 858 (1959).
(60) R. W. Fair and B. A. Thrush, *Trans. Faraday Soc.*, **65**, 1550 (1969).
(61) H. A. Kazmi and D. J. LeRoy, *Can. J. Chem.*, **42**, 1145 (1964).
(62) N. Basco, D. G. L. James, and F. C. James, *Int. J. Chem. Kinet.*, **4**, 129 (1972).
(63) A. Good and J. C. J. Thynne, *Trans. Faraday Soc.*, **63**, 2708 (1967).
(64) N. Imai and O. Toyama, *Bull. Chem. Soc. Jap.*, **33**, 652 (1960).
(65) R. J. Cvetanovic and R. S. Irwin, *J. Chem. Phys.*, **46**, 1694 (1967).

Recoil Tritium Reactions with Methylcyclohexene. A Test of the Assumption of Energy Randomization Prior to Unimolecular Decomposition[1a]

Darrell C. Fee*[1b] and Samuel S. Markowitz

Department of Chemistry and Lawrence Berkeley Laboratory, University of California, Berkeley, California 94720

(Received July 2, 1973)

The reactions of recoil tritium atoms with the three methylcyclohexene isomers have been studied in the gas phase at 135°. T was produced by ^{3}He(n,p)T. Recoil tritium atom abstraction, addition, or T-for-H substitution reactions accounted for 90% of the gas-phase products. Following activation by T-for-H substitution, the unimolecular decomposition of 4-methylcyclohexene-*t* (to give propylene-*t* or butadiene-*t*) and the unimolecular decomposition of 3-methylcyclohexene-*t* (to give ethylene-*t* or 1,3-pentadiene-*t*) was established from the pressure dependence of the product yield in the 300–1200-Torr pressure range. The apparent rate constants for these unimolecular decomposition processes was determined as 1×10^7 and 3×10^6 sec^{-1}, respectively. The rate constants for the unimolecular decomposition of cyclohexene-*1-t* and cyclohexene-*3-t* (formed by T-for-methyl substitution on 1-methylcyclohexene and 3-methylcyclohexene, respectively) were nearly equivalent. In addition, the average energy of excitation following T-for-methyl substitution is the same in cyclohexene-*1-t* and cyclohexene-*3-t*, namely, 6.0 to 6.5 eV. It was concluded that the RRKM (Rice, Ramsperger, Kassel, and Marcus) assumption of energy randomization prior to unimolecular decomposition is valid for the recoil tritium initiated unimolecular decomposition of cyclohexene.

Introduction

For many years, the role of translational energy in promoting virtually all chemical reactions has been emphasized. One method of producing translationally excited ("hot") atoms for chemical studies is by nuclear reaction and resulting recoil. Recoil tritium atom reactions have now been observed with over 100 parent molecules.[2-4] The main reaction channels are as follows. (1) *Addition.* Recoil tritium atom addition to a double bond forms an alkyl-*t* radical. The alkyl-*t* radical is capable of further reaction by abstraction of a hydrogen atom from the hydrocarbon system to form a tritiated alkane; by addition to the double bond of the parent compound to initiate a (tritiated) radical chain; or by unimolecular decomposition/isomer-

ization processes. (2) *Abstraction.* Recoil tritium atom abstraction forms HT. (3) *Substitution.* Recoil T-for-H atom substitution forms a tritiated parent molecule. The tritiated parent molecule possesses an average excitation energy of 5 eV (1 eV = 23 kcal mol^{-1}) following recoil T-for-H substitution.[5,6] This large energy of excitation often produces characteristic unimolecular decomposition of the tritiated parent molecule as a secondary process following recoil T-for-H substitution. In this respect recoil T-for-H substitution may be viewed as a chemical activation process.

We are interested in the reaction of recoil tritium atoms with the positional isomers of methylcyclohexene. The characteristic unimolecular decomposition reactions of the

methylcyclohexene isomers as determined by pyrolysis,[7-9] shock tube,[10] and mercury-sensitized photolysis[11,12] studies are shown in eq 1-3. These studies have been largely (mc = methylcyclohexene)

$$k_{4mc} = 10^{14.54} \exp(-64,900/kT) \quad [10]$$
$$k_{4mc} = 10^{15.13} \exp(-66,600/kT) \quad [11]$$
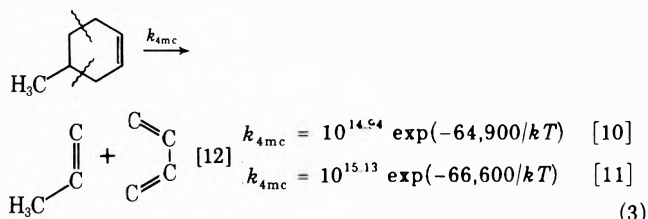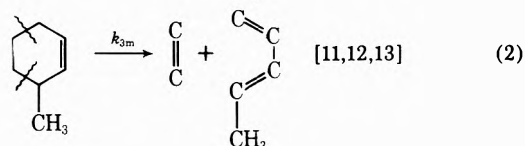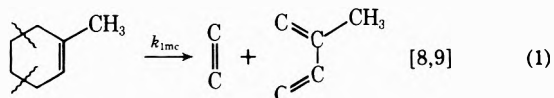
limited to determining that the reaction indicated in eq 1-3 is the principle unimolecular reaction for each isomer. Only for the unimolecular decomposition of 4-methylcyclohexene has a full kinetic study (leading to determination of the rate constant) been made. Nevertheless, a comparison of the decomposition products indicates that the principle unimolecular process is retro-Diels-Alder cleavage as shown.

composition in each ring was equally probable. However, analysis showed that regardless of the isotopic labeling of the added methylene, the newly formed ring is more probable to decompose. The conclusion was that energy nonrandomized unimolecular decomposition was occurring.

We propose to test the RRK-RRKM[13] assumption of energy randomization prior to unimolecular decomposition with reaction Scheme I for recoil T + methylcyclohexene reactions. If $k_{1c} = k_{3c}$, excited cyclohexene-t molecules decompose with the same probability regardless of the site of energy input. That is, energy randomization occurs prior to unimolecular decomposition. If $k_{1c} \neq k_{3c}$, energy nonrandomized unimolecular decomposition occurs.

In the postulation and discussion of the reaction scheme shown in eq 6 and 7, there are several necessary assumptions.

(a) *T-for-methyl substitution occurs as indicated*, without a shift of the double bond. Chemical degradation to determine the intramolecular tritium content has shown recoil T-for-X substitution in disubstituted benzenes (where X = alkyl, -NH$_2$, -COOH) to occur with 85-95% of the T being bonded at the position within the molecule recently occupied by the X species.[16]

(b) *The only reaction of excited cyclohexene-t molecules is* either stabilization or retro-Diels-Alder cleavage as indicated to give butadiene-t. The unimolecular decomposition of cyclohexene to give primarily ethylene and butadiene has been well established in pyrolysis,[9,17-21] shock tube,[10,22,23] photolysis,[24,25] and mercury-sensitized pho-

Our interest in recoil T + methylcyclohexene reactions was chiefly in studying unimolecular decomposition following T-for-H substitution *and* in testing the RRK-RRKM[13] assumption of energy randomization prior to unimolecular decomposition. Recently Rynbrandt and Rabinovitch[14] reported the first positive example of energy nonrandomized unimolecular decomposition. Their reaction sequence is shown in eq 4. In chemical activation studies such as this, k_a, the apparent rate constant of unimolecular decomposition, is determined from[14]

$$k_a = \omega(D/S) = Z(D/S)P \quad (5)$$

where $\omega = ZP$ = collision frequency: Z is the collision number;[15] P is the sample pressure in Torr; D is the yield of decomposition product; and S is the yield of collisionally stabilized product; that is, S is the yield of activated molecules which were collisionally stabilized prior to unimolecular decomposition. Hence the stabilization $(S)/$ decomposition (D) ratio should vary linearly with pressure for a unimolecular process. A plot of S/D vs. pressure is usually extrapolated to $S/D = 1$. At the pressure where $S/D = 1$, k_a equals ω.

In the reaction scheme shown in eq 4, if energy was randomized prior to decomposition, $k_{a1} = k_{a2}$. That is, de-

tolysis[11] studies. Of the total unimolecular decompositions, 96% occur giving ethylene and butadiene, 3% occur by H$_2$ elimination to give cyclohexadienes and benzene,

Scheme I
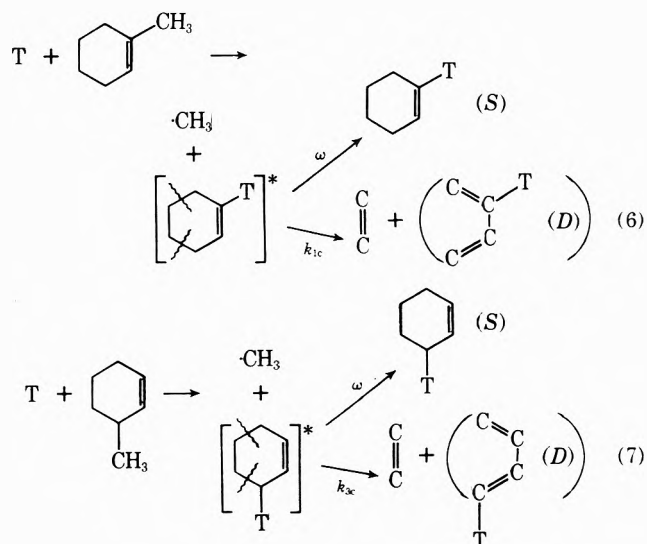
and the remaining 1% give C_5 and smaller hydrocarbons presumably through a free-radical mechanism.[20,21,25] A possible radical contribution to the ethylene and butadiene yield has been proposed from cyclohexyl radicals *via* H-atom addition to cyclohexene.[10,22] However, addition of scavenger does not affect the ethylene and butadiene yield.[11,20,25] The unimolecular rate constant for cyclohexene decomposition

$$k_a = 10^{15.3} \exp(-66,900 \text{ cal}/kT) = A \exp(-E_0/kT) \quad (8)$$

has been so well determined that cyclohexene is used as an internal standard in shock tube studies.[22,23]

Strong evidence for the retro-Diels–Alder cleavage of cyclohexene comes from the photolysis of cyclohexene-*3,3,6,6-d4*. The photolysis of cyclohexene-*3,3,6,6-d4* occurred as shown in eq 9 to give C_2H_4 and $C_4H_2D_4$ in 98%
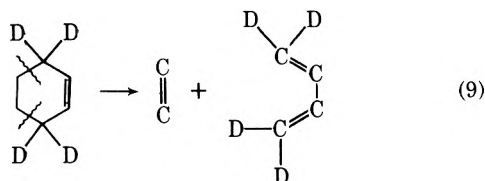
of the decompositions at 4.9-eV photolysis energy and 86% of the decompositions at 8.4-eV photolysis energy. At 8.4 eV the remaining 14% of the decompositions gave $C_2H_2D_2$ and $C_4H_4D_2$.[25] Further evidence for the retro-Diels–Alder cleavage of cyclohexene comes from the pyrolysis of cyclohexene-*1-t* and cyclohexene-*3-t* to give primarily butadiene-*t* and the pyrolysis of cyclohexene-*4-t* to give primarily ethylene-*t*.[17]

(c) *The reaction sequence shown in eq 6 and 7 is the only* reaction channel leading to the formation of butadiene-*t* from recoil T + 1-methylcyclohexene reactions and recoil T + 3-methylcyclohexene reactions. This assumption is supported by the retro-Diels–Alder cleavage of the methylcyclohexenes shown in eq 1–3.

(d) *Corrections can be made for possible* differences in the average energy of excitation of cyclohexene-*1-t vs.* cyclohexene-*3-t* formed by T-for-methyl substitution in eq 6 and 7, respectively. Differences in the average energy of excitation of cyclohexene-*1-t vs.* cyclohexene-*3-t* may arise from (i) differences in the average energy of the recoil T atom initiating the T-for-methyl substitution (This effect should be very small. Changes in structure from 1-methylcyclohexene to 3-methylcyclohexene should not drastically affect the recoil tritium atom energy distribution.)[2-4]; (ii) differences in the average energy carried away by the unlabeled methyl radical in eq 6 *vs.* 7; (iii) differences in the C–CH_3 and C–T bond strengths. A crudely estimated differential of as much as 1 eV more energy may be required to break the C–CH_3 bond in 1-methylcyclohexene (in comparison to 3-methylcyclohexene). The difference in the ΔH of cyclohexene-*t* formation in eq 6 and 7 is probably small, however. An estimated energy differential of as much as 1 eV more energy may be released by the formation of the C–T bond in cyclohexene-*1-t* (in comparison to cyclohexene-*3-t*). The possible difference in the ΔH of cyclohexene-*t* formation in eq 6 and 7 is certainly small compared to the estimated 6- to 7-eV energy excitation deposited in the tritiated molecule following recoil T-for-methyl substitution.[27] The chief concern is that the low-energy cut-off point for the recoil T-for-methyl substitution reaction may be as much as 1 eV higher for 1-methylcyclohexene than 3-methylcyclohexene.

We assumed that this ambiguity concerning possible

differences in the average energy of excitation of cyclohexene-*1-t vs.* cyclohexene-*3-t* could be resolved using the RRK formulation of the energy dependence of the unimolecular rate constant.[28-31] Namely

$$k_a = A[(E - E_0)/E]^{s-1} \quad (10)$$

where k_a is alternately k_{1c} or k_{3c} which are determined from the stabilization (S)/decomposition (D) ratios from eq 6 and 7, respectively; E_0 and A for the unimolecular decomposition of cyclohexene are given in eq 8; the s parameter is taken as $s = 24$ from the unimolecular decomposition of cyclohexene-*t* following recoil T-for-H substitution;[32] and E is the average energy deposited in the cyclohexene-*t* molecule following recoil T-for-methyl substitution on methylcyclohexene. If E_{1c} and E_{3c} (from reactions 6 and 7, respectively) are nearly equal, the small difference may be attributed to the energy factors discussed previously (i to iii). If E_{1c} and E_{3c} are different by more than 1 eV (reflecting large differences in k_{1c} and k_{3c}) this difference can be attributed solely to energy nonrandomized unimolecular decomposition of cyclohexene-*t* following recoil T-for-methyl substitution on methylcyclohexene.

We point out that in this treatment energy nonrandomization is reflected in a difference in excitation energy for each system. Energy nonrandomization, in general, could also be reflected in a different number of effective oscillators, s, for each system.

Experimental Section

The samples were prepared in 1720 Pyrex glass capsules (14 ml internal volume) with a vacuum line technique similar to that employed in other laboratories.[33] Further details of sample preparation are provided elsewhere.[34] The ^3He (Mound Laboratories) was certified as 99.7 mol % ^3He with a tritium content of 1.0 × 10^{-11} mol %. A standard radio gas chromatographic analysis[35] of an unirradiated aliquot of ^3He containing at least twice the moles normally sealed in the 1720 Pyrex capsules showed no measurable tritiated contaminant. The ^3He was used directly from the Mound Laboratories' container without further purification. The parent methylcyclohexene isomers were API Standard Reference Materials certified at greater than 99.8% chemically and isomerically pure. All other materials used were research grade.

The samples were irradiated in the Hohlraum of The Berkeley Campus Nuclear Reactor in a specially designed irradiation container.[36] Temperature control during irradiation was maintained at 135 ± 0.5°. The samples were irradiated for 24 hr at a flux of 3.9 × 10^8 n cm^{-2} sec^{-1}. Radiolysis damage due to recoils following the $^3He(n,p)T$ reactions was less than 1%.

The samples were analyzed on a specially designed radio gas chromatographic system described elsewhere.[35] Good resolution of major peaks was obtained in an analysis time of 15 hr. "Polymer-t" is defined as high molecular weight tritiated hydrocarbons not eluted in the normal radio gas chromatographic analysis. The recovery and analysis of polymer-t was similar to that previously described.[37] Reported here are the results from the analysis of two identical samples that agreed to within 5% on major products unless otherwise stated.

Results and Discussion

The reactions of recoil tritium atoms with gas-phase 1-methylcyclohexene, 3-methylcyclohexene, and 4-methyl-

cyclohexene are studied at 135°. The major gas-phase products observed from each methylcyclohexene isomer were (a) *methylcyclohexane-t* formed by recoil tritium atom addition to the double bond of methylcyclohexene to form a methylcyclohexyl-*t* radical (The methylcyclohexyl-*t* radical then abstracts a hydrogen atom from the bulk hydrocarbon system to form methylcyclohexane-*t*.); (b) *HT* formed by the recoil tritium atom abstracting a hydrogen atom from methylcyclohexene; (c) *tritiated methylcyclohexene* formed by a T-for-H substitution reaction. These three products composed 90% of the total observed gas-phase tritiated products.

Among the tritiated products observed in small yield were those which may have resulted from the retro-Diels–Alder cleavage of the methylcyclohexene-*t* isomers following recoil T-for-H substitution. Activation (energization) by T-for-H substitution and the resultant unimolecular decomposition of 4-methylcyclohexene is shown in eq 11.

$$T + \begin{array}{c} \text{[C}_7\text{H}_{12}] \end{array} \longrightarrow \begin{array}{c} \text{H·} \\ + \\ \text{[C}_7\text{H}_{11}\text{T]*} \end{array} \overset{\omega}{\underset{k_{4mc}}{\rightleftarrows}} \begin{array}{c} \text{4-methylcyclohexene-}t \ (S) \\ (C_3H_5T + C_4H_6) \text{ or} \\ (C_3H_6 + C_4H_5T) \end{array}$$

$$D = C_3H_5T \ (\text{propylene-}t) + C_4H_5T \ (\text{butadiene-}t) \quad (11)$$

Analogous equations can easily be written for 1-methylcyclohexene and 3-methylcyclohexene from eq 1 and 2. The pressure dependences of the stabilization (S)/decomposition (D) ratios from the retro-Diels–Alder cleavage of 4-methylcyclohexene-*t* and 3-methylcyclohexene-*t* are shown in Figures 1 and 2, respectively. The data in Figures 1 and 2 may be represented by a linear pressure dependence. The analogous plot of S/D vs. pressure from the unimolecular decomposition of 1-methylcyclohexene-*t* to ethylene-*t* or isoprene-*t* is not shown. The data points were widely scattered and a pressure effect was not observed. The lack of a linear dependence of S/D on pressure may result from the extreme reactivity of isoprene-*t*. Isoprene polymerization[38] may prevent an accurate determination of the isoprene-*t* yield from the unimolecular decomposition of 1-methylcyclohexene-*t*.

The abscissa in Figures 1 and 2 is the effective collisional deactivation pressure in the sample defined as

$$P_{\text{eff}} = 1.0 P_{C_7H_{12}} + 0.17 P_{^3He} \quad (12)$$

Each sample contained 300 Torr of ^{3}He (at 135°) and a variable amount of methylcyclohexene isomer (C_7H_{12}). On a pressure for pressure basis, ^{3}He is estimated to be only 17% as effective as methylcyclohexene in collisionally deactivating excited methylcyclohexene-*t* molecules.[39] The use of the effective pressure for the P in eq 5 is an attempt to correct for the effect of a weak collider in the system, ^{3}He. Otherwise, it is assumed that only a single collision between an activated methylcyclohexene-*t* molecule and an unlabeled methylcyclohexene molecule is necessary for complete deactivation of the excited methylcyclohexene-*t* species. We point out that this "strong collision"[13] assumption may not be valid at the high energies of excitation encountered in recoil tritium experiments. No correction was made for the effect of changing the mole fraction of ^{3}He from 0.5 in the lowest pressure samples to 0.2 in the highest pressure samples. Changes in the tritium atom energy with added moderator are usually only observed with the moderator in great excess of the parent hydrocarbon.[2,3]

Figure 1. The unimolecular decomposition of 4-methylcyclohexene-*t* to give propylene-*t* or butadiene-*t*; unscavenged data at 135°. Activated 4-methylcyclohexene-*t* molecules are formed by recoil T-for-H substitution. The abscissa is the effective collisional deactivation pressure (in the same capsule) defined as effective pressure = 4-methylcyclohexene pressure + 0.17 (helium-3 pressure).

Figure 2. The unimolecular decomposition of 3-methylcyclohexene-*t* to give ethylene-*t* or pentadiene-*t*; unscavenged data at 135°. Activated 3-methylcyclohexene-*t* molecules are formed by recoil T-for-H substitution. The abscissa is the effective collisional deactivation pressure (in the sample capsule) defined as effective pressure = 3-methylcyclohexene pressure + 0.17 (helium-3 pressure).

The plot of S/D vs. effective pressure (actually log (S/D) vs. log (effective pressure)) was extrapolated to S/D = 1. From Figure 1, S/D = 1 at 1.3 Torr; $k_{4mc} = 1.5 \times 10^7$ sec^{-1}. From Figure 2, S/D = 1 at 0.29 Torr; $k_{3mc} = 3.4 \times 10^6$ sec^{-1}. Extrapolation over the large pressure range is a standard hot atom technique.[5] Nevertheless, large uncertainties (−0.4, +1.3 Torr) result from this extrapolation. This uncertainty is inherent in hot atom chemistry where low-pressure regions (below 20 Torr) are not experimentally accessible.[2,3] The value of the methylcyclohexene collision diameter used to calculate Z in eq 5 was estimated[39] at 6.12×10^{-8} cm. Using this value of

k_{4mc} for k_a in eq 10 and the average of the rate parameters from eq 3, the s parameter in the RRK formulation of the rate constant for the unimolecular decomposition of 4-methylcyclohexene was determined as $s = 22$. E, in this case, was set at 5 eV, the average energy of excitation following a recoil T-for-H substitution.[7,8] For a fixed $s = 25 \approx (1/2)(3N - 6)$, E was determined as 5.4 eV. For a fixed $s = 34 \approx (3/4)(3N - 6)$, E was determined as 6.8 eV. N is the number of atoms in the methylcyclohexene molecule.

The data in Figures 1 and 2 are for unscavenged samples. Scavenging with butadiene-d_6 revealed that the butadiene-t yield was not depleted by reactions with radiolysis produced H atoms. This result is similar to recoil T + cyclohexene reaction results at 25°.[40,41] Nitric oxide scavenging at the lowest methylcyclohexene pressure displayed in Figures 1 and 2 showed (a) a 15% radical contribution to the propylene-t yield but a 14% radical contribution to the ethylene-t yield in Figure 2. The data in Figures 1 and 2 were crudely "corrected" by subtracting a yield and a 14% radical contribution from the ethylene-t yield at all pressures. The resultant plots of "corrected" S/D ratio vs. pressure were extrapolated to $S/D = 1$ at 4.2 and 0.48 Torr for "corrected" data from Figures 1 and 2, respectively. Because the assumption of a constant radical contribution may not be valid, we chose to use the unscavenged data for further calculations.

Other interesting scavenger effects were noted.

(a) *Methylcyclohexane-t.* The proposed methylcyclohexyl-t radical precursors to the methylcyclohexane-t yield were intercepted by 9 mol % nitric oxide (NO) scavenger. With nitric oxide scavenging, the methylcyclohexane-t yield decreased to 1–4% of the unscavenged yield value. Similar concentrations of H_2S, O_2, and SO_2 scavenger did not affect the methylcyclohexane-t yield. This may indicate bulk chemical reactions between the parent hydrocarbon and the scavenger similar to those previously postulated in the T + cyclohexene system.[40] The methylcyclohexane-t yields from T + 3-methylcyclohexene reactions and T + 4-methylcyclohexene reactions were nearly equal. The yield of methylcyclohexane-t from T + 1-methylcyclohexene reactions was only about one-half that from T + 3- and 4-methylcyclohexene reactions. This is consistent with the methylcyclohexyl-t radical formed by tritium atom addition to 1-methylcyclohexene being less reactive via H-atom abstraction than the methylcyclohexyl-t radicals formed by tritium atom addition to 3- and 4-methylcyclohexene. In tritium atom addition to 1-methylcyclohexene, formation of the tertiary radical may be favored over the formation of the secondary radical by as much as twenty to one.[42] The adjacent methyl group by the tertiary methylcyclohexyl-t radical from T + 1-methylcyclohexene reactions probably hinders H-atom abstraction compared to H-atom abstraction by the secondary methylcyclohexyl-t radicals from T + 3- and 4-methylcyclohexene reactions.

(b) *Methylcyclohexene-t Isomers Other Than the Parent.* The parent isomers were API Standard Reference Materials certified at greater than 99.8% chemically and isomerically pure. The radio gas chromatographic system employed for analysis[35] would not resolve small amounts of 3-methylcyclohexene from a larger 4-methylcyclohexene peak and vice-versa. The 1-methylcyclohexene peak was well resolved from the 3-/4-methylcyclohexene peak. The mass tracing during the radio gas chromatographic analysis did not reveal the presence of any methylcyclohexene

isomers other than the parent compound. However, tritiated methycyclohexene isomers other than the parent compound were observed in greater than 0.2% abundance compared to the tritiated parent compound.

For example, T + 4-methylcyclohexene reactions gave 1-methylcyclohexene-t in both unscavenged and nitric oxide scavenged samples. The 1-methylcyclohexene-t yield from T + 4-methylcyclohexene reactions was (a) 4.8% as large as the 4-methylcyclohexene-t yield in unscavenged samples and (b) decreased by 60% with nitric oxide scavenging. This is consistent with a high-energy and a thermal route to 1-methylcyclohexene-t formation from T + 4-methylcyclohexene reactions. The high-energy (unscavengeable) route is probably hydrogen atom "scrambling" following a high-energy recoil T-for-H substitution reaction. The low-energy (scavengeable) route is probably via loss of a hydrogen atom from a methylcyclohexyl-t radical formed by tritium atom addition to 4-methylcyclohexene. Similar H-atom loss mechanisms have been postulated in other recoil tritium reaction studies.[43]

In unscavenged T + 1-methylcyclohexene reactions, the combined 3- and 4-methylcyclohexene-t yield was 9% as large as the 1-methylcyclohexene-t yield. In unscavanged T + 3-methylcyclohexene reactions, the 1-methylcyclohexene-t yield was only 3% as large as the 3-methylcyclohexene yield. In both T + 3-methylcyclohexene and T + 1-methylcyclohexene reactions the yield of the nonparent methylcyclohexene-t isomer(s) doubled with nitric oxide scavenging. Similar anomolous increases with nitric oxide scavenging have been observed in the recoil T + *trans*-2-butene system.[44]

(c) *Methane-t.* The yield of methane-t in nitric oxide scavenged systems is roughly the same from recoil tritium atom reactions with 3- and 4-methylcyclohexene and roughly twice the yield of methane-t from nitric oxide scavenged T + 1-methylcyclohexene reactions. The methane-t yield in nitric oxide scavenged methylcyclohexene systems probably results from a direct T-for-cyclohexene substitution process.[2-4] This trend of the methane-t yields is consistent with decreased probability for T-for-cyclohexene substitution to give methane-t when the cyclohexene-CH_3 bond strength is increased.

A Test of the RRK–RRKM Assumption of Energy Randomization Prior to Unimolecular Decomposition. The formation of cyclohexene-t (S) and butadiene-t (D) by the reaction pathways shown in eq 6 and 7 was a small reaction channel (less than 3% of the gas-phase tritiated products) in the recoil tritium reactions with 1- and 3-methylcyclohexene. The pressure dependence of the S/D ratio in eq 6 and 7 could not be determined in high-pressure unscavenged T + 1-methylcyclohexene and T + 3-methylcyclohexene systems, respectively. The adjacent methylcyclohexene-t peak[35] was broadened by column overloading in the high-pressure samples. Consequently, the cyclohexene-t peak could not be resolved from the methylcyclohexane-t peak. Good resolution of the cyclohexene-t peak and the methylcyclohexane-t peak was obtained at the lowest pressure samples. A comparison of unscavenged and nitric oxide scavenged samples at the lowest methylcyclohexene pressure showed that the yield of cyclohexene-t and butadiene-t was unaffected by scavenger. The results of the determination of the S/D ratios from eq 6 and 7 in nitric oxide scavenged samples are shown in Table I. Considering the range of unimolecular rate constants[15] and the uncertainties of this method, k_{1c} and k_{3c} are nearly equivalent.

TABLE I: Unimolecular Decomposition of Cyclohexene-t at 135° [a]

Effective pressure,[b] Torr	S/D (eq 6)	S/D (eq 7)	k_{1c}, 10^9 sec^{-1}	k_{3c}, 10^9 sec^{-1}	E_{1c}, eV	E_{3c}, eV
360	2.8	1.7	1.6[c]	2.7	6.4[d]	6.5
970	3.2	1.6	3.4	6.7	5.9	6.1

[a] Activated cyclohexene-t molecules formed by recoil T-for-methyl substitution with methylcyclohexene. [b] Effective pressure = $1.0P(C_7H_{12})$ + $0.17P(3He)$ + $0.24P(NO)$. [c] Determined with an estimated[19] collision diameter for cyclohexene of 5.47×10^{-8} cm and 6.12×10^{-8} cm for methylcyclohexene. [d] Determined from eq 10 with $A = 10^{15.3}$, $E_0 = 2.9$ eV, and $s = 24$.

The near equivalence of the unimolecular rate constants and the average energies of excitation for cyclohexene-1-t and cyclohexene-3-t (from T-for-methyl substitutions on 1-methylcyclohexene and 3-methylcyclohexene, respectively) shows the following. (a) The RRK–RRKM assumption of energy randomization prior to unimolecular decomposition is valid for the recoil-tritium-initiated unimolecular decomposition of cyclohexene. (b) A T-for-methyl substitution reaction leaves an average energy of excitation of 6.0 to 6.5 eV in the resultant tritiated molecule. The energy of the C–CH$_3$ bond broken in the T-for-methyl substitution process apparently has little effect on the average energy deposited in the resultant tritiated molecule.

The proven RRK–RRKM assumption of energy randomization prior to unimolecular decomposition can now be put to use. There are ten possible T-for-H substitution sites in cyclohexene. Assuming retro-Diels–Alder cleavage of cyclohexene, T-for-H substitution at four of the sites results in ethylene-t; at six of the sites in butadiene-t. By analogy to T-for-methyl substitution in methylcyclohexenes, the average energy of excitation in cyclohexene-t following T-for-H substitution is probably independent of the strength of the C–H bond that was broken. This means that the cyclohexene-t molecule formed by T-for-H substitution has the same average energy of excitation, regardless of the site of the T label. Because all cyclohexene-t molecules have the same average excitation energy and energy is randomized in cyclohexene prior to unimolecular decomposition, cyclohexene-t molecules should decompose with equal probability regardless of the site of the T label. Consequently, the ethylene-t/butadiene-t ratio should be 4 to 6 from the retro-Diels–Alder cleavage of cyclohexene-t formed in T + cyclohexene reactions.

The ethylene-t/butadiene-t ratio from scavenged T + cyclohexene systems was 1.00 at 25° and 1.05 at 135°. Similarly the ethylene-t/1,3-pentadiene-t ratio at 135° in scavenged T + 3-methylcyclohexene reactions (see eq 2) was 1.48 (*vs.* 4 to 8 statistically). However, the propylene-t/butadiene-t ratio at 135° in scavenged T + 4-methylcyclohexene reactions (see eq 11) was 0.84 (*vs.* 6 to 6 statistically). Only when ethylene-t is not the smaller of the assumed retro-Diels–Alder cleavage products does the ratio of the tritiated products approach the statistical prediction based of equal unimolecular decomposition per T-for-H substitution site. An explanation consistent with this observation is the production of ethylene-t from a nonretro-Diels–Alder reaction. Ethylene-t from a non-retro-Diels–Alder cleavage pathway has been observed in cyclohexene-$3,3,6,6$-d_4 decompositions[25] (see eq 9). The postulated non-retro-Diels–Alder cleavage of methylcyclohexene-t is supported by the observation of a 1,3-pentadiene-t

peak 14% as large as the butadiene-t peak in nitric oxide scavenged T + 4-methylcyclohexene reactions.

Summary and Conclusions

In the reactions of recoil tritium atoms with the three methylcyclohexene isomers 90% of the reactions which gave gas-phase products can be attributed to (a) *abstraction* to form HT; (b) *addition* to form a methylcyclohexyl-t radical which may abstract a hydrogen atom to form methylcyclohexane-t; (c) *substitution* of T-for-H to form the tritiated parent isomer. Small yield reaction channels have also been observed. (i) *Unimolecular Decomposition.* The unimolecular decomposition of 4-methylcyclohexene-t to give propylene-t or butadiene-t; and the unimolecular decomposition of 3-methylcyclohexene-t to give ethylene-t or 1,3-pentadiene-t has been established from the pressure dependence of the tritiated products. The apparent rate constants of these unimolecular decomposition processes are 1×10^7 and 3×10^6 sec^{-1}, respectively. (ii) *T-for-Methyl Substitutions.* The average energy of excitation following recoil T-for-methyl substitution is the same for cyclohexene-1-t and cyclohexene-3-t, namely, 6.0 to 6.5 eV. From this we concluded that the energy of the C–CH$_3$ bond broken in T-for-methyl substitution has little effect on the average energy deposited in the resultant molecule. In addition, the rate constants for the unimolecular decomposition of cyclohexene-t were nearly the same for cyclohexene-1-t and cyclohexene-3-t (formed by recoil T-for-methyl substitution on 1-methylcyclohexene and 3-methylcyclohexene, respectively).

We therefore conclude that the RRK–RRKM assumption of energy randomization prior to unimolecular decomposition is valid for the recoil tritium initiated unimolecular decomposition of cyclohexene.

References and Notes

(1) (a) Work performed under the auspices of the U. S. Atomic Energy Commission. (b) Submitted in partial fulfillment of Ph.D. requirements, University of California, Berkeley, June 1973. Thesis reference, Lawrence Berkeley Laboratory Report No. LBL-1687 (unpublished).
(2) F. S. Rowland, "Molecular Beams and Reaction Kinetics," Ch. Schlier, Ed., Academic Press, New York, N. Y., 1970, p 108.
(3) D. S. Urch, *MTP Int. Rev. Sci., Inorg. Chem. Ser.*, **8**, 149 (1972).
(4) F. S. Rowland, *MTP Int. Rev. Sci., Phys. Chem. Ser.*, **9**, 109 (1972).
(5) E. K. C. Lee and F. S. Rowland, *J. Amer. Chem. Soc.*, **85**, 897 (1963).
(6) A. Hosaka and F. S. Rowland, *J. Phys. Chem.*, **75**, 3781 (1971).
(7) F. O. Rice and M. T. Murphy, *J. Amer. Chem. Soc.*, **66**, 765 (1944).
(8) M. Krans and V. Bazant, *Collect. Czech. Chem. Commun.*, **25**, 2695 (1960).
(9) T. Sakai, T. Nakatani, T. Takahashi, and T. Kungi, *Ind. Eng. Chem., Fundam.*, **11**, 529 (1972).
(10) W. Tsang, *J. Chem. Phys.*, **42**, 1805 (1965).
(11) G. R. De Mare, O. P. Strausz, and H. E. Gunning, *Can. J. Chem.*, **43**, 1329 (1965).
(12) G. R. De Mare, *Bull. Soc. Chim. Belg.*, **81**, 459 (1972).
(13) Rice, Ramsperger, Kassel, and Marcus. See R. A. Marcus, *J. Chem. Phys.*, **20**, 359 (1952); R. A. Marcus and O. K. Rice, *J. Phys. Colloid. Chem.*, **55**, 894 (1951), and ref 28–31.
(14) J. D. Rynbrandt and B. S. Rabinovitch, *J. Phys. Chem.*, **75**, 2164 (1971).
(15) P. J. Robinson and K. A. Holbrook, "Unimolecular Reactions," Wiley-Interscience, New York, N. Y., 1972, p 164.
(16) R. M. White and F. S. Rowland, *J. Amer. Chem. Soc.*, **82**, 4713 (1960).
(17) R. F. Nystrom, S. S. Rajan, N. H. Nam, and D. Gurne, *Proc. Int. Conf. Methods Prep. Stor. Label. Compounds, 2nd, 1966*, 407 (1968).
(18) N. D. Zelinskii, B. M. Mikhailov, and Y. A. Arbuzov, *J. Gen. Chem. (USSR)*, **4**, 856 (1934).
(19) L. Kuchler, *Trans. Faraday Soc.*, **35**, 874 (1939).
(20) S. R. Smith and A. S. Gordon, *J. Phys. Chem.*, **65**, 1124 (1961).
(21) M. Uchiyama, T. Tomioka, and A. Amano, *J. Phys. Chem.*, **68**, 1178 (1964).

(22) W. Tsang, *Int. J. Chem. Kinet.*, **2**, 311 (1970).
(23) W. Tsang, *J. Phys. Chem.*, **76**, 143 (1972).
(24) R. D. Doepker and P. Ausloos, *J. Chem. Phys.*, **42**, 3746 (1965).
(25) R. Lesclaux, S. Searles, L. W. Sieck, and P. Ausloos, *J. Chem. Phys.*, **53**, 336 (1970).
(26) See the bond dissociation data in "The Handbook of Chemistry and Physics," 53rd ed, Chemical Rubber Publishing Co., Cleveland, Ohio, 1972, p F-189 *ff*.
(27) Estimated from the stabilization (S)/decomposition (D) ratio of methylcyclobutane-f following T-for-H substitution on 1,3-dimethyl-cyclobutane. See C. T. Ting and F. S. Rowland, *J. Phys. Chem.*, **74**, 445 (1970).
(28) O. K. Rice and H. C. Ramsperger, *J. Amer. Chem. Soc.*, **49**, 1617 (1927).
(29) O. K. Rice and H. C. Ramsperger, *J. Amer. Chem. Soc.*, **50**, 617 (1928).
(30) L. S. Kassel, *J. Phys. Chem.*, **32**, 225 (1928).
(31) L. S. Kassel, *J. Phys. Chem.*, **32**, 1065 (1928).
(32) D. C. Fee and S. S. Markowitz, *J. Phys. Chem.*, **78**, 347 (1974).
(33) See the reference in footnote 27 and references therein.

(34) D. C. Fee, Ph.D. Thesis, University of California, Berkeley, June 1973, LBL-1687.
(35) D. C. Fee and S. S. Markowitz, *Anal. Chem.*, **45**, 1827 (1973).
(36) D. C. Fee and S. S. Markowitz, *Nucl. Instrum. Methods.* **109**, 445 (1973).
(37) J. K. Garland, *Anal. Lett.*, **1**, 273 (1968).
(38) T. Tabata, R. Shimazawa, and H. Sobue, *J. Polym. Sci.*, **54**, 201 (1961).
(39) Estimated from tabulated collisional deactivation efficiency data and collision diameters found in S. C. Chan, B. S. Rabinovitch, J. T. Bryant, L. D. Spicer, T. Fujimoto, Y. N. Lin, and S. P. Pavlou, *J. Phys. Chem.*, **74**, 3160 (1970).
(40) D. C. Fee, J. K. Garland, and S. S. Markowitz, *Radiochim. Acta.* **17**, 135 (1972).
(41) D. C. Fee and S. S. Markowitz, *J. Inorg. Nucl. Chem.*, **35**, 2153 (1973).
(42) W. M. Ollison and J. Dubrin, *Radiochim. Acta.* **14**, 111 (1970).
(43) K. I. Mahan and J. K. Garland, *J. Phys. Chem.*, **73**, 1247 (1969).
(44) F. S. Rowland, J. K. Lee, B. Musgrave, and R. M. White, "Chemical Effects of Nuclear Transformations," Vol. 1., IAEA, Vienna, 1960, p 67.

Effect of Iodine and Other Scavengers on the γ Radiolysis of Liquid Perfluorocyclohexane

George A. Kennedy and Robert J. Hanrahan*

Department of Chemistry, University of Florida, Gainesville, Florida 32611 (Received August 4, 1972; Revised Manuscript Received November 8, 1973)

The major radiolysis products of liquid F-cyclohexane are F-bicyclohexyl (G = 0.95), F-cyclohexylhexene (G = 0.48), and F-cyclohexylhexane (G = 0.12). The production of these compounds is eliminated in the radiolysis of F-cyclohexane–iodine mixtures, and the following iodides are formed: F-cyclohexyl iodide (G = 3.1), F-hexenyl iodide (G = 0.8), F-hexyl iodide (G = 0.15), and a diiodide, $C_6F_{12}I_2$ (G = 0.12). It is concluded that the major end products from the radiolysis of F-cyclohexane are formed by free-radical reactions. Comparison of yields with and without added iodine indicates that the total G value for radical production is ca. 5.8. Yields estimated for particular radicals are as follows: G(F-cyclohexyl) = 3.0 ± 0.2; G(F-hexenyl) = 0.8 ± 0.2; G(F-hexyl) = 0.1 ± 0.05; and G(F-1,6-hexamethylene diradical) = 0.1 ± 0.05. Hydrogen iodide is apparently a poor radical scavenger in the F-cyclohexane system. Yields of the products expected from the scavenging process were found to be much lower than the radical yields estimated above. This low efficiency may be due to unfavorable polar effects in the transition state formed during the scavenging reaction. Bromine appears to be an efficient scavenger in irradiated F-cyclohexane, but the high reactivity of the bromine atoms produced may result in further reactions that complicate interpretation of the observed results. There appear to be two products with the formula $C_6F_{11}Br$, two products with the formula $C_6F_{12}Br_2$, and smaller amounts of several other C_1, C_2, and C_6 bromides.

Introduction

The present work is an investigation of the effects of free-radical scavengers on the radiation chemistry of liquid F-cyclohexane,[1] with the object of identifying free-radical intermediates and determining their contributions to the formation of the radiolysis products. A subsequent paper[2] will describe similar work on mixtures of cyclohexane and F-cyclohexane. These investigations are extensions of earlier work in this laboratory on the same systems.[3,4]

A number of papers have appeared in the literature describing the radiation chemistry of F-cyclohexane[3,5] as well as other fluorocarbon compounds.[6-10] Although it has frequently been suggested that free radicals play an important role in the mechanism of radiolysis of these compounds, especially as regards formation of the ultimate products, relatively little work has been done toward establishing this point. Kevan and coworkers found that the yield of CF_4 was reduced and the production of C_3F_8 and n-C_4F_{10} was eliminated when oxygen was present in the radiolysis of C_2F_6 in either the gas[8] or liquid phase.[9] Heckel and Hanrahan[10] found that the addition of O_2 eliminated most of the heavier products from the gas-phase radiolysis of F-cyclobutane.

Although iodine has not been used to study free-radical intermediates in the radiolysis of fluorocarbons, there is

TABLE I: Yields of Radiolysis Products of Perfluorocyclohexane

Products[a]	G values[b]
C_1–C_6	(0.3)
C_7–C_{11}	(0.4)
F-Cyclohexylhexane	0.11 (0.13)
F-Cyclohexylhexene	0.43 (0.53)
F-Bicyclohexyl	0.95
>C_{12}	(0.1)

[a] Detailed minor product yields are given in Table II. [b] G values in parentheses were calculated using estimated gas chromatograph detector responses factors; see text. Other values were calculated using the response to F-bicyclohexyl for all C_{12} products.

TABLE II: Estimated Distribution of Minor Radiolysis Products of Perfluorocyclohexane

| Products	G values	Products	G values
CF_4	Not measured	C_8F_{16}	0.1
C_2F_6	0.1	C_9F_{18}	0.04
C_3F_8	0.1	$C_{10}F_{20}$	0.02
C_4F_{10}	0.03	$C_{11}F_{22}$	0.03
$C_5(?)$	0.01	$C_{13}F_{26}$	0.05
C_6F_{14}	0.01	$C_{14}F_{28}$	0.03
C_7F_{14}	0.2	C_{15} and above	0.01

evidence, based on reactions of CF_3 radicals, that iodine should be an efficient scavenger in these systems. The value for $D(CF_3-I)$ has been reported to be 53.5 kcal/mol,[11] which is approximately the same as $D(CH_3-I)$.[12] Assuming that there is no large change in the C–I bond strength in going to other perfluoro radicals, the energetics for radical scavenging are favorable, since $D(I-I)$ is about 36 kcal/mol. Amphlett and Whittle[13] have reported that the rate constant for reaction of $CF_3\cdot$ with I_2 is 2.6 × 10^9 M^{-1} sec^{-1}, which is comparable to the rate constants reported for radical scavenging by iodine in hydrocarbon systems.

The scavengers used in the present work were I_2, Br_2, and HI. Arguments for the efficiency of Br_2 as a scavenger in fluorocarbons parallel those given above for I_2. There appear to be problems involved in the use of HI as a scavenger in F-cyclohexane radiolysis; this will be considered in the Discussion section.

Experimental Section

Reagents. F-Cyclohexane from Imperial Smelting Limited was purified using preparative gas chromatography. The purified material contained a single impurity, amounting to about 0.5 mol %, eluting just before the parent on a silica gel column. It is believed to be a fluorocarbon. Hydrogen iodide was prepared by dehydrating Baker analyzed reagent grade hydriodic acid with P_2O_5, and purified by trap-to-trap distillation. F-Cyclohexyl iodide was prepared by a slight modification of the method of Krespan[14] and purified by preparative gas chromatography. Other materials were used as available in the best commercial grades.

Sample Preparation and Irradiation. All samples were prepared using conventional vacuum line techniques; the details are given elsewhere.[15] Irradiations were carried out at 65 ± 1° using a cobalt-60 γ ray source which has been described previously.[16] Radiolysis vessels for 0.5- or 1.0-ml samples were prepared from 8-mm Pyrex tubing; Pyrex absorption cells made from precision rectangular bore 10 mm × 2.5 mm i.d. tubing were attached when spectro-
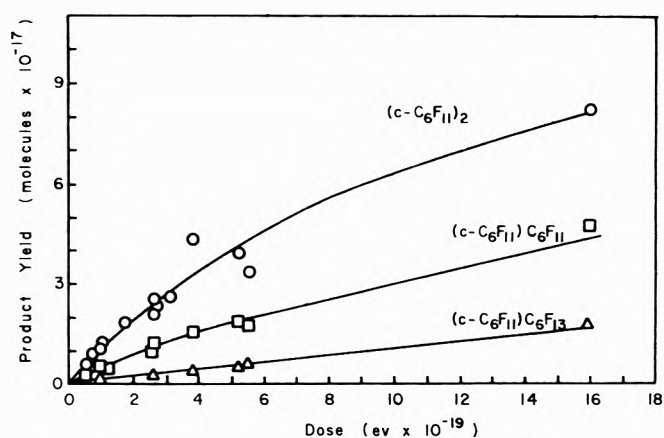
Figure 1. Yields of the major radiolysis products of c-C_6F_{12} as a function of dose.

photometric measurement was desired. Sample cells for 0.15-ml samples to be analyzed by glc were constructed of 6-mm diameter Pyrex tubing. Dose rates were measured by Fricke dosimetry [$G(Fe^{3+})$ = 15.5]. For sample vessels of 1.0 and 0.5 ml, respectively, the dose rates were 2.3 × 10^{18} and 2.65 × 10^{18} eV ml^{-1} min^{-1}. For the 0.15-ml glc samples, dosimetry was done both by measuring the H_2 yield from cyclohexane (G = 5.6) and the Fe^{3+} yield in the Fricke solution. Results agree within 2%. A dose rate of 3.34 × 10^{18} eV ml^{-1} min^{-1} was found. The ratio of energy absorption in the sample and in the dosimeter was taken to be equal to the ratio of electron densities. The density of F-cyclohexane was found by experimental measurement to be 1.67 g/cc at 65°.

Analytical Procedures. Radiolysis products were identified by combined mass spectrometry-gas chromatography using a Bendix Model 14-107 time-of-flight mass spectrometer and a flame ionization gas chromatograph with the column effluent split between the flame detector and a quadruple trapping facility with provisions for sampling to the mass spectrometer.[15] Quantitative gas chromatography was done using a flame ionization detector and a SE-30 column. Sufficient pure fluorocarbon standards were available to confirm reasonably well the observation reported for hydrogenated (rather than fluorinated) compounds that flame response is a linear function of carbon number.[17] Unfortunately, only the single perfluoroiodide c-$C_6F_{11}I$ was available for calibration purposes. Accordingly, alternate interpretations of the yields of iodine-containing products are reported, based either on the use of the sensitivity coefficient found for c-$C_6F_{11}I$ or an extrapolation line drawn parallel to the fluorocarbon line but through the point for c-$C_6F_{11}I$.

Optical absorption measurements were made using a Beckman Model DU spectrophotometer; for I_2 in F-cyclohexane at 65°, we found λ_{max} 524 nm and ϵ 865 M^{-1} cm^{-1}.

Results

Pure Perfluorocyclohexane. Preliminary experiments were carried out to reexamine the radiolysis products of F-cyclohexane for the purpose of comparison with experiments using added scavengers. Major products are recorded in Table I, and minor products in Table II. Yields of the three major products as a function of absorbed dose are shown in Figure 1. The initial yields of the major products are somewhat lower than those published earlier by Fallgatter and Hanrahan[3,4] but agree well with some
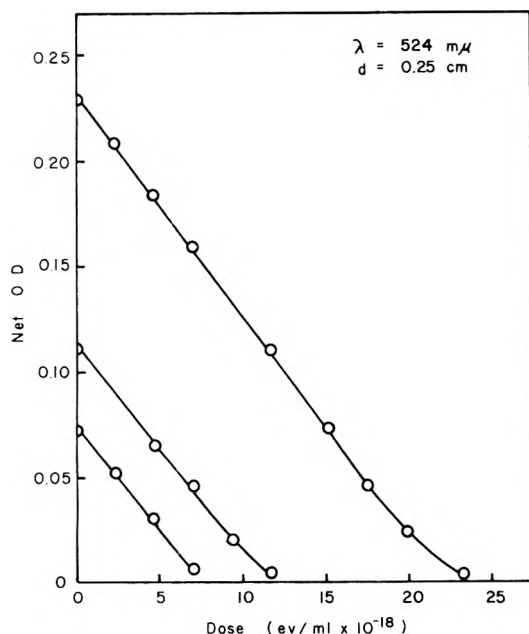
Figure 2. Iodine consumption in the radiolysis of c-C_6F_{12}-I_2 mixtures. Initial iodine concentrations reading top to bottom were 1.0, 0.5, and 0.3 mM.

TABLE III: Yields of Major Radiolysis Products of Perfluorocyclohexane–Iodine Mixtures

Products	G values[a]
F-Cyclohexyl iodide	3.1
F-Hexenyl iodide	0.68 (0.97)
F-Hexyl iodide	0.13 (0.18)
F-1,6-Hexamethylene diiodide	0.11 (0.13)

[a] Yields in parentheses were calculated using estimated gas chromatograph detector response factors; see text. Other yields were calculated using the response to c-$C_6F_{11}I$ for all products.

preliminary unpublished data taken by Fallgatter in this laboratory. It appears that incorrect dosimetry data were used in the published results.

In addition to reconfirming the identification of F-bicyclohexyl by comparison with a known standard, and of F-cyclohexylhexane from its fragmentation pattern, a further confirmation of the identification of F-cyclohexylhexene was made by isolating this product and observing an infrared band in the region between 5 and 6 μ, attributed to C=C absorption. There is a problem concerning quantitative determination of yields of the dimeric products since a standard was available only for F-bicyclohexyl. Table I lists the values determined in two ways: calculations were made for all three compounds based on the sensitivity coefficient for F-bicyclohexyl and in addition results were calculated using extrapolated sensitivity coefficients determined from several fluorocarbon compounds. The latter figures are given in parentheses. Table II gives the G values of several minor products from the radiolysis of pure F-cyclohexane; sensitivity coefficients were obtained from the linear extrapolation graph in all cases.

Iodine Scavenging. The irradiation of solutions of iodine in F-cyclohexane results in the fading of the iodine color in the solution, as in the analogous case of the radiolysis of solutions of iodine in hydrocarbon. Typical results are shown in Figure 2. The rate of the radiation-induced uptake of iodine was studied by measuring the change in optical density at 524 nm as a function of dose. Samples were prepared with initial iodine concentrations of 0.3, 0.5, and 1.0 mM. It can be seen in Figure 2 that curves for the three different initial iodine concentrations have the same initial slope. From this slope and an extinction coefficient of 865 M^{-1} cm^{-1}, the calculated initial G value for loss of iodine is 2.9.

The gas chromatograph-mass spectrometer combination was used to separate and identify products from the radiolysis of iodine-F-cyclohexane mixtures. Only four peaks of significant size were observed in the gas chromatogram. Three of these had retention times rather similar to the three C_{12} products from the radiolysis of pure compounds,

and the fourth peak was retained about twice as long as the first three. In addition, several small peaks were observed. These peaks were neither as numerous nor as large as the minor products from the pure compound.

The four major iodine-containing organic products were analyzed by mass spectrometry. The first in the group of three products has an empirical formula $C_6F_{13}I$, and the spectrum is consistent with its identification as n-perfluorohexyl iodide. The second and third were found to have the same empirical formula, namely, $C_6F_{11}I$. Of these two, the latter was identified as perfluorocyclohexyl iodide, both on the basis of its mass spectrum and on the comparison of its retention time with a standard sample. The second compound in the group of three is believed to be F-hexenyl iodide, based upon a detailed consideration of its mass spectrum. The fourth product, eluting much later than the other three, is thought to be 1,6-$C_6F_{12}I_2$, based on a detailed consideration of its mass spectrum as well as on the plausibility of rupture of a C–C bond to give a 1,6 diradical.

Radiolysis yields of the four organic iodide products are listed in Table III. G values were calculated both using the sensitivity coefficient of F-cyclohexyl iodide for all four compounds, and using sensitivity coefficients as derived from a linear extrapolation graph. The yields of the four products were measured as a function of total dose in the range from 0.3 × 10^{19} to 2.0 × 10^{19} eV absorbed in a 0.15-ml sample. Good straight line graphs were obtained in all cases, as shown in Figures 3 and 4. The G values as listed in Table III were obtained from the slopes.

As noted above, the group of three iodine-containing products eluted from the SE-30 column at nearly the same position normally occupied by the three major dimeric products from the pure compound. However, experiments with several more polar columns (which completely retained the iodides) showed no residual yield of C_{12} fluorocarbons. In addition, no evidence for a residual yield of the fluorocarbon dimers was seen in the mass spectrum of the iodine-containing compound; it appears that residual yields are very small or nonexistent. As will be seen below, a quantitative interpretation of yield data is consistent with the assumption that the perfluoro dimers were removed essentially quantitatively. As noted above, a smaller number of minor products was observed in the iodine-containing system, and at least some of these are probably minor iodine-containing products. Accordingly, it is clear that the yields of many of the minor fluorocarbon products were reduced with added iodine. However, a detailed investigation of this aspect of the radiolytic behavior of the system was not made.

HI Scavenging. Several experiments were carried out to study the radiolysis of F-cyclohexane with added hydrogen iodide. Gas chromatographic analyses were made on several samples, and very little c-$C_6F_{11}H$ was observed.

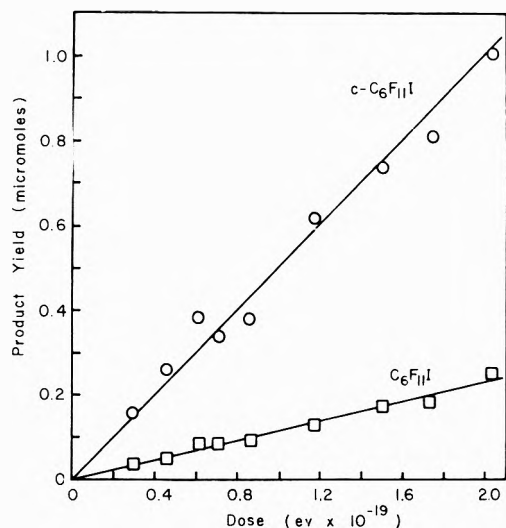**Figure 3.** Yields of c-$C_6F_{11}I$ and $C_6F_{11}I$ as a function of dose.

Figure 4. Yields of $C_6F_{13}I$ and $C_6F_{12}I_2$ as a function of dose.

There were three peaks which had the same retention time as the C_6 iodides (and, unfortunately, as the C_{12} dimers); identification of these products was not attempted. Figure 5 shows the results of spectrophotometric observation of iodine production from samples containing 2.8 and 5.2 μmol of HI in 0.5 ml of F-cyclohexane. Unlike the analogous case with the corresponding hydrocarbon, cyclohexane, the apparent G value for I_2 production was different in the two experiments (G = 1.3 and 1.9, respectively), and was substantially smaller than the yield for I_2 consumption in this system. Accordingly, it appears that HI is not a satisfactory scavenger for quantitative work in F-cyclohexane.

Bromine Scavenging. Several samples of bromine in F-cyclohexane were irradiated and analyzed using the ms–glc apparatus. Although complete analyses were not made in all cases, molecular formulae could be obtained from the highest mass ions and ions containing bromine were obvious because of the isotope abundances. Two relatively large peaks eluting shortly after the F-cyclohexane parent were found, both corresponding to the formula $C_6F_{11}Br$. When the column was warmed to 150°, two more substantial peaks appeared, both having the formula $C_6F_{12}Br_2$. Other minor products were observed, corresponding to the following formulas: CF_2Br_2, C_2F_5Br, $C_2F_4Br_2$, $C_2F_3Br_3$, $C_6F_{10}Br_2$, $C_6F_{13}Br$, and $C_6F_{11}Br_3$. Although free-radical scavenging obviously occurs, the rather reactive nature of Br_2 and Br· apparently complicates the results. Accordingly, bromine scavenging will not be discussed further.

Discussion

It is concluded from the results of the present studies on the radiolysis of pure F-cyclohexane and F-cyclohexane with added iodine that the majority of the radiolysis products of the pure material have free-radical precursors. Supporting evidence is the fact that, in the presence of millimolar concentrations of iodine, the production of the perfluorinated products is eliminated and iodine-containing products are formed instead. Since $G(-I_2)$ is independent of iodine concentration (Figure 2) it is clear that the reaction of iodine with radicals can compete effectively with radical–radical combination at iodine concentrations at least as low as 10^{-4} M. The linearity of the plots of the yields of the iodide products vs dose, and the fact that the lines pass through the origin (Figures 3 and 4), indicates
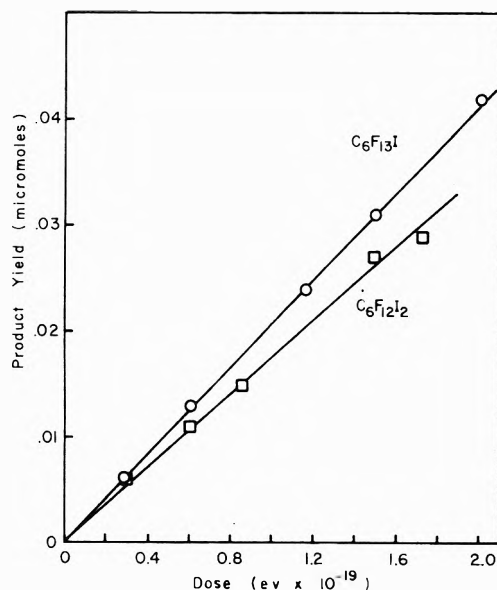
both that these compounds are first-generation products and that they are not subject to decomposition during further radiolysis (in the dose range investigated). The former point is important with respect to F-hexyl iodide, since it shows that this compound is not formed by reaction of F· or F_2 with F-hexenyl iodide. Similarly, it rules out the possibility that F-1,6-hexamethylene diiodide could be formed by addition of F· to F-hexenyl iodide, followed by reaction of the resultant radical with I_2.

The repetition of the chemical groups F-cyclohexyl, F-hexenyl, and F-hexyl in both the C_{12} products from pure F-cyclohexane and the C_6 iodides from the scavenged system suggests that the corresponding free radicals are important reactive intermediates in the radiolysis of F-cyclohexane. The total radical yield measured as $G(-I_2)$ should be equal to the sum of the yields of the observed F-alkyl iodide products. Furthermore, estimates of individual radical yields as detected in specific iodide products should correlate with radical yields inferred from the product yields measured in the pure perfluorocarbon. (Although plots of the yields in the pure compound are curved, indicating that secondary reactions are occuring, the plots are essentially linear at low doses, and initial G values can readily be obtained; see Figure 1.)

In making the comparison of total radical yields as described above, we note that the initial G value of 2.9 for iodine uptake in F-cyclohexane corresponds to a total radical yield of 5.8. This value can be compared with a total radical yield calculated from the yields of the radiolysis products of pure F-cyclohexane (see eq 11, 12, and 13 below). If it is assumed that all products having more than six carbon atoms are formed by the combination of two radicals, the total radical yield can be estimated with the expression

$$G(\text{total radicals}) = 2\sum G(\text{products} > C_6) \qquad (1)$$

using the product yields given in Table I, G(total radicals) = 4.0 or 4.2, depending upon the gas chromatograph detector responses that were used. Since all products were not measured, the total radical yield calculated by the summation of the radiolysis product yields is probably a lower limit; some back reaction of radicals with F or F_2 in the steady state may also occur. Accordingly, the total

TABLE IV: Yields of Perfluoro C_6 Radicals

Radical	G values[a] calculated from iodine products	G values[a] calculated from c-C_6F_{12} products
F-Cyclohexyl	3.1	2.8 (2.9)
F-Hexenyl	0.68 (0.97)	0.6 (0.7)
F-Hexyl	0.13 (0.18)	0.1 (0.1)
F-1,6-Hexa-methylene diradical	0.1 (0.1)	

[a] Values in parentheses are based on product yields calculated using estimated gas chromatograph detector response factors; see text.

radical yield in F-cyclohexane can be accepted as 5.8, about the same total radical yield reported for a number of hydrocarbons. This implies that F-cyclohexane is not especially stable to ionizing radiation even though the C–F bond is much stronger than the C–H bond.

Yields of the individual C_6 radicals can be estimated from the yields of the corresponding C_6 iodide products, and compared with radical yields estimated from the products in pure F-cyclohexane. For the latter purpose, it is assumed that C_7–C_{11} and $> C_{12}$ products contain F-cyclohexyl and F-hexenyl groups, and that these are distributed in the same ratio ($ca.$ 2 to 1) as are the yields of F-bicyclohexyl and F-cyclohexylhexene. The radical yields are then estimated by the following expressions
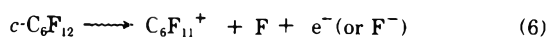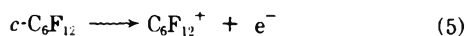
$$G(F\text{-cyclohexyl}) = 2G(F\text{-bicyclohexyl}) +$$
$$G(F\text{-cyclohexylhexene}) +$$
$$G(F\text{-cyclohexylhexane} + {}^2/_3 G(C_7\text{-}C_{11}, > C_{12}) \quad (2)$$

$$G(F\text{-hexenyl}) = G(F\text{-cyclohexylhene}) +$$
$$\quad {}^1/_3 G(C_7\text{-}C_{11}, > C_{12}) \quad (3)$$

$$G(F\text{-hexyl}) = G(F\text{-cyclohexylhexane}) \quad (4)$$

As in earlier calculations, two sets of values are obtained, depending on the gas chromatograph detector response data that are used. The yields of the C_6 radicals that were calculated by the methods described above are summarized in Table IV. The agreement of the values listed in Table IV is surprisingly good considering the approximations that had to be made. From the data in Table IV, reasonable yields of the C_6 radicals are $G(F$-cyclohexyl$) = 3.0 \pm 0.2$, $G(F$-hexenyl$) = 0.8 \pm 0.2$, $G(F$-hexyl$) = 0.1 \pm 0.05$, and $G(F$-1,6-hexamethylene diradical$) = 0.1 \pm 0.05$.

Although the results of our scavenging experiments indicate that the major radiolysis products of F-cyclohexane are formed by radical–radical combination reactions, the initial radiolytic processes must involve ionized and excited species. The principal positive ions could be $C_6F_{11}^+$ and $C_6F_{12}^+$

$$c\text{-}C_6F_{12} \longrightarrow C_6F_{12}^+ + e^- \quad (5)$$

$$c\text{-}C_6F_{12} \longrightarrow C_6F_{11}^+ + F + e^-(\text{or } F^-) \quad (6)$$

While the abundance of the parent ion is very low in the mass spectrum of F-cyclohexane, this does not necessarily rule out its importance in the liquid phase. Carbon tetrachloride also does not give a parent ion in the mass spectrometer, but evidence has been reported that the CCl_4^+ ion is produced by irradiation of the liquid.[18] Natalis[19] has suggested that the structure of the $C_6F_{11}^+$ ion is an open chain, suggesting a route to formation of the F-hexenyl radical. Judging from the substantial yield of c-C_6F_{11} radicals, however, a considerable portion of the ions
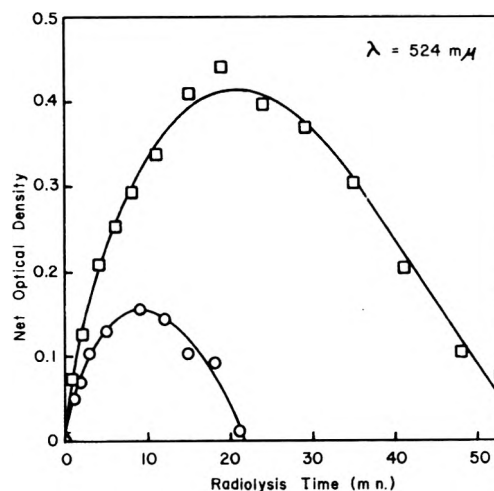
Figure 5. Iodine production in the radiolysis of c-C_6F_{12}–HI mixtures. Initial HI concentrations reading top to bottom were 10.0 and 5.6 mM, if all of the HI was dissolved in the liquid phase.

formed in reactions 5 and 6 must have the cyclic structure.

The important negatively charged species in irradiated F-cyclohexane are expected to be F^- and c-$C_6F_{12}^-$ rather than the electron. Estimating from the measured electron attachment rate of 6×10^{13} M^{-1} sec^{-1} for the related compound F-methylcyclohexane,[20] the half-life for the electron capture would be about 10^{-14} sec, considerably shorter than the positive ion–electron neutralization times of 10^{-7} to 10^{-11} sec estimated by Buchanan and Williams for cyclohexane.[21] If the electron energy exceeds 1.8 eV, dissociative electron capture is also possible. Thus we have

$$e^- + c\text{-}C_6F_{12} \longrightarrow c\text{-}C_6F_{12}^- \quad (7)$$

$$e^- + c\text{-}C_6F_{12} \longrightarrow c\text{-}C_6F_{11} + F^- \quad (8)$$
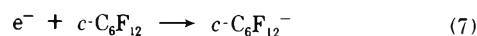
Neutralization of the positive ions formed in reactions 5 and 6 would involve the negative species formed in reactions 7 and 8. The corresponding neturalization energies would be less than in electron neutralization, by the amount of the electron affinity of the F atom and the F-cyclohexane molecule, respectively. The former is known to be 80 kcal/mol, and the latter can be estimated to be between 30 and 50 kcal/mol by comparison with other efficient electron capture agents such as SF_6, CCl_4, and N_2O.[22] The energy difference in neutralization by F^- and by c-$C_6F_{12}^-$ would thus be 30 kcal/mol or greater, and this may well affect the probability of C–F $vs.$ C–C bond rupture, since their bond strengths differ by about 30 kcal/mol.

Since F-cyclohexane is transparent above 220 nm (corresponding to 120 kcal/mol), the energy of the lowest accessible excited state appears to be sufficient to break either C–C or C–F bonds. MacKenzie, et $al.$,[5] suggested that F-cyclohexyl radicals might be formed by C–F bond rupture of an excited molecule, followed by attack of the F atom on the substrate to give F-hexyl radicals

$$c\text{-}C_6F_{12}^* \longrightarrow c\text{-}C_6F_{11} + F \quad (9)$$

$$F + c\text{-}C_6F_{12} \longrightarrow n\text{-}C_6F_{13} \quad (10)$$
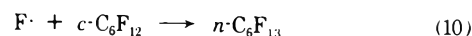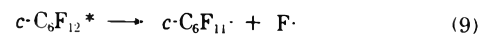
However, the yield of n-hexyl radicals is insufficient to account for all of the fluorine atoms which must be formed. As in most fluorocarbon radiolysis systems reported to

date, there is a considerable deficit of fluorine atoms ($G \cong 3$). Presumably fluorine is lost to the walls of the radiolysis vessel.

Formation of the net products in the radiolysis of pure F-cyclohexane is readily explained by radical combination processes

$$2c\text{-}C_6F_{11}\cdot \longrightarrow (c\text{-}C_6F_{11})_2 \tag{11}$$

$$c\text{-}C_6F_{11}\cdot + C_6F_{11}\cdot \longrightarrow (c\text{-}C_6F_{11})C_3F_{11} \tag{12}$$

$$c\text{-}C_6F_{11}\cdot + C_6F_{13}\cdot \longrightarrow (C_6F_{11})C_6F_{13} \tag{13}$$
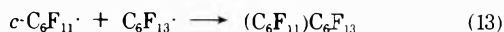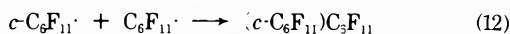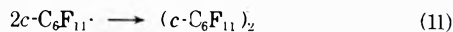
where $c\text{-}C_6F_{11}\cdot$ is the F-cyclohexyl radical, $C_6F_{11}\cdot$ is the F-hexenyl radicals, and $C_6F_{13}\cdot$ is the F-n-hexyl radical. In addition, similar reactions with small F-alkyl radicals appear to be responsible for most of the minor products.

It is suggested that the curvature of the product yield vs. dose graph for $(c\text{-}C_6F_{11})_2$ and also for $(c\text{-}C_6F_{11})C_6F_{11}$ is a function of the concentration of the respective compounds in the radiolysis mixture. The curvature of (c-$C_6F_{11})_2$ is only moderately obvious when 3×10^{17} molecules have been produced, and essentially nonobservable when 1×10^{17} molecules have been produced. Correspondingly, only a slight effect is seen over the entire production range for $(c\text{-}C_6F_{11})C_6F_{11}$, which terminates with 3×10^{17} molecules produced, and essentially no curvature is seen for the graph of $(c\text{-}C_6F_{11})C_6F_{13}$, which terminates with 1×10^{17} molecules produced. It is possible that these compounds are attacked by fluorine atoms present in steady-state concentrations during the radiolysis.

Hydrogen iodide should scavenge $c\text{-}C_6H_{11}\cdot$ radicals according to

$$c\text{-}C_6F_{11}\cdot + HI \longrightarrow c\text{-}C_6F_{11}H + I\cdot \tag{14}$$
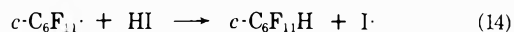
It is clear that HI is not a good scavenger in this case, however, since $G(+I_2)$ with added HI was less than $G(-I_2)$ with added I_2. In addition, the yield of $c\text{-}C_6F_{11}H$ as measured by gas chromatography was considerably less than the expected value of 3.1. The problem can not involve energetics; bond strength considerations show that reaction 14 is about 25 kcal exothermic. A likely explanation is found in an investigation by Amphlett and Whittle[13] of competitive scavenging of $CF_3\cdot$ radicals by HBr and Br_2. Their value of k_{Br_2}/k_{HBr} would be 120 at room temperature, much larger than in a comparable case involving hydrocarbon radicals. Amphlett and Whittle interpreted the low efficiency of HBr to an unfavorable

polar effect in the transition state

$$\begin{array}{cccc} \delta- & \delta+ & \delta+ & \delta- \\ F_3 & - & C\cdots H\cdots Br \end{array}$$
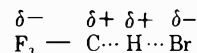
In the present work, a low solubility of the polar molecule HI in highly nonpolar liquid $c\text{-}C_6F_{12}$ could also be a factor. Possibly most of the HI was in the gas phase, rather than in the liquid.

It is concluded that formation of the final products in F-cyclohexane radiolysis proceeds by a straightforward mechanism. In addition, I_2 was found to be a good scavenger in this fluorocarbon system, while both HI and Br_2 were unsatisfactory for various reasons.

References and Notes

(1) The prefix F- will be used as an abbreviation for prefluoro.
(2) G. A. Kennedy and R. J. Hanrahan, *J. Phys. Chem.*, **78**, 366 (1974).
(3) M. B. Fallgatter and R. J. Hanrahan, *J. Phys. Chem.*, **69**, 2059 (1965).
(4) M. B. Fallgatter and R. J. Hanrahan, *J. Phys. Chem.*, **74**, 2806 (1970).
(5) D. R. MacKenzie, F. W. Bloch, and R. H. Wiswall, Jr., *J. Phys. Chem.*, **69**, 2526 (1965).
(6) J. Fajer, D. R. MacKenzie, and F. W. Bloch, *J. Phys. Chem.*, **70**, 935 (1966).
(7) W. C. Askew, T. M. Reed, III, and J. C. Mailen, *Radiat. Res.*, **33**, 282 (1968).
(8) L. Kevan and P. Hamlet, *J. Chem. Phys.*, **42**, 2255 (1965).
(9) A. Sokolowska and L. Kevan, *J. Phys. Chem.*, **71**, 2220 (1967).
(10) E. Heckel and R. J. Hanrahan, *Advan. Chem. Ser.*, **No. 82**, 120 (1968).
(11) R. K. Boyd, G. W. Downs, J. S. Gow, and C. Horrex, *J. Phys. Chem.*, **67**, 719 (1963).
(12) T. L. Cottrell, "The Strengths of Chemical Bonds," 2nd ed, Academic Press, New York, N. Y., 1968.
(13) J. C. Amphlett and E. Whittle, *Trans. Faraday Soc.*, **62**, 1662 (1966).
(14) C. G. Krespan, *J. Org. Chem.*, **27**, 1813 (1962).
(15) G. A. Kennedy, Ph.D. Dissertation, University of Florida, 1969.
(16) R. J. Hanrahan, *Int. J. Appl. Radiat. Isotopes*, **13**, 254 (1962).
(17) L. S. Ettre in "The Practice of Gas Chromatography," L. S. Ettre and A. Zlatkis, Ed., Interscience, New York, N. Y., 1967, pp 394-399.
(18) R. Cooper and J. K. Thomas, *Advan. Chem. Ser.*, **No. 82**, 351 (1968).
(19) P. Natalis, *Bull. Soc. Roy. Sci. Liege*, **29**, 94 (1960).
(20) B. H. Mahan and C. E. Young, *J. Chem. Phys.*, **44**, 2192 (1966).
(21) J. W. Buchanan and F. Williams, *J. Chem. Phys.*, **44**, 4377 (1966).
(22) G. R. Freeman, *Radiat. Res. Rev.*, **1**, 16 (1968).

Effect of Iodine as a Radical Scavenger in the γ Radiolysis of Liquid-Phase Cyclohexane–Perfluorocyclohexane Solutions

George A. Kennedy and Robert J. Hanrahan*

Department of Chemistry. University of Florida, Gainesville, Florida 32611   (Received August 4, 1972; Revised Manuscript Received November 8. 1973)

An investigation has been made of the effects of I_2 as a radical scavenger in the γ radiolysis of liquid-phase c-C_6H_{12}–c-C_6F_{12} mixture at 65°. Both iodine consumption (with added I_2) and iodine production (with added HI) appear to give reliable radical counting over most of the concentration range. The total radical yields were found to be about 6.0 for both of the pure compounds and to maximize at about 9.0 for solutions containing 30 electron % c-C_6F_{12}. With respect to the hydrocarbon products, both the qualitative and quantitative effects of added I_2 agree with simple expectations; the disproportionation/combination products (cyclohexene and dicyclohexyl) from cyclohexyl radicals are sharply reduced, and a substantial yield of c-$C_6H_{11}I$ is formed, showing a maximum yield of 7.2 which is nearly constant from 10 to 60 electron % c-C_6F_{12}. The H_2 yield, which is strongly depressed by the fluorocarbon, shows little further effect of the added I_2. Remarkably, the yield of c-$C_6F_{11}H$ is essentially unaffected by added I_2, in spite of the fact that I_2 is a good scavenger of c-C_6F_{11} radicals in pure C-C_6F_{12}. It appears that the (thermal) c-C_6F_{11} radical is not a precursor of c-$C_6F_{11}H$ in the irradiated mixtures. This result apparently requires reevaluation of previous suggestions concerning the mechanism of C–F bond rupture in irradiated fluorocarbon–hydrocarbon mixtures. Additional photolytic experiments on solutions containing HI (as a source of H atoms) and triphenylamine (as a source of photoelectrons) suggest, respectively, that H atoms are not involved, and that electrons or negative ions are involved, in C–F bond rupture.

Introduction

The radiation chemistry of gas-phase and liquid-phase mixtures of hydrocarbon and fluorocarbon compounds has been a subject of numerous publications over the past several years.[1-8] Rajbenbach and coworkers[2,3,7] and Sagert and coworkers[4,5] have primarily been concerned with systems containing small amounts of the fluorocarbon (1% or less) and an excess of hydrocarbon. Work in this laboratory has involved studies of the entire composition range from 100% hydrocarbon to 100% fluorocarbon.[1,6,8,9] Much of the earlier work was concerned with the role of added fluorocarbons as electron scavengers in irradiated hydrocarbon systems. In particular, a sharp decrease of the H_2 yield of cyclohexane and other hydrocarbons was interpreted as being due to nondissociative electron capture by an added fluorocarbon compound[2] such as F-cyclohexane[10]
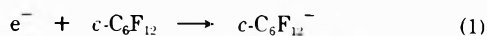
$$e^- + c\text{-}C_6F_{12} \longrightarrow c\text{-}C_6F_{12}^- \qquad (1)$$

It was assumed that the energy available from the neutralization of the parent positive ion of the hydrocarbon by the c-$C_6F_{12}^-$ ion would be rather low, so that sufficient energy to produce H_2 or H atoms would not be available

$$c\text{-}C_6H_{12}^+ + c\text{-}C_6F_{12}^- \longrightarrow (\text{no H or } H_2) \qquad (2)$$
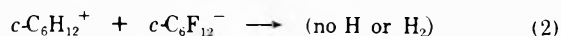
A more elaborate interpretation of the radiolysis of fluorocarbon–hydrocarbon systems became necessary when it was observed that, even in solutions containing less than 1% fluorocarbon, efficient rupture of CF bonds occurs.[1,5] In the cyclohexane system, c-$C_6F_{11}H$ is produced with a G value which exceeds 2 over the entire range 10 to 90% fluorocarbon, and shows a broad maximum of about $G = 3.5$. In order to interpret the formation of c-$C_6F_{11}H$, Sagert proposed[5]

$$c\text{-}C_6H_{12}^+ + c\text{-}C_6F_{12}^- \longrightarrow c\text{-}C_6H_{11}\cdot + c\text{-}C_6F_{11}\cdot + HF \quad (3)$$
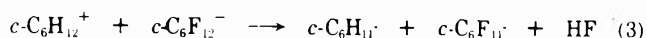
We have mentioned the decrease of the H_2 yield and the production of c-$C_6F_{11}H$; other products in the radiolysis of cyclohexane–F-cyclohexane mixtures include a substantial yield of c-C_6H_{10} and $(c$-$C_6H_{11})_2$.[5,8] Production of these compounds was assumed to be due to disproportionation–combination of c-$C_6H_{11}\cdot$ radicals, which were presumed to be formed from hydrocarbon substrate by attack of c-$C_6F_{11}\cdot$ radicals

$$c\text{-}C_6F_{11}\cdot + c\text{-}C_6H_{12} \longrightarrow c\text{-}C_6F_{11}H + c\text{-}C_6H_{11}\cdot \qquad (4)$$
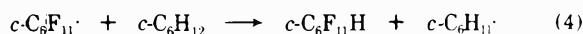
The original purpose of the present work was to investigate the postulated role of free-radical chemistry in the radiolysis of cyclohexane–F-cyclohexane solutions as described briefly above. For this purpose, HI and I_2 were selected as free-radical scavengers, since they have been used extensively in the radiation chemistry of cyclohexane. We have previously described the effects of these scavengers, as well as Br_2, on the radiolysis of pure c-C_6F_{12}.[9] As will be seen below, the results of the present work are entirely consistent with the postulated formation of cyclohexene and bicyclohexyl by free-radical reactions. We are forced to question the role of reactions 3 and 4 in this system, however, since the yield of c-$C_6F_{11}H$ seems to be quite insensitive to added scavengers.

Experimental Section

The radiolysis source, dosimetry, irradiation conditions, purification of the F-cyclohexane, and several aspects of the sample preparation and analysis procedures were described previously.[8,9,11] The cyclohexane used was Phillips Research Grade; it was passed through a 12-in. column of silica gel, dried over BaO, degassed, and transferred into a storage vessel on the vacuum line. F-Cyclohexane was metered as a gas. A concentrated stock solu-

Figure 1. Densities of c-C_6F_{12}–c-C_6H_{12} mixtures at 65°.

Figure 2. Production of c-$C_6H_{11}I$ and c-$C_6F_{11}H$ in the radiolysis of c-C_6F_{12}–c-C_6H_{12} mixtures with added iodine.

tion of I_2 in cyclohexane was metered from a vacuum line buret[12] and additional cyclohexane was added from a second buret as needed.

Dosimetry calculations for the γ irradiations, which were conducted at 65°, require a knowledge of the densities of cyclohexane–F-cyclohexane solutions at that temperature. Since the necessary data were not found in the literature, the densities were measured by observing the liquid level in a calibrated glass vessel, occupied by a weighed quantity of solution. Slight corrections (ca. 2%) for material present in the vapor phase were necessary. The results of the density measurements are shown in Figure 1.

Product identification using a gas chromatograph interfaced to a Bendix mass spectrometer via a multiple peak-trapping manifold is described elsewhere.[11] Hydrogen yields were measured in a combined Toepler pump–McLeod gauge apparatus. Other products were analyzed using a MicroTec GC 2000-R gas chromatograph. Fluorocarbon–hydrocarbon mixtures containing less than 25 wt % F-cyclohexane are miscible at room temperature, and were injected into the chromatograph using a microliter syringe. More concentrated solutions were irradiated in 6-mm Pyrex ampoules and injected into the chromatograph using a bulb-crushing apparatus. Most products were analyzed on columns of SE-30 on Chromosorb W; however, a column of β,β'-oxydipropionitrile on Chromosorb W was used for the measurement of cyclohexene yields. Further details of the procedures for gas chromatographic analysis are given elsewhere.[9,11]

Measurements of the uptake of I_2 in irradiated F-cyclohexane–cyclohexane solutions were done spectrophotometrically, using irradiation vessels with attached optical cells. Analyses were done using a Beckman DU spectrophotometer, thermost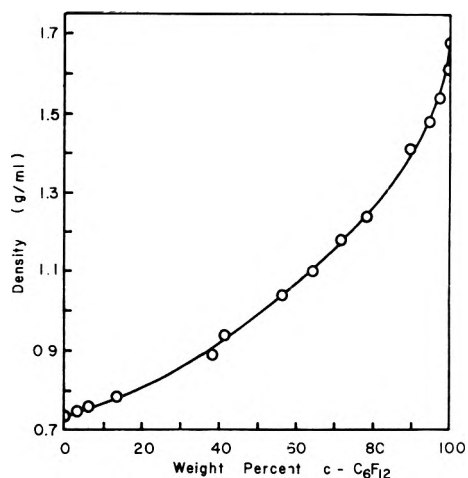atted to 65°, at a wavelength of 524 nm. Samples of 1.0 ml volume were prepared with initial iodine concentrations of 4 mM and various F-cyclohexane concentrations.

Measurements of the HF yields in unscavenged F-cyclohexane–cyclohexane solutions were performed using a potentiometric titration with $La(NO_3)_2$ in a 65% $EtOH$–H_2O solution, following a procedure recently described by Heckel.[13]

Photochemical experiments to check for H atom attack on c-C_6F_{12} were done at about 60° using a 2537-Å Hg resonance lamp. Samples were dissolved in a minimum amount of CCl_4 and analyzed by gas chromatography.
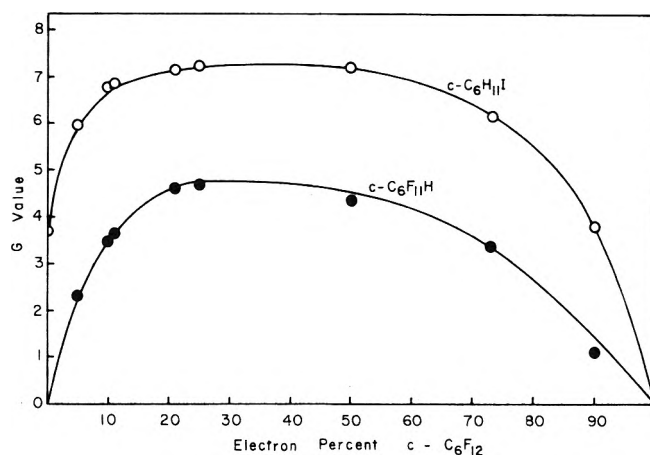
Photochemical experiments involving triphenylamine as a photoionizing agent were also done at 2537-Å using a Hg resonance lamp. In a series of experiments involving end product analysis, solutions were prepared with 0.3 M F-cyclohexane and 0.05 M triphenylamine, or benzene, in Phillips pure grade cyclohexane. Samples of 2.0 ml were placed in 6-mm o.d. quartz test tubes, degassed, and sealed. The photolysis times and geometries were as close to identical as possible for all samples. For measurement of photoinduced currents in triphenylamine solutions, a conductivity cell was constructed.[11] This consisted of a pair of plane-parallel nickel electrodes sealed about 3 mm apart in a quartz optical cell. A Heath EUW-15 power supply was used to supply a voltage (V_A) across the electrodes, and the current (I_x) was measured with a General Radio 1230-A dc amplifier and electrometer.

Results

Radiolysis Experiments. Mixtures with iodine concentrations of 5 ± 1 mM were irradiated to a dose of 5.1×10^{19} eV/ml and analyzed for the major products, which were found to be c-$C_6F_{11}H$, c-$C_6H_{11}I$, $(c$-$C_6H_{11})_2$, c-C_6H_{10}, and H_2. Apparently, c-$C_6F_{11}I$ is not produced. This species eluted on the tail of the large c-C_6H_{12} peak, and we probably would have been unable to see a small amount of the compound. If its yield approximated the amount expected from efficient scavenging of c-$C_6F_{11}\cdot$ radical, however, we should have seen some evidence of it, at least in solutions of high F-cyclohexane concentration. This was never the case. Furthermore, the entire expected yield of c-$C_6F_{11}\cdot$ appears as c-$C_6F_{11}H$, and there would be a stoichiometric problem if a substantial yield of the iodide also appeared. Finally, the suggestion that c-$C_6F_{11}I$ was lost in the chromatography process is ruled out by the fact that we were able to analyze for it routinely in the radiolysis of pure F-cyclohexane with I_2 scavenger.

Graphs of product yields as a function of mixture composition are shown in Figures 2 and 3. For comparison, the yields of hydrogen and c-$C_6F_{11}H$ as a function of mixture composition are shown in Figures 4 and 5 for systems with and without added iodine. The data for systems without iodine were taken from ref 8. In the mixtures containing iodine, the yields of c-$C_6F_{11}H$ and c-$C_6H_{11}I$ increase sharply with increasing F-cyclohexane content up to 20–40 electron %. Beyond this region, the yields gradually decrease to about 80 electron % and then decrease more rapidly. The maximum G values are 7.3 for c-$C_6H_{11}I$ and 4.7
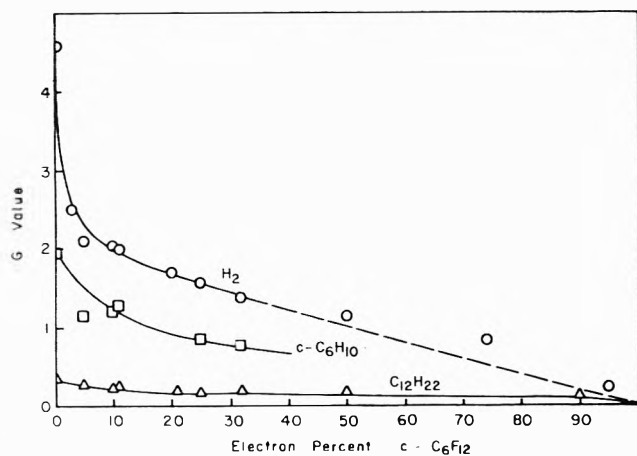
Figure 3. Production of H_2, c-C_6H_{10}, and c-$C_{12}H_{22}$ in the radiolysis of c-C_6F_{12}-c-C_6H_{12} mixtures with added iodine.
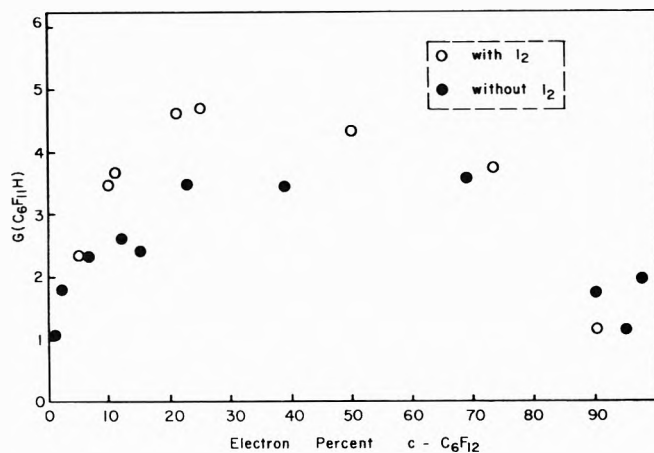
Figure 5. Production of c-$C_6F_{11}H$ in the radiolysis of c-C_6F_{12}-c-C_6H_{12} mixtures with and without added iodine.
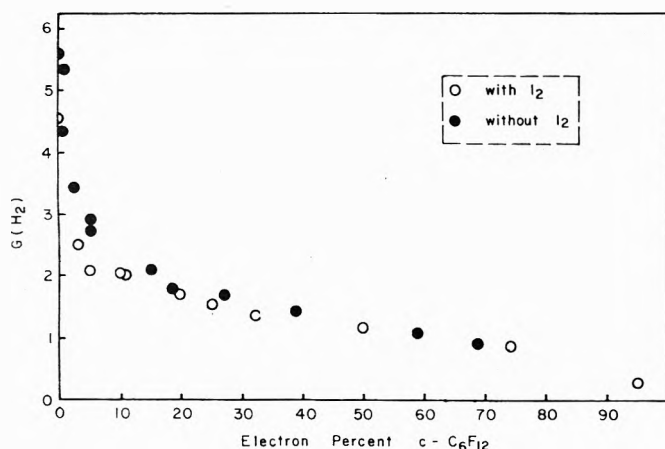
Figure 4. Hydrogen production in the radiolysis of c-C_6F_{12}-c-C_6H_{12} mixtures with and without added iodine.
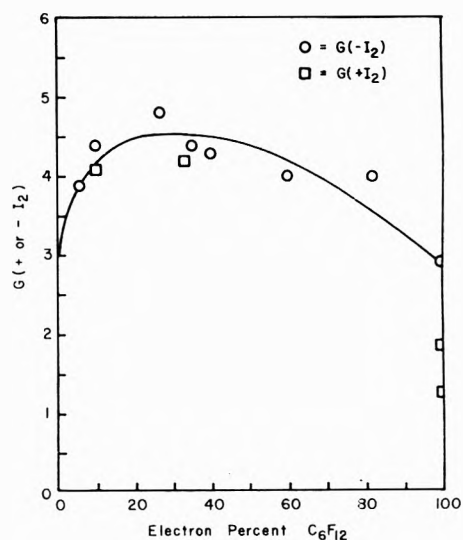
Figure 6. Iodine consumption or production in the radiolysis of c-C_6F_{12}-c-C_6H_{12} mixtures with added iodine or hydrogen iodide.

for c-$C_6F_{11}H$. The yields of hydrogen, cyclohexene, and bicyclohexyl all decrease with increasing F-cyclohexane content, with the hydrogen yield decreasing more sharply than the latter two. Analytical difficulties prevented reliable measurements of cyclohexene yields beyond those shown. The curves for both hydrogen and bicyclohexyl appear to have very broad inflection regions between 30 and 90 electron % with sharper slopes in the more dilute and concentrated regions.

Inspection of the data in Figure 4 shows that above 20 electron % F-cyclohexane, the hydrogen yield does not appear to be affected by the presence of iodine. Below this concentration, the systems with iodine show slightly lower hydrogen yields than the systems without iodine. It can be seen from the data in Figure 5 that the c-$C_6F_{11}H$ yields in systems with iodine appear to be somewhat greater than the yields in the absence of iodine. However, most of the difference between the two sets of data is believed to be due to differences in the method used for glc sample injection.

In the experiments done to measure I_2 uptake as a function of dose, for various concentrations of F-cyclohexane and cyclohexane, all of the optical density $vs.$ dose plots were concave upward. This type of behavior is seen in similar plots for pure cyclohexane,[14] and implies that there is a decrease in the net scavenging with increasing dose. In pure cyclohexane the behavior has been interpret-

ed as due to a buildup of HI in the system with increasing dose; the HI then competes with the iodine for free radicals.[14] $G(-I_2)$ values were calculated from the initial slopes of the optical density $vs.$ dose curves and are shown in Figure 6 as a function of the mixture composition. The value of $G(-I_2)$ for pure cyclohexane was taken from ref 14. Samples containing about 10 electron % F-cyclohexane were prepared with initial iodine concentrations of 0.7, 1, and 4 mM. The initial $G(-I_2)$ values for all of these were the same, indicating that there is no dependence of the initial rate of iodine uptake on the iodine concentration.

Experiments were also carried out to study the effects of HI. The initial $G(+I_2)$ values were determined and these points are also shown in Figure 6. At low perfluorocarbon content, the agreement between the $G(+I_2)$ and $G(-I_2)$ values is fairly good.

Subsequent to the investigations of the radiolysis of F-cyclohexane-cyclohexane solutions done earlier in this laboratory by Fallgatter and Hanrahan[8] a practical method for the analysis of micromolar amounts of HF radiolysis product was developed by Heckel.[13] Using this technique, HF yields were measured as a function of composition in unscavenged F-cyclohexane-cyclohexane solutions. The results are given in Figure 7.
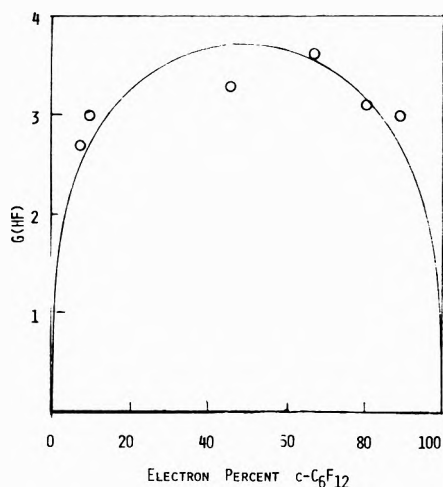
Figure 7. Production of HF in the radiolysis of unscavenged c-C_6F_{12}–c-C_6H_{12} mixtures.

Photolysis Experiments. Other experiments were carried out to attempt to gain additional information about possible reactions in the fluorocarbon–hydrocarbon mixtures.

The abstraction of fluorine from F-cyclohexane by H atoms (reaction 5) is a possible means of forming F-cyclo-

$$H + c\text{-}C_6F_{12} \longrightarrow HF + c\text{-}C_6F_{11}\cdot \qquad (5)$$
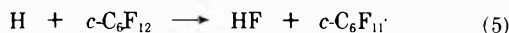
hexyl radicals. Thermochemical arguments have been given[2] against this reaction occurring with thermal H in the gas phase. In order to check the possibility of the occurrence of the reaction in the liquid phase, HI in F-cyclohexane was photolyzed with a 2537-Å Hg resonance lamp. At this wavelength the fluorocarbon does not absorb light, while the HI is readily decomposed, as evidenced by a substantial production of I_2. No c-$C_6F_{11}H$ was detected by gas chromatography. Since the CCl_4 solvent, used to dissolve the samples for analysis, eluted in the same region where c-$C_6F_{11}I$ and $C_{12}F_{22}$ were expected, the absence of these products can not be conclusively determined. However, there were no shoulders or breaks in the tailing solvent peak which are seen in the gas chromatograms of irradiated c-C_6F_{12}–I_2 mixtures dissolved in CCl_4. It does not appear that reaction 5 occurs to a significant extent.

The photolysis of solutions of triphenylamine in n-hexane has been shown to produce short-lived charged species, presumably by the photoionization of the amine (reaction 6).[15] In the studies reported, a full mercury arc

$$(C_6H_5)_3N + h\nu \longrightarrow (C_6H_5)_3N^+ + e^- \qquad (6)$$
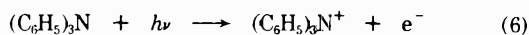
($\lambda > 200$ nm) was used to produce the photoionization. By filtering the light, it was found that electrical conductivity of the solution was greatest with light below 250 nm, but charged species were still formed with light of longer wavelengths. Since C–F bond rupture in the radiolysis of low concentrations of F-cyclohexane in cyclohexane has been proposed to occur *via* electron capture,[2–8] it was decided to see if evidence for such a process could be found in the photolysis of solutions of triphenylamine and F-cyclohexane in cyclohexane. To check for C–F bond rupture due to a direct or Hg-photosensitized effect, a solution without the amine was photolyzed. To check for possible energy transfer effects, a solution of benzene and F-cyclohexane was photolyzed. After photolysis, the samples were opened and analyzed for c-$C_6F_{11}H$ by gas chromatography. The results are given in Table I.

TABLE I: Photolysis of c-C_6H_{12}–c-C_6F_{12} Mixtures

Sample	[c-$C_6F_{11}H$], mM
c-C_6F_{12} + c-C_6H_{12}	0.3
c-C_6F_{12} + c-C_6H_{12} + C_6H_6	0.2
c-C_6F_{12} + c-C_6H_{12} + $(C_6H_5)_3N$	1.4
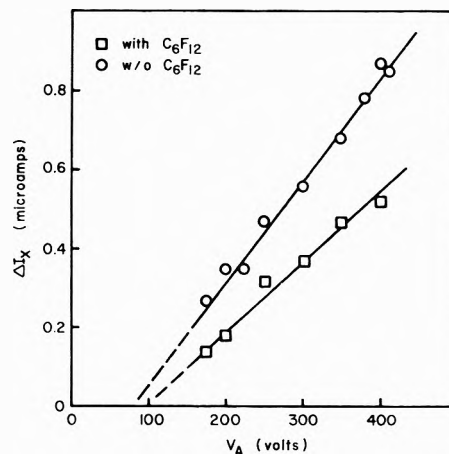
Figure 8. Current increases observed upon exposure of solutions of triphenylamine in cyclohexane to uv light, as a function of applied voltage, with and without added c-C_6F_{12}.

An experiment was also carried out to see if a photoinduced current could be detected in the solution with triphenylamine. With the Hg lamp off, a small current was observed as soon as the voltage was applied across the electrodes. In the amine solutions, this current was reduced when three sides of the optical cell were darkened by painting with black ink. In pure cyclohexane, a small current was also observed. This "dark" current is probably due to circuit leakage plus some photoionization of the amine by the room lights. Very distinct differences in current were noted between amine solutions exposed to the uv light source and those shielded from it. Plots of the increase in current upon removing the light shield *vs.* the applied voltage are shown in Figure 8 for triphenylamine (0.1 mM) in cyclohexane and for the same solution with 0.3 mM F-cyclohexane added.

Discussion

The kinetic scheme given below has been useful as a basis for discussion of the effect of added c-C_6F_{12} on the radiolysis of c-C_6H_{12}.[5,8]

$$c\text{-}C_6H_{12} \rightsquigarrow (c\text{-}C_6H_{12}^+ + e^-) \longrightarrow c\text{-}C_6H_{12}^* \qquad (7)$$

$$c\text{-}C_6H_{12} \rightsquigarrow c\text{-}C_6H_{12}^* \qquad (8)$$

$$c\text{-}C_6H_{12}^* \longrightarrow c\text{-}C_6H_{10} + H_2 \qquad (9)$$

$$c\text{-}C_6H_{12}^* \longrightarrow c\text{-}C_6H_{11}\cdot + H\cdot \qquad (10)$$

$$H\cdot + c\text{-}C_6H_{12} \longrightarrow H_2 + c\text{-}C_6H_{11}\cdot \qquad (11)$$

$$2c\text{-}C_6H_{11}\cdot \longrightarrow C_{12}H_{22} \qquad (12)$$

$$2c\text{-}C_6H_{11}\cdot \longrightarrow c\text{-}C_6H_{10} + c\text{-}C_6H_{12} \qquad (13)$$
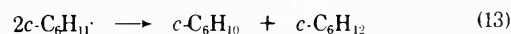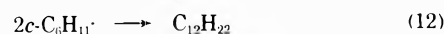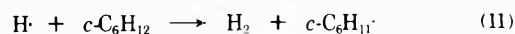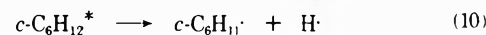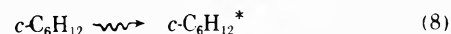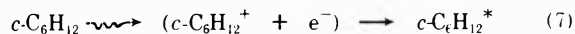
Added F-cyclohexane apparently captures electrons, thereby interfering with reaction 7. The reactions that have been proposed are[2,5,8]

$$c\text{-}C_6F_{12} + e^- \longrightarrow c\text{-}C_6F_{12}^- \qquad (14)$$

$$c\text{-}C_6F_{12}^- + c\text{-}C_6H_{12}^+ \longrightarrow c\text{-}C_6F_{11}\cdot + c\text{-}C_6H_{11}\cdot + HF \qquad (15)$$

and/or

$$c\text{-}C_6F_{12} + e^- \longrightarrow c\text{-}C_6F_{11}\cdot + F^- \tag{16}$$

$$F^- + c\text{-}C_6H_{12}{}^+ \longrightarrow HF + c\text{-}C_6H_{11}\cdot \tag{17}$$

followed by

$$c\text{-}C_6F_{11}\cdot + c\text{-}C_6H_{12} \longrightarrow c\text{-}C_6F_{11}H + c\text{-}C_6H_{11}\cdot \tag{18}$$
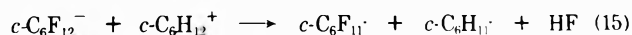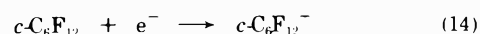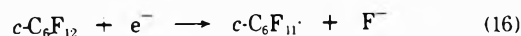
and reactions 12 and 13. The equality of the yields of c-$C_6F_{11}H$ and HF, implicit in the above reaction scheme, has been confirmed in the present work (compare Figures 5 and 7).

In the present studies on F-cyclohexane–cyclohexane systems, the results from the uv photolyses of triphenylamine solutions support arguments that production of c-$C_6F_{11}H$ results from electron capture by F-cyclohexane. The lower yields observed in the photolysis of samples without the amine and with benzene replacing the amine seem to indicate that little C–F bond rupture occurs due to direct or Hg-sensitized photolysis or by energy transfer from an exicted aromatic molecule. The higher yield in the presence of triphenylamine coupled with the observation of a net increase in current upon exposure of the amine solutions to uv light are consistent with photoionization of the amine followed by electron capture by c-C_6F_{12}. The details of the mechanism by which the c-$C_6F_{11}H$ is produced cannot be ascertained from these experiments.

The results of the radiolysis of F-cyclohexane and cyclohexane mixtures containing iodine parallel the results of the studies of systems without iodine. The hydrogen yield is reduced sharply upon addition of F-cyclohexane, c-$C_6F_{11}H$ is formed, and $G(c$-$C_6H_{11}\cdot)$ is increased compared to the pure hydrocarbon. In the studies without iodine, the increase in $G(c$-$C_6H_{11}\cdot)$ was manifested as an increased $C_{12}H_{22}$ yield. In the present studies, the cyclohexyl radicals are removed by reaction 19, and the yield of c-

$$c\text{-}C_6H_{11}\cdot + I_2 \longrightarrow c\text{-}C_6H_{11}I + I \tag{19}$$
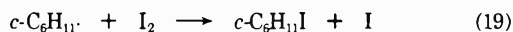
$C_6H_{11}I$ is increased above the value observed in the absence of F-cyclohexane. The presence of iodine does not completely eliminate $C_{12}H_{22}$ production. As in the case of the pure hydrocarbon, the residual yield may be radical-radical combination in spurs.

Comparison of the hydrogen yields from systems with and without iodine (see Figure 4) shows that there is a slightly lower hydrogen production in the systems with iodine between 0 and 15 electron % F-cyclohexane. Such a reduction of H_2 may be due to the scavenging of thermal hydrogen atoms by iodine (reaction 20), thereby preventing

$$H + I_2 \longrightarrow HI + I\cdot \tag{20}$$
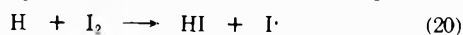
ing the occurrence of reaction 11. A similar situation was reported by Rajbenbach[3] who used olefins to scavenge hydrogen atoms in the radiolysis of n-hexane–F-cyclobutane mixtures. As was mentioned in the Results section, the optical density $vs.$ dose curves were all concave upward. This behavior is attributed to competition between I_2 and HI in the radiolysis of cyclohexane with iodine,[14] and might indicate that HI was being formed in the systems studied in the present work.

The apparent lack of a significant reduction in the c-$C_6F_{11}H$ yields in the systems containing iodine (see Figure 5) presents a problem. Although there are multiple possibilities for C–F bond rupture in the radiolysis of F-cyclohexane and cyclohexane mixtures, both Fallgatter and Hanrahan[8] and Sagert[5] have proposed that c-$C_6F_{11}H$ is formed by abstraction of hydrogen from cyclohexane by

the c-$C_6F_{11}\cdot$ radical (reaction 18). If these radicals are present, they should be susceptible to scavenging by iodine. The competition between hydrogen abstraction and reaction with iodine of small perfluoroalkyl radicals has been studied by Infelta and Schuler.[16]

$$R_f\cdot + I_2 \longrightarrow R_fI + I\cdot \tag{21}$$

$$R_f\cdot + c\text{-}C_6H_{12} \longrightarrow R_fH + c\text{-}C_6H_{11}\cdot \tag{22}$$
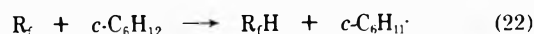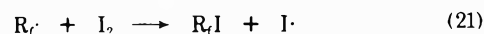
These researchers found that $k_{22}/k_{21} = 3.16 \times 10^{-5}$ for $R_f\cdot = CF_3\cdot$ and $k_{22}/k_{21} = 1.63 \times 10^{-5}$ for $R_f\cdot = C_2F_5\cdot$ in studies made at room temperature. The radicals were generated as a result of the electron capture reaction (23)

$$R_fBr + e^- \longrightarrow R_f\cdot + Br^- \tag{23}$$
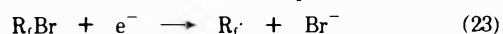
in the radiolysis of solutions of the bromides in cyclohexane with added radioiodine (used to increase the analytical sensitivity). The fraction of radicals produced which were scavenged by iodine was determined over the iodine concentration range from 10^{-4} to 10^{-2} M. It was found that over 80% of the radicals were scavenged at an iodine concentration of 5×10^{-3} M ($i.e.$, the concentration used in the present work).

Now, consider the present study. For samples of 90 electron % F-cyclohexane, the cyclohexane concentration is about 1.5 M. Assuming that $k_{22}/k_{21} = 1.6 \times 10^{-5}$ for $R_f = c\text{-}C_6F_{11}$.

$$\frac{d[c\text{-}C_6F_{11}H]}{d[c\text{-}C_6F_{11}I]} = \frac{k_{22}[c\text{-}C_6H_{12}][c\text{-}C_6F_{11}\cdot]}{k_{21}[I_2][c\text{-}C_6F_{11}\cdot]} =$$
$$1.6 \times 10^{-5}\frac{(1.5)}{(0.005)} = 4.8 \times 10^{-3}$$

At 50 electron %, the same assumption about k_{22}/k_{21} leads to the prediction that the ratio of the yields of c-$C_6F_{11}H$ and c-$C_6F_{11}I$ should be 0.01. The trend going from CF_3Br to C_2F_5Br suggests that k_{22}/k_{21} might well be less than 1.6×10^{-5} for $R_f\cdot = c\text{-}C_6F_{11}$. But our results would be incompatible with the calculation even if the ratio were taken as 100 times larger, or 1.6×10^{-3}. (This would suggest c-$C_6F_{11}H \simeq c$-$C_6F_{11}I$, or a 50% decrease in yield in the 50 electron % solution.) Thus, assuming any plausible value of k_{22}/k_{21}, the observed lack of reduction of the c-$C_6F_{11}H$ yields in the presence of iodine is inconsistent with the suggested radical mechanism (reaction 18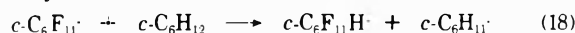) for formation of this compound (there should be a large decrease in the c-$C_6F_{11}H$ yield, which was not observed).

The apparent failure of the c-$C_6F_{11}H$ yields to be reduced in the presence of iodine suggests that production of this compound by means other than reaction of F-cyclohexyl radicals is occurring. Rajbenbach[3] has proposed an alternate mechanism in a report on the radiolysis of fluorocarbons in n-hexane. The mechanism, written below for the F-cyclohexane–cyclohexane system, does not involve any neutral c-$C_6F_{11}\cdot$ radicals that would be subject to scavenging by iodine.

$$c\text{-}C_6F_{12}{}^- + c\text{-}C_6H_{12} \longrightarrow c\text{-}C_6F_{11}{}^- + HF + c\text{-}C_6H_{11}\cdot \tag{24}$$

$$c\text{-}C_6F_{11}{}^- + c\text{-}C_6H_{12}{}^+ \longrightarrow c\text{-}C_6F_{11}H + c\text{-}C_6H_{11}\cdot \tag{25}$$
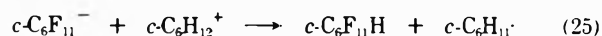
Presumably, even if some complex species might arise from the reaction of iodine with the c-$C_6F_{11}{}^-$ radical ion before neutralization occurred, the weaker C–I bond would be replaced by the stronger C–H bond in reaction 25. The problem with this scheme as an explanation of the observed results lies in the energetics of reaction 24. The C–H bond strength in c-C_6H_{12} is approximately 94

kcal/mol, and the H–F bond strength is approximately 136 kcal/mol.[17] Assuming a C–F bond strength of 120 kcal/mol, the energy required for reaction 24 to occur with neutral species is $120 + 94 - 136 = 78$ kcal/mol. The difference in the electron affinities of $c\text{-}C_6F_{12}$ and $c\text{-}C_6F_{11}$ may change the energy requirement somewhat, but in view of the electron affinities reported[18] for SF_6, SF_5, CCl_4, and CCl_3 it seems likely that reaction 24 would still be at least 30 kcal/mol endothermic.

After an extended search, we are unable to present an acceptable alternative to the three schemes already presented (reactions 14–15, 16–17, and 24–25) for the radiolytic behavior of the F-cyclohexane–cyclohexane system, and similar fluorocarbon–hydrocarbon mixtures. The relationships between fluorocarbon and hydrocarbon energetics are such that practically any process devised to transfer radiation effect from a hydrocarbon (as solvent) to a fluorocarbon (as solute) is strongly endoergic, hence probably of low efficiency. Yet C–F bonds are broken, even in rather dilute fluorocarbon solutions, with good efficiency ($G > 3$). We conclude that one of the three schemes is probably correct.

We have reexamined these three proposals, which we designate as the Sagert mechanism (reactions 14–15), the dissociative capture mechanism (reactions 16–17), and the Rajbenbach mechanism (reactions 24–25). Of these three, the dissociative capture mechanism is dismissed not only because it is 41 kcal/mol endoergic, but also because it distinctly would give thermal F-cyclohexyl radicals, which are unacceptable in the light of the present experiments. Both the Sagert and Rajbenbach schemes can be allowed if appropriate specific assumptions are made about the way in which they occur.

Considering the Sagert mechanism, reaction 14 is satisfactory, but reaction 15 needs modification, since we disallow production of thermal F-cyclohexyl radicals. We suggest that it could occur in two steps, as a proton transfer reaction

$$c\text{-}C_6F_{12}^- + c\text{-}C_6H_{12}^+ \longrightarrow (c\text{-}C_6F_{12}H)^* + c\text{-}C_6H_{11} \quad (15a)$$

$$(c\text{-}C_6F_{12}H)^* \longrightarrow (c\text{-}C_6F_{11})^* + HF \quad (15b)$$
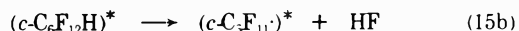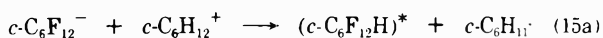
It is suggested that most of the excess energy of reaction 15 resides in the intermediate $(c\text{-}C_6F_{12}H)^*$ where it is vibrationally distributed before HF is eliminated.[19] In consequence, the product F-cyclohexyl radical would be "hot," and might easily abstract hydrogen from substrate cyclohexane. This would solve the dilema about the rate constant ratio k_{22}/k_{21}.

The energetic problem with the Rajbenbach scheme arises in the assumption that the reactant species $c\text{-}C_6F_{12}^-$ is "relaxed," that is, that the rather substantial attachment energy has been dissipated to the medium. It will be seen to be energetically possible if viewed as a concerted process

$$e^- + c\text{-}C_6F_{12} + c\text{-}C_6H_{12} \longrightarrow$$
$$c\text{-}C_6F_{11}^- + HF + c\text{-}C_6H_{11} \quad (24a)$$
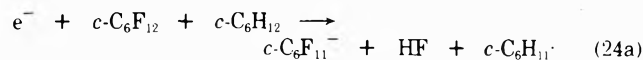
Alternatively, the reactant $c\text{-}C_6F_{12}^-$ ion can be designated as "excited," indicating that the attachment energy is available (probably in vibrational modes)

$$(c\text{-}C_6F_{12}^-)^* + c\text{-}C_6H_{12} \longrightarrow$$
$$c\text{-}C_6F_{11}^- + HF + c\text{-}C_6H_{11} \quad (24b)$$
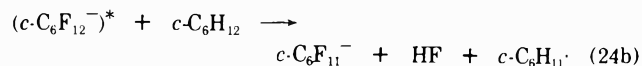
In either case, the product $c\text{-}C_6F_{11}^-$ must be relaxed since its electron affinity is needed to drive the reaction. Reaction 25 would follow in any event.

We have also given some consideration to a reaction involving hydride transfer from cyclohexane to the $c\text{-}C_6F_{11}^+$ ion

$$c\text{-}C_6F_{11}^+ + c\text{-}C_6H_{12} \longrightarrow c\text{-}C_6F_{11}H + c\text{-}C_6H_{11}^+ \quad (26)$$
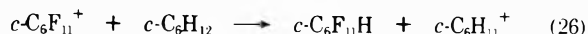
This reaction appears energetically favorably, and Heckel has in fact observed an analogous reaction between CF_3^+ and C_2H_6 using a high-pressure Bendix mass spectrometer in our laboratory. We are not able to propose a reasonable, efficient route to the $c\text{-}C_6F_{11}^+$ ion, however.

We conclude that either the Sagert or Rajbenbach mechanisms, as modified, would account for these and previous related experimental results. Although a choice between them is difficult we tend to favor the Rajbenbach proposal, for the negative reason that $G(c\text{-}C_6F_{11}H) \simeq 4$ seems too high even for an efficient hot radical process.

References and Notes

(1) M. B. Fallgatter and R. J. Hanrahan, Paper No. 127, Division of Physical Chemistry, 148th National Meeting of the American Chemical Society, Chicago, Ill., Sept 1964.
(2) L. A. Rajbenbach, *J. Amer. Chem. Soc.*, **88**, 4275 (1966).
(3) L. A. Rajbenbach and U. Kaldor, *J. Chem. Phys.*, **47**, 242 (1967).
(4) N. H. Sagert and A. S. Blair, *J. Chem. Phys.*, **46**, 3284 (1968).
(5) N. H. Sagert, *Can. J. Chem.*, **46**, 95 (1968).
(6) E. Heckel and R. J. Hanrahan, *Advan. Chem. Ser.*, **No. 82**, 120, (1968).
(7) L. A. Rajbenbach, *J. Phys. Chem.*, **73**, 356 (1969).
(8) M. B. Fallgatter and R. J. Hanrahan, *J. Phys. Chem.*, **74**, 2806 (1970).
(9) G. A. Kennedy and R. J. Hanrahan, *J. Phys. Chem.*, **78**, 360 (1974).
(10) The prefix F- will be used to indicate perfluoro-.
(11) G. A. Kennedy, Ph.D. Dissertation, University of Florida, 1969. Available from University Microfilms, Ann Arbor, Mich.
(12) R. H. Hanrahan, *J. Chem. Educ.*, **41**, 623 (1964).
(13) E. Heckel and P. F. Marsh, *Anal. Chem.*, **44**, 2347 (1972).
(14) I. Mani and R. J. Hanrahan, *J. Phys. Chem.*, **70**, 2233 (1966).
(15) (a) H. Ruppel and H. T. Witt, *Z. Phys. Chem. (Frankfurt am Main)*, **15**, 321 (1958); (b) H. Ruppel, U. Krug, and W. T Witt, *J. Electrochem. Soc.*, **107**, 966 (1960).
(16) P. P. Infelta and R. H. Schuler, *J. Phys. Chem.*, **73**, 2083 (1969).
(17) J. G. Calvert and J. N. Pitts, "Photochemistry," Wiley, New York, N. Y., 1966, pp 824–826.
(18) G. R. Freeman, *Radiat. Res. Rev.*, **1**, 16 (1968).
(19) The intermediate $(c\text{-}C_6F_{12}H)^*$ might be thought of as an intimate ion-pair or charge-transfer complex $(c\text{-}C_6F_{12}^- \cdots H^+)$.

Chemical States of Sulfur-35 Formed by the ^{35}Cl(n,p)^{35}S Process in Potassium Chloride[1,2]

James L. Giulianelli[2] and John E. Willard*

Department of Chemistry, University of Wisconsin, Madison, Wisconsin 53706 (*Received June 1, 1973; Revised Manuscript Received November 21, 1973*)

Using neutron-irradiated KCl crystals pretreated to maximize the "labile" fraction of ^{35}S formed by the ^{35}Cl(n,p)^{35}S process, the chemical reactions of this fraction upon dissolution have been examined using different scavengers, reductants, and carriers. This 85% component is oxidized to ^{35}SO$_4^{2-}$ when dissolved in carrier-free aqueous NaOH and appears as ^{35}S^{2-} when only S^{2-} carrier is present. When only SO$_3^{2-}$ carrier is present, it appears in three fractions: 20% S$_2$O$_3^{2-}$, 50% S^{2-}, and 15% SO$_3^{2-}$, indicating the presence of (1) S$_1^0$, (2) a species reduced by SO$_3^{2-}$, and (3) a species which exchanges with SO$_3^{2-}$. Tests in the presence of CN$^-$ and allyl alcohol are consistent with these findings. Experiments on the effect of temperature of dissolution of the KCl on the distribution of the ^{35}S activity and on the production of S$_1^0$ in water by photolysis of OCS are also described.

Introduction

The chemical identity of the sulfur species produced as a result of the ^{35}Cl(n,p)^{35}S reaction during neutron irradiation of alkali chloride crystals has been the subject of a variety of investigations,[3-7] including studies of the effects of crystal purity, pre- and postirradiation γ doses, thermal annealing, doping, and carriers used in the dissolution solution. With KCl which has been sublimed *in vacuo*, γ irradiated, irradiated with neutrons, and dissolved in water, *ca.* 90% of the ^{35}S is found as SO$_4^{2-}$ when the mixed carriers S^{2-}, SO$_3^{2-}$, and SO$_4^{2-}$ are subsequently added and separated.[3a,b] If, however, S^{2-} carrier is present at the time of dissolution and the other carriers are added subsequently, *ca.* 90% of the ^{35}S may be found as S^{2-}. It has been suggested[3a,b] that this indicates that *ca.* 80% of the ^{35}S in the irradiated KCl is present as S$_1^0$ which is oxidized by water (S$_1^0$ + 4H$_2$O → 2H$^+$ + SO$_4^{2-}$ + 3H$_2$), or, in the presence of S^{2-}, exchanges to give ^{35}S^{2-} (^{35}S$_1^0$ + S^{2-} → ^{35}S^{2-} + S$_1^0$). However, the same effects might be observed if the ^{35}S were in the crystal as one of several other species (*e.g.*, S$^+$, S$^-$, SCl, SCl$_2$) which could be oxidized by H$_2$O (or by oxidants from the irradiated crystals) or be reduced by S^{2-} and exchange with it. This paper reports tests which show that species in the "labile" fraction from the dissolving crystals undergo three different types of reaction which imply three different reactive entities.

Experimental Section

The KCl crystals used were Merck reagent grade, prepared for neutron irradiation by sublimation at 10^{-3} Torr and 700° from the bottom to the sides of quartz ampoules, sealing under vacuum, and exposure to 2.3 × 10^{21} eV g^{-1} of ^{60}Co γ radiation. They were irradiated with a flux of *ca.* 2 × 10^9 n cm^{-2} sec^{-1} for 6 hr in the thermal column of the University of Wisconsin nuclear reactor. The fast neutron flux was negligible and the γ flux was estimated as less than 200 rads hr^{-1}.

Weighed amounts of the neutron-irradiated KCl crystals were dissolved in 0.3 M NaOH with and without one or more of the solutes S^{2-}, S$_2$O$_3^{2-}$, SO$_3^{2-}$, SO$_4^{2-}$, CN$^-$,

while nitrogen was bubbled through the solution to maintain an oxygen-free system. In some cases solutions of additional solutes were added subsequent to the dissolution. The final volume (4 ml) and the final concentration of each solute used (2.2 × 10^{-2} M in 0.3 M NaOH) were always the same. Solutions containing S$_2$O$_3^{2-}$ were maintained below 5° until the S$_2$O$_3^{2-}$ was separated, to prevent exchange reactions.

Analysis was accomplished by separating the S^{2-}, S$_2$O$_3^{2-}$, SO$_3^{2-}$, and SO$_4^{2-}$, converting each to SO$_4^{2-}$, precipitating as BaSO$_4$, centrifuging onto planchets, weighing, and counting with a mica window Geiger counter. Corrections were made for any loss of carrier in the analytical process. Duplicate analyses on KCl samples from the same batch regularly agreed within 5%.

To separate sulfide from the mixed anion carriers, ZnS was precipitated by addition of zinc acetate and washed with ammonium acetate. Separation of SO$_3^{2-}$ and SO$_4^{2-}$ from S$_2$O$_3^{2-}$ was then accomplished by precipitation from each of two aliquots of the remaining solution by addition of SrCl$_2$ and absolute alcohol, followed by addition of more SO$_3^{2-}$ and SO$_4^{2-}$ and a second precipitation to ensure complete removal of the ^{35}SO$_3^{2-}$ and ^{35}SO$_4^{2-}$ activity. One SrSO$_3$-SrSO$_4$ precipitate was treated with HCl to remove SO$_3^{2-}$, following which both were treated with ammoniacal H$_2$O$_2$ and converted to BaSO$_4$ for counting by adding HCl and BaCl$_2$. The sulfite was determined by difference. The thiosulfate in the supernatant from the SrSO$_3$-SrSO$_4$ precipitates was oxidized to sulfate using alkaline hydrogen peroxide and the ^{35}S recovered for counting as BaSO$_4$.

As a check on the strontium method of separating SO$_3^{2-}$ and SO$_4^{2-}$ from S$_2$O$_3^{2-}$, a second procedure was used in which Ni(en)$_3$(NO$_3$)$_2$ was added after removal of ZnS to precipitate Ni(en)$_3$S$_2$O$_3$, leaving SO$_3^{2-}$ and SO$_4^{2-}$ in solution. A second precipitation with additional S$_2$O$_3^{2-}$ carrier assured complete removal of labeled S$_2$O$_3^{2-}$. Ni(en)$_3$S$_2$O$_3$ was oxidized to sulfate with alkaline H$_2$O$_2$. One aliquot from the supernatant of the Ni(en)$_3$S$_2$O$_3$ precipitate was acidified and the second oxidized to allow de-

TABLE I: Comparison of Ni(en)$_3$(NO$_3$)$_2$ and Strontium Methods of Separation of S$_2$O$_3{}^{2-}$ from SO$_3{}^{2-}$ and SO$_4{}^{2-}$ [a]

Analytical method	S^{2-}	S$_2$O$_3{}^{2-}$	SO$_3{}^{2-}$	SO$_4{}^{2-}$
Strontium	58.6 ± 1.1	22.9 ± 0.5	14.3	4.2
Ni(en)$_3$(NO$_3$)$_2$	55.9 ± 1.5	24.6 ± 0.3	16.1	3.4

[a] Similar samples of vacuum-sublimed, neutron-irradiated KCl were dissolved in alkaline SO$_3{}^{2-}$ solution. The remaining carriers were added after dissolution.

TABLE II: Distribution of ^{35}S Activity after Dissolution of Vacuum-Sublimed, Neutron-Irradiated KCl in Solutions of Different Compositions [a]

Carriers present at 4.3 × 10^{-2} M prior to KCl dissolution	S^{2-}	S$_2$O$_3{}^{2-}$	SO$_3{}^{2-}$	SO$_4{}^{2-}$
None	11.0	1.2	1.8	85.9
SO$_3{}^{2-}$	58.6	22.9	14.3	4.2
S^{2-}, SO$_3{}^{2-}$, S$_2$O$_3{}^{2-}$, SO$_4{}^{2-}$ [b]	91.0	2.0	4.1	2.9

[a] All solutions contained 0.3 M NaOH. Following KCl dissolution each solution was made 2.2 × 10^{-2} M in all four carrier anions. [b] Essentially this same distribution was found in prior experiments when only S^{2-} carrier was present during KCl dissolution.

TABLE III: Effect of Carriers Used and Their Order of Addition on the Chemical Form of ^{35}S Activity Recovered from Neutron-Irradiated KCl Dissolved in SO$_3{}^{2-}$ Solution [a]

Carriers in order of addition after KCl dissolution	^{35}S, %			
	S^{2-}	S$_2$O$_3{}^{2-}$	SO$_3{}^{2-}$	SO$_4{}^{2-}$
S$_2$O$_3{}^{2-}$, S^{2-}, SO$_4{}^{2-}$	58.6	22.9	14.3	4.2
—, S^{2-}, SO$_4{}^{2-}$	62.9	14.4 [b]	22.7	0
S^{2-}, SO$_4{}^{2-}$, S$_2$O$_3{}^{2-}$	62.1	18.7	15.4	3.7

[a] All solutions contained 0.3 M NaOH and 4.3 × 10^{-2} M SO$_3{}^{2-}$ prior to dissolution of the KCl. [b] Activity in supernatant after removal of S^{2-}, SO$_3{}^{2-}$, and SO$_4{}^{2-}$ carrier precipitates.

TABLE IV: ^{35}SCN$^-$ Formation During Dissolution of Neutron-Irradiated KCl in Alkaline Cyanide Solution

Solutes present prior to dissolving KCl [a]	^{35}S, %		
	S^{2-}	SCN$^-$	Other
None	17		83
4 × 10^{-2} M CN$^-$	67	23	11
4 × 10^{-2} M S^{2-}	95		5

[a] All solutions were 0.3 M in NaOH.

termination of ^{35}SO$_4{}^{2-}$ and the total of ^{35}SO$_3{}^{2-}$ + ^{35}SO$_4{}^{2-}$. The Ni(en)$_3$(NO$_3$)$_2$ and strontium methods of analysis gave equivalent results (Table I). The latter was used in the subsequent work of this paper.

Analysis for ^{35}SCN$^-$ formed on dissolution of irradiated KCl in solutions containing CN$^-$ was made by subsequent addition of S^{2-}, SO$_3{}^{2-}$, SO$_4{}^{2-}$, and SCN$^-$ as carriers, precipitation of ZnS, BaSO$_3$, and BaSO$_4$, and oxidation of the supernatant with alkaline hypobromite to allow precipitation of its ^{35}S as BaSO$_4$. Correction was made for the ^{35}S appearing in the SCN$^-$ fraction as a result of the solubility of ZnS in CN$^-$ solution, as determined in a control experiment.

Results

Table II allows comparison of the distribution of recovered ^{35}S activity between S^{2-}, S$_2$O$_3{}^{2-}$, SO$_3{}^{2-}$, and SO$_4{}^{2-}$ for samples of the same neutron-irradiated KCl dissolved in 0.3 M NaOH with no carriers present, with only SO$_3{}^{2-}$ present, and with all four carriers present. In these and all other experiments the carriers not present at the time of dissolution were added prior to the subsequent analysis. Table III contains data for experiments in which the irradiated KCl crystals were dissolved in 0.3 M NaOH containing 4.3 × 10^{-2} M SO$_3{}^{2-}$ as the only carrier, following which additional carriers were added one at a time in the sequence indicated. These data show that the distribuion of activity is independent of the order of addition of the carriers S^{2-} and S$_2$O$_3{}^{2-}$ and is not greatly influenced by the presence of thiosulfate carrier. An experiment to test whether any of the ^{35}S from crystals dissolved in solutions containing CN$^-$ as the only carrier would form ^{35}SCN$^-$ is reported in Table IV where the relative yields from dissolution of samples of the same irradiated KCl without carrier or reactant and with S^{2-} present are also shown.

In an experiment where the KCl was dissolved in aqueous 0.3 M NaOH containing 10 mol % allyl alcohol, 50% of the ^{35}S was recovered as sulfide, compared to 14% when the allyl alcohol was not present. The sulfide fraction includes the organic sulfide which forms from the scavenging of S$_1{}^0$ by allyl alcohol.[8]

Discussion

The data of Tables II and III indicate that when irradiated KCl crystals, prepared as described, are dissolved in deaerated carrier-free alkaline solutions 11% of the ^{35}S appears as ^{35}S^{2-} and ca. 85% as species which are oxidized to SO$_4{}^{2-}$. It is not known whether this oxidation is caused by radiation produced species from the crystals (e.g., Cl or Cl$_2{}^-$) or by H$_2$O. When SO$_3{}^{2-}$ is present during dissolution, the activity which otherwise would have been oxidized to SO$_4{}^{2-}$ (the differences between lines 1 and 2 of Table II) appears as S^{2-} (48% of the S^{35}), S$_2$O$_3{}^{2-}$ (22%), and SO$_3{}^{2-}$ (12%). The similarity of the S$_2$O$_3{}^{2-}$ yields from the dissolution in the presence of SO$_3{}^{2-}$ (Table III) and the SCN$^-$ yield from the dissolution in the presence of CN$^-$ (Table IV) are strong evidence that about 20% of the ^{35}S in the crystals enters solution as neutral monatomic sulfur (^{35}S$_1{}^0$), the scavenging reactions being ^{35}S$_1{}^0$ + SO$_3{}^{2-}$ → ^{35}SSO$_3{}^{2-}$ and ^{35}S$_1{}^0$ + CN$^-$ → ^{35}SCN$^-$. Evidence that the thiosulfate activity does not come from an exchange reaction with S$_2$O$_3{}^{2-}$ carrier is given by the observations that when irradiated KCl was added to sulfite carrier solution to which no S$_2$O$_3{}^{2-}$ was ever added, 14.4% of the ^{35}S could not be separated as S^{2-}, SO$_3{}^{2-}$, or SO$_4{}^{2-}$, and is therefore presumably S$_2$O$_3{}^{2-}$ (Table III, line 2). Also, we have determined experimentally that ^{35}SSO$_3{}^{2-}$ does not exchange radiosulfur with S^{2-} under the conditions of this work[2] and rate constants in the literature indicate negligible exchange of ^{35}S^{2-} with S$_2$O$_3{}^{2-}$ [9] or ^{35}SO$_3{}^{2-}$ with S$_2$O$_3{}^{2-}$ [10] under these conditions.

The increase in the ^{35}S^{2-} yield from ca. 10 to 60% when a reducing agent (SO$_3{}^{2-}$ (Tables I and II), CN$^-$ (Table IV), or allyl alcohol) is present seems to indicate that the irradiated KCl contains one or more ^{35}S species in addition to ^{35}S$_1{}^0$ which can be reduced to S^{2-} or to a species which will exchange with S^{2-} added after the dissolution. Alternatively the reducing agents may react with oxidiz-

ing species released by the irradiated KCl, thus preventing these from oxidizing the ^{35}S species to forms unexchangeable with S^{2-}. The 12% of the ^{35}S which appears as SO_3^{2-} when SO_3^{2-} is the only carrier may result from a specific exchange reaction between SO_3^{2-} and a product of the dissolution of the irradiated KCl (e.g., S^+, S^-, SCl, SCl_2, or one of their hydrolysis products). Since exchange of the two sulfur atoms in the $^{35}SSO_3^{2-}$ anion does not occur,[10] $^{35}SSO_3^{2-}$ cannot be the precursor of this sulfite activity. Nor does it seem that it can be the product of attack of "hot" S_1^0 on SO_3^{2-} as has been postulated[11] as the origin of the $^{37}SO_3^{2-}$ activity from the $^{37}Cl(n,p)^{37}S$ reaction following neutron irradiation of Cl^- solutions containing SO_3^{2-}.

When S^{2-} is present in the dissolving solution with or without other additives, >90% of the ^{35}S is converted to S^{2-} (Table II, line 3). This 90% includes the 11% present as S^{2-} when no carriers are present at dissolution, the 22% which dissolves as S_1^0, the 48% prevented from oxidation by the reducing power of S^{2-} and the 12% which reacts with SO_3^{2-} if the latter is present in the absence of S^{2-} (Table I and II). As far as we know, this investigation is the first to show that the labile fraction of the ^{35}S from neutron-irradiated KCl contains species which can react with SO_3^{2-} in three different ways, i.e., as monatomic sulfur giving rise to thiosulfate activity, as an ^{35}S species which appears as sulfide, and in a form which is recovered as sulfite. Evidence for the formation of neutral monatomic sulfur by the $^{35}Cl(n,p)^{35}S$ reaction in KCl crystals using 2 M CN^- as scavenger in the dissolving solution has been obtained previously.[7] Enhancement of the sulfide fraction from irradiated crystals by the presence of ethyl alcohol in the dissolving solution has also been reported.[6,7] In the present work the enhancement of the activity in the sulfide fraction when irradiated crystals were dissolved in allyl alcohol-containing solutions is attributed to either (1) the scavenging of oxidizing entities from the crystals analagous to the mechanisms suggested for the effect of ethyl alcohol,[6,7] (2) the known scavenging of sulfur atoms by the olefinic bond of allyl alcohol,[8] (3) a combination of 1 and 2. More definitive experiments are needed to distinguish between these alternatives.

When it was thought that the total labile fraction of ^{35}S from KCl might enter solution as S_1^0, experiments were conducted by A. A. Adams of our laboratory in which neutron-irradiated KCl was dissolved in S^{2-} carrier solutions at temperatures from 0 to 100°.[2] Low carrier concentrations (4×10^{-4} and 4×10^{-5} M) in the region where carrier effectiveness begins to decrease were used on the hypothesis that the two reactions: $^{35}S_1^0 + 4H_2O \rightarrow H_2^{35}SO_4 + 3H_2$ and $^{35}S_1^0 + S^{2-} \rightarrow ^{35}S^{2-} + S_1^0$ might then compete effectively, and produce a systematic change in ^{35}S distribution with increasing temperature due to differing energies of activation. No systematic change occurred. The $^{35}S^{2-}$ yield was higher for the higher S^{2-} concentration but remained constant over most of the temperature range save for surprising minima at 27 and 68° at both concentrations. The constancy seems more consistent with oxidation by highly reactive species from the crystals than with oxidation by H_2O.

Exploration of Other Sources of S_1^0. It is well established that S atoms can be produced by the photolysis of OCS in the gas phase[8] and some similar investigations have been made in liquid alkanes and alcohols[12] and in rare gas and hydrocarbon matrices.[8,13] We have explored the possibility of producing S_1^0 in aqueous solution by photolysis of OCS for the purpose of studying its oxidation by water and reaction with additives studied.[2] To provide low enough concentrations to minimize the reaction S + OCS $\rightarrow S_2$ + CO, high specific activity $OC^{35}S$ was synthesized. Photolysis of 10^{-5} M solutions produced SO_3^{2-} and SO_4^{2-} and data were obtained on the analytical procedures, absorption spectra of aqueous OCS, hydrolysis, and polymer formation.[2] Photolysis of an OCS concentration of *ca.* 10^{-6} mole fraction produced polymeric sulfur, but that this did not occur in the presence of allyl alcohol, suggesting that (a) S atoms have a lifetime of the order of 10^6 collisions or more with H_2O without oxidation (as suggested by carrier experiments with KCl[3b]) and (b) that allyl alcohol scavenges S atoms as indicated in the experiments with neutron-irradiated KCl.

References and Notes

(1) This work has been supported in part by the U. S. Atomic Energy Commission under Contract No. AT(11-1)-1715 and by the W. F. Vilas Trust of the University of Wisconsin.

(2) Additional details of this investigation are given in the Ph.D. Thesis of J. L. Giulianelli, University of Wisconsin, 1969.

(3) (a) R. C. Milham, Ph.D. Thesis, University of Wisconsin, Madison, Wis., 1952; (b) R. C. Milham, A. Adams, and J. E. Willard in "Chemical Effects of Nuclear Transformation," Vol. II, IAEA, Vienna, 1965, p 31; (c) A. G. Maddock and R. M. Mirsky in "Chemical Effects of Nuclear Transformations," Vol. II, IAEA, Vienna, 1965, p 41.

(4) C. Chiotan, I. Zamfir, and M. Szabo, *J. Inorg. Nucl. Chem.*, **26**, 1132 (1964); C. Chiotan, M. Szabo, I. Zamfir, and T. Costia, *J. Inorg. Nucl. Chem.*, **30**, 1377 (1968).

(5) C. W. Owens and J. R. Hobbs, *J. Phys. Chem.*, **73**, 1956 (1969).

(6) K. Yoshihara, Ting-Chia Huang, H. Ebihara, and N. Shibata, *Radiochim. Acta*, **3**, 185 (1964).

(7) M. Kasrai and A. G. Maddock, *J. Chem. Soc. A*, 1105 (1970).

(8) H. E. Gunning and O. P. Strausz in "Advances in Photochemistry," Vol. 4, Interscience, New York, N. Y., 1966, p 143.

(9) C. Ciuffarin and W. A. Pryor, *J. Amer. Chem. Soc.*, **86**, 3621 (1964).

(10) D. P. Ames and J. E. Willard, *J. Amer. Chem. Soc.*, **73**, 164 (1951).

(11) J. P. Adloff and J. P. Meyer, *Radiochim. Acta*, **7**, 15 (1967).

(12) K. Gollnick and E. Leppin, *J. Amer. Chem. Soc.*, **92**, 2217 (1970); E. Leppin and K. Gollnick, *ibid.*, **92**, 2221 (1970).

(13) D. A. Stiles, R. Kewley, O. P. Strausz, and H. E. Gunning, *Can. J. Chem.*, **43**, 2442 (1965).

Solid-State Study of the Potassium Nitrosodisulfonate Radical

Thomas E. Gangwer[1]

Department of Chemistry and Physics, Wake Forest University, Winston-Salem, North Carolina 27106 and Department of Chemistry, University of Notre Dame, Notre Dame, Indiana 46556 (Received May 21, 1973; Revised Manuscript Received October 5, 1973)

The esr and optical properties of the potassium nitrosodisulfonate radical trapped in the host potassium hydroxylaminedisulfonate crystal matrix are reported. Evidence is presented which indicates room temperature near-neighbor proton and low-temperature radical pair interactions occur in the X-irradiated crystals. These interactions are estimated to involve approximate distances of 2.3 and 6.4 Å, respectively. A broad absorption in the 360-nm range produced upon irradiation at 77°K is correlated with the radical pairs. A hydrogen-bonded configuration for the potassium hydroxylaminedisulfonate molecules in single crystals is proposed which correlates with the esr results.

Introduction

The esr properties of the nitrosodisulfonate radical, $(KSO_3)_2NO$, in single crystals of potassium hydroxylaminedisulfonate, $(KSO_3)_2NOH$, have been reported.[2] Parke, et al.,[3] reported the first esr study of the nitrodisulfonate radical. In aqueous solutions, Fremy's salt dissociates to form the $(SO_3^+)_2NO$ radical which has three equal intensity peaks with isotropic splitting of 13.0 G.[4] Equivalent esr spectra are obtained from dilute solid solutions of $(KSO_3)_2NO$ in $(KSO_3)_2NOH$ and room temperature X-irradiated $(KSO_3)_2NOH$. Thus, X-irradiation of single crystals of $(KSO_3)_2NOH$ and its deuterated analog yield radicals identical with the $(KSO_3)_2NO$ radical prepared by chemical means. Decomposition of this radical, observed in solution, is found also in the solid state. The single crystal esr spectra, which showed site splitting, were consistent with crystal X-ray diffraction data[5] where the host $(KSO_3)_2NOH$ compound was determined to be monoclinic. The hyperfine coupling constants and g values for this system, X-irradiated at room temperatures, have been reported.[2a]

Zeldes and Livingston[6] reported the first esr study on the simultaneous change in spin state of an unpaired electron and neighboring nuclei. They assigned the satellite lines in the spectra of atomic hydrogen trapped in frozen acids to the simultaneous flip of the atomic hydrogen electron spin and a neighboring hydrogen nuclear spin. Trammell, et al.,[7] developed a theoretical interpretation of this phenomenon. Proton satellite lines have been reported in various esr studies.[8] The esr spectra of the $(KSO_3)_2NO$ radical trapped in $(KSO_3)_2NOH$ contains satellite lines which are shown to be due to near-neighbor proton interactions and are treated using Trammell's equations.

Kurita and Kashiwagi[9] reported the first esr study on intermolecular exchange interaction between free-radical pairs. Intermolecular radical pair exchange interactions, giving rise to a triplet state, have been subsequently investigated for various systems.[10,11] Low-temperature irradiation of crystals of hydroxyurea has shown esr spectral splittings attributed to pair-wise trapping of free radicals.[11] X-irradiation of $(KSO_3)_2NOH$ at 77°K yields $[(KSO_3)_2NO]_2$ radical pairs. The esr and ultraviolet-visible spectra of these radical pairs will be discussed.

The crystal structure of Fremy's salt was determined by Moser and Howie.[12] Using this closely related system as a model, the environment of the $(KSO_3)_2NO$ radical trapped in crystalline $(KSO_3)_2NOH$ is discussed.

Experimental Section

Potassium nitrosoaminedisulfonate (Fremy's salt) was prepared by the method of Moser and Howie.[12] Potassium hydroxylaminedisulfonate was prepared by the method of Palmer.[13] Both salts were recrystallized from a pH 8 buffered solution of potassium acetate–acetic acid and stored in a refrigerator. Potassium deuterioxylaminedisulfonate was prepared by repeated recrystallization of the hydroxyl salt from pH 8 anhydrous potassium acetate buffered D_2O. The extent of deuteration was determined to be greater than 90% by comparison of the areas of the infrared hydroxyl and deuterioxyl absorptions.

Single crystals of sufficient size for easy manipulation (4–8 mm long and 1–1.5 mm thick) were prepared by slow evaporation (in a refrigerated desiccator containing P_2O_5) of pH 8 potassium acetate–acetic acid buffered solutions saturated with the appropriate salt. The mixed crystals of $(KSO_3)_2NO$ trapped in $(KSO_3)_2NOH$ were prepared by dissolving sufficient amounts of Fremy's salt to give a deep blue color to the $(KSO_3)_2NOH$ saturated solution. Needle-shaped crystals were grown in 2–5 days.

Comparison of the infrared spectra of these crystals with the literature[12,14] confirmed their composition. X-Ray crystallographic data for these monoclinic crystals previously reported[2a] was improperly labeled. The reported values correspond to the d_{hkl} spacings. The unit cell dimensions, which are related to the d_{hkl} spacings through the angle $\beta = 150°\ 50'$, are $a = 10.12$ Å, $b = 6.51$ Å, and $c = 14.69$ Å.[5] Figure 1a shows the appearance of the crystal and the experimental orthogonal axes.

The potassium hydroxylaminedisulfonate and potassium deuterioxylaminedisulfonate are colorless, transparent crystals before X-irradiation, but have the same blue color as the mixed crystals after being damaged at room temperature. Irradiation at 77°K yielded yellow crystals.

The crystals were irradiated on a Picker X-ray machine operating at 20 mA and 50 kV giving an estimated dosage of 60,000 R/min. For low temperature work, single crystals were mounted on optical or esr cryotip apparatus,[11] cooled to liquid nitrogen temperature and X-irradiated *in situ*. Visible spectra were recorded on a Beckmann DK-2A
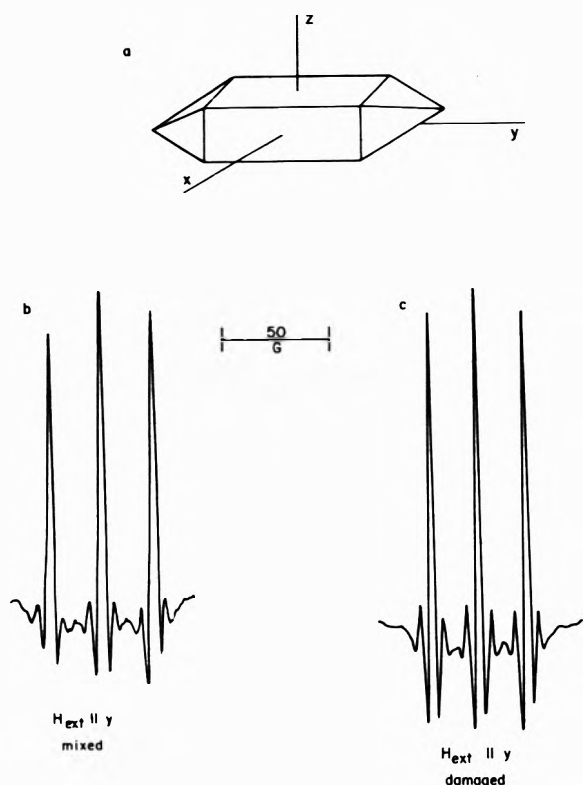
Figure 1. Crystal habit, assigned orthogonal axes, and second derivative esr spectra of the $(KSO_3)_2NOH$ crystals. The spectra confirm the assignment of the X-irradiated radical as equivalent to $(KSO_3)_2NO$.

Figure 2. Absorption spectra of the $(KSO_3)_2NO$ radical. The spectra have been shifted vertically for clarity in presentation: (a) baseline for matched crystal halves; (b) X-irradiated $(KSO_3)_2$-NOH single crystal at room temperature; (c) X-irradiated $(KSO_3)_2NOH$ single crystal at $-197°$; (d) $(KSO_3)_2NO$ in water.

Figure 3. Second derivative spectra of $(KSO_3)_2NO$ generated in $(KSO_3)_2NOH$ and $(KSO_3)_2NOD$ single crystals by X-irradiation.

spectrometer, infrared spectra on a Perkin-Elmer 521 grating spectrometer, and esr spectra on a Varian X Band spectrometer. The investigation of the crystalline state in the visible region was conducted by using matched halves of single crystals in the sample and reference chambers. Esr spectra were recorded by rotating the magnetic field about the axes shown in Figure 1a using a Varian V4533 rotating cavity.

The $(KSO_3)NOH$ and $(KSO_3)_2NOD$ single crystals prepared in this study decompose. The crystals first appear cloudy in the center, with decay proceeding outward, yielding a white, opaque, sticky residue. The stability of the crystals is increased by repeated recrystallization from acetate buffer solution and refrigeration. The purest salts decompose (in the presence or absence of air) within 2 days at room temperature but decay slowly over several months when refrigerated. Crystal halves irradiated with X-rays decomposed uniformly throughout the whole crystal within 12 hr while unirradiated halves decomposed from the center outward over several days at room temperature. An infrared study of the solid products formed by decomposition of $(KSO_3)_2NOH$ in solution and of unirradiated and irradiated $(KSO_3)_2NOH$ single crystals showed them to be composed mainly of potassium sulfate.

Results

The esr spectra of the radicals trapped by growing mixed crystals of $(KSO_3)_2NO$ and $(KSO_3)_2NOH$ and by X-irradiating $(KSO_3)_2NOH$ are given in Figure 1b and 1c for the orientation of the external magnetic field along the y crystal axis. The esr spectra for these two types of crystals have a one-to-one correspondence for all orientations of the crystals. The mixed and irradiated crystals exhibit
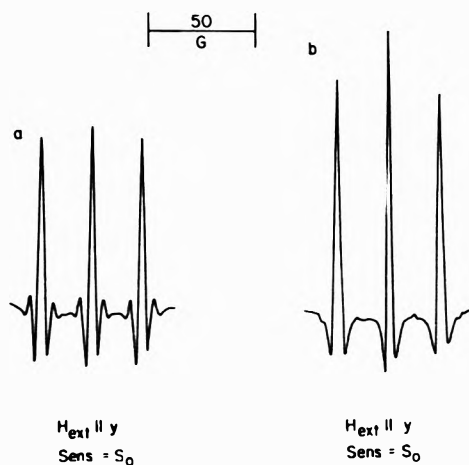
the blue color characteristic of the nitroso radical. The visible absorption spectrum of the aqueous solution of Fremy's salt and of irradiated $(KSO_3)_2NOH$ crystals are identical as shown in Figure 2.

The comparison in Figure 3 of corresponding esr spectra for $(KSO_3)_2NO$ trapped in $(KSO_3)_2NOH$ and $(KSO_3)_2$-NOD shows that satellite lines accompany each ^{14}N triplet line in the light hydrogen system. Due to the small hyperfine coupling of a deuterium nucleus as compared to a hydrogen nucleus, no satellite lines are resolved in the deuterioxylamine system. By varying the magnetic field sweep rate, the intensity of the high-field satellite line relative to the twin low-field line could be changed. Figure 4 shows the esr spectra and Figure 5 the resultant saturation curve of a microwave power study. Within the experimental error of the relative intensity measurements, the three main ^{14}N lines saturated along curve 1 and the outermost high- and low-field satellite lines saturated along curve 2. The microwave magnetic field H_1 was calculated using the relation given by Varian for their rotating cavity. The central ^{14}N lines progressively saturate as the satellite lines first increase (Figure 4a,b,c) before beginning to saturate (Figure 4d,e) slightly at high microwave powers. The spacing between each satellite and its main triplet line is, within experimental error, 5.2 G at a field
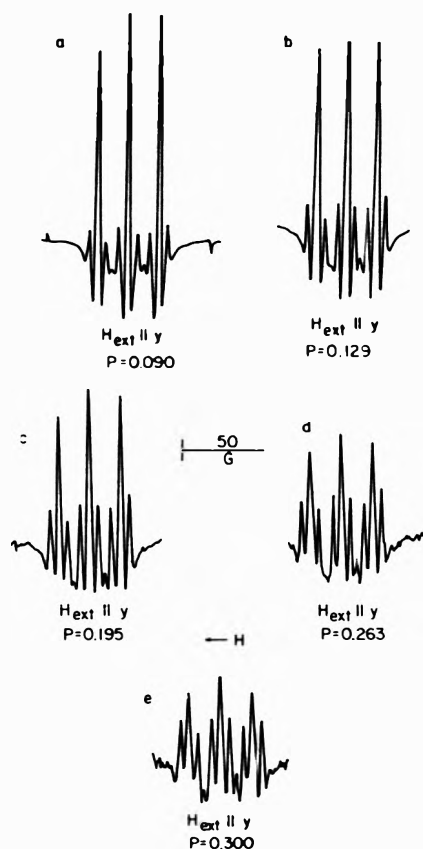
Figure 4. Microwave power saturation spectra.

Figure 5. The saturation behavior of the ^{14}N triplet (curve 1) and proton satellite (curve 2) transitions.

strength of 3370 G over all observed orientations. Over the microwave power range investigated the line widths of the satellite lines are constant and their line-shape parameters[15a,b] (ratio of maximum positive and negative slopes) approximate that for a Gaussian curve.

Upon X-irradiation of single crystals of (KSO3)2NOH or its deuterated analog at 77°K evidence of radical pairs was observed in the optical and esr spectra. The crystals have a yellowish color when irradiated at 77°K which disappears upon warming to room temperature. The broad optical absorption with λ(max) $\sim$360 nm shown in Figure 2 for these low-temperature studies is removed by annealing the crystal to room temperature. As shown in Figure 6 the esr spectra of the radical pairs were resolved upon conditioning the spectrometer to maximize the wings of the main triplet. Theoretically hyperfine patterns of intensities 1:2:3:2:1 should occur in the wings of the isolated radical absorption due to the interaction of the total radical pair spin with their ^{14}N nuclei. The low-temperature spectra are complex due to second-order interactions and site splitting as shown in Figure 6a,b. In orientations where site splittings do not occur, the theoretically predicted five-line radical pair peaks of 1:2:3:2:1 relative intensity are resolved as shown in Figure 6c,d. In accord with theory,[16] the ^{14}N hyperfine splitting in the (KSO3)2NO radical is twice the corresponding splitting of the radical pairs. Upon annealing, the esr spectrum shows a disappearance of the radical pair quintet and an increase in the isolated radical intensity. This behavior indicates nondestructive separation of some of the paired radicals occurs. Similar results have been reported for the hydroxyurea system.[11]

In addition to the satellite lines, orientation dependent proton splitting of the nitrogen triplet lines are observed.
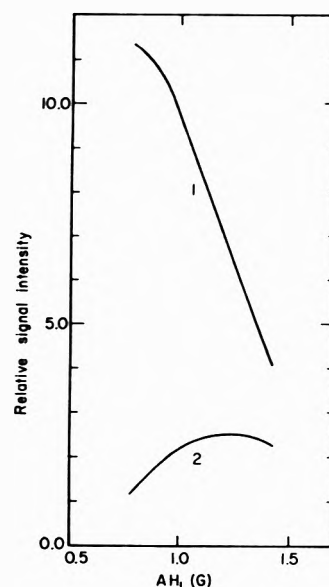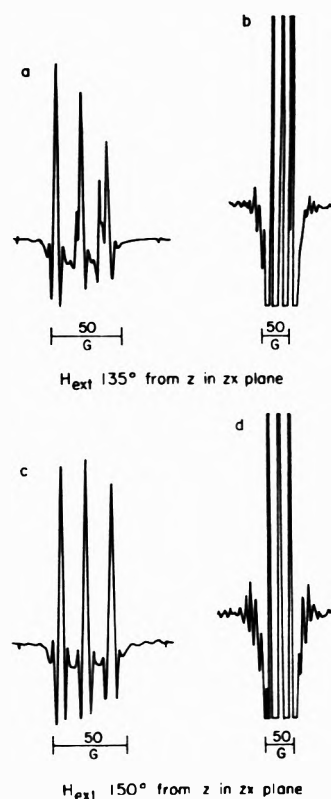
Figure 6. Second derivative spectra of a (KSO3)2NOH crystal X-irradiated at 77°K. The spectrometer was adjusted for maximum resolution of the radical pair coupling in spectra b and d.

Figure 7 shows esr spectra for an equivalent orientation of X-irradiated (KSO3)2NOH and its deuterated analog. The maximum proton splitting is resolved for the second and fourth lines in this orientation. From the small magnitude of the splitting and crystal structure considerations, this proton splitting is attributed to hydrogen bonding in (KSO3)2NOH dimer units. From crystal structure considerations, the near-neighbor and hydrogen bond splittings appear to arise from the same proton.
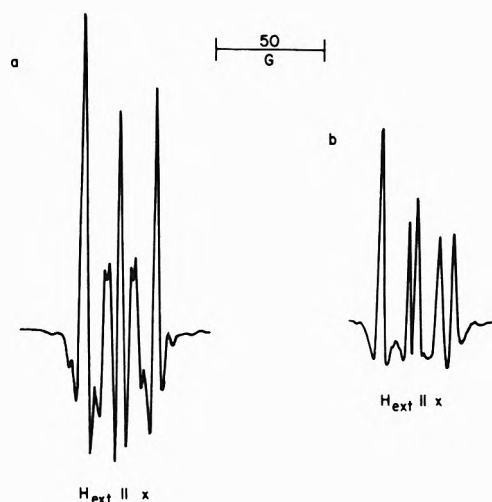
Figure 7. Comparative spectra of X-irradiated $(KSO_3)_2NOH$ and $(KSO_3)_2NOD$ for the orientation where the maximum hydrogen bonded proton coupling occurs.

Discussion

The radical and its environment created by irradiating $(KSO_3)_2NOH$ is equivalent to the $(KSO)_2NO$ radical trapped in this host crystal from solution as shown by the esr (Figure 1) and optical (Figure 2) spectra. The magnetic equivalence of these two systems shows the predominant mode of cleavage under X-irradiation occurs in the O–H bond as opposed to the N–O or N–S bond. The observed unpaired spin density on the ^{14}N is 0.40 indicating delocalization onto the oxygen.

The satellite lines, shown by deuteration studies (Figure 3) to arise from interaction with hydrogen nuclei, exhibit the behavior given by Zeldes and Livingston[6] for second-order hydrogen nucleus interactions. Theoretically,[7] this spacing is $\pm g_n B_n H$ corresponding to the proton resonance frequency in the experimental magnetic field H. The experimental 5.2 G compares well with the calculated 5.1-G spacing. In the present system only one near-neighbor proton per $(KSO_3)_2NO$ radical was detected. Applying Trammell's theory for near-neighbor interactions to this system, a distance of 2.3 Å is calculated for the effective distance r_{eff} between the atoms on which the unpaired electron spin density is concentrated and the hydrogen nucleus giving rise to satellite lines.[17] Values of r_{eff} in frozen acid systems fall in the 1.7–1.9-Å range.[6,8b,e] The transition probabilities for such spin-flip transitions have been established[7] and experimentally found[18] to be appreciable for distances out to ~ 3 Å.

The saturation behavior of the line width and line shape in Figure 4 and saturation curve in Figure 5 for the satellite lines approximates ideal inhomogeneous line broadening.[15] The unpaired electron–near neighbor proton configuration of the present system is consistent with this interpretation since inhomogeneous broadening involves interactions arising outside the unpaired electron spin system which vary slowly with respect to the average spin transition times of the unpaired electron. Dipolar, anisotropic hyperfine interaction between the unpaired electron spin and the adjacent hydrogen nuclear spin gives rise to the main part of the broadening. The proton, strongly coupled to the lattice *via* its chemical bond in the neighboring $(KSO_3)_2NOH$ molecule, results in a short spin lattice relaxation time T_1 such that the satellite lines do not readily saturate at high power.

At 77°K the optical (Figure 2) and esr (Figure 6) transitions for radical pairs are observed. The yellow crystal color and 360-nm absorption correlate with the esr spectral change upon annealing showing these properties arise from the radical pairs. The radical pair consists of two $(KSO_3)_2NO$ radicals in proximity such that exchange interaction between the unpaired electrons of the two radicals occurs.[16] Similar color and esr spectral changes with annealing were reported for the radical pairs observed in hydroxyurea crystals.[11]

The paramagnetic properties arising from these radical pairs are readily studied by esr. The large doublet splitting in Figure 6 is due to the anisotropic dipole–dipole interaction of the two electron spins and the hyperfine quintet structure arises from coupling with the two ^{14}N nuclei. From the dipolar splitting[11] a distance of 6.4 Å is calculated for the separation between the unpaired electron spin density sites of the coupled radicals in the present system.

The visible spectra of a single crystal of $(KSO_3)_2NOH$ X-irradiated at 77°K (Figure 2) shows a broad absorption in the 360-nm range which disappears upon annealing and is attributed to an electronic transition of the radical pair. The origin of this absorption is probably a charge transfer transition since this interaction would be expected to be dominant in radical pairs.[19a] Wiersma, *et al.*,[19] correlated an absorption in the visible region with the diphenylamino radical pair using annealing techniques and theoretical calculations. A charge transfer transition analogous to the diphenylamino system[19b] is proposed to explain the 360-nm band in the present system.

A detailed crystal structure determination of $(KSO_3)_2$NOH was not attempted due to the chemical instability of the crystals. Crystallographic studies on systems containing hydroxylamine (R_2NOH) groups reveal a common intermolecular structural arrangement of the NOH groups[20-23] shown in Figure 8 where the nitrogen and oxygen atoms of the hydrogen bonded network are approximately coplanar.

Studies of the closely related $(KSO_3)_2NO$ crystals revealed a dimorphic behavior.[12] Spectroscopic results on crystals grown from solution at temperatures below 30° have been interpreted in terms of a dimer formed through a peroxide linkage of two $(KSO_3)_2NO$ molecules.[12,14] For crystals grown above 30°, a crystallographic study[12b] showed the molecules to be paired *via* their nitroso groups forming a coplanar network analogous to that of Figure 8 if the hydrogen atoms are eliminated. Although separated by large distances, other molecules containing nitroso groups display a similar head-to-tail arrangement of their nitrogen and oxygen atoms in the crystalline state.[24]

Although only differing in chemical composition by a hydrogen atom, the present $(KSO_3)_2NOH$ system does not exhibit any dimorphic character.[25] Considering the tendency toward a head-to-tail arrangement of the nitroso groups in crystals and the formation of hydrogen bonded networks in molecules containing hydroxylamine groups, it seems reasonable to propose the existence of the hydrogen bonded dimer unit shown in Figure 8 for the $(KSO_3)_2$-NOH crystals.

The unirradiated, high-temperature form of Fremy's salt is paramagnetic and, from susceptibility studies, a weak covalent bond between the two molecules forming the dimer is proposed.[12] This exchange of electron density supports the proposed hydrogen bonded dimer of $(KSO_3)_2$-NOH. Inclusion of hydrogen atoms in the $(KSO_3)_2NO$
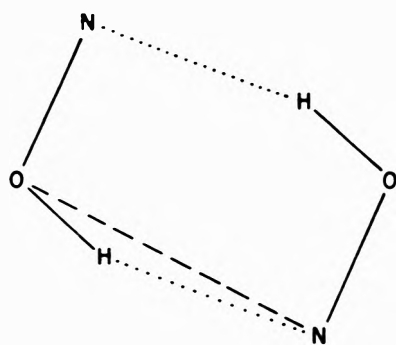
Figure 8. The coplanar head-to-tail configuration in crystals for the nitrogen and oxygen atoms of the dimer unit $(R_2NOH)_2$. The R substituents are not shown.

dimer provides an improved path for electron exchange which eliminates the paramagnetic behavior (*i.e.*, $(KSO_3)_2$-NOH crystals are diamagnetic). The availability of hydrogen atoms for hydrogen bonding stabilizes the intermolecular head to tail configurations of the nitroso groups of molecules in their crystalline state. Upon room temperature X-irradiation, one hydrogen atom leaves the dimer unit and results in a paramagnetic site whose interactions can be correlated with this interpretation of $(KSO_3)_2NOH$ crystal structure. Thus the configuration parameters estimated for the hydrogen bonded network based on the present esr data are consistent with the crystal structure data for the high temperature form of Fremy's salt.

The orientational dependent splitting of the nitrogen triplet by the near-neighbor proton indicates the proton interaction is not pure second order. In certain orientations the angle between the resultants of the external magnetic field and the electronic magnetic field is such that the first-order transitions of this proton occur with appreciable probability. This supports the hydrogen bonding scheme since for purely second-order interaction the nuclei do not share the electron for a significant time. Delocation of unpaired spin density onto the nitroso oxygen atom provides increased coupling to the near-neighbor proton. Thus the proposed hydrogen bonded network in Figure 8 is consistent with the esr data indicating the hydrogen bonded proton and near-neighbor proton are one in the same.

Acknowledgment. The author would like to thank Wake Forest University for the graduate assistanceship. Discussions concerning the experimental portion of this research with Dr. P. J. Hamrick are acknowledged. Thanks are due Dr. W. Baird for assistance with the X-ray crystal data.

References and Notes

(1) Present address. Department of Chemistry, Brookhaven National Laboratory. Upton, N. Y. 11973.
(2) (a) P. J. Hamrick, H. Shields, and T. Gangwer. *J. Chem. Phys.*, **57,** 5029 (1972); (b) S. I. Weissman and D. Banfill, *J. Amer. Chem. Soc.*, **75,** 2534 (1953).
(3) G. E. Parke, J. Townsend, and S. I. Weissman, *Phys. Rev.*, **85,** 683 (1952).
(4) M. S. Blois, Jr., "Free Radicals in Biological Systems," Academic Press, New York, N. Y., 1961, p 186.
(5) W. Baird and T. Gangwer, data reported in ref 1.
(6) H. Zeldes and R. Livingston, *Phys. Rev.*, **96,** 1702 (1954).
(7) G. T. Trammell, H. Zeldes, and R. Livingston, *Phys. Rev.*, **110,** 630 (1958).
(8) (a) W. Snipes and W. Bernhard, *J. Chem. Phys.*, **43,** 2921 (1965); (b) W. Kohnlein and J. H. Venable, *Nature (London),* **215,** 618 (1967); (c) W. Bernhard and W. Snipes, *J. Chem. Phys.*, **44,** 2817 (1966); (d) M. T. Rogers and L. D. Kispert, *J. Chem. Phys.*, **46,** 221 (1967); (e) J. Helbert and L. Kevan, *J. Chem. Phys.*, **58,** 1205 (1973); (f) L. J. Libertin and O. H. Griffith, *J. Chem. Phys.*, **53,** 1359 (1970).
(9) Y. Kurita and M. Kashiwagi, *J. Chem. Phys.*, **44,** 1727 (1966).
(10) R. W. Fessenden and R. H. Schuler, *Advan. Radiat. Chem.*, **2,** 1 (1970).
(11) K. Reiss and H. Shields, *J. Chem. Phys.*, **50,** 4368 (1969).
(12) (a) W. Moser and R. A. Howie, *J. Chem. Soc. A*, 3039 (1968); (b) W. Moser and R. A. Howie, *ibid.*, 3043 (1968).
(13) W. G. Palmer, "Experimental Inorganic Chemistry," Cambridge University Press, London, 1959, p 279.
(14) S. Yamada and R. Tsuchida, *Bull. Chem. Soc. Jap.*, **32,** 721 (1956).
(15) (a) J. Zimbrick and L. Kevan, *J. Chem. Phys.*, **47,** 2364 (1967); (b) J. Zimbrick and L. Kevan, *ibid.*, **47,** 5000 (1967); (c) S. K. Wong and J. K. S. Wan, *ibid.*, **55,** 4940 (1971).
(16) W. Gordy and R. Moorehouse, *Phys. Rev.*, **151,** 207 (1966).
(17) Following the submission of the present manuscript, it was brought to my attention by Dr. L. Kevan that the calculation of the near-neighbor proton distance *r* from the satellite–main line intensity ratio data should be based on unsaturated data. Such data for the ^{14}N line were not experimentally accessible. The value of $r = 2.3$ Å is based on the intensity ratio occurring when the ^{14}N intensity is a maximum. This procedure results in the *r* value being a lower limit. Since *r* is proportional to the sixth root of the intensity ratio, it is not extremely sensitive to errors in the ratio. For the present system an error in the intensity ratio of 300% results in a change in r of 20% which should be an upper limit for the error in the data.
(18) A. Horsfield, J. R. Morton, J. R. Rowlands, and D. H. Witten, *Mol. Phys.*, **5,** 241 (1962).
(19) (a) D. A. Wiersma and J. Kommandeur, *Mol. Phys.*, **13,** 241 (1967); (b) D. A. Wiersma, J. H. Lichtenbelt, and J. Kommandeur, *J. Chem. Phys.*, **50,** 2794 (1969).
(20) W. C. Hamilton, *Acta Crystallogr.*, **14,** 95 (1961).
(21) I. K. Larsen and B. Jerslev, *Acta Chem. Scand.*, **20,** 983 (1966).
(22) T. K. Bierlein and E. C. Lingafelter, *Acta Crystallogr.*, **4,** 450 (1951).
(23) E. A. Meyers and W. N. Lipscomb, *Acta Crystallogr.*, **8,** 583 (1955).
(24) (a) P. G. Tsoucaris, *Acta Crystallogr.*, **14,** 914 (1961); (b) E. L. Eichhorn, *ibid.*, **9,** 787 (1956); (c) K. Folting, B. Jerslev, and W. N. Lipscomb, *ibid.*, **17,** 1263 (1964).
(25) The esr spectra of X-irradiated $(KSO_3)_2NOH$ are equivalent for crystals grown over the temperature range 5–40°.

Effect of Dimer Formation of the Electronic Absorption and Emission Spectra of Ionic Dyes. Rhodamines and Other Common Dyes

Richard W. Chambers,[1] Takashi Kajiwara, and David R. Kearns*

Department of Chemistry, University of California, Riverside, California 92502   (Received August 24, 1973)

Publication costs assisted by the U. S. Public Health Service

The visible absorption, excitation, fluorescence, and phosphorescence spectra have been measured for the monomeric and dimeric forms of rhodamine B and sulforhodamine B (Figure 1). Dimer fluorescence and phosphorescence spectra were assigned through the use of excitation spectroscopy, and polarized excitation spectra were used to determine the polarization of the dimer absorption bands relative to the dimer fluorescence and phosphorescence emission. The most unexpected finding of these studies is that all major bands associated with the lowest $S_0 \rightarrow S_1$ transition of the dimer have the same polarization. Simple exciton theory in which vibronic interactions are neglected cannot account for the polarization of the dimer absorption spectra, but with the inclusion of vibronic interaction it is possible to account for the polarization of all bands except the origin band. To account for the "anomalous" polarization properties of the origin band it is suggested that the two molecules in the dimer are not equivalent, perhaps due to different orientation of phenyl substituents. The theoretical interpretation of the absorption automatically accounts for the anomalous intensity distribution in the dimer emission and the $\sim$10-fold increase in the fluorescence lifetime produced by dimerization. Less complete results obtained with some eosin, and acridine dyes serve to confirm the generality of the effects observed with the rhodamine dyes.

Introduction

The widespread use of dyes in dye lasers[2-7] and in various photosensitized reactions[8-13] has generated a renewed interest in the excited-state properties of dyes. Since many of the commonly used dyes tend to aggregate and form dimers in solutions, a number of the studies carried out during the past 10 years have been concerned with understanding the spectral effects produced by dimerization.[14-33]

In the experimental studies which have been carried out so far, the emphasis has been on measurement of spectral shifts of bands, hypochromism, and changes in vibronic structure produced by dimerization. Insofar as we are aware, there has been no measurement of the polarization of the electronic transitions in the dimers, despite the fact that most theoretical treatments of dimer spectra give strong predictions regarding the polarization of transitions in the dimer. Thus, an important experimental parameter for testing theories of dimer spectra has not previously been measured. Perhaps an even more serious problem was recently raised by the studies of Ferguson and Mau,[33] who demonstrated that many spectral changes previously attributed to dimerization were actually the result of an acid–base equilibrium.

In the present study we have reexamined the conditions which we previously used to obtain dye monomer and dimer spectra[26,27] and have specifically tested for the role of pH on the spectra. Polarized emission and excitation spectra have been used to determine the relative polarizations of bands in both the monomer and dimer absorption spectra. As we shall show, the simple exciton theory in which vibronic interactions are neglected cannot account for the polarized dimer spectra. With the inclusion of interactions between vibronic levels of the lowest excited singlet state, it is possible to account for the polarization of the major dimer absorption bands. In order to account for the polarization of the origin band of the dimer fluorescence, however, it is necessary to invoke some sort of local asymmetry.

Materials and Methods

Chemicals. In the present study we have used the following dyes: sulforhodamine and rhodamine B (Chroma-Gesellschaft Schmid Co.), eosin B (MCB), eosin Y (Eastman), acriflavine (K and K Laboratories), proflavine (nutritional Biochemicals), and acridine Orange (Baker Chemical). The structures of these different dyes are shown in Figure 1. Generally the dyes were used as received from the manufacturer after a chromatographic examination indicated that impurities present had no deleterious effect on the spectral measurements.

Spectroscopic Measurements. Most of the spectroscopic studies were carried out using a previously described fluorophosphorimeter[26,27] which permitted both fluorescence and phosphorescence excitation spectra as well as emission spectra to be measured. Polarized excitation and emission spectra were obtained by incorporating a Glan-Thompson polarizer on the output side of the exciting monochromator and a polarizing sheet in front of the detector. Although a 90° configuration with respect to the exciting and emitted light was used for most of the experiments, a 180° configuration was used in the polarization experiments. Most spectroscopic measurements were carried out at 77°K (although some room temperature data are reported) and several different solvent systems were used. In order to obtain monomer spectra, the dyes were dissolved in either a 9:1 mixture of ethanol and methanol or in EPA (diethyl ether, isopentane, and ethanol in a ratio of 5:5:2). To obtain dimer spectra, aqueous solutions containing 10 M LiBr or 10 M LiCl were used since the dyes have a greater tendency to aggregate in this solvent at low temperature.

All excitation spectra reported in this paper have been corrected for the nonuniform spectral distribution of the exciting light from the monochromator, but only the rhodamine B and sulforhodamine B fluorescence spectra have been corrected for the spectral response of the detector system (0.25 M Jarrel Ash monochromator and RCA 7265 photomultiplier).
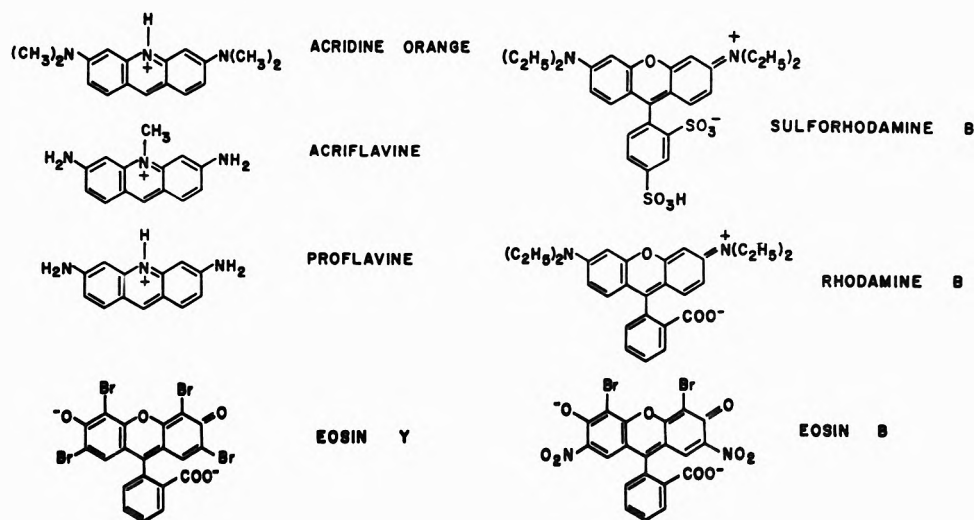
Figure 1. Structures of the dyes studied.

In order to have high sensitivity in the polarized fluorescence and phosphorescence excitation spectra measurements and to eliminate polarization effects in the detection system, the emission (phosphorescence or fluorescence) was monitored through a band pass filter rather than a monochromator.

Fluorescence lifetime measurements were obtained with a nanosecond lifetime apparatus constructed in this laboratory according to the design of Ware.[34] Interference filters were used to separate fluorescence emission from the exciting light.

Authentication of Monomer and Dimer Spectra. Depending upon the dye concentration, solvent, and temperature used in the experiments, it is possible to have dyes present as monomers and/or dimers. It was necessary, therefore, to determine which species was responsible for the emission and to establish conditions where monomer or dimer emission could be observed separately. Furthermore, the results of Ferguson and Mau[33] regarding pH effects on dye spectra raised serious questions regarding some spectra previously attributed to dimers. For this reason the effect of pH on some low-temperature spectra was also studied.

Monomer absorption spectra were easily obtained at room temperature in dilute (10^{-5} M) alcohol solutions and upon cooling these samples to 77°K there were no changes in the spectra except for expected improvement in the resolutions. From earlier work we know that dimer formation is promoted in aqueous 10 M LiCl or LiBr solutions at 77°K.[26,27] From comparison of our low-temperature spectra obtained with previously published and assigned dimer spectra, we conclude that the dyes were almost exclusively present in the dimeric state in the concentrated salt solutions at 77°K.

The effect of pH on the spectral properties of rhodamine B, sulforhodamine B, and proflavine and the results of these experiments are shown in Figure 2. From a comparison of these spectra with the dimer spectra discussed below, it is clear that the spectra which we attribute to the dimer are not due to a change in the state of protonation of the monomeric form of the dye. In the aqueous solutions which we used to form the dimers at low temperatures, there is little change in the spectra of the rhodamines over a range of pH extending from about 4 to 12. In the case of the proflavine spectrum the range is smaller,
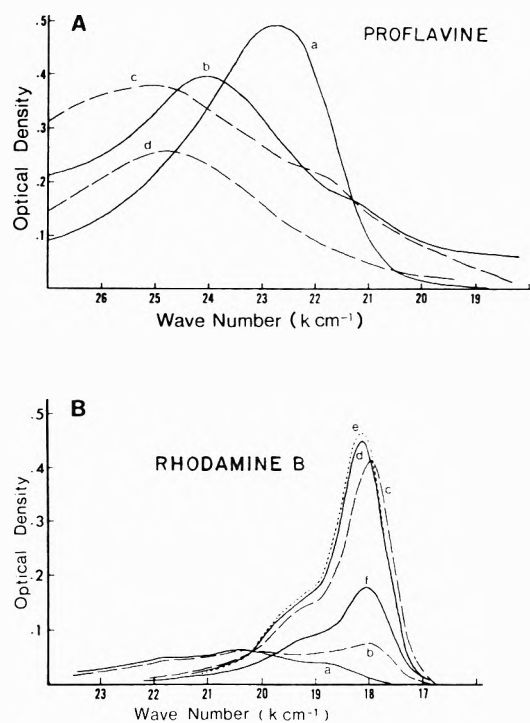
Figure 2. A. Effect of pH and temperature on the proflavine absorption spectrum: a, 1.8 × 10^{-5} M in H$_2$O–10 M LiCl, pH 3–5 at room temperature, monomer; b, 1.8 × 10^{-5} M in H$_2$O–10 M LiCl, pH ~3 at 77°K, dimer; c, 10^{-4} M in H$_2$O–13 N NaOH at 77°K; d, 10^{-4} M in H$_2$O–13 N NaOH at room temperature. B. Effect of pH on the absorption spectrum of rhodamine B (3.6 × 10^{-6} M) in H$_2$O at room temperature; a, 5 N HCl; b, pH − 0.2; c, pH 1.0; d, pH 3.7; e, pH 13.0; f, 5 N NaOH. Only slight changes in the spectra are observed in the pH range 3.7–13.0.

but it is clear that the spectra of the basic form is different from the dimer spectrum which are obtained in dilute solutions at low temperature. We therefore conclude that the problems which Ferguson and Mau encountered using *anhydrous* alcohol solutions appear to be absent in the aqueous solution we used.

Once authentic monomer and dimer absorption spectra were obtained, the emitting species were easily identified by measuring the fluorescence or phosphorescence excitation spectra of optically dilute samples. In the phosphorescence excitation measurements, the intensity of the
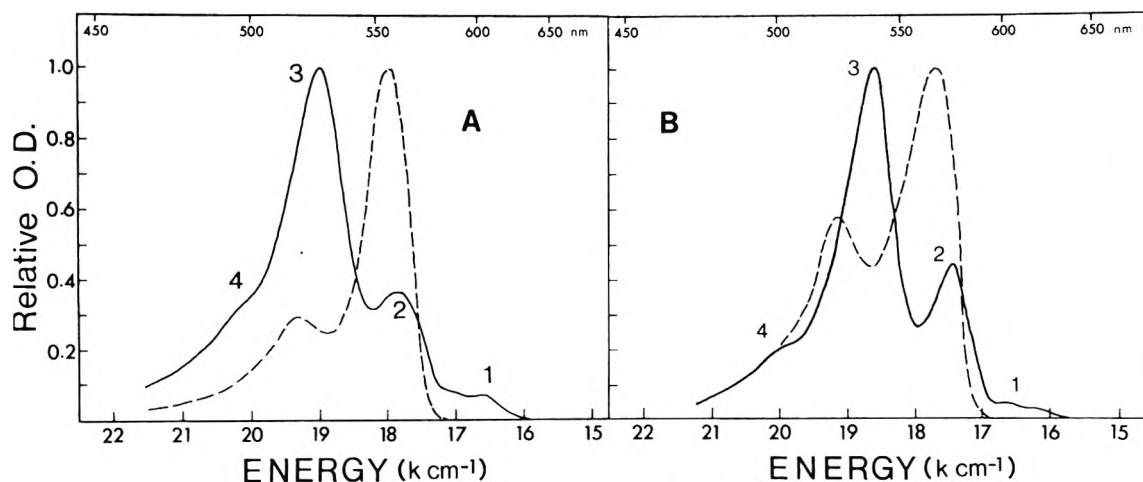
Figure 3. The 77°K absorption spectra of rhodamine B (10^{-4} M) and sulforhodamine B (10^{-4} M) dimers in 10 M LiCl–water (solid curve) and monomers in 9:1 ethanol:methanol solution (broken curve). Solutions were approximately 10^{-5} M. Individual bands (numbered 1–4) are discussed in the text: A, rhodamine B; B, sulforhodamine B.
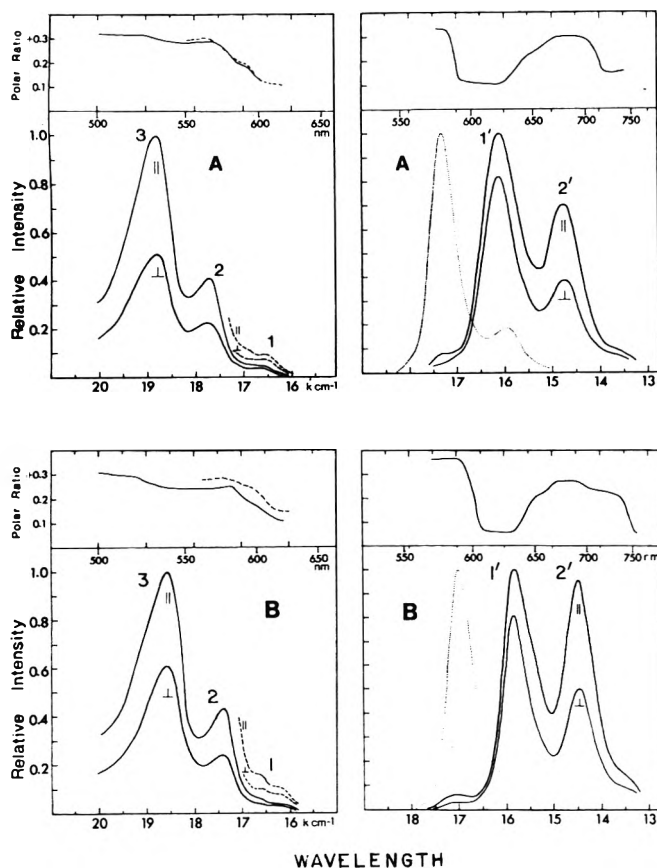
Figure 4. The polarized fluorescence excitation and emission spectra of rhodamine B and sulforhodamine B dimers in 10 M LiCl–water solutions at 77°K: A, rhodamine B; B, sulforhodamine B. The monomer emission spectra (shown by the dotted curves) were obtained using 50% ethanol–50% 9 M LiCl water solutions at 77°K. The polarization ratios of the dimer excitation and emission spectra are shown at the top of the figure. In the fluorescence excitation measurements the second fluorescence band was monitored (650–710 nm). A part of the spectra measured at higher sensitivity is also shown by broken lines to show the detailed structure at lower energy region. The small band which is observed at the high energy side of the dimer fluorescence, and which gives a high polarization ratio, is due to residual monomer fluorescence. The small shoulder on the lower energy side which gives a low polarization ratio is due to dimer phosphorescence.

phosphorescence was monitored at the peak of the phosphorescence while the wavelength of the exciting light was continuously varied throughout the visible region of the spectra. Fluorescence excitation spectra were obtained in a similar manner.

Results and Discussion

Using the procedures described above, monomer and dimer absorption and emission spectra were obtained and these results are presented in Figures 3–6. In each case we find that the long wavelength maximum of the absorption spectrum is *blue* shifted by dimerization and one or two relatively weak shoulders appear on the long wavelength side of the strong dimer band. Once the monomer and dimer absorption spectra were obtained, fluorescence and phosphorescence excitation spectroscopy were used to establish the authentic monomer and dimer emission spectra (compare Figures 3 and 4).

It is well known that dimerization or aggregation of dyes usually leads to a great reduction in the fluorescence quantum yield.[14,35] However, in the case of rhodamine B and sulforhodamine B some residual fluorescence was still observable even though the molecules were almost completely dimerized.[36] Through the use of excitation spectroscopy this residual fluorescence, which is shown in Figure 4, was established as authentic dimer fluorescence.[36] (Compare Figures 3 and 4.) Rhodamine B and sulforhodamine B appear to be unusual in this regard since none of the other dyes we studied exhibited measurable dimer fluorescence. The fact that dimer fluorescence was observed from these two dyes provided us with a unique opportunity to study the polarization properties of the dimer absorption spectra, and a preliminary account of this work has already been presented.[36]

Relative polarizations of the absorption and emission bands are a valuable source of information about the nature of the excited states of the dye monomers and dimers. Photoselection measurements were therefore carried out using phosphorescence and fluorescence emission on both monomers and dimers of the various dyes and the results of these experiments are presented in Figures 4 and 6. Since the measurements were conducted at 77°K, depolarization effects due to molecular rotation are absent and dye concentrations (10^{-5} M) were sufficiently low
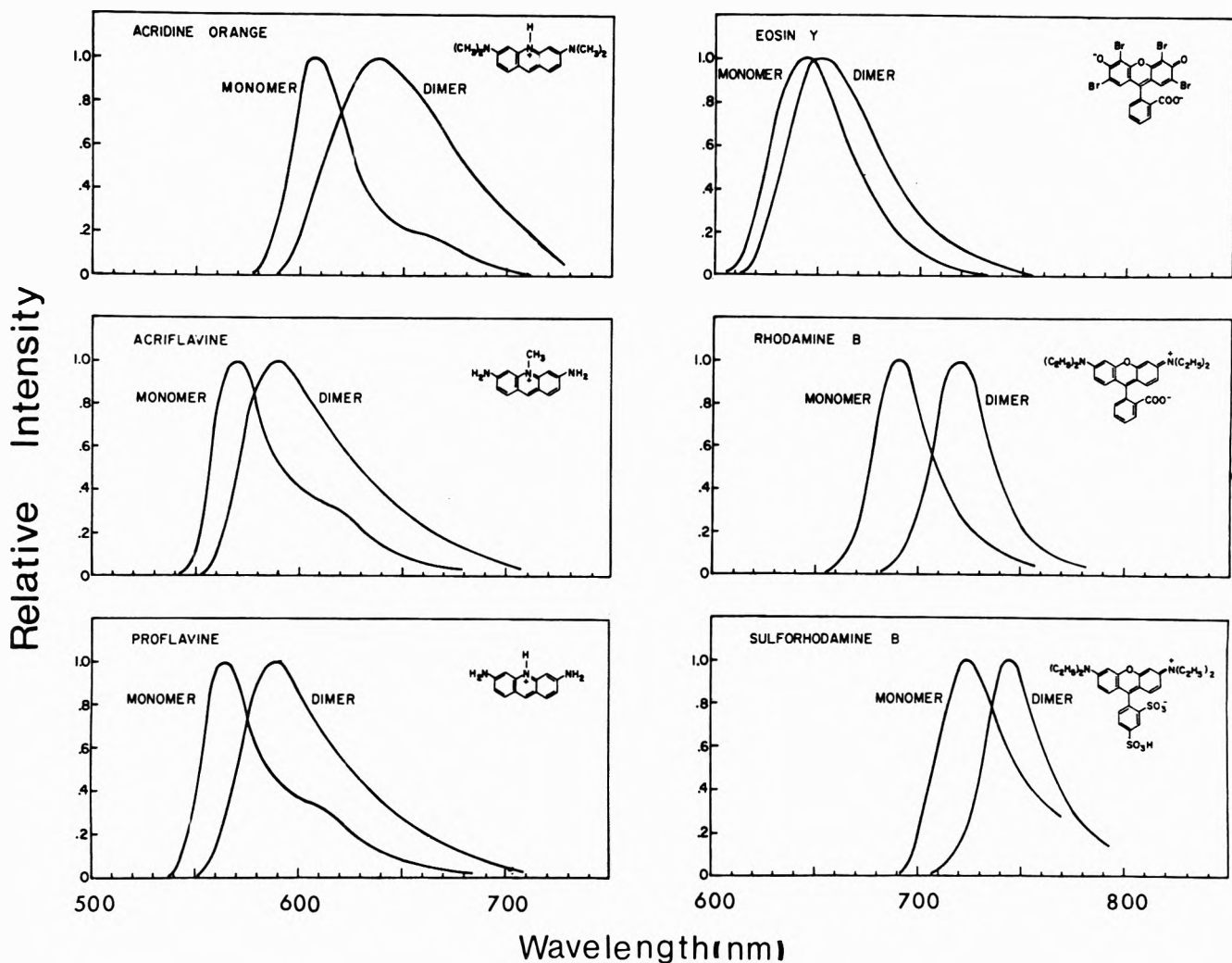
Figure 5. A comparison of the monomer and dimer 77°K phosphorescence emission spectra of six representative dyes. The monomer spectra were obtained using 10^{-5} M solutions in 1:1 ethanol–water containing 10 M LiBr. The dimer spectra were obtained using 10^{-5} M in water containing 10 M LiBr.
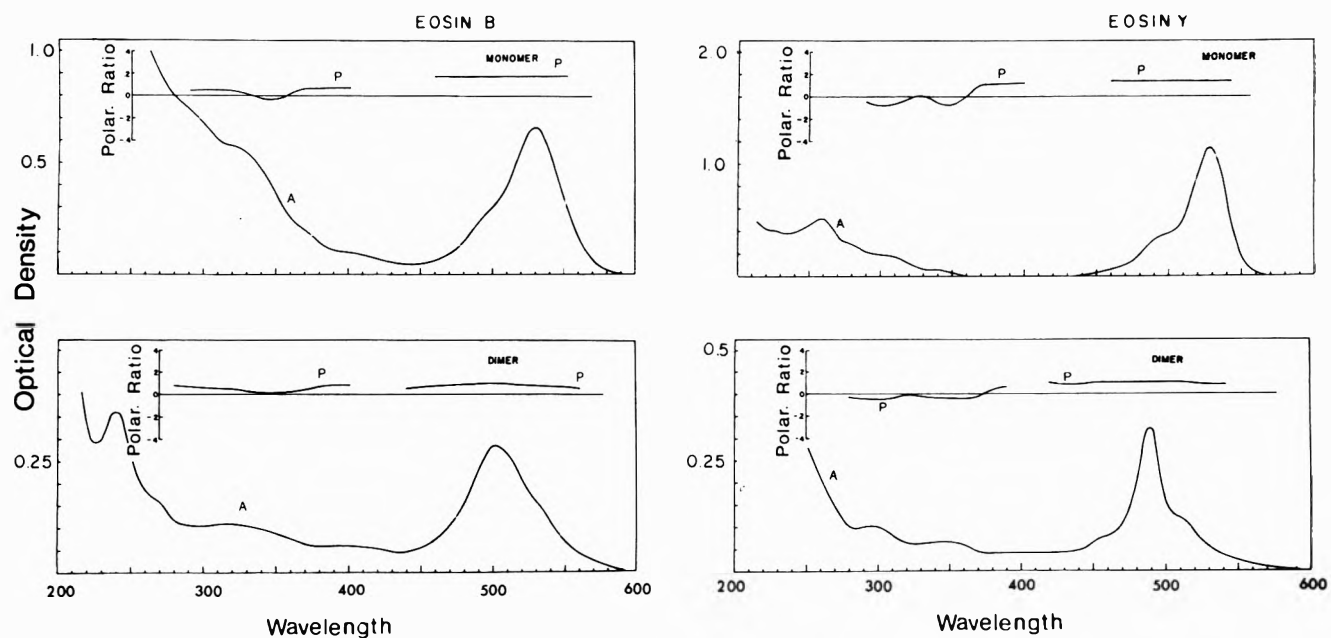
Figure 6. A comparison of the polarized phosphorescence excitation for the monomer and dimer of eosin B and eosin Y at 77°K. The monomer spectra were obtained using an aqueous alcohol solution and the dimer spectra were obtained using a 10 M LiCl aqueous solution: A, direct absorption spectrum; P, polarization ratio of the phosphorescence excitation spectrum.

Figure 7. A schematic drawing illustrating the effect of dimer formation on the spectroscopic properties of a dye according to simple exciton theory. In the dimeric state (D) the transition to the upper state is strong and polarized perpendicular to the weaker, lower energy transition.

that depolarization of the emission due to reabsorption effects was eliminated. A comparison of fluorescence polarization data obtained in an EPA glass at 77°K and in glycerol at room temperature demonstrated that uncracked EPA glass does not significantly depolarize the emission. With slow cooling, good quality glasses of aqueous 10 M LiCl were also obtained and used to obtain polarized dimer emission spectra.

Interpretation of the Rhodamine B and Sulforhodamine B Dimer Spectra. Since our most complete experimental results were obtained with rhodamine B and sulforhodamine B we discuss these two molecules first.

The absorption spectra of the monomeric and dimeric forms of rhodamine B and sulforhodamine B shown in Figure 3 illustrate the spectral changes which are typically noted with many dyes. Dimerization leads to a blue shift of the main absorption band, a slight loss of intensity in the low energy portion of the spectrum (hypochromism), and a reduction in the fluorescence quantum yield (usually complete quenching). Previously dimer spectra such as these have usually been interpreted in terms of a simple exciton model,[14,35,37-39] the results of which are schematically depicted in Figure 7. According to this theory the strong band in the dimer spectrum (band 3 in Figures 3 or 4) would be assigned to the allowed transition to the Ψ_+ state and the weaker, lower energy band in the dimer spectrum (band 2 in Figures 3 or 4) should have the opposite polarization and would be assigned as the "forbidden" transition to the Ψ_- state. Band 1, which is easily observed only in the low-temperature dimer spectrum of both sulforhodamine B and rhodamine B had not previously been reported since most of the earlier measurements were carried out at room temperature. The polarized fluorescence excitation and emission spectra for the dimer forms of these two molecules are shown in Figure 4.

In the absence of polarization data it appeared that the dimer absorption spectra could be qualitatively accounted for in terms of a simple exciton picture where the dimer symmetry is sufficiently low that there is incomplete cancellation of the transition dipole moment for the transition to the Ψ_- state.

Insofar as the theoretical interpretation of the dimer is concerned, however, the most significant observation is that the two strong absorption bands (bands 2 and 3) in the dimer spectra are positively polarized with respect to the 2' band in fluorescence. Furthermore, the origin band in absorption (band 1) is obliquely polarized with respect to bands 2 and 3 in absorption, and band 2' in emission.

Figure 8. A schematic diagram showing the relation between the energy levels of a sandwich dimer (D) and two monomers (M). This diagram has been drawn based on the zeroth-order resonance coupling theory which includes the vibronic effects but not configuration interaction between zeroth-order wave functions. The actual forms of zeroth-order wave functions are given in Table I. The positions of levels were determined based on absorption and fluorescence spectra of rhodamine B, the strongest absorption band and the weakest absorption band being fitted to level 5 and level 4, respectively. Relative intensities for various transitions are indicated by the thickness of the arrows and the polarizations of the transitions (relative to the strongest band) are indicated by $\pm$.

These polarization properties are simply not consistent with the simple exciton model. Since the true origin band has now been observed, band 1 might be reassigned as the transition to the Ψ_- state, but this assignment raises a problem with regard to the interpretation of the two stronger absorption bands (bands 2 and 3) since only one can be assigned as the transition to the Ψ_+ state. The dimer emission properties also pose serious problems for the simple exciton theory in two other important respects. First of all, the relative intensities of the $0 \rightarrow 0$ and $0 \rightarrow 1$ bands in the dimer emission spectrum (bands 1' and 2') are quite different from those found in the monomer emission spectrum. Secondly, the polarization properties of bands 1' and 2' differ from one another.

In order to account for these "anomalies" it is necessary to modify the simple exciton theory by taking into consideration the role of molecular vibrations and the vibronic coupling between various states of the dimer. Several different treatments of the effects of vibronic interaction on the electronic spectra of dimers have been published[40-46] so that only the essential results of these treatments need to be summarized here. Depending upon the strength of the electronic coupling between the two molecules there are two different theoretical limits that should be considered. In the weak coupling limit the electronic coupling is assumed to be smaller than the spacing between vibronic levels of the monomer, whereas in the strong coupling limit, the electronic coupling is larger than the spacing between vibronic levels. In view of the large changes which occur on dimerization, it would appear that the strong coupling limit is more appropriate to the case at hand. A schematic diagram showing how the monomer states correlate with those of the dimer in the strong coupling limit are shown in Figure 8. In this diagram the rel-

TABLE I: Wave Functions Used to Describe the Dimer States in the Strong Coupling Limit (see Figure 8)[a]

Ground Electronic States

$$\Psi_1{}^+ = \Phi_0{}^+(0,0;+) = \varphi_a{}^0\varphi_b{}^0\chi_a{}^{(0,0)}\chi_b{}^{(0,0)}$$

$$\Psi_2{}^+ = \Phi_0{}^+(1,0;+) = \frac{1}{\sqrt{2}}\,\varphi_a{}^0\varphi_b{}^0[\chi_a{}^{(0,1)}\chi_b{}^{(0,0)} + \chi_a{}^{(0,0)}\chi_b{}^{(0,1)}]$$

$$\Psi_3{}^- = \Phi_0{}^-(1,0;+) + \frac{1}{\sqrt{2}}\,\varphi_a{}^0\varphi_b{}^0[\chi_a{}^{(0,1)}\chi_b{}^{(0,0)} - \chi_r{}^{(e,0)}\chi_b{}^{(0,1)}]$$

Excited Electronic States

$$\Psi_4{}^- = \Phi_1{}^-(0,0;-) = \frac{1}{\sqrt{2}}(\varphi_a{}^1\varphi_b{}^0 - \varphi_a{}^0\varphi_b{}^1)\chi_a{}^{(1,0)}\chi_b{}^{(1,0)}$$

$$\Psi_5{}^+ = \Phi_1{}^+(0,0;+) = \frac{1}{\sqrt{2}}(\varphi_a{}^1\varphi_b{}^0 + \varphi_a{}^0\varphi_b{}^1)\chi_a{}^{(1,0)}\chi_b{}^{(1,0)}$$

$$\Psi_6{}^- = \Phi_1{}^-(1,0;-) = \tfrac{1}{2}(\varphi_a{}^1\varphi_b{}^0 - \varphi_a{}^0\varphi_b{}^1)\,[\chi_a{}^{(1,1)}\chi_b{}^{(1,0)} + \chi_a{}^{(1,0)}\chi_b{}^{(1,1)}]$$
$$\Psi_7{}^+ = \Phi_1{}^+(1,0;-) = \tfrac{1}{2}(\varphi_a{}^1\varphi_b{}^0 - \varphi_a{}^0\varphi_b{}^1)\,[\chi_a{}^{(1,1)}\chi_b{}^{(1,0)} - \chi_a{}^{(1,0)}\chi_b{}^{(1,1)}]$$
$$\Psi_8{}^+ = \Phi_1{}^+(1,0;-) = \tfrac{1}{2}(\varphi_a{}^1\varphi_b{}^0 + \varphi_a{}^0\varphi_b{}^1)\,[\chi_a{}^{(1,1)}\chi_b{}^{(1,0)} + \chi_a{}^{(1,0)}\chi_b{}^{(1,1)}]$$
$$\Psi_9{}^- = \Phi_1{}^-(1,0;+) = \tfrac{1}{2}(\varphi_a{}^1\varphi_b{}^0 + \varphi_a{}^0\varphi_b{}^1)\,[\chi_a{}^{(1,1)}\chi_b{}^{(1,0)} - \chi_a{}^{(1,0)}\chi_b{}^{(1,1)}]$$

[a] $\varphi_a{}^0$ is the electronic wave function for the ground state of molecule a, and $\varphi_a{}^n$ is the nth excited-state function. $\chi_a(n,\nu)$ is the vibrational wave function for molecule a in its nth electronic state, and νth vibrational level. The corresponding wave functions for molecule b are indicated in a similar fashion. The complete wave functions for the dimer are described by the functions $\Phi_n{}^\pm(\nu,0,\pm)$ where the $\pm$ superscript indicates the overall (electronic + vibrational) symmetry.

ative intensities of the various transitions and their polarization with respect to the strongest band in the absorption spectra have also been indicated to facilitate comparison with the experimental data. (Also see Table I.)

The strongest band in the dimer absorption spectrum is assigned as a transition to state Ψ_5 and the polarizations of all other transitions are specified relative to this transition. (In the simple exciton theory this would correspond to a transition to the Ψ_+ state.) Since Ψ_5 is the *second* electronic state there is no band in the emission spectrum corresponding to this absorption band. The moderately intense longer wavelength in the dimer absorption spectra (band 2) is correspondingly assigned as the transition to the vibrationally excited state of the lowest electronic state of the dimer. In the strong coupling model this is a transition to Ψ_7 and it receives its intensity by vibronic coupling with the higher energy Ψ_5 state. It therefore is predicted to have the same polarization as band 3, in agreement with experiment. The corresponding band in emission corresponds to the transition from Ψ_4 to the vibrationally excited ground state Ψ_3 and it too should have a positive polarization. Band 2′ in the emission spectrum can clearly be identified as this transition. This assignment also permits us to understand the anomalous intensity of this band as is discussed below.

The weak origin band in the dimer absorption and emission spectrum can be assigned as a transition between states Ψ_1 and Ψ_4. If the dimer has a center of symmetry or a plane of symmetry, theory predicts that this transition should be forbidden or partially allowed and polarized opposite to the intense band 3. The fact that this transition is polarized *obliquely* to the main dimer band is therefore not accounted for, and as long as the dimer is assumed to have some symmetry there is no way that positive polarization can be introduced into this transition so that it would have roughly equal contributions from positive and negative polarizations. Conceivably the weak origin band could be a vibrationally induced band made allowed by a small-frequency mode belonging to a nontotally symmetric representation of dimer symmetry. However, the maximum of this weak band and the maximum of the higher energy band of dimer fluorescence are separated by only about 300–400 cm⁻¹ and this is nearly the same as the Stokes shift for corresponding

monomer bands. Also, the absorption and fluorescence bands are not as sharp as expected for vibronically induced forbidden band. Thus, this mechanism seems to be unlikely. It is unlikely that this weak origin band and the corresponding higher energy fluorescence band are respectively superposition of two bands which have mutually perpendicular transition dipole moments, because of the facts discussed above and because the intensity ratio of the higher energy band to the lower energy band of dimer fluorescence is smaller than that of monomer fluorescence. We are forced to conclude that the two molecules in the dimer complex are slightly different from each other. The angular orientation of the phenyl substituents offers one obvious source of assymetry. This may result in a slightly different transition probability for the same transition in the two different molecules, and together with slight deviation from parallel arrangement, will result in an oblique orientation of the transition dipole moment for the transition to the Ψ_4 state of the dimer.

Finally, we have to explain the anomalous intensity of the 0–1 band of the dimer fluorescence (at 678 nm for rhodamine B and at 690 nm for sulforhodamine B). As we noted above, the polarization of this band is easily accounted for if we assume that it corresponds to a vibronically induced transition from Ψ_4 to Ψ_3. This assignment also accounts for the large increase in intensity of the 0–1 band relative to the 0–0 band, which occurs on dimerization (0.6 for the dimer compared to 0.19 for the monomer of rhodamine B and 0.9 compared with 0.25 for sulforhodamine B) as the following analysis indicates.

The intensity of band 2 in the absorption spectrum is derived from vibronically induced mixing between the Ψ_7 and Ψ_5 states which, experimentally, are separated from each other by only about 1000 cm⁻¹. The corresponding vibronically induced band in emission (band 2′) corresponds to a transition between states Ψ_4 and Ψ_3 and it derives intensity *via* vibronic coupling between state Ψ_4 and state Ψ_9 which is located over 3000 cm⁻¹ away. Because of this larger separation (factor of over 3) vibronic coupling effects on the 0–1 band in emission are reduced by a factor of about 10 compared with the corresponding absorption band. In the dimer *absorption* spectrum the 0–1 band is about 10 times stronger than the 0–0 band. However, because of the factor of 10 difference arising

from the ΔE factor, we predict that the two bands would be about equal in intensity in the *emission* spectrum. Experimentally, the ratio of the intensity of the 0–1 band to the intensity of the 0–0 band is 0.6 for rhodamine B and 0.8 for sulforhodamine B, in reasonably good agreement with our approximate estimate. Our interpretation of the dimer absorption spectrum is thus found to give a reasonable account of the enhancement of the 0–1 band relative to the 0–0 band in the dimer emission spectrum as compared with the monomer emission spectrum.

Our interpretation is that the emission spectrum is comprised of a weak electronic transition which corresponds to the 0–0 band and a vibronically induced transition which corresponds to the 0–1 band. In view of this assignment and the relationship between absorption coefficients and radiative lifetimes, we further predict that the radiative lifetime of the dimer should be a factor of 8–10 times longer than the monomer, based on a comparison of the integrated intensity in the monomer spectrum. The observed lifetime of the monomer fluorescence of rhodamine B is reported as 6.2 nsec in ethanol and the quantum yield 0.97.[47] Experimentally, we find a value of 3.4 nsec at room temperature in ethanol–glycerol and 5.3 nsec at 77°K. By comparison, the lifetime of the dimer in an aqueous solution is 38 nsec at 77°K, corresponding to at least a sevenfold increase in the *radiative* lifetime as a result of dimer formation. This agrees quite well with the estimated value, and confirms that the strong band 3 in the dimer absorption spectrum corresponds to a transition to an upper electronic state of the dimer which is not involved in the emission spectrum.[35]

Monomer and Dimer Phosphorescence from Acridine and Xanthene Dyes. Some time ago we reported the observation of dimer phosphorescence from acridine orange, rhodamine B, and eosin Y.[26] These observations have now been extended to several other dyes and these results are presented in Figure 5 along with corresponding results for the monomer.

The comparison of the monomer and dimer phosphorescence spectra presented in Figure 5 reveals that dimer formation generally leads to a ~30-nm red shift in the peak of the phosphorescence. Because of this spectral shift it was of interest to determine whether or not dimerization affected the phosphorescence decay times. Phosphorescence lifetimes were measured for both monomers and dimers of acridine orange, eosin Y, and sulforhodamine B. Within experimental error dimerization has no effect on the phosphorescence lifetime of these three dyes indicating that either dimerization has no effect on either the radiative or nonradiative transition rates from the triplet state or (less likely) that the rates are fortuitously changed in such a manner that they exactly cancel one another. The phosphorescence lifetime for acridine orange and sulforhodamine B were also measured at 1.8°K and found to be virtually identical with those measured at 77°K. The motivation for this latter experiment lay in the possibility that the triplet states of the dimer might be slightly split due to an exciton interaction, and therefore at low temperatures emission might be observed from the lower component with an altered lifetime. The observation that there is no change in lifetime indicates that either the splitting of the triplets is less than 2 cm^{-1} or that the radiative lifetimes of both triplet components are comparable. Spin polarization effects also appear to be absent.

As with the rhodamines, direct absorption spectra were

compared with the phosphorescence excitation spectra to establish the authenticity of the emitting species. In general, the phosphorescence from these compounds is polarized out-of-plane so that it is not possible to learn anything about the relative polarization of the in-plane polarized singlet–singlet transitions of the dimers. The halogenated xanthenes are exceptions to this generalization since they exhibit an in-plane polarized phosphorescence. With eosin Y and eosin B the monomer phosphorescence is polarized positively ($P = +0.1$) with respect to the first strong singlet–singlet band of the monomer (Figure 6). In the dimer the polarization of the phosphorescence is slightly reduced, but it is nevertheless still a positive polarization with respect to the two bands in the dimer absorption spectrum which appear to be the counterparts of bands 2 and 3 in the dimer absorption spectra of the rhodamines (see Figure 6). The true origin band (counterpart of band 1) is apparently too weak to be seen in the eosin Y dimer spectrum and this is consistent with the fact that the no dimer fluorescence is observed from this compound. Consequently, we believe that our interpretation of the dimer spectra is not restricted to the rhodamines, which are special in exhibiting dimer fluorescence as well as dimer phosphorescence, but rather that we are dealing with a rather general phenomenon which applies to many other similar dye systems.

Summary

In this paper we have presented the results of measurements on the polarized absorption and emission of several dyes in the dimeric state. The rhodamine dyes are unusual in that the dimers are fluorescent, and this permitted us to determine for the first time the relative polarizations of various dimer absorption and emission bands. We find that neither the dimer absorption nor the emission spectrum can be accounted for in terms of the simple exciton model commonly used to interpret the electronic spectra of dye dimers. The spectra can, however, be satisfactorily interpreted in terms of a strong coupling model in which vibronic interactions are included. The fact that the 0–1 band in fluorescence is intensified compared to the 0–0 band as a result of dimerization raises some question about the frequently discussed stabilization energies of excimers of some aromatic hydrocarbons such as perylene and pyrene.[48] These stabilization energies have usually been evaluated based on the energy difference between the maximum of the monomer fluorescence and the maximum of the excimer fluorescence. The present study suggests that the maximum of the excimer fluorescence might correspond to a "0–1" band rather than the "0–0" band, and this leads to ~1300 cm^{-1} smaller values of stabilization energy than those usually accepted.

References and Notes

(1) Submitted in partial fulfillment of the requirements for the Ph.D. degree in Chemistry at the University of California, Riverside.
(2) P. P. Sorokin, *et al.*, *IBM J.*, **11**, 139, 148 (1967).
(3) (a) D. A. Leonard, *Appl. Phys. Lett.*, **7**, 4 (1965); (b) D. A. Leonard, R. A. Neal, and E. T. Gerry, *ibid.*, **7**, 175 (1965).
(4) M. Bass, T. F. Deutsch, and M. J. Weber, *Appl. Phys. Lett.*, **13**, 120 (1968).
(5) G. I. Farmer, B. G. Huth, L. M. Taylor, and M. R. Kagan, *Appl. Opt.*, **8** (2), 363 (1969).
(6) H. Samelson, *Electronics*, 142 (1968).
(7) R. A. Keller, *IEEE J. Quantum Electron.*, **6** (7), 411 (1970).

(8) D. R. Kearns, *Chem. Rev.*, **71**, 395 (1971).

(9) J. D. Spikes and R. Livingston, *Advan. Radiat. Biol.*, **3**, 29 (1969).

(10) D. C. Chatterjee and E. A. Noltmann, *Eur. J. Biochem.*, **2**, 9 (1967).

(11) E. Scoffone, G. Galiazzo, and G. Jori, *Biochem. Biophys.*, **38**, 16 (1970).

(12) H. E. A. Kramer and A. Maute, *Photochem. Photobiol.*, **15**, 25 (1972).

(13) F. Leterrier and P. Douzou, *Photochem. Photobiol.* **8**, 369 (1968).

(14) T. Forster and E. Konig, *Z. Elektrochem.*, **61**, 344 (1957).

(15) L. V. Levshin and V. K. Gorshkov, *Opt. Spektrosk.*, **10**, 401 (1961).

(16) L. A. Ignat'eva, L. V. Levshin, T. D. Osipova and Y. M. Polukhin, *Opt. Spektrosk.*, **13**, 219 (1962).

(17) K. L. Arvan and N. E. Zaitseva, *Opt. Spektrosk.*, **11**, 38 (1961).

(18) G. P. Gurinovich and T. I. Stelkova, *Biofizika*, **8**, 229 (1963).

(19) L. V. Levshin and I. S. Lonskaya, *Opt. Spektrosk.*, **11**, 148 (1961).

(20) L. V. Levshin and E. G. Baranova, *Opt. Spektrosk.*, **6**, 31 (1959).

(21) L. V. Levshin and V. G. Bocharov, *Opt. Spektrosk.*, **10**, 330 (1961).

(22) V. G. Bocharov and L. V. Levshin, *Izv. Akad. Nauk SSSR, Ser. Fiz.*, **27**, 591 (1963).

(23) L. V. Levshin, *Izv. Akad. Nauk SSSR, Ser Fiz.*, **29**, 1299 (1965).

(24) L. V. Levshin and D. M. Akbarova, *Zh. Prikl. Spektrosk.*, **2**, 43 (1965).

(25) L. V. Levshin and D. M. Akbarova, *Zh. Prikl. Spektrosk.*, **3**, 326 (1965).

(26) R. W. Chambers and D. R. Kearns, *J. Phys. Chem.*, **72**, 4718 (1968).

(27) R. W. Chambers and D. R. Kearns, *Fhotochem. Photobiol.*, **10**, 215 (1969).

(28) D. J. Blears and S. S. Danyluk, *J. Amer. Chem. Soc.*, **89**, 21 (1967).

(29) S. J. Davidson and W. P. Jencks, *J. Amer. Chem. Soc.*, **91**, 225 (1969).

(30) R. E. Ballard and C. H. Park, *J. Chem. Soc., A*, 1340 (1970).

(31) K. K. Rohatgi and A. K. Mukhopadhyay, *Photochem. Photobiol.*, **14**, 551 (1971).

(32) E. Braswell, *J. Phys. Chem.*, **72**, 2477 (1968).

(33) J. Ferguson and A. W. H. Mau, *Chem. Phys. Lett.*, **17**, 543 (1972).

(34) W. R. Ware, "Creation and Detection of the Excited State," A. Lamola, Ed., Marcel Dekker, New York, N. Y. 1970.

(35) E. G. McRae and M. Kasha, *J. Chem. Phys.*, **28**, 721 (1958).

(36) T. Kajiwara, R. W. Chambers, and D. R. Kearns, *Chem. Phys. Lett.*, **22**, 37 (1973).

(37) E. G. McRae and M. Kasha, "Physical Processes in Radiation Biology," Academic Press, New York, N. Y., 1964, p 23.

(38) M. Kasha, H. R. Rawls, and M. Ashraf El-Bayoumi, *Pure Appl. Chem.*, **11**, 371 (1965).

(39) A. S. Davydov, "Theory of Molecular Excitons," translated by M. Kasha and M. Oppenheimer, Jr., McGraw-Hill, New York, N. Y., 1962.

(40) W. T. Simpson and D. L. Peterson, *J. Chem. Phys.*, **26**, 588 (1957).

(41) A. Witkowski and W. Moffitt, *J. Chem. Phys.*, **33**, 872 (1960).

(42) R. L. Fulton and M. Gouterman, *J. Chem. Phys.*, **35**, 1059 (1961).

(43) R. L. Fulton and M. Gouterman, *J. Chem. Phys.*, **41**, 2280 (1964).

(44) M. G. Sucre, F. Geny, and R. Lefebvre, *J. Chem. Phys.*, **49**, 458 (1968).

(45) J. H. Young, *J. Chem Phys.*, **49**, 2566 (1968).

(46) E. G. McRae, *Aust. J. Chem.*, **14**, 329 (1961).

(47) S. J. Strickler and R. A. Berg, *J. Chem. Phys.*, **37** 814 (1962).

(48) J. B. Birks, "Photophysics of Aromatic Molecules," Wiley-Interscience, London, 1970.

Theory of Circularly Polarized Emission from Molecules Displaying Rotary Brownian Motion[1]

Joseph Snir and John A. Schellman*

Chemistry Department, University of Oregon, Eugene, Oregon 97403   (Received September 18, 1973)

Publication costs assisted by the University of Oregon

Formulas are obtained for the extent of circular polarization of light produced by fluorescence emission. Photoselection and its relaxation by rotary Brownian movement are taken into account. For simplicity, the model is restricted to spherical molecules and a simple dipole coupling mechanism. On the basis of this model, it is shown that the ratio of circularly polarized emission to total emission is independent of the relaxation of photoselection. The dependence of the absolute intensity of circularly polarized emission is evaluated as a function of the optical parameters and the relaxation time for rotary Brownian movement. The relaxation correction is small.

Introduction

The use of optical activity as a reflection of molecular conformation and changes in molecular conformation has been established for many years. The measurement and interpretation of optical activity came into particular prominence when it became convenient to measure optical rotation and later circular dichroism within absorption bands. In measuring circular dichroism, one determines the difference in absorbance by the molecule of left and right circularly polarized light. Recently, interest has developed in the possibilities of the reverse process, *i.e.*, the measurement of the circularly polarized component of emitted light from asymmetric molecules. Experimental observations have been obtained with crystals of sodium uranyl acetate[2] and with solutions of both organic compounds (hydrandindone and thiohydrandindone) and inorganic complexes $[Cr(en)_3](ClO_4)_3$ by Emeis and Oosterhof.[3] These pioneering investigations have mostly been made with systems which guaranteed a fairly strong signal of circularly polarized light in the emission process.[4]

Recently, an instrument has been developed by Steinberg and Gafni which provides the capability of measuring circularly polarized light when it comprises only one part in 10^4 of the total intensity.[5a] The first application of this method (which uses stress modulation techniques now common in CD measurements) has been to the difficult problem of molecules bound to enzymes.[5b] This technical development, which requires only relatively simple modifications of a spectrofluorimeter, widely extends the applicability of the method. The principal question of interest at the present time is the nature of the new information which will come from the new measure-

ments. It is to this problem that the present paper is directed.

Emeis and Oosterhof have discussed the theory of the effect.[3] From considerations of coefficients for spontaneous emission, they draw the conclusion that circularly polarized emission is governed by matrix elements of the same structure as those for circular dichroism, namely, the rotatory strength

$$R_{fo} = \sum_w \text{Im}(\langle fw|\mu|0v\rangle \cdot \langle 0v|\mathbf{m}|fw\rangle) \qquad (1)$$

μ and $\mathbf{m}$ are the electric and magnetic transition moment operators, respectively. Here f and 0 indicate the fluorescent and ground electronic states, respectively, while v and w indicate the vibronic state. An explicit description of the states that contribute to R_{fo} will follow shortly.

By defining an anisotropy factor for emission $g_e = (I_L - I_R)/I \equiv \Delta I/I$ (where I_L and I_R are the intensity of emission of left and right polarized light, respectively), all of the constants of the spontaneous emission probabilities (including the frequency dependence) cancel out. If the shape of the CPE spectrum is the same as that of the total emission spectrum, the anisotropy factor is a multiple of the ratio of the rotatory strength (R) to dipole strength (D) for the emission process. In particular $\Delta I/I = 4R/D$ as in ordinary CD and absorption. Thus, as usual, the essential problem is the evaluation and/or interpretation of the rotatory strength.

Emeis and Oosterhof further point out that in addition to vibrational considerations, the rotatory strength for emission will differ from that for absorption because of changes in molecular geometry, molecular association, ionization reactions, excimer formation, etc. in the excited state. These are all well established in the case of ordinary fluorescence spectroscopy and it is by virtue of events which take place in the time interval between absorption and emission that new information is expected to be obtained from CPE.

Emeis and Oosterhof developed their theoretical discussion for the case where the emitting molecules have random orientations. Such a theory does not apply to crystals and applies to solutions only to the extent that the relaxation time for rotary Brownian movement is small compared to the lifetime of the excited state. The work of Schlessinger and Steinberg[5b] on enzymes makes this question particularly pertinent since it is well known that the rotary relaxation time of protein molecules is commensurate with the lifetime of the excited electronic states. This aspect of protein fluorescence has been thoroughly exploited *via* measurements of fluorescence depolarization. Consequently, a general discussion must take cognizance of the fact that the emitting molecules have been photoselected and that this photoselection may be intact, relaxed, or partially relaxed at the time of emission. The first case would apply to very large molecules or viscous solutions, the second to small molecules in solution, and the third to biopolymers in the 10^4–10^6 range of molecular weight in solvents of moderate viscosity. We will attempt to solve the general case, *i.e.*, partially relaxed, for a simple model. The other two cases then become limiting forms.

As soon as one considers the case of a photoselected distribution, a new feature arises. Tinoco and Hamerle[6] have demonstrated that for nonrandom orientation, the usual rotatory strength is not applicable since the discard of quadrupole contributions is not permitted. To meet this problem, our work will be carried out in two stages. In the first, equations will be developed for the CPE of mole-

cules with oriented excitations. In the second, equations will be developed for the effect of the relaxation of photoselection by rotary Brownian movement.

A Coupling Mechanism for CPE

The magnitude of the electric transition moment for fluorescence $\langle fw|\mu|0v\rangle$ is related to the Einstein coefficient for spontaneous emission $A = (32\pi^3/3\hbar\lambda^3) \cdot \langle fw|\mu|0v\rangle^2$. Typical lifetimes of fluorescence run from 1 to 10 nsec. The fluorescence efficiency (Q) of chromophores normally varies from 1 to 99%. The radiative lifetime is related to the observed lifetime by the relation $\tau^0 = \tau/Q$, where τ is the observed lifetime which involves nonradiative as well as radiative processes and τ^0 is the lifetime associated with the radiative process alone.[7] Assuming a 5-nsec lifetime and a 20% quantum yield, we calculate a midrange fluorescence transition moment of the order of 3 D at 400 nm. Transition moments of fluorescing dyes will be considerably larger. In the theory of ordinary optical activity, electric transition moments of this order of magnitude usually contribute most effectively to the rotatory strength by way of a correlative coupling of the transition dipoles. In the following we shall treat this as the dominant mechanism for CPE. Other contributions resulting from the one electron mechanisms, dissymmetric chromophores, etc. can be added to the theory by means which are already well established for ORD–CD.[8]

To simplify the discussion we will make the following assumptions. (1) The molecule contains only two chromophores each with only a single excited state. (2) The energy levels of the chromophore are sufficiently separated that their bands do not overlap. The lower energy chromophore will be treated as the absorber and emitter of energy; the other chromophore will be considered to interact with the emitter/absorber in a coupling mechanism. This assumption evades the question of energy transfer between the chromophores which can be taken up later. (3) In the fluorescing chromophore, the emission transition dipole is parallel to the absorption dipole. Energy levels of the fluorescing and perturbing group are indicated in Figure 1. For the fluorescent group, the absorption process is from low or zero vibrational excitation in the ground state to high vibrational excitation in the excited state. In the emission process, the situation is reversed. For simplification, we will use the following notation

$$\langle 0v|\mathcal{O}|fw\rangle = (\mathcal{O})_{0'f'}, \qquad v, w, \neq 0. \ \mathcal{O} = \text{any operator}$$

i.e., states with primed indices are in vibrationally excited vibronic levels. In this notation the electric transition moment for fluorescence will be $(\mu)_{f0'}$. The perturbing group wave functions will be labeled α and its singly excited states j. The fluorescing group wave function will be labeled ϕ. The zero-order wave functions for the molecule are the products of the two group wave functions. Of the eight symbolic product functions, only four contribute to dynamic coupling of the two groups. These are given in Table I. Zero-order wave functions are indicated by rounded kets.

With this limited basis set, the necessary matrix elements could be calculated by diagonalizing the Hamiltonian matrix and employing the same similarity transformation to the optical matrix elements.[9] In this communication we will use perturbation theory. The formal resemblance to Kirkwood's coupling mechanism for optical activity will be apparent.

Using angular kets for first-order wave functions we find
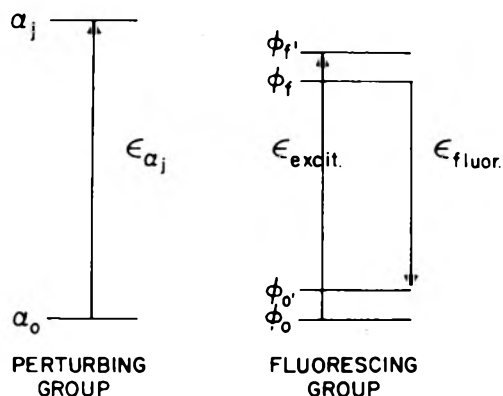
Figure 1. Electronic states of perturber and emitter involved in producing CPE. See text.

for the ground state and vibrationally relaxed fluorescent state

$$|00'\rangle = |00'\rangle - \frac{(00'|V|jf)}{\epsilon_j + \epsilon_f} \cdot |jf\rangle$$

$$|0f\rangle = |0f\rangle - \frac{(0f|V|j0')}{\epsilon_j - \epsilon_f} \cdot |j0'\rangle \qquad (2)$$

The zero of energy has been taken as the state $|00'\rangle$ as indicated in Table I. V is the interaction energy between the two groups. Because of the commutation of operators involving coordinates alone, the two matrix elements containing V are identical and will be symbolized by $V_{0f, j0'}$.

The matrix element of a vector or tensor operator $\mathfrak{O}$ will be given by

$$\langle 0f|\mathfrak{O}|00'\rangle = (0f|\mathfrak{O}|00') - V_{0f, j0'}\left(\frac{(j0'|\mathfrak{O}|00')}{\epsilon_j - \epsilon_f} + \frac{(0f|\mathfrak{O}|jf)}{\epsilon_j + \epsilon_f}\right) (3)$$

Operators in which we will be interested are the electric dipole moment operator μ and the diad operator $\mathbf{pr}$ where $\mathbf{p}$ is the momentum and $\mathbf{r}$ the position vector. $\mathbf{pr}$ is a one electron operator summed over all the electrons in both groups. Placing the origin of the coordinate system on the fluorescing group and ignoring local contributions to the matrix elements (local magnetic and quadrupole moments) we find

$$\langle 0f|\mu|00'\rangle = (f|\mu|0') - \frac{2\epsilon_j V_{0f, j0'}}{\epsilon_j^2 - \epsilon_f^2}(j|\mu|0) \qquad (4)$$

$$\langle 00'|\mathbf{pr}|0f\rangle = V_{0f, j0'}\left[\frac{(j|\mathbf{p}|0)}{\epsilon_j - \epsilon_f} + \frac{(0|\mathbf{p}|j)}{\epsilon_j + \epsilon_f}\right]\mathbf{R}^\alpha =$$

$$\frac{2\epsilon_f V_{0f, j0'}}{\epsilon_j^2 - \epsilon_f^2}(j|\mathbf{p}|0)\mathbf{R}^\alpha \qquad (5)$$

where $\mathbf{R}^\alpha$ is the position vector of the perturbing group. With real wave functions $(0|\mathbf{p}|j) = -(j|\mathbf{p}|0)$.

The rotatory strength tensor is given by

$$\mathbf{R}_{f0'} = \frac{3e}{2mc}\text{Im}\{\mu_{f0'} \times (\mathbf{pr})_{0'f}\} \qquad (6)$$

A typical product of matrix elements entering into it is

$$(\mu_\beta)_{f0'}(p_\gamma r_\delta)_{0'f} = \frac{2\epsilon_f V_{0f, j0'}}{\epsilon_j^2 - \epsilon_f^2}(\mu_\beta)_{f0'}{}^0(p_\gamma)_{j0}{}^0 R_\delta{}^\alpha \qquad (7)$$

where β, γ, and δ represent any of the three cartesian coordinates and the notation has been contracted such that the presence and absence of superscript 0 indicates zero- and first-order matrix elements, respectively. The term containing V^2 has been neglected.

TABLE I: Zero-Order Wave Functions of a Fluorescing and Perturbing Group

Product function	Ket symbol	Energy[a]
$\alpha_0\phi_0'$	$|00'\rangle$	0
$\alpha_0\phi_f$	$|0f\rangle$	ϵ_{ϕ_f}
$\alpha_j\phi_0'$	$|j0'\rangle$	ϵ_{ϕ_j}
$\alpha_j\phi_f$	$|jf\rangle$	$\epsilon_{\alpha_j} + \epsilon_{\phi_f}$

[a] Subsequently we will omit the group index, i.e., $\epsilon_{\alpha_j} = \epsilon_j$ and $\epsilon_{\phi_f} = \epsilon_f$.
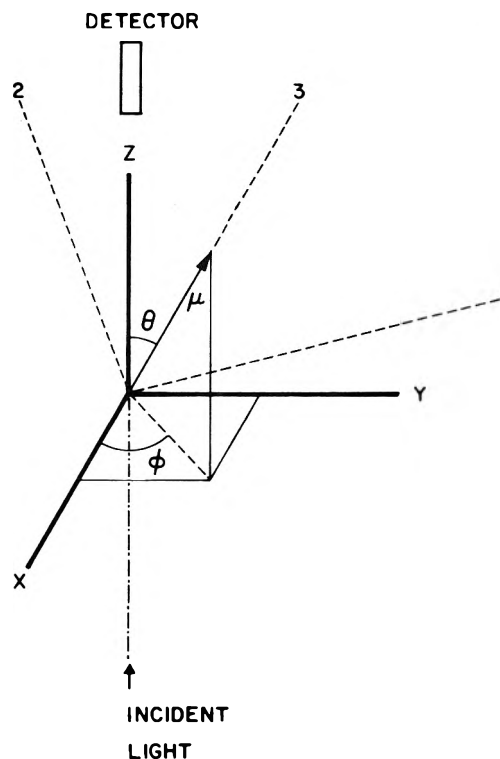
Figure 2. Representation of the laboratory and molecular coordinate systems. See text.

Using the relation $(p_\gamma)_{j0}{}^0 = (i\epsilon_j m/\hbar e) (\mu_\gamma)_{j0}{}^c$ eq 7 becomes

$$(\mu_\beta)_{f0'}(p_\gamma r_\delta)_{0'f} = \frac{2im}{\hbar e}\frac{\epsilon_f \epsilon_j}{\epsilon_j^2 - \epsilon_f^2}(V_{0f, j0'})(\mu_\beta)_{f0'}{}^0(\mu_\gamma)_{j0}{}^0 R_\delta{}^\alpha \qquad (8)$$

CPE from an Oriented Molecule

In discussing the predictions of the theory, it will be necessary to shuttle back and forth between coordinate systems appropriate for the experimental apparatus and for the emitting molecule. For the laboratory system we shall assume the geometry of the apparatus of Steinberg which detects CPE in the forward direction of the exciting beam. The advantage of this arrangement is that there is no linear polarization of fluorescence for light emitted in this direction, which can otherwise produce severe artifacts in the measurement of CPE.[10] The coordinate system is represented in Figure 2. The unpolarized excitation beam is assumed to come from the negative Z direction and the forward emission is measured in the positive Z direction. Since the experimental arrangement is isotropic about the Z axis, all dependence of the phenomenon on the choice of the X and Y axes must eventually disappear. To avoid confusion the molecular coordinates will be specified by the integers 1, 2, and 3. We assume that the origin

of the laboratory and molecular coordinate systems coincide.

If the molecular coordinate system is chosen such that the Z axis is directed along the electric transition moment of the fluorescing group, $(\mu_1 = \mu_2 = 0)$ the rotatory strength matrix (eq 6) reduces to

$$R_{f0'} = \frac{3e}{2mc} \text{Im} \begin{Bmatrix} -(\mu_3)(p_2 r_1) & -(\mu_3)(p_2 r_2) & -(\mu_3)(p_2 r_3) \\ (\mu_3)(p_1 r_1) & (\mu_3)(p_1 r_2) & (\mu_3)(p_1 r_3) \\ 0 & 0 & 0 \end{Bmatrix}_{f0'.0'f}$$

(9)

where the indices outside the optical matrix indicate the state labels for the transition matrix elements within.

The molecules are assumed to be randomly oriented so that once the 3 axis has been set along the direction of the emitting transition moment there is no preferred orientation of the molecule about this axis. Averaging over all orientations about the 3 axis by a procedure that has been described elsewhere[11]

$$\mathbf{R}_{f0'} = +\frac{3e}{4mc} \times$$

$$\text{Im} \begin{Bmatrix} (\mu_3)_{f'0}(p_2 r_1 - p_1 r_2)_{0f'} & (\mu_3)_{f'0}(p_1 r_1 + p_2 r_2)_{0f'} & 0 \\ -(\mu_3)_{f'0}(p_1 r_1 + p_2 r_2)_{0f'} & (\mu_3)_{f'0}(p_2 r_1 - p_1 r_2)_{0f'} & 0 \\ 0 & 0 & 0 \end{Bmatrix} (10)$$

Substituting from eq 8

$$\mathbf{R}_{f0'} = \begin{Bmatrix} A & B & 0 \\ -B & A & 0 \\ 0 & 0 & 0 \end{Bmatrix}$$

(11)

where

$$A = \frac{3}{2\hbar c} \frac{\epsilon_f \epsilon_j}{\epsilon_j{}^2 - \epsilon_f{}^2} V_{0f.j0}(\mu_3)_{f0'}{}^0 [(\mu_2)_{j0}{}^0 R_1{}'' - (\mu_1)_{j0}{}^0 R_2{}''] =$$

$$\frac{3}{2} \frac{\epsilon_f V_{0f.j0'}}{\epsilon_j{}^2 - \epsilon_f{}^2} \text{Im}[(\mu)_{f'0}{}^0 \cdot (\mathbf{m})_{j0}{}^0] =$$

$$\frac{3}{2\hbar c} \frac{\epsilon_f \epsilon_j}{\epsilon_j{}^2 - \epsilon_f{}^2} V_{0f.j0} \mathbf{R}'' \cdot (\mu)_{j0}{}^0 \times (\mu)_{f'0}{}^0 \quad (12)$$

$$B = \frac{3}{2\hbar c} \frac{\epsilon_f \epsilon_j}{\epsilon_j{}^2 - \epsilon_f{}^2} V_{0f.j0'}(\mu_3)_{f0'}{}^0 [(\mu_1)_{j0}{}^0 R_1{}'' + (\mu_2)_{j0}{}^0 R_2{}''] =$$

$$\frac{3}{2\hbar c} \frac{\epsilon_f \epsilon_j}{\epsilon_j{}^2 - \epsilon_f{}^2} V_{0f.j0'}(\mu_3)_{f0'}{}^0 [(Q_{11})_{j0}{}^0 + (Q_{22})_{j0}{}^0]$$

where m is the magnetic moment and Q the quadrupole moment. In the last two forms of writing A the coordinate system has disappeared from the formula though the origin must remain on the fluorescing group. To evaluate A and B, the position and orientation of the perturbing transition moment μ_{j0} must be known as well as the absorption frequency of the perturber and the emission frequency of the perturbing group. *The formula becomes general for this mechanism by considering the prime and j as summation indices, thereby summing over all vibronic sublevels, and all excited states of all perturbing groups.*

As can be seen, the A and B terms contain the magnetic and quadrupole contributions, respectively. Furthermore, with our very simple model and special coordinate system, it is the fluorescent chromophore which contributes the electric moment to the rotatory strength, and the environmental chromophore(s) which contribute the magnetic and quadrupole terms. With other coordinate systems, the results would be physically equivalent but less readily perceived. The classical physical interpretation of

this result is that the emitting electric dipole induces currents in neighboring chromophoric groups which circulate around its own axis in such a way as to produce magnetic and quadrupole moments relative to this axis. Currents parallel to the emitting dipole are contained in the perturbation theory but do not contribute to the dipole strength and lead to an attenuation or enhancement of emission which is akin to hypo- and hyperchromic effects in absorption spectroscopy.

Transformation to Laboratory Coordinates

Expression 11 gives the rotatory strength tensor in the molecular coordinate system. The transformation from particle to laboratory coordinates can be represented as a general coordinate rotation. The orthogonal unitary matrix S describing the transformation is the matrix of the direction cosines between the particle axes 1, 2, and 3 and the laboratory axes X, Y, and Z. The rotatory strength tensor transforms under rotation like a second rank tensor. In the lab system

$$(\mathbf{R}_{f0'})_{\text{lab}} = (S)(\mathbf{R}_{f'0})(\tilde{S}) \quad (13)$$

The measured quantity in the experiment with the geometry described in Figure 2 is

$$(\mathbf{R}_{f0'})_{\text{lab}} = R_{ZZ} = \mathbf{k} \cdot (S)(\mathbf{R}_{f0'})(\tilde{S}) \cdot \mathbf{k} \quad (14)$$

where $\mathbf{k}$ is a unit vector in the direction of propagation of the light which is the Z direction in the experimental setting. As defined above

$$S = \begin{pmatrix} \alpha_1 & \alpha_2 & \alpha_3 \\ \beta_1 & \beta_2 & \beta_3 \\ \gamma_1 & \gamma_2 & \gamma_3 \end{pmatrix}$$

with $\alpha_1 = \cos(X1)$, $\alpha_2 = \cos(X2)$, $\alpha_3 = \cos(X3)$, etc. The dot products with $\mathbf{k}$ select the third row and column of S and $\tilde{S}$, respectively, so

$$R_{ZZ} = (\gamma_1, \gamma_2, \gamma_3) \begin{pmatrix} A & B & 0 \\ -B & A & 0 \\ 0 & 0 & 0 \end{pmatrix} \begin{pmatrix} \gamma_1 \\ \gamma_2 \\ \gamma_3 \end{pmatrix} = A(\gamma_1{}^2 + \gamma_2{}^2) =$$

$$A[\cos^2(Z1) + \cos^2(Z2)] = A(\sin^2\theta(\sin^2\phi + \sin^2\phi)) =$$

$$A\sin^2\theta \quad (15)$$

θ is the angle between the directions 3 and Z, and is also the angle between $\mu_{f0'}$ and Z as follows from the definition of the molecular coordinate system. The expression $(A \sin^2\theta)$ has to be averaged over the distribution of the moments $\mu_{f0'}$ at the time of emission. The form of this distribution will be discussed in the next section.

It can be shown that only the symmetric parts of the rotatory strength tensor contribute to optical activity or CPE. This is the reason that the B terms have dropped out of the final formula. This means that for this simple model and coordinate system the quadrupole terms make no contribution. In general this is not true.[6,11]

The Moment Distribution Function

The problem of the orientation of the transition moments of molecules that are in rotary Brownian motion has been discussed extensively in connection with fluorescence depolarization theory.[12,13] This theory has been extended by Tao[14] in two aspects: his discussion includes the case where the molecule is considered a completely

asymmetric rotor, and the time dependent distribution is obtained.

In what follows, we shall use Tao's definitions and notation in applying his method and results for CPE. We define $W(\theta, \phi, t)$ as the probability that the vector μ_{f0}' is in the direction (θ, ϕ) at time t in the lab coordinate system (Figure 2). $G(\theta_0, \phi_0|\theta, \phi, t)$ is the probability evolution function for $W(\theta, \phi, t)$, i.e., it will give the probability that the moment $\mu_{f0'}$, which was in direction (θ_0, ϕ_0) at time $t = 0$, will be in direction (θ, ϕ) at time t. From the definitions it follows that

$$W(\theta, \phi, t) = \int_0^{2\pi} d\phi_0 \int_0^{\pi} \sin\theta_0 \, d\theta_0 \, W(\theta_0, \phi_0) G(\theta_0, \phi_0|\theta, \phi, t)$$

(16)

where $W(\theta_0, \phi_0)$ is the initial distribution of the transition directions, i.e.

$$W(\theta_0, \phi_0) = W(\theta, \phi, 0)$$

The probability that a molecule with transition moment μ will be excited by unpolarized light traveling in the Z direction is proportional to $(\mu \sin\theta)^2$ where θ is the angle between μ and Z. The normalized initial distribution will be, therefore

$$W(\theta_0, \phi_0) = \frac{3}{8\pi} \sin^2\theta_0 = \frac{1}{4\pi}[1 - P_2(\cos\theta_0)] \quad (17)$$

where $P_2(\cos\theta_0)$ is the Legendre polynomial of order 2.

Expanding $G(\theta_0, \phi_0|\theta, \phi, t)$ in terms of the surface harmonics

$$G(\theta_0, \phi_0|\theta, \phi, t) = \sum_{l=0}^{\infty} \sum_{m=-l}^{l} C_{l,m}(t) Y_{l,m}^*(\theta_0, \phi_0) Y_{l,m}(\theta, \phi) \quad (18)$$

This expansion involves the addition theorem for spherical harmonics with time dependent coefficients. Using the appropriate normalization and boundary conditions for G (ref 14), and substituting eq 17 and 18 in the definition 16 gives

$$W(\theta, \phi, t) = \frac{1}{4\pi}[1 - C_{2,0}(t) P_2(\cos\theta)] \quad (19)$$

Because of the orthogonality of the surface harmonics the only coefficient that contributes to $W(\theta, \phi, t)$ is $C_{2,0}(t)$. The value of this coefficient depends on the shape of the molecules and the specific mechanism by which redistribution of the moments takes place.

Assuming that $C_{2,0}(t)$ is known, we can proceed to substitute (19) into (15) and average over the distribution arising from photoselection and Brownian relaxation.

$$R_{ZZ}(t) = \int_0^{2\pi} d\phi \int_0^{\pi} \sin\theta \, d\theta \cdot A \sin^2\theta \, W(\theta, \phi, t) =$$

$$A \cdot \frac{2\pi}{4\pi} \int_0^{\pi} \sin^3\theta[1 - C_{2,0}(t) P_2(\cos\theta)] \, d\theta =$$

$$2A\left[\frac{1}{3} + \frac{1}{15} C_{2,0}(t)\right] \quad (20)$$

$R_{ZZ}(t)$ is defined as the contribution to R_{ZZ} of a molecule which emits at time t. If we assume that the mechanism of redistribution is the rotary diffusion of spheres of volume V in a solution of viscosity η then as was shown by Favro[15] the coefficients $C_{l,m}(t)$ are $= e^{-l(l+1)\theta t}$ where $\Theta = kT/6V\eta$. This result was obtained by solving the equation for the probability distribution function.[16] Therefore $C_{2,0}(t) = e^{-6\theta t}$ and $\bar{R}_{ZZ}(t) = 2A[(1/3) + (1/15) \cdot e^{-6\theta t}]$. The steady-state CPE is obtained by taking the time av-

erage over the emission decay. The probability of emission at time t of a molecule which is excited at $t = 0$ is given by $\rho(t) = k_0 e^{-t/\tau}$ where $k_0 = 1/\tau_0$ is the rate constant for the emission process, τ is the relaxation time for all processes, and $e^{-t/\tau}$ is the probability that the molecule remains excited at time t. Integration over all times give τ/τ_0 which is the fluorescence efficiency. To get the time average rotatory strength, $R_{ZZ}(t)$ must be integrated over, time weighted by $\rho(t)$

$$R_{ZZ} = k_0 \int_0^{\infty} R_{ZZ}(t) e^{-t/\tau} \, dt =$$

$$2A(\tau/\tau_0)\left(\frac{1}{3} + \frac{1}{15}\frac{1}{6\theta\tau + 1}\right) \quad (21)$$

If $\theta\tau \gg 1$, i.e., if the molecules reach a random distribution before emission, then R_{ZZ} reduces to the expression for a randomly oriented sample, $R_{ZZ} \rightarrow (2/3)A$; in the other extreme, i.e., the initial distribution exists at the time of emission, the expression reduces to $2A[(1/3) + (1/15)] = 2A(2/5) = (4/5)A$. The coefficient 4/5 is specific to the special geometry of our case. The direct calculation of R_{ZZ} for the extreme cases of no Brownian movement and for uniformly distributed excitation gives the same results.

The fluorescence intensity, and therefore the dipole strength, also depend on the rate of relaxation of the photoselection process. The elements of the dipole strength tensor D are of the form $3(\mu_\beta)_{f0} \cdot (\mu_\gamma)_{f0}$. The factor of 3 in this definition cancels out the factor of 3 that is contained in intensity formulas because of the assumed averaging over all orientations. The elements of the diad are to be obtained from eq 4. The principal part of the fluorescing dipole is in the z direction because of the selection of the coordinate system, so the only elements of D which do not vanish in first-order perturbation theory are those with indices 13, 31, 23, 32, and 33 in the molecular coordinate system 1, 2, and 3. Averaging over all orientations about the 3 axis causes all but the 33 element to vanish leaving the dipole strength tensor with only this single element on the diagonal. D_{33} can be evaluated as the product of the z components of eq 4 with the elimination of terms in V^2

$$D_{33} = 3\left\{|(\mu_3)_{f'0}|^2 - \frac{4\epsilon_j V_{0f,j0'}}{\epsilon_j^2 - \epsilon_f^2}(\mu_3)_{f0'}(\mu_3)_{j0}\right\} \quad (22)$$

The second term in eq 22 has the form, origin, and significance of the hypo(hyper)chromicity terms of absorption spectroscopy. It describes a dipolar coupling mechanism which leads to the enhancement or attenuation of emission intensity. The scalar dipole strength, $D_{f0'}$, is given by the product $|\langle 0f|\mu|00'\rangle|^2$ and so to the first order in perturbation theory is identical with the term in braces in the above equation. The dipole strength may be evaluated from eq 22 though it will, in general, be more direct and accurate to obtain it from the relationship which exists between the dipole strength, the fluorescence lifetime, and the fluorescence efficiency. At any rate the dipole strength tensor in the molecular coordinate system has the form

$$\mathbf{D}_{f0'} = 3\left\{\begin{matrix} 0 & 0 & 0 \\ 0 & 0 & 0 \\ 0 & 0 & D_{f0'} \end{matrix}\right\} \quad (23)$$

after averaging about orientations around the transition dipole.

This discussion of the dipole strength brings out the nature of one of the approximations of this calculation.

Strictly speaking the system should be averaged about an axis defined by the direction of the absorbing transition dipole. We have averaged around the direction of the zeroth order emitting dipole. The manner in which one must alter fluorescence polarization formulas to account for the difference in direction between the absorbing and emitting dipole has been the subject of careful study and the appropriate corrections can be added to a more complete formulation.

The dipole strength of the radiation which is emitted in the forward direction will be taken as the sum of the dipole strengths for x and y polarizations, i.e.

$$D_{ZZ} = D_x + D_y = (\mathbf{i} \cdot \mathbf{S}(\mathbf{D}_{f0'})(\tilde{\mathbf{S}}) \cdot \mathbf{i}) + (\mathbf{j} \cdot \mathbf{S}(\mathbf{D}_{f0'}) \cdot \tilde{\mathbf{S}} \cdot \mathbf{j})$$

where $\mathbf{i}$ and $\mathbf{j}$ are unit vectors in the direction of the X and Y axes of the laboratory coordinate system. We obtain

$$D_{ZZ} = 3 \sin^2 \theta D_{f0'} \tag{24}$$

This is, however, of precisely the same form as (15) but with $3D_{f0'}$ instead of A. Consequently the treatment of rotary Brownian movement follows the same course as that for the rotatory strength with the final result

$$D_{ZZ} = 6D_{f0'} \frac{\tau}{\tau_0} \left(\frac{1}{3} + \frac{1}{15} \frac{1}{6\theta\tau + 1} \right) \tag{25}$$

We thus see that the decay of photoselection leads to an attenuation of the emission intensity which is of the same form as the decay in the CPE signal. Consequently if the ratio $\Delta I/I = 4R_{ZZ}/D_{ZZ}$ is used as the experimental quantity, the decay of photoselection has no effect on the result. This is, in fact, a much simpler experiment than obtaining the magnitude of ΔI itself. We state the complete final result

$$\frac{\Delta I}{I} = \frac{8A}{3D_{f0'}} = \frac{4}{D_{f0'}} \frac{\epsilon_f V_{0f,j0'}}{\epsilon_j^2 - \epsilon_f^2} \mathrm{Im}\{(\mu)_{f0'}^{0} \cdot (\mathbf{m})_{j0}\} \tag{26}$$

or

$$\frac{\Delta I}{I} = \frac{4}{\hbar c D_{f0'}} \frac{\epsilon_f \epsilon_j}{\epsilon_0^2 - \epsilon_f^2} V_{0f,j0'} (\mathbf{R}^a \cdot (\mu)_{j0}^{0} \times (\mu)_{f0'}^{0})$$

Note that the relaxation times have cancelled out.

Discussion

The principal results of the paper are 21 and 26 which give explicit results for the forward component of the rotatory strength and for the fraction of fluorescent light that is circularly polarized. The first formula shows that the intensity of circularly polarized light is diminished by only a sixth by the rotational relaxation of the photoselected molecules. The second formula shows that the total emitted intensity and the intensity of circularly polarized

emission follow the same laws of averaging in space and time so that the relaxation process does not affect their ratio. Since this ratio is the quantity which is usually measured, the indication is that considerations of photoselection and relaxation can be bypassed. This will often be a desirable simplification.

The results apply only to spheres but can be generalized to other shapes by procedures which have already been established for the linear polarization of fluorescence by Perrin, Weber, Favro, and Tao. These generalizations include molecules of other shapes (ellipsoids in particular) and the possibility that the transition moment at the time of emission no longer has the same orientation as at the time of absorption. Processes which change the direction of the active transition dipole other than rotary diffusion are internal conversion of electronic states, energy transfer, and local motions of the emitting chromophore.

The quantum-optical part of the calculation can also be generalized utilizing the formalism available for the calculation of the rotatory strength of absorption processes. The inclusion of all possible extensions of the model will yield formulas of unwieldy complexity, so we have dealt only with the simplest case. Complications appropriate for given systems can be grafted onto this basic system.

We have not yet investigated the manner in which these generalizations might affect the cancellations leading to eq 26.

References and Notes

(1) This research was supported in part by Grant No. GB-27399X2 of the National Science Foundation and Grant No. GM-20195 of the National Institutes of Health.
(2) (a) R. N. Samojlov, J. Exp. Theor. Phys., 18, 1030 (1948); (b) M. S. Brodin and V. Reznichenko, Ukr. Phys. J., 10, 178 (1965).
(3) C. A. Emeis and L. J. Oosterhof, Chem. Phys. Lett., 1, 129 (1967).
(4) The initials CPL have been used by several authors to designate circularly polarized luminescence. Since the initials cpl are already fairly well established as signifying circularly polarized light, we find it preferable to designate by CPE the process of circularly polarized emission.
(5) (a) I. Z. Steinberg and A. Gafni, Rev. Sci. Instrum., 43, 409 (1972); (b) J. Schlessinger and I. Steinberg, Proc. Natl. Acad. Sci. U. S., 69, 769 (1972).
(6) I. Tinoco and W. G. Hamerle, J. Phys. Chem., 60, 1619 (1956).
(7) D. M. Hercules, Ed., "Fluoescence and Phosphorescence Analysis," Interscience, New York, N. Y., 1966, Chapter 1.
(8) J. Schellman, Accounts Chem. Res., 1, 144 (1968).
(9) P. M. Bayley, E. Nielsen, and J. A. Schellman, J. Chem. Phys., 73, 228 (1969).
(10) H. J. Hofrichter, Ph.D. Thesis, University of Oregon, Eugene, Oreg., 1971.
(11) J. Snir and J. A. Schellman, J. Phys. Chem., 77, 1653 (1973).
(12) F. Perrin, J. Phys. Radium, 5, 497 (1934).
(13) G. Weber, Biochem. J., 51, 145 (1952).
(14) T. Tao, Biopolymers, 8, 609 (1969).
(15) L. D. Favro, Phys. Rev., 119, 53 (1960).
(16) P. Debye, "Polar Molecules," Dover, New York, N. Y., 1945, Chapter 5.

Application of the Semicontinuum Model to Temperature Effects on Solvated Electron Spectra and Relaxation Rates of Dipole Orientation Around an Excess Electron in Liquid Alcohols

Kenji Fueki, Da-Fei Feng, and Larry Kevan*

Department of Chemistry. Wayne State University, Detroit, Michigan 48202 (*Received August 16, 1973*)

A method is developed for calculation of relaxation times for dipole orientation in liquid alcohols induced by localized excess electrons. A microscopic model is used which utilizes quantities calculated from the Fueki, Feng, Kevan semicontinuum model of solvated and trapped electron energy levels. Calculated results for methanol, ethanol, and 1-propanol *vs.* temperature agree well with the limited experimental data available. The semicontinuum model has also been applied to the calculation of temperature effects on solvated electron spectra in liquid methanol, ethanol, and 1-propanol. The temperature dependence of the quasifree electron state, V_0, and of the effective dipole moment of molecules in the first solvation shell around the electron are considered for the first time. The calculated results account for about 70% of the observed temperature dependence.

Introduction

In our previous work[1-4] we have developed a semicontinuum model for solvated or trapped electrons in polar liquids and solids and have shown that the semicontinuum model can satisfactorily account for various physical properties of solvated or trapped electrons in a wide range of matrices. Copeland, Kestner, and Jortner have developed a similar model for solvated electrons in water and liquid ammonia.[5-8] In the Fueki, Feng, Kevan model, a self-consistent field approximation is used to obtain the potential, while in the Copeland, Kestner, Jortner model a modified adiabatic approximation is used to obtain the potential. The mathematical differences between these two models have recently been discussed and compared in detail.[9]

Recent developments in pulse radiolysis techniques have made it possible to directly observe changes in solvated electron spectra with time on nano- to picosecond time scales.[10-12] A theoretical calculation has recently been made of the formation time of solvated electrons in a model system which represents a very dilute solution of a polar solute in a nonpolar solvent.[13] However, such a model is not representative of actual experimental conditions to date and is not directly applicable to the interpretation of the reported time-dependent spectral changes of solvated electrons. We report in this paper the first calculation of relaxation times for dipole orientation induced by localized excess electrons in alcohols on the basis of a microscopic model which utilizes quantities calculated from the Fueki, Feng, Kevan semicontinuum model. In connection with this relaxation time calculation, we have also applied the Fueki, Feng, Kevan semicontinuum model to the calculation of temperature effects on solvated electron spectra in liquid methanol, ethanol, and 1-propanol. Previously, Iguchi has made a calculation of the temperature dependence of solvated electron spectra in alcohols based on an oriented dipole model.[14] In his calculation, however, the configurational stability of the solvated electron was not established and the cavity radius was chosen arbitrarily.

Outline of Calculation

A. Temperature Effect. A formulation of the semicontinuum model for the solvated electron is given in ref 1 and 4. It is assumed that the solvated electron interacts with the dipoles of oriented alcohol molecules in the first solvation shell by a short-range charge dipole attractive potential. The solvent molecules beyond the first solvation shell are treated as a continuous dielectric medium with which the electron interacts by a long-range polarization potential. The number of solvent molecules in the first solvation shell is taken to be 4 or 6. These molecules are arranged symmetrically around the center of a cavity containing the electron.

The total ground and excited state energies are given by the sum of the kinetic energy of the electron, the electronic energy for short-range attractive charge dipole interactions, the short-range medium rearrangement energy from dipole–dipole interactions, the electronic energy for long-range polarization interactions, the medium rearrangement energy for long-range polarization interactions, the energy required to form a void in the medium, and the short-range interaction energy arising from a Wigner–Seitz model.

In the calculation of an energy level with the semicontinuum model the obvious temperature dependent factors are the static dielectric constant and the Langevin factor which determines the degree of dipole orientation at thermal equilibrium. In addition to the above factors, which have not given satisfactory results previously,[5] we here consider the temperature dependence of the quasifree electron state, V_0, and of the effective dipole moment of the molecules in the first solvation shell. If either of these latter quantities is assumed to be temperature independent, the agreement of calculated with experimental results is worse, so both are clearly important. The temperature dependence of these factors have not been previously considered in electron solvation.

The values of the physical constants used in the present calculation are listed elsewhere; see paragraph at end of paper regarding supplementary material. The energy V_0

was estimated as a function of temperature, or actually medium density, by the following approach. (1) At room temperature V_0 is found with which the calculated optical transition energy fits the experimental value at that temperature. (2) The hard-core radius, $\bar{a}$, is calculated by the Wigner–Seitz method,[3,15] i.e., from

$$\tan k_0(r_{ws} - \bar{a}) = k_0 r_{ws} \tag{1}$$

where r_{ws} is the Wigner–Seitz radius which equals $(\frac{3}{4} \pi n)^{1/3}$ and k_0 is the electron wave vector. (3) V_0 is calculated for various medium densities from eq 2 by using this value of $\bar{a}$

$$V_0 = T + U_p$$

$$T = \hbar^2 k_0^2 / 2m$$

$$U_p = -(3\alpha e^2/2r_{ws}^4)\{(8/7) + [1 + (1/3)(8\pi\alpha n)]^{-1}\} \tag{2}$$

where α is the isotropic polarizability of a solvent molecule and n is the number density of solvent molecules. V_0 changes with temperature because n, r_{ws}, and k_0 do; the values of V_0 obtained in this way are given elsewhere: see paragraph at end of paper. In methanol V_0 varies from 0.00 eV at 140 K to -0.26 eV at 358 K. In ethanol V_0 varies from 0.58 eV at 140 K to 0.08 eV at 343 K. In 1-propanol V_0 varies from 0.83 eV at 129 K to 0.32 eV at 298 K.

The effective permanent dipole moment, μ, of a given molecule in polar liquids is different from the gas-phase dipole moment, μ_0. This effect was treated from a molecular point of view by Kirkwood[16] who introduced a correlation factor g defined by (3). To treat the specific case of

$$\mu = \mu_0 g^{1/2} \tag{3}$$

alcohols, we will consider a model in which an equilibrium between monomeric molecules and hydrogen-bonded dimeric molecules exist. We will also assume free rotation about the hydrogen bond. We will neglect trimers and higher nmers for simplicity. The effective dipole moment of a monomeric molecule is taken to be the gas-phase value with $g_1 = 1$. For the dimeric molecules we take $g_2 = 1.40$ based on Dannhauser and Cole's treatment of the dielectric properties of liquid alcohols.[17] We can then define an average correlation factor $\bar{g}$ by (4) in which α is the fraction of monomeric molecules.

$$\bar{g} = 1.40 - 0.40\alpha \tag{4}$$

We now introduce a temperature dependence via the equilibrium constant defined by (5) where $\Delta F^\circ = \Delta H^\circ - T\Delta S^\circ$

$$\exp(-\Delta F^\circ/RT) = (1 - \alpha^{1/2})\alpha^{-1} \tag{5}$$

$T\Delta S^\circ$ and the thermodynamic quantities refer to hydrogen bonding. The values of ΔH° used are given in Table I and are taken as one-half the values reported for hydrogen bonding with two hydrogen bonds per alcohol molecule.[18] Values of ΔS° for hydrogen bonding have also been reported[18] for a model in which equilibria between various nmers and with restricted rotation about the hydrogen bonds have been considered. However, ΔS° will be rather sensitive to the particular hydrogen bonding model chosen, so we have treated ΔS° as a limited parameter constrained to values near those reported for the model described above. An appreciable temperature dependence for μ is only found for ΔS° values more negative than given in ref 18; the ΔS° values used are summarized elsewhere: see paragraph at end of paper. The consequent temperature dependence of μ varies from 2.01 (140 K) to 1.77 (358 K) in methanol, from 2.00 (140 K) to 1.69 (343

K) in ethanol, and from 2.00 (129 K) to 1.70 (298 K) in 1-propanol.

Once V_0 and μ have been found as a function of temperature, the energy levels and optical transition energy are then calculated as a function of temperature by the Fueki, Feng, Kevan semicontinuum model.

B. Relaxation Time of Dipole Orientation. In this section we describe a method of calculation for the orientational relaxation time of molecular dipoles in the first solvation shell around a solvated electron. The rate of change in dipole orientation angle, θ, is given by Debye[19] as

$$\zeta \frac{d\theta}{dt} = -\mu \frac{C_{1s}e}{r_d^{02}} \sin\theta \tag{6}$$

where e is the electronic charge; μ is the permanent dipole moment; ζ is the internal friction constant, $\zeta = 8\pi\eta a^3$ (η is the microscopic viscosity and a is the rotational radius of the molecule); r_d^0 is the distance between the center of a cavity and the center of a dipole in the first solvation shell at the configurational minimum; and C_{1s} is the charge enclosed with radius r_d^0 for the ground state of a solvated electron. In a previous study[2] we have shown that r_d^0 and C_{1s} are nearly independent of θ when θ is less than 80°. Therefore. to a good approximation, we may regard C_{1s}/r_d^{02} in eq 6 as a constant characteristic of an individual system. Then, eq 6 can be readily integrated to give

$$\tau_r = -\frac{\zeta r_d^{02}}{\mu C_{1s}e} \int_{\theta_0}^{\theta_{th}} \frac{d\theta}{\sin\theta} = \frac{\zeta r_d^{02}}{\mu C_{1s}e} \ln\left[\frac{\tan(\theta_0/2)}{\tan(\theta_{th}/2)}\right] \tag{7}$$

Equation 7 gives the time required for dipole rotation from an initial orientation angle, θ_0, to the orientation angle at thermal equilibrium. Here we define the relaxation time of dipole orientation by eq 7. In eq 7, r_d^0, C_{1s}, and θ_{th} can be obtained from the semicontinuum model calculation described in the previous section, and they are given in Tables I and II. θ_0 is taken to be a parameter which is varied over angles less than 80°. ζ can be calculated by using η approximated by the macroscopic viscosity.[20,21] The rotational radii, a, used in the calculation were 1.8, 2.0, and 2.2 Å for methanol, ethanol and 1-propanol, respectively[22,23]; these values are larger than the corresponding values of r_s, the molecular radius, by about 10%.

Results and Discussion

A. Temperature Effect. The results of the temperature dependence calculations are given in Tables I and II. For the solvated electron in methanol the calculated 1s → 2p transition energy, $h\nu$, decreases with increasing temperature, and the calculated temperature coefficient of $h\nu$ is 72% of the experimental values.[24] Likewise, the calculated threshold energy for photoconductivity, I, decreases significantly with increasing temperature. The calculated oscillator strength, f, only decreases slightly with increasing temperature. The magnitude of f is about 75% larger than recently revised experimental values;[24] this is a larger discrepancy than previously believed,[4] but the experimental values are probably lower limits due to the uncertainty in the spectral extrapolation to short wavelengths. The heat of solution, ΔH, behaves in a complicated way but generally decreases with increasing temperature. The orientation angle, θ_{th}, of molecular dipoles in the first solvation shell at thermal equilibrium increases with increasing temperature as expected. The cavity radius, r_d^0, is constant over the temperature range studied. The calculated

TABLE I: Temperature Effect on the Properties of the Solvated Electron in Methanol, Ethanol, and 1-Propanol for $N = 4$

T, K	r_d^0, Å	f	I, eV	ΔH, eV	θ_{th}, deg	$h\nu$(calcd), eV	$h\nu$(obsd),[a] eV
				Methanol			
140	2.28	0.723	3.788	2.220	10.1	2.268	
160	2.28	0.720	3.751	2.230	10.9	2.243	
183	2.28	0.717	3.692	2.234	11.7	2.205	2.22
195	2.28	0.713	3.662	2.234	12.1	2.183	2.20
243	2.28	0.707	3.514	2.209	13.8	2.080	2.07
294	2.28	0.702	3.362	2.169	15.7	1.974	1.95
320	2.28	0.702	3.287	2.154	16.6	1.923	1.90
336	2.28	0.702	3.246	2.144	17.1	1.897	1.84
358	2.28	0.702	3.193	2.134	17.8	1.865	1.75
				Ethanol			
140	2.56	0.805	3.708	1.845	11.1	2.201	
155	2.56	0.797	3.659	1.850	11.7	2.172	2.27
173	2.56	0.783	3.581	1.842	12.5	2.123	2.23
195	2.51	0.737	3.467	1.816	13.4	2.072	2.13
234	2.51	0.716	3.275	1.777	15.3	1.936	2.03
296	2.51	0.702	3.086	1.776	17.6	1.816	1.80
323	2.51	0.708	3.006	1.783	18.5	1.767	1.73
343	2.51	0.697	2.943	1.788	19.1	1.730	1.66
				1-Propanol			
129	2.83	0.888	3.555	1.623	11.5	2.049	
147	2.83	0.868	3.480	1.628	12.3	2.015	2.25
173	2.77	0.816	3.363	1.616	13.5	1.978	
195	2.77	0.787	3.231	1.592	14.7	1.898	
227	2.77	0.755	3.081	1.576	16.3	1.805	
249	2.77	0.744	3.005	1.577	17.3	1.759	
273	2.77	0.731	2.929	1.584	18.2	1.713	
298	2.77	0.720	2.849	1.590	19.2	1.668	1.67[b]

[a] Reference 24. [b] Reference 25.

TABLE II: Charge Distribution of the Solvated Electron in the Ground State

	Methanol			Ethanol			1-Propanol	
	$C_{1s}(r_d^0)$			$C_{1s}(r_d^0)$			$C_{1s}(r_d^0)$	
T, K	$N = 4$	$N = 6$	T, K	$N = 4$	$N = 6$	T, K	$N = 4$	$N = 6$
140	0.667	0.728	140	0.713	0.762	129	0.743	0.785
160	0.666	0.724	155	0.711	0.759	147	0.740	0.782
183	0.662	0.722	173	0.706	0.755	173	0.729	0.774
195	0.661	0.720	195	0.694	0.748	195	0.722	0.766
243	0.652	0.711	234	0.684	0.732	227	0.713	0.754
294	0.642	0.701	296	0.672	0.720	249	0.709	0.750
320	0.637	0.695	323	0.668	0.716	273	0.706	0.746
336	0.635	0.693	343	0.665	0.712	298	0.700	0.742
358	0.632	0.688						

$h\nu$, I, and ΔH for molecular dipole coordination number N = 6 are smaller than those for $N = 4$ and are given elsewhere; see paragraph at end of paper. Trends in the calculated temperature dependence of various physical properties of the solvated electron in ethanol are very similar to those in methanol. The calculated temperature coefficient of $h\nu$ is 72% of the experimental value.[24] The calculated results on the solvated electron in 1-propanol are similar. The calculated temperature coefficient of $h\nu$ is 60% of the experimental value. It is noted that the experimental data at different temperatures are taken from two sources.[10,25]

Table II presents the fraction of charge, $C_{1s}(r_d^0)$, enclosed within radius r_d^0 for the ground state of the solvated electron in methanol, ethanol, and 1-propanol. The values of $C_{1s}(r_d^0)$ decrease somewhat with increasing temperature for all cases. $C_{1s}(r_d^0)$ increases, as does r_d^0 for methanol to ethanol to 1-propanol.

We would like to stress the importance of the temperature dependence of the permanent dipole moment, μ, on the calculated temperature dependence of the transition energy. Using the temperature independent gas-phase value, μ_0, of the permanent dipole moment and keeping all the other physical constants the same, we obtain a calculated temperature coefficient of $h\nu$ which accounts for only 50% of the experimental values. It is interesting to note that the oriented dipole model,[14] in which the gas-phase value of the permanent dipole moment is used, also accounts for only 50% of the experimental temperature coefficient of $h\nu$ for the solvated electron in alcohols. Thus it appears that the temperature dependence of μ should be considered. Although our estimate of the temperature dependence of μ is based on a very simple model, the success of our calculation suggests that a more general treatment of μ is desirable in order to improve the semicontinuum model for excess electrons.

Previous applications of the semicontinuum model[1-8] have used the gas-phase dipole moment μ_0 in the charge-dipole potential. In the condensed phase it is probably more appropriate to use the effective dipole moment μ
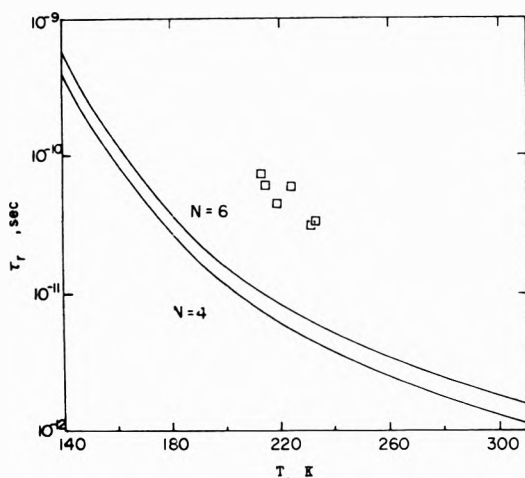
Figure 1. Calculated relaxation times of dipole orientation by a solvated electron in methanol vs. temperature: $\theta_0 = 80°$. Experimental data points ($\square$) are from Gilles, Aldrich, and Hunt.[12]

Figure 2. Calculated relaxation times of dipole orientation by a solvated electron in ethanol vs. temperature: $\theta_0 = 80°$. Experimental data points are from Gilles, Aldrich, and Hunt ($\square$),[12] Baxendale and Wardman (O),[10] and Beck and Thomas (I).[11]

which involves the Kirkwood correlation factor. Then this correlation factor is included in the semicontinuum model in a natural way. The Kirkwood correlation factor was previously invoked without any theoretical consideration to correlate empirically transition energies at absorption maxima in solvated electron spectra in polar solvents with some physical properties of solvents.[26]

Kestner, Jortner, and Gaathon[7] have recently discussed the temperature dependence of the optical absorption maximum for electrons in ammonia and water. Their original theoretical results[5] gave poor agreement with experiment because they only considered the temperature dependence of the Langevin factor which determines the degree of dipole orientation at thermal equilibrium and of the static dielectric constant. They did not originally consider the temperature dependence of V_0, which depends on density, so their calculation was done for constant density conditions. They have now corrected this in an *ad hoc* fashion[7] and obtain good agreement between experiment and theory for ammonia, but poor agreement still exists for water (only 20% of the experimental temperature dependence is calculated). Their correction is not applicable to our calculation because we explicitly consider the temperature dependence of V_0 and do not constrain the calculation to constant density. We feel that their poor agreement for water occurs primarily because the water molecule is small and the charge-dipole interaction with the first solvation shell is large. Consequently, the temperature dependence of the Langevin term is small. Also a temperature-dependent μ should improve the results for water.

Nilsson[27] has given a purportedly successful calculation for the temperature dependence of the optical band maximum of electrons in water and ice. He uses a modified semicontinuum model, as originally introduced by Fueki, Feng, and Kevan,[28] in which the configurational stability of the ground state is *not* established. Nilsson assumed that the thermal expansion of the cavity containing the electron is proportional to the thermal expansion of bulk ice and water. To us, the apparent good agreement between theory and experiment that Nilsson finds is probably largely fortuitous since configurational stability calculations show that the cavity radius is almost independent of temperature (see Table I).

B. Relaxation Time of Dipole Orientation. The results
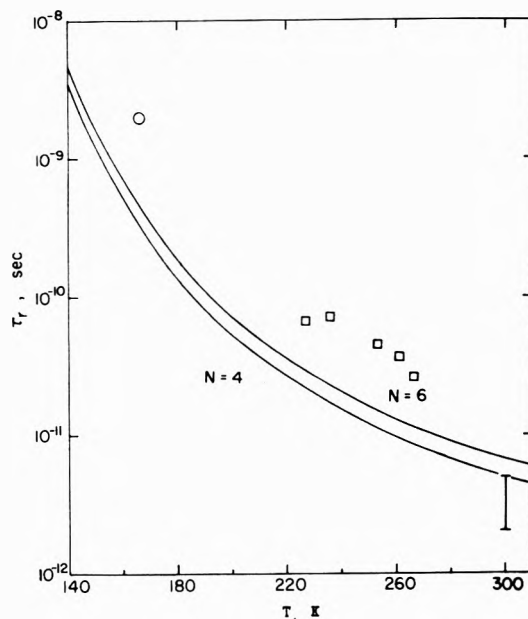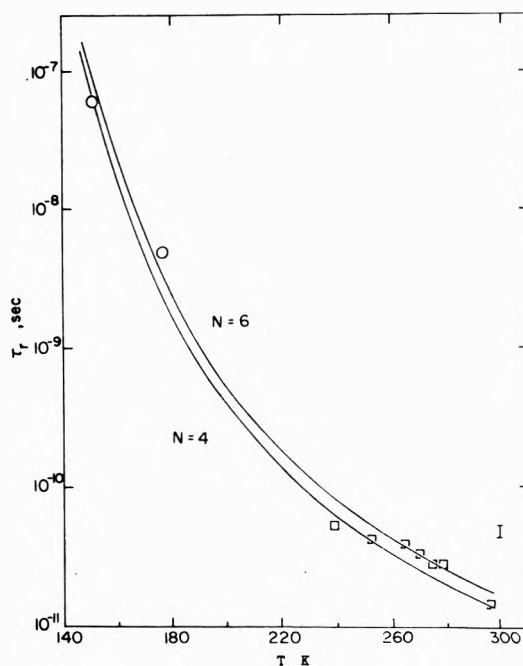
Figure 3. Calculated relaxation times of dipole orientation by a solvated electron in 1-propanol vs. temperature: $\theta_0 = 80°$. Experimental data points are from Gilles, Aldrich, and Hunt ($\square$),[12] Baxendale and Wardman (O),[10] and Beck and Thomas (I).[11]

of the calculations are given in Figures 1-6. Figures 1-3 show the relaxation time, τ_r, of dipole orientation in the presence of the solvated electron as a function of temperature for methanol, ethanol, and 1-propanol, respectively. The initial dipole orientation angle, θ_0, is taken to be 80° in these figures. The results for coordination number $N = 4$ and 6 are given in each figure, from which it is seen that τ_r is somewhat less for $N = 4$ than for $N = 6$ at the same temperature.

The only experimental data for comparison to our results in methanol are e_{sol}^- formation times by Gilles, Al-
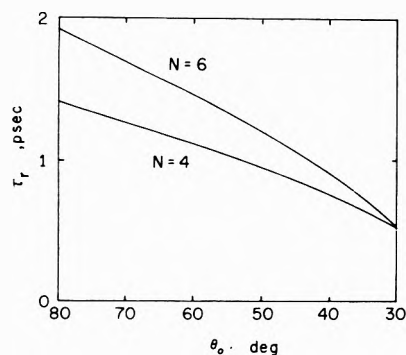
Figure 4. Relaxation time of dipole orientation by a solvated electron in methanol at 294 K vs. initial orientation angle.
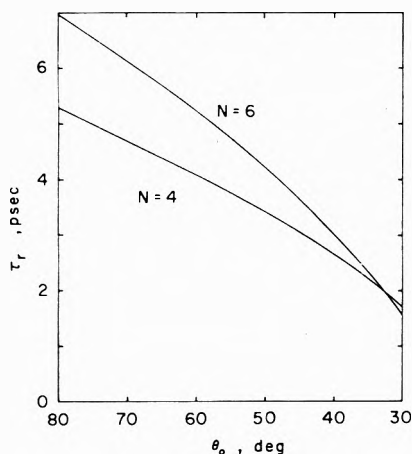
Figure 5. Relaxation time of dipole orientation by a solvated electron in ethanol at 296 K vs. initial orientation angle.

Figure 6. Relaxation time of dipole orientation by a solvated electron in 1-propanol at 298 K vs. initial orientation angle.

drich, and Hunt[12] over a 20° temperature range which are about 6 times longer than the calculated values. More formation time data over a wider temperature range exist for ethanol[10-12] where the agreement with theory seems quite reasonable and in propanol[10-12] where the agreement between experiment and theory is excellent. Although the experimental data are quite limited, comparison with theory suggests that our model holds best for higher alcohols.

Figures 4–6 show the relaxation time of dipole orientation at room temperature in the presence of the solvated electron as a function of initial dipole orientation angle, θ_0, for methanol, ethanol, and 1-propanol, respectively. Similar results are found at other temperatures. The relaxation times are less for $N = 4$ than for $N = 6$ at the same value of θ_0 except for $\theta_0 \leq 35°$. Note that the dependence of τ_r on θ_0 is rather small; for example, τ_r varies from 0.5 to 1.4 psec for methanol, 1.7 to 5.2 psec for ethanol, and 3.8 to 13.2 psec for 1-propanol over $\theta_0 = 30$ to 80° for $N = 4$. Thus the difference in solvation time for electrons that become localized in different depths of the fluctuating potential in a liquid appears to be small.

Since ζ is proportional to the viscosity η, the temperature dependence of ζ is that of η and is expressed by $\exp[B/(T - T_0)]$, where B and T_0 are constants characteristic of the solvent.[21] The temperature dependencies of the other quantities in eq 7 are small. Therefore, the temperature dependence of τ_r should be of the form, $\exp[B/(T - T_0)]$ and follow the temperature dependence of the viscosity. The agreement with experiment in Figure 3 suggests that this form of temperature dependence is ob-

served experimentally. It was previously noted that electron solvation times in 1-propanol are well described by the form, $\exp[B/(T - T_0)]$.[10] Within the model presented here it appears appropriate to compare the temperature dependence of electron solvation with that of viscosity. It also appears that use of the macroscopic viscosity is a good approximation to the microscopic viscosity, at least for the liquid alcohols studied here.

Supplementary Material Available. The physical constants used in the calculations, the detailed temperature dependence of μ and V_0, and temperature effects on the properties of solvated electrons in methanol, ethanol, and 1-propanol for $N = 6$ will appear following these pages in the microfilm edition of this volume of the journal. Photocopies of the supplementary material from this paper only or microfiche (105 × 148 mm, 24× reduction, negatives) containing all of the supplementary material for the papers in this issue may be obtained from the Journals Department, American Chemical Society, 1155 16th St., N.W., Washington, D. C. 20036. Remit check or money order for $3.00 for photocopy or $2.00 for microfiche, referring to code number JPC-74-393.

References and Notes

(1) K. Fueki, D. F. Feng, L. Kevan, and R. Christoffersen, *J. Phys. Chem.*, **75**, 2297 (1971).
(2) K. Fueki, D. F. Feng, and L. Kevan, *J. Chem. Phys.*, **56**, 5351 (1972).
(3) D. F. Feng, K. Fueki, and L. Kevan, *J. Chem. Phys.*, **57**, 1253 (1972).
(4) K. Fueki, D. F. Feng, and L. Kevan, *J. Amer. Chem. Soc.*, **95**, 1398 (1973).
(5) D. A. Copeland, N. R. Kestner, and J. Jortner, *J. Chem. Phys.*, **53**, 1189 (1970).
(6) J. Logan and N. R. Kestner, *J. Phys. Chem.*, **76**, 2738 (1972).
(7) N. R. Kestner, J. Jortner, and A. Gaathon, *Chem. Phys. Lett.*, **19**, 328 (1973).

(8) N. R. Kestner and J. Jortner, J. Phys. Chem., **77**, 1040 (1973).
(9) L. Kevan in "Advances in Radiation Chemistry," M. Burton and J. L. Magee, Ed., Wiley-Interscience, New York, N. Y., 1973.
(10) J. H. Baxendale and P. Wardman, Nature (London), **230**, 449 (1971); J. Chem. Soc., Faraday Trans. 1, **69**, 584 (1973).
(11) G. Beck and J. K. Thomas, J. Phys. Chem., **76**, 3856 (1972).
(12) L. Gilles, J. E. Aldrich, and J. W. Hunt, Nature (London), Phys. Sci., **243**, 70 (1973).
(13) A. Mozumder, J. Phys. Chem., **76**, 3824 (1972).
(14) K. Iguchi, J. Chem. Phys., **48**, 1735 (1968); **51**, 3137 (1969).
(15) B. E. Springett, J. Jortner, and M. H. Cohen, J. Chem. Phys., **48**, 2720 (1968).
(16) J. G. Kirkwood, J. Chem. Phys., **7**, 911 (1939); G. Oster and J. G. Kirkwood, ibid., **11**, 175 (1943).
(17) W. Dannhauser and R. H. Cole, J. Chem. Phys., **23**, 1762 (1955).
(18) W. Dannhauser and L. W. Bahe, J. Chem. Phys., **40**, 3058 (1964).

(19) P. Debye, "Polar Molecules," Dover Publications, New York, N. Y., 1929, p 81.
(20) R. C. Weast, Ed., "Handbook of Chemistry and Physics," 50th ed, Chemical Rubber Publishing Co., Cleveland, Ohio, 1969.
(21) M. R. Carpenter, D. B. Davies, and A. J. Matheson, J. Chem. Phys., **46**, 2451 (1967).
(22) Reference 19, p 102.
(23) S. Mizushima, Phys. Z., **28**, 418 (1927).
(24) K. N. Jha, G. L. Bolton, and G. R. Freeman, J. Phys. Chem., **76**, 3876 (1972).
(25) M. C. Sauer, Jr., S. Arai, and L. M. Dorfman, J. Chem. Phys., **42**, 708 (1965).
(26) G. R. Freeman, J. Phys. Chem., **77**, 7 (1973).
(27) G. Nilsson, J. Chem. Phys., **56**, 3427 (1972).
(28) K. Fueki, D. F. Feng, and L. Kevan, J. Phys. Chem., **74**, 1976 (1970).

Model Calculations of the Hydrogen/Deuterium Kinetic Isotope Effect in the H + Si₂H₆ Reaction

I. Safarik, T. L. Pollock, and O. P. Strausz*

Department of Chemistry, University of Alberta, Edmonton, Alberta, Canada (Received July 12, 1973)

Model studies within the framework of transition state theory have been carried out for the computation of the H/D kinetic isotope effect in the displacement reaction of H atoms with disilane, H + SiH₃SiH₃ → SiH₄ + SiH₃. The results obtained using full normal coordinate analysis suggest that the displacement of the silyl radical proceeds *via* a bridged activated complex (I) and not a linear intermediate. The isotope effect is shown to arise from force constant changes during passage from reactants to the activated complex as a result of three different sources: (a) geometrical alterations, (b) an increase in the number of normal modes, and (c) cancellation of interaction forces.

Hydrogen atoms react with disilane *via* hydrogen abstraction and a simultaneous, competing displacement type process[1]

$$H + Si_2H_6 \longrightarrow H_2 + Si_2H_5 \qquad (1)$$

$$H + Si_2H_6 \longrightarrow SiH_4 + SiH_3 \qquad (2)$$
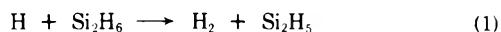
The rate constant of reaction 2 has been determined for disilane and disilane-d_6 and a direct isotope effect with a value of $k_H/k_D = 1.4$ established. Kinetic isotope effects have been reported for many similar types of S_N2 reactions in the liquid phase[2] but this represents the first gas-phase measurement. Since the gas-phase reaction is free from complications arising from solvent effects, reaction 2 appeared to be particularly inviting for a theoretical study of the origin of the isotope effect and the structure of the activated complex. With regard to the latter question two alternative models can be considered. One of these features a linear structure, Figure 1, and the other a bridged one

I
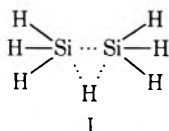
which is supported by certain experimental observations.[3]

Meaningful calculations can only be carried out on the linear model and therefore computations were not attempted on the bridged model.

The method of calculation of the kinetic isotope effect within the framework of the transition state theory has been worked out in detail by Biegeleisen,[4] Wolfsberg, and coworkers.[5] In the present study as in previous studies from this laboratory the computational procedure of Wolfsberg[5] was followed.

The isotopic rate ratio can be derived as a product of three factors

$$k_H/k_D = (MMI)(EXC)(ZPE)$$

where MMI, EXC, and ZPE represent the contributions from the translational and rotational energies, vibrational energies, and the zero point energies, respectively. Extensive model calculations with this method led to the conclusion that the kinetic isotope effect is caused by force constant changes at the sites of isotopic substitution in the transition from reactant to activated complex.[5]

Results

In the linear model, as depicted in Figure 1, the H atom attacks in the direction of the Si–Si bond. The Si¹H₃ group assumes a planar configuration and the Si²H₃ retains its

TABLE I: Diagonal Elements of the F Matrix for the Cases of C_{3v} and D_{3d}[a] Symmetry

i,j	F	F
1,1	f_d	f_d
2,2	$f_r + 2f_{rr}$	$f_r + 2f_{rr} + f'_{rr} + 2f'_{rr'}$
3,3	$^1/_2(f_\beta + f_\gamma) + f_{\beta\beta} + f_{\gamma\gamma} - f_{\beta\gamma} - 2f^*_{\beta\gamma}$	$^1/_2(f_\alpha + f_\beta) + f_{\alpha\alpha'} + f_{\beta\beta'} + ^1/_2(f'_{\alpha\alpha} + f'_{\beta\beta}) + f'_{\alpha\alpha'} + f'_{\beta\beta'} - f_{\alpha\beta} - 2f_{\alpha\beta'} - f'_{\alpha\beta} - 2f'_{\alpha\beta'}$
4,4	$f_{r'} + 2f_{r'r'}$	$f_r + 2f_{rr'} - f'_{rr} - 2f'_{rr'}$
5,5	$^1/_2(f_{\alpha'} + f_{\beta'}) + f_{\alpha'\alpha'} + f_{\beta'\beta'} - f_{\alpha'\beta'} - 2f^*_{\alpha'\beta'}$	$^1/_2(f_\alpha + f_\beta) + f_{\alpha\alpha'} + f_{\beta\beta'} - ^1/_2(f'_{\alpha\alpha} + f'_{\beta\beta}) + f'_{\alpha\alpha'} - f'_{\beta\beta'} - f_{\alpha\beta} - 2f_{\alpha\beta'} + f'_{\alpha\beta} + 2f'_{\alpha\beta'}$
6,6	$f_{d'}$	
7,7	$f_r - f_{rr}$	$f_r - f_{rr'} + f'_{rr} - f'_{rr'}$
8,8	$f_\alpha - f_{\alpha\alpha}$	$f_\alpha - f_{\alpha\alpha'} + f'_{\alpha\alpha} - f'_{\alpha\alpha'}$
9,9	$f_\beta - f_{\beta\beta}$	$f_\beta - f_{\beta\beta'} + f'_{\beta\beta} - f'_{\beta\beta}$
10,10	$f_{r'} - f_{r'r'}$	$f_r - f_{rr'} - f'_{rr} + f'_{rr'}$
11,11	$f_{\alpha'} - f_{\alpha'\alpha'}$	$f_\alpha - f_{\alpha\alpha'} - f'_{\alpha\alpha} + f'_{\alpha\alpha'}$
12,12	$f_{\beta'} - f_{\beta'\beta'}$	$f_\beta - f_{\beta\beta'} - f'_{\beta\beta} + f'_{\beta\beta'}$
13,13	$f_\gamma - f_{\gamma\gamma}$	

[a] Derived with the symmetry coordinates of disilane in ref 7.
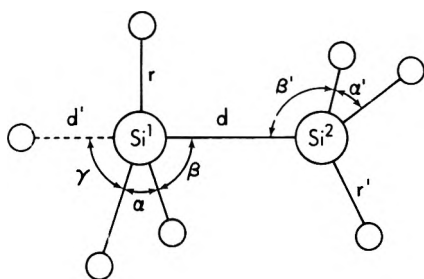
Figure 1. Geometry of the assumed model for the activated complex.

tetrahedral structure. The H$\cdots$Si^1 and Si–Si bonds become somewhat stretched but all the other Si–H bond lengths remain identical with those in the disilane molecule. This structure is essentially the same as that applied successfully in isotope effect calculations for S$_N$2 bimolecular nucleophilic substitution reactions in general.[2,5]

With this structure the MMI factor is evaluated as 1.079.

The assumed activated complex has C_{3v} symmetry and the $3N - 6 = 21$ normal vibrations divide into 6A$_1$, 1A$_2$, and 7 doubly degenerate E species. We carried out a full normal coordinate analysis of the activated complex using the standard Wilson FG matrix method[6] to calculate the normal coordinates and vibrational frequencies. Applying projection operators to the appropriate internal coordinate, the following symmetry coordinates can be obtained for C_{3v} symmetry

$$S_1 = d$$
$$S_2 = (r_1 + r_2 + r_3)/\sqrt{3}$$
$$S_3 = (\beta_1 + \beta_2 + \beta_3 - \gamma_1 - \gamma_2 - \gamma_3)/\sqrt{6}$$
$$S_4 = (r_1' + r_2' + r_3')/\sqrt{3}$$
$$S_5 = (\alpha' + \alpha_2' + \alpha_3' - \beta_1' - \beta_2' - \beta_3')/\sqrt{6}$$
$$S_6 = d'$$
$$S_{7a} = (2r_1 - r_2 - r_3)/\sqrt{6}$$
$$S_{7b} = (r_2 - r_3)/\sqrt{2}$$
$$S_{8a} = (2\alpha_1 - \alpha_2 - \alpha_3)/\sqrt{6}$$
$$S_{8b} = (\alpha_2 - \alpha_3)/\sqrt{2}$$

$$S_{9a} = (2\beta_1 - \beta_2 - \beta_3)/\sqrt{6}$$
$$S_{9b} = (\beta_2 - \beta_3)/\sqrt{2}$$
$$S_{10a} = (2r_1' - r_2' - r_3')/\sqrt{6}$$
$$S_{10b} = (r_2' - r_3')/\sqrt{2}$$
$$S_{11a} = (2\alpha_1' - \alpha_2' - \alpha_3')/\sqrt{6}$$
$$S_{11b} = (\alpha_2' - \alpha_3')/\sqrt{2}$$
$$S_{12a} = (2\beta_1' - \beta_2' - \beta_3')/\sqrt{6}$$
$$S_{12b} = (\beta_2' - \beta_3')/\sqrt{2}$$
$$S_{13a} = (2\gamma_1 - \gamma_2 - \gamma_3)/\sqrt{6}$$
$$S_{13b} = (\gamma_2 - \gamma_3)/\sqrt{2}$$

Since the torsional mode in disilane is both ir and Raman inactive and the corresponding vibrational frequency is not known, we omitted the A$_2$ normal mode from the calculation of the vibrational frequencies of the activated complex.

As the magnitude of the kinetic isotope effect is closely related to the values of the force constants, the diagonal elements of the F matrix for C_{3v} and D_{3d} symmetries are shown in Table I, which illustrates the changes in the force field between the reactant and the activated complex. The force field for the activated complex was computed using the force constants of the disilane molecule from the literature[7] and the values assigned to the H–Si^1–H (α), H–Si^1–Si^2 (β), and H$\cdots$Si^1–H (γ) bending force constants were varied to generate isotope effects.

The calculated vibrational frequencies of the activated complex listed in Table II were obtained using the following force constant values: f(H–Si^1–H) = 0.3 mdyn Å, f(H–Si^1–Si^2) = 0.2 mdyn Å, f(H$\cdots$Si^1–H) = 0.1 mdyn Å. The corresponding force constant values in the disilane molecule are 0.46 and 0.41 mdyn Å, respectively. The force constants related to the Si^{2}H$_3$ group were assumed to be identical with those of the disilane molecule. Only diagonal force constants were used in the calculations of the activated complex frequencies. Inclusion of the off-diagonal elements from the disilane force field caused about 6% change in the results.

Contributions to the EXC and ZPE factors by the individual normal modes of the activated complex are shown in Table III. Since the Si–H stretching force constants were not altered, the corresponding normal modes with

TABLE II: Vibrational Frequencies, cm⁻¹

	Si₂H₆ᵃ	Si₂D₆ᵃ		H⋯Si₂H₆ᵇ	H⋯Si₂D₆ᵇ
A₁g	434.2	407.5	A₁	0.0ᶜ	0.0ᶜ
	2152.0	1547.5		2144.4	1540.9
	909.0	683.1		488.1	362.4
A₂u	2154.3	1549.3		2152.1	1538.0
	843.5	624.9		870.5	623.5
				1642.0	1637.0
E₂u	2178.6	1585.0	E	2184.0	1578.6
	939.6	682.9		931.2	666.1
	379.3	277.0		517.2	378.2
E₁g	2155.0	1569.0		2160.3	1571.1
	929.3	667.0		852.2	615.9
	625.2	474.7		473.1	355.9
				178.3	167.1

ᵃ From ref 7. ᵇ Calculated. ᶜ Reaction coordinate.

TABLE III: Calculated Values of the EXC and ZPE Factorsᵃ

Vibrations, cm⁻¹		EXC	ZPE	EXC × ZPE
Si₂H₆	H⋯Si₂H₆			
A				
434.2		1.041	1.072	1.116
909.0	488.1	0.917	1.150	1.055
843.5	870.5	1.003	0.989	0.992
E				
939.6	931.2	1.001	0.993	0.994
379.3	517.2	1.094	0.911	0.997
929.3	852.2	0.987	1.129	1.114
625.2	473.1	0.921	1.132	1.043
	178.3	0.918	0.966	0.887
Π		0.875	1.362	1.193

ᵃ MMI × EXC × ZPE = 1.079 × 0.875 × 1.362 = 1.286.

practically unchanged frequencies did not contribute to the isotope effect and are not listed. The overall kinetic isotope effect is $k_H/k_D = 1.29$, compared to the experimental value of 1.4.

The potential energy distribution in the normal modes among the internal coordinates for the activated complex and the disilane molecule is given in Table IV. They were calculated by the expression

$$(L_{ij}{}^2 F_{ii}/\lambda_j)100$$

where L is the eigenvector matrix obtained by solving the secular equation in internal coordinates, F the force field matrix, and λ_j is the eigenvalue for normal mode j. The extent of participation of the H–Si¹–H (α), H–Si¹–Si² (β), and H⋯Si¹–H (γ) bending coordinates in the different normal modes is explicitly indicated by the fractional contributions of the diagonal terms of the force field to the potential energy.

Discussion

The computed value of the overall isotope effect, 1.29, approaches closely the experimental value of 1.4. This computed value, however, represents an upper limit since it is based on an activated complex in which the extreme geometry is designed to yield upper bound isotope effects and it is not free from internal contradictions as will be shown below.

In the computation the normal mode assigned to the H⋯Si¹–Si² asymmetric stretching was taken as the reaction coordinate. Since the Si–Si stretching mode in disilane-d_6 has a small isotope shift, the breaking of this bond generates a small primary isotope effect, $k_H/k_D \simeq 1.12$ as seen from Table III.

TABLE IV: Potential Energy Distribution of the Diagonal Elements of the F Matrix in Disilane and in the Activated Complexᵃ

Vibrations, cm⁻¹	H–Si¹–H bend	H–Si¹–Si² bend	H⋯Si¹–H bend	H–Si²–H bend	H–Si²–Si¹ bend
A					
909.0	25	25		25	25
(488.1)		(66.7)	(33.3)		
843.5	25	25		25	25
(870.5)				(50)	(50)
E					
939.6	50			50	
(931.2)				(100)	
379.3		50			50
(517.2)					(100)
929.3	50			50	
(852.2)	(100)				
625.2		50			50
(473.1)		(50)	(50)		
(178.3)		(44)	(56)		

ᵃ Values are given in per cent. Bracketed figures refer to the activated complex.

Bond formation between the H and Si atoms in the activated complex creates three new vibrations. The A₁ species, which can be assigned to the H⋯Si¹ stretching motion, does not change with deuterium substitution in disilane and consequently does not contribute to the isotope effect. The doubly degenerate E species is only slightly isotopically sensitive, the ratio of the corresponding frequencies is 1.063. Analysis of the eigenvectors revealed that this normal mode can be approximately described as the linear bending of the H⋯Si¹–Si² skeleton. The latter two vibrations created by the addition of the H atom generate an inverse isotope effect, as observed previously in other addition reactions.[8]

It is seen from Table IV that the vibrations of the Si²H₃ group are independent of those of the rest of the activated complex since this part of the complex retained its original structure. The only force constant change which influences these frequencies is the cancellation of the interaction force constants between the two silyl groups in the activated complex; this caused a slight increase in the corresponding frequencies and accordingly generated a small inverse isotope effect.

Since isotope effects are generated by variations in the force constants of the H–Si¹–H, H–Si¹–Si², and H⋯Si¹–H bending motions, it is necessary to know how these internal coordinates are related to the normal frequencies of the complex. This can be obtained from a knowledge of the potential energy distribution, Table IV. It is apparent that the differences between the normal frequencies of the reactant disilane and those of the activated complex do not reflect only changes of the force constants but also changes of the normal modes associated with structural variations. In order to reproduce the experimental isotope effect the force constants of the disilane molecule must be reduced in the activated complex. It is seen from the data in Table IV that there is only one, namely, the $\nu = 852.2$ cm⁻¹ doubly degenerate vibration related to the Si¹ atom in the activated complex, which is affected by the change in the H–Si¹–H bending force constant. The magnitudes of the others are determined by the sum of the H–Si¹–Si² and H⋯Si¹–H bending force constants. This means that if these two force constants are assumed to vary simultaneously, i.e., the increase in f(H⋯Si¹–H) is accompanied by the simultaneous decrease in f(H–Si¹–Si²), keep-

ing their sum constant, the corresponding vibrational frequencies will not change and will not contribute to the isotope effect. A substantial direct isotope effect can only be expected if both of these force constants have low values.

The structure of the SiH$_3$ radical is not yet known in detail, but it seems certain from epr[9] and ir[10] studies that, unlike the CH$_3$ radical, it has a nonplanar structure. In view of this the configuration assigned to the activated complex with the three Si^1–H bonds in one plane must represent a rather strained structure. Therefore the low values of both the H–Si^1–Si^2 and H$\cdots$Si^1–H bending force constants (0.2 and 0.1 mdyn Å, respectively) required to reproduce the experimentally observed isotope effect do not appear to be realistic and the extremely loose structure that these force constants represent cannot be accepted as "reasonable" for the activated complex.

To this point the effect generated by the possible change in the rotational energy barrier about the Si–Si bond has been neglected. There are no data available on the rotational energy barrier in disilane. A direct isotope effect could be produced as a result of a substantial lowering of the rotational energy barrier when the Si–Si bond is lengthened. However, when the Si^{1}H$_3$ group adopts a planar configuration the H atoms are displaced by 0.49 Å in the direction of the Si^{2}H$_3$ group and the same increase in the Si–Si bond would reduce the Si–Si stretching force constant to 15% of its original value, according to the Badger rule. This structural change still leaves the distance between the H atoms on Si^{1}H$_3$ and those on the Si^{2}H$_3$ moieties unaltered and consequently the rotational barrier in the complex is expected to be almost the same as that in disilane.

The results of the present calculations lead to the conclusion that, on the basis of the suggested model for the activated complex, the observed isotope effect can only be reproduced by assuming simultaneously very low values for all the bending force constants of the Si^{1}H$_3$ group, which does not seem possible in view of the known geometry of the SiH$_3$ radical. Therefore it seems more likely that the H atom attacks the disilane molecule in a plane perpendicular to the Si–Si bond and the activated complex has a three-membered bridged structure. In a model of this type, the H atom is linked to both Si atoms and

brings about force constant changes in both SiH$_3$ groups affecting almost all of the normal vibration. Furthermore, as the SiH$_3$ groups are not forced into a planar configuration the small reduction of the Si–H bending force constants necessary to generate the direct isotope effect seems more reasonable.

It is concluded that the isotope effect in the present reaction is generated by three more or less distinct sources: (a) changes in the force constants which accompany the geometrical changes in the passage from reactants to the activated complex, (b) an increase in the number of normal modes owing to the larger size of the activated complex compared with either of the two reactants, and (c) force constant changes resulting from the cancellation of the interaction forces between the two identical silyl groups. It should be pointed out that b, in addition to altering the force field, also generates an isotope effect by increasing the magnitude of the moment of inertia.

Finally it is emphasized that a detailed analysis of the normal modes and the distribution of the potential energy in the activated complex is a very useful tool to locate the origin of the isotope effect. Especially in the case of secondary isotope effect which generally arise as the result of the simultaneous and frequently opposing action of numerous factors, the comparison of force constants alone does not reveal the cause of the isotope effect in its entire complexity.

References and Notes

(1) T. L. Pollock, H. S. Sandhu, A. Jodhan, and O. P. Strausz, *J. Amer. Chem. Soc.*, **95**, 1017 (1973).
(2) A. V. Willi, *Can. J. Chem.*, **44**, 1889 (1966).
(3) M. A. Ring, M. J. Puenter, and H. E. O'Neal, *J. Amer. Chem. Soc.*, **92**, 4845 (1970).
(4) J. Bigeleisen and M. Wolfsberg, *Advan. Chem. Phys.*, **1**, 15 (1958).
(5) M. Wolfsberg and M. J. Stern, *Pure Appl. Chem.*, **8**, 225, 325 (1964).
(6) E. B. Wilson, J. C. Decius, and P. C. Cross, "Molecular Vibrations," McGraw-Hill, New York, N. Y., 1955.
(7) E. A. Clark and A. Weber, *J. Chem. Phys.*, **45**, 1759 (1966).
(8) I. Safarik and O. P. Strausz, *J. Phys. Chem.*, **76**, 3613 (1972).
(9) J. H. Sharp and M. C. R. Symons, *J. Chem. Soc. A*, 3084 (1970).
(10) D. E. Milligan and M. E. Jacox, *J. Chem. Phys.*, **52**, 2594 (1970).

Isotopic Exchange Reactions between Nitrogen Oxides and Oxyhalides

H. D. Sharma* and S. P. Sood

Department of Chemistry, University of Waterloo, Waterloo, Ontario, Canada   (Received August 14, 1973)

Publication costs assisted by the Department of Chemistry, University of Waterloo

The kinetics of atom exchange reactions among ClNO, NO, and NO_2 have been studied by using a time-of-flight mass spectrometer in two reactors of different surface-to-volume ratio, over a temperature range of $0-23°$. The reactions proceed according to the equations $Cl^{14}NO + {}^{15}NO_2 \rightarrow Cl^{15}NO_2 + {}^{14}NO$, $Cl^{14}NO + {}^{15}NO_2 \rightarrow Cl^{15}NO + {}^{14}NO_2$, $Cl^{14}NO + {}^{15}NO \rightarrow Cl^{15}NO + {}^{14}NO$, with the second-order rate constant, $k = (1.78 \pm 0.04) \times 10^5 \exp[-(3350 \pm 150)/T] \ M^{-1} \ sec^{-1}$ for the first two reactions and $k = (1.64 \pm 0.10) \times 10^6 \exp[-(3145 \pm 150)/T] \ M^{-1} \ sec^{-1}$ for the last reaction. Bimolecular mechanisms for the reactions have been proposed similar to those for the corresponding reactions in $NO-NO_2$ and NO_2-NO_2 systems. However, the rates of reactions in the present systems are slower by a factor of $\sim 10^6$ at $23°$.

Introduction

In a previous paper,[1] it was shown that bimolecular exchange reactions occur in $N^{18}O_2-N^{16}O_2$ and ${}^{15}NO_2-{}^{14}NO$ systems with the rate constants $k = (3.0 \pm 0.1) \times 10^6$ and $(4.9 \pm 0.8) \times 10^7 \ M^{-1} \ sec^{-1}$, respectively, at $25°$. It was concluded that the atom transfer reaction takes place through an associative mechanism. Freiling, Johnston, and Ogg[2] studied the kinetics of the reaction

$$ClNO_2 + NO = NO_2 + ClNO \tag{1}$$
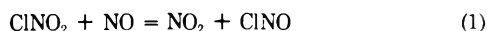
and proposed an elementary bimolecular mechanism with a rate constant, $k = 0.83 \times 10^9 \exp(-6900/RT) \ M^{-1} \ sec^{-1}$. However, they noted that there existed an ambiguity with respect to the path of the reaction, *i.e.*, nitryl chloride could pass an oxygen atom or a chloride atom to nitric oxide with the same chemical results. They suggested that isotopic exchange studies may be helpful in clarifying the ambiguity. In this paper we report the results of isotopic exchange studies of the reactions

$$Cl^{14}NO + {}^{15}NO \rightarrow Cl^{15}NO + {}^{14}NO \tag{2}$$

$$Cl^{14}NO + {}^{15}NO_2 \rightarrow Cl^{15}NO + {}^{14}NO_2 \tag{3}$$
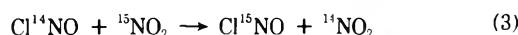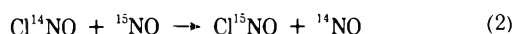
Attempts to obtain rate data on reaction 2 by Kuhn and Butkiewicz[3] were unsuccessful because of the speed of the exchange reaction.

Experimental Section

Preparation of Gases. ClNO obtained from Matheson Co. was purified by the methods of Ray and Ogg[4] and Burns and Dainton.[5] About 20 ml of liquid ClNO along with 2 ml of NO was condensed in a glass vessel. The mixture was kept at $-60°$ in a dimethylformamide slush for 6-8 hr with occasional stirring. It was fractionally distilled with the middle 60% condensed onto P_2O_5. The condensate was allowed to melt and ClNO distilled under vacuum. Several purification cycles resulted in a pure ClNO sample which was stored at liquid N_2 temperature in a dark vessel. ${}^{15}NO$ gas was prepared by the reduction of $H^{15}NO_3$ with Fe^{2+} ions in 4 M HCl and purified according to a method described by Sharma, *et al.*[1] The preparation and purification of ${}^{15}NO$ and $N^{18}O_2$ was also carried out in a manner similar to that described by Sharma, *et al.*[1]

Static Reactor Experiments. The vacuum line used for the transfer of metered gases in all experiments has previously been described.[1] Two reactors were used. One of the reactors was a 2-l. flask with a three-way stopcock which provided access to the inlet system of a time-of-flight mass spectrometer. The other reactor was made by fusing six 1 m × 22 mm o.d. glass tubes to a 33-mm o.d. glass tube. Each 22-mm tube had a 12-mm o.d. tube inside it to provide a large surface-to-volume ratio. The reactors were exposed to appropriate gas mixtures prior to a run. Experiments were performed in the absence of light to avoid any photodecomposition.

The exchange kinetics was followed by measuring peak heights in mass spectra in the mass range of 46 to 52. A small volume of gas from the reactor was trapped periodically such that the total pressure did not change significantly during the course of the reaction. The gas was allowed to leak into the inlet system of the mass spectrometer through a 75-μ pinhole. The residual gases were removed after the mass spectrum had been recorded. The change in the m/e 46 and 47 for the ${}^{15}N$ exchange and 46, 48, and 50 for the ${}^{18}O$ exchange provided the rate data, except for one case in which NO_2 was not present, the peak heights due to m/e 30 and 31 were followed. The peak heights due to ClN^+ at m/e 49, 50, 51, and 52 were small and therefore the rate data on the exchange kinetics showed a large scatter. Nevertheless, the latter measurements provided additional data on the progress of the exchange kinetics.

Experimental Results and Discussion

The experimental results are summarized in Table I, giving the total pressure, P, and the initial concentrations, $[ClNO]_0$, $[NO]_0$, and $[NO_2]_0$. Corrections for the presence of the dimer of NO_2 have been applied by using the data of Giauque and Kemp.[6] The isotopic exchange rate, R, for ${}^{15}N$ and ${}^{18}O$ has been obtained by using the expression[7]

$$Rt = -\frac{[ClNO]\{[NO] + n[NO_2]\}}{[ClNO] + [NO] + n[NO_2]} \ln(1 - F)$$

and

$$F = (f^0 - f')/(f^0 - f^\infty)$$

TABLE I: Summary of Experimental Data and R Values

Run no.	Temp, °C	P, mm	$[NO_2]_0 \times 10^6\,M$	$[NO]_0 \times 10^6\,M$	$[ClNO]_0 \times 10^6\,M$	$R \times 10^9\,M$	k_2, M^{-1} sec^{-1}	k_3, M^{-1} sec^{-1}
1	23	2.57	72.5	0.00	78.60	14.72 ± 0.28	40.56 ± 0.09	2.18 ± 0.03
2	23	5.12	57.6	0.00	243.50	14.06 ± 0.24		
3	23	2.89	50.1	0.00	119.90	17.01 ± 0.68		
4	23	7.79	44.8	0.00	413.70	62.25 ± 1.02		
5	23	1.45	53.3	0.00	32.10	4.37 ± 0.07		
6	23	1.93	55.4	0.00	58.00	8.18 ± 0.12		
7	23	2.85	109.8	0.00	58.00	15.66 ± 0.80		
8	23	3.34	138.6	0.00	58.00	18.89 ± 0.19		
9	23	2.24	53.3	0.00	78.60	11.29 ± 0.12		
10	23	1.37	38.4	0.00	42.00	4.21 ± 0.09		
11	23	1.79	52.2	5.60	47.70	15.89 ± 0.19		
12	23	1.75	49.0	12.90	41.00	25.90 ± 0.52		
13	23	2.46	46.2	22.70	76.10	75.94 ± 1.51		
14	23	3.18	32.0	45.00	109.90	209.18 ± 3.10		
15	23	3.10	35.2	80.80	66.40	221.70 ± 8.75		
16	23	2.29	0.0	51.80	83.20	175.58 ± 4.31		
17[a]	23	5.69	56.4	0.00	278.40	52.59 ± 0.76		
18[a]	23	3.06	59.0	0.00	121.20	21.32 ± 0.22		
19[a]	23	3.41	70.2	0.00	130.20	28.47 ± 0.39		
20	11	1.91	52.2	12.90	47.30	19.78 ± 0.49	27.76 ± 0.27	1.32 ± 0.03
21	11	2.98	53.3	11.48	110.69	42.91 ± 1.41		
22	11	4.25	59.7	0.00	190.46	19.09 ± 0.57		
23	0	2.20	64.0	14.60	51.10	14.90 ± 0.15	16.71 ± 0.08	0.84 ± 0.02
24	0	2.09	52.2	12.90	58.0	14.76 ± 0.48		
25	0	3.10	74.6	0.00	107.6	6.97 ± 0.08		

[a] Runs were made in reactor B.

where f^0 is the fraction of ^{15}N or ^{18}O in the labeled gas, f^t is the fraction of ^{15}N or ^{18}O at time t, f^∞ is the fraction of ^{15}N or ^{18}O at equilibrium, and n is the number of exchangeable atoms in the labeled molecule. The values of R and the associated errors (Table I) for each run have been computed by a least-square-fitting program from the exchange rate data after the chemical equilibrium among the species has been reached. The concentration of ClNO at equilibrium has been evaluated from the kinetics and equilibrium data of Ray and Ogg,[4] Freiling, et al.,[2] and Martin and Kohnlein.[8]

If the trial assumption is made that the exchange takes place through bimolecular associations and that the exchange rate constants differ from those for the chemical reactions, since the exchange can take place without producing a net chemical change, the exchange reactions can be depicted by the following equations

$$Cl^{14}NO + {}^{15}NO_2 \underset{k_{-1}}{\overset{k_1}{\rightleftharpoons}} Cl^{15}NO_2 + {}^{14}NO \quad (4)$$

$$Cl^{14}NO + {}^{15}NO_2 \overset{k'}{\rightleftharpoons} Cl^{15}NO + {}^{14}NO_2 \quad (5)$$

$$Cl^{14}NO + {}^{15}NO \overset{k_3}{\rightleftharpoons} Cl^{15}NO + {}^{14}NO \quad (6)$$

$$^{14}NO + {}^{15}NO_2 \overset{rapid}{\rightleftharpoons} {}^{15}NO + {}^{14}NO_2 \quad (7)$$
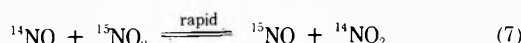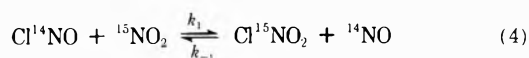
where k_1 and k_{-1} are the rate constants for the forward and the reverse reactions for (4), $k_1 + k' = k_2$ is the combined rate constant for exchange reactions 4 and 5 and k_3 is the rate constant for reaction 6. The expression for $[ClNO_2]$ can be derived from eq 8.

$$d[ClNO_2]/dt = k_1\{[NO_2] - [ClNO_2]\}\{[ClNO]_0 - [ClNO_2]\} - $$
$$k_{-1}\{[NO]_0 + [ClNO_2]\}[ClNO_2] \quad (8)$$

$$[ClNO_2] = [ClNO_2]_{eq}\{\tanh\,(0.5at)\} \times$$
$$\{(a + b)\{a + b\,\tanh\,(0.5at)\}^{-1}\} \quad (9)$$

where

$$[ClNO]_{eq} = (a - b)[2(k_{-1} - k)]^{-1} \quad (10)$$

$$a = \{b^2 + 4k_1(k_{-1} - k_1)[NO_2]_0[ClNO]_c\} \quad (11)$$

$$b = k_1\{[NO_2]_0 + [ClNO]_0\} - k_{-1}[NO]_0 \quad (12)$$

The expression for R for the entire range of t can be derived from eq 9 and 13

$$R = -\frac{[ClNO]\{[NO] + n[NO_2]\}}{[ClNO] + [NO] + n[NO_2]}\frac{d\ln(1 - F)}{dt} =$$
$$k_2[ClNO][NO_2] + k_3[ClNO][NO] \quad (13)$$

for the case when

$$[NO]_0 = 0 \text{ and } (a + b)\{a + b\,\tanh\,(0.5at)\}^{-1} \approx 1 \quad (14)$$

$$Rt = k_2\{[NO_2]_0 - [ClNO_2]_{eq}\}\{[ClNO]_0 - [ClNO_2]_{eq}\}t +$$
$$k_3\{[ClNO] - [ClNO_2]_{eq}\}[ClNO_2]_{eq}t - [\{k_3[ClNO]_0 - $$
$$k_2([NO_2]_0 + [ClNO]_0)\}[ClNO_2]_{eq}][t - 2a^{-1}\ln\cosh(0.5at)] +$$
$$2\{k_3 - k_2\}a^{-1}[ClNO_2]_{eq}^2\,\tanh\,(0.5at) \quad (15)$$

and for the case when $[NO]_0 \gg [ClNO_2]_{eq}$ and

$$(a + b)[a + b\,\tanh\,(0.5at)]^{-1} \approx 2\{1 + \tanh\,(0.5at)\}^{-1} \quad (16)$$

$$Rt = k_2\{[NO_2]_0 - [ClNO_2]_{eq}\}\{[ClNO]_0 - [ClNO_2]_{eq}\}t +$$
$$\{k_3[NO]_0 + [ClNO_2]_{eq}\}\{[ClNO]_0 - [ClNO_2]_{eq}\}t +$$
$$a^{-1}\exp(-at)\{[k_3([ClNO]_0 - [NO]_0) - k_2([NO_2]_0 +$$
$$[ClNO]_0)][ClNO_2]_{eq} + (k_3 -$$
$$k_2)[ClNO_2]_{eq}^2[0.5\exp(-at) - 2]\} \quad (17)$$

The values of k_2 and k_3 are evaluated by following eq 9 from R values (after the chemical equilibrium has been reached). The $\ln(1 - F)$ values for each run are then calculated as a function of t over the entire range of t and compared with the experimental data (Figure 1). The assumptions given in eq 14 and 16 have been justified by calculating $[ClNO_2]$ as a function of t according to eq 9 and by evaluating the values of $\ln(1 - F)$ vs. t by numerical integration of eq 13. The complex factors in eq 15 and 17 serve to show the effect of initial nonequilibrium condition on R with respect to time for the reactions. In this

Figure 1. Ln $(1 - F)$ vs. time: run no. 4, $\triangle$ (with ^{15}N); run no. 12, $\square$ with ^{15}N; run no. 2, O (with ^{18}O); —, according to eq 10 and 16.

system, the chemical equilibrium is reached long before isotopic species attain statistical distribution among the molecules (Figure 1). The errors associated with k_2 and k_3 have been evaluated by using a least-square-fitting program.

The rate data for any given run fit the appropriate expressions. It can, therefore, be surmised that the exchange reactions are first order with respect to each reactant. The initial concentration of the reactants has been varied fourfold and the second-order rate constants are given in Table I. Runs 17 to 19 made in reactor B, having a tenfold change of surface-to-volume ratio, have been found to give the same rate constants within the experimental errors. This provides evidence for the homogeneity of the exchange reactions.

In order to determine the activation energy, runs were made in the temperature range 0-23°. A plot of log k vs. T^{-1} is shown in Figure 2. The rate constants can be expressed by the Arrhenius equation for reactions 4 and 5 as $k_2 = (1.78 \pm 0.04) \times 10^5 \exp[-3350 \pm 150/T]$ and for reaction 6 as $k_3 = (1.64 \pm 0.10) \times 10^6 \exp[-(3145 \pm 150)/T]$. The value of the activation energy for reactions 4 and 5 is similar to that found for the chemical reaction[8] for the oxidation of ClNO by NO$_2$. It is, however, interesting to note that k_2 is 2.5 times larger than k_1 for both ^{15}N and ^{18}O exchange and that k_2 has the same value for both ^{15}N and ^{18}O transfer reactions. It appears that the exchange can occur through another path which does not lead to the oxidation of ClNO. In the N^{16}O$_2$-N^{18}O$_2$ system, it has been shown that the transfer of oxygen atom can only occur through the formation of a bridged "intermediate dimer" of NO$_2$.[1] In ClNO-NO$_2$ system, the possibility of the formation of such a bridged species is indicated. The "intermediate species" (not differentiated from a "transition state" configuration) may be depicted as follows

Figure 2. Log k_2 vs. T^{-1} ($\triangle$) and log k_3 vs. T^{-1} (O).

If the intermediate species involved one or two oxygen atoms, as shown in II and III and particularly III, k_2 for ^{18}O atom transfer should have been higher. Failure to observe any significant difference in ^{15}N and ^{18}O exchange rate implies that the chlorine atom is involved in forming the intermediate species as shown in I and IV. In ClNO, the N-Cl bond length (1.95 Å)[9] is longer than the normal N-Cl bond length (1.73 Å). The low value of the NQR coupling constant[10] and high value of dipole moment indicate that the electron density is shifted toward the chlorine atom. In a bimolecular collision the Cl atom will orient itself toward the positive end of NO$_2$, i.e., toward the nitrogen atom, thus leading to I. The evidence, though inconclusive, favors the path which involves transfer of the Cl atom rather than the oxygen atom in the oxidation of ClNO by NO$_2$. Further evidence can perhaps be obtained by spectroscopic studies of the unstable species by the matrix isolation technique. The possibility of a dissociative mechanism involving NO and Cl radicals can be excluded on the grounds that the reaction has a very high value for the activation energy (158.8 kJ mol^{-1}).

An intermediate species, V, involving the chlorine atom

for N transfer in ClNO-NO system similar to that postu-

lated for $NO-NO_2$[1,11] can provide satisfactory explanation for the exchange rate.

It is interesting to note that the atom transfer reactions between oxides of nitrogen proceed $\sim 10^6$ times faster than those between the corresponding oxide and oxyhalide at room temperature. In the former cases the activation energy is almost 0 while in the latter cases the value is ~ 27 kJ. It may, however, be noted that in oxides both the reactants can be considered as radicals whereas in the latter cases the reaction is between a radical and a molecular species. It will be of interest to investigate whether isotope exchange will occur between oxyhalides by the double labeling technique.

References and Notes

(1) H. D. Sharma, R. E. Jervis, and K. Y. Wong, *J. Phys. Chem.*, **74**, 923 (1970).
(2) E. C. Freiling, H. S. Johnston, and R. A. Ogg, Jr., *J. Chem. Phys.*, **20**, 327 (1952).
(3) L. P. Kuhn and C. Butkiewicz, *J. Phys. Chem.*, **65**, 1084 (1961).
(4) J. D. Ray and R. A. Ogg, Jr., *J. Chem. Phys.*, **26**, 984 (1957).
(5) W. G. Burns and F. S. Dainton, *Trans. Faraday Soc.*, **48**, 21 (1952).
(6) W. F. Giauque and J. D. Kemp, *J. Chem. Phys.*, **6**, 40 (1938).
(7) H. A. C. McKay, *J. Amer. Chem. Soc.*, **65**, 702 (1943).
(8) H. Martin and E. Kohnlein, *Z. Phys. Chem.*, **17**, 375 (1958).
(9) L. E. Sutton, *Chem. Soc. Spec. Pub.*, **No. 11** (1958); **No. 18** (1965).
(10) D. J. Millen and J. Pannel, *J. Chem. Soc.*, 1322 (1961).
(11) F. S. Klein, W. Spindel, and M. J. Stern, *J. Chim. Phys.*, **60**, 148 (1963).

Isotherm for Mobile Physisorption of Noble Gases[1a]

E. Bergmann[1b]

Department of Physical Chemistry, The Hebrew University, Jerusalem, Israel, and Battelle Institute, Advanced Studies Center 1227 Carouge, Switzerland (Received August 2, 1973)

The solution of the scaled particle theory for hard disks is used with the temperature-dependent diameter corresponding to the R^{-12} repulsive potential. This is combined with the contribution of the attractive potential to the second virial coefficient to an improved equation of state for mobile adsorbed layers on homogeneous surfaces. For the intermolecular potential the parameters determined from surface gas virial data are used. The equation of state is thermodynamically related to an isotherm. Both the critical temperatures and the isotherm show satisfactory agreement with measurements.

I. Introduction

The recent physisorption experiments of Thomy and Duval[2a] on exfoliated graphite have raised new interest in the fluid phase transitions on such surfaces.[2b] The data are currently interpreted in terms of the De Boer–Hill isotherm, which is based on the simple two-dimensional van der Waals equation. Tsien and Halsey[3] have combined this isotherm with the Langmuir isotherm for localized adsorption and were thus able to explain the whole coverage range. Earlier, Stebbins and Halsey[4] pointed out that one could use results for the virial coefficients of hard disks to improve the treatment of the repulsive short-range interaction. Claiming the short-range interaction to reproduce the second virial coefficient correctly, they derived the adjusted Volmer equation. In contrast to this McAlpin and Pierotti[5] used the significant structure model of liquids to obtain also an equation of state for adsorbed layers. Meanwhile greatly improved solutions of the hard disk problem are available, e.g., the Padé approximant of Ree and Hoover[6] which agrees excellently with the results of molecular dynamics calculations up to the liquid–solid transition.

One purpose of this study is to use improved hard disk results. To avoid unnecessary complication, we will however use the simpler scaled particle result[7] which also gives very good results at not too high densities. The long-range contribution to the equation of state is taken from the second virial coefficient. The approximations involved herein are discussed in section III. For the interaction between adsorbed atoms we use the potential obtained by Everett[8] from fitting of second virial data. The equation of state so obtained is integrated *via* thermodynamic relations to an isotherm whose integration constant is determined by comparison with Hill's classical result.[9]

II. Short-Range Interaction

We choose as usual the short-range potential as an inverse power.

$$V(R) = V_0 / R^{12} = 4V_{min}(R_0/R)^{12} \qquad (1)$$

As Everett[8] we take for V_{min} and R_0 the parameters of the bulk gas, thus plugging the entire perturbation of the intermolecular potential by the adsorbent into the long-range repulsion. There is no real justification for this, nor for the special form chosen in (1), e.g., theoretical calculations fit much better to an exponential,[10] but the small amount of experimental results of intermolecular forces of adsorbed atoms precludes for the moment any improvement.

Equation 1 leads to a specially simple form for the repulsive part of the second virial coefficient

$$b = -\frac{1}{2}\int d^2R\left\{\exp\left[-\frac{\beta V_0}{R^{12}}\right]-1\right\} = \frac{\pi}{2}(\beta V_0)^{1/6}\Gamma\left(\frac{5}{6}\right) \quad (2)$$

The comparison with the expression for hard disks, $b = (\pi/2)\sigma^2$ suggests the definition of a temperature-dependent hard-disk diameter

$$\sigma = R_0\sqrt{\Gamma\left(\frac{5}{6}\right)}\left(\frac{4V_{min}}{kT}\right)^{1/12} \quad (3)$$

The hard-disk model system has been treated repeatedly. Since there exists no solution for the PY or HNC equation in two dimensions, the best one can take are the results of Ree and Hoover[6] obtained as Pade approximants from the first seven virial coefficients. But since this is very close to the scaled particle theory[7] (1.8% at $\theta = 0.8$) we will choose the latter because its simple form makes the integrals necessary to obtain the pressure-coverage relation very simple. It should however be noted that this result does not reproduce correctly the higher virial coefficients. An expansion similar to eq 13 of ref 4 is therefore again not possible. We have for the spreading pressure ϕ_0 corresponding to (1)

$$\phi_0 A / NKT = 1/\left(1 - \frac{\theta}{2}\right)^2 \quad (4)$$

where A is the surface area and N the number of molecules adsorbed. The definition of the coverage θ in terms of the surface excess Γ is the usual van der Waals definition

$$\theta = \Gamma b \qquad \Gamma = N/A \quad (5)$$

It is not identical with the empirical definition of θ.

$$\theta = N(\text{absorbed})/N(\text{full coverage}) \quad (6)$$

If we identify full coverage as Stebbins and Halsey with the densest solid phase, we would have

$$\theta' = (\sqrt{3}/\pi) = \theta \quad (7)$$

III. Long-Range Interaction

The long-range interaction cannot in general be represented by a simple two particle potential, since dispersion forces are not additive.[10] The nonadditive contribution to the pressure, for example, has been found to be of the order of 7% in the bulk gas phase.[11] If it is neglected the long-range potential of two molecules can be written as[8]

$$V_1(R) = -\frac{C_6}{R^6} - \frac{C_3}{R^3} = -4V_{min}\left[\left(\frac{R_0}{R}\right)^6 - \chi\left(\frac{R_0}{R}\right)^3\right] \quad (8)$$

The repulsive R^{-3} term is used as a representation of the perturbation by the adsorbent. Its main contribution comes from the three-body dispersion interaction, the third being the surface.[12] To the lowest order in density the contribution of the attractive forces, (8), to the free energy is

$$\beta F_1 = \frac{N^2}{-2A}\int_0^\infty d^2R \exp[-\beta V(R)]\{\exp[-\beta V_1(R)]-1\} \quad (9)$$

The integral in (9) is simply related to the total second virial coefficient B_2, so that we can write this contribution of (8) to the spreading pressure as

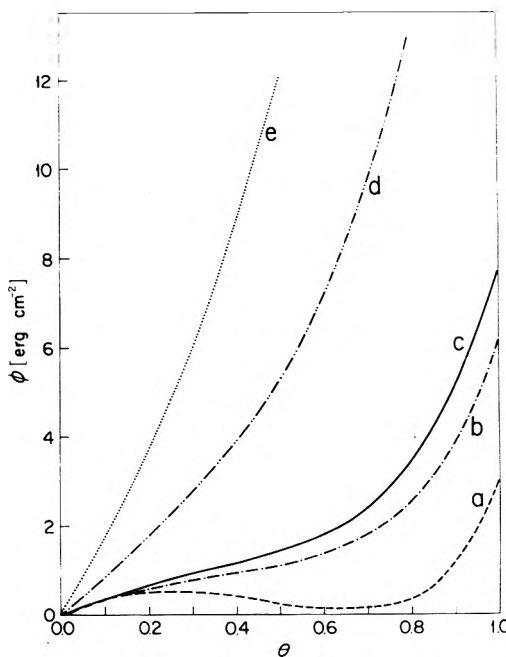$$\phi_1 = \beta F_1/A = \Gamma^2(B_2 - b)kT \quad (10)$$

Figure 1. Spreading pressure as a function of coverage for argon: (a) 59.9°K, (b) 65°K, (c) 70°K, (d) 119.8°K, (e) 199.67°K.

and if, following van der Waals, we introduce a function $a(T)$ as

$$a(T) = kT(B_2 - b) \quad (11)$$

we have for the total spreading pressure

$$\phi = \phi_0 + \phi_1 = \frac{\theta kT}{b}\frac{1}{[1-(\theta/2)]^2} - \theta^2\frac{a(T)}{b^2} \quad (12)$$

This can be rearranged to the conventional form of an equation of state.

$$\left[\phi + \frac{N^2}{A^2}a(T)\right]\left[A - \frac{Nb}{2}\right]^2 = ANkT \quad (13)$$

Compared with the simple two-dimensional van der Waals equation, (13) shows two changes. The second factor reproduces the singularity of the pressure at high density with the correct power 2 and the value is well approximated, $\pi/4$ instead of $\sqrt{3}/2$ of eq 7. The two coefficients are temperature dependent. The virial coefficients corresponding to (1) and (8) have been tabulated for various χ values by Johnson and Klein.[13] We have used the χ parameters of Everett and interpolated linearly in the tables to obtain the corresponding B_2's. For $T = 100$ and 90 in the case of krypton and $T = 65$ and 70 in the case of argon we interpolated graphically on a plot of $a(T)$ obtained from Johnson and Klein's table. The results of this are plotted in Figure 1 for argon and in Figure 2 for krypton. The kink appearing below the critical temperatures has to be interpreted as usual in terms of the Maxwell construction. The figures indicate that for argon the critical temperature should lie somewhat below 65°K. This agrees well with the experimentally observed values 64-67°K listed in ref 2b. The good agreement may however be due to a partial cancellation of the errors introduced by the approximations (use of eq 9 for the attractive contribution and neglect of many-body forces). The agreement in the case of krypton is less satisfactory, since we find a critical temperature of more than 90°K compared with the experimental value of 86°K. However, many-body forces are
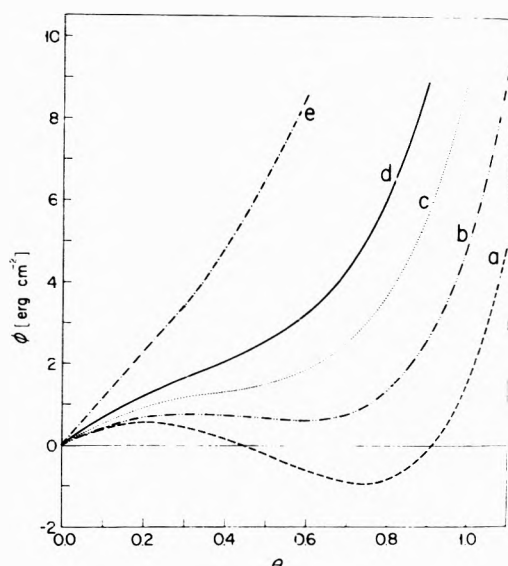
Figure 2. Spreading pressure as a function of coverage for krypton: (a) 85.5°K, (b) 90°K, (c) 100°K, (d) 114°K, (e) 171°K.

known to be stronger for larger molecules[11] and, on the other hand, the parameters used for krypton are less reliable.[8]

IV. The Isotherm

The isotherm corresponding to (11) can be obtained through thermodynamic relations.[9] Following Hill we take, since on the isotherm $p = p(\Gamma)$ and $\phi = \phi(\Gamma)$

$$\phi = kT \int_0^\Gamma \Gamma \frac{d\ln p}{d\Gamma} d\Gamma \qquad (14)$$

and differentiate it.

$$kT \frac{d\ln p}{d\Gamma} = \frac{kT}{[1-(\Gamma b/2)]} + \frac{b\Gamma kT}{[1-(\Gamma b/2)]^3} - 2a(T)\Gamma \qquad (15)$$

This can be integrated straightforwardly and leads to

$$p = \frac{P_0 e^2}{b} \frac{\theta}{1-(\theta/2)} \exp\left\{\frac{(\theta/2)[3-(\theta/2)]}{[1-(\theta/2)]^2} - 2\frac{a(T)}{bkT}\theta\right\} \qquad (16)$$

The integration constant has been chosen in the same way as by Hill. Therefore we have by comparison with his result

$$p = \frac{(2\pi m)^{1/2}(kT)^{3/2}}{hbj_n} \exp\left[-\frac{\epsilon_1}{kT}\right] \frac{\theta}{1-(\theta/2)} \times$$
$$\exp\left\{\frac{\theta[3-(\theta/2)]}{2[1-(\theta/2)]^2} - 2\frac{a(T)}{bkT}\theta\right\} \qquad (17)$$

where j_n is the partition function for the motion normal to the surface and ϵ_1 the adsorption energy. For practical purposes it is however convenient to introduce[4]

$$p^* = \frac{pb}{p_0 e^2} = \frac{\theta}{1-(\theta/2)} \exp\left\{\frac{(\theta/2)[3-(\theta/2)]}{[1-(\theta/2)]^2} - \frac{2a(T)}{bkT}\theta\right\} \qquad (18)$$

V. Comparison with Experiment and Conclusion

The direct comparison of (18) with the results of Thomy and Duval present difficulties, since even if we could identify p^*/p as the slope in the linear region of the isotherm, there remains the calibration of θ, which seems ambiguous in this case.[14] We therefore prefered the argon
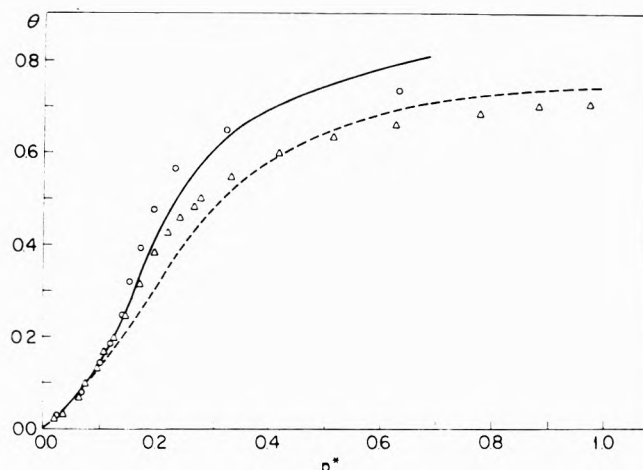

Figure 3. The isotherm of argon adsorption on P 33(2700) for 77.5 (solid line) and 90.1°K (broken line): experimental points, O for 77.5°K and △ for 90.1°K, from ref 15.

data of Ross and Olivier[15] who have determined the θ scaling and the constant $K' = p^*/p$. The result is plotted in Figure 3. Agreement was only obtained after changing the scaling constant K'. We found as best values K' (77.5°) = 2.745 mm (originally 1.84 mm) and K' (90.1°) = 15.411 mm (originally 14.8 mm). The temperature dependence of this adjustment can be understood from eq 17 or. eq 6a of ref 15. Exploiting it would lead us to a slight modification of the adsorption energy and entropy.

If one takes into account our neglect of the surface inhomogeneity (for P 33(2700), however, rather small) the agreement is very satisfactory. It shows that experiments on such surfaces and their interpretation have reached a high degree of consistency since our potential parameters were obtained from fitting of the virial data of Sams, Constabaris, and Halsey[16] and lead to an explanation of the full adsorption isotherm. This means that it is now possible in principle to improve the use of adsorption isotherms for obtaining of surface data like area and adsorption energy by the use of standardized parameters for the intermolecular interaction in the adsorbate which reduces the final uncertainty considerably. It would require however confirming repetitions of the virial experiments.

References and Notes

(1) (a) Supported by N.B.S. Grant No. 2-35724. (b) On leave from Battelle Institute.
(2) (a) A. Thomy and X. Duval, *J. Chim. Phys.*, **66**, 1966 (1969), **67**, 286, 1101 (1970); (b) S. Ross, *Progr. Surface Membrane Sci.*, **4**, 377 (1971).
(3) F. Tsien and G. D. Halsey, *J. Phys. Chem.*, **71**, 4012 (1967).
(4) J. R. Stebbins and G. D. Halsey, *J. Phys. Chem.*, **68**, 3863 (1964).
(5) J. J. McAlpin and R. A. Pierotti, *J. Chem. Phys.*, **41**, 68 (1964).
(6) F. H. Ree and W. G. Hoover, *J. Chem. Phys.*, **46**, 4181 (1967).
(7) E. Helfand, H. L. Frisch, and J. L. Lebowitz, *J. Chem. Phys.*, **34**, 1037 (1961).
(8) D. H. Everett, *Discuss. Faraday Soc.*, **40**, 177 (1965)
(9) T. L. Hill, *J. Chem. Phys.*, **14**, 441 (1946).
(10) See, e.g., H. Margenau and N. R. Kestner, "Theory of Intermolecular Forces," Pergamon Press, Elmsford, N. Y., 1969.
(11) S. Baer and A. Ben Shaul, *J. Chem. Phys.*, **56**, 1238 (1972).
(12) A. D. McLachlan, *Mol. Phys.*, **7**, 381 (1964); T. B. MacRury and B. Linder, *J. Chem. Phys.*, **54**, 2056 (1971).
(13) J. D. Johnson and M. L. Klein, *Trans. Faraday Soc.*, **60**, 1964 (1964).
(14) The last section of ref 2b contains a full discussion of this problem.
(15) S. Ross and J. P. Olivier, *J. Phys. Chem.*, **65**, 608 (1960).
(16) J. R. Sams, G. Constabaris, and G. D. Halsey, *J. Chem. Phys.*, **36**, 1334 (1962).

Transport Properties of Hydrophilic Polymer Membranes. The Influence of Volume Fraction Polymer and Tortuosity on Permeability

H. W. Osterhoudt

Research Laboratories, Eastman Kodak Company, Rochester, New York 14650 (Received June 25, 1973)

Publication costs assisted by Eastman Kodak Company

Relationships between the permeability of a solvent-containing polymer membrane to a solute and the amount of polymer present in the membrane have been derived by Yasuda, *et al.*, and by Mackie and Meares. Yasuda and coworkers considered the influence of the free volume in the membrane on permeability, whereas Mackie and Meares related diffusivity in the membrane to the tortuosity present and then described a relationship between the tortuosity and the volume fraction of polymer (v_2). Data are presented which show that, for low-molecular-weight permeants (such as ethylene glycol and ethanol) in moderately to highly water-swollen membranes from gelatin and poly(vinyl alcohol), both the Yasuda and the Mackie–Meares equations agree reasonably well with experimental data. In the v_2 range studied here ($0.08 \leq v_2 \leq 0.59$), the Mackie–Meares equation is the better approximation. Also, the Mackie–Meares equation can be used to describe the permeabilities of different kinds of membranes, including those with very low tortuosities, because it considers explicitly tortuosity as a variable.

Introduction and Theoretical Section

It is important for those working with solvent-containing polymer membranes to know how transport through such membranes is regulated. There are many parameters that might be needed for an adequate description of transport in a given membrane. High on the list of these parameters are those that describe the amount and disposition of the polymer in the membrane. Indeed, knowledge of how the polymer present governs the transport of a low-molecular-weight, uncharged permeant can serve as a basis for comparing how other properties, such as the size, charge and chemical characteristics of a permeant, or the charge and composition of the membrane, influence the transport of a solute.

The present report, therefore, is concerned with the influence of the amount of polymer in and tortuosity of a membrane on permeability. Data will be presented which show that often the tortuosity is directly related to the amount of polymer present. This, however, is not always the case and, because of the exceptions, it is useful to consider tortuosity itself as a variable.

There are at least two credible treatments that relate permeability to polymer content. These have been provided by Mackie and Meares[1] and by Yasuda, Lamaze, and Ikenberry.[2] In dealing with the permeability of low-molecular-weight, uncharged solutes, the treatment of Yasuda, *et al.*, considers but one variable, the free volume in the membrane. For membranes that are highly diluted with solvent (which is frequently water) or for membranes in which the diffusant is excluded from the polymer in the membrane, the free volume is proportional to the volume fraction of solvent (H) in the membrane. Yasuda, *et al.*, wrote for D', the diffusivity in such membranes

$$D' = D_0 \exp[- k(1/H - 1)] \qquad (1)$$

in which D_0 is the diffusivity in the solvent and k is a constant that includes the "characteristic volume required to accommodate the diffusing permeant molecules" and the free volume of the solvent. In making dialysis measurements, one often measures, instead of the diffusion coefficient only, the permeability coefficient, $P = D'K$. Here K is the partition coefficient between the membrane and solution phases which, for low-molecular-weight, uncharged permeants, can be approximated by $K = H$. Equation 1, therefore, can be transformed into a definition of the permeability coefficient which can be rewritten as a series expansion in H

$$\ln\ D'K = \ln\ D_0 + k - k/H + (H - 1) -$$
$$(H - 1)^2/2 + (H - 1)^3/3 \cdots \quad (2)$$

It turns out that k is approximately 2 or 3 and, for values of $H > 0.5$, the term in $1/H$ is dominant. Equation 2 becomes, with the use of logarithms and the substitution of $H = (1 - v_2)$, where v_2 is the volume fraction polymer in the membrane

$$\log\ D'K = \log\ D_0 + \frac{k}{2.303} - \frac{k}{2.303(1 - v_2)} \quad (3)$$

Yasuda, *et al.*, have presented data for the permeation of water-swollen synthetic polymer membranes by NaCl[2] and other solutes[3] that agree with eq 3.

In contrast to the approach of Yasuda and coworkers, Mackie and Meares considered first the relation of diffusivity in the membrane to θ, the tortuosity of the membrane. They defined θ as the ratio of the distance a diffusant must travel in traversing the membrane to the distance the diffusant would travel in traversing a lamella of solvent whose thickness equals the membrane thickness. They related D', the diffusion coefficient that one obtains experimentally for the diffusant in the membrane, to D_0 as

$$D' = D_0/\theta^2 \qquad (4)$$

The tortuosity appeared as a squared term because it was thought to diminish diffusivity in two ways. The diffusant is required to travel a greater distance in order to zig and zag around the polymer chains in the swollen membrane and the concentration gradient is decreased by the presence of the polymer.

Mackie and Meares then related tortuosity to the volume fraction polymer by assuming a lattice representation

for a polymer array, letting the lattice be partially filled in a random manner and inquiring how many steps (jumps) are required for a diffusant to move through the maze. Their result is $\theta = (1 + v_2)/(1 - v_2)$. By substituting this in eq 4, one obtains

$$D' = D_0 \left(\frac{1 - v_2}{1 + v_2}\right)^2 \tag{5}$$

This relation was tested by monitoring coion diffusion across ion-exchange membranes and the agreement between theory and experiment was generally good.[4]

In order to transform eq 5 into one suitable for comparison to dialysis rate measurements, the same relations between diffusivity and permeability that were used previously, viz., $P = D'K = D'(1 - v_2)$, can be used. The result for a random polymer array is

$$\log D'K = \log D_0 + \log \left[\frac{(1 - v_2)^3}{(1 + v_2)^2}\right] \tag{6}$$

Experimental Section

The permeabilities of several different membrane materials, whose volume fractions covered a range 0.08-0.59, were examined. These materials included sol-dried gelatin films and poly(vinyl alcohol) films (which are good representatives of homogeneous swollen polymers), Eastman cellulose acetate membranes (whose structures are not completely understood but thought to be at least partially heterogeneous), and a Millipore mixed cellulose ester membrane (which has a heterogeneous structure as shown by scanning electron microscopy). Also examined were the permeabilities of several gel-dried gelatin films. These were different from the sol-dried gelatin films in that they were allowed to dry in the gel state and their swelling in water was almost entirely in the thickness direction. All of these membrane materials are listed in Table I.

The gelatin films were made from commercial-lime-processed-ossein gelatin. The degree of swell in them was controlled by crosslinking the gelatin with varying amounts of formaldehyde. With the poly(vinyl alcohol) films, for which the starting polymer was Du Pont Elvanol 71-30 (acetyl content, 0.5-1.8%), the crosslinking was introduced by using terephthalaldehyde or by annealing a film to achieve a moderate level of crystallinity.

Dialysis rate measurements were made for the aforementioned materials and two additional ones. These are General Electric Nuclepore filters whose mean pore diameters were approximately 0.5 μ. They are not listed in Table I because these filters are known to have straight pores which run perpendicularly across the plane of the film. Nuclepore filters, therefore, are representatives of the very special (and limiting) case in which $\theta = 1.00$.

The technique for determining the volume fraction polymer in the wet membrane, v_2, was dictated by the nature of the membrane. For the gelatin and poly(vinyl alcohol) membranes, v_2 was determined by measuring the dry dimensions and the swollen dimensions of the membrane and taking the ratio of the former to the latter. The volume fraction polymer in the Eastman and Millipore membranes was determined by weighing and measuring the wet membrane, drying the membrane, and weighing it again to find the weight of water lost. For the Nuclepore membranes, v_2 was calculated from data provided by General Electric, which gave the average pore size and pore density of the membrane.

It should be noted that v_2 values obtained from swelling measurements [such as those for poly(vinyl alcohol)]

TABLE I: Summary of Permeability Data for Membranes

Material	Symbol	v_2	$D'K(10^7)$ Ethanol	$D'K(10^7)$ Glycol
Gelatin (sol-dried)	O	0.080		64.3
Gelatin (sol-dried)		0.156		45.5
Gelatin (sol-dried)		0.122		59.8
Gelatin (sol-dried)		0.188		36.4
Gelatin (sol-dried)		0.144		51.0
Gelatin (sol-dried)		0.240		31.5
Gelatin (gel-dried)	●	0.143		60.2
Gelatin (gel-dried)		0.226		41.0
Gelatin (gel-dried)		0.155		49.5
Gelatin (gel-dried)		0.289		33.4
Gelatin (gel-dried)		0.195		39.8
Gelatin (gel-dried)		0.320		23.9
Poly(vinyl alcohol)	☐	0.228	36.1	
Poly(vinyl alcohol)		0.303	24.2	
Poly(vinyl alcohol)		0.513	4.99	
Poly(vinyl alcohol)		0.592	6.08	
Eastman cellulose acetate	△	1/3	22	
Millipore RA	▲	0.12	64.2	

should carry an error of ± 0.03. The values determined from weight-loss measurements are frequently accompanied by errors of thrice this amount, i.e., ± 0.10. No estimate of the errors in v_2 for the Nuclepore membranes is presently available because these are related to the variabilities in the Nuclepore preparation procedure.

All permeability data in Table I were taken using distilled water as solvent. The permeants were either ethylene glycol ($D_0 = 117(10^{-7})$ cm^2 sec^{-1}, cf. ref 5) or ethanol ($D_0 = 124(10^{-7})$ cm^2 sec^{-1}, cf. ref 6). These two permeants are water soluble, of small molecular size, and uncharged. The permeability coefficients were determined using one of the two dialysis-rate experiments that have been described previously.[5,7] The error in the $D'K$ values is estimated to be at most, 20%. Some of this error is due to uncertainties in determining membrane thickness and some is due to stagnant layers at the membrane-solution interfaces.

Results and Discussion

The data in Table I can be compared to the predictions of the Yasuda and Mackie-Meares derivations by making plots of log $(D'K)$ vs. $(1 - v_2)^{-1}$ and log $(D'K)$ vs. log $[(1 - v_2)^3/(1 + v_2)^2]$, respectively. These plots are shown in Figures 1 and 2. In neither of these figures are the Nuclepore data plotted because the Yasuda derivation would not be expected to be applicable to Nuclepore and the
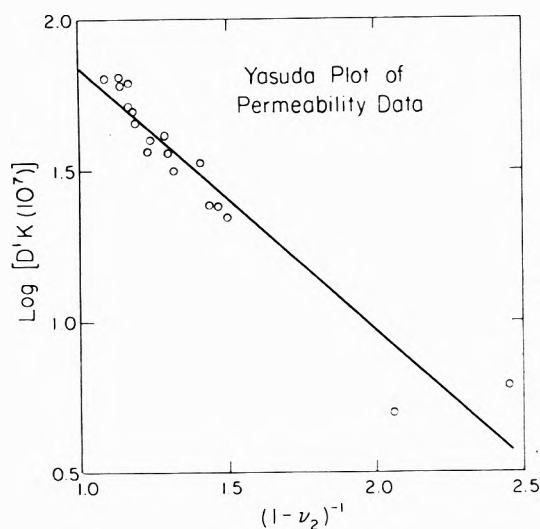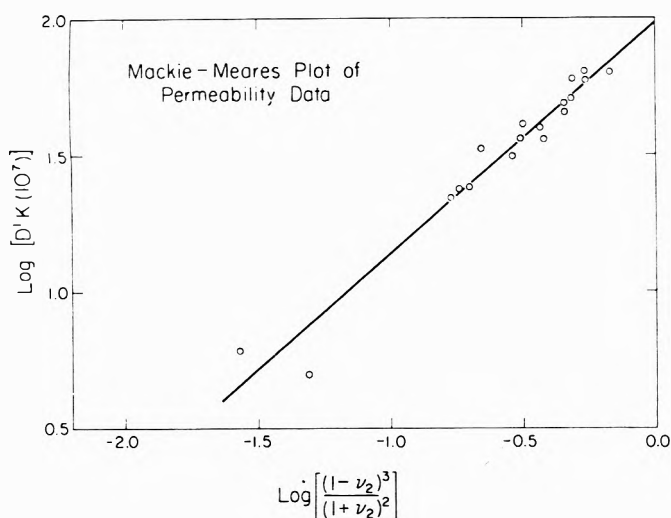
Figure 1.

Yasuda Plot of Permeability Data

Figure 2.

Mackie–Meares Plot of Permeability Data

Figure 3.

Mackie–Meares Plots of Permeability Data

$\theta = 1.0$ ———

$\theta = (1 + v_2)/(1 - v_2)$ ------

TABLE II: Comparison of the Fits of the Permeability Data Plots

Case	Slope	Correlation coefficient	Standard deviation	Log ($D'K \times 10^{7}$) at $v_2 = 0$
Yasuda, et al.	−0.8677	−0.9582	0.0876	1.8369
Yasuda (perfect)		−1.0000	0.0000	2.079
Mackie–Meares	0.8455	0.9776	0.0644	1.9885
Mackie–Meares (perfect)	1.0000	1.0000	0.0000	2.079

Mackie–Meares prediction would be only with $\theta = 1.00$ rather than $\theta = (1 + v_2)/(1 - v_2)$.

The plots in Figures 1 and 2 appear to be represented fairly well by straight lines. In order to appraise how well a linear representation applies to each, a least-squares analysis was performed on each set of data. The solid line in each figure represents the results of the least-squares fit. In Table II the parameters that describe the lines are summarized. Also presented are the parameters that would have been observed had the fit been perfect. .

From the comparisons in Table II it can be concluded that the modified Mackie–Meares equation is in better agreement with the permeability data than is the Yasuda equation. Of particular significance is the better agreement between the value of D_0 obtained from the extrapolation of the data according to the Mackie–Meares equation and the actual value of D_0, $120(10^{-7})$ cm^2 sec^{-1}.

Just how well the Mackie–Meares prediction and the data in Table I agree can be seen from the plot of $(D'K/D_0)$ vs. v_2 presented in Figure 3. The dashed line (lower curve) in this figure gives the locus of points predicted by eq 7, which is another form of the Mackie–Meares equation
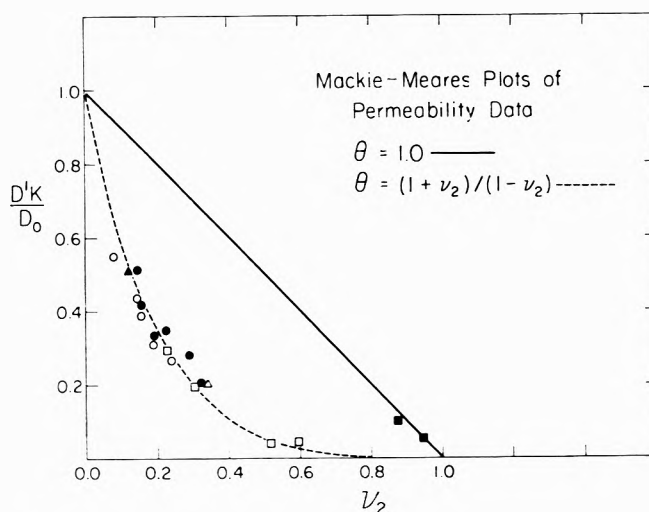
$$(D'K)/D_0 = (1 - v_2)^3/(1 + v_2)^2 \qquad (7)$$

tion for random polymer arrays. The agreement between theory and experiment is remarkably good, and it can be concluded that, in the volume fraction range that was examined ($0.08 \leq v_2 \leq 0.59$), the Mackie–Meares derivation did an acceptable job of predicting the permeability coefficients in the swollen polymer membranes.

There has been at least one study in which D' was shown to be related to D_0 as $D'\theta = D_0$.[8] This is contrary to what was postulated by Mackie and Meares, viz., $D'\theta^2 = D_0$. The data in Figure 3 tend to confirm the validity of the Mackie and Meares assumption in that they lie well below the curve (not shown) described by $D'K/D_0 = (1 - v_2)/\theta = (1 - v_2)^2/(1 + v_2)$.

One of the potential advantages of the Mackie–Meares expression, given in its general form by eq 8, is the explic-

$$D'K = D_0(1 - v_2)/\theta^2 \qquad (8)$$

it way in which the tortuosity of the membrane is included. This potential is realized in dealing with the Nuclepore membranes, for which $\theta = 1.00$. When $\theta = 1.00$, $(D'K/D_0)$ should be equal to $(1 - v_2)$. This is the source of the solid line (upper plot) in Figure 3. It is gratifying to observe that the two Nuclepore permeability data lie very near the line.

The discussion so far has considered the validity of the Yasuda or the Mackie–Meares treatment under very special circumstances, viz., only distilled water as solvent and a low-molecular-weight, uncharged solute as permeant. It turns out that each treatment can serve as a useful approximation in certain situations well removed from these. For instance, it has been observed in this lab-

oratory that eq 7 predicts rather well the permeabilities of gel-dried gelatin films swollen (v_2 = 0.25) in simulated Kodak DK-50 developer solution to ethylene glycol, hydroquinone, and Elon (monomethyl-p-aminophenol sulfate). With gelatin films swollen in simulated Kodak F-5 fixer solution (v_2 = 0.40), the Mackie–Meares prediction was observed experimentally for $Na_2S_2O_3$ but was not realized with either ethylene glycol or NaI.

Turning to the data of Wong, et al.,[9] for the diffusivity of D-fructose in diethylene glycol swollen poly(β-hydroxyethylmethacrylate) gels, the Mackie–Meares prediction is acceptable for $v_2 \leq 0.2$. At v_2's higher than 0.3, however, the measured diffusivities are substantially less than the predicted values. This divergence in the less swollen gels is not suprising inasmuch as D-fructose is an appreciably larger molecule than water or a small ion (*i.e.*, species for which the Mackie–Meares equation was derived) and would be expected to encounter a greater tortuosity than $(1 + v_2)/(1 - v_2)$ at higher v_2's. On the other hand, the plot of these same data according to log D' *vs.* $1/(1 - v_2)$ yielded a straight line that could be extrapolated to the (estimated) diffusion coefficient of the solute in solvent only at $1/(1 - v_2) = 1.0$. Thus, the data of Wong, et al., suggest that the Yasuda treatment is the more appropri-

ate one for a diffusant of appreciable size in swollen, random polymer matrixes.

References and Notes

(1) J. S. Mackie and P. Meares, *Proc. Roy. Soc.. Ser. A.* **232**, 498 (1955).
(2) H. Yasuda, C. E. Lamaze, and L. D. Ikenberry, *Makromol. Chem.,* **118**, 19 (1968).
(3) H. Yasuda. L. D. Ikenberry, and C. E. Lamaze, *Makromol. Chem..* **125**, 108 (1969).
(4) P. Mears in "Diffusion in Polymers," J. Crank and G. S. Park, Ed., Academic Press, London. 1968, pp 404–408 [also see J. S. Mackie and P. Meares, *Proc. Roy Soc.. Ser. A.* **232**, 510 (1955)].
(5) C. M. Little and H. W. Osterhoudt, *Ion Exchange Membranes,* **1**, 75 (1972).
(6) L. G. Longsworth in "American Institute of Physics Handbook," 2nd ed, D. E. Gray, Ed., McGraw-Hill, New York, N. Y., 1963, pp 2–209.
(7) H. W. Osterhoudt, *J. Appl. Polym. Sci..* **15**, 597 (1971).
(8) H. Ferguson, C. R. Gardner, and R. Paterson, *J. Chem. Soc., Faraday Trans. 1.* **68**, 2021 (1972).
(9) C.-P. Wong, J. L. Schrag, and J. D. Ferry, *J. Polym. Sci.. Part A-2.* **9**, 1725 (1971).

Cation Exchange in Mixed Solvent Media. I. The Equilibrium Swelling of Polystyrenesulfonate Resins in Dimethyl Sulfoxide–Water Media

Harold E. Van Wart and Gilbert E. Janauer*

Department of Chemistry, State University of New York at Binghamton. Binghamton. New York 13901 (Received June 1, 1973)

Total solvent uptake and solvent selectivity were determined as a function of external solvent composition for the H^+, Li^+, Na^+, K^+, Rb^+, and $N(Me)_4^+$ forms of Bio-Rad AG 50W-X8 resin in dimethyl sulfoxide–water mixtures at 25°. Similar data were obtained at 25, 45, and 65° for the H^+, Li^+, K^+, and $N(Me)_4^+$ forms of Bio-Rad AG 50W-X4, and for the H^+ and Li^+ forms of the X12 resin at 25°. As expected, total solvent uptake (SU) decreased with increasing crystal ionic radius for the homologous group I counterions in both X4 and X8 resins. Increase in degree of resin cross-linkage produced a decrease in SU but only slight changes in resin solvent selectivity (SS). The H^+ and Li^+ resins exhibited consistently high SU with a flat maximum between 30 and 50 mol % dimethyl sulfoxide (DMSO) in the binary solvent mixtures. The Na^+, K^+, and Rb^+ resins showed at 25° reversals in solvent selectivity as the mole percentage of DMSO increased in the external solvent phase. At elevated temperatures SU was reduced for all resins while SS shifted slightly toward a preference for DMSO. It is noteworthy that the H^+ resins exhibited only very weak SS and the Li^+ resins showed virtually no SS at any of the cross-linkages or temperatures studied. Intrinsic differences in solvation tendency among the counterions in conjunction with the solvent properties peculiar to the DMSO–water system account for the major trends observed. The strongly exenthalpic, temperature sensitive association equilibrium $2nH_2O + nDMSO \rightleftharpoons [DMSO-(H_2O)_2]_n$ is believed to influence significantly both resin SU and SS in DMSO–water media.

Introduction

It is a well recognized fact that quantitative information on solvent uptake (SU) and solvent selectivity (SS) of ion-exchange materials is a necessary prerequisite for the elucidation of the factors which govern ion-exchange equilibria (and kinetics) in mixed solvent media.[1] Two recent

studies with strongly basic anion-exchange resins shed new light on various factors and interactions which can control resin swelling and ion-exchange selectivity in mixed solvent systems (MSS).[2,3] Most of this work as well as earlier work (see literature cited in ref 1-3) with cation-exchange resins (similar to the ones used in our study) was carried out in the more common MSS (such as

ROH–water, acetone–water, and dioxane–water). Since water was the more polar component in these mixtures it was preferentially imbibed by the ion-exchange resins over almost the entire composition range. The extent to which water was preferred depended on the polarity of the particular organic component, the nature of the counterions and functional groups in the resin, and the degree of cross-linkage.

Enhanced differences in ion-exchange selectivities in MSS are frequently exploited for the purpose of more selective analytical separations.[4-6] Among the factors which have been considered important in conventional MSS, the significantly lowered bulk dielectric constants of the solutions in conjunction with solvent selectivity (SS) of the ion-exchange resins have often been invoked as the major sources of observed selectivity changes.[1,7,8] The factors which affect ion-exchange equilibria and kinetics in MSS will be discussed in subsequent papers. However, it should perhaps be mentioned here that the introduction of an organic solvent may affect cation- and anion-exchange equilibria somewhat differently. It was found in two recent studies of anion-exchange selectivity that sizeable initial (aqueous) resin selectivity differences for homologous series of univalent anions were actually decreased, removed, or even reversed by introducing organic solvent components of low polarity,[3,9] while significantly different selectivity patterns are frequently obtained for simple cation-exchange equilibria in MSS, as well as for cation- and anion-exchange equilibria involving complex formation.[6,10]

There has been a longstanding need for systematic ion-exchange studies in MSS containing organic solvent components of high enough polarity to minimize or completely eliminate SS of ion-exchange resins. It was suggested[11] that under these conditions—namely in the absence of the gross, classical effects of low bulk solution dielectric constants and strong resin SS—one can hope to identify and study other factors which may affect ion-exchange selectivity but would otherwise be hard to single out. Some of the considerations which prompted our choice of the dimethyl sulfoxide–water system for a systematic investigation of all aspects of cation-exchange behavior have been mentioned earlier.[12] Somewhat similar ideas have been the basis of a very recent study of Rb^+/H^+ and Mg^{2+}/H^+ exchanges on Dowex 50W-X8 resin in this solvent medium.[13] The interesting properties of dimethyl sulfoxide (DMSO), its peculiar interactions in aqueous mixtures, and properties of solutions of inorganic and organic species in DMSO media have been studied extensively.[13-38] A review of the extensive literature published on this subject would be impossible and inappropriate here, although this knowledge is essential for understanding resin swelling and ion exchange in DMSO media. We will draw upon information concerning DMSO and DMSO–water mixtures wherever we believe it to be relevant for the discussion and interpretation of our experimental data.

This paper reports the results of resin swelling measurements obtained at 25° for Bio-Rad AG 50W resins (H^+, Li^+, Na^+, K^+, Rb^+, and $N(Me)_4^+$ forms) in DMSO–water mixtures as a function of solvent composition. Effects of variation in temperature or cross-linkage upon SU and SS were also determined. The results are discussed with reference to the swelling behavior of similar resins in other binary solvent systems and may be understood from a consideration of the solvent properties of the DMSO–H_2O system.

Experimental Section

Analytical grade, recycled polystyrenesulfonate resins (AG 50W, Bio-Rad Laboratories, Richmond, Calif.) of nominal cross-linkages of 4, 8, and 12% divinylbenzene (DVB) were obtained in the hydrogen form (200–400 mesh bead size range) and converted to other ionic forms as needed. All data were obtained and recorded relative to the anhydrous state of the hydrogen resins (vacuum oven, at 105° to constant resin weight). However, because of the possibility of cracking of resin beads when "bone-dry" resins swell, and in order to avoid excessive precautions during weighing (of the extremely hygroscopic anhydrous resins) we used air-dry resins in all actual experiments. The capacities of the hydrogen resins were determined in the usual way[39] by acid–base titration and were found to be for the bone-dry exchangers 5.15 mequiv/g (H^+-X4), 4.86 mequiv/g (H^+-X8), and 5.04 mequiv/g (H^+-X12). The same resins had, after equilibration with air, typical "air-dry" capacities of 4.46 mequiv/g (X4), 3.65 mequiv/g (X8), and 3.46 mequiv/g (X12). Because of changes in ambient conditions (air humidity) the latter capacities varied slightly with time and were checked (redetermined by triplicate analyses) every time when a series of swelling experiments was run. Chemicals and solvents were all reagent grade (Fisher certified ACS) except for the tetramethylammonium chloride (Fisher, "highest purity") and were used without further purification. Dimethyl sulfoxide (DMSO) contained 0.2% water (as specified by the manufacturer and analyzed by gas chromatography using a Poropak Q column[11]). No attempt was made to remove this small concentration of water since the large majority of swelling experiments were made with solvent mixtures containing no more than a maximum of 90 vol % DMSO (X_{DMSO} = 0.695). Even for "100%" DMSO points the solvent was used without further treatment, since no special effects of small concentrations of water ("edge effects") on swelling (or for that matter, ion-exchange) equilibria had been observed in preliminary studies over the 90–100 vol % DMSO composition range. This is, of course, what one would expect from the general lack of sensitivity of various other properties of DMSO toward the addition of small amounts of water.[26] Moreover, all the significant changes found in ion-exchange behavior (to be discussed in a subsequent paper) occur in the intermediate range of solvent compositions and always below 90 vol % ($X_{DMSO} \leq$ 0.695). This—and the fact that solvent mixtures containing 10 vol % water (or more) pick up water very slowly—permitted transfer and storage without elaborate precautions and made it rational and convenient to carry out most of our experimental work in mixtures containing DMSO concentrations up to, but not exceeding, 90 vol %, although some measurements were also made at 95 vol % and in essentially water-free DMSO (0.2% water); "100% DMSO" points were important in that they provided a stringent test for the quantitative recovery of DMSO from all the resins studied. Recovery of DMSO in mixtures was tested as described earlier.[11] The small amount of water present necessitated a small correction in calculating the solvent composition of the DMSO-rich mixtures but was negligible in the water-rich region of the binary solvent systems. All the water used was deionized and distilled from an all-Pyrex still. Large quantities of all solvent mixtures for swelling experiments were prepared and characterized by refractive index,[11] which was then checked before each run.

The analytical and equilibration procedures for the determination of SU and SS have all been described. The precision of SU data reported here was ±4–5% relative when performing the elution of DMSO from centrifuged resins with hot water and using refractive index measurement for quantitative determination. SU and SS obtained at 25° with the H+ form of the AG 50W-X8 resin in this study reproduced very closely the corresponding results obtained earlier with the regular grade Dowex 50W-X8 (H+) resin.[11] In all swelling measurements air-dry hydrogen resin was first weighed into the filter tubes and conversion (to other ionic forms) was carried out by treatment with 0.5 M solutions of the appropriate electrolyte directly in the filter tubes. In this way transfer losses were completely precluded. Completeness of conversion was routinely checked in control tubes and was confirmed in all cases but in one when the X8 resin in the N(Me)₄+ form was found to contain 9% H+ ions. This series of experiments was repeated after full conversion had been accomplished by treating the resin with a larger quantity of N(Me)₄Cl solution. Solvent pretreatment of the resins (after conversion in the filter tubes) with approximately 100 ml of the particular mixture, followed by equilibration with a large excess of the same mixture (40 ml/g of resin), ensured that no noticeable changes occurred in bulk solvent compositions (external phase). Equilibration of resins with solvent mixtures at elevated temperatures was, with slight modifications, performed as described for room temperature experiments (polyethylene bottles in thermostated water bath shaker)[11] although care had to be taken to prevent loss of solvent by evaporation. After rapid transfer, centrifugation was carried out inside a large drying oven which contained also a large open beaker with the appropriate solvent mixture at the specified temperatures (45 or 65°). Variations in temperature of ±4° or less were estimated for these measurements as compared to variations of only ±0.5° at 25°.

Results and Discussion

All experimentally determined total SU data (Figures 1, 2, and 4 and Table I) as well as the calculated resin phase solvent compositions (Figures 3 and 5 and Tables I and II) have been shown as a function of the mole fraction of DMSO in the external phase (X_{DMSO}). SU has for all resins been expressed as grams of imbibed solvent per gram "bone-dry" hydrogen resin (X4, X8, X12). Solvent uptake per milliequivalent may be calculated for any ionic form of a resin by simply dividing the bone-dry capacity of the appropriate H+ resin into the reported SU values. Experimental data in graphs and tables have been shown just once with the only exception of the SU results obtained with X4 resins at 25°. These were shown first in Figure 1 to illustrate the effect of variation of cross-linkage and again in Figure 4 to show the influence of increased temperature. Figure 2 compares the swelling of the H+-X4 resin in DMSO-water with swelling of a similar resin in acetone-water. Table I presents SU for Na+ and Rb+ forms of the AG 50W-X8 resin and solvent partition data for the Li+ (X8) and (X12), H+ (X12), and K+ (X8) resinates at 25°. Internal solvent compositions for various X4 resinates as a function of X_{DMSO} at 45° are shown in Table II.

The major driving forces which produce swelling of an ion-exchange resin in contact with a solvent S are commonly taken to arise from primary and secondary solvation of fixed ions and counterions, from a general trend to
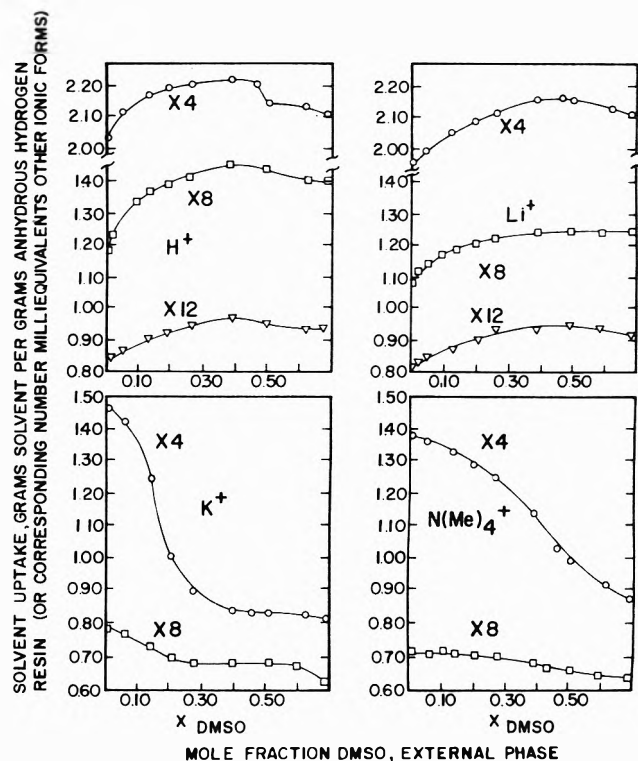
Figure 1. Solvent uptake with different forms of Bio-Rad AG 50W resins in DMSO–water media at 25° as a function of solvent composition.
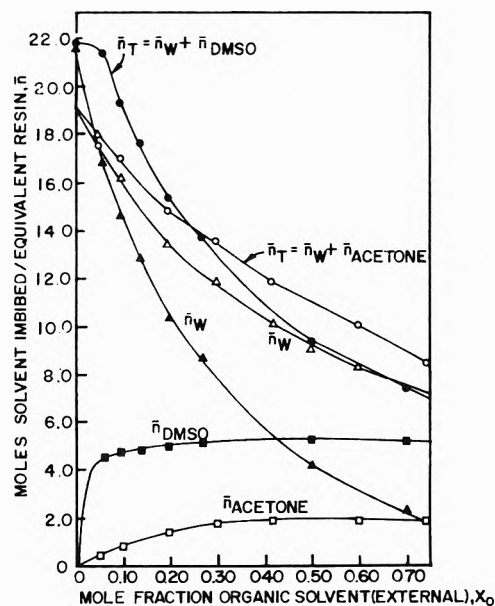
Figure 2. Swelling of AG 50W-X4 H+ resin in DMSO–water (this work: ●, ▲, and ■) and of Dowex 50-X5.5 H+ resin in acetone–water (from ref 46: ○, △, and □).

disperse charge,[3] and from the need to separate incompletely screened fixed-ion charges of equal sign which repel each other at nearby positions in the polymer network. Resin swelling will be favored by attractive interactions between S and the organic resin matrix (van der Waals' and London forces, π–π interactions). Furthermore, significant differences in the type and/or extent of solvent–solvent interactions (association) between the bulk solvent phase and the resin phase liquid may be important. The currently accepted picture for imbibed sol-

Figure 3. Solvent selectivities of univalent ionic forms of Bio-Rad AG 50W-X8 resin in DMSO–water mixtures at 25°: ■, H^+ form; ♦, Na^+ form; O, Rb^+ form; ▼, $N(CH_3)_4^+$ form. (Li^+ form not shown; SS very small; see Table I.)

Figure 5. Solvent selectivity of different forms of Bio-Rad AG 50W-X4 resin in DMSO–water media at 25 and 65°.

Figure 4. Solvent uptake with different forms of Bio-Rad AG 50W-X4 resin in DMSO–water media at 25, 45, and 65°.

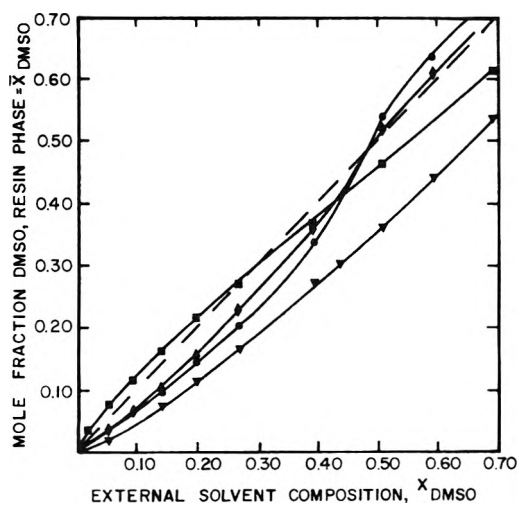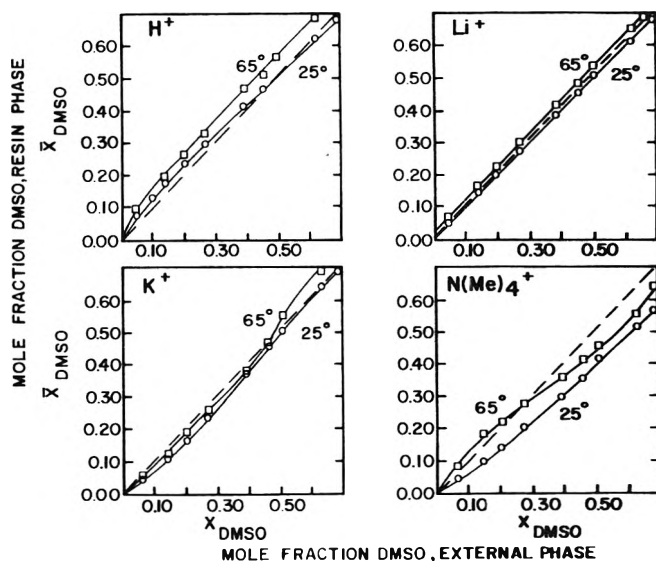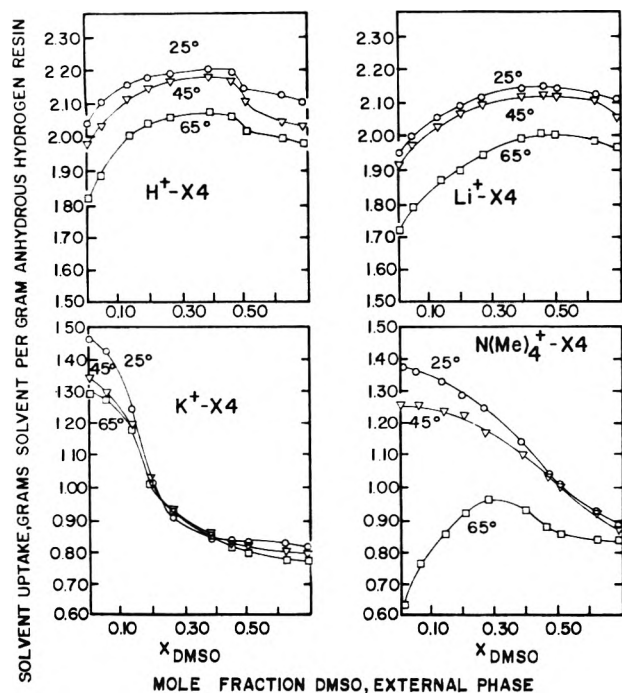vents[2,3,9] is that of rather broken-up, noncooperative (unstructured) pore liquids. In the absence of superimposed ion exchange equilibria one might expect that a strongly associated solvent $(S_1)_x$ would probably be taken up less than an essentially unassociated solvent S_2, assuming S_1 and S_2 have "otherwise identical properties," a situation which is, of course, almost impossible to achieve in practice.

The physical–chemical characteristics of a solvent which govern its uptake into an ion-exchange resin include its permanent dipole moment, the size and shape of the solvent molecule and its aggregates (if any), and possibly the presence of particular groups of atoms and/or electron configurations which may engage in specific interactions.[1] The combined forces which produce resin

swelling are, at equilibrium, balanced by the forces which hold together the polyelectrolyte with the degree of cross-linkage obviously being a very important factor.[40]

The difference between the observed total swelling of a particular ion-exchange resin (of given cross-linkage and ionic form) in two different individual solvents S_1 and S_2 will be a function of the relative tendencies of S_1 and S_2 to interact with the constituents of the polyelectrolyte (S-fixed ion, S-counterion, and S-matrix interactions) and their relative success in fulfilling the general needs of dispersing and separating charges in the resin phase (also influenced by size and shape of S_1 and S_2).

The swelling of a resin in a binary mixture of S_1 and S_2 will, in principle, be controlled by the same forces and factors already discussed, but now the two solvent components will also interact and compete with each other and produce changes in the bulk solvent medium (external phase) and possibly also in the local solvent environment in the vicinity of fixed ions, counterions, and polymer chains within the resin matrix. The "selective swelling" or "solvent selectivity" (SS) exhibited by a particular resin (i.e., its preference for S_1 over S_2) thus results from a complex interplay of many factors, although differences in polarity of S_1 and S_2 and the relative solvation tendencies of the fixed ions and counterions present in the resin are always of prime importance.

We have seen[23] that the proton may achieve more favorable interactions in DMSO–water mixtures than in pure water (certain transition metal ions have been shown to be preferentially solvated with DMSO[41,42]) and we know that all the univalent cations of the alkali group are solvated well by DMSO[43]—the small Li^+ ion considerably more than the rest.[18] Therefore, the cation-exchange resins will imbibe considerable quantities of water *and* DMSO in order to satisfy the solvation needs of the counterions,[1,2] absorb some water plus relatively much less DMSO for the solvation of the fixed group sulfonate ions and, in addition, some "free solvent" (water *and* DMSO). A recent report on selective solvent uptake by a strong base anion-exchange resin from DMSO–water mixtures showed a distinct, albeit modest, preference of the chloride resin for water[44] which is in accord with what one

TABLE I: Variation of Total Solvent Uptake (SU)^a or Resin Phase Solvent Composition $(\bar{X}_{DMSO})$ with External Solvent Composition (X_{DMSO}) for Various Resinates at 25°

Mole fraction of DMSO in external solvent = X_{DMSO}	SU		$\bar{X}_{DMSO}$			
	X8-Na$^+$	X8-Rb$^+$	X8-Li$^+$	X8-K$^+$	X12-H$^+$	X12-Li$^+$
0.059	0.908	0.724	0.055	0.037	0.075	0.046
0.098	0.896	0.722	0.077	0.067	0.13	0.092
0.140	0.879	0.688	0.12	0.10	0.16	0.12
0.200	0.869	0.660	0.18	0.15	0.22	0.17
0.270	0.860	0.641	0.25	0.22	0.29	0.24
0.500	0.863	0.653	0.49	0.52	0.50	0.46
0.695	0.885	0.600	0.67	0.73	0.65	0.63
1.00	0.554	0.347	1.0	0.98	0.980	1.0

^{a} SU = grams of solvent mixture per gram of anhydrous H$^+$ resin.

TABLE II: Resin Phase Solvent Composition $(\bar{X}_{DMSO})$ for Different Resinates of (Dowex) AG 50W-X4 as a Function of Bulk Solvent Composition (X_{DMSO}) at 45°

$X_{DMSO}/$ $\bar{X}_{DMSO}$	H$^+$	Li$^+$	K$^+$	(CH$_3$)$_4$N$^+$
0.059	0.077	0.060	0.048	0.044
0.098	0.12	0.099	0.078	0.053
0.140	0.16	0.14	0.13	0.11
0.200	0.23	0.20	0.18	0.16
0.270	0.29	0.26	0.26	0.21
0.500	0.52	0.50	0.52	0.41
0.695	0.68	0.69	0.72	0.61
1.00	0.99	1.00	0.99	1.00

might anticipate by analogy to the solvent selectivities reported for Cl$^-$ resins in various aqueous-organic mixtures by Marcus and Naveh.[2] Other factors which may affect the uptake of DMSO into an ion-exchange resin are the possibility of interaction with aromatic rings (via the lone pair of electrons on the sulfur) and dispersion forces between the methyl groups of the solvent and the resin matrix similar to what has been suggested for the case of aliphatic alcohols.[2,45] Of major importance in this highly associated solvent system may be differences between the solvent-solvent interactions in the resin phase and in the external binary mixture in equilibrium with the exchanger[2,3,9] as will be shown below.

Our solvent uptake data at 25° (Figures 1 and 4 and Table I) for H$^+$ and Li$^+$ resins reflect the extremely strong solvation tendencies of these counterions over the entire range of solvent compositions. The curves plotted for various resinates represent the total weight of solvents imbibed per gram of bone-dry H$^+$ resins and thus give also a fair idea of the total swelling of the resins as a function of external solvent composition. When, instead, the number of moles solvent $(\bar{n})$ in the resin is calculated and plotted for the same data, a marked deviation from the familiar pattern[45,46] of gradually increasing $\bar{n}_{org}$ (accompanied by fast decrease of $\bar{n}_w$ and $\bar{n}_{total}$) is observed. In cases where comparison is possible, such as for H$^+$ resins (with swelling in acetone-water[46]—see Figure 2) and alkali resinates (in ethanol-water[45]) it is seen that $\bar{n}_{DMSO}$ rises much more steeply and reaches much higher values than $\bar{n}_{org}$, and $\bar{n}_w$ and $\bar{n}_{total}$ drop faster in DMSO-water than in other systems. Overall SU as well as SS for DMSO remain high even at large external X_{DMSO} in this system. The general swelling trend for the X8 alkali resinates in DMSO-water (see Figures 1 and 2 and Table I) follows the expected order Li$^+$ > Na$^+$ > K$^+$ > Rb$^+$, although the differences between the K$^+$ and Rb$^+$ resinates are fairly small. The SU for the N(CH$_3$)$_4$$^+$ form of the X8 resin falls

between the corresponding K$^+$ and Rb$^+$ curves and SU of the Na$^+$ resinate between Li$^+$ and K$^+$ (but closer to K$^+$). It may be recalled that the flat maximum in SU for the H$^+$ resins (upper left of Figure 1) is coincident with the mole fraction range of strongest interaction for the proton in the binary system. In general, the similarity of the SU curves for H$^+$ and Li$^+$ resins is in good correlation with expected solvation tendencies as seen by comparison with the results of solvation studies by Arnett and McKelvey.[18]

Unfortunately, no comparable swelling studies have so far been reported for the 50W-X8 and X12 resins in other highly polar aprotic solvents. One recent study in DMF-water was performed with the Dowex 50W-X1 resin,[8] and the results suggest trends somewhat similar to the ones found in this work. However, as pointed out correctly by these authors,[47] resins of such low cross-linkage cannot be expected to exhibit any strong trends in solvent preferences.

The solvent selectivities of univalent X8-resinates (Figure 3) are interesting from several points of view. First of all, the solvent selectivity (defined as SS = $\bar{X}_{DMSO}/X_{DMSO}$, or the slope of $\bar{X}_{DMSO}$ vs. X_{DMSO}, independent of n) of the H$^+$ resin was found to be closer to one than any SS found so far for any cation-exchange resin of intermediate cross-linkage in any binary solvent medium. The preference of this resin for DMSO at low DMSO concentrations seems noteworthy and is tentatively attributed to a specific interaction between the proton and DMSO with possible participation of the fixed sulfonate group. In this connection it should be recalled that DMSO by itself is a much stronger base vs. proton than is water[23,25,26]—although this is not necessarily true in its aqueous mixtures—and also that the formation of well defined and stable DMSO·HX adducts has been reported.[25,29] Also noteworthy is the fact that the largest value for SS of the H$^+$-X8 resin for DMSO coincides with a 1:1 ratio of H$^+$ to DMSO imbibed (i.e., 1 mol of DMSO/mol of hydrogen resinate). The possibility that DMSO is rejected by the dilute aqueous bulk phase because of structure-making properties (negative entropy effect) and therefore "put away" into the much less structures resin phase seems unlikely. Such an effect would have to be the same for all ionic forms studied. Actually, only the H$^+$ form exhibits SS for DMSO in this region (Figure 2). The strongly exenthalpic interaction between DMSO and water to some extent counterindicates "water-structure making" as found for small amounts of alcohols in water.[34]

The Li$^+$-X8 resin shows an even smaller solvent selectivity than the H$^+$ resin. Thus, the experimental points (determined at the same mole fractions as for the H$^+$ resin) fell very close to the (dashed) "ideal" partition line (SS = 1.0) in Figure 3 and are not shown (but see Table

I). Both the H^+ and the Li^+-X8 resins make it possible to carry out ion-exchange studies in the virtual absence of solvent selectivity as hoped for originally. It should be stressed however, that a SS $\cong 1$ for the Li^+-X8 resin does *not* mean "ideal conditions" exist in the resin phase. It means only that the net composition of the solvent mixtures happens to be virtually identical in both phases.

The very small preference for water shown by the other univalent X8-resinates at low mole fractions of DMSO in the bulk solvent phase is in sharp contrast to the SS shown by similar alkali resinates in conventional alcohol-water mixtures[45] where resin phases are always highly enriched with water. Our observed relative order of SS resembles the one found by Starobinets and Novitskaya[48] in water-acetone mixtures. The absolute differences between the individual SS (Na^+, K^+, Rb^+) are quite small, but the general trend, *viz.*, the reversal of solvent selectivity (going from water toward DMSO) and the crossover for the Na^+ and Rb^+ resins deserve attention. It may be timely to recall now the existence of the $[DMSO(H_2O)_2]_n$ aggregates in DMSO-water and to consider possible differences between the DMSO-water interactions inside and outside the resin phase. Due to the high molality of electrolyte inside the resin (greater than 3 in all cases) and because of the expected disruptive effect of the cross-linked resin matrix on any cooperative solvent-solvent interactions one can, in general, expect solvent-solvent association to be much more extensive in the external solvent phase. (This would be equally true whether the DMSO-water aggregates be linear polymers, rings, or three dimensional. It should, perhaps, be repeated that the existence of a water-like structure in the stoichiometric 2:1 DMSO-water mixtures does not appear very likely). Since a large amount of experimental evidence indicates that the DMSO-water medium attains maximum association at about $X_{DMSO} = 0.33$, the following interesting effect may become important for resin swelling equilibria in this solvent system. The introduction of a disruptive resin phase (disruptive from the point of view of solvent association in the pore liquid) to mixtures of varying percentages of DMSO affords these mixtures the opportunity to change composition so as to better attain maximum DMSO-water interaction (*i.e.*, a minimum in the excess free energy of the mixture): below a DMSO-water ratio of 1:2 "excess" water is transferred into the resin, and above this ratio "excess" DMSO is transferred into the resin phase. (This is, of course, possible only because of the excellent solvation characteristics of both solvents with respect to counterions and fixed ions). Thus, the resin would act, to some extent, as a "buffer" for the maintenance of maximum solvent association in the external solvent phase. This effect will be referred to as the solvent association effect (SAE). Either "excess" water ($X_w \geq 0.67$) or "excess" DMSO ($X_{DMSO} \geq 0.33$) is better accommodated in the resin because there, the primary solvation of counterions and fixed ions engages the solvent in strong ion-solvent interactions, and geometric restrictions by themselves may oppose the formation of DMSO-H_2O aggregates. Thus, the SAE would contribute to minimize the excess free energy of the external binary solvent phase due to the favorable enthalpic interaction around the stoichiometric 1:2 composition of the system and must be clearly distinguished from entropy-driven effects identified as important for ion exchange[9,49,50] and swelling[3] equilibria in other solvent systems. The postulated SAE has its apparent origin in the external solvent phase and

must be superimposed upon all other factors affecting SU and SS in this system.

Returning now to Figures 3 and 5, one sees that up to an external DMSO concentration of about 33 mol %, the preference of the Na^+, K^+, and Rb^+ resins for water at 25° is increasing. When $X_{DMSO} = 0.33$ the influence of the SAE upon SS should be minimal. At this composition, the order of SS of the resins for DMSO is found to be $H^+ > Li^+ > Na^+ > K^+ > Rb^+$, which is also the order for SU and the expected order for maximum ion-solvent interaction. Thus, the SS and SU of the alkali resinates at 25° can be consistently explained over the entire composition range of solvent mixtures by considering the interplay between the relative solvation tendencies of the resin phase ions and the SAE. The difference in the thermodynamic stability between DMSO-water and alcohol-water associates can explain SU and SS differences between DMSO-rich and *e.g.*, alcohol-rich binary solvent systems.[45]

The solvent selectivity curve shown for the $N(CH_3)_4^+$-X8 resin was accidentally obtained with a resin still containing 9% H^+ counterions, but a repeat with a fully converted $N(CH_3)_4^+$ resin fell virtually on the same experimental SS curve. This result is of considerable interest in that it suggests the feasibility of ion-exchange experiments at virtually constant swelling conditions when the exchange fraction is kept small.

Figure 4 presents the results of total swelling studies of four different ionic forms of the X4 resin at three different temperatures. It is observed that total swelling generally decreases with increasing temperature which probably reflects mainly the temperature effect upon ion-solvation equilibria in the resin phase. The SAE should decrease in magnitude at temperatures above 45° as the thermo-labile DMSO-water aggregates are being broken up.[36] This would not affect SU very much, but should influence the SS of resins at elevated temperatures.

The data presented in Figure 5 and Table I represent the selective swelling behavior on the four ionic forms of the X4 resin studied at 25, 45, and 65°. The effect on SS of increasing the temperature from 25 to 45° is only slight and is to increase preference for DMSO. In going from 45 to 65°, however, the effect of increased preference for DMSO is enough to cause selectivity reversals for all four ions over at least part of the range. This correlates well with the larger decrease in viscosity of DMSO water mixtures between 45-65° as compared to the 25-45° interval. The swelling behavior at elevated temperatures probably reflects the temperature dependence of preferential ion solvation and progressive removal of the postulated SAE.

In summary it can be said that a detailed consideration of the physical and thermodynamic properties of DMSO-water mixtures makes possible a consistent explanation of the somewhat unusual SU and SS of cation exchangers observed in these media.

It may be of interest that Starobinets and Novitskaya[48] have pointed out that SS of ion-exchange resins in common solvent mixtures is most extreme for those binary systems showing the greatest positive deviations from ideality. The fact that the DMSO-water system shows a rather sizable negative deviation cannot alone explain all the differences between swelling behavior in alcohol-water or acetone-water mixtures and DMSO-water mixtures. The ability of DMSO to compete effectively with water in cation solvation is certainly a most important factor and

it seems safe to conclude that the structural effects in this system must be viewed as different from the typical structural effects acting upon swelling equilibria in binary solvent systems thus far studied. The implications for ion-exchange equilibria and kinetics of the singularly small SS of the cation exchange resins studied will become apparent in the discussion of work now being completed.

References and Notes

(1) F. Helfferich, "Ion Exchange," McGraw-Hill, New York, N. Y., 1962, p 507.
(2) Y. Marcus and J. Naveh, *J. Phys. Chem.*, **73**, 591 (1969).
(3) C. H. Jensen and R. M. Diamond, *J. Phys. Chem.*, **75**, 79 (1971).
(4) G. E. Janauer, J. Korkisch, and S. A. Hubbard, *Talanta*, **18**, 767 (1971).
(5) H. F. Walton, *Anal. Chem.*, **42**, 86R (1970).
(6) J. Korkisch, "Modern Methods for the Separation of Rarer Metal Ions," Pergamon Press, New York, N. Y., 1969.
(7) J. Korkisch, *Progr. Nucl. Energy Ser. 9*, **6** (1966).
(8) A. Ghodstinat, J. L. Pauley, Teh-Hsuen Chen, and G. Quark, *J. Phys. Chem.*, **70**, 521 (1966).
(9) G. E. Janauer and I. M. Turner, *J. Phys. Chem.*, **73**, 2194 (1969).
(10) J. Penciner, I. Eliezer, and Y. Marcus, *J. Phys. Chem.*, **69**, 2955 (1965).
(11) G. E. Janauer, H. E. Van Wart, and J. T. Carrano, *Anal. Chem.*, **42**, 215 (1970).
(12) G. E. Janauer, *Mikrochim. Acta*, 1111 (1968).
(13) R. Smits, P. Van den Winkel, D. L. Massart, J. Juillard, and J. P. Morel, *Anal. Chem.*, **45**, 339 (1973).
(14) D. Martin, A. Weise, and H. J. Niclas, *Angew. Chem., Int. Ed. Engl.*, **6**, 318 (1967).
(15) J. N. Butler, *J. Electroanal. Chem.*, **14**, 89 (1967).
(16) H. L. Schläfer and W. Schaffernicht, *Angew. Chem.*, **72**, 618 (1960).
(17) C. V. Krishnan and H. L. Friedman, *J. Phys. Chem.*, **73**, 1572, 3934 (1969).
(18) E. M. Arnett and D. R. McKelvey, *J. Amer. Chem. Soc.*, **88**, 2598 (1966).
(19) D. E. Arrington and E. Griswold, *J. Phys. Chem.*, **74**, 123 (1970).
(20) A. J. Parker, *Int. Sci. Technol.*, 28 (Aug 1965).
(21) J. Kenttamaa, *Suom. Kemistilehti*, **33**, 179 (1960).
(22) J. M. G. Cowie and P. M. Toporowski, *Can. J. Chem.*, **39**, 2240 (1961).
(23) R. K. Wolford, *J. Phys. Chem.*, **68**, 3392 (1964).
(24) J. C. Synott and J. N. Butler, *J. Phys. Chem.*, **73**, 1470 (1969).
(25) I. M. Kolthoff, M. K. Chantooni, Jr., and S. Bhowmik, *J. Amer. Chem. Soc.*, **90**, 23 (1968).
(26) I. M. Kolthoff and T. B. Reddy, *Inorg. Chem.*, **1**, 189 (1962).
(27) A. J. Parker, *Quart. Rev. Chem. Soc.*, **16**, 163 (1962).
(28) J. Miller and A. J. Parker, *J. Amer. Chem. Soc.*, **83** 117 (1961).
(29) J. A. Olabe, M. C. Giordana, and A. J. Arvia, *Electrochim. Acta*, **12**, 907 (1967).
(30) R. G. Fessler and H. A. Strobel, *J. Phys. Chem.*, **67**, 2562 (1963).
(31) G. Yagil, *J. Phys. Chem.*, **73**, 1610 (1969).
(32) S. A. Schichman and R. L. Amey, *J. Phys. Chem.*, **75**, 98 (1971).
(33) J. J. Lindberg, *Suom. Kemistiseuran Tiedonantoja*, **70**, 33 (1961).
(34) F. Franks and D. J. G. Ives, *Quart. Rev. Chem. Soc.*, **20**, 1 (1966).
(35) G. E. Walrafen, *J. Chem. Phys.*, **52**, 4176 (1970).
(36) G. J. Safford, P. C. Schaffer, P. S. Leung, G. F. Doebbler, G. W. Brady, and E. F. X. Lyden, *J. Chem. Phys.*, **50**, 2140 (1969).
(37) G. Brink and M. Falk, *J. Mol. Struct.*, **5**, 27 (1970).
(38) D. D. MacDonald and J. B. Hyne, *Can. J. Chem.*, **49**, 611 (1971).
(39) See ref 1, p 91.
(40) M. P. Gregor, D. Noble, and M. H. Gottlieb, *J. Phys. Chem.*, **59**, 10 (1955).
(41) L. P. Scott, T. J. Weeks, Jr., D. E. Bracken, and E. L. King, *J. Amer. Chem. Soc.*, **91**, 5219 (1969).
(42) A. G. Kosak, G. E. Janauer, and H. E. Van Wart, Abstracts, 160th National Meeting of the American Chemical Society, Chicago, Ill., Sept 1970, Division of Inorganic Chemistry, No. 187.
(43) J. Kenttamaa, *Suom. Kemistilehti*, **33**, 179 (1960).
(44) L. S. Frankel, *Can. J. Chem.*, **48**, 2433 (1970).
(45) H. Rückert and O. Samuelson, *Acta Chem. Scand.*, **11**, 303 (1957).
(46) C. W. Davies and B. D. R. Owen, *J. Chem. Soc.*, 1676 (1956).
(47) J. L. Pauley, D. D. Vietti, C. C. Ou-Yang, D. A. Wood, and R. D. Shevill, *Anal. Chem.*, **41**, 2047 (1969).
(48) G. L. Starobinets and L. V. Novitskaya, *Kolloid Zh.*, **25**, 689 (1963).
(49) G. E. Boyd and Q. V. Larson, *J. Amer. Chem. Soc.*, **89**, 6038 (1967).
(50) G. E. Janauer, *Monatsh. Chem.*, **103**, 605 (1972).

On Certain Aspects of Charge Dependence of Free Energy of Adsorption at the Electrode–Solution Interphase

Liliana Rampazzo

Institute of Chemistry, University of Rome, Faculty of Engineering, Rome, Italy (Received December 15, 1972; Revised Manuscript Received October 19, 1973)

Adsorption isotherms in which polarization energy of adsorbed ions is taken into account are examined. Under some extrathermodynamic assumptions, the dependence of the isotherm parameters $\ln \beta$ and A upon the electrode coverage and charge density q_M are evaluated. Whereas the zero-polarization assumption of Levine, Bell, and Calvert leads to a linear dependence of $\ln \beta$ on q_M, a quadratic dependence appears in the extended theory as a natural consequence of electrostatic interactions. Experimental data on $(BPh_4)^-$ ion adsorption are in reasonable agreement with the above analysis.

Introduction

In a previous communication,[1] we reported that in aqueous solutions of x M NaBPh$_4$ + (0.916 − x) M NaF, the free energy of adsorption of $(BPh_4)^-$ anion at the mercury electrode exhibits a quadratic dependence on the electrode charge density.

It was observed that the system obeys a Frumkin-type[2] isotherm, and that such an isotherm is congruent[3] with respect to the charge taken as the electrical variable. The $(BPh_4)^-$ ion is centrosymmetrical (zero dipole moment) and its radius is comparatively high with respect to simpler ions as I^-. Therefore, it seems likely that, in deriving

the isotherm, the contribution from anion polarization in the electrical field acting between the metal and solution must be computed. The equivalence of the Frumkin and Levine, Bell, and Calvert[4,5] isotherms was also demonstrated.[1] The latter isotherm foresees a linear dependence of the free energy of adsorption on the charge, if, as the authors pointed out,[4] the polarization energy of the adsorbed ion can be neglected. In what follows, an attempt is made to show that if such energy is taken into account, a quadratic dependence of the free energy of adsorption on the charge is obtained. Moreover, one topic of discussion will be the effects of a particular case of functional dependence of the dielectric constant on the number of ions adsorbed at the interphase.

Theoretical

Following the usual method, the condition for adsorption equilibrium is expressed by equating the chemical potential of an adsorbed ion at $x = \beta$ ($x = 0$ is the plane of the electrode) to that of an ion of the same kind in the bulk of the solution. Preliminary assumptions are that the ion is neither oxidized nor reduced in the potential range examined; moreover, d (the distance of outer Helmholtz layer from the electrode) is constant. Ions of one type only are involved in adsorption. Symbols used are: I.H.P. = inner Helmholtz plane; O.H.P. = outer Helmholtz plane; ϕ_M = mean electrostatic potential in the metal; ϕ_β = mean electrostatic potential at the I.H.P.; ϕ_d = mean electrostatic potential at the O.H.P.; $\gamma = d - \beta$; a = ion activity in the bulk of the solution; q_M = mean charge density in the metal; q_β = mean charge density at the I.H.P.; Γ = concentration of adsorbed ions at $x = \beta$ (mol cm^{-2}); Γ_m = maximum concentration of adsorbed ions (mol cm^{-2}); $\theta = \Gamma/\Gamma_m$ electrode coverage; ϵ_0, ϵ_1, $\epsilon(\theta)$ = mean[6] dielectric constants, for $\theta = 0$, $\theta = 1$, and θ respectively, of the region between metal and O.H.P.; and r = number of solvent molecules displaced by an adsorbed ion. The chemical potential of 1 g-ion in the solution interior is given by

$$\mu_S = \mu_S^0 + RT \ln a \qquad (1)$$

The chemical potential of 1 g-ion adsorbed at $x = \beta$, μ_β, can be expressed by

$$\mu_\beta = \mu_\beta^0 + RT \ln \frac{\theta}{(1 - \theta)^r} + zF\phi_1 + z^2F^2\Gamma_m \frac{4\pi\gamma^2}{\epsilon d} + zF \frac{4\pi\gamma}{\epsilon} q_M - \frac{d}{8\pi\Gamma_m} \left(\frac{\phi_M - \phi_d}{d}\right)^2 \frac{\partial\epsilon}{\partial\theta} \qquad (2)$$

All the terms on the right-hand side of eq 2 except the last one are the same as in the Levine-Bell-Calvert theory. The last term describes the polarization energy of the ion (of zero dipole moment) in the field acting at the center of the ion itself.[4,7]

At equilibrium, $\mu_S = \mu_\beta$ and therefore

$$\ln \frac{\theta}{(1 - \theta)^r} = \frac{\mu_S^0 - \mu_\beta^0}{RT} - \frac{zF}{RT}\phi_d - \frac{zF}{RT}\frac{4\pi\gamma}{\epsilon}q_M + \frac{d}{8\pi RT\Gamma_m}\left(\frac{\phi_M - \phi_d}{d}\right)^2 \frac{\partial\epsilon}{\partial\theta} + \ln a - \frac{z^2F^2}{RT}\Gamma_m \frac{4\pi\gamma^2}{\epsilon d}\theta \qquad (3)$$

On the other hand[4,5]

$$\phi_M - \phi_d = \frac{q_M}{K} + \frac{\gamma q_\beta}{K} \qquad (4)$$

where $K = \epsilon/4\pi d$. Writing

$$\ln \beta^0 = \frac{\mu_S^0 - \mu_\beta^0}{RT} \qquad (5)$$

one has

$$\ln \frac{\theta}{(1 - \theta)^r} = \ln \beta^0 - \frac{zF}{RT}\phi_d - \frac{zF}{RT}\frac{4\pi\gamma}{\epsilon}q_M + \frac{2\pi d}{RT\Gamma_m\epsilon^2}\left(q_M + zF\Gamma_m\frac{\gamma}{d\theta}\right)^2\frac{\partial\epsilon}{\partial\theta} - \frac{z^2F^2}{RT}\Gamma_m\frac{4\pi\gamma^2}{\epsilon}\theta + \ln a \qquad (6)$$

which is equivalent to

$$\ln \frac{\theta}{(1 - \theta)^r} = \ln \beta^0 - \frac{zF}{RT}\phi_d - \frac{zF}{RT}\frac{4\pi\gamma}{\epsilon}q_M + \frac{2\pi d}{RT\Gamma_m}\frac{1}{\epsilon^2}\frac{\partial\epsilon}{\partial\theta}q_M^2 + \frac{zF}{RT}4\pi\gamma\frac{1}{\epsilon^2}\frac{\partial\epsilon}{\partial\theta}q_M\theta - \frac{z^2F^2}{RT}\Gamma_m\frac{4\pi\gamma^2}{d\epsilon}\theta + \frac{z^2F^2}{RT}\frac{2\pi\gamma^2}{d}\Gamma_m\frac{1}{\epsilon^2}\frac{\partial\epsilon}{\partial\theta}\theta^2 + \ln a \qquad (7)$$

Generally, at q_M = constant, ϵ and $\partial\epsilon/\partial\theta$ are unknown functions of θ. Moreover, since ϕ_d depends on θ, congruent isotherms cannot be expected.

Let us consider the particular case in which the following conditions are fulfilled: (a) ϕ_d is negligible, as it can be assumed for solutions at high ionic strength; (b)

$$\frac{1}{\epsilon^2}\frac{\partial\epsilon}{\partial\theta} = \text{constant} \qquad (8)$$

It is easily verified that, by integrating eq 8 under the conditions $\epsilon = \epsilon_0$ ($\theta = 0$), $\epsilon = \epsilon_1$ ($\theta = 1$), one has

$$\frac{1}{\epsilon} = \left(\frac{1}{\epsilon_1} - \frac{1}{\epsilon_0}\right)\theta + \frac{1}{\epsilon_0} \qquad (9)$$

$$\frac{1}{\epsilon^2}\frac{\partial\epsilon}{\partial\theta} = \frac{1}{\epsilon_0} - \frac{1}{\epsilon_1} \qquad (10)$$

Taking eq 9 and 10 into account, it follows therefore from eq 7 that, under conditions a and b

$$\ln \frac{\theta}{(1 - \theta)^r} = \ln \beta^0 - \frac{zF}{RT}\frac{4\pi\gamma}{\epsilon_0}q_M + \frac{2\pi d}{\Gamma_m RT}\left(\frac{1}{\epsilon_0} - \frac{1}{\epsilon_1}\right)q_M^2 + \ln a - \frac{z^2F^2}{RT}\Gamma_m\frac{4\pi\gamma^2}{d\epsilon_0}\theta - \frac{zF}{RT}8\pi\gamma\left(\frac{1}{\epsilon_1} - \frac{1}{\epsilon_0}\right)q_M\theta - \frac{z^2F^2}{RT}\Gamma_m\frac{6\pi\gamma^2}{d}\left(\frac{1}{\epsilon_1} - \frac{1}{\epsilon_0}\right)\theta^2 \qquad (11)$$

It can be concluded that strictly congruent isotherms are not obtained even if conditions a and b hold good. (Cf. Appendix.) Anyhow, the quadratic dependence from the electrode charge in eq 11 stands out. It is interesting to note that, according to hypothesis b, the coefficient of the term which is quadratic in the charge density q_M depends only on d and on $1/\epsilon_0 - 1/\epsilon_1$, and is independent of z (which can be ± 1, etc.); in other words, if $\epsilon_1 < \epsilon_0$ ($\partial\epsilon/\partial\theta < 0$) such a coefficient is always negative irrespective of the fact that adsorbed ion is a cation or an anion.

Returning to the general case, we observe that eq 11 can be written as

$$\ln \frac{\theta}{(1 - \theta)^r} = \ln \beta + \ln a - A(\theta, q_M)\theta \qquad (12)$$

i.e., in the form of a Frumkin isotherm. It is seen that $\ln \beta$ can be written as

$$\ln \beta = \ln \beta^0 + A'q_M + B'q_M^2 \qquad (13)$$

that is, it is independent of θ, whereas the interaction parameter is expressed by

$$A(\theta, q_M) =$$

$$A_0 \left[1 + \frac{2a'}{zF\Gamma_m\gamma} \left(\frac{\epsilon_0}{\epsilon_1} - 1 \right) q_M + \frac{3}{2} \left(\frac{\epsilon_0}{\epsilon_1} - 1 \right)\theta \right] \quad (14)$$

where

$$A_0 = \frac{z^2 F^2}{RT} \Gamma_m \frac{4\pi\gamma^2}{d} \frac{1}{\epsilon_0} \quad (15)$$

Hence

$$\lim_{\substack{q \to 0 \\ \theta \to 0}} A(\theta, q_M) = A_0$$

It means that, at q_M = constant, the interaction parameter varies linearly with θ

$$\frac{A}{A_0} = m\theta + h \quad (16)$$

where

$$m = \frac{3}{2} \left(\frac{\epsilon_0}{\epsilon_1} - 1 \right) \quad (17)$$

Figure 1 represents the behavior of A/A_0 as a function of θ, for various values of q_M, in the case $\epsilon_1/\epsilon_0 = 2/3$ and $z =. -1$ and fixed values of β, Γ_m, and $d(\beta = 4.2$ Å, $d = 6.3$ Å, $\Gamma_m = 2.6 \times 10^{-10}$ mol × cm^{-2}).

Comparison with Experimental Data and Discussion

In this way, the adsorption isotherm for the case under discussion, as written in the form of eq 12, should exhibit: (a) the term $\ln \beta$ (eq 13), which is quadratic in the charge and independent of θ; this term describes ion–electrode interactions; (b) the term $A(\theta, q_M)\theta$ with $A(\theta, q_M)$ given by eq 14. This term describes ion–ion interactions at $x = \beta$ as modified by ion polarization from the electric field acting at the center of the ion.

For the practical cases, if the values of the product q_M θ are not too high, "pseudo congruent" isotherms can be experimentally observed. In such a case, and neglecting the term in θ^2 ($0 < \theta < 1$) in eq 11, the isotherm becomes

$$\ln \frac{\theta}{(1-\theta)^r} = \ln \beta^0 - \frac{zF}{RT} \frac{4\pi\gamma}{\epsilon_0} q_M +$$

$$\frac{2\pi d}{\Gamma_m RT} q_M^2 - \frac{z^2 F^2}{RT} \Gamma_m \frac{4\pi\gamma^2}{d} \frac{1}{\epsilon_0} \theta + \ln a \quad (18)$$

which is a Frumkin type isotherm, *i.e.*

$$\ln \frac{\theta}{(1-\theta)^r} = \ln \beta - A\theta + \ln a \quad (19)$$

where

$$\ln \beta = \ln \beta^0 + A'q_M + B'q_M^2 \quad (20)$$

$$A = \frac{z^2 F^2}{RT} \Gamma_m \frac{4\pi\gamma^2}{d} \frac{1}{\epsilon_0} \quad (cf. \text{ eq } 15) \quad (21)$$

$$A' = -\frac{zF}{RT} \frac{4\pi\gamma}{\epsilon_0} \quad (22)$$

$$B' = \frac{2\pi d}{\Gamma_m RT} \left(\frac{1}{\epsilon_0} - \frac{1}{\epsilon_1} \right) \quad (23)$$

In the case of $(BPh_4)^-$ ion, a satisfactory agreement between calculated and experimental values of coefficients A and A' was found,[1] with $\Gamma_m = 2.6 \times 10^{-10}$ mol cm^{-2} (from experimental data) and assuming $\beta = 4.2$ Å, $d = 6.3$ Å, $\epsilon_0 = 6(T = 298$ K). The experimentally observed dependence of $\ln \beta$ on q_M was expressed by[1]

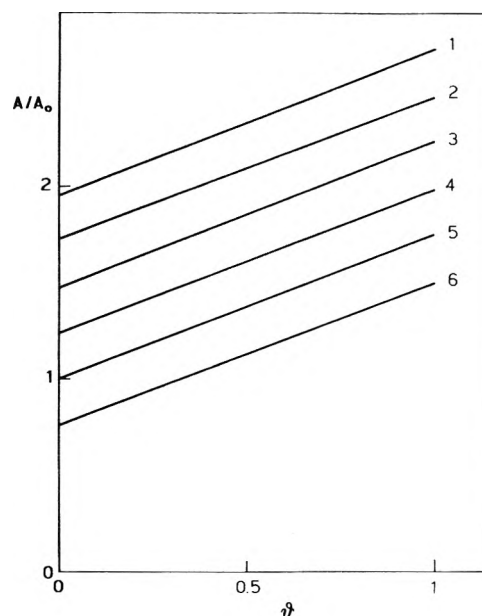**Figure 1.** Interaction parameter A/A_0 relative to a Frumkin isotherm, calculated according to eq 14, as a function of electrode coverage θ. Values of electrode charge density q_M (μC cm^{-2}): (1) -8; (2) -6; (3) -4; (4) -2; (5) 0; (6) $+2$; $z = -1$; $\epsilon_1/\epsilon_0 = 2/3$.

$$\log \beta - \log \beta^0 - 0.022 = 0.2981q_M - 0.0197q_M^2 \quad (24)$$

Therefore, if the above mentioned assumptions are valid, it follows that

$$\frac{B'}{2.3} = \frac{1}{2.3} \frac{2\pi d}{\Gamma_m RT} \left(\frac{1}{\epsilon_0} - \frac{1}{\epsilon_1} \right) = -0.0197 \text{ cm}^4/(\mu C)^2 \quad (25)$$

With the same values for Γ_m, d, and ϵ_0 we used previously for A and A', and assuming $\epsilon_1 = 4$, the calculated value of $B'/2.3$ (eq 25) becomes $B'/2.3 = -0.02$ cm$^4/(\mu C)^2$, which agrees with the experimental value of -0.0197. This fact confers some reliability to hypothesis b, by which the functional dependence of ϵ from θ is expressed by eq 9. Moreover, the value of $\epsilon_1 = 4$ can be compared with the value $\epsilon = 2.27$ for benzene.[8] These results imply that, in the adsorption of $(BPh_4)^-$ ion, the dielectric properties of the interphase at $\theta = 1$ are controlled mainly by the phenyl group, in the inner zone $0 < x < \beta$ of the inner region, which some contribution from the arrangement of water molecules in the outer zone $\beta < x < d$ of the inner region.[5,9,10]

The assumption that d = constant has been made throughout. Variation of d with θ cannot be excluded in principle, especially for adsorbed ions of large radius. The major difficulty is to locate the O.H.P. and to evaluate the value of d ($d = 4$–6 Å), even in the absence of adsorbed ions. In the presence of adsorbed ions, the O.H.P. probably represents a leveling of local variations in thickness,[5] which in turn will depend from the size of adsorbed ions and from the extent of solvation of the diffuse layer ions in the outer zone of the inner double layer. Moreover, the adsorbed ions will displace the solvation sheet of the electrode. Variation of d with coverage, if any, will be of minor importance with respect to dielectric constant effects. Thus the thickness d may well be assumed to be a constant, at least as a first approximation. This will be not the case if the adsorbed ions assume different orientations as θ is varied.

Appendix

Let the isotherm be congruent with respect to q_M; one can then write such an isotherm in the form[11a,b]

$$\ln G + \ln a = \ln f(\theta) \quad (A1)$$

where G is some function of q_M alone and $f(\theta)$ is some function of θ alone. It follows from the pure thermodynamic arguments developed by Parsons[11a] (see also Frumkin, et al.,[11b]) that

$$E = E_0(1 - \theta) + E_1\theta \quad (q_M = \text{constant}) \quad (A2)$$

Here E, E_0, and E_1 are the values of the applied electrode potentials, at q_M = constant, in the presence of adsorbed ions, in their absence and for $\theta = 1$, respectively. At q_M = 0, and the same θ, eq A2 yields

$$E^z = E_0{}^z(1 - \theta) + E_1{}^z\theta \quad q_M = 0 \quad (A3)$$

where E^z, $E_0{}^z$, and $E_1{}^z$ are the potentials of the electrocapillary maximum at θ, at $\theta = 0$, and $\theta = 1$ respectively.

From (A2) and (A3) it follows that

$$E - E^z = (E_0 - E_0{}^z)(1 - \theta) + (E_1 - E_1{}^z)\theta \quad (A4)$$

i.e.

$$\frac{E - E^z}{q_M} = \frac{E_0 - E_0{}^z}{q_M}(1 - \theta) + \frac{E_1 - E_1{}^z}{q_M}\theta \quad (A5)$$

Hence

$$\frac{1}{K} = \frac{1}{K_0}(1 - \theta) + \frac{1}{K_1}\theta \quad (A6)$$

or, being $K = \epsilon/4\pi d$, $K_0 = \epsilon_0/4\pi d$, and $K_1 = \epsilon_1/4\pi d$

$$\frac{1}{\epsilon} = \frac{1}{\epsilon_0}(1 - \theta) + \frac{1}{\epsilon_1}\theta \quad (A7)$$

i.e., if the isotherm is congruent with respect to q_M, and d = constant, $1/\epsilon$ is a linear function of θ.

Let us now see if the reverse is also true. Supposing that

$$\frac{1}{\epsilon} = \frac{1}{\epsilon_0}(1 - \theta) + \frac{1}{\epsilon_1}\theta \quad (A7)$$

it follows that

$$\frac{1}{K} = \frac{1}{K_0}(1 - \theta) + \frac{1}{K_1}\theta \quad (A8)$$

Hence

$$\frac{E - E^z}{q_M} = \frac{E_0 - E_0{}^z}{q_M}(1 - \theta) + \frac{E_1 - E_1{}^z}{q_M}\theta \quad (A9)$$

which is equivalent to (q_M = constant)

$$E = E_0(1 - \theta) + E_1\theta + E^z - E_0{}^z(1 - \theta) - E_1{}^z\theta \quad (A10)$$

Here now E^z is an unknown function of θ. Deriving (A10) with respect to θ at q_M = constant, it follows that

$$\left(\frac{\partial E}{\partial \theta}\right)_{q_M} = (E_1 - E_0) + \frac{dE^z}{d\theta} - (E_1{}^z - E_0{}^z) \quad (A11)$$

On the other hand, it is known that the following thermodynamic relation holds[12]

$$\left(\frac{\partial E}{\partial \theta}\right)_{q_M} = \Gamma_m RT \left(\frac{\partial \ln a}{\partial q_M}\right)_\theta \quad (A12)$$

and eq A11 becomes

$$\Gamma_m RT \left(\frac{\partial \ln a}{\partial q_M}\right)_\theta = (E_1 - E_0) + \frac{dE^z}{d\theta} - (E_1{}^z - E_0{}^z) \quad (A13)$$

where $dE^z/d\theta$ is an unknown function of θ, say $g(\theta)$, and $E_1 - E_0$ is some function of q_M, say $\chi(q_M)$. In other words, from eq A13 it follows that

$$\Gamma_m RT \left(\frac{\partial \ln a}{\partial q_M}\right)_\theta = \chi(q_M) + g(\theta) - (E_1{}^z - E_0{}^z) \quad (A14)$$

In order for the isotherm to be congruent with respect to the charge q_M, the following equation must hold (cf. eq A1)

$$RT \left(\frac{\partial \ln a}{\partial q_M}\right)_\theta = - RT \frac{d \ln G}{dq_M} \quad (A15)$$

where G and hence $d \ln G/d q_M$ must be a function of q_M alone. Since the right-hand side of eq A14 is a function of both q_M and θ, it is concluded that the isotherm with the condition (A7) is, in general, not congruent with respect to q_M.

From the arguments developed above it is demonstrated that eq (A7) i.e., eq 9 of the text, is a necessary but not a sufficient condition for the congruence of the isotherms with respect to q_M.

References and Notes

(1) C. Giomini and L. Rampazzo, J. Phys. Chem., 76, 707 (1972).
(2) A. N. Frumkin, Z. Phys., 35, 792 (1926).
(3) R. Parsons, Trans. Faraday Soc., 51, 1518 (1955).
(4) S. Levine, G. M. Bell, and D. Calvert, Can. J. Chem., 40, 518 (1962).
(5) S. Levine, J. Mingins, and G. M. Bell, J. Electroanal. Chem., 13, 280 (1967).
(6) V. A. Kir'yanov, Sov. Electrochem., 6, 1143 (1970).
(7) (a) M. J. Sparnaay, Recl. Trav. Chim., Pays-Bas. 77, 872 (1958); (b) I. Prigogine, P. Mazur, and R. Defay, J. Chim. Phys., 50, 146 (1953).
(8) "Handbook of Chemistry and Physics," 50th ed, The Chemical Rubber Co., Cleveland, Ohio, 1970.
(9) J. R. Macdonald and C. A. Barlow, Jr., J. Chem. Phys., 44, 202 (1966).
(10) In the text it was assumed that ϵ_0 = constant, ϵ_1 = constant in the inner layer: in fact, ϵ_0 is to be intended as a mean value,

$$\epsilon_0 = \frac{1}{d} \int_0^d \epsilon_0(x) dx$$

of the unknown $\epsilon_0(x)$ profile, and similarly for ϵ_1. Moreover, it was tacitly assumed that g = 1 (for the significance of g see ref 4 and 5), which is a good approximation, especially in the case of solutions of high ionic strength. After this paper was submitted, S. Levine and K. Robinson [J. Electroanal. Chem., 41, 159 (1973)] have presented a generalized discreteness of charge theory (with ϵ_0 = ϵ_{01} for $0 < x < \beta$, ϵ_0 = ϵ_{02} for $\beta < x < d$). Their conclusions are, inter alia, that a "perturbation" term in the discreteness of charge potential may lead to a slight variation of g with θ. The authors estimated that the contribution of this perturbation term is a minor one. The value ϵ_0 = 6 used in our calculations is to be recognized as tentative: possibly, ϵ_0 = 12 would be preferable. In this case, and retaining the same ϵ_1/ϵ_0, value (cf. Figure 1), the calculated values for A' and B' are $A'/2.3$ = 0.33 cm^2/μC and $B'/2.3$ = -0.01 cm^4/$(\mu$C$)^2$, respectively.
(11) (a) R. Parsons, Trans. Faraday Soc., 55, 999 (1959); (b) A. N. Frumkin, B. B. Damaskin, V. M. Gerovich, and R. I. Kaganovich, Dokl. Akad. Nauk SSSR. 158, 706 (1964).
(12) Cf. P. Delahay, "Double Layer and Electrode Kinetics," Interscience, New York, N. Y., 1964, p 28.

Determination of Acidity in 80% Dimethyl Sulfoxide-20% Water[1]

Ernest H. Baughman and Maurice M. Kreevoy*

University of Minnesota, Chemical Dynamics Laboratory, Minneapolis, Minnesota 55455 (Received June 21, 1973)

Dissociation constants have been measured by the "ladder" technique for a series of buffer acids and a series of acid-base indicators in 80% DMSO-20% water. The whole range, between dilute HCl and dilute KOH, has been spanned. The latter measurements permit the determination of pK_{HA} for water in this solvent. It has a value of 18.38 which correlates well with values in other DMSO-water mixtures. The indicators provide a convenient method for reasonably accurate pH measurements in this solvent mixture in which reliable electrometric pH determination is inconvenient.

Mixtures of dimethyl sulfoxide (DMSO) with water have recently become increasingly popular and useful as reaction media. It has been apparent in our own and other work that a rapid and reliable method of determining pH in such solvent mixtures would be desirable. Unfortunately, the conventional glass electrode-calomel electrode pH meter responds slowly and sometimes irreproducibly in such mixtures.[2,3] We have therefore calibrated a set of indicators for use in 80% DMSO-20% water, by weight. This is a convenient solvent for many purposes because it dissolves many ionic and molecular substances freely. It has a dielectric constant (72) only a little below that of pure water.[4] It is not highly hygroscopic and shows solvent acid-base properties quite different from those of pure water.

The calibration was carried out by the "ladder" technique,[5] starting with dilute HCl. For the most part colorless and indicator acids were alternated on the "ladder." The overlap is sufficient so that at least one indicator, capable of giving quantitative results, is available at any pH. The indicators used all have absorptions characteristic of both the acidic and basic forms so that the pH can be determined from a ratio of absorbances, without an exact knowledge of the indicator concentration. The ladder was continued until the pH of dilute KOH solutions could be determined. These latter measurements permit the determination of the autoprotolysis constant of water in this solvent.

The dissociation constants, K_{HA}, of the acids, HA, are represented by eq 1. Charges are not shown for HA and A

$$K_{HA} = \frac{(H^+)(A)}{(HA)} \frac{\gamma_H \cdot \gamma_A}{\gamma_{HA}} \qquad (1)$$

because various charge types were used. Activity coefficients are represented by γ. For each indicator two wavelengths, λ_1 and λ_2, were chosen. Extinction coefficients of A and HA were designated $\epsilon_A{}^1$, $\epsilon_A{}^2$, $\epsilon_{HA}{}^1$, and $\epsilon_{HA}{}^2$, respectively. The wavelengths were chosen so as to minimize the ratios $\epsilon_{HA}{}^2/\epsilon_A{}^1$ and $\epsilon_A{}^2/\epsilon_A{}^1$ which were designated R_1 and R_2. R_3 is $\epsilon_{HA}{}^1/\epsilon_{HA}{}^2$. The R values were determined from spectra of solutions in which the indicators are completely in the acidic or basic form. When the absorbance at each wavelength, A_n, is given by

$$A_n = \epsilon_A{}^n(A) + \epsilon_{HA}{}^n(HA) \qquad (2)$$

K_{HA} is given by eq 3a

$$K_{HA} = \frac{(H^+)(A_1 - R_3 A_2)R_1}{A_2 - A_1 R_2} \frac{\gamma_H \cdot \gamma_A}{\gamma_{HA}} \qquad (3a)$$

$$(H^+)\frac{\gamma_H \cdot \gamma_A}{\gamma_{HA}} = \frac{K_{HA}(A_1 R_2 - A_2)}{(A_2 - R_1 A_1)R_3} \qquad (3b)$$

When $\epsilon_{HA}{}^1$ is not significantly different from zero, which is the case for many of our indicators, eq 3a simplifies to eq 4a

$$K_{HA} = \frac{(H^+)A_1 R_1}{A_2 - A_1 R_2} \frac{\gamma_H \cdot \gamma_A}{\gamma_{HA}} \qquad (4a)$$

$$(H^+)\frac{\gamma_H \cdot \gamma_A}{\gamma_{HA}} = K_{HA}\frac{(A_2 - A_1 R_2)}{A_2 R_1} \qquad (4b)$$

Equation 3a or 4a was used to determine all the indicator dissociation constants reported in this paper. Ionic strength, u, in these measurements ranged between 2×10^{-3} and 4×10^{-4} M. Equation 5, a form of the Debye-

$$\log \gamma_i = \frac{-A(Z_i)^2 u^{1/2}}{1 + Bdu^{1/2}} \qquad (5)$$

Hückel limiting law,[6] was used to estimate the activity coefficients of ionic species. In this solvent A is 0.710 when concentrations are expressed as moles per liter, and Bd was taken as 1.42.[7] The activity coefficients of neutral species were assumed to be unity. All these activity coefficients refer, of course, to infinite dilution *in this solvent mixture,* as the standard state. In all these solutions (H^+) was known, either from the concentration of HCl or from the composition of a buffer. In the case of a buffer the value of K_{HA} for the buffer was previously determined.

Equations 3a and 4a are readily rearranged to 3b and 4b so as to make them more convenient for the determination of (H^+) from the, now known, K_{HA} values and measured absorbances. They were used in this form to determine (H^+) for nonindicator buffers to which a very small amount of indicator was added. Since the buffer ratio was known or separately determined in these solutions, K_{HA} could be calculated. In this way the "ladder" was extended.

Experimental Section

DMSO (Aldrich Chemical Co.) was twice distilled under vacuum from calcium hydride, discarding the first and last 15% each time. Such DMSO was shown by Karl

TABLE I: pK_{HA} for Buffer Acids

Compound	pK_{HA} (80% DMSO)	ΔpK_a	R_1	R_2	λ_2	λ_1	pK_{HA}(H$_2$O)
Cl$_2$CHCOOH	3.87 ± 0.01	2.61					1.26[a]
ClCH$_2$COOH	5.69 ± 0.01	2.82					2.87[b]
CH$_3$COOH	8.00 ± 0.02	3.24					4.76[c]
p-CNC$_6$H$_4$OH[g]	9.83 ± 0.01	1.88	27.22	0.0623	289	250	7.95[d]
p-ClC$_6$H$_4$OH	11.98 ± 0.01	2.60	0.6155	0.2866	312	284	9.38[e]
2,4,6-(CH$_3$)$_3$C$_6$H$_2$OH	13.83 ± 0.03	2.95	0.4321	0.3536	309	282	10.88[f]
H$_2$O	18.38 ± 0.02[h]	4.38					14.00

[a] M. Rondell and C. F. Failey, *Chem. Rev.*, **4**, 291 (1927). [b] D. J. G. Ives and J. H. Pryor, *J. Chem. Soc.*, 2104 (1955). [c] H. S. Harned and R. W. Ehlers, *J. Amer. Chem. Soc.*, **55**, 652 (1933). [d] G. W. Wheland, R. M. Brownell, and E. C. Mayo, *ibid.*, **70**, 2492 (1948). [e] C. M. Judson and M. Kilpatrick, *ibid.*, **71**, 3110 (1943). [f] G. R. Sprengling and C. W. Lewis, *ibid.*, **75**, 5709 (1953). [g] R_3 is 0.0263. [h] For water K_{HA} is taken as (H$^+$)(OH$^-$)$\gamma_\pm^2$.

TABLE II: pK_{HA} for Indicators

Compound	pK_{HA} (80% DMSO)	R_1	R_2	R_3	λ_2	λ_1	pK_{HA}(H$_2$O)
2,4-Dinitrophenol	4.16 ± 0.00	0.6692	0.0524		419	303	4.09[c]
Bromcresol Green	5.73 ± 0.02	0.2528	0.0046		615	444	4.90[b]
Bromcresol Purple	7.63 ± 0.01	0.2157	0.00647		590	424	6.30[a]
Bromthymol Blue	8.95 ± 0.01	0.192	0.0107		620	454	7.30[b]
Cresol Red	10.68 ± 0.02	0.2417	0.00269		581	419	8.20[a]
2,4-Dinitrodiphenylamine	11.79 ± 0.01	0.2073	0.01527	1.065	495	357	
2,6-Dichloro-4-nitro-analine	14.46 ± 0.01	0.3970	0.0198		465	362	

[a] W. R. Brode, *J. Amer. Chem. Soc.*, **46**, 589 (1924). [b] I. M. Kolthoff and T. B. Reddy, *Inorg. Chem.*, **1**, 189 (1962). [c] H. V. Halban and G. Kortüm, *Z. Phys. Chem.*, **A170**, 351 (1934).

Fischer titration and by nmr measurements to have a residual water content of about 0.1%.[8] The water used was deionized and then distilled.[9] Hydrochloric acid solutions were made up by dilution of constant boiling HCl.[10] Reagent grade acetic acid (E. I. du Pont de Nemours & Co., Inc.) was redistilled before use. Both 4-chlorophenol (Aldrich Chemical Co.) and 2,4,6-trimethylphenol (Aldrich Chemical Co.) were distilled under vacuum (mp 40-41 and 71-71.5°, respectively; lit. mp 41[11] and 69°[12]). 4-Cyanophenol (Aldrich Chemical Co.) was recrystallized from benzene (mp 112.6-113.6°; lit. mp 112.0-112.4°[13]). Both 2,4-dinitrophenol (Eastman Kodak Co.) and 2,4-dinitrodiphenylamine (Aldrich Chemical Co.) were recrystallized from ethanol (mp 112.6-113.6 and 156.6-157.0°; lit. mp 112-113[14] and 154.2-155.5°,[15] respectively). 2,6-Dichloro-4-nitroaniline (Aldrich Chemical Co.) was used without purification (mp 190-191°; lit. mp 189°[16]). Bromcresol Green, Bromcresol Purple, Bromthymol Blue, Methyl Red, and Cresol Red were dissolved in aqueous 5% NaHCO$_3$ solution and precipitated from the hot solution by drop-wise addition of aqueous HCl.[17] The process was repeated until no further increase in the extinction coefficient was noted. No attempt was made to duplicate the literature values of λ_{max} or ϵ's as these are solvent dependent.[18] (The commercial products appeared to be about 25% indicator and 75% low molecular weight acid which was not identified.)

In the future these indicators will all be made available, as concentrated solutions, by the Ventron Corporation through Alfa Products.

The ratios, R_1, R_2, and R_3, required by eq 3 and 4, were determined after taking spectra in successively more basic or more acidic solutions till further changes in pH produced no further changes in the spectra. In these solutions, and also in the solutions used to determine K_{HA} values, total indicator concentrations were around 5 × 10^{-6} M.

In the buffer solutions the total concentration of buffer constituents was around 10^{-3} M. The buffer constituents were nearly nonabsorbing in the visible, except for 2,4,6-trimethylphenol, in which case its absorbance was can-

celled by using, as reference, solution containing the buffer but not the indicator. Thus they did not interfere with the indicator measurements, which were made in 10-cm cells. The indicator concentrations, on the other hand, were so low that absorption by the indicators was less than 1% that of the phenolic buffer constituents at their maxima in the uv. For the phenolic buffers this enables us to determine the buffer ratios, also, from eq 3 and 4, without *a priori* knowledge of the composition of the solution, using 0.1-cm cells. The buffer ratios so determined were always in reasonable agreement with those given by the *a priori* compositions of the solutions, however.

The buffer ratios in the carboxylic acid buffers were determined from the stoichiometric compositions of the solutions. These were less subject to error than the buffer ratios in the phenolic buffers because the carboxylic acid buffers are acidic, and, therefore, less prone to absorb CO$_2$ from the atmosphere.

Spectrophotometric measurements were made with a Beckman DK-2 spectrophotometer, calibrated at 536.4, 453.6, 385.8, 360.8, 333.8, 287.6, and 279.3 nm with holmium oxide (Beckman Std.). All measurements were made at ambient temperature, but room temperature was maintained within 2° of 25° by air-conditioning, and temperature fluctuations are not thought to contribute significantly to the inaccuracy of the reported K_{HA} values.

Results

Table I gives the mean pK_{HA} values for the (nonindicator) buffer acids. In the case of the phenols λ_1, λ_2, R_1, R_2, and, where necessary, R_3, are also given. Table II gives the same information for the indicators. In each case the value is the mean of at least five separate determinations. The cited uncertainty is the probable error of the mean value. Table III shows a typical set of determinations. The largest deviations from the mean pK_{HA} values were around 0.1 and the average deviations from the mean values around 0.02, so that it ought to be possible to use these indicators to determine pH with about that precision.
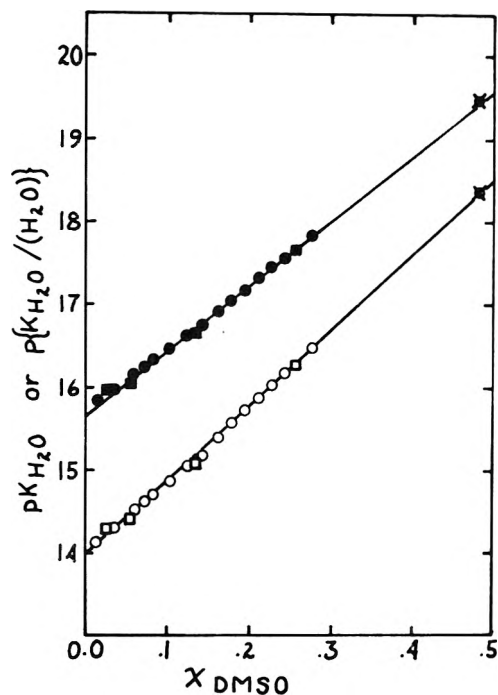
Figure 1. pK_{H_2O} as a function of χ_{DMSO}, the mole fraction of DMSO in the solvent. Values of Wooley and Hepler are indicated by circles, those of Das and Kundu by squares, the present values by crossed circles. Open figures are for pK_{H_2O}; closed figures are for $p\{K_{H_2O}/(H_2O)\}$. If either function of K_{H_2O} is extrapolated to the present χ_{DMSO}, a value similar to the present one is obtained.

TABLE III: K_{HA} Determinations for 2,6-Dichloro-4-nitroaniline

$[H^+]^a$	A^{465}	A^{365}	$K_{HA} \times 10^{16}$
2.52×10^{-14}	0.123	0.358	3.30
1.77×10^{-14}	0.160	0.331	3.43
1.27×10^{-14}	0.215	0.313	3.52
5.90×10^{-15}	0.371	0.266	3.60
4.87×10^{-15}	0.401	0.249	3.22
4.17×10^{-5}	0.458	0.222	3.56
2.62×10^{-15}	0.595	0.178	3.72
$\sim 10^{-13b}$	1.010	0.020	
$\sim 10^{-18c}$	0.000	0.401	

^{a} Determined from the uv spectra of $2.05 \times 10^{-3} M$ $(CH_3)_3C_6H_2OH$ solutions. ^{b} Used to determine the spectrum of HA. ^{c} Used to determine the spectrum of A.

Discussion

There are two points at which our results can be subjected to critical, external checks. The pK_{HA} of acetic acid has been previously determined, conductometrically, by Morel.[19] He obtained a value of 8.00. This is in excellent agreement with the value given in Table I. Two recent papers have given pK_{HA} values for water in DMSO-water mixtures, 0 to 60% DMSO.[20,21] For water K_{HA} was defined as $(H^+)(OH^-)\gamma_{\pm}^2$ rather than by eq 1. Plots of pK_{HA} or $pK_{HA} + \log (H_2O)$, are, empirically, linear functions of the mole fraction DMSO. Figure 1 shows that such plots extrapolate to our present value of the pK_{HA} for water quite acceptably. Since the pK_{HA} for water depends on all the others, this supports all the present results. In addition, the reported values of pK_{HA} for chloroacetic acid and dichloroacetic acid are reasonably related to those reported[22] at an ionic strength of $0.2 M$. These correspondences suggest that the inaccuracy of the pK_{HA} values reported are not much worse than their impreci-
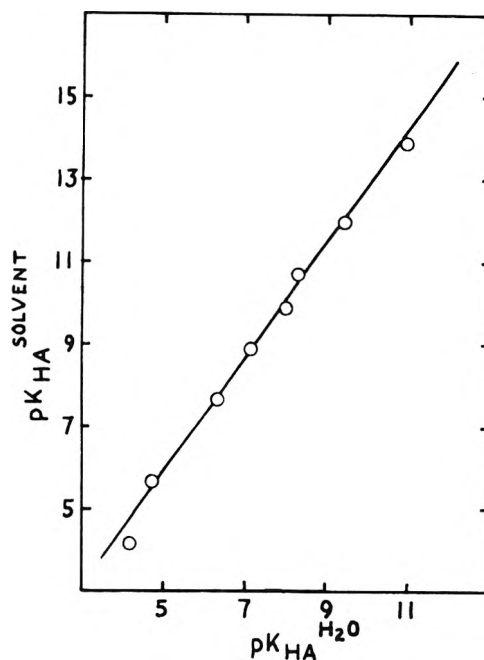

Figure 2. The relation between pK_{HA} values in the present solvent and those in water. The slope of the linear relation is 1.4.

sion, and pH values obtained with the aid of the indicators will have a corresponding reliability.

Internal consistency of the present data is further supported by Figure 2. The linear plot of pK_{HA}(solvent) against pK_{HA}(water) is expected[23] and observed. The nonunit slope of this plot has certain implications for acidity functions which will be discussed elsewhere.

Further, approximate, use of the indicators can be made in DMSO-water mixtures having 0-80% by weight DMSO, if it is assumed that their pK_{HA} values are linear functions of the mole fraction of DMSO. Such relations have been found to have a wide, approximate, validity.[22]

References and Notes

(1) Supported, in part, by the U. S. National Science Foundation through Grant No. GP-31360X.
(2) T. B. Reddy, Ph.D. Thesis, University of Minnesota, 1960.
(3) C. D. Ritchie and R. E. Uschold, J. Amer. Chem. Soc., 89, 1721 (1967).
(4) E. Tommila and A. Pajunen, Suom. Kemi. B, 41, 172 (1968).
(5) W. Bover and P. Zuman, J. Amer. Chem. Soc., 95, 2531 (1973).
(6) H. S. Harned and W. B. Owen, "The Physical Chemistry of Electrolytic Solutions," 3rd ed, Reinhold, New York, N. Y., 1958, p 66.
(7) J. Kielland, J. Amer. Chem. Soc., 59, 1675 (1937).
(8) We are indebted to Sister Lavonne Abts for the nmr measurements.
(9) J. E. C. Hutchins, Ph.D. Thesis, University of Minnesota, 1969.
(10) G. A. Hulett and W. D. Bonner, J. Amer. Chem. Soc., 31, 390 (1909).
(11) W. J. Wohlleben, Berichte. 42, 4373 (1909).
(12) C. W. Porter and E. H. Thurber, J. Amer. Chem. Soc., 43, 1194 (1921).
(13) G. W. Wheland, R. M. Brownell, and E. C. Mayo, J. Amer. Chem. Soc., 70, 2493 (1948).
(14) W. E. Bachman, J. M. Chenenda, N. C. Deno, and E. C. Horning, J. Org. Chem., 13, 390 (1948).
(15) E. J. Hoffman and P. A. Dane, J. Amer. Chem. Soc., 41, 1016 (1919).
(16) R. L. Datta and H. K. Miller, J. Amer. Chem. Soc., 41, 2036 (1919).
(17) W. R. Orndorff and A. C. Purdy, J. Amer. Chem. Soc., 48, 2216 (1926).
(18) R. Stewart and J. D. O'Donnell, Can. J. Chem., 42, 1681 (1964).
(19) J. P. Morel, Bull. Soc. Chim., Fr., 1406 (1967).
(20) A. Das and K. Kundu, J. Phys. Chem., 69, 730 (1973).
(21) E. Woolley and L. Hepler, Anal. Chem., 44, 1520 (1972).
(22) N. M. Ballash, E. B. Robertson, and M. D. Sokolowski, Trans. Faraday Soc., 66, 2622 (1970).
(23) R. P. Bell, "The Proton in Chemistry," Cornell University Press, Ithaca, N. Y., 1959, Chapter III.

Metal Ion Association in Alcohol Solutions. III. Erbium Chloride in Aqueous Methanol[1,2]

Jeffry Reidler and Herbert B. Silber*

Department of Chemistry, University of Maryland Baltimore County, Baltimore, Maryland 21228   (Received August 20, 1973)

As water is added to methanolic solutions of $ErCl_3$, the distribution of complexes shifts from predominantly inner-sphere to outer-sphere complexes. The rate constants for complexation were essentially the same at two different water compositions and in agreement with aqueous solution results for the reaction of Er(III) with a univalent anion.

A question of continuing interest in lanthanide chemistry has been the determination of the environment surrounding each cation in solution, coupled with the possibility that a change in coordination numbers occurs within the middle region of the series. Freed and his group used spectroscopic measurements on lanthanide nitrates and chlorides to probe the environments surrounding selected lanthanide cations.[3-6] The existence of different environments around Eu(III) was found for the nitrate and the chloride salts in water. Upon dilution of the nitrate salt, there was a change in spectral peaks to those present in the aqueous chloride solutions. When the spectroscopic measurements were carried out in anhydrous and aqueous alcohol solutions other differences between the two salts were observed. In the aqueous alcohol solutions the spectral changes which occurred were attributed to the existence of more than one environment surrounding the cation in the mixed solvents. We have used the ultrasonic relaxation technique to study aqueous alcohol solutions of $ErCl_3$ and $Er(NO_3)_3$ to determine what causes the major spectral differences between these ligands.[1,2,7] In aqueous solutions Freed's spectral measurements can be explained in terms of the predominant species present in the chloride being outer-sphere complexes, while the nitrate salt has significant quantities of inner-sphere complexes. As the nitrate concentration decreases, the outer-sphere complex becomes favored and the spectra resemble those of the chloride solutions. Ultrasonic relaxation measurements in aqueous alcohol solutions of erbium chloride and nitrate solutions have also been used to interpret results in the mixed solvents. An analysis of the change in the amplitude as well as the frequency of the sound absorbance as a function of water composition led to the conclusion that a change in solvation number occurred during complexation for $Er(NO_3)_3$ in aqueous methanol, which was essentially complete at 25% water.[1] In the case of the chloride no change which could be attributed to a coordination number change was observed as water was added, thereby establishing that any coordination number changes that occur within the lanthanide series are not due to the solvated cation alone, but involve a major dependence upon the ligand.[2] Because the relaxation frequency change for $ErCl_3$ as water was added was very unusual, it was decided to continue the earlier investigation in order to determine the complexation rate constants in alcohol solutions containing only a small per cent water.

Experimental Section

The erbium chloride solutions were made from the oxide or the chloride salts obtained from American Potash & Chemical Corp. In some cases the solutions made from the commercial chloride were not as soluble as expected. To obtain the correct concentration it was necessary to add a small quantity of aqueous HCl to the methanol solution of $ErCl_3$, heat for dissolution, and then to heat to dryness several times, adding methanol before cooling. The solutions made from the oxide were made in a similar manner. The water content was determined by Karl Fisher titration. For some solutions the quantity of water exceeded that reported here and this was most easily picked up by the ultrasonic measurements because a small quantity of water decreased both the relaxation amplitude and especially the relaxation frequency. The concentration of all $ErCl_3$ stock solutions were determined using ion exchange.[8] The methanol was prepared by distillation from a solution containing Mg metal to remove the excess water.

The ultrasonic relaxation apparatus and techniques employed were similar to those described earlier.[1] All calculations were carried out using a Wang 700 programmable calculator.

Results and Discussion

No excess ultrasonic absorption was observed over the frequency range 10-250 MHz for a solution composed of $ErCl_3$ in water, indicating that in aqueous solution the complex is almost completely outer-sphere, because these complexes are not detectable in these cation complexation reaction systems. However, $ErCl_3$ solutions with methanol or aqueous methanol exhibited an excess absorption over the experimental frequency range, indicating the existence of at least one chemical reaction whose time constant was in the frequency range under observation. For a system undergoing chemical relaxation, the measured sound absorption α/f^2, fits a standard curve defined by

$$\alpha/f^2 = B + \sum_i \frac{A_i}{1 + (f/f_i)^2} \tag{1}$$

where f is the frequency, f_i is the relaxation frequency of each independent chemical relaxation step, A_i is the amplitude of the relaxation, and B is the experimental background which is characteristic of the solvent medium. The excess absorbance, μ, is defined as the quantity $(\alpha/f^2 - B)f^2\lambda$. The absorbance data are typical of systems which have one low-frequency relaxation coupled to a high-frequency process. This is illustrated in Figure 1 where the data are presented in methanol containing 0.03 and 0.70 mol fraction of water (X_{H_2O}), respectively.

A summary of the relaxation results for solutions 0.096 M in $ErCl_3$ as a function of water composition is present-

TABLE I: Relaxation Results for 0.096 M ErCl$_3$ as a Function of Water Composition

X_{H_2O}	0.03	0.07	0.22	0.37	0.60	0.70	1.00
Single relaxation calculation							
A^a	237 ± 6	413 ± 33	357 ± 22	227 ± 17	92.0 ± 7.4	53.7 ± 4.3	No excess ab-
f_R, MHz	18.1 ± 0.5	8.1 ± 0.5	9.9 ± 0.5	12.1 ± 0.7	15.9 ± 1.2	17.2 ± 1.4	sorbance
B^a	37.3 ± 0.8	43.0 ± 0.8	39.8 ± 0.7	42.5 ± 0.4	40.5 ± 0.5	36.2 ± 0.3	
$10^4\mu_{max}$	24.1	19.2	22.0	18.0	10.9	7.1	
Double relaxation, $B^a = 25$							
Low frequency							
A^a	239 ± 6	461 ± 46	402 ± 24	281 ± 18	116 ± 9	67.3 ± 6.3	
f_R, MHz	17.6 ± 0.6	7.3 ± 0.5	8.8 ± 0.4	10.1 ± 0.5	12.0 ± 0.8	12.8 ± 1.1	
$10^4\mu_{max}$	23.6	19.4	21.9	18.6	10.4	6.7	
High frequency							
A^a	14.3 ± 1.7	21.1 ± 1.5	21.1 ± 1.0	20.7 ± 0.6	19.1 ± 0.6	13.8 ± 0.5	
f_R, MHz	413 ± 161	251 ± 58	271 ± 33	274 ± 23	248 ± 19	252 ± 23	
$10^4\mu_{max}$	33.2	30.6	35.4	37.2	35.3	26.8	

^{a} Units = 10^{17} nepers cm^{-1} sec^2.
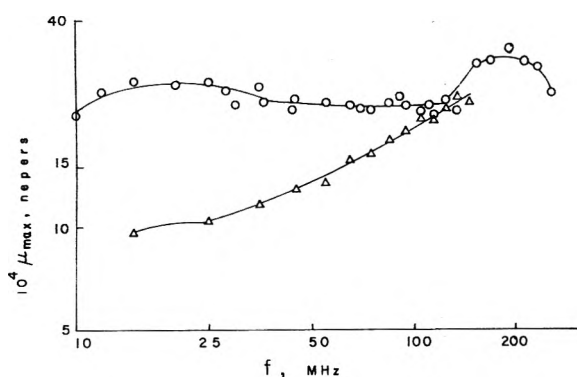

Figure 1. Excess absorbance for 0.096 M ErCl$_3$ in aqueous methanol: (O) $X_{H_2O} = 0.03$; ($\triangle$) $X_{H_2O} = 0.70$.

ed in Table I. The relaxation data can be calculated in two ways. The first way is to assume that only one chemical relaxation process is present within the experimental frequency range, and to include any high-frequency relaxations along with the solvent background. We do not believe this procedure is correct. As in aqueous solutions,[7] a calculated value of B significantly in excess of that characteristic of the solvent system alone is attributed to the presence of at least one additional high-frequency relaxation. We have carried out ultrasonic measurements on different water–methanol solutions in the absence of salts, measuring B to be $(25 \pm 2) \times 10^{-17}$ nepers cm^{-1} sec^2 for these solutions. We have assumed this value to hold for each of our solvent compositions. Early measurements made at a constant frequency for water–methanol solutions have been reported to be independent of water mole fraction,[9] a result which is expected only if no relaxation is present in the vicinity of the frequency measurements and if B is essentially the same for all compositions of aqueous methanol. This was not the case with aqueous ethanol or the higher aqueous alcohol systems,[9] and it was on this basis that aqueous methanol was chosen for our solvent systems. The possibility that the presence of a nonassociating salt changes the solvent structure sufficiently so as to change the value of B was investigated by making ultrasonic measurements on a solution of dilute NaClO$_4$ in the aqueous methanol. There was essentially no variation in the absorption with frequency and the background was approximately 25×10^{-17} nepers cm^{-1} sec^2, consistent with the results in the absence of salt. Therefore, the

effects that are observed must be correlated with a high-frequency relaxation that is present in all of the experimental solutions that were investigated in the mixed solvents. Thus, the data were also calculated in terms of a double relaxation program. This has the effect of decreasing the relaxation frequency of the low-frequency relaxation compared with the calculation assuming only a single relaxation is present. This result is typical of the observations reported under similar conditions in other systems.[7] The reported errors in the high-frequency relaxation are very large, and hence, make it impossible to obtain accurate rate constants for the high-frequency steps. In aqueous systems composed of lanthanide(III) ions and ligands, this high-frequency relaxation is usually attributed to the formation of an outer-sphere complex coupled to the loss of water from the ligand solvation shell. A similar desolvation process occurring in these aqueous alcohol solutions would not be unreasonable.

The amplitude of the low-frequency relaxation provides information about the thermodynamic properties of this reaction, specifically ΔV, the volume change occurring during reaction. Through an analysis of the variation in maximum excess absorbance as a function of water mole fraction, it was demonstrated that the solvation number change occurring upon association for ErNO$_3^{2+}$ was absent for ErCl^{2+}.[2] The variation in experimental relaxation frequency, f_R, for the low-frequency relaxation process was also different for the chloride and nitrate salts. The nitrate value increased from the methanol result, reached a region in which f_R was essentially constant, and then increased as further water was added. The variation of f_R with water mole fraction for constant concentrations of ErCl$_3$ is shown in Figure 2. Here we have plotted the results in terms of the double relaxation data. Although the numerical values of the frequencies are different from that calculated from single relaxation programs, the trends are the same either way. For ErCl$_3$ containing only a low water mole fraction, the relaxation frequency was approximately 18 MHz, a range which would have been expected for the aqueous system if an inner-sphere complex had been formed. However, as additional water was added the relaxation frequency dropped very rapidly to a value around 10 MHz at $X_{H_2O} = 0.07$. Further additions of water, at constant ErCl$_3$ concentrations, resulted in a regular increase in relaxation frequency with mole fraction of water. Because this result was much different than in the nitrate case, we carried out concentration dependence
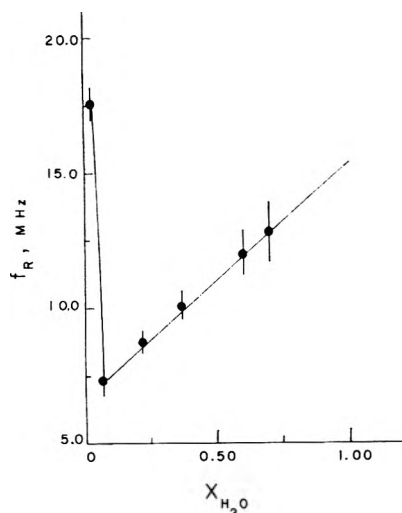
Figure 2. Variation in relaxation frequency with water composition for 0.096 M $ErCl_3$.

studies of the relaxation frequency for two series of $ErCl_3$ solutions, each of which was low in water content. From an analysis of the rate constants at each of the two water compositions we hoped to determine the cause of this unusual behavior.

The relaxation data are tabulated in Tables II and III respectively for solutions consisting of 1.5 and 2.9% water. The per cent water was determined by Karl Fischer titrations, utilizing solutions of methanol with known amounts of water. In a study of lanthanide(III) complexation of murexide in 50% aqueous ethanol solutions, it was demonstrated that the complexation constant was greater than in the water system,[10] and hence, the complex formation constants had to be determined for both water compositions. No complexation constants have been reported for the lanthanide chlorides in methanol solutions, but there have been several for some of the lanthanides in aqueous solutions. Although K_f for $ErCl^{2+}$ has not been reported, one can estimate the result from the value for other lanthanides to a first approximation. For $ErCl^{2+}$ in water, the following results have been obtained: K_f = 0.82 at ionic strength 1.00 and 1 M acid at 25°;[11] K_f = 0.9 at ionic strength 1.00 and 22°;[12] and 0.71 at ionic strength 4.00 in $NaClO_4$ at 25°.[13] Based on all of these results it was anticipated that the complexation constant in the low water content methanol solutions would be somewhat larger than 1.

The analysis of the equilibrium constant was carried out by spectroscopic measurements. Although for most peaks in the visible and uv range, Beer's law was obeyed, there were some peaks where significant deviations from Beer's law were observed. The most sensitive of these appeared to be at 255 nm, and this was utilized to calculate K_f at room temperature, 22°. In other lanthanide ultrasonic studies, it had been demonstrated that at least the complexation rate constant is independent of the choice of K_f,[9,14] and hence a technique was used which gives approximate values for the stability constants.[15]

For a system in which only the one to one complex is formed ($ErCl^{2+}$), and where the extinction coefficients of the free cation and complex are unknown, the value of K_f can be obtained from a plot of ϵ against log $[Cl^-]$ from the point at which either a maximum or minimum slope is obtained. Based on the assumption that free Cl^- does not absorb at 255 nm, the quantity ϵ is given by the absorb-
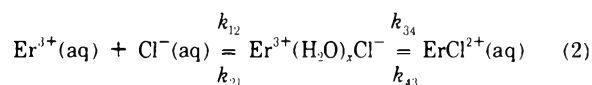
TABLE II: Kinetic Data for the 1.5%
Water $ErCl_3$ Solutions

C, M	$10^{17}A_{III}$[a]	$f_{R_{III}}$, MHz	$10^{17}B$[a]
	A. Single Relaxation Data		
0.0691	182 ± 5	17.9 ± 0.6	35.9 + 0.6
0.0456	158 ± 7	16.0 ± 0.8	33.1 ± 0.6
0.0319	118 ± 7	16.3 ± 0.9	31.8 ± 0.6
0.0223	96.0 ± 5.7	15.8 ± 0.9	31.1 ± 0.5

C, M	$10^{17}A_{III}$[a]	$f_{R_{III}}$, MHz	$10^{17}A_{12}$[a]	$f_{R_{12}}$, MHz
	B. Double Relaxation Data, B = 25 × 10^{-17} nepers cm^{-1} sec^2			
0.0691	190 ± 5	16.2 ± 0.5	15.7 ± 1.1	215 ± 26
0.0456	175 ± 9	13.4 ± 0.8	14.1 ± 1.6	154 ± 22
0.0319	130 ± 8	13.8 ± 1.0	11.0 ± 1.4	177 ± 32
0.0223	110 ± 7	12.7 ± 0.9	10.4 ± 1.0	159 ± 21

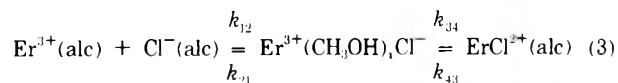[a] Units are nepers cm^{-1} sec^2.

ance at 255 divided by the concentration of $ErCl_3$ divided by the path length. At the point where the slope of the curve is a maximum or minimum, log K_f is equal to $-$log $[Cl^-]$. An iterative calculation was carried out starting with the assumption that the free chloride was three times the concentration of $ErCl_3$ in each solution. When K_f was obtained, an improved value of $[Cl^-]$ was calculated. This process was continued until K_f did not change by more than 1%. For the solutions containing 1.5 and 2.9% water respectively, K_f was equal to 9 and 8. These numbers appear quite reasonable since the amplitude of the ultrasonic absorbance was similar to that observed in the aqueous solutions of the rare earth nitrates, where K_f, obtained by conductivity measurements, varied from about 7 to 17.[9,16]

In the aqueous solutions, the mechanism of rare earth complexation reactions involves at least two steps, corresponding to

$$Er^{3+}(aq) + Cl^-(aq) \underset{k_{21}}{\overset{k_{12}}{=}} Er^{3+}(H_2O)_xCl^- \underset{k_{43}}{\overset{k_{34}}{=}} ErCl^{2+}(aq) \quad (2)$$

Here the $Er^{3+}(H_2O)_xCl^-$ represents a solvent-separated outer-sphere ion pair, which reacts in a slow step corresponding to the low-frequency relaxation to form a solvated inner-sphere complex. The analogous reaction in methanol, consistent with a double relaxation process would be

$$Er^{3+}(alc) + Cl^-(alc) \underset{k_{21}}{\overset{k_{12}}{=}} Er^{3+}(CH_3OH)_xCl^- \underset{k_{43}}{\overset{k_{34}}{=}} ErCl^{2+}(alc) \quad (3)$$

Although we write the structure of the outer-sphere complex with only methanol solvent molecules, in the mixed solvents under investigation there probably is some water in the solvation shell. Since the absorption at 255 nm corresponds to both free Er^{3+} and to complex, the formation constants reported are analogous to those obtained by conductivity measurements in that the concentration of complex will correspond to the sum of the inner- and outer-sphere complexes. If we let K_{12} represent the equilibrium constant for the formation of the outer-sphere complex and K_{III} that for the inner-sphere complex, then

$$K_f = K_{12}(1 + K_{III}) \quad (4)$$

or

$$K_f = [ErCl^{2+}]/[Er^{3+}][Cl^-] \quad (5)$$

These expressions differ from those used in the aqueous

TABLE III: Kinetic Data for the 2.9% Water ErCl₃ Solutions

C, M	$10^{17}A_{III}{}^a$	$f_{R_{III}}$, MHz	$10^{17}B^a$	
	A. Single Relaxation Data			
0.0960	237 ± 6	18.1 ± 0.5	37.3 ± 0.8	
0.0822	252 ± 6	16.3 ± 0.4	35.8 ± 0.5	
0.0571	200 ± 4	15.3 ± 0.3	34.6 ± 0.3	
0.0403	143 ± 5	15.8 ± 0.5	33.1 ± 0.4	

C, M	$10^{17}A_{III}{}^a$	$f_{R_{III}}$, MHz	$10^{17}A_{12}{}^a$	$f_{R_{12}}$, MHz
	B. Double Relaxation Data,			
	$B = 25.0 \times 10^{-17}$ nepers cm^{-1} sec^2			
0.0960	239 ± 6	17.6 ± 0.6	16.3 ± 1.7	413 ± 161
0.0822	257 ± 6	15.7 ± 0.4	12.9 ± 1.1	343 ± 85
0.0571	202 ± 4	14.9 ± 0.3	12.4 ± 0.5	555 ± 145
0.0403	147 ± 5	15.1 ± 0.6	9.5 ± 0.8	355 ± 96

TABLE IV: Equilibrium Data for the ErCl₃ Solutions

C, M	[Er³⁺], M	[ErCl²⁺], M	[Cl⁻], M	$\theta(c)$, M	$\phi(c)$
	A. Solutions with 1.5% Water,				
	$K_f = 9$ ($X_{H_2O} = 0.026$)				
0.0691	0.0277	0.0414	0.166	0.194	0.433
0.0456	0.0225	0.0231	0.114	0.136	0.327
0.0319	0.0183	0.0136	0.0821	0.101	0.263
0.0223	0.0146	0.0077	0.0592	0.0737	0.208
	B. Solutions with 2.9% Water,				
	$K_f = 8$ ($X_{H_2O} = 0.050$)				
0.0960	0.0342	0.0618	0.226	0.260	0.493
0.0822	0.0320	0.0502	0.196	0.228	0.461
0.0571	0.0268	0.0303	0.141	0.168	0.386
0.0403	0.0221	0.0181	0.103	0.125	0.318

nitrate study,[7] because the constants determined by conductivity measurements are in terms of activities of species, whereas the spectrophotometric measurements are in terms of concentrations.

For reaction 3, assuming step 12 is significantly more rapid than III[17]

$$\tau_{12}^{-1} = 2\pi f_{R_{12}} = k_{21} + k_{12}\theta(c) \tag{6}$$

$$\tau_{III}^{-1} = 2\pi f_{R_{III}} = k_{43} + k_{34}\phi(c) \tag{7}$$

where $\theta(c)$ calculated in this case in terms of concentration is[18]
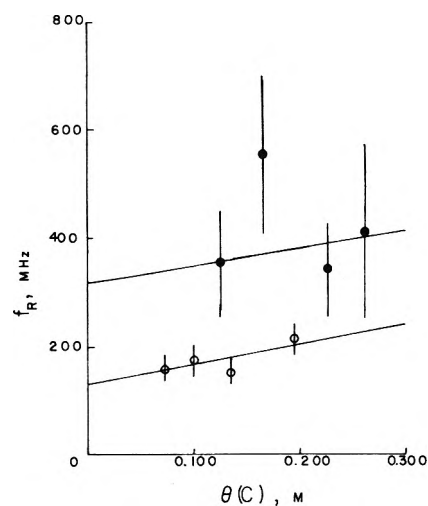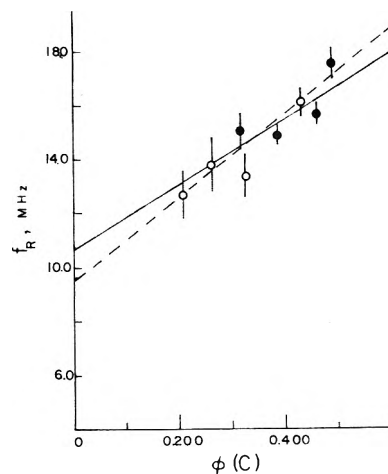
$$\theta(c) = [\text{Er}^{3+}] + [\text{Cl}] \tag{8}$$

and

$$\phi(c) = \theta(c)/(K_{12}^{-1} + \theta(c)) \tag{9}$$

The equilibrium concentrations and the numerical values of $\theta(c)$ and $\phi(c)$ are listed in Table IV. Figure 3 is a plot of the high-frequency relaxation times as a function of $\theta(c)$ for both sets of data and Figure 4 is a similar plot of the relaxation items as a function of $\phi(c)$ for the low-frequency signal.

For the solutions consisting of 1.5% water, the high-frequency data resulted in a calculated k_{12} of $(2.3 \pm 1.2) \times 10^9 \, M^{-1} \, \text{sec}^{-1}$ and k_{21} of $(8.1 \pm 1.7) \times 10^8 \, \text{sec}^{-1}$ with $K_{12} = 2.8$ from this data. Rather than propagate the large errors in the relaxation frequency a new K_{12} was calculated from the more accurate low-frequency data according to a technique developed earlier.[14] The low-frequency data resulted in the following values of the rate constants with $k_{34} = (10 \pm 4) \times 10^7 \, \text{sec}^{-1}$ and $k_{43} = (5.9 \pm 1.1) \times 10^7$

Figure 3. ErCl₃ high-frequency rate data: (O) 1.5% water; (●) 2.9% water.

Figure 4. ErCl₃ low-frequency rate data: (O) 1.5% water; (●) 2.9% water.
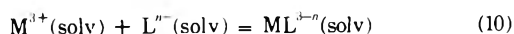
sec^{-1}. The experimental values of the equilibrium constants are $K_{12} = 3.3$ and $K_{III} = 1.8$, in close agreement to the results calculated from the high-frequency data.

For the higher water content solutions containing 2.9% water, k_{12} was equal to $(1.8 \pm 2.8) \times 10^9 \, M^{-1} \, \text{sec}^{-1}$ and k_{21} was $(2.0 \pm 0.6) \times 10^9 \, \text{sec}^{-1}$, with K_{12} calculated to be 0.94. As before a new K_{12} was calculated from the low-frequency data, yielding $k_{34} = (7.7 \pm 4.1) \times 10^7 \, \text{sec}^{-1}$, $k_{43} = (6.7 \pm 1.7) \times 10^7 \, \text{sec}^{-1}$, $K_{12} = 3.7$, and $K_{III} = 1.1$. We believe the calculated K_{12} result based on step III is more accurate because the relaxation data are better defined for the low-frequency relaxations.

For the solutions containing a smaller quantity of water, the complexation rate constant appeared to be somewhat larger than the one with more water. However, this difference is not great, and considering the experimental errors involved in the determination of these rate constants, it may not be a real difference. In a similar manner, the dissociation rate constant is smaller the less water is present in the solution, but this difference is also very small. Because the complex which is present in aqueous solutions of the chloride is predominantly outer sphere, no information is available in water. The reaction between Er(III) and nitrate has been studied, however, and this will provide a means of comparison. In water at

25°, using the ultrasonic relaxation technique, the rate constant k_{34} was determined to be $(6 \pm 1) \times 10^7$ sec^{-1} [9] in close agreement with the chloride results in the aqueous methanol solutions. This agreement may be fortuitous, as the rate-determining step in aqueous solutions is the rate of bond formation between the cation and the ligand.[14]

More conclusive evidence that the complexation rate constant is independent of solvent composition in aqueous alcohol solutions comes from Bear's study of murexide complexation with selected lanthanides in 50% ethanol.[10] Although Er(III) was not studied, the next lanthanide in the series, Ho(III) was. In the aqueous alcohol, Bear found a complexation rate constant at 12° of 1.8×10^7 M^{-1} sec^{-1}, which is slightly greater than Geier's value in water of 1.4×10^7 M^{-1} sec^{-1}.[19] The major differences in the 50% ethanol study occur in the dissociation rate constant where the rate was a factor of 5 slower in the alcoholic solution. Because the murexide results, measured by temperature jump, measure a rate constant corresponding to a modification of reaction 3 given by

$$M^{3+}(\text{solv}) + L^{n-}(\text{solv}) = ML^{3-n}(\text{solv}) \qquad (10)$$

the numerical results cannot be directly compared. However, the trends in this study are in agreement with the trends reported in 50% ethanol. Based on these observations, it appears that the complexation rate constant for lanthanide complexation is approximately the same in aqueous or aqueous alcohol solutions. Because the complexation rate constant from reaction 10, k_f, is related to the k_{34} results in this study by

$$k_f = K_{12}k_{34} \qquad (11)$$

and since k_f was the same in both solvents, this requires that K_{12} be independent of whether alcohol is present in the solution. Both water composition series resulted in essentially the same value of K_{12} between 3.3 and 3.7. Although K_{12} was not determined for ErNO$_3{}^{2+}$, the corresponding NdNO$_3{}^{2+}$ complex had K_{12} equal to 2.9,[7] in reasonable agreement with the chloride results. This observation that a solvent change does not influence the outer-sphere ion pair formation constant, K_{12}, is not unique to lanthanide systems. In the study of the association of Mn(II) with sulfate, Atkinson and Kor observed that essentially no difference was obtained in the outer-sphere association constants and rate constants when the solvent was shifted from water to aqueous dioxane to aqueous methanol, with the major kinetic differences occurring in the step III parameters.[20]

Thus, the major difference in the mechanism of ErCl^{2+} complexation in water and aqueous methanol is the increased stability of inner-sphere complex as the methanol composition increases. Because methanol has a much lower dielectric constant than water, this effect is not unexpected. We have been unable to carry out these measurements in absolute alcohol, where no water molecules can be in the cation solvation shell. In aqueous solutions, the slow step was found to be the bond formation between the lanthanide and the ligand rather than the cation–sol-

vent exchange process.[14,21] In the presence of only a small mole fraction of water, the same complexation rate constant is expected if the cation–ligand bond formation remains the slow step. Thus, our measurements require that the lanthanide(III)–methanol solvent exchange rate be more rapid than this bond formation rate or that sufficient water is present in the cation solvation shell to allow bond formation in positions vacated by water molecules.

A possible explanation for the high value of the relaxation frequency observed as the water content approaches the lower limit is that in a solvent of low dielectric constant significant concentrations of the bischloride complex, ErCl$_2{}^+$, are present. In aqueous solutions of dysprosium acetate it had been demonstrated that the kinetic effect of forming the 1:2 complex was an increase in observed relaxation time.[22] As water is added, the concentration of bis complex decreases toward zero, with a resulting rapid decrease in relaxation time.

This study has demonstrated that the spectroscopic observations of Freed are indeed caused by the presence of significantly different environments surrounding rare earth nitrate and chloride salts in water and in aqueous and anhydrous alcohols. The extension of this work to other rare earth systems is in order to determine which lanthanides possess the solvation number change in mixed solvents.

References and Notes

(1) Part I: J. Reidler and H. B. Silber, *J. Inorg. Nucl. Chem.*, **36**, 175 (1974).
(2) Part II: J. Reidler and H. B. Silber, *J. Chem. Soc., Chem. Commun.*, 354 (1973).
(3) S. Freed, *et al., J. Chem. Phys.*, **6**, 297, 654, 655 (1938).
(4) S. Freed and S. I. Weissman, *Phys. Rev.*, **60**, 440 (1941).
(5) S. Freed, *Rev. Mod. Phys.*, **14**, 105 (1942).
(6) E. V. Sayre, D. G. Miller, and S. Freed, *J. Chem. Phys.*, **26**, 109 (1957).
(7) H. B. Silber, N. Scheinin, G. Atkinson, and J. J. Grecsek, *J. Chem. Soc., Faraday Trans. 1*, **68**, 1200 (1972).
(8) H. B. Silber, *J. Chem. Educ.*, **50**, 720 (1973).
(9) L. R. O. Storey, *Proc. Phys. Soc., Ser. B*, **65**, 943 (1952); C. J. Burton, *J. Acoust. Soc. Amer.*, **20**, 186 (1948).
(10) J. L. Bear and C. T. Lin, *J. Inorg. Nucl. Chem.*, **34**, 2368 (1972).
(11) G. R. Choppin and P. J. Unrein, *J. Inorg. Nucl. Chem.*, **25**, 387 (1963).
(12) D. F. Peppard, G. W. Mason, and I. Hucher, *J. Inorg. Nucl. Chem.*, **24**, 881 (1962).
(13) T. Sekine, *Acta Chem. Scand.*, **19**, 1435 (1965).
(14) J. Reidler and H. B. Silber, *J. Phys. Chem.*, **77**, 1275 (1973).
(15) F. J. C. Rossotti and H. Rossotti, "The Determination of Stability Constants," McGraw-Hill, New York, N. Y., 1961, p 276.
(16) R. Garnsey and D. W. Ebdon, *J. Amer. Chem. Soc.*, **91**, 50 (1969).
(17) K. Tamm, "Dispersion and Absorption of Sound by Molecular Processes," D. Sette, Ed., Academic Press, New York, N. Y., 1963, pp 175–222.
(18) R. A. Robinson and R. H. Stokes, "Electrolyte Solutions," 2nd ed, Butterworths, London, 1959, pp 161–163, 468.
(19) G. Geier, *Ber. Bunsenges. Phys. Chem.*, **69**, 617 (1965).
(20) G. Atkinson and S. K. Kor, *J. Phys. Chem.*, **69**, 128 (1965).
(21) H. B. Silber, *J. Chem. Soc., Chem. Commun.*, 731 (1971).
(22) M. Doyle and H. B. Silber, *J. Chem. Soc., Chem. Commun.*, 1067 (1972).

A Calorimetric and Spectrophotometric Comparison of Adducts of Phenol and Deuteriophenol

John W. Boettcher and Russell S. Drago*

The William A. Noyes Laboratory, University of Illinois, Urbana, Illinois 61801 (Received June 13, 1973)

The literature is filled with conflicting reports on the effect of deuteration upon the thermodynamic data describing the hydrogen bonding interaction. In earlier work in this laboratory involving a spectral and thermodynamic study of the hydrogen bonding of chloroform, it became necessary to employ $CDCl_3$ in the infrared work. Accordingly, it became necessary to resolve the questions concerning the effects of deuteration. Calorimetrically measured enthalpies of the hydrogen bonding interaction of C_6H_5OH and C_6H_5OD with acetone and quinuclidine showed no detectable difference in the enthalpies of adduct formation of a given donor with either acid. An infrared analysis of the shift in the OH and OD vibrations upon hydrogen bonding leads us to conclude that no difference is to be expected in the enthalpy of adduct formation for interactions in the range from 0 to 10 kcal mol^{-1}.

Introduction

Hydrogen bonding is one of the more completely studied and understood type of specific intermolecular interaction. A successful potential function describing this interaction has been proposed originally by Lippincott and Schroeder[1] and refined by Reid.[2] One of the still unresolved questions in this area involves the effect of deuteration on the bond strength, bond length, infrared force constant, and Lewis acid strength.

Ubbelohde[3] observed that the substitution of deuterium for hydrogen in oxalic acid dihydrate brought about a significant increase in the unit cell parameters. He concluded that this increase was due to the bond lengthening of R_{A-B} (in fragment A-H-B) by as much as 0.04 Å. Since that time, many other systems have been found which display the same behavior. These are nicely summarized by Hamilton.[4] To complement this data, there is also good evidence that this lengthening is also operative in the gaseous state.[5] On the basis of this structural data, it would seem that deuterium substitution weakens and lengthens the hydrogen bond.

In order to determine the consequences of this weakening, various workers have studied the thermodynamics of deuterium bonding in dilute solution. The first of these studies was reported by using fluorine nuclear magnetic resonance. The enthalpy of H bonding of fluoroform and fluoroform-d to tetrahydrofuran was determined.[6] The deuterated acid gave the larger enthalpy, 4.95 kcal mol^{-1} compared to 4.77 kcal mol^{-1} for the protium isotope. The equilibrium constants fell in the same order also. The differences were concluded to be significant.

A few years later Bellon[7] published the results of a systematic study of chloroform and chloroform-d interacting with a variety of Lewis bases. Although reporting no raw data, he claims no difference in the enthalpies of H bonding or in the equilibrium constants for the protium and deuterium isotope.

Another study with quite different results is that of Singh and Rao.[8] Using infrared spectroscopy they determined the enthalpies and equilibrium constants for phenol and phenol-d interacting with various bases. Their results confirm the expected weakening of the H bond upon deuteration with startling differences between the corre-

sponding enthalpies for the two isotopes. In all cases the enthalpies of adduct formation of the protium isotope are *at least* three times *greater* than that of the deuterium isotope. They also report no linear relationship between the infrared frequency shift $\Delta\nu_{OD}$ and the enthalpies of formation of the deuterium adducts. Also in contrast to R_{AO}, comparable enthalpies for phenol-h and phenol-d have been reported from spectroscopic studies.[9] In view of the described difficulties[10] that are associated with the procedures for obtaining and calculating thermodynamic data from spectroscopic studies, the conflicting reports are not surprising.

At the start of the present work, this laboratory had just confirmed the nonexistence of a linear relationship between the enthalpy and the infrared frequency shift for the weak hydrogen bonding acid, chloroform.[10] Because of the interfering C-H vibrations of the bases used, the values of $\Delta\nu_{CH}$ could not be determined. Instead, the frequency shifts of the deuterated acid were used. We thus became interested in the effect of deuteration on the adduct frequency shifts and thermodynamic data.

The purpose of this research was to determine by using a calorimetric procedure if there is any difference in the measured enthalpies of adduct formation between phenol-h and phenol-d with a given base. The bases acetone and quinuclidine were chosen for this research for two reasons. First, there is a large difference in the strength of these two bases toward phenol increasing the generality of the conclusions. Secondly, it is for acetone that the reported[8] enthalpies of adduct formation for the two isotopes differ the most.

An infrared study of the O-D stretching region of the infrared spectrum was also made to compare with the OH stretching vibration. The relative values of the corresponding frequency shifts should provide information as to the change in the potential function for proton motion with isotopic substitution. Comparisons of this type in various neat liquids have been reported.[11,12]

Experimental Section

A. Preparation and Purification of Materials. The Lewis bases used in this study were purified and dried as previously reported.[10,13]

TABLE I: Enthalpies of Adduct Formation (kcal mol^{-1})

| | | Acid | |
| | | Mixture[c] | |
Base	C$_6$H$_5$OH	Assuming pure C$_6$H$_5$OD	Assuming pure C$_6$H$_5$OH
Acetone	4.9 ± 0.1[a]	5.1 ± 0.1	5.0 ± 0.1
Quinuclidine	9.1 ± 0.2[b]	9.4 ± 0.2	9.3 ± 0.2

[a] Reference 15. [b] Reference 13. [c] The molecular ratio of phenol-d/phenol-h is 3.8 for the acetone study and 1.5 for quinuclidine.

The solvents used, cyclohexane and carbon tetrachloride, were dried by allowing them to stand over Linde 4A molecular sieves for at least 1 week prior to use.

The partially deuterated phenol samples were prepared by slightly modifying a literature procedure[14] for the preparation of deuterated thiophenol. A slurry of 2.8 g (0.1+ mol) of sodium hydride in 50 ml of anhydrous ether was prepared. To this was added drop-wise a solution of 9.4 g (0.1 mol) of phenol in 50 ml of anhydrous ether. Upon completion of this addition and cessation of hydrogen evolution, 8.0 ml of 99.5% D$_2$O was slowly added and the mixture was stirred for 1 to 2 hr. Carbon dioxide was then bubbled into this mixture at a moderate rate for approximately 0.5 hr. The solution was then filtered to remove the precipitate, and the filtrate was dried over anhydrous sodium sulfate. The solvent was removed through use of a rotary evaporator. The phenol was then purified by two vacuum sublimations.

The molecular ratio of phenol-d to phenol-h was determined by mass spectroscopy of the purified samples. This ratio is simply the ratio of the intensity of the peak occurring at mass number 95, minus the natural abundance of phenol-h, ^{13}C, to the intensity of the peak occurring at mass number 94. The average of several runs determine the reported values.

B. *Infrared Spectroscopy.* The infrared spectra were obtained on a Beckman IR-7 grating spectrometer. The region from 2000 to 2800 cm^{-1} was scanned at a rate of 40 cm^{-1}/min with a spectral slit width of 4 cm^{-1} at 2000 cm^{-1}. The wave number calibration of the instrument was checked using polystyrene film.

A stock solution was diluted to give a free phenol-d O–D stretching absorption of approximately 30% transmittance in the 0.5-mm sodium chloride solution cells used in this experiment. Numerous concentrations of each base were employed and checked for absorption in this region.

C. *Calorimetry.* The calorimeter used in this study has been described previously.[10]

The H'''s obtained from the calorimeter are corrected for the heat of dilution of the same phenol stock solution in pure solvent. These H'_{corr} along with concentrations of acid and base, and the total volume of solution were used as input to a computer program which simultaneously determines both ΔH and K.[9]

There is some uncertainty as to the exact phenol concentration due to it being an isotopic mixture. To place boundaries on the enthalpy and equilibrium constant, the data from both systems studied were treated using two different sets of acid concentrations. The first assumes pure phenol-h (mol wt = 94.11), and the second assumes pure phenol-d (mol wt = 95.12). The differences between the two enthalpies is, as one might expect and is shown in Table I, negligible.

Results

The ΔH's and K's along with the raw data obtained for the phenol-d,h mixture interacting with acetone and quinuclidine are presented in the microfilm edition along with the Rose–Drago plots[15] which provide the reader with an indication of the precision of the experiments (Table II and III and Figure 1 and 2). See paragraph at end of paper regarding supplementary material. The thermodynamic data are summarized in Table IV.

The free, or uncomplexed, O–D stretching band of deuteriophenol is a prominent peak in the spectrum at 2667 cm^{-1}. A listing of the $\Delta\nu_{OD}$'s and the corresponding $\Delta\nu_{OH}$'s is given in Table IV.

Discussion

In Figure 3 is shown a plot of $\Delta\nu_{OH}$ vs. $\Delta\nu_{OD}$. The equation of the least-squares line, shown by the dotted line in this figure, is $\Delta\nu_{OH} = 1.45\Delta\nu_{OD} + 3.3$. This linear relationship is interesting. The error limits on the slope of this line, 1.45 ± 0.12 (90% confidence level), make it, within experimental error, equivalent to a line with slope equal to 1.414 and zero intercept. This is the equation of the bold, solid line shown in Figure 3. The slope of 1.414 is what one would expect if no change in the force constant governing the motion of the proton occurs upon its replacement with a deuteron. The ratio of the two vibrational frequencies would simply be the inverse of the square root of the ratio of the mass of hydrogen to deuterium. Thus it would seem that the change in the infrared spectrum of H-bonded phenol in these adducts that occurs upon deuteration can be explained quite simply on the basis of their mass differences alone. It is not necessary to invoke a change in the force constant governing the proton's motion. Since the shape of this potential has not changed upon isotopic substitution, it seems unreasonable that the overall energetics of H-bond formation will change upon isotopic substitution. Thus the infrared evidence would seem to predict that there should be no difference in the enthalpies of formation of the corresponding adducts of phenol-h and phenol-d.

The value of $\Delta H = -4.99$ kcal/mol obtained for the phenol-d,h mixture interacting with acetone is in excellent agreement with the value obtained by Epley for pure phenol-h of -4.94. This same value is also in fair agreement with Rao's value of -4.5 for the undeuterated species. However, the -0.8 reported by Singh and Rao[8] for the enthalpy of interaction of deuteriophenol with acetone is in considerable disagreement with our result.

There is some reason to place doubt on all the enthalpies for phenol-d adduct formation given by Rao. First of all, in the description of the experiment given by Rao, he states that both phenol and deuteriophenol were present in solution and competing for the available base. The algebra necessary to treat this situation of competing equilibrium is complicated, and the interdependence of K_H, K_D, ΔH_H, and ΔH_D cannot but result in large uncertainties being placed on their calculated values. This is disregarding the errors any simplifying assumptions would make.

Secondly, a method of curve resolution was used to determine the intensity of the band due to uncomplexed phenol-d. The overlapping peak is due to the analogous O–D stretching band in the complex. Although a listing of Rao's values of enthalpies for phenol-h agree quite well with those obtained by calorimetry, one must remember that $\Delta\nu_{OD}$ is smaller than $\Delta\nu_{OH}$ and, for bands with simi-

TABLE IV:

Base	ν_{OD}, cm^{-1}	ν_{ODH}, cm^{-1}	$\Delta\nu_{OD}$, cm^{-1}	$\Delta\nu_{OH}$, cm^{-1}
1. Benzene	2667	2633	34 ± 2	50 ± 5[b]
2. Acetonitrile	2667	2555	112 ± 3	150 ± 5[a]
3. Acetone	2667	2509	158 ± 5	240 ± 20[a]
4. Tetrahydrothiophene	2667	2487	180 ± 5	274 ± 5[a]
5. N,N-Dimethylacetamide	2667	2440	227 ± 10	345 ± 5[b]
6. Pyridine	2667	2317	350 ± 10	500 ± 20[a]

[a] See ref 16. [b] See ref 17.
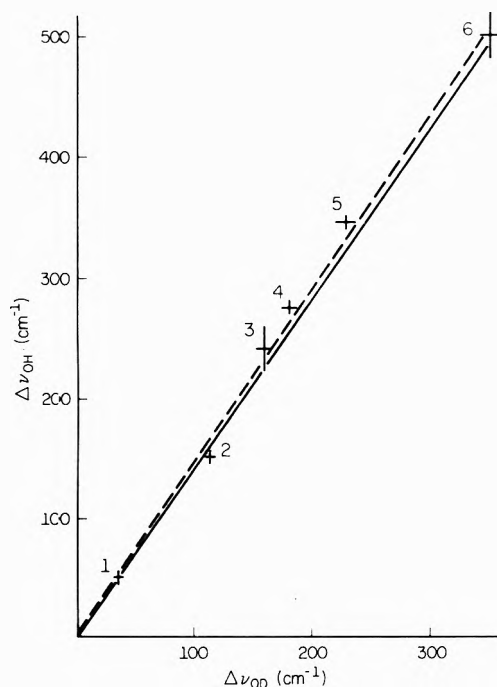
Figure 3. Plot of hydrogen bonding frequency shift, $\Delta\nu_{OH}$, vs. deuterium bonding frequency shift, $\Delta\nu_{OD}$, for the bases in Table IV. Dotted line is least-squares fit. Bold line is the theoretically expected line.

lar half-widths, the overlap in his study of deuterated phenol will be more serious. Thus this method may give numbers with large errors.

The enthalpy of interaction of the phenol-d,h mixture with quinuclidine, $\Delta H = 9.28$, is in good agreement with the calorimetric value[13] of -9.05 for the phenol-h adduct. The fact that the two enthalpies of formation obtained in this study for partially deuterated phenol samples agree so closely with those obtained for pure phenol-h seems to bear out our earlier prediction of this fact based on the infrared evidence. This agreement is also consistent with the X-ray diffraction data. The isotope effect on the R_{AB} distance as measured using X-ray crystallography is significant only for those systems which R_{AB} is less than 2.5 Å. Using Lippincott's model[1] and his reported correlation of R_{AB} with H-bond strength, a R_{AB} distance of 2.5 Å would imply a H-bond strength of 14 kcal/mol. If the enthalpies obtained in solution in this study can be used in conjunction with the diffraction data obtained in the solid state, no isotope effect and hence no difference in enthalpies of formation of the corresponding isotopic adducts should be expected in this study and in the study of

Singh and Rao. Although our results conclusively show no difference (within our error limits) for interactions as large as 9.0 kcal/mol, this does not eliminate the possibility that for stronger interactions (>14 kcal/mol) differences in the enthalpies of the two isotopes could be observed. These results are not of the accuracy reported for an earlier study[6] of CHF$_3$ and CDF$_3$ which claimed to distinguish differences in the strength of interaction. A recalculation of their[6] data, however, indicates the authors have grossly overestimated their precision. Errors of the order of magnitude of 20% in their equilibrium constants (at 90% confidence) result.

Supplementary Material Available. Tables II and III and Figures 1 and 2 will appear following these pages in the microfilm edition of this volume of the journal. Photocopies of the supplementary material from this paper only or microfiche (105 × 148 mm, 24× reduction, negatives) containing all of the supplementary material for the papers in this issue may be obtained from the Journals Department, American Chemical Society, 1155 16th St., N.W., Washington, D. C. 20036. Remit check or money order for $3.00 for photocopy or $2.00 for microfiche, referring to code number JPC-74-429.

References and Notes

(1) E. L. Lippincott and R. Schroeder, *J. Chem. Phys.*, **23**, 1099 (1955).
(2) C. Reid, *J. Chem. Phys.*, **30**, 182 (1958).
(3) A. R. Ubbelohde and J. M. Robertson. *Proc. Roy. Soc.. Ser. A*, **170**, 222 (1939).
(4) W. C. Hamilton and J. A. Ibers, "Hydrogen Bonding in Solids," W. A. Benjamin, New York, N. Y., 1968.
(5) C. C. Costain and G. P. Srivastava, *J. Chem. Phys.*, **41**, 1620 (1964).
(6) C. J. Creswell and A. L. Allred, *J. Amer. Chem. Soc.*, **84**, 3966 (1962).
(7) L. Bellon and J. L. Abbuud, *C. R. Acad. Sci.*, **261**, 3106 (1965).
(8) S. Singh and C. N. R. Rao, *Can. J. Chem.*, **44**, 2611 (1966).
(9) (a) S. N. Vinogradov and R. H. Linnell, "Hydrogen Bonding," Van Nostrand-Reinhold, New York, N. Y., 1971, p 225; (b) D. Plourde, Ph.D. Thesis, University of Wisconsin, 1969.
(10) R. S. Drago, F. L. Slejko, and D. Brown, *J. Amer. Chem. Soc.*, **94**, 9120 (1972).
(11) M. T. Forel, *et al.*, *J. Chim. Phys.*, 1103 (1960).
(12) P. V. Huong, *et al.*, *C. R. Acad. Sci.*, **266**, 172 (1968), and references therein.
(13) F. L. Slejko and R. S. Drago, *Inorg. Chem.*, **12**, 176 (1973).
(14) D. Plant, D. S., Tarbell, and C. Whiteman, *J. Amer. Chem. Soc.*, **77**, 1572 (1955).
(15) T. D. Epley and R. S. Drago, *J. Amer. Chem. Soc.*, **89**, 5770 (1967).
(16) G. C. Vogel and R. S. Drago, *J. Amer. Chem. Soc.*, **92**, 5347 (1970).
(17) R. S. Drago, G. C. Vogel, and T. E. Needham, *J. Amer. Chem. Soc.*, **93**, 6014 (1971).

Complexes of Hydrogen Chloride with Ethers in Carbon Tetrachloride and Heptane. Effects of Induction on the Basicity of Ethers

Sherril D. Christian* and Basil M. Keenan

The University of Oklahoma, Norman, Oklahoma 73069 (*Received June 4, 1973; Revised Manuscript Received October 15, 1973*)

Publication costs assisted by the Petroleum Research Fund

Thermodynamic constants for formation of ether–HCl adducts have been calculated from vapor-pressure data for mixtures of ethers and HCl in the solvents heptane and carbon tetrachloride. Equilibrium constants and enthalpies are reported for the formation of 1:1 and 1:2 ether–HCl adducts; it is suggested that in the 1:2 complex both HCl molecules are attached to the ether oxygen. The stability of the 1:2 complexes is discussed in relation to the effect of induction on the basicity of the nonbonded electrons of the ether oxygen.

Introduction

In spite of the fact that hydrogen chloride is a relatively simple molecule, which may be expected to function primarily as a proton donor in hydrogen-bonding interactions, relatively little is known about specific complexes between HCl and organic oxygen bases. There have been several reports of solid complexes of HCl with ethers, ketones, and alcohols.[1-4] In addition, evidence for formation of complexes between HCl and various electron donors in organic solutions is provided by calorimetric,[3,4] infrared[5] and Raman[6] spectral, and vapor pressure[7] data, although formation constants are generally lacking. Vapor density,[8,9] infrared,[8] and proton magnetic resonance[10] results have yielded thermodynamic constants for 1:1 complexes of HCl with acetone and methyl ether in the gas phase. An infrared study of $H_2O \cdot HCl$ in a nitrogen matrix at 15°K has recently been reported.[11]

The present report provides thermodynamic information about the 1:1 HCl–*n*-butyl ether complex in CCl_4, inferred from partition and solubility measurements. In addition, related thermodynamic results for several HCl–ether complexes have been obtained from vapor pressure data reported previously.[12]

Experimental Section

Aqueous solutions of hydrochloric acid (10.35 and 12.35 *M*) were allowed to equilibrate with solutions of *n*-butyl ether (Bu_2O) in CCl_4 (0–0.30 *M*). Ordinary beverage bottles, covered with a layer of Saran Wrap and bottled with a hand-operated bottle-capper, served as air-tight equilibrator vessels. Each bottle contained 50 ml of Bu_2O in CCl_4 and 100 ml of aqueous HCl; the systems were brought to equilibrium by intermittent shaking for at least 4 hr in a constant temperature bath. Samples of the organic phase were withdrawn using a calibrated 5-ml Hamilton syringe with an 8-in. needle. To prevent contamination of the CCl_4 solutions during sampling (by droplets of the aqueous phase) the pipet needle was inserted through a sealed disposable pipet resting on the bottom of the bottle. The tip of the pipet could be broken by applying moderate downward pressure on the syringe, permitting removal of organic phase samples uncontaminated by the aqueous phase. To find out if water is extracted from the concentrated aqueous HCl solutions into CCl_4, Karl Fischer titrations were performed with the

Beckman KF-3 aquameter. The analytical concentration of water in the CCl_4 solutions (~0.0005 *M*) was not detectably greater than that in CCl_4 which had been dried as completely as possible. (This contradicts the observation by Mitamura, *et al.*,[13] that the solubility of water in CCl_4 equilibrated with aqueous HCl remains constant at about 0.004 *M* at HCl concentrations in CCl_4 greater than 0.05 *M*.) To check the possibility that some of the Bu_2O might transfer from CCl_4 into the aqueous HCl solutions, the absorbance of the CH-stretching band of the ether in the organic phase was measured before and after equilibration, using a Beckman IR-10 spectrophotometer; no observable loss of Bu_2O from the CCl_4 phase occurred to within the sensitivity of the instrument (about 1% in absorbance). To determine whether or not HCl is lost by reaction with the soft glass containers, HCl titrations were performed on samples equilibrated for only 4 hr and on samples left in the bath for 10 days. Total HCl concentrations in these samples agreed to within experimental error with those determined for samples which had been equilibrated overnight.

Results and Discussion

Figure 1 shows partition/solubility results, plotted as formal concentration of HCl in CCl_4 (f_A) against formal concentration of ether in CCl_4 (f_E). Aqueous HCl molarities were fixed at 10.35 and 12.35 *M*, respectively, in the sets of measurements shown in the figure.

The linearity of the plots of f_A vs. f_E suggests that it is reasonable to fit the data in terms of the formation of a 1:1 complex between HCl and Bu_2O. Assuming that the HCl, ether, and complex molecules individually obey Henry's law in the CCl_4 phase and that the excess solubility of HCl in the presence of the ether owes solely to the formation of $Bu_2O \cdot HCl$, equations may be derived for calculating the formation constant (K_{11}) for the reaction HCl + Bu_2O = $Bu_2O \cdot HCl$. The solid curves in the figure have been calculated by fitting data at each temperature to the relation

$$f_A = C_A + \frac{f_E K_{11} C_A}{1 + K_{11} C_A} \tag{1}$$

using both K_{11} and C_A as least-squares parameters and assuming that all the experimental error resides in the f_A values.[14] The constant C_A at each temperature represents
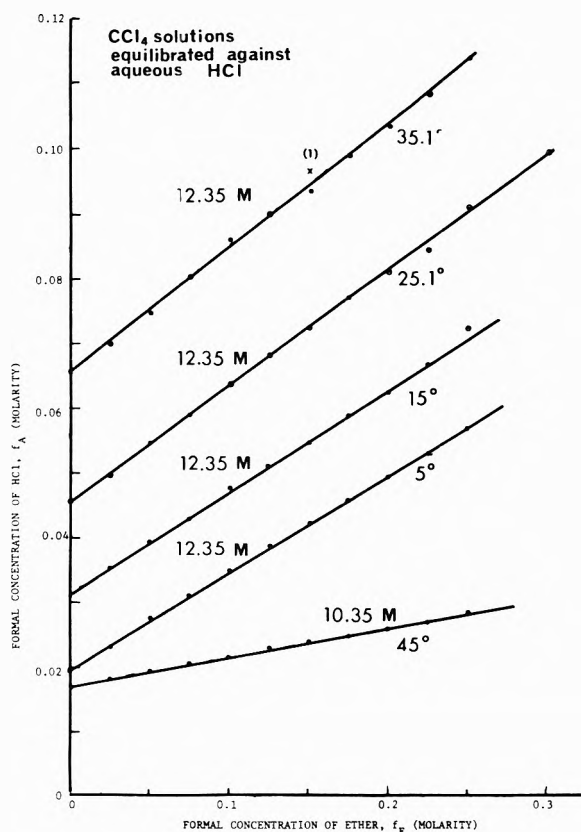
Figure 1. Distribution data for HCl(aq)/dibutyl ether (CCl_4) system; points represent HCl molarities in CCl_4 at given ether molarities. The diameter of each circle indicates the range of three to five values of HCl molarity determined for the same solution, except for the point marked (1), which represents a single measurement. Lines are calculated from least-squares constants.

the solubility of monomeric HCl in pure CCl_4 at a fixed molarity of HCl in the aqueous phase. Values of C_A in equilibrium with 12.35 M aqueous HCl are 0.0197 M at 5.0°; 0.0310 M at 15.0°; 0.0457 M at 25.1°; 0.0657 M at 35.1°. At 45.0°, C_A = 0.0171 M in equilibrium with 10.35 M aqueous HCl. Both K_{11} and C_A vary with temperature as predicted by the van't Hoff relation.[15] Table I lists thermodynamic constants derived for the complex formation reaction in CCl_4. To supplement information about the solubility of HCl and CCl_4 gained from fitting data to eq 1, values of C_A were determined at other temperatures, using pure CCl_4 equilibrated with 10.35 M aqueous HCl. Calculated enthalpies for the transfer of HCl from 10.35 and 12.35 M aqueous solution to the ideal dilute solution in CCl_4 are −7.94 ± 0.20 and −7.82 ± 0.46 kcal/mol, respectively.

Strohmeier and Echte[12] have reported partial pressure-concentration data for HCl above pure n-heptane and solutions of various monobasic ethers in n-heptane (1:20 mole ratio) at temperatures ranging from 200 to 273°K. From the values of limiting Henry's law constants of HCl in the ether solutions, the order of basicity of the ethers was inferred and compared with estimates of basicity obtained from other vapor-pressure, partition, and infrared spectral results. However, we thought it would be worthwhile to attempt to calculate thermodynamic constants for the association of HCl with ethers from the extensive data of Strohmeier and Echte by using the method of analysis described above. In interpreting these results, it is necessary to assume that an adduct involving more

TABLE I: Thermodynamic Constants for Formation of Dibutyl Ether·HCl in Carbon Tetrachloride[a]

Temp, °K	K_{11}, M^{-1}	$\Delta H_{11}°$, kcal/mol
278.15	8.69 ± 0.07	
288.20	6.09 ± 0.09	
298.25	4.80 ± 0.05	−5.2 ± 0.2
308.25	3.61 ± 0.05	
318.15	2.71 ± 0.03	

[a] Standard states 1 M ideal dilute solution.

than one HCl molecule exists along with the 1:1 complex. Data can be correlated adequately by assuming that both 1:1 and 1:2 ether–HCl complexes exist in solution along with the monomers. The method of fitting Strohmeier and Echte's data is described in the Appendix. Table II summarizes equilibrium constants calculated for the complex formation reactions at several temperatures, for comparison with the results of the present study.

Table III lists ΔH_{11} values for a number of ether–proton donor complexes of HCl, phenol, and isothiocyanic acid in CCl_4, n-heptane, and the gas phase. Several generalizations may be drawn from the comparative enthalpy values: (1) HCl is a somewhat better proton donor than phenol, but a poorer donor than HNCS; (2) the effect of the solvent is to reduce $-\Delta H_{11}$ from the gas-phase value (CCl_4 is apparently somewhat more effective than n-heptane in opposing complex formation); and (3) the order of basicity of the ethers (as indicated by the progression of $-\Delta H_{11}$ values) is essentially that deduced from previous studies of ether complexes. Similar conclusions are reached by considering K_{11} or $-\Delta S_{11}°$ values for the same complexes. The effect of nonpolar solvents in decreasing $-\Delta H_{11}$ is similar to that noted for numerous hydrogen-bonding reactions, but more data will be needed to elucidate the effects of solvation on the individual monomeric and complex species. The energy of solvation of the 1:1 ether–HCl complexes is somewhat less (in magnitude) than the sum of solvation energies of the separate donor and acceptor molecules. We estimate that the solvation fraction, α, is about 0.9 for the $Bu_2O·HCl$ complex.[16]

The necessity of including K_{12} in the treatment of Strohmeier and Echte's results opens the question of the validity of assuming that only the 1:1 ether–HCl complex is present under the conditions of the present study. Given that K_{11} = 11.33 M^{-1} and K_{12} = 6.73 M^{-1} for the Bu_2O–HCl–n-heptane system at 0°, and assuming that the corresponding constants for the Bu_2O–HCl–CCl_4 system at 5° are no greater in magnitude, it is possible to estimate that the ratio of the concentration of the 1:2 complex to that of the 1:1 complex is only about 0.001 at the relatively low activity of HCl employed in the present experiments.

By considering the relative magnitudes of thermodynamic constants for the ether–HCl complexes, it is possible to suggest a plausible geometry for the 1:2 adduct. The 1:1 complex very likely involves a linear O···H–Cl hydrogen bond; however, the 1:2 complex could conceivably form either by attachment of a second HCl proton at the non-bonded lone-pair of the ether

$$\begin{array}{c} \diagdown \\ \diagup \end{array} O \cdots \begin{array}{c} \cdots HCl \\ \cdots HCl \end{array}$$

I
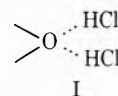
or by bonding of the second HCl to the Cl of the 1:1 complex

TABLE II: Calculated Equilibrium Constants for Systems Ether–HCl–n-Heptane[a]

| Ether		200.8	209.6	220.3	230.8	241.6	258.4	272.9
					Temp, °C			
Tetrahydrofuran	K_{11}	3,150 ± 290	1,031 ± 80	675 ± 47	295 ± 9	152.4 ± 2.8	68.9 ± 0.9	34.3 ± 0.4
	K_{12}	56,200 ± 14,200	20,200 ± 3780	7140 ± 1060	1620 ± 130	394 ± 23	114.1 ± 5.2	42.6 ± 1.9
Tetrahydropyran	K_{11}	1,973 ± 123	607 ± 58	322 ± 16	187 ± 7.4	100.8 ± 2.4	49.3 ± 0.7	25.7 ± 0.3
	K_{12}	19,500 ± 3800	5,580 ± 1480	1980 ± 260	535 ± 69	245 ± 17	59.3 ± 3.5	27.6 ± 1.0
Diethyl ether	K_{11}	975 ± 33	517 ± 27	231 ± 4	122 ± 2	65.6 ± 1.7	32.0 ± 0.4	16.5 ± 0.2
	K_{12}	5,590 ± 600	1,640 ± 200	598 ± 38	236 ± 14	135 ± 10	31.1 ± 1.8	15.3 ± 0.7
Dipropyl ether[b]	K_{11}	516 ± 20	256.1 ± 6.6	136.5 ± 3.4	77.0 ± 0.9	41.6 ± 0.3	19.88 ± 0.30	11.36 ± 0.09
	K_{12}	2,210 ± 280	893 ± 72	364 ± 27	138.6 ± 5.1	51.2 ± 1.2	21.0 ± 1.1	7.17 ± 0.26
Dibutyl ether[b]	K_{11}	516 ± 20	256.1 ± 6.6	136.5 ± 3.4	77.0 ± 0.9	41.6 ± 0.3	19.86 ± 0.30	11.33 ± 0.09
	K_{12}	2,190 ± 280	884 ± 71	358 ± 21	135 ± 5	49.6 ± 1.2	20.3 ± 1.1	6.73 ± 0.26
Dibenzyl ether	K_{11}						7.23 ± 0.20	4.22 ± 0.05
	K_{12}						8.11 ± 0.80	3.22 ± 0.16
β,β'-Dichlorodiethyl ether	K_{11}						1.87 ± 0.19	1.175 ± 0.046
	K_{12}						2.79 ± 0.73	1.18 ± 0.15
Anisole	K_{11}		5.94 ± 0.17	4.08 ± 0.05		1.95 ± 0.01	1.336 ± 0.009	0.823 ± 0.062
	K_{12}		8.17 ± 0.92	4.31 ± 0.21		1.48 ± 0.04	0.714 ± 0.029	1.00 ± 0.19
Diphenyl ether	K_{11}						0.647 ± 0.015	0.469 ± 0.050
	K_{12}						0.327 ± 0.061	

[a] Data taken from ref 12. Units for K_{11}, M^{-1}; units for K_{12}, M^{-2}. Standard state, 1 M ideal dilute solution. [b] Identical data are given for the dipropyl and dibutyl ether systems in ref 12.

TABLE III: Standard Heats of Formation for Hydrogen-Bonded Ether Systems

Ether	Proton donor	State	$-\Delta H_{11}°$, kcal/mol	Ref
Methyl ether	HCl	Gas	7.6	9
	HCl	Gas	6.3 to 7.9	10
Ethyl ether	Phenol	CCl₄	4.3	a
	Phenol	CCl₄	5.0[b]	c
	Phenol	CCl₄	3.7	8[b]
	HCl	Heptane	6.4 ± 0.1[b]	12
	HNCS	CCl₄	6.3	d
n-Propyl ether	HCl	Heptane	5.9 ± 0.1[b]	12
	Phenol	CCl₄	4.4[b]	c
	HNCS	CCl₄	6.7	d
Isopropyl ether	Phenol	CCl₄	5.6[b]	c
	HNCS	CCl₄	7.4	d
n-Butyl ether	HCl	CCl₄	5.2	e
	HCl	Heptane	5.9 ± 0.1[b]	12
	Phenol	CCl₄	5.5[b]	c
	HNCS	CCl₄	6.5	d
n-Amyl ether	HNCS	CCl₄	6.50	d
Benzyl ether	HCl	Heptane	5.4 ± 0.4[b]	12
	Phenol	CCl₄	4.1[b]	c
	HNCS	CCl₄	5.4	d
Anisole	HCl	Heptane	3.7 ± 0.1[b]	12
	Phenol	CCl₄	3.5[b]	c
	HNCS	CCl₄	3.7	d
Tetrahydro-furan	HCl	Heptane	6.5 ± 0.3[b]	12
	Phenol	CCl₄	5.9[b]	d
	Phenol	CCl₄	5.5	a
	HNCS	CCl₄	6.3	d
Tetrahydro-pyran	HCl	Heptane	6.4 ± 0.3[b]	12
	Phenol	CCl₄	6.1[b]	c
	HNCS	CCl₄	6.2	d

[a] G. Sellier and B. Wojtkowiak, *Bull. Soc. Chim. Fr.*, 936 (1968). [b] Calculated from published data. [c] T. Gramstad, *Spectrochim. Acta*, 19, 497 (1963). [d] T. M. Barakat, M. J. Nelson, S. M. Nelson, and A. D. E. Pullin, *Trans. Faraday Soc.*, 62, 2674 (1966). [e] This work.
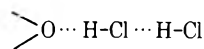
$$\diagdown\!\!\!O \cdots H\text{-}Cl \cdots H\text{-}Cl$$

II

If structure II is the correct one, thermodynamic constants for the reaction E·HCl + HCl = E·(HCl)₂ should provide evidence for progressively stronger bonding as the base strength of the ether increases, since a purely inductive effect would stabilize that structure. However, the effect of increasing base strength on the addition of the second HCl is less easy to predict if structure I is correct. The inductive effect of the first HCl should cause a decrease in the basicity of the non-bonded lone-pair electrons; in the more basic ethers, induction will be more effective in reducing the lone-pair electronegativity. Therefore, the variation with base strength of the thermodynamic constants for the addition of a second HCl to the 1:1 complex should be much less than the variation of these constants with basicity in the case of the 1:1 formation reaction. Table IV lists values of $-\Delta H°$ and $-\Delta G°$ for adding HCl to the 1:1 complex, calculated from constants in Table II for the 1:2 and 1:1 formation reactions. The most striking feature of these results is that there is little variation in $-\Delta H°$ and $-\Delta G°$ and no simple correlation of these values with the base strength of the ethers. This supports the conclusion that I is the more plausible of the two structures proposed for the 1:2 complex. The unbound lone-pair electrons of the more basic ethers apparently suffer a large loss in donor ability upon formation of a strong first bond; this leveling effect appears all the more remarkable when it is considered that $-\Delta G_{11}°$ and $-\Delta H_{11}°$ for the 1:1 complex formation reaction increase by

TABLE IV: Enthalpies and Gibbs Free Energies for the Reaction E·HCl + HCl = E·(HCl)$_2$ in Heptane[a]

Ether	$-\Delta H°$, kcal/mol	$-\Delta G°$, kcal/mol
Tetrahydrofuran	3.31	0.12
Tetrahydropyran	3.98	0.04
Ethyl ether	2.82	−0.04
n-Propyl ether	3.07	−0.25
n-Butyl ether	3.14	−0.28
Benzyl ether	3.87	0.06
β,β'-Dichlorodiethyl ether	3.79	0.00
Anisole	2.07	0.11

[a] Standard states, 1 M ideal dilute solution.

1.6 and 2.7 kcal/mol, respectively, as the base is varied from anisole to tetrahydrofuran. Thus, for example, the 1:1 complexes of tetrahydropyran with HCl and benzyl ether with HCl are equally good bases (as judged by the enthalpy and free energy changes accompanying addition of a second HCl molecule) in spite of the fact that tetrahydropyran is a much stronger base than benzyl ether (in adding the first HCl molecule).

The present study provides quantitative information about the reduction in donor strength of ethers which accompanies formation of a hydrogen bond to one of the ether oxygen lone pairs. Because HCl functions primarily as a proton donor, the interpretation of inductive effects is considerably simpler than in systems of hydroxylic compounds, which can function simultaneously as donors and acceptors of electrons. Recently, structures similar to II have been proposed for the 1:2 complexes of diethylamine and methanol or water[17] and of tetramethylurea with various phenols.[18] The second hydroxylic proton donor in each of these complexes is assumed to attach to the oxygen of the first, which is apparently rendered considerably more basic by the inductive effect. In the case of the diethylamine–methanol system, it has been argued that the basicity of the methanol oxygen in the 1:1 complex is so enhanced that it becomes a better proton acceptor than the lone-pair nitrogen of a free diethylamine molecule.[17] Undoubtedly induction effects are important in stabilizing trimers and larger aggregates in solutions of hydroxylic compounds;[19] however, the present study suggests that induction is far less effective in augmenting the electron donor strength of chlorine. The electronic distribution about Cl is more diffuse than that about atoms of first row elements such as O and N, and the hydrogen bonding of ethers at the HCl proton apparently does not cause the Cl to become a good proton acceptor.

Appendix

The HCl vapor pressure data of Strohmeier and Echte[12] can be correlated by assuming that the complex equilibria E + A = EA and E + 2A = EA$_2$ occur in solution and that the formal concentrations of HCl and ether, respectively, in solution are given by

$$f_A = C_A + K_{11}C_EC_A + 2K_{12}C_EC_A{}^2$$

and

$$f_E = C_E + K_{11}C_EC_A + K_{12}C_EC_A{}^2$$

where C_E and C_A are the monomer concentrations of ether and HCl and K_{11} and K_{12} are the formation constants for the 1:1 and 1:2 complexes from the ether and HCl monomers. Values of C_A were inferred directly from partial pressures of HCl and the Henry's law constants of HCl in pure n-heptane; f_A and f_E (in molar units) were computed from Strohmeier and Echte's mole fraction data, using available molar volumes of heptane and reasonable estimates of the partial molar volumes of the dissolved HCl and ethers. ($\bar{V}_{HCl}$ is assumed to be 10% greater than the molar volume of liquid HCl; the partial molar volumes of the ethers and solvent are assumed to be equal to the respective molar volumes of the pure liquids.) Non-linear least-squares methods described previously[14] were employed to compute values of C_E for each data set, as well as K_{11}, K_{12}, and the standard errors in these constants. The constants reported in Table II are least-squares values with standard errors.

References and Notes

(1) G. Friedel, *Bull. Soc. Chim. Fr.*, **24**, 160, 241 (1875).
(2) E. H. Archibald and D. McIntosh, *J. Chem. Soc.*, **85**, 919 (1904).
(3) O. Maass and D. McIntosh, *J. Amer. Chem. Soc.*, **34**, 1273 (1912).
(4) O. Maass and D. McIntosh, *J. Amer. Chem. Soc.*, **35**, 535 (1913).
(5) W. Gordy and P. C. Martin, *J. Chem. Phys.*, **7**, 99 (1939); W. Gordy and P. C. Martin, *ibid.*, **9**, 215 (1941); M. L. Josien and G. Sourisseau, *Bull. Soc. Chim. Fr.*, **178** (1955); P. Grange and J. Lascombe, *J. Chim. Phys.*, **60**, 1119 (1963); J. E. Bertie and D. J. Millen, *J. Chem. Soc.*, 497 (1965); J. E. Bertie and M. V. Falk, International Conference on Hydrogen Bonding, Ottawa, Aug 21–25, 1972, Abstract 17; J. Lascombe, J. C. Lassegues, and P. V. Huong, *ibid.*, Abstract 16.
(6) G. Briegleb and W. Lauppe, *Z. Phys. Chem. B*, **37**, 260 (1937); A. R. Gantmacher, M. V. Vol'kenshtein, and Ya. K. Syrkin, *Acta Physiochem. URSS*, **12**, 786 (1940); *Chem. Abstr.*, **35**, 976 (1941); G. L. Vidale and R. C. Taylor, *J. Amer. Chem. Soc.*, **78**, 294 (1956).
(7) S. J. O'Brien, C. L. Kenney, and R. A. Zuercher, *J. Amer. Chem. Soc.*, **61**, 2504 (1939); S. J. O'Brien, *ibid.*, **63**, 2709 (1941); H. C. Brown and J. D. Brady, *ibid.*, **74**, 3570 (1952).
(8) S. D. Christian, E. Tucker, and H. E. Affsprung, *Spectrochim. Acta, Part A*, **23**, 1185 (1967).
(9) A. T. Gladishev and Ya. K. Syrkin, *C. R. Acad. Sci. URSS*, **20**, 145 (1938).
(10) G. Govil, A. D. H. Clague, and H. J. Bernstein, *J. Chem. Phys.*, **49**, 2821 (1968).
(11) B. S. Ault and G. C. Pimentel, *J. Phys. Chem.*, **77**, 57 (1973).
(12) W. Strohmeier and A. Echte, *Z. Electrochem.*, **61**, 549 (1957).
(13) R. Mitamura, I. Tokura, S. Nishimura, Y. Kondo, and N. C. Li, *J. Inorg. Nucl. Chem.*, **30**, 1019 (1968).
(14) Details of the data analysis are given by B. M. Keenan, M.S. Thesis, The University of Oklahoma, 1969. See also R. D. Grigsby, S. D. Christian, and H. E. Affsprung, *J. Phys. Chem.*, **72**, 2465 (1968); S. D. Christian, *J. Chem. Educ.*, **42**, 604 (1965).
(15) Enthalpies for complex formation reactions are calculated from the relation $\Delta H = RT^2[d \ln K_c/dT + \Delta n\alpha_s]$, where α_s is the coefficient of thermal expansion of the medium and Δn is the change in number of moles of species. See E. M. Woolley, J. C. Travers, B. P. Erno, and L. G. Hepler, *J. Phys. Chem.*, **75**, 3591 (1971).
(16) See S. D. Christian, A. A. Taha, and B. W. Gash, *Quart. Rev., Chem. Soc.*, **24**, 20 (1970), for a discussion of solvent effects and use of the parameter α.
(17) E. E. Tucker, Ph.D. Dissertation, The University of Oklahoma, 1969.
(18) J. P. Muller, G. Vergruysse, and Th. Zeegers-Huyskens, *J. Chim. Phys.*, **69**, 1439 (1972).
(19) E. E. Tucker and E. D. Becker, *J. Phys. Chem.*, **77**, 1783 (1973); E. E. Tucker, S. B. Farnham, and S. D. Christian, *ibid.*, **73**, 3820 (1969).

Cyclopentene Decomposition in Shock Waves

David K. Lewis,* Michael Sarr, and Mark Keil

Department of Chemistry, Colgate University, Hamilton, New York 13346   (*Received August 29, 1973*)

Publication costs assisted by Colgate University

The rate of thermal dehydrogenation of cyclopentene was studied in a single-pulse shock tube. Reactant mixtures consisted of 0.25 and 1.00% cyclopentene in argon, and total gas pressures were about 1 atm. Reaction temperatures were determined *via* the comparative rate technique, using the decomposition of *tert*-butyl alcohol as the internal standard reaction. Over the temperature range 1020–1189°K the data support a first-order rate equation, with rate constants in units of $\sec^{-1}$ given by $\log k(C_5H_8 \rightarrow C_5H_6 + H_2) = 13.35 - [60.0 \times 10^3/4.58 T°K]$. The reaction was essentially free of complications over this temperature range, but significant concentrations of side products were formed at higher temperatures. A separate study of the products formed from cyclopentadiene decomposition suggests that these side products were produced primarily from cyclopentene. Possible mechanisms are discussed.

Introduction

This paper reports a shock tube study of the homogeneous gas-phase thermal reactions of cyclopentene. The dehydrogenation of cyclopentene to form cyclopentadiene has been studied extensively in static systems over the temperature range 690–800°K.[1-4] The experimental conditions and results of three rate studies and a measurement of the equilibrium constant are summarized in Table I. The reaction was found to be unimolecular over the pressure range studied, and as can be seen from the table, there is good agreement on the Arrhenius parameters, despite the relatively narrow temperature range covered. However, there is some disagreement concerning the extent of ring fragmentation that takes place concurrently with dehydrogenation. Vanas and Walters,[1] who obtained their rate data from pressure measurements, believed that their products consisted of only cyclopentadiene and hydrogen up to at least 25% conversion of cyclopentene. Shoemaker and Garland[5] recommend this reaction as excellent for study in an undergraduate physical chemistry laboratory experiment because it is supposedly free of complications up to 50% conversion. However, Tanji, *et al.*,[2] and Knecht[3] found considerable amounts of ethene and propene in their reaction products. The latter observed that, at the quarter time of the reaction, these side products accounted for 5-6% of the loss of cyclopentene. Grant and Walsh[4] also found substantial quantities of ethene and propene plus cyclopentane and smaller quantities of methane and other hydrocarbons after 50% conversion of cyclopentene at 774°K.

With this background of studies, it appeared worthwhile to extend the cyclopentene dehydrogenation rate measurements to higher temperatures and also to determine extents of ring fragmentation, under the strictly homogeneous conditions attainable in a shock tube. In this study, we have made dehydrogenation and ring fragmentation rate measurements *via* the comparative rate technique developed by Tsang,[6] using the decomposition of *tert*-butyl alcohol to isobutene and water as the internal standard reaction, and also *via* the absolute rate method in which reaction temperatures are deduced from incident shock speeds. Measurements have also been made of the extent of ring fragmentation of cyclopentadiene in the same temperature range.

Experimental Section

Materials. The cyclopentene and *tert*-butyl alcohol were both Reagent Grade from Analabs and Brothers Chemical Co., respectively. Cyclopentadiene was prepared from the dimer (Matheson Coleman and Bell Practical grade, >95%) by distillation at atmospheric pressure. All reagents were subjected to a purification process *in vacuo* involving three consecutive freeze–pump–thaw–distill cycles. At each distillation, the first and last 10-20% fractions were discarded. Gas chromatographic analysis of the purified reagents showed no detectable impurities (estimated limit for detection ~0.1%). Nmr analysis of the cyclopentadiene at the time of gas sample preparation showed no detectable dimer.

Matheson Ultra-High Purity argon (99.999%) was used as the diluent gas for the reactant samples. Linde helium was used as the driver gas.

Matheson ethene (CP grade, 99.5%), propene (CP grade, 99%), allene (97%), isobutene (CP grade, 99%), and other hydrocarbons were used as obtained from the tanks for preparation of gas chromatograph calibration samples.

Apparatus. A 10-cm j.d. stainless steel single-pulse shock tube was used in this study. This apparatus and details of its operation have been described previously.[7] Methods of reagent purification and sample preparation were also described in that earlier report. Reaction times behind reflected shocks ranged from 800 to 900 μsec.

Analyses. Reactant and product samples were analyzed on a Varian Aerograph 1440 chromatograph with hydrogen flame detector. A 1.8 m × 0.32-cm column of 20% DEGS on 60-80 mesh Chromosorb W at 40° was used for the relative rate experiments run during 7/71. This was replaced by a 3.0 m × 0.32 cm column of 20% polypropylene glycol saturated with silver nitrate on 80-100 mesh Chromosorb W at 50°, for the relative rate experiments run during 8/72 and for all experiments from which extents of side product formation were determined. Peak areas were determined by the "cut and weigh" method. Multiple analyses were run on the products of each shock, and calculated rate constants were averaged. Gas chromatograph calibrations were checked before and after each day's experiments and at intervals during the day.

Conditions. Two series of comparative rate experiments were run on mixtures containing 0.25% cyclopentene,

TABLE I: Summary of Previous Studies of Cyclopentene Dehydrogenation

Ref	T range, °K	P range, Torr	A, sec^{-1}	E_a, kcal./mol	K, atm
1	730–800	39–249	$10^{13.04}$	58.8	...
2	690–800	12–30	$10^{13.34}$	59.9	...
3	750–800	4–34	$10^{12.77}$	57.7	...
4	774.4	...	...	...	0.424 (±0.059)

0.25% *tert*-butyl alcohol and 99.50% argon, and another series was run on a mixture containing 1.00% cyclopentene, 0.25% *tert*-butyl alcohol and 98.75% argon. These series are referred to hereafter as sets A, B, and C, respectively. Three other groups of experiments were run on 0.25% and 1.00% mixtures of cyclopentene (sets D and E) and a 0.25% mixture of cyclopentadiene (set F) in argon. Experimental conditions for all sets are summarized in Table II.

Calculations. Reflected shock temperatures in the comparative rate experiments (sets A, B, and C) were calculated from measured extents of *tert*-butyl alcohol decomposition to isobutene and water, based upon the previously reported parameters for that reaction,[7] log k = 14.6 − [66.2 × 10³/4.58T°K]. For absolute rate experiments (sets D, E, and F), temperatures were computed from measured incident shock velocities on the basis of ideal one-dimensional treatment of the shock process. Thermodynamic data for cyclopentene and cyclopentadiene were calculated from vibrational assignments and structural data listed by Furuyama, Golden, and Benson.[8]

Rate constants for cyclopentene dehydrogenation and *tert*-butyl alcohol decomposition were calculated from the integrated form of the rate expression for an irreversible first-order reaction. At these low sample pressures, negligible error is introduced by the assumption of irreversibility up to large extents of reaction. For example, although the reaction $C_5H_{10} \rightleftarrows C_5H_8 + H_2$ has an equilibrium constant K_p = 0.424 at 774°K,[4] the value becomes $K_p \approx 100$ at 1200°K (standard states are 1 atm). Thus equilibrium will be achieved when about 99.998% of the cyclopentene has been converted to the diene, under the experimental conditions of this study.

Results

The cyclopentadiene dehydrogenation was observed to proceed cleanly up to 1150°K, and the *tert*-butyl alcohol decomposition has been previously shown to be well behaved up to that temperature.[7] The rate constants for formation of cyclopentadiene and isobutene in experiments of sets A–C are listed in Table III and are shown together in the comparative rate plot, Figure 1. All rate constants are in units of sec^{-1}. The line, resulting from linear least-squares treatment of the data up to 1189°K, has a slope of 0.906 and an intercept of 0.51. Based on the Arrhenius parameters for *tert*-butyl alcohol decomposition[7] listed earlier, rate constants for cyclopentene dehydrogenation are given by

$$\log k(C_5H_8 \longrightarrow C_5H_6 + H_2) = 13.35(\pm 0.27) -$$

$$[60,000(\pm 1350)/4.58T°K] \quad (1020\text{–}1189°K) \quad (1)$$

The low-temperature limit of this study, 1020°K, was determined by limitations in the product gas analysis; we were not able to obtain reproducible measurements of very small cyclopentadiene peaks because of overlap with the large reactant peak. The upper limit of 1189°K was
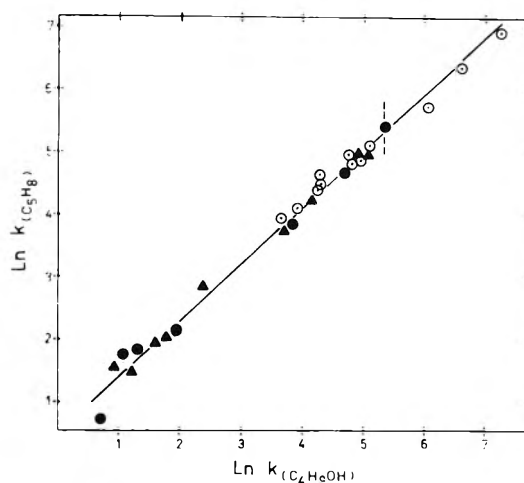
Figure 1. Relative rate plot; rate constants for formation of cyclopentadiene *vs.* rate constants for formation of isobutene: ⊙, set A; ●, set B; ▲, set C. See Table I for experimental conditions.

chosen because significant concentrations of side products were produced by both reactants above that temperature. The three experiments run at higher temperatures are included in Figure 1 to show that the influence of side reactions on the two primary reactions is not extreme up to 60% conversion of cyclopentene and 70% conversion of *tert*-butyl alcohol.

The uncertainties given in eq 1 represent one standard deviation in the least-squares analysis and do not reflect the total uncertainty in these values. The uncertainty in the parameters for *tert*-butyl alcohol should also be considered as should the uncertainties in the parameters for cyclohexene decyclization, the reaction with respect to which *tert*-butyl alcohol decomposition was compared.[7] However, it is reasonable to expect that random errors will cancel to some extent, so a realistic estimate of uncertainties in the parameters in eq 1 is about twice the magnitudes listed.

The products of cyclopentene ring fragmentation were monitored in the experiments of sets D and E. The major side products detected over the range 1170–1490°K were ethene, propene, allene, and 1,3-butadiene, in a fairly constant ratio 6:3:2:3. Methane, acetylene, and a lesser amount of ethane were also formed. The methane:ethene ratio rose from ½:6 at $T < 1300°K$ to 6:6 at 1450°K. The acetylene:ethene ratio also rose rapidly with temperature; the observed concentrations of acetylene can be attributed to dehydrogenation of ethene at these temperatures.[9] Total amounts of these six side products and amounts of cyclopentene and cyclopentadiene detected in product gas samples, as a function of reflected shock temperature, are shown in Figure 2. These values are for an initial 0.25% cyclopentene in argon sample (set D). Also included are predicted concentration *vs.* temperature curves for cyclopentene and cyclopentadiene, based on the Arrhenius parameters determined for cyclopentene dehydrogenation (eq 1) and assuming no loss of either compound due to side reactions. With reference to Figure 2, two conclusions can be drawn: (1) under the homogeneous conditions in the shock tube, side reactions do not account for more than 2% of the loss of reactant up to about 1250°, at which temperature the dehydrogenation goes 50% to completion in the 800 μsec reaction time; (2) there is an apparent drop in temperature of the reacting gas in experiments run

TABLE II: Summary of Experimental Conditions[a]

Set	Symbol (Figure 1)	Date	$\overset{\cdot\cdot}{\bigcirc}$	$\overset{\cdot\cdot}{\bigcirc}$	% C_4H_9OH	T range, °K
A	⊙	7/71	0.25	. . .	0.25	1121–1258
B	●	8/72	0.25	. . .	0.25	1020–1189
C	▲	8/72	1.00	. . .	0.25	1028–1178
D		7/71,6/72	0.25	. . .	. . .	1080–1490
E		6/72	1.00	. . .	. . .	1325–1450
F		7/71	. . .	0.25	. . .	1120–1460

[a] Initial pressure range: 20–40 Torr; reaction pressures ≈ 1 atm; reaction dwell times ≈ 800 μsec.

TABLE III: Rate Constants for Formation of Cyclopentadiene and Isobutene in Relative Rate Experiments, Sets A, B and C[a]

Set A (*)6.36, 6.59; (*)5.72, 6.06; 5.09, 5.10; 4.85, 4.95; 4.80, 4.81; 4.95, 4.75; 4.51, 4.31; 4.39, 4.24; 4.65, 4.28; 4.13, 3.92; 3.95, 3.65; (*)6.93, 7.26

Set B 0.72, 0.70; 2.17, 1.94; 1.86, 1.31; 1.73, 1.07; 4.66, 4.69; 5.40, 5.33; 3.84, 3.86

Set C 1.96, 1.61; 2.05, 1.79; 1.55, 0.95; 2.87, 2.38; 1.49, 1.23; 4.94, 4.89; 4.25, 4.16; 3.74, 3.71; 4.97, 5.07

[a] Number pairs are ln $k(C_5H_6)$, ln $k(C_4H_9OH)$. Experiments noted with an asterisk (*) were not included in the least-squares reduction. Dwell time for all experiments, 800 μsec.

at temperatures above 1200°K. Temperature values of 1350 and 1450°K calculated from shock speed measurements appear to be 50 and 100°, respectively, higher than the actual effective gas temperatures determined from measured extents of cyclopentene dehydrogenation and the Arrhenius parameters in eq 1. This discrepancy is probably due largely to endothermicity of the reactions occurring at these temperatures, although unimolecular falloff and/or systematic experimental errors may also be contributing factors. One may speculate that the dehydrogenation reaction is not entirely within the high-pressure regime under conditions of the experiments of set D above 1200°K, but it is difficult to attribute the entire factor of 5 decrease in the rate constant at 1450°K to unimolecular falloff. Recall that there was no observable dependence of the rate constant upon reactant concentration up to 1189°K in the experiments of sets A–C. It is also unlikely that this discrepancy arises solely from unreliable shock speed measurements; in sets A–C, temperatures determined from shock speed measurements generally agreed with the relative rate values within experimental error (±25°K).

The ring fragmentation experiments on the 1.00% cyclopentene mixture (set E) gave very similar results in terms of identities and ratios of concentrations of species formed. Although there was greater scatter in total amounts of fragmentation for different experiments at a given temperature, a comparison with the 0.25% cyclopentene experiments indicated that the rate of ethene formation shows about first-order dependence on cyclopentene concentration.

The extent of cyclopentadiene ring fragmentation over the temperature range 1120–1460°K was investigated in the experiments of set F. The C_1–C_4 products and their *ratios* of concentrations were similar to those found when cyclopentene was shocked to the same temperatures, except that only very small quantities of 1,3-butadiene were produced and that there were small quantities of an additional unidentified (probably C_5) alkene. However, at a given temperature, the total concentrations of all these products were only about one-third as great as concentra-
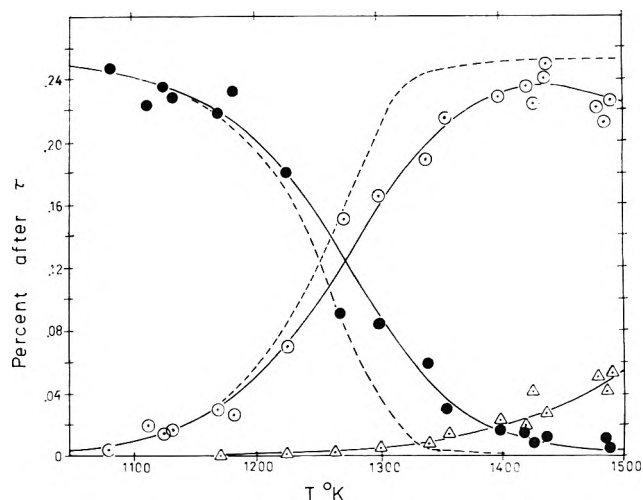
Figure 2. Percentage of reactant and products (as analyzed by vpc) vs. reflected shock temperature (evaluated from shock speeds), after residence time τ (≈ 800 μsec) for experiments of set D (initial composition 0.25% cyclopentene in argon): ●, cyclopentene; ⊙, cyclopentadiene; △, sum of all C_1–C_4 side products. Solid lines, drawn through experimental points; dotted lines, expected cyclopentene and cyclopentadiene concentration after τ vs. reflected shock temperature, assuming no formation of side products or cooling of gas due to endothermicity of reactions.

tions produced by shocking cyclopentene to the same temperature.

There was no measurable cyclopentane formed from either cyclopentene or cyclopentadiene at any temperature. This is not surprising as the low sample partial pressures resulted in a very low rate of biomolecular hydrogenation.

Discussion

The Arrhenius parameters deduced for the cyclopentene dehydrogenation from this relative rate study are in excellent agreement with those reported from the lower temperature studies,[1-3] but particularly with the highest values of E_a and A, reported by Tanji, et al.[2] Thus kinetic parameters of this reaction are well established over the range 690–1190°K.

There is ample evidence that the dehydrogenation is a concerted process. The Woodward–Hoffman rules[10] predict that concerted 1,4 elimination should be allowed, whereas 1,2 elimination should not, and Baldwin[11] has reported, from experiments on monodeuterated cyclopentene at 823°K, that 1,4 elimination is favored over 1,2 elimination by a ratio of 6:1. Recently, Anet and Leyendecker,[12] studying the reverse process, reported that reaction of deuterium with cyclopentadiene at 823°K results in a predominantly suprafacial 1,4 molecular addition. Isotopic labeling to check the mechanism was not performed in the

present study, but the consistency of the Arrhenius parameters with the low-temperature work, the freedom from side reactions below 1150°K, and the absence of cyclopentane at all temperatures are strong arguments that the concerted process is maintained to high temperatures.

Side product formation was more extensive from mixtures initially containing cyclopentene than from mixtures containing cyclopentadiene, at comparable reflected shock temperatures. The difference in rate of ring fragmentation is somewhat greater than the apparent 3:1 ratio because the cyclopentene mixtures were cooled more than the cyclopentadiene mixtures by the endothermic dehydrogenation process. Tanji, et al.,[2] reported finding that most side products in their samples were produced from cyclopentene. Comparing ring fragmentation of tetrahydrothiophene (thiocyclopentane) and thiophene (thiocyclopentadiene), Bauer, et al.,[13] found the rate of the former to be considerably greater than the rate of the latter at comparable temperatures. However, in this study, because of the rapid depletion of cyclopentene by dehydrogenation at high temperatures, and the resulting presence of molecular hydrogen, the source of the side products cannot be determined with certainty. Cyclopentane can be ruled out as the major contributor because the rates of collisions between cyclopentene and the liberated hydrogen were far too low for enough cyclopentane to have been formed under our experimental conditions. The complete absence of cyclopentane in the product samples and the apparently first-order kinetics for side product formation support this argument. While the results of this study seem to rule out cyclopentadiene as the major source, they do not exclude the possibility that the side products are formed from nascent cyclopentadiene. Newly formed product molecules, certainly highly excited, ought to undergo ring fragmentation more rapidly than thermalized cyclopentadiene. This possibility ought to be subject to experimental verification; a manyfold increase in pressure should result in more rapid thermalization of the nascent product and a subsequent reduction in side products formed from it. Also selective pumping of cyclopentadiene vibrations with a tunable laser might give information on the tendency of these excited molecules to fragment. Experimental limitations precluded our testing these hypotheses. Weighing the available evidence, we feel that the most likely source of the bulk of the side products was cyclopentene.

If cyclopentene ring fragmentation is the source of most of the side products, then there are two possible initial steps by which this fragmentation can occur: (a) bimolecular hydrogen atom transfer to form a cyclopentyl and a cyclopentenyl radical and (b) C–C bond rupture to form a biradical alkene. The results of earlier studies[14-16] suggest that if process a were operative, the cyclic monoradicals would quickly decyclize as follows
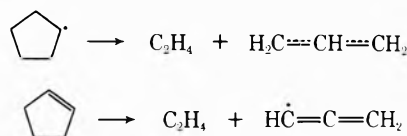
Subsequent hydrogen abstraction reactions would result in formation of stable ethene, propene and allene, in the ratio 2:1:1. While this is not far removed from the experimental ratio of these constituents, this process does not explain the presence of considerable amounts of 1,3-butadiene. Also, the hydrogen atom transfer step ought to be rate limiting. This would lead to second-order kinetics for side product formation contrary to experiment. Finally, the C–H bond energy is considerably higher than the C–C bond energy in cyclopentene, so the formation of the biradical ought to be favored energetically over the hydrogen atom transfer process. Assuming that the side products are formed directly from cyclopentene, we conclude that ring fragmentation via biradical formation is probably the dominant side reaction.

References and Notes

(1) D. W. Vanas and W. D. Walters. *J. Amer. Chem. Soc.*, **70**, 4035 (1948).
(2) H. Tanji, M. Uchiyama, A. Amano, and H. Tokuhisa, *J. Chem. Soc. Jap., Ind. Chem. Sect.*, **70**, 307 (1967).
(3) D. A. Knecht. Ph.D. Thesis, University of Rochester, 1968.
(4) C. J. Grant and R. Walsh, *Chem. Commun.*, 667 (1969).
(5) D. P. Shoemaker and C. W. Garland, "Experiments in Physical Chemistry," 2nd ed, McGraw-Hill, New York. N. Y., 1967, pp 228–236.
(6) W. Tsang, *J. Chem. Phys.*, **40**, 1171 (1964); **41**, 2487 (1964); **42**, 1805 (1965).
(7) D. Lewis, M. Keil, and M. Sarr, submitted for publication in *J. Amer. Chem. Soc.*
(8) S. Furuyama, D. M. Golden, and S. W. Benson, *J. Chem. Thermodyn.*, **2**, 161 (1970).
(9) G. B. Skinner, R. C. Sweet, and S. K. Davis, *J. Phys. Chem.*, **75**, 1 (1971).
(10) R. B. Woodward and R. Hoffman, "The Conservation of Orbital Symmetry," Verlag Chemie, Weinheim, West Germany, 1970, p 141.
(11) J. E. Baldwin, *Tetrahedron Lett.*, 2953 (1966).
(12) F. A. L. Anet and F. Leyendecker, *J. Amer. Chem. Soc.*, **95**, 156 (1973).
(13) S. H. Bauer, R. A. Fifer, P. Jeffers, A. Lifshitz, S. Matsuda, G. E. Millward, R. Moreau, and B. P. Yadava, "SO₂—Its Odessy in a Combustion Chamber," paper presented at 165th National Meeting of the American Chemical Society, Dallas, Tex., April 1973.
(14) H. E. Gunning and R. L. Stock, *Can. J. Chem.*, **42**, 357 (1964).
(15) A. S. Gordon, *Can. J. Chem.*, **43**, 570 (1965).
(16) T. F. Palmer and F. P. Lossing, *Can. J. Chem.*, **43**, 565 (1965).

Conformational Analysis and Electronic Structure of Para-Substituted Phenyl Vinyl Ethers

R. H. Donnay and F. Garnier*

Laboratoire de Chimie Organique Physique, associé au CNRS (LA 34), Université Pairs VII, 75005, Paris, France
(Received August 14, 1973)

The conformational analysis of para-substituted phenyl vinyl ethers $XPhOCH=CH_2$ (X = H, Me, MeO, OH, F, NO_2) has been performed by the INDO method. The same conformation is obtained for all of the compounds, in which the trend to maximum conjugation by coplanarity of the two unsaturated systems is blocked by steric hindrance. Analysis of the electronic structure of the ground state demonstrates the transmission of the conjugative effect through the oxygen atom to the ethylenic bond. However, in the course of an electrophilic reaction the role of the O atom as a transmitter of the conjugative effect must be diminished by the participation of the electron pair in the stabilization of the transition state.

Introduction

The study of the modification of the physical and chemical properties of a molecular site by its environment is of particular interest in chemistry. It leads first to an understanding of the mechanism by which the property operates and also to a prediction of the behavior of homologous compounds. The most frequently investigated model consists of a carbon atom chain, where the transmission of structural effects has been analyzed in terms of inductive effect, resonance, hyperconjugation, etc. However, results dealing with the transmission of structural effects through a heteroatom are very limited in spite of the growing interest paid to this class of compounds.

We undertook the study of the case where a heteroatom bearing lone pairs of electrons is placed α to a carbon–carbon double bond; previously, we analyzed comparatively the systems $C=CCR$ and $C=COR$ with R = alkyl.[1] The work presented here deals with para-substituted phenyl vinyl ethers $C=COArX$, which involve the conjugation between two unsaturated systems through the oxygen orbitals.

The problem of such conjugation has already been the subject of some controversy in the literature, in which two trends can be distinguished. Fueno,[2] for hydrolysis reactions, and Kennedy,[3] for cationic copolymerization reactions, do not discern the existence of any conjugation. This is the case also in the series of articles reviewed by Montanari[4] and Frolov.[5] On the other hand, Koch, from uv spectroscopic results,[6] observes an interaction between phenyl rings through a sulfur atom which he calls "quasi-conjugation." Finally, on the basis of more detailed spectroscopic studies on phenyl rings linked by N, P, Pb, As, and Bi atoms, Jaffé[7] proposed the existence of a weak conjugative interaction between the π systems when the heteroatoms possess unshared electrons.

In order to obtain a more precise view of the transmission of such conjugation through a heteroatom, we have undertaken the study of the para-substituted phenyl vinyl ethers $XPhOCH=CH_2$ (X = H, Me, MeO, OH, NO_2, F) using a quantum mechanical method. The prefered conformation of these compounds was first determined by energy minimization. The substituent effect and the electronic structure of the double bond were then analyzed using gross and partial atomic populations and localization and energies of the highest occupied molecular orbital. We shall discuss here the fundamental state of the molecule and the cationic species involved in the rate-determining step of electrophilic addition.

Conformational Analysis

The conformation of the para-substituted phenyl vinyl ether has been determined by the minimization of the total molecular energy with respect to the two angular parameters Φ_1 and Φ_2 shown in Figure 1. Several quantum chemical methods have already been proposed for such a theoretical conformation analysis: variational methods such as EHT by Hoffmann,[8] CNDO and INDO by Pople,[9] and perturbation methods such as PCILO by Malrieu.[10] As pointed out by Hall,[11] these different methods can lead to contradictory results for the same compound. Since we felt it necessary to justify the use of the INDO method, we have chosen to test its validity on a homologous compound whose structure has been determined experimentally: divinyl ether. In view of the similarity of its structure and interactions to those of phenyl vinyl ether, as shown in Figure 2, this compound may be regarded as a suitable test case. Using microwave data, Hirose and Curl[12] reached the following conclusions: the *cis–trans* divinyl ether possesses two energetically equivalent conformations corresponding to mirror-image molecules, separated by a saddle whose maximum represents the planar form. The internal rotation angles corresponding to the preferred conformation are found to be $\Phi_1 \simeq 50°$ and $\Phi_2 \simeq 10°$. Our calculations in this compound, based on the INDO method, lead to the results presented in Figure 3. Two symmetrical potential minima are found, separated by a saddle corresponding to the planar form, and the angles are $\Phi_1 = 56.25°$, $\Phi_2 = 11.25°$. The satisfactory agreement with experimental data justifies the use of the INDO method for the conformational analysis of these compounds.

Computing Conditions

The angle Φ_1 (Figure 2) corresponds to the C_3O internal rotation angle with clockwise rotation positive, looking inward from C_3 to O. The angle Φ_2 (Figure 2) corresponds to the C_2O internal rotation angle with clockwise rotation positive, looking inward from C_2 to O.

The variation intervals considered for the two internal rotation angles are the following: $0° < \Phi_1 < 180°$ and $-90°$
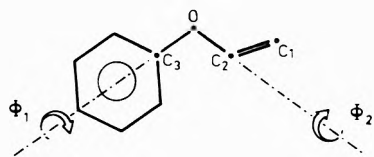
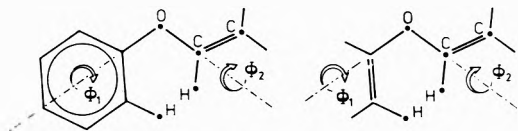**Figure 1.** Internal rotation parameters for conformational analysis.

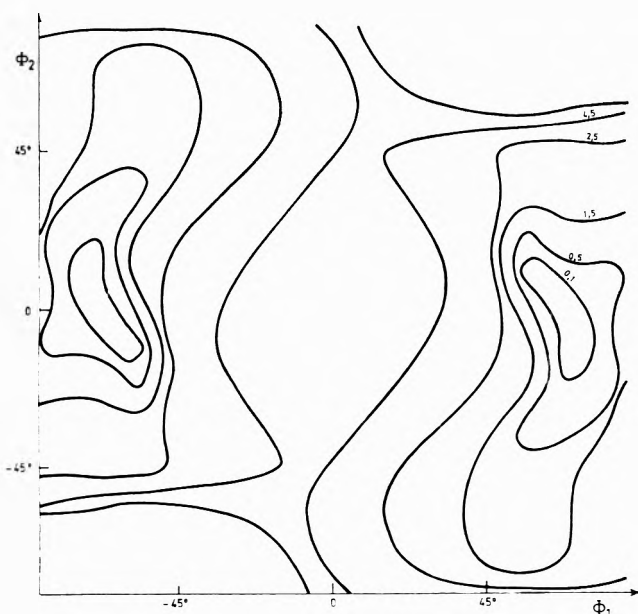**Figure 2.** Comparison of interactions in phenyl vinyl ether and divinyl ether.

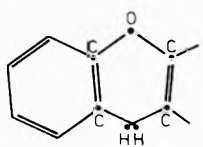**Figure 3.** Conformational map of divinyl ether; contours are in kcal/mol above the absolute minimum.

Figure 4. Forbidden structure; phenyl ring "inside" the double bond.

$< \Phi_2 < 90°$, the values $\Phi_1 = \Phi_2 = 0$ corresponding to the planar form. These two intervals take into account the symmetry of the para-substituted phenyl rings and do not consider the sterically hindered structure in which the phenyl ring would be "inside" the double bond (Figure 4). The bond lengths and bond angles used in the calculations are standard values given by Pople,[13] which have been average from available experimental data.

Results

The potential surfaces obtained for the unsubstituted phenyl vinyl ether are represented in Figure 5. The surface is symmetrical with respect to origin, with two equivalent minima corresponding to mirror-image molecules, as in the divinyl ether case. Similarly, the planar form corre-
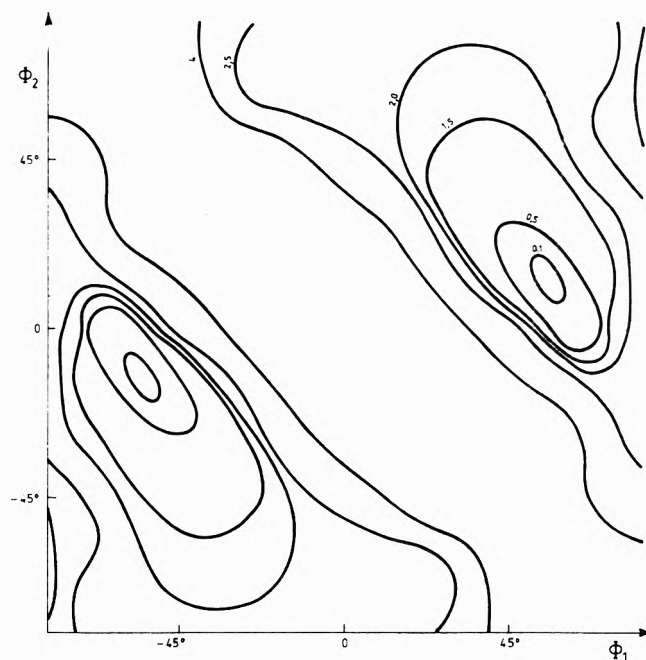
Figure 5. Conformational map of phenyl vinyl ether.

sponds to a saddle point between the two minimum energy structures.

These remarks on the symmetry lead us to consider only the first quadrant of the calculated potential surfaces of para-substituted phenyl vinyl ethers. The complete potential surfaces determined for the para-substituted phenyl vinyl ethers (which are included in the microfilm edition of this journal[14]) demonstrate that the potential minima are obtained for same values of Φ_1 and Φ_2, whatever the para substituent. These values are $50° < \Phi_1 < 60°$ and $10° < \Phi_2 < 20°$, this $10°$ range being due to the fact that the potential well is rather large.

Two opposite effects may be argued for these results: a tendency towards maximum conjugation between the two unsaturated systems in a planar configuration; and steric hindrance between the two hydrogens H_1 of the ethylenic bond and H_2 on the phenyl ring (Figure 11). In fact, for a planar structure, the allowed distance between the two hydrogen atoms H_1 and H_2 is only 1.3 Å, whereas the sum of the van der Waals radii for these atoms is 2.2 Å. In the calculated preferred conformation, the interatomic distance H_1H_2 is found to be 2.2 Å.

Thus for these compounds, the tendency to a maximum conjugation operates up to the limit determined by the steric repulsion between the H_1 and H_2 hydrogen atoms. Having determined the minimum energy conformation, we shall analyze in what follows the precise electronic structure of these compounds, taking into account for the π-orbital electronic population, the total electronic population, and the ionization potential.

Electronic Structure of Para-Substituted Phenyl Vinyl Ethers. The electronic structure of the reaction center (the olefinic bond) of these compounds has been analyzed. Two features will be discussed, first, the absolute electrical modification of the double bond induced by the α heteroatom—π-orbital delocalization, bond polarization, and secondly, the transmission of the effect of a para substituent through the heteroatom to the olefinic bond.

Application of population analysis of the Mulliken[15] type to phenyl vinyl ether leads to the atomic populations
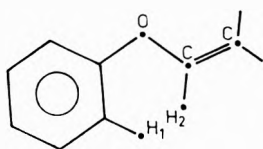
Figure 11. Origin of the nonplanarity of the molecular system: steric hindrance.
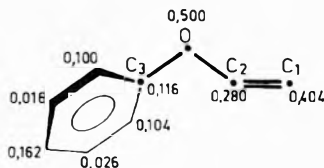

Figure 12. Localized electronic populations in the highest π orbital.

of the highest occupied molecular orbital as shown in Figure 12. The values obtained indicate that this orbital is essentially delocalized on three centers, the two carbon atoms of the double bond and the oxygen atom. The charges on atoms C_1 and C_2 in the π orbital indicate that the C_1-C_2 π bond is polarized, the C_1 carbon atom being the negative end of the π-electron dipole.

Using a valence bond scheme, this result may be visualized by the mesomeric structures

$$CH_2=CHO^- \quad \longleftrightarrow \quad {}^+CH_2CH=O^-$$

The C_1-C_2 bond polarization is directly related to the contribution of the ionic mesomer. In order to determine the extent transmission of the substituent effect through the oxygen atom to the ethylenic bond, we use the calculated gross atomic populations and the energies of the highest occupied molecular orbitals E_{HOMO}. *The total charges* on the two carbon atoms C_1 and C_2 of the double bond, on the oxygen atom, and on the C_3 carbon atom of the phenyl ring bound to oxygen are listed in Table I.

The relative variation found for the charges borne on the C_3 carbon atom in relation to the substituent agrees with the classical resonance structures. Thus, for a *p*-hydroxy substituent, there is π donation from the oxygen p orbital lone pair into the ring
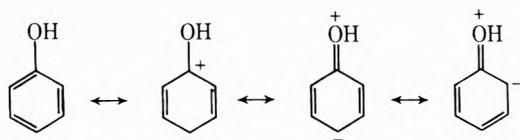
On the other hand, the electron-withdrawing nitro substituent leads to a decrease in the C_3 charge
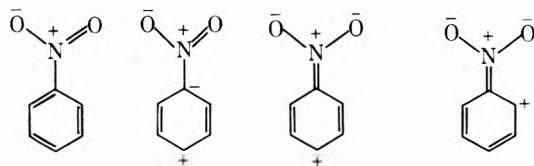
The relative variation of the charges on the two carbon atoms C_1 and C_2 is $0.011e$ for C_1 and $0.008e$ for C_2. This structure effect appears to be more sensitive on the C_1 carbon atom, whose charge variation for instance reaches $0.007e$ in going from H to NO_2.

Although sensitive, the overall effect is weak. This phenomenon may be interpreted first by the rather large distance between the substituent and the C_1 carbon atom,

TABLE I: Gross Atomic Populations on the Carbon Atoms of the Double Bond, the Oxygen Atom, and the α-Carbon Atom of the Ring

Charges	C_1	C_2	O	C_3
H	6.055	5.785	8.247	5.771
Me	6.054	5.790	8.242	5.776
MeO	6.058	5.780	8.248	5.797
OH	6.059	5.782	8.247	5.794
F	6.056	5.784	8.245	5.789
NO_2	6.048	5.790	8.241	5.749

TABLE II: Ionization Potentials of Para-Substituted Phenyl Vinyl Ethers

X	E, eV
H	10.90
Me	10.73
MeO	10.49
OH	10.59
F	10.84
NO_2	11.40

and secondly by the nonplanarity of the π system, which reduces the ease of conjugation.

The E_{HOMO} energies listed in Table II are directly related to the ionization potentials by Koopmans' theorem[16] and to a measure of the chemical reactivity of these compounds.[17] The sensitivity to substituent effects is expressed by the following relationship between these E_{HOMO} energies and the values of the kinetic parameters σ^+[18] determined by Brown for the solvolysis of para-substituted *tert*-cumyl chlorides (Figure 13)

$$E_{eV} = 0.58\,\sigma^+ + 10.92$$

On account of the uncertainty of the σ_{OH}^+ value, which could not be determined for the same reference reaction, the corresponding point has not been included in the correlation and in fact lies off the line. The value of the slope, 0.58, is to be compared to those obtained by Crable and Kearnes[19] for mono- and disubstituted benzenes. These authors observed the existence of linear relationships between the experimental ionization potentials and σ^+ substituent parameters. The slopes obtained are, using same units, 0.70, 0.75, 0.86, 0.95, respectively, for para-substituted anilines, toluenes, benzenes, and nitrobenzenes.

Thus these results clearly show that, in spite of the great distance between the substituent and the double bond in phenyl vinyl ethers, the modification of the electronic structure of the reaction center by conjugation is similar to that observed in substituted benzenes. This conclusion agrees with nmr chemical shift data of the trans β protons in phenyl vinyl ethers and allylbenzenes:[20] two comparable relationships have been obtained between chemical shifts and inductive effect substituent parameters.

Is this conjugation maximal? The preceding conclusion refers to the minimum energy conformation where the nonplanarity is due to steric hindrance between two hydrogen atoms. The relationship $E = f(\sigma^+)$ calculated for a hypothetical planar conformation and for the corresponding energies gives a higher slope value of 0.66. This result confirms that two opposite effects operate in the minimum energy conformation, conjugation and steric repulsion, the latter imposing the same conformation on the ethers irrespective of the substituent.
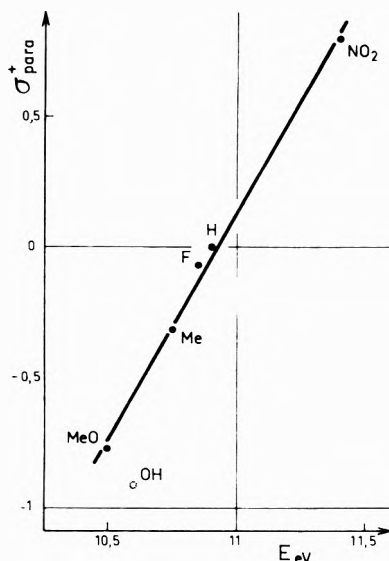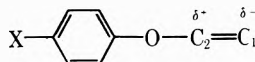
**Figure 13.** Linear relationship $E_{\text{eV}} = f(\sigma^+)$.

Thus the results obtained for the isolated molecule in its ground state show that the conjugation between the two unsaturated systems does exist and therefore that the oxygen atom acts as a transmitter of the mesomeric effect towards a polarized reaction center

$$X-\langle \text{ring} \rangle-O-\overset{\delta^+}{C_2}=\overset{\delta^-}{C_1}$$

Considering now the kinetic behavior of these para-substituted phenyl vinyl ethers, we have to analyze the structural effect on the transition state of the reaction. The approach of an electrophilic reagent E^+ toward the ethylenic bond will increase the electronic dissymmetry of the double bond and lead to a cationic intermediate of the carbocation type

$$-\overset{+}{C_2}-\overset{|}{\underset{|}{C_1}}-$$
$$E$$
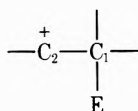
Taking this structure as an extreme model of the reaction transition state, we must consider the unshared electrons of the neighboring oxygen atom, which will participate in this unsaturation and will lead to the following mesomeric structure

$$X-\langle \text{ring} \rangle-O-\overset{+}{C}H-CH_2E \longleftrightarrow$$

$$X-\langle \text{ring} \rangle-\overset{+}{O}=CH-CH_2E$$
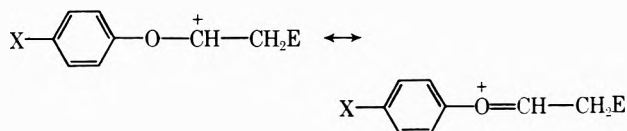
The loss of these lone pairs decreases the probability of direct conjugation between the substituted phenyl ring and the vinyl group and it can be presumed that the para-substituent effect on the transition state of the reaction will be weaker than that on the ground state.

This analysis leads us to the conclusion that, in the course of a reaction, there is a small structural effect on the kinetic constants. This discussion allows us to understand why in the case of electrophilic reactions, the conjugative effect is absent.[21]

Conclusion

This study of para-substituted phenyl vinyl ethers by the INDO method demonstrates that in the ground state of the isolated molecule there is conjugation between the unsaturated system through the oxygen atom. This is in agreement with previous spectroscopic results.

For the transition state of an electrophilic reaction, we are led to propose that the conjugative effect is canceled by the participation of the oxygen lone pairs to the stabilization of the carbocation in accordance with kinetic measurements on these compounds.

Supplementary Material Available. Calculated potential surfaces for the para-substituted phenyl vinyl ethers (Figures 6-10) will appear following these pages in the microfilm edition of this volume of the journal. Photocopies of the supplementary material from this paper only or microfiche (105 × 148 mm, 24× reduction, negatives) containing all of the supplementary material for the papers in this issue may be obtained from the Journals Department, American Chemical Society, 1155 16th St., N.W., Washington, D. C. 20036. Remit check or money order for $3.00 for photocopy or $2.00 for microfiche, referring to code number JPC-74-440.

References and Notes

(1) R. H. Donnay, F. Garnier, and J. E. Dubois, *J. Chim. Phys.*, **4**, 549 (1972).
(2) T. Fueno, I. Matsumura, T. Okuyama, and J. Furukawa. *Bull. Chem. Soc. Jap.*, **41**, 818 (1968).
(3) J. P. Kennedy in "Copolymerization," G. E. Ham, Ed., Interscience, New York, N. Y., 1964, p 308.
(4) F. Montanari, *Boll. Scient. Fac. Chim. Ind. Bologna*, **16**, 31 (1958).
(5) Y. L. Frolov, A. V. Kalabina, and A. K. Filippova, *Zh. Strukt. Khim.*, **6** (3), 397 (1965).
(6) H. Koch, *J. Chem. Soc.*, 387 (1949).
(7) J. J. Jaffé, *J. Chem. Phys.*, **22**, 1430 (1954).
(8) R. Hoffmann, *J. Amer. Chem. Soc.*, **90**, 1475 (1968).
(9) (a) J. A. Pople, D. P. Santry, and G. A. Segal, *J. Chem. Phys.*, **43**, S129 (1965); (b) J. A. Pople, D. L. Beveridge, and P. A. Dobosh, *ibid.*, **47**, 2026 (1967).
(10) S. Diner, J. P. Malrieu, and P. Claverie, *Theoret. Chim. Acta*, **13**, 1 (1969).
(11) W. C. Herndon, J. Feuer, and L. H. Hall, *Tetrahedron Lett.*, 2025 (1968).
(12) C. Hirose and R. F. Curl, Jr., *Mol. Spectrosc.*, **38**, 358 (1971).
(13) J. A. Pople and D. L. Beveridge, "Approximate Molecular Orbital Theory," McGraw-Hill, New York, N. Y., 1970, p 111.
(14) See paragraph at end of paper regarding supplementary material.
(15) R. S. Mulliken, *J. Chem. Phys.*, **23** (10), 1833 (1955).
(16) T. Koopmans. *Physica*, **1**, 104 (1933).
(17) A. Streitwieser, Jr., H. A. Hammond, R. H. Jagow, R. M. Williams, R. G. Jesaitis, C. J. Chang, and R. Wolf, *J. Amer. Chem. Soc.*, **92**, 5141 (1970).
(18) H. C. Brown and Y. Okamoto, *J. Amer. Chem. Soc.*, **80**, 4979 (1958).
(19) G. F. Crable and G. L. Kearnes, *J. Phys. Chem.*, **66**, 436 (1962).
(20) O. Kajimoto, T. Fueno, Symposium on the Hammett Relationship, Kyoto, 1967.
(21) T. Fueno, T. Okuyama, I. Matsumura, and J. Furukawa, *J. Polym. Sci., Part A1*, **7** (6), 1447 (1969).

Time-Dependent Hartree Calculations of the Sequence Dependence of DNA Hypochromism

James S. Balcerski and E. S. Pysh*

Department of Chemistry, Brown University, Providence, Rhode Island 02912   (Received August 6, 1973)

By a direct comparison with experimental data we show that time-dependent Hartree calculations of DNA hypochromism are accurate enough to show some of the sequence dependence that is experimentally observed.

Introduction

Brown and Pysh[1a,b] have shown that if a self-consistent field nucleotide basis set is used, the observed overall base composition dependence of DNA hypochromism, *i.e.*, the behavior of poly dA:dT compared with that of poly dG:dC, can be reproduced by a time dependent Hartree (TDH) calculation of the hypochromism. Pysh and Richards[2] reported, moreover, that such TDH calculations are accurate enough to show some of the sequence dependence that is experimentally observed. In making such a correspondence they used an empirical parameterization of nearest neighbor interactions of the type developed by Tinoco, *et al.*[3-6] Having completed additional calculations we are here able to demonstrate the correspondence between the TDH method and experimental and empirical data directly.

Calculations and Results

The details of the calculations are the same as in the earlier work.[1,2] We have examined decamer segments of double-stranded polydeoxyribonucleotides for which experimental absorption results are available. The calculations were carried out for double-stranded structures in the B-conformational form of fibrous DNA lithium salt with base pairs in planes perpendicular to the tenfold screw axis and separated by 3.36 Å.

The results are combined with earlier results[2] in Table I in terms of the hypochromism of the low-energy absorption band near 260 nm. The calculated results of column three include contributions to hypochromism from the coupling of the low-energy electronic transitions above 190 nm, but not the contributions from the higher energy monomer transitions or the solvent transitions. The observed values in column four are therefore substantially more positive in every case.

Discussion

These calculations are in no sense fitted to the polymer data. The calculated results are determined by the self-consistent field monomer wave functions, which are obtained without reference to the polymer data,[1] and by the formalism of TDH theory.[1,2,7] TDH theory is equivalent to the generalized susceptibility formalism of Rhodes, *et al.*[8,9]

The salient feature of Table I is that the TDH results correctly order the hypochromism for four pairs of synthetic polynucleotides representing the entire range of %A-T content: poly dG:dC > poly dGC:dGC (0% A-T);

poly dAG:dCT > poly dAC:dGT (50% A-T); poly dTAC:dGTA > poly dATC:dGAT (67% A-T); and poly dA:dT > poly dAT:dAT (100% A-T). Thus, the double strand of the alternating sequence poly dGC:dGC is significantly less hypochromic than the double strand of complementary homopolymers, although this difference is greater in the calculated results than in the experimental results. The double strand of the alternating sequence of poly dAT:dAT is also less hypochromic than the corresponding double strand of complementary homopolymers, but this difference is much smaller than in the GC case according to both the calculated results and the experimental data. The double strand of the alternating sequence poly dGC:dGC is the least hypochromic of all sequences compared.

The results for these eight sequences can be combined with the earlier results[2] for six other sequences to determine the parameters of an empirical relation which has been shown[6] to describe DNA hypochromism

$$\epsilon' = -H\epsilon^0 \equiv \Sigma f_i \epsilon_i' \qquad (1)$$

where ϵ^0 is the contribution from isolated A-T and G-C base pairs taken here as[10]

$$\epsilon^0 = 11,300 f_{AT} + 10,500 f_{GC} \qquad (2)$$

ϵ_i' is the contribution from the ith nearest neighbor paired base pair interaction, and f_i is the mole fraction of each type of paired base pair. There are ten independent contributions to ϵ' from the ten independent nearest neighbor interactions,[5] shown in the first column of Table II.

The second column of Table II shows the derived set of ϵ_i'(TDH) describing the TDH results. The third column shows the parameterization ϵ_i'(exp) reported earlier[2] and derived from experimental data on 15 double-stranded polynucleotides whose nearest-neighbor frequency distributions are known. The set of ϵ_i'(exp) include contributions from the high-energy monomer states and solvent states, which are not included in the set of ϵ_i'(TDH).

That the TDH results display to a substantial degree the correct sequence dependence is shown in this comparison through the partial similarity in the two sets of ϵ_i'. In both sets the largest contributors to hypochromism are the paired base pairs corresponding to ϵ_1, ϵ_2, ϵ_3, ϵ_9, and ϵ_{10}. Next in order are the contributions from ϵ_4 and ϵ_6. The lowest contributions to hypochromism come from ϵ_5, ϵ_7, and ϵ_8.

The correspondence between these extensively detailed TDH calculations and the observed experimental results

TABLE I: Time-Dependent Hartree Calculated Hypochromism and Experimentally Measured Hypochromism[2,6] for Double-Strand Polydeoxyribonucleotides

	% A–T	$\%H_{TDH}$	$\%H_{exp}$
Poly dG:dC	0.0	10	33
Poly dGC:dGC	0.0	−38	22
Poly dAC:dGT	50.0	7	40
Poly dAG:dCT	50.0	19	48
Poly dATC:dGAT	66.7	16	37
Poly dTAC:dGTA	66.7	18	51
Poly dAT:dAT	100.0	26	42
Poly dA:dT	100.0	27	47

TABLE II: The Ten Independent Paired Base Pair Interactions and Our Parameterization of Eq 1 Using the TDH Calculated Hypochromism (Column 2) and the Experimentally Measured Hypochromism[1] (Column 3)[a]

Paired base pair	$\epsilon_i{}'$(TDH)	$\epsilon_i{}'$(exp)
1 ↑ AT ↓ ↑ AT ↓	−3.10	−5.50
2 ↑ CG ↓ ↑ AT ↓	−1.80	−6.30
3 ↑ GC ↓ ↑ AT ↓	−2.15	−5.50
4 ↑ CG ↓ ↑ TA ↓	−1.35	−4.50
5 ↑ GC ↓ ↑ TA ↓	+0.30	−2.90
6 ↑ GC ↓ ↑ GC ↓	−0.80	−3.44
7 ↑ CG ↓ ↑ GC ↓	+2.20	−3.30
8 ↑ GC ↓ ↑ CG ↓	+3.05	−1.30
9 ↑ TA ↓ ↑ AT ↓	−4.00	−4.80
10 ↑ AT ↓ ↑ TA ↓	−1.80	−4.60

[a] The parameters $\epsilon_i{}'$(exp) include hypochromism contributions from high-energy monomer transitions and solvent transitions.

is therefore significant, and the probability that such a degree of correspondence is exhibited fortuitously is very small.

There is nevertheless significant scatter in the results shown in Table I. The three most likely sources of this scatter, however, can all be treated by further refinements in the calculations.

(1) The contribution to the hypochromism from high-energy monomer transitions and from solvent transitions is not included in the TDH calculations. Some of the scatter in Table I could come from a base sequence dependence in these contributions. It is possible to calculate these contributions in terms of macroscopic polarizabilities, but a first-order perturbation description of this coupling is probably not adequate, and the inclusion of these polarizabilities in the framework of a TDH study of the sequence dependence has not yet been carried out. Such a refinement is nevertheless feasible and could in fact be the first step in determining the solvent contribution to hypochromism in less structured polynucleotides.

The correspondence we find between our TDH calculations and the experimental data nevertheless indicates that the sequence dependence in the omitted terms is smaller than the sequence dependence in the terms we

have included. The solvent sphere around double-stranded polynucleotides in the B conformation is probably similar for all sequences, and the bases are furthermore separated from the solvent sphere by the phosphate and sugar moieties. Of the two types of term omitted, therefore, there is probably more sequence dependence in the contributions from the high-energy monomer states than from the solvent states.

(2) The monomer basis set we used is accurate enough to describe some of the sequence dependence observed, but part of the remaining scatter that is observed could arise from the inaccuracy of these wave functions, and it may be that future refinements in the basis set would decrease the scatter.

The choice of monomer basis set affects the polymer calculations in several ways. First, the choice establishes the number of electronic transitions in each monomer between 190 and 280 nm and the transition energies. The basis set must be chosen to be consistent with all experimental absorption data available for the monomers. Usually, as in our own calculations, the monomer basis is scaled to reproduce the magnitude of each transition moment. As additional experimental data on nucleotide bases become available the very number of low energy transitions assigned to a given base could change.[11]

Furthermore, the basis set determines the distributed monopoles used to evaluate the interaction potential. Some indication of the accuracy of the basis set can be established by comparing the transition moment directions calculated from the selected basis set with experimentally determined transition moment directions, but a unique set of monopoles cannot be derived directly from the experimental directions. That is, only a consistency can at best be shown. The alternative, however, is to describe the interaction potential in the point dipolar approximation which in the case of these relatively closely stacked bases is less likely ever to be adequate.

(3) These calculations have been carried out for double-stranded polynucleotides in the B-conformational form of fibrous DNA lithium salt with base pairs in planes perpendicular to the tenfold screw axis and separated by 3.36 Å. Comparing the results with experimental data, as is done in Table I, carries an implicit assumption that the data correspond to the same polynucleotide structure. Peticolas, et al.,[12-14] concluded (from their laser Raman work) that the polydeoxyribonucleotides they studied do not take up the A conformation, since the Raman band near 800 cm^{-1} characteristic of the A conformation is never observed in these cases. It is possible, however, that some polydeoxyribonucleotides take up variants of the B conformation, such as the D conformation,[15] under some experimental conditions in solution. Such a case would lead to some scatter in Table I. However, the work of Ivanov, et al.,[15] indicates that variants of the B conformation have very similar absorption characteristics near 260 nm.

Conclusions

We have shown by a direct comparison with experimental data that time-dependent Hartree calculations of DNA hypochromism are accurate enough to show some of the sequence dependence that is experimentally observed. The same conclusion is reached when calculated and experimental results are compared indirectly, in that both sets of results can be parameterized in terms of the contributions from nearest-neighbor paired base pair interactions to give somewhat similar parameters.

References and Notes

(1) (a) E. Brown and E. S. Pysh, *J. Chem. Phys.*, **56**, 31 (1972); (b) E. Brown, Ph.D. Thesis, Brown University, April 1971.
(2) E. S. Pysh and J. L. Richards, *J. Chem. Phys.*, **57**, 3680 (1972).
(3) C. R. Cantor and I. Tinoco, *J. Mol. Biol.*, **13**, 65 (1965).
(4) W. C. Johnson and I. Tinoco, *Biopolymers*, **7**, 727 (1969).
(5) D. M. Gray and I. Tinoco, *Biopolymers*, **9**, 223 (1970).

(6) F. S. Allen, D. M. Gray, G. P. Roberts, and I. Tinoco, *Biopolymers*, **11**, 853 (1972).
(7) A. S. Schneider and R. A. Harris, *J. Chem. Phys.*, **50**, 5204 (1969).
(8) W. Rhodes and M. Chase, *Rev. Mod. Phys.*, **39**, 348 (1967).
(9) W. Rhodes, *J. Chem. Phys.*, **53**, 3650 (1970).
(10) D. Voet, W. B. Gratzer, R. A. Cox, and P. Doty, *Biopolymers*, **1**, 193 (1963).
(11) H. Chen and L. B. Clark, *J. Chem. Phys.*, **58**, 2593 (1973).
(12) E. W. Small and W. L. Peticolas, *Biopolymers*, **10**, 1377 (1971).
(13) S. C. Erfurth, E. J. Kiser, and W. L. Peticolas, *Proc. Nat. Acad. sci. U. S.*, **69**, 938 (1972).
(14) K. G. Brown, E. J. Kiser, and W. L. Peticclas, *Biopolymers*, **11**, 1855 (1972).
(15) V. I. Ivanov, L. E. Minchenkova, A. K. Schyolkina, and A. I. Poletayev, *Biopolymers*, **12**, 89 (1973).

Laser Flash Photolysis of Substituted Stilbenes in Solution

D. V. Bent* and D. Schulte-Frohlinde

Institut für Strahlenchemie im Max-Planck-Institut für Kohlenforschung. D-4330 Mulheim an der Ruhr. West Germany
(Received September 4, 1973)

Laser flash photolysis of nitro-substituted stilbenes (4-nitrostilbene, 4,4'-dinitrostilbene, 4-nitro-4'-methoxystilbene, and 4-nitro-4'-dimethylaminostilbene) permits the observation of transients. The lifetimes of the transients (around 100 nsec) and their spectra vary strongly with the polarity of the solvent for 4-nitro-4'-methoxystilbene and for 4-nitro-4'-dimethylaminostilbene, but less so for the other nitrostilbenes. No transients were observed from 4-cyano-4'-dimethoxystilbene, 4,4'-dimethoxystilbene, 4-aminostilbene, and 4,4'-diaminostilbene. It is assumed that the transients are the triplet states of the nitrostilbenes. This is supported by the fact that (1) the transients of the nitrostilbenes are quenched at a diffusion-controlled rate by such triplet quenchers as oxygen, azulene, and ferrocene, (2) the transient from 4-nitro-4'-dimethylaminostilbene is formed by interaction with the triplet state of triphenylene (rate constant for the energy transfer $k = 8 \times 10^9 \ M^{-1} \ sec^{-1}$, and (3) the lifetime of the transient from 4-nitro-4'-methoxystilbene is identical with the lifetime of the expected triplet intermediate derived from the influence of added quenchers (azulene or ferrocene) on the position of the cis–trans photostationary state (*cf.* subsequent paper). Under our experimental conditions the transients produced from the cis and the trans form of 4-nitro-4'-methoxystilbene and two other nitrostilbenes have identical spectra and lifetimes. The λ_{max} values of the transients produced in nonpolar liquid solvents show a blue shift in comparison to the values measured in the glassy state in EPA at 77°K. The λ_{max} values of nitronaphthalene and other nitroaromatics do not show this shift. In agreement with Dainton, *et al.*, this result is explained by assuming that the triplet intermediate may be in a somewhat more twisted form in the liquid than it is in the glass state.

Introduction .

The triplet states of stilbenes were first observed in absorption in 1967[1] and 1968[2] in glassy frozen solutions at 77°K. Recently, Dainton, *et al.*,[3] were able to show by nanosecond pulse radiolysis studies that the triplet state of stilbene has a lifetime of about 100 nsec in benzene solutions.

However, we have been unable to observe the triplet state of stilbene in solution by flash photolysis. The purpose of this paper is to show that it is possible to observe transients of stilbenes with the laser flash photolysis technique if the stilbene molecule has at least one nitro group as substituent.

It is the property of nitro groups to enhance the $S_1 \rightarrow T$ transition rate without changing the $T \rightarrow S_0$ transition rate appreciably[4] and it is probably this property which allows the transient to appear. In the absence of nitro groups in the stilbene molecule no transient was observable with our technique.

Experimental Section

The laser photolysis system (Applied Photophysics, London) consisted of a frequency doubled ruby laser emitting a single 30-nsec pulse of about 50 mJ intensity at 347 nm. By means of a beam splitting prism analyzing light from a pulsed 250-W xenon lamp was focused onto the reaction cell collinearly with the laser pulse. After passing through a Jarrell-Ash ¼-m monochromator the change in analyzing light intensity was monitored by means of an 1 P 28 or R 406 (red sensitive) photomultiplier and the sig-

nal was fed to a Textronix 549 storage oscilloscope. Experiments were carried out in degassed or argon-saturated solutions using 1- or 2-cm path lengths.

The low-temperature conventional flash photolysis apparatus will be described elsewhere.[5] All measurements were made using the single-wavelength kinetic technique. Typical energies used were 400 J and the shortest time that observations could be made was 1 msec after the flash at 77°K.

Materials. *trans*-Stilbenes were prepared by standard methods involving a piperidine-catalyzed condensation of the 4-substituted phenylacetic acid with the appropriate aromatic aldehyde[6,7] or in the case of 4,4′-dinitrostilbene by reaction of 4-nitrobenzylchloride with alcoholic KOH.[8] Purification was by two recrystallizations from glacial acetic acid and then from ethanol. The cis isomers were prepared by irradiation of the *trans*-stilbenes followed by separation on a neutral alumina column and then recrystallization.

A magnesium oxide column was found to give a better separation of *cis*-4,4′-dinitrostilbene. All solvents used in the results section were analytical reagent grade. In addition, ethanol was dried by distillation over magnesium ethoxide. Azulene was sublimed twice under vacuum and other reagents were purified by several recrystallizations.

Results

The nitro-substituted stilbenes have strong absorptions in the region of 347 nm and are therefore well suited for study with frequency-doubled light from a ruby laser. It was found that laser irradiation at 347 nm of 4,4′-dinitrostilbene, 4-nitrostilbene, 4-nitro-4′-methoxystilbene, and 4-nitro-4′-dimethylaminostilbene produced strongly absorbing short-lived transients in each case. Both the cis and the trans isomers of the first three stilbenes were studied. The cis and the trans forms yielded identical transient spectra. From 4-nitro-4′-dimethylaminostilbene only the trans isomer was studied. Experiments in various solvents have revealed that as the intramolecular charge-transfer character of the stilbene is increased then an increasingly large effect of solvent polarity on the lifetime and position of the transient absorption spectra occurs.

Transient Spectra. (a) In Liquid Solvents. Figure 1 (curve a) shows the transient absorption spectrum produced from *trans*- or *cis*-4,4′-dinitrostilbene in cyclohexane at room temperature. The absorption maximum and the shape of the spectrum (λ_{max} 500 nm) was found to be insensitive to solvent polarity. Irradiation of *trans*-4-nitrostilbene in cyclohexane produced a transient absorbing at 540 nm (Figure 2, curve a). The absorption maximum was shifted 20 nm to higher values in dimethylformamide. However, when a nitrostilbene containing a strongly electron donating group as in *trans*- or *cis*-4-nitro-4′-methoxystilbene was irradiated, the transient spectra produced showed substantial differences between nonpolar and polar solvents (Figure 3, curves a and c).

An absorption band centered at 600 nm was observed in nonpolar solvents but in polar solvents an absorption at 600 nm together with an additional much larger absorption with a maximum around 700 nm was observed. Only approximate values were obtained for the absorbance in the region 600–710 nm because of scattered light problems due to the inability to filter out completely all of the 694-nm laser fundamental.

Irradiation of *trans*-4-nitro-4′-dimethylaminostilbene in cyclohexane produced a transient absorption with a maxi-
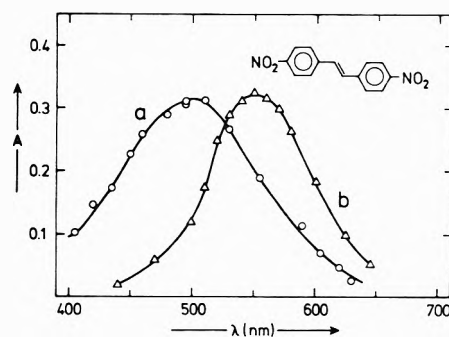

Figure 1. Transient absorption spectra obtained from irradiated *trans*-4,4′-dinitrostilbene: a (O), in cyclohexane or methanol at room temperature; b (△), in an EPA glass at 77°K.
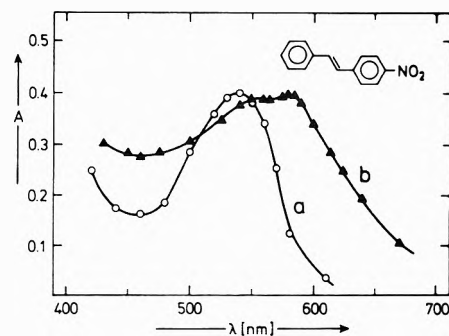

Figure 2. Transient absorption spectra obtained from irradiated *trans*-4-nitrostilbene: a (O), in cyclohexane at room temperature; b (▲), in an EPA glass at 77°K.
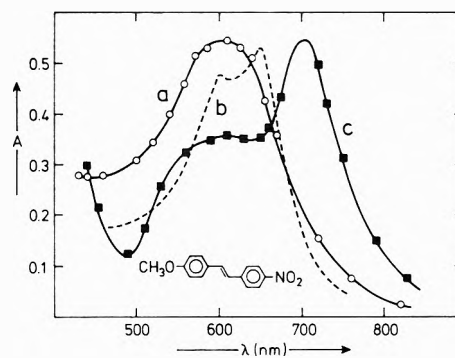

Figure 3. Transient absorption spectra obtained from irradiated *trans*-4-nitro-4′-methoxystilbene: a (O), in cyclohexane; c (■), in methanol at room temperature; and b (- - - -), in an *n*-pentane /2,2-dimethylbutane (3:8) glass at 77°K.

mum at 735 nm and evidence of a shoulder around 650 nm (Figure 4, curve a). This transient absorption was shifted strongly in benzene solution to give a spectrum with a maximum at 800 nm and a shoulder at 745 nm. However, irradiation in polar solvents failed to produce any observable transients. This problem was overcome by means of triplet energy transfer experiments using triphenylene as the sensitiser. Degassed solutions of 10^{-2} M triphenylene in dimethylformamide were irradiated at 347 nm in the presence of 4-nitro-4′-dimethylaminostilbene in various concentrations in the range 5×10^{-5} to 5×10^{-4} M. Under these conditions triphenylene absorbs most of the laser energy at 347 nm. The growth of a strongly absorbing transient having maxima at 820 and 910 nm was observed and the rate of its growth was found to increase with increasing stilbene concentration. From these data a value for the second-order rate constant of transient for-
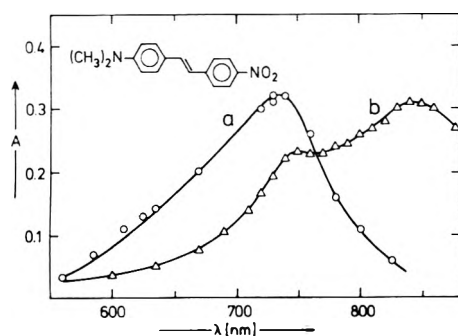
Figure 4. Transient absorption spectra obtained from irradiated *trans*-4-nitro-4'-dimethylaminostilbene: a (O), in cyclohexane at room temperature; b (△), in an *n*-pentane/2,2-dimethylbutane (3:8) glass at 77°K.

Figure 5. Transient absorption spectra obta ned from irradiated 4-nitrobiphenyl: a, (O) in benzene; b (✕), in dimethylformamide at room temperature; c (- - - -), in an EPA glass.

mation of 8×10^9 M^{-1} sec^{-1} was calculated. Unfortunately, no comparative observations of the triphenylene triplet absorption at 428 nm could be made because of the high stilbene ground-state absorption at this wavelength. If triphenylene alone was irradiated in dimethylformamide no absorbing species were observed in the 700–900-nm region. In order to show that the transient produced by sensitization is of the same nature as that produced on direct irradiation of the stilbene an energy transfer experiment, again using triphenylene as the sensitizer and 4-nitro-4'-dimethylaminostilbene as acceptor, was performed in benzene solution. Concentrations were adjusted so that the triphenylene absorbed over 80% of the laser energy at 347 nm. The growth of a transient intermediate was observed which had an absorption spectrum and lifetime exactly the same as that observed immediately after the laser flash in experiments involving irradiation of the stilbene directly in the absence of sensitizer.

(*b*) *Spectra in Glassy Matrices at 77°K*. In order to obtain further information regarding the nature of the transients, conventional flash photolysis experiments in EPA and *n*-pentane 2,2-dimethylbutane (3:8) glasses at 77°K were carried out.

The long-lived transient absorptions produced from the trans isomers of each stilbene are shown in Figures 1–4, curves b. No difference in the transient absorption spectra was observed in *trans*-4-nitro-4'-dimethylaminostilbene on changing from the hydrocarbon glass to EPA. Similarly, a comparison with the literature[1] shows that there is no difference between the transient absorption spectra from *trans*-4-nitro-4'-methoxystilbene in the two glasses. Flash photolysis of the cis isomer of 4,4'-dinitrostilbene in an EPA glass produced no transient absorption, in agreement with similar observations with *cis*-stilbene[1] and *cis*-4-nitro-4'-methoxystilbene.[1] Owing to scattered light problems, we were unable to make observations at times under a millisecond and so we cannot rule out the possibility that a transient having a shorter lifetime may still be produced from the cis isomer.

The shift of the transient spectra to longer wavelengths in the glassy matrices at 77°K (Figures 1–4) is unusual and we therefore decided to see whether a similar shift occurred in the triplet absorption spectrum of 4-nitrobiphenyl, a compound which has no ethylenic double bond. In an EPA glass at 77°K a long-lived transient with absorption peaks at 520 and 550 nm was observed (Figure 5, curve c). The decay of the 4-nitrobiphenyl phosphorescence at 490 nm[9] matched that of the transient absorption decay, thus indicating that the absorption was due to a
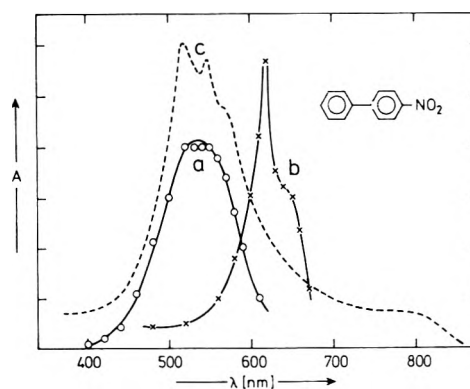
triplet state. In laser absorption studies of 4-nitrobiphenyl at room temperature a very short-lived transient (lifetime ∼ 10 nsec) was observed in benzene solutions. The transient absorption spectrum (Figure 5, curve a) had a λ_{max} at 540 nm and was at the same position as the absorption observed in the glasses. Since there is no appreciable difference, other than fine structure, in the absorption spectra observed in benzene and in the glass it seems fairly certain that the short-lived transient observed in benzene is the triplet state of 4-nitrobiphenyl. Furthermore, there is no red shift between the spectra in the glass and the liquid. Laser irradiation of 4-nitrobiphenyl in polar solvents also produced short-lived transients but the absorption spectra of these transients were substantially shifted to higher wavelengths. Figure 5, curve b shows the transient absorption spectrum with λ_{max} at 620 nm, observed in dimethylformamide.

Transient Lifetimes. (*a*) *Nitro-Substituted Stilbenes.* The measured reaction rate constants for the decay of transients are summarized in Table I. An increase in lifetime (by lifetime we mean the reciprocal of the first-order rate constants in Table I) of the transients was produced with 4,4'-dinitrostilbene and 4-nitrostilbene on increasing the solvent polarity; *e.g.*, for *trans*-4,4'-dinitrostilbene the lifetime of the transient is 80 nsec in cyclohexane and 208 nsec in dimethylformamide.

However, in the case of *trans*-4-nitro-4'-methoxystilbene the transient lifetime, 90 nsec in cyclohexane, increased more strongly with solvent polarity so that it reached a value of 570 nsec in dimethylformamide. In glycerol a combination of solvent polarity and viscosity combined to lengthen the transient lifetime of *trans*-4-nitro-4'-methoxystilbene to 6.2 μsec.

The values in Table II show that an even stronger solvent effect was observed in *trans*-4-nitro-4'-dimethylaminostilbene. As previously explained, no transient species were observed on direct irradiation in ethanol or dimethylformamide but these could be produced by sensitization experiments using triphenylene.

If the observed transients are triplet states then they should be strongly quenched by oxygen. The values of the second-order rate constants obtained in air-saturated benzene solutions assuming $[O_2]$ = 1.63 $\times$ 10^{-3} M[10] are shown in Table II. These values represent diffusion-controlled rates.

Additional quenching experiments using various concentrations of azulene and ferrocene were carried out on the transient produced from 4-nitro-4'-methoxystilbene. Second-order quenching rate constants of 6.0 $\times$ 10^9 M^{-1}

TABLE I: First-Order Rate Constants $(k_1 \times 10^{-6} \text{ sec}^{-1})$ **for the Decay of Transient Intermediates in the Laser Flash Photolysis of** *cis-* **and** *trans-***Nitro-Substituted Stilbenes in Various Solvents at Room Temperature**[a]

	4-NO$_2$ stilbene		4-NO$_2$-4'-NO$_2$ stilbene		4-NO$_2$-4'-OCH$_3$ stilbene		4-NO$_2$-4'-N(CH$_3$)$_2$ trans
	Cis	Trans	Cis	Trans	Cis	Trans	
Cyclohexane	13	16	12.1	12.5	12.3	11.3	2.3
Benzene	12	15		9.8	8.0	7.2	0.48
Ethanol			9.6	9.2	3.6	3.5	0.25[b]
Methanol	12	12				3.0	
Dimethylform-amide	8.9	9.6	5.1	4.8	1.75	1.75	0.047[b]

[a] All values are subject to an error of up to 10%. [b] Values obtained from transients produced by triplet energy transfer from triphenylene.

sec^{-1} and 4.5×10^9 M^{-1} sec^{-1} for azulene and ferrocene, respectively, were obtained in benzene solutions.

(b) *Stilbenes Substituted with Groups Other Than the Nitro Group.* Stilbenes substituted with polar groups other than NO$_2$ fail to give any observable transient intermediates in the region 400–800 nm. The stilbenes studied include 4-methoxystilbene, 4,4'-dimethoxystilbene, 4-aminostilbene, 4,4'-diaminostilbene, and 4-cyano-4'-methoxystilbene. *trans*-Stilbene absorbs very weakly at 347 nm and no transient was observed above 400 nm. With our present detection configuration we are unable to observe below 400 nm, the region where the triplet state of the unsubstituted stilbene absorbs.[1-3] However, we should have been able to observe the triplet states of 4-methoxystilbene (λ_{max} 400 nm in EPA at 77°K) and of 4-cyano-4'-methoxystilbene.

Irradiation of a 1.0 M solution of *cis*-stilbene in benzene gave only a long-lived absorption centered around 450 nm. It was formed during the laser flash and is attributed to dihydrophenanthrene. We have also noted that laser irradiation of azobenzene and several nitroazobenzenes has failed to produce any observable short-lived transients.

Other Nitroaromatics. In the absence of phosphorescence data from the stilbenes it is important to observe and identify the triplet states of nitroaromatic molecules in solution so that a comparison with the nitrostilbene transients can be made. Kanamaru, *et al.*,[11] have shown in the case of 1-nitronaphthalene and 2-nitronaphthalene that the short-lived transients observed in liquids are indeed triplet states. They also state that no difference in absorption between EPA glasses and liquids was observed. We have determined the lifetime of the 1-nitronaphthalene triplet as 1.5 μsec in cyclohexane and 3.5 μsec in methanol. In order to have a further example we chose to study 4-nitrobiphenyl. In benzene solutions an extremely short-lived transient with a lifetime of about 10 nsec was observed at 540 nm (Figure 5). However, in dimethylformamide the transient absorption shifted to 620 nm and the lifetime increased to 50 nsec.

Discussion

(a) *Nature of the Transients.* We should discuss first the nature of the observed transients. Since the transients are only observed when nitro groups are present in the molecule, it has to be considered what the influence of the nitro group could be. From spectroscopic investigations it is known that nitro groups enhance the rate of the $S_1 \rightarrow T_1$ transition in nitroaromatics so that very often only phosphorescence and no fluorescence is observed. Saltiel, *et al.*,[12] have shown that the photochemical cis–trans isomerization of stilbenes proceeds *via* a single route in liquid solvents. Therefore we would not expect to observe a triplet in solution. However, in the presence of nitro

TABLE II: Second-Order Rate Constant (k_{O_2}) **for the Quenching by Oxygen of the Transients Produced in the Laser Flash Photolysis of Nitro-Substituted Stilbenes in Benzene**[a]

	$k_{O_2} \times 10^9$ M^{-1} sec^{-1}
4-NO$_2$ stilbene	7.0
4-NO$_2$-4'-NO$_2$ stilbene	6.0
4-NO$_2$-4'-OCH$_3$ stilbene	6.8
4-NO$_2$-4'-N(CH$_3$)$_2$ stilbene	5.3

[a] All values are subject to an error of up to 20%.

groups as substituents it is possible that the $S_1 \rightarrow T_1$ transition is enhanced to such a degree that triplet states are populated.

On the other hand, nitroaromatics are photochemically active compounds and can undergo a variety of different photochemical reactions.[13] Therefore two possibilities exist. The transient could be a triplet state or a photochemical intermediate of an unknown nature.

For the following reasons we assume that the transients are triplet states.

1. The transients of stilbene and 4-nitro-4'-methoxystilbene observed by the flash photolysis technique in glassy matrices at 77°K have previously been identified as triplet states.[1,2] The spectrum of the transient we observed from 4-nitro-4'-methoxystilbene in a nonpolar liquid solvent has a similar shape and absorption maximum (shift 50 nm) as in the frozen solution. The other three nitrostilbenes studied gave similar results.

2. Triplet states should be quenched by oxygen and by compounds with lower lying triplet states. Indeed we observed diffusion-controlled quenching of all transients by oxygen (Table II). Quenching studies with azulene and ferrocene on 4-nitro-4'-methoxystilbene also revealed quenching at a diffusion-controlled rate. Ferrocene[14] and azulene[12] are known triplet quenchers.

3. The transient obtained from 4-nitro-4'-dimethylaminostilbene by direct excitation can also be obtained by triplet sensitization employing triphenylene as a triplet sensitizer.

4. No photochemical reactions other than cis–trans isomerization and cyclization leading to dihydrophenanthrene have been observed in nitrostilbenes. The quantum yields for the photocyclization are very low for 4-nitrostilbene ($\phi \sim 0.0007$) and 3-nitrostilbene ($\phi < 0.0001$).[15] They are around three orders of magnitude lower than the values obtained for 3-aminostilbene ($\phi = 0.28$).[15] From this it follows that in the nitrostilbenes the illumination does not lead to a free radical intermediate because otherwise further photochemical products should have been found.

5. The photostationary states of the cis and the trans form of the four nitrostilbenes mentioned in this paper are strongly influenced by the addition of azulene and ferrocene. Assuming that an intermediate is quenched at a diffusion-controlled rate one should be able to calculate the lifetime of such an intermediate. If we take as rate constants for the quenching the values obtained by laser photolysis for the quenching of the transient from 4-nitro-4'-methoxystilbene, then the calculated lifetimes of the intermediate are in good agreement with the directly measured values (for a detailed discussion of this point see the following paper[16]). This result provides evidence that the observed transients are intermediates in the photochemical cis-trans isomerization of the nitrostilbenes.

(b) *Is the Transient a Common Intermediate Reached from the Cis and the Trans Form?* The question if the transients are really common intermediates as the experimental results suggest (formation of the same transient from the cis and the trans form) is still open to doubt since it seems possible that during the laser flash the cis form is converted to the trans form and the trans form after absorbing a further light quantum produces the transient. The laser flash has enough quanta to do so. This would mean that the cis → trans isomerization has to be a very fast process; otherwise not enough trans form is produced from the cis form during the duration of the laser flash ($\sim$ 30 nsec). Further investigations are in progress to clarify this point.

Mechanism of the Cis → Trans and the Trans → Cis Isomerization. It is very likely that the cis → trans isomerization of substituted stilbene occurs in the excited singlet state by rotation about the C=C double bond since the lifetime of the excited singlet state of the cis form is extremely short[17] and it is most unlikely that during that time a S_1 → T transition can occur. The reason for the short lifetime of the cis form in the excited singlet state is believed to be the steepness of the potential curve as calculated from Borrel and Greenwood[18] for unsubstituted stilbene, in contrast to the flat minimum in the excited singlet trans form. It is probable that the same holds for the nitrostilbenes despite the fact that the nitro groups enhance the S_1 → T transition. This means that the rotation in the cis → trans photoisomerization of the nitrostilbenes occurs in the excited singlet state and the rotation in the trans → cis isomerization after S_1 → T transition in the triplet state. For a more detailed discussion of this point see the following paper.[16]

Substituent and Solvent Shift of the Transient Absorption. The S_0 → S_1 absorption of stilbene spectra depends on the degree of the internal charge-transfer properties introduced to the molecules by the substituents. A similar but larger shift is observed for the transient absorption as a function of substitution (Figures 1-4). In order to explain this strong solvent shift it seems possible to assume that a change in dipole moment occurs during excitation. However, in the case of 4-nitro-4'methoxystilbene and 4-nitro-4'-dimethylaminostilbene the solvent shift of the transients is unusually large and is accompanied by a

change in the shape of the spectra. In order to explain the solvent shift of the position of the photostationary state of this class of compounds, Fischer and coworkers[19] assumed that the lowest triplet state changes from (n,π^*) to (π,π^*) in character as the solvent polarity increases. More experimental facts are needed for a detailed interpretation.

Comparison of Transient Spectra in Liquid and Frozen Solutions. The absorption spectra of the transients of nitroaromatic compounds which are believed to be triplet states[11] are not strongly shifted on going from liquid solvents at room temperature to amorphous frozen glassy solutions at 77°K (for our own experiments see Figure 5). The behavior of the transient spectra of the nitrostilbenes, however, is somewhat different. In solid matrices the absorption maxima are found at longer wavelength than the corresponding spectra in nonpolar liquid solvents. A similar observation has been made with the triplet state of the unsubstituted stilbene. In frozen solution in EPA at 77°K the triplet of stilbene has an absorption maximum at 379 nm.[1] Dainton and coworkers[3] observed the absorption spectrum of the triplet stilbene at 350-360 nm in liquid benzene at room temperature. The solvent polarity is not expected to have an influence on the absorption maximum in this case. Dainton, *et al.*,[3] suggested that this shift is due to a greater twisting about the double bond of triplet stilbene in liquid benzene as compared with the frozen solution. This is in accordance with calculations of Borrell and Greenwood[18] which showed that the twisted form should absorb at shorter wavelength. If we make identical assumptions then we can only conclude that the triplet states of the *trans*-nitrostilbenes are indeed more twisted in the liquid state than in frozen solution.

References and Notes

(1) G. Heinrich, H. Blume, and D. Schulte-Frohlinde, *Tetrahedron Lett.*, **47**, 4693 (1967).
(2) W. G. Herkstroeter and D. S. McClure, *J. Amer. Chem. Soc.*, **90**, 4522 (1968).
(3) F. S. Dainton, E. A. Robinson, and G. A. Salmon, *J. Phys. Chem.*, **76**, 3897 (1972).
(4) S. P. Mc Glynn, R. Ajumi, and M. Kinoshita, "Molecular Spectroscopy of the Triplet State," Prentice-Hall, Englewood Cliffs, N. J., 1969, pp 251-266.
(5) S. Toki and D. Schulte-Frohlinde, to be published.
(6) P. Pfeiffer, *Ber. Deut. Chem. Ges.*, **48**, 1777 (1916).
(7) G. Riezebos and E. Havinga, *Recl. Trav. Chim.*, **80**, 446 (1961).
(8) P. Walden and K. Kernbaum, *Ber. Deut. Chem. Ges.*, **23**, 1958 (1890).
(9) D. S. McClure, *J. Chem. Phys.*, **17**, 905 (1949).
(10) Landolt-Bornstein, "Zahlenwerte und Functionen," New Series, Group II, Vol. 3, Springer-Verlag, Berlin, 1967, p 302.
(11) N. Kanamaru, S. Okajima, and K. Kimura, *Bull. Chem. Soc. Jap.*, **45**, 1273 (1972).
(12) J. Saltiel and E. D. Megarity, *J. Amer. Chem. Soc.*, **94**, 2742 (1972).
(13) O. L. Chapman, *et al.*, *J. Pure Appl. Chem.*, **9**, 585 (1964).
(14) G. S. Hammond and P. A. Leermakers, *J. Phys. Chem.*, **66**, 1148 (1962).
(15) H. Jungmann, H. Gusten, and D. Schulte-Frohlinde, *Chem. Ber.*, **101**, 2690 (1968).
(16) D. V. Bent and D. Schulte-Frohlinde, *J. Phys. Chem.*, **78**, 451 (1974).
(17) D. Schulte-Frohlinde, H. Blume, and H. Gusten, *J. Phys. Chem.*, **66**, 2486 (1962).
(18) P. Borrel and H. H. Greenwood, *Proc. Roy. Soc.*, *Ser. A*, **298**, 453 (1967).
(19) D. Gegiou, K. A. Muszkat, and E. Fischer, *J. Amer. Chem. Soc.*, **90**, 3907 (1968).

Evidence for the Triplet Route in the Photochemical Trans → Cis Isomerization of Nitrostilbenes in Solution

D. V. Bent* and D. Schulte-Frohlinde

Institut fur Strahlenchemie im Max-Planck-Institut fur Kohlenforschung. D-4330 Mulheim an der Rhur. West Germany
(Received September 4, 1973)

Added azulene or ferrocene shift the position of the photostationary state in the photochemical cis–trans isomerization of 4-nitro-4'-methoxystilbene, 4-nitrostilbene, and 4,4'-dinitrostilbene in solution toward the trans form. These shifts occur at concentrations well below the beginning of the fluorescence quenching. No such influence is observed for 4-cyano-4'-methoxystilbene. From these results it is concluded that the photochemical trans → cis isomerization of nitrostilbenes occurs *via* triplet states as intermediates. The lifetime of the intermediate from 4-nitro-4'-methoxystilbene measured directly by laser flash photolysis matches the lifetime calculated from the effects of azulene and ferrocene on the photostationary state assuming a triplet route for the trans → cis isomerization and a singlet route for cis → trans isomerization. There is no common intermediate in the direct trans → cis and the cis → trans isomerization of the nitrostilbenes.

Introduction

With the help of the triplet quenching technique, Saltiel and coworkers[1] have shown that the photochemical cis–trans isomerization of stilbene in solution occurs *via* a singlet route since no long-lived triplet intermediate could be detected. We applied these techniques to study the isomerization of 4-nitrostilbene, 4,4'-dinitrostilbene, 4-nitro-4'-methoxystilbene, and 4-cyano-4'-methoxystilbene because laser flash photolysis studies[2] have shown that transients are formed from the nitrostilbenes which could not be found, *e.g.*, in 4-cyano-4'-methoxystilbene and other stilbenes not containing nitro groups. In this paper it will be shown that the observed transients are, indeed, intermediates in the direct trans → cis isomerization of the nitrostilbenes.

Experimental Section

The steady-state irradiation employed an HBO 200 W/4 high-pressure Hg lamp. The 366-nm line of the radiation was isolated by means of the following combination: a Schott glass filter 2 W-PIL gave over 1% transmission only in the range 366 ± 15 nm. A gray filter of 10% transmittance was employed to reduce the light intensity further.

Optical absorbance measurements were made at regular intervals up to and after photoequilibrium using a Zeiss PMQ II spectrophotometer. Stilbene concentrations employed were $\sim 10^{-5}$ M and the samples were irradiated in standard 1-cm cells containing ~ 4 ml of solution. The optical density of pure azulene and ferrocene did not change during the irradiation time indicating that no strong photodecomposition of the quencher occurred. Samples were argon or oxygen saturated by bubbling with solvent-saturated gas for 30 min and where necessary corrections were made for any small solvent losses incurred. The oxygen content of the solution has no influence on the photostationary state.

At the light intensities employed equilibrium was reached in 40–60 min and in all cases further irradiation for 3 hr produced no change in this equilibrium value. Dihydrophenanthrene formation occurs apparently with very small quantum yields and was not taken into consider-ation in the calculations. (For a listing of the materials used, refer to the preceding article.[2])

Results and Discussion

Effect of Triplet Quenchers on the Position of the Photostationary State. Hammond, *et al.*,[3] have shown that by the addition of small amounts of azulene it is possible to alter the position of the photostationary state of stilbene isomerization when this is induced by means of triplet sensitization. In all cases the final mixture becomes richer in *trans*-stilbene. The effect of azulene on the position of the photostationary state induced by direct irradiation of the stilbene is small by comparison and is assumed to be due to singlet quenching.[1] If substituents which enhance intersystem crossing such as the nitro group are introduced into the molecule, a triplet mechanism for the trans → cis photoisomerization becomes possible.[1,2,4] We have therefore studied the effect of different quenchers on the position of the photostationary state of several nitro-substituted stilbenes. Isomerization was induced by direct irradiation of the stilbenes.

(a) *Effects of Oxygen.* We initially studied the effect of oxygen on the position of the photostationary state of 4-nitro-4'-methoxystilbene and 4,4'-dinitrostilbene. The solvent employed was benzene and it was found that argon, air (1.6×10^{-3} M), or oxygen (8×10^{-3} M) saturated solutions yielded identical photostationary states. In the preceding paper[2] it was shown that oxygen is able to quench strongly the lifetime of the triplet transients of the nitrostilbenes.

(b) *Effects of Azulene and Ferrocene.* These two molecules are known to be good quenchers of triplet states and furthermore they have a "window" in their absorption spectra around 400 nm. Since the nitrostilbenes absorb strongly in this region it has been possible to study the photoisomerization changes by optical absorption methods in the presence of azulene. In each case irradiation was at 366 nm.
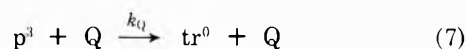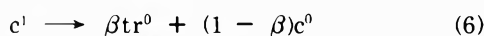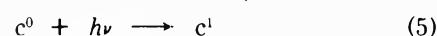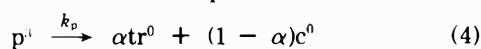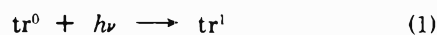
Ferrocene and azulene were both found to quench strongly the position of the photostationary state of 4-

nitro-4'-methoxystilbene in argon-saturated benzene solutions. In Figure 1, the percentage of cis isomer in the photostationary state is plotted against ferrocene concentration; equilibrium was approached from the trans side. In order to show that this observation was not due to singlet quenching we carried out a study of the effect of ferrocene on the quantum yield of fluorescence of *trans*-4-nitro-4'-methoxystilbene in air-saturated benzene. The fluorescence was quenched by ferrocene, but as can be seen in Figure 1 this effect occurs at much too high a concentration to account for the observed effect on the position of the photostationary state. The added ferrocene therefore can only be interacting with a long-lived intermediate in order to influence the position of the photostationary state.

(c) *Triplet Mechanism.* Previous work on the sensitized photoisomerization of stilbene has indicated that the reaction proceeds *via* a common twisted intermediate known as "phantom triplet."[3] In the direct trans → cis photoisomerization of nitro-substituted stilbenes a triplet pathway may predominate. Two possibilities are discussed.

In mechanism A the cis → trans isomerization occurs *via* a singlet pathway, that is the cis → trans isomerization occurs by rotation about the C=C double bond in the excited singlet state, and when a twisting angle of 90° is reached radiationless deactivation leads *via* the potential curve of the singlet ground state to the cis and trans ground state. The first step of the trans → cis isomerization is an S_1 → T transition before rotation has set in. The rotation about the C=C double bond then proceeds in the triplet state which is assumed to have the lowest energy minimum at an angle of 90°. From this point a radiationless transition to the singlet ground state occurs, and by following the singlet ground-state potential curve the cis and the trans ground state at 180 and 0° is reached. These assumptions lead to Scheme A.

Scheme A

$$tr^0 + h\nu \longrightarrow tr^1 \tag{1}$$

$$tr^1 \longrightarrow tr^3 \tag{2}$$

$$tr^3 \longrightarrow p^3 \tag{3}$$

$$p^3 \xrightarrow{k_p} \alpha tr^0 + (1 - \alpha)c^0 \tag{4}$$

$$c^0 + h\nu \longrightarrow c^1 \tag{5}$$

$$c^1 \longrightarrow \beta tr^0 + (1 - \beta)c^0 \tag{6}$$

$$p^3 + Q \xrightarrow{k_Q} tr^0 + Q \tag{7}$$

In mechanism B it is assumed that the trans → cis and the cis → trans isomerization occurs *via* a common triplet intermediate. This assumption leads to Scheme B. In this

Scheme B

$$tr^0 + h\nu \longrightarrow tr^1 \tag{1}$$

$$tr^1 \longrightarrow tr^3 \tag{2}$$

$$tr^3 \longrightarrow p^3 \tag{3}$$

$$p^3 \xrightarrow{k_p} \alpha tr^0 + (1 - \alpha)c^0 \tag{4}$$

$$c^0 + h\nu \longrightarrow c^1 \tag{5}$$

$$p^3 + Q \xrightarrow{k_Q} tr^0 + Q \tag{6}$$

$$c^1 \longrightarrow p^3 \tag{7}$$
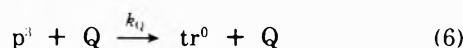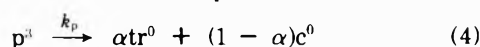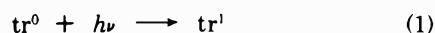
scheme it is an open question whether c^1 first is transformed to c^3 and afterward rotation leads to p^3 or whether
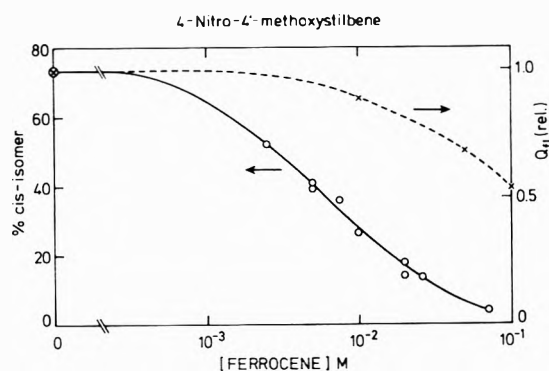

Figure 1. Position of the photostationary state of 4-nitro-4'-methoxystilbene in argon-saturated benzene solutions as a function of ferrocene concentration (O). Irradiation with λ 366 nm. The effect of ferrocene concentration on the quantum yield of fluorescence of 4-nitro-4'-methoxystilbene, Q_{fl} (X).

the rotation occurs in the S^1 state followed by a fast S^1 → T transition in the twisted state leading to p^3.

In Schemes A and B tr^0 and c^0 stand for the planar *trans*- and the nearly planar *cis*-stilbenes, respectively, in their ground states, and the superscripts 1 and 3 indicate the excited singlet and triplet states; p^3 represents the twisted triplet intermediate and α is the fraction of p^3 decaying to tr^0, and β is the fraction of c^1 decaying to tr^0. In Schemes A and B steps other then those leading to isomerization, such as fluorescence and dihydrophenanthrene formation, have been omitted. In the presence of quencher, Q, an additional step (reaction 6) must be added. Equation 6 is only applicable for azulene and ferrocene.

By making the normal steady state assumptions from Scheme A, eq 8 can be obtained for the effect of Q on the ratio $[tr^0]_s/[c^0]_s$, where the subscript s indicates the stationary state condition; ϵ_c and ϵ_{tr} are the extinction coefficients of the cis and trans isomers, respectively. Scheme B leads to eq 9.

$$\frac{[tr^0]_s}{[c^0]_s} = \frac{\epsilon_c}{\epsilon_{tr}} \left[\frac{\beta}{(1 - \alpha)} + \frac{\beta k_Q[Q]}{(1 - \alpha)k_p} \right] \tag{8}$$

$$\frac{[tr^0]_s}{[c^0]_s} = \frac{\epsilon_c}{\epsilon_{tr}} \left[\frac{\alpha}{(1 - \alpha)} + \frac{k_Q[Q]}{(1 - \alpha)k_p} \right] \tag{9}$$

It follows from eq 8 that a plot of $[tr^0]_s/[c^0]_s$ against [Q] should yield a straight line whose slope/intercept ratio is equal to k_Q/k_p. A similar procedure is possible for eq 9 leading to a slope/intercept ratio equal to $k_Q/\alpha k_p$. Since α and β can be obtained from the intercept or from the quantum yields together with ϵ_c and ϵ_{tr} and a value for k_Q can be proposed, it is possible to obtain a value for k_p, the first-order decay constant of p^3.

Figure 2 shows a plot of $[tr^0]_s/[c^0]_s$ against quencher concentration for the isomerization of 4-nitro-4'-methoxystilbene in argon-saturated benzene solutions. Azulene and ferrocene can be seen to give very similar plots. In order to calculate k_p we have taken values for k_Q of 4.5 × 10^9 M^{-1} sec^{-1} and 6.0 × 10^9 M^{-1} sec^{-1} for ferrocene and azulene, respectively.[2] These values were determined from quenching studies of an intermediate assigned to p^3, which was observed in the laser flash photolysis of 4-nitro-4'-methoxystilbene[2] and represent diffusion controlled values similar to those obtained in other triplet quenching studies.[5-7]

In Table I we have shown the values of k_p derived from Schemes A and B which were obtained from the photosta-
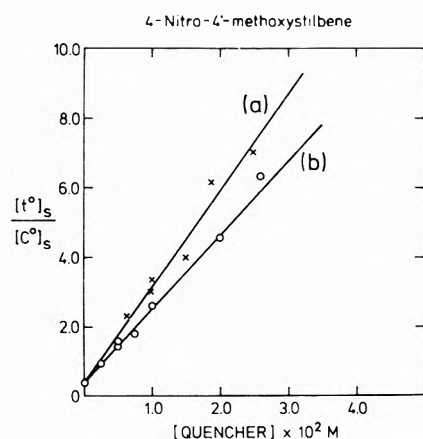
4-Nitro-4'-methoxystilbene

Figure 2. Position of the photostationary state of 4-nitro-4'-methoxystilbene in benzene as a function of azulene and ferrocene concentration. Irradiation with uv light wavelength λ 366 nm: (a) azulene, argon-saturated solution; (b) ferrocene, argon-saturated solution.

TABLE I: Values of k_p for 4-Nitro-4'-methoxystilbene in Benzene[a]

Quencher	Slope/intercept, M^{-1}	$k_p \times 10^{-7}$, sec^{-1} (a)	(b)	(c)
Azulene	665	0.79	1.32	0.72 ± 20%
Ferrocene	520	0.77	1.28	0.72 ± 20%

[a] Obtained (a) from the slope/intercept ratio of Figure 2, calculated using mechanism A, (b) the same, calculated using mechanism B, and (c) by laser flash photolysis.[2,4]

tionary-state studies and as a comparison we have listed the k_p values obtained from our laser studies.[2] The results in Table I show that agreement between the directly and indirectly determined values for k_p is only reached in the case of mechanism A. We conclude from this result that: (1) the observed transients are intermediates in the direct photochemical trans → cis isomerization of nitrostilbenes; (2) the observed transients are triplet states; and (3) only the trans → cis but not the cis → trans isomerizations of nitrostilbenes proceed through triplet states as intermediates.

Figure 3 shows the plots of $[tr^0]_s/[c^0]_s$ against [Q] obtained from argon-saturated benzene solutions of trans-4-nitrostilbene and trans-4,4'-dinitrostilbene. The slope/intercept ratios of Figure 3 are given in Table II. The cis isomers of these stilbenes were also studied and were found to give the same photostationary states as the trans isomers.

The following result is in agreement with the assumption that the cis → trans isomerization of the nitrostilbenes occurs in the singlet state and practically no triplet transient is produced from excitation of the cis form. We observe that the addition of ferrocene (direct illumination of the stilbene) only influences the quantum yield of the trans → cis isomerization ($\phi_{tr \to c}$). The quantum yield of the cis → trans isomerization ($\phi_{c \to tr}$) is not affected. If on illumination of the cis form in the presence of a quencher $\phi_{c \to tr}$ is not shifted then no quenchable transient is being produced from the cis form. This result also shows that the assumption[8] that azulene was acting as a catalyst and enhancing only the rate of the cis → trans interconversion is not correct.

Results which apparently are not in complete agree-

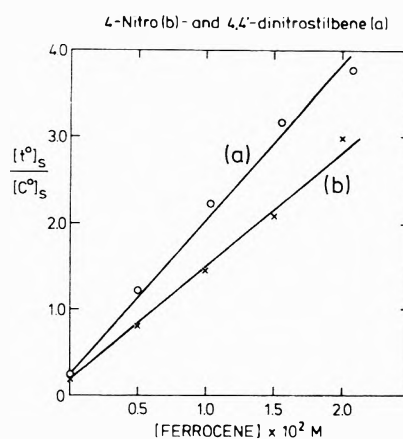4-Nitro(b)- and 4,4'-dinitrostilbene (a)

Figure 3. Position of the photostationary state of (a) 4,4'-dinitrostilbene and (b) 4-nitrostilbene as a function of ferrocene concentration in argon-saturated benzene solutions.

TABLE II: Values of k_p Obtained in Benzene by Flash Photolysis[a] and Slope/Intercept Values for Ferrocene as Quencher

	Slope/intercept, M^{-1}	$k_F \times 10^{-7}$, sec^{-1}
4-Nitrostilbene	820	1.2
4,4'-Dinitrostilbene	760	0.98

[a] See ref 2 and 4.

ment with these conclusions are those of the observed transient produced during laser irradiation of the cis form of 4-nitro-4'-methoxystilbene.[2] As was pointed out in the preceding paper,[2] it is possible that the transient is produced by a two-quanta process. The first absorbed quantum is used to convert the cis form to the trans form and the second quantum to produce the transient from the trans form. The laser beam has enough quanta to do so. Another possibility is that in a side reaction a few per cent of the twisted excited singlet produces some twisted triplet which could be the transient observed on flashing the cis form. This problem is under further investigation.

(d) *Singlet Mechanism.* We have shown by other means that the photoisomerization of 4-cyano-4'-methoxystilbene follows a different pathway to that of 4-nitro-4'-methoxystilbene[4] and we have verified these observations by studying the effect of ferrocene and azulene on the position of the photostationary state. In contrast to the results with the nitrostilbenes the effect of quencher was very low. The slope/intercept ratio of ~2.5 M^{-1} obtained is very similar to the value of ~15 M^{-1} obtained in similar studies with stilbene where a singlet mechanism is applicable.[1] Therefore the effect of quencher on the cis-trans isomerization of 4-cyano-4'-methoxystilbene supports the assumption that in this case a singlet pathway is applicable.

(e) *Interpretation of the Results.* The effect of azulene on the photostationary state of 4-nitro-4'-methoxystilbenes at concentrations occurring well before the fluorescence quenching show that there must be a long-lived intermediate present during illumination of the nitrostilbenes. Since the lifetime of the intermediates determined directly by laser flash photolysis and indirectly from the effect of added quenchers on the position of the photostationary state coincide, it has to be concluded that the observed transients are intermediates in the direct photo-

chemical trans → cis isomerization. The transients are produced only (or overwhelmingly) from the trans form and not from the cis form. The reason for this is most probably the small barrier to rotation which is present in the excited singlet trans form and absent in the corresponding cis form. This barrier prolongs the lifetime of the excited singlet state in the planar trans forms and allows the S_1 → T transition to occur, whereas in the excited singlet state of the cis form such barriers do not exist according to calculations of Borrel and Greenwood,[9] in agreement with the unusual short lifetime of the S_1 state of cis form.[10] Furthermore, the spectra show that the transients are probably in a twisted state; that is, they should be the phantom triplets.

References and Notes

(1) J. Saltiel and E. C. Megarity, J. Amer. Chem. Soc., **94**, 2742 (1972).
(2) D. V. Bent and D. Schulte-Frohlinde, J. Phys. Chem., **78**, 446 (1974).
(3) G. S. Hammond, J. Saltiel, A. A. Lamola, N. J. Turro, J. B. Bradshaw, D. O. Cowan, R. C. Coursell, V. Vogt, and C. Dalton, J. Amer. Chem. Soc., **86**, 3197 (1964).
(4) D. Schulte-Frohlinde and D. V. Bent, Mol. Photochem., in press.
(5) G. S. Hammond and P. A. Leermakers, J. Phys. Chem., **66**, 1148 (1962).
(6) A. J. Fry, R. S. H. Liu, and G. S. Hammond, J. Amer. Chem. Soc., **88**, 4781 (1966).
(7) W. Ware, J. Chem. Phys., **37**, 923 (1962).
(8) E. Fischer, Mol. Photochem., **5**, 227 (1973).
(9) P. Borrel and H. H. Greenwood, Proc. Roy. Soc., Ser A, **298**, 453 (1967).
(10) D. Schulte-Frohlinde, H. Blume, and H. Güsten, J. Phys. Chem., **66**, 2486 (1962).

Extension of Models for Evaluating Solvent Transfer Enthalpies

R. Martin Guidry[1] and Russell S. Drago*

The William A. Noyes Laboratory, University of Illinois, Urbana, Illinois 61801 (Received May 31, 1973; Revised Manuscript Received October 18, 1973)

Recently we have proposed and tested a model, called ESP (elimination of solvation procedure), for estimating solvation contributions to enthalpy data in weakly basic, nonpolar, and weakly polar solvents. In this work, we have considerably extended the range of solvent polarity employed by investigating equilibria in the polar solvent nitrobenzene. The strong hydrogen-bonding acid 1,1,1,3,3,3-hexafluoro-2-propanol (HFIP) has been investigated to extend the range of acids used in evaluating our model. The data collected also permit a test of a solvent transfer model proposed by Christian, et al. By expanding the narrow range of solvents previously employed to include the much more polar nitrobenzene as a solvent, the ESP model was found to predict the correct results, but the alternative model was less successful. The extension of the ESP model to include nitrobenzene is significant for other reasons. If the results for some acid–base system insoluble in poorly solvating solvents can be studied in two or more quite different polar basic solvents and corrected to the same solvation free value, one will have more confidence that the base employed is not interacting with the polar solvents and, therefore, that the corrected enthalpy is reasonable.

Introduction

In recent publications, we have described a procedure, called ESP (elimination of solvation procedure), for converting enthalpies measured in polar solvents into solvation minimized data that one would obtain in the solvents carbon tetrachloride or hexane.[2-4] When investigating a series of bases toward a common acid, the individual enthalpies of adduct formation, ΔH_f, measured in a basic solvent, are combined to produce the enthalpy for the displacement reaction

$$AB + B' \rightleftarrows AB' + B \qquad (1)$$
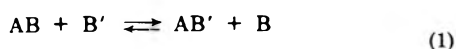
$$(\Delta H \text{ displacement} = \Delta H_f AB' - \Delta H_f AB)$$

By subtracting the two enthalpies of formation to produce eq 1, one eliminates from the displacement reaction the free acid, which is interacting in a specific manner with the basic solvent. The nonspecific solvation energies of the products and reactants are expected to cancel when the free bases and adducts do not interact in a specific man-

ner with the basic solvent. This can be understood by observing the solvation of products and reactants on a molecular level. If the active site on B undergoes similar, nonspecific interactions with the solvent as the active site on B', if the packing around the remainder of B and B' remain unchanged in the adduct and free state, and if there is no change around the coordinated acid, then all other nearest-neighbor interactions should cancel. The above assumptions should hold if both B and B' do not change geometry significantly upon coordination and if A does not coordinate in a different manner to B' than it does to B. If the gas-phase enthalpy for the reaction

$$A_{(g)} + B_{(g)} \longrightarrow AB_{(g)} \qquad (2)$$
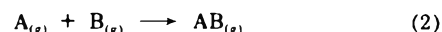
is known, then one can add eq 1 and 2 to produce the gas-phase enthalpy for the reaction

$$A_{(g)} + B'_{(g)} \longrightarrow AB'_{(g)} \qquad (3)$$
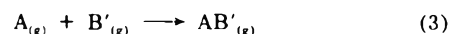
assuming there are no solvation contributions to eq 1. The counterpart of eq 3 is expected if a carbon tetrachloride or

cyclohexane solvent minimized enthalpy is used instead of a gas-phase enthalpy. For example, if the acid hydrogen bonds to CCl_4 to the extent of -0.2 kcal mol^{-1}, the enthalpy of eq 2 will be too large (i.e., not negative enough) and that of eq 3 will also be too large by the same amount.

This approach has been checked out on reactions for which the Lewis acids are m-fluorophenol[2,4] and bis(hexafluoroacetylacetonate)copper(II)[3] and the solvents are benzene and o-dichlorobenzene. The solvent, 1,2-dichloroethane, was found to be unsuitable.[4] The bases studied involved dimethyl sulfoxide, ethyl acetate, di-n-butyl ether, and triethylamine. The agreement of the enthalpies for eq 1 in the solvents benzene and o-dichlorobenzene with data obtained in CCl_4 or hexane as solvent was taken as support for the model. On such systems we were able to show that the enthalpies measured in the solvating solvents for the whole series of bases obeying eq 1 were related to those in CCl_4 or hexane by a constant. Thus, in the absence of specific interactions, some new base insoluble in CCl_4 or hexane could be studied in benzene or o-dichlorobenzene and the constant used to produce the enthalpy expected in CCl_4 or hexane. Similar considerations can be employed on systems in which the base is held constant and the acids varied in an acidic solvent.[5]

At the present level of understanding of intermolecular interactions, the name ESP also stands for the extrasensory perception one needs in order to know when the bases or adducts interact specifically with a basic solvent. For example, pyridine interacts with the solvents CCl_4, benzene, and o-dichlorobenzene. Accordingly, it is desirable to have several different polar basic solvents for study. If the corrected results for a new base in two or more different polar solvents were identical, one might have confidence that the base is not interacting with the solvent. This conclusion would be in error only if the new base interacted with the solvent to the same extent in both solvents. The probability of this coincidence is decreased by selecting very different types of solvents. This provided part of the motivation for extension of our earlier work to the solvent nitrobenzene.

A second aim of this study is directed toward evaluating an alternative proposal for predicting the effect of solvent on thermodynamic data. It has been proposed by Christian, et al.,[6-8] that the enthalpy of transferring an adduct from solvent I to solvent II is proportional to the sum of the enthalpies of transfer of the acid and base from solvent I to solvent II. A quantitative statement of this is

$$\Delta H^\circ{}_C = \alpha(\Delta H^\circ{}_A + \Delta H^\circ{}_B) \qquad (4)$$
$$I \longrightarrow II \quad I \longrightarrow II \quad I \longrightarrow II$$

where $\Delta H^\circ{}_C$, $\Delta H^\circ{}_A$, and $\Delta H^\circ{}_B$ are the enthalpies of transfer from solvent I to solvent II for the adduct, acid, and base, respectively. The quantity α should be nearly constant for a given acid-base pair and is not strongly dependent upon either the temperature or the choice of solvents.

In a previous report[4] from this laboratory, it was shown that the enthalpy for formation of the adducts of the acid m-fluorophenol with a variety of bases in the solvents carbon tetrachloride, cyclohexane, benzene, and o-dichlorobenzene (with dielectric constants at 20° of 2.24, 2.02, 2.28, and 10.40, respectively) missed the value predicted by eq 4 in several instances. It was also felt that the range of solvents used in the earlier studies[2-4] was too narrow to be definitive. The real test of eq 4 involves studying a given acid-base system in a wide variety of solvents to see

if α truly is a constant (it is almost certain to be constant for three closely related solvents). The real test of ESP is to use a wide variety of acids and bases which do not undergo specific interactions between the free base or adduct and solvent. This study was designed to extend the range of systems that could be used to test both models. Nitrobenzene was selected as the solvent because, with a dielectric constant of 35.74 at 20°, it greatly extends the range of solvents employed. The acids used were extended to include the strong hydrogen-bonding acid 1,1,1,3,3,3-hexafluoro-2-propanol (HFIP). The bases employed included the oxygen donors ethyl acetate, N,N-dimethylacetamide, and hexamethylphosphoramide as well as the nitrogen donors 1-methylimidazole and pyridine.

Experimental Section

Purification of Materials. Mallinckrodt Analytical Reagent carbon tetrachloride, Phillips 66 Pure Grade n-hexane, Eastman Organic o-dichlorobenzene, and Baker Analyzed Reagent benzene were dried over Linde 4A molecular sieves and used without further purification. Baker Analyzed Reagent nitrobenzene was vacuum distilled at ~ 1 Torr with only the middle fraction, collected at 50–51°, being retained. Mallinckrodt nitromethane was dried overnight over anhydrous calcium sulfate and then distilled with only the middle fraction, collected at 95–96°, being retained.

1,1,1,3,3,3-Hexafluoro-2-propanol (HFIP) (Peninsular Chemresearch, Inc.) was purified as previously described.[9]

N,N-Dimethylacetamide (DMA, Eastman Organic), ethyl acetate (EtOAc, Baker Analyzed Reagent), and pyridine (Baker Analyzed Reagent) were purified as previously described.[10] Hexamethylphosphoramide (HMPA, Aldrich Chemical Corp.) was twice vacuum distilled at ~ 10 Torr from calcium hydride with only the middle fraction being retained in each distillation. The boiling range of the middle fraction of the second distillation was 100.0–101.0°. 1-Methylimidazole (1-MeIm, Aldrich Chemical Corp.) was twice vacuum distilled from calcium hydride at ~ 15 Torr with only the middle fraction being retained in each distillation. The boiling range of the middle fraction on of the second distillation was 77.5–78.5°.

Apparatus and Calculations. The description of the modified calorimeter and the procedure for performing the experiments and calculating the results have been reported.[10-14]

Results

The experimental data appear immediately following this article in the microfilm edition of the journal.[15] The heats of solution of the different donors, as well as 1,1,1,3,3,3-hexafluoro-2-propanol, in various solvents are reported in Table I. In Table I, most heats of solution represent an average value of several experimental trials; however, for these cases where a definite concentration dependence was observed, the heats of solution reported were determined by extrapolation to infinite dilution. In all cases, though, the values reported were obtained over a range of low concentrations. In general, the heat of solution of HFIP is more endothermic than that of the individual bases in the corresponding media.

A summary of the calorimetric results for the interaction of HFIP with the various bases in the different solvents is contained in Table II. The calculated uncertainty limits for the enthalpies were always less than 0.1 kcal mol^{-1}. Previously,[10] it has been shown that, because the

TABLE I: Partial Molar Heats of Solution $(\Delta H_s$, kcal mol^{-1}) **of Various Compounds in Different Solvents at High Dilution**[a]
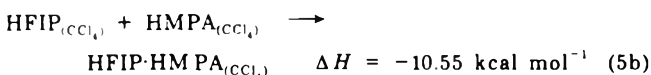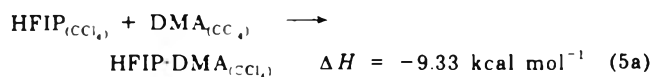
Solvent	HFIP	Ethyl acetate	Hexamethyl-phosphoramide	Dimethyl-acetamide	1-Methyl-imidazole	Pyridine
Carbon tetrachloride	4.78[b]	0.04[c]	−1.39[c]	0.33[d]		0.36[c]
n-Hexane	5.15[b]				3.18	2.00
Benzene	2.25	0.11[c]	−0.94[c]	0.07[c]	0.55[d]	0.00[c]
o-Dichlorobenzene	3.45	−0.12[c]	−2.44[c]	−0.42[c]	0.63	0.16[c]
Nitrobenzene	0.13	−0.11[c]	−1.09	−0.36	0.24	0.13
Nitromethane	0.92					

[a] Precision is ±0.01 kcal mol^{-1} or somewhat better. [b] From ref 10. [c] F. L. Slejko, Ph.D. Thesis, University of Illinois, 1972. [d] Measured in this laboratory by other investigators.

acid 1,1,1,3,3,3-hexafluoro-2-propanol undergoes H---F intramolecular bonding, all calorimetrically measured enthalpies of interaction of HFIP with a base must be corrected by subtracting 1.1 kcal mol^{-1} from the calorimetrically measured exothermic enthalpy. That is to say, the calorimetrically measured enthalpy is made more negative by 1.1 kcal mol^{-1}. The enthalpies reported in Table II do not reflect this correction for the intramolecular interaction. For oxygen donors, carbon tetrachloride is used as the "poorly solvating" medium while the "poorly solvating" medium for nitrogen donors is n-hexane.

Discussion

The data in Table II can be combined to produce a whole series of displacement reactions analogous to eq 1. Illustrated below is an example involving dimethylacetamide (DMA) and hexamethylphosphoramide (HMPA) interacting with HFIP in CCl$_4$

$$\text{HFIP}_{(CCl_4)} + \text{DMA}_{(CCl_4)} \longrightarrow$$
$$\text{HFIP·DMA}_{(CCl_4)} \qquad \Delta H = -9.33 \text{ kcal mol}^{-1} \quad (5a)$$

$$\text{HFIP}_{(CCl_4)} + \text{HMPA}_{(CCl_4)} \longrightarrow$$
$$\text{HFIP·HMPA}_{(CCl_4)} \qquad \Delta H = -10.55 \text{ kcal mol}^{-1} \quad (5b)$$

Multiplying eq 5a by −1 and adding it to (5b) yields eq 6a.

$$\text{HMPA}_{(CCl_4)} + \text{HFIP·DMA}_{(CCl_4)} \longrightarrow$$
$$\text{DMA}_{(CCl_4)} + \text{HFIP·HMPA}_{(CCl_4)} \qquad \Delta H = -1.2 \text{ kcal mol}^{-1} \quad (6a)$$
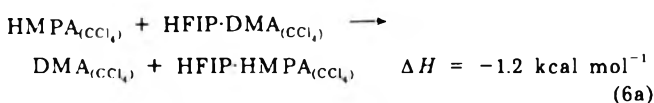
In Table III are summarized the results for displacement reactions of other acid–base combinations in different solvents.

It has been previously observed[4] that the base pyridine interacts with the aromatic solvents benzene and o-dichlorobenzene to the extent of 0.9 kcal mol^{-1}. Thus, 0.9 kcal mol^{-1} was added to the pyridine enthalpies measured in benzene and o-dichlorobenzene when they were used to calculate the enthalpies for the displacement reactions in Table III. Comparison of eq 6e″ and 6g″ with the other solvents for these displacement reactions indicates that when a similar correction is applied in the pyridine–nitrobenzene system, good agreement results.

The 6b, b′, and b″ series as well as 6d, d′, and d″ series illustrate that the ESP procedure can be extended to the acid HFIP and to the base HMPA. Similar displacement enthalpies are obtained for these systems in CCl$_4$ and in the solvents, benzene and o-dichlorobenzene, used in the earlier ESP papers. Although we have used the 1-methylimidazole enthalpies directly in calculating the data in Table III, the displacement reactions provide no

information directly about whether or not 1-methylimidazole interacts to the same extent with all the aromatic solvents studied as pyridine did. However, they do show that 1-methylimidazole does work well with HFIP in the ESP procedure.

The results in Table III show that, regardless of the solvent employed, a constant value of ΔH (to ±0.2 kcal mol^{-1}) is obtained for any of the given pairs of bases undergoing the displacement reaction (eq 1). For example, if one observes the set of eq 6i, 6i′, 6i″, and 6i‴ which employ the bases DMA and HMPA and the solvents carbon tetrachloride, benzene, o-dichlorobenzene, and nitrobenzene, he discovers that the enthalpy for the displacement reaction in all four solvents is −1.2 ± 0.1 kcal mol^{-1}. Even when the very polar solvent nitrobenzene is employed with a pair of bases as widely differing in polarity as DMA and pyridine, the enthalpy of the displacement reaction is still found to be independent of the solvent and dependent only on the acid and base pairs chosen.

Furthermore, the data in Table II reveal the fact that all enthalpies for various bases measured in a single polar solvent, e.g., nitrobenzene, differ by a constant amount from the corresponding enthalpies measured in carbon tetrachloride or hexane. A quantitative statement of the above is

$$-\Delta H_{(\text{poorly solvating medium})} = -\Delta H_{(\text{polar solvent})} + S \quad (7)$$

where S is the constant difference between the enthalpies measured in the inert media and those measured in the polar solvent. In earlier papers it was shown that eq 7 is a direct consequence of obtaining constant enthalpies for eq 1 for a series of bases in a solvent. Thus, if the acid is held constant in a given polar basic solvent and a series of bases studied, the assumption that solvation contributions to the general eq 1 cancel is analogous to the assumption that the enthalpies measured in the polar basic solvent will differ by a constant amount from those measured in the poorly solvating media. In weakly basic solvents, the value of S is dependent only on the acid and the solvent employed and is independent of the base if it does not interact specifically with the solvent. For 1,1,1,3,3,3-hexafluoro-2-propanol in benzene, o-dichlorobenzene, and nitrobenzene, the constant S is 1.7 ± 0.2, 0.7 ± 0.2, and 3.5 ± 0.1 kcal mol^{-1}, respectively. The constant S has contributions to it from the difference in nonspecific solvation of the adducts and the corresponding acids and bases in the polar solvent. It also includes the energy required to overcome the specific interactions of the acid with the solvent.

If the correction factors described above are applied to the donor pyridine in the various aromatic solvents, the corrected enthalpy of adduct formation of pyridine with

TABLE II: Thermodynamic Data for the System 1,1,1,3,3,3-Hexafluoro-2-propanol Base in Different Solvents
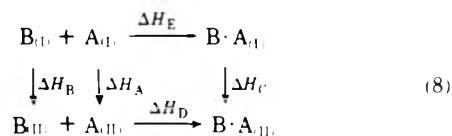
Solvent	Lewis base									
	Ethyl acetate		Hexamethylphosphoramide		Dimethylacetamide		1-Methylimidazole		Pyridine	
	K^a	$-\Delta H^b$	K^a	$-\Delta H^b$	K^a	$-\Delta H^b$	K^a	$-\Delta H^b$	K^a	$-\Delta H^b$
Carbon tetrachloride	37 ± 1^b	5.92 ± 0.03^c	∞	9.45 ± 0.03^c	825 ± 63^c	8.23 ± 0.03^c		10.00 ± 0.20^d	731 ± 101	9.78 ± 0.05^c
n-Hexane										
Benzene	7.6 ± 0.3	4.09 ± 0.07	$1,334 \pm 106$	7.78 ± 0.02	268 ± 14	6.67 ± 0.03	855 ± 185	8.32 ± 0.04	175 ± 3	6.93 ± 0.01^e
o-Dichlorobenzene	22 ± 1	5.05 ± 0.03	$17,385 \pm 2780$	8.66 ± 0.02	800 ± 26	7.58 ± 0.01	3016 ± 92	9.44 ± 0.01	504 ± 59	8.20 ± 0.03^e
Nitrobenzene	f	f	373 ± 26	5.91 ± 0.03	58 ± 1	4.70 ± 0.02	434 ± 20	6.57 ± 0.02	37 ± 1	5.34 ± 0.02^e
Nitromethane	f	f	39 ± 2	4.30 ± 0.05	f	f	f		14 ± 1	4.89 ± 0.05

^{a} In units of M^{-1}. ^{b} These enthalpies are in units of kcal mol^{-1} and are not corrected for the 1.1 kcal mol^{-1} enthalpy of intramolecular bonding in 1,1,1,3,3,3-hexafluoro-2-propanol. Errors are marginal standard deviations at 67% confidence. ^{c} From ref 10. ^{d} Calculated from the E and C parameters. ^{e} These enthalpies do not reflect the 0.9 kcal mol^{-1} correction of free pyridine interacting specifically with aromatic solvents (vide infra). ^{f} The solvent competed so effectively with the base for the acid that accurate measurement was difficult.

HFIP differs from the value measured in n-hexane by the 0.9 kcal mol^{-1} previously ascribed to the pyridine-solvent donor-acceptor interaction. In order to gain further support for the specific interaction of pyridine with aromatic solvents, pyridine was investigated as a base in nitromethane. Nitromethane is apparently a more basic solvent than nitrobenzene and, consequently, the equilibrium constants and enthalpies are much lower in this solvent. The HMPA-HFIP system was investigated to produce the solvent correction constant S. It was assumed that nitromethane would obey ESP with this donor because it works well in nitrobenzene and all of the other ESP solvents reported. When the pyridine-HFIP system was investigated, the correction constant found for HMPA-HFIP system yielded the pyridine-HFIP enthalpy in hexane implying no specific interaction of the pyridine with this nonaromatic solvent. Employing these two systems, one obtains a correction constant S for HFIP in nitromethane of 5.0 kcal mol^{-1}. This result supports all of our previous conclusions about pyridine interacting with CCl_4 and aromatic solvents.

When the enthalpy data in aromatic solvents for the donor 1-methylimidazole are corrected by adding S (which is a negative number), the enthalpy measured in n-hexane results. Thus, 1-methylimidazole is not undergoing an appreciable donor-acceptor interaction with the aromatic solvents studied.

Next, we shall evaluate the approach proposed by Christian,[6-8] et al., for predicting thermodynamic data in a range of solvents represented by eq 4. Utilizing this approach, it is claimed that one can predict thermodynamic data in a range of solvents as long as the specific interactions are not large. The thermodynamic cycle in eq 8 illustrates the processes that the various enthalpies in eq 4

$$
\begin{array}{ccc}
B_{(I)} + A_{(I)} & \xrightarrow{\Delta H_E} & B \cdot A_{(I)} \\
\downarrow{\scriptstyle\Delta H_B} \quad \downarrow{\scriptstyle\Delta H_A} & & \downarrow{\scriptstyle\Delta H_C} \\
B_{(II)} + A_{(II)} & \xrightarrow{\Delta H_D} & B \cdot A_{(II)}
\end{array} \qquad (8)
$$

lustrates the processes that the various enthalpies in eq 4 represent. The experimental value for the enthalpy of transferring the adduct from solvent I to solvent II is calculated by utilizing eq 9. We now have all of the enthalpy

$$\Delta H_C = \Delta H_A + \Delta H_B + \Delta H_D - \Delta H_E \qquad (9)$$

data needed to test the basic assumption upon which eq 4 is based. Table IV contains the experimental enthalpies of transferring the acid (ΔH_A), the base (ΔH_B), and the adduct (ΔH_C) from one solvent to another. The value of α for each acid-base system is graphically determined by plotting ΔH_C vs. ($\Delta H_A + \Delta H_B$) for that pair being transferred between all pairs of solvents. The "constant" α is then the slope of the best least-squares line through all of the plotted points (which must include the origin). The value of α for each acid-base pair is reported in Table V. According to this model, the α values for a particular acid-base system should be nearly the same regardless of which solvents are involved in the transfer. Using the value of α graphically determined for each acid-base pair and the enthalpies of acid and base transfer, ΔH_C (I → II) was calculated using eq 4. These calculated adduct transfer enthalpies, which are reported in Table V, are to be compared with the experimentally determined complex transfer enthalpies also reported in Table V. Of the 27 systems reported, 17 miss outside of a generous estimate of the precision of ±0.2 kcal mol^{-1}. This is to be contrasted

TABLE III: Summary of the Enthalpy of the Reactions for AB + B' → AB' + B Type Interactions

Eq no.	Solvent	AB	+	B'	→	AB'	+	B	ΔH^a
6a	C_6H_6	HFIP·EtOAc	+	C_5H_5N	→	HFIP·C_5H_5N	+	EtOAc	−3.7
6a'	o-$Cl_2C_6H_4$	HFIP·EtOAc	+	C_5H_5N	→	HFIP·C_5H_5N	+	EtOAc	−4.0
6b	CCl_4	HFIP·EtOAc	+	DMA	→	HFIP·DMA	+	EtOAc	−2.3
6b'	C_6H_6	HFIP·EtOAc	+	DMA	→	HFIP·DMA	+	EtOAc	−2.6
6b''	o-$Cl_2C_6H_4$	HFIP·EtOAc	+	DMA	→	HFIP·DMA	+	EtOAc	−2.5
6c	C_6H_6	HFIP·EtOAc	+	1-MeIm	→	HFIP·1-MeIm	+	EtOAc	−4.2
6c'	o-$Cl_2C_6H_4$	HFIP·EtOAc	+	1-MeIm	→	HFIP·1-MeIm	+	EtOAc	−4.4
6d	CCl_4	HFIP·EtOAc	+	HMPA	→	HFIP·HMPA	+	EtOAc	−3.5
6d'	C_6H_6	HFIP·EtOAc	+	HMPA	→	HFIP·HMPA	+	EtOAc	−3.7
6d''	o-$Cl_2C_6H_4$	HFIP·EtOAc	+	HMPA	→	HFIP·HMPA	+	EtOAc	−3.6
6e	C_6H_6	HFIP·C_5H_5N	+	DMA	→	HFIP·DMA	+	C_5H_5N	1.2
6e'	o-$Cl_2C_6H_4$	HFIP·C_5H_5N	+	DMA	→	HFIP·DMA	+	C_5H_5N	1.5
6e''	$NO_2C_6H_5$	HFIP·C_5H_5N	+	DMA	→	HFIP·DMA	+	C_5H_5N	1.5
6f	C_6H_{14}	HFIP·C_5H_5N	+	1-MeIm	→	HFIP·1-MeIm	+	C_5H_5N	−0.2
6f'	C_6H_6	HFIP·C_5H_5N	+	1-MeIm	→	HFIP·1-MeIm	+	C_5H_5N	−0.5
6f''	o-$Cl_2C_6H_4$	HFIP·C_5H_5N	+	1-MeIm	→	HFIP·1-MeIm	+	C_5H_5N	−0.3
6f'''	$NO_2C_6H_5$	HFIP·C_5H_5N	+	1-MeIm	→	HFIP·1-MeIm	+	C_5H_5N	−0.3
6g	C_6H_6	HFIP·C_5H_5N	+	HMPA	→	HFIP·HMPA	+	C_5H_5N	0.1
6g'	o-$Cl_2C_6H_4$	HFIP·C_5H_5N	+	HMPA	→	HFIP·HMPA	+	C_5H_5N	0.4
6g''	$NO_2C_6H_5$	HFIP·C_5H_5N	+	HMPA	→	HFIP·HMPA	+	C_5H_5N	0.3
6h	C_6H_6	HFIP·DMA	+	1-MeIm	→	HFIP·1-MeIm	+	DMA	−1.7
6h'	o-$Cl_2C_6H_4$	HFIP·DMA	+	1-MeIm	→	HFIP·1-MeIm	+	DMA	−1.9
6h''	$NO_2C_6H_5$	HFIP·DMA	+	1-MeIm	→	HFIP·1-MeIm	+	DMA	−1.9
6i	CCl_4	HFIP·DMA	+	HMPA	→	HFIP·HMPA	+	DMA	−1.2
6i'	C_6H_6	HFIP·DMA	+	HMPA	→	HFIP·HMPA	+	DMA	−1.1
6i''	o-$Cl_2C_6H_4$	HFIP·DMA	+	HMPA	→	HFIP·HMPA	+	DMA	−1.1
6i'''	$NO_2C_6H_5$	HFIP·DMA	+	HMPA	→	HFIP·HMPA	+	DMA	−1.2
6j	C_6H_6	HFIP·1-MeIm	+	HMPA	→	HFIP·HMPA	+	1-MeIm	0.6
6j'	o-$Cl_2C_6H_4$	HFIP·1-MeIm	+	HMPA	→	HFIP·HMPA	+	1-MeIm	0.8
6j''	$NO_2C_6H_5$	HFIP·1-MeIm	+	HMPA	→	HFIP·HMPA	+	1-MeIm	0.7

^{a} In units of kcal mol^{-1}.

TABLE IV: Transfer Energies for Acids (ΔH_A), **Bases** (ΔH_B), **and Adducts** (ΔH_C) **from Solvent I to Solvent II (kcal mol^{-1})**

Substance	$CCl_4 \to C_6H_6$	$CCl_4 \to o\text{-}Cl_2C_6H_4$	$CCl_4 \to NO_2C_6H_5$	$C_6H_{14} \to C_6H_6$	$C_6H_{14} \to o\text{-}Cl_2C_6H_4$	$C_6H_{14} \to NO_2C_6H_5$	$C_6H_6 \to o\text{-}Cl_2C_6H_4$	$C_6H_6 \to NO_2C_6H_5$	$o\text{-}Cl_2C_6H_4 \to NO_2C_6H_4$
HFIP	−2.53	−1.33	−4.65	−2.90	−1.74	−5.02	1.20	−2.12	−3.32
EtOAc	0.07	−0.16					−0.23		
HFIP·EtOAc	−0.63	−0.62					0.01		
HMPA	0.45	−1.05	0.30				−1.50	−0.15	1.35
HFIP·HMPA	−0.41	−1.59	−0.81				−1.18	−0.40	0.78
DMA	−0.26	−0.75	−0.69				−0.49	−0.43	0.06
HFIP·DMA	−1.23	−1.43	−1.81				−0.20	−0.58	−0.38
1-MeIm				−2.63	−2.55	−2.94	0.08	−0.31	−0.39
HFIP·1-MeIm				−3.85	−3.69	−4.53	0.16	−0.68	−0.84
Pyridine				−2.00	−1.84	−1.87	0.16	0.13	−0.03
HFIP·pyridine				−2.95^a	−2.86^a	−3.35^a	0.09	−0.40	−0.49

^{a} Corrected for the specific interaction of free pyridine with the aromatic solvent of 0.9 kcal mol^{-1}.

with our Δk values (deviation from k); all of which are less than or equal to 0.2 kcal mol^{-1}. If one could find a plausible explanation for why eq 4 misses so badly in many of systems, then possibly some of the data could be rejected or the model corrected. It would be interesting, for example, to find suitable answers to the following questions. In the transfer of the pyridine complex from o-dichlorobenzene to nitrobenzene, the specific interactions of the free pyridine with the aromatic solvents should cancel; however, this is not the case in the transfer of the pyridine complex from n-hexane to nitrobenzene. Why then should the transfer from n-hexane to nitrobenzene for this complex be predicted reasonably well with this model while the transfer from o-dichlorobenzene to nitrobenzene be predicted so poorly? Furthermore, why should the transfer energy of the ethyl acetate adduct from carbon tetrachloride to o-dichlorobenzene be predicted so well while the

exact same transfer energy for the DMA complex, which also involved an oxygen donor, misses so badly? Why, for one acid–base pair, e.g., HFIP–DMA, does the model based on eq 4 predict some transfer energies so accurately and yet misses others so badly? This happens even when no specific interactions between free base and solvent are involved.

By employing the very polar solvent nitrobenzene in this study, we have vastly extended the range of solvents previously[2-4] studied and thus put both solvation models through a more rigid test. Furthermore, a new hydrogen-bonding acid, 1,1,1,3,3,3-hexafluoro-2-propanol, and a wide range of Lewis bases (both oxygen donors and nitrogen donors) have been used. The ESP model has again worked exceptionally well while the model based on eq 4 has proven to be less than desirable. It may be of interest to correct the data used to test eq 4 for the specific inter-

TABLE V: Comparison of the ΔH_C Values Obtained from α with that of the ESP Constant, k

Complex	Solvent transfer	α_{av}[a]	ΔH_C(calcd), kcal mol^{-1}	ΔH_C(meas), kcal mol^{-1}	$\|(\Delta H_C)\|$,[b] kcal mol^{-1}	k_{meas},[c] kcal mol^{-1}	$\|\Delta k\|$,[d] kcal mol^{-1}
HFIP·EtOAc	$CCl_4 \rightarrow C_6H_6$	0.42	-1.03	-0.63	0.40	-0.70	0.14
	$CCl_4 \rightarrow o\text{-}Cl_2C_6H_4$		-0.62	-0.62	0.00	-0.46	0.10
	$C_6H_6 \rightarrow o\text{-}Cl_2C_6H_4$		0.40	0.01	0.39	0.24	0.07
HFIP·HMPA	$CCl_4 \rightarrow C_6H_6$	0.27	-0.56	-0.41	0.15	-0.86	0.02
	$CCl_4 \rightarrow o\text{-}Cl_2C_6H_4$		-0.64	-1.59	0.95	-0.54	0.02
	$CCl_4 \rightarrow NO_2C_6H_5$		-1.17	-0.81	0.36	-1.11	0.01
	$C_6H_6 \rightarrow o\text{-}Cl_2C_6H_4$		-0.08	-1.18	1.10	0.32	0.15
	$C_6H_6 \rightarrow NO_2C_6H_5$		-0.61	-0.40	0.21	-0.25	0.08
	$o\text{-}Cl_2C_6H_4 \rightarrow NO_2C_6H_5$		-0.53	0.78	1.31	-0.57	0.09
HFIP·DMA	$CCl_4 \rightarrow C_6H_6$	0.37	-1.03	-1.23	0.20	-0.97	0.13
	$CCl_4 \rightarrow o\text{-}Cl_2C_6H_4$		-0.77	-1.43	0.66	-0.68	0.12
	$CCl_4 \rightarrow NO_2C_6H_5$		-1.98	-1.81	0.17	-1.12	0.00
	$C_6H_6 \rightarrow o\text{-}Cl_2C_6H_4$		0.26	-0.20	0.46	0.29	0.12
	$C_6H_6 \rightarrow NO_2C_6H_5$		-0.44	-0.58	0.36	-0.15	0.18
	$o\text{-}Cl_2C_6H_4 \rightarrow NO_2C_6H_5$		-1.21	-0.38	0.83	-0.44	0.04
HFIP·1-MeIm	$C_6H_{14} \rightarrow C_6H_6$	0.59	-3.26	-3.85	0.59	-1.22	0.13
	$C_6H_{14} \rightarrow o\text{-}Cl_2C_6H_4$		-2.53	-3.69	1.16	-1.14	0.06
	$C_6H_{14} \rightarrow NO_2C_6H_5$		-4.70	-4.53	0.17	-1.59	0.05
	$C_6H_6 \rightarrow o\text{-}Cl_2C_6H_4$		0.76	0.16	0.60	0.08	0.09
	$C_6H_6 \rightarrow NO_2C_6H_5$		-1.43	-0.68	0.75	-0.37	0.04
	$o\text{-}Cl_2C_6H_4 \rightarrow NO_2C_6H_5$		-2.14	-0.84	1.35	-0.45	0.03
HFIP·pyridine	$C_6H_{14} \rightarrow C_6H_6$	0.38	-1.86	-2.05^f	0.19	-0.95^e	0.14
	$C_6H_{14} \rightarrow o\text{-}Cl_2C_6H_4$		-1.36	-1.96^f	0.60	-1.02^e	0.06
	$C_6H_{14} \rightarrow NO_2C_6H_5$		-2.62	-2.45^f	0.17	-1.48^e	0.06
	$C_6H_6 \rightarrow o\text{-}Cl_2C_6H_4$		0.52	0.09	0.43	-0.07	0.24
	$C_6H_6 \rightarrow NO_2C_6H_5$		-0.76	-0.40	0.36	-0.53	0.20
	$o\text{-}Cl_2C_6H_4 \rightarrow NO_2C_6H_5$		-1.27	-0.49	0.78	-0.46	0.02

[a] α_{av} is determined from the slope of the plot of ΔH_C vs. $\Delta H_A + \Delta H_B$. The origin has to be a point on the graph according to this equation and the best least-squares line is then constructed. [b] The absolute value of the difference between ΔH_C(meas) and ΔH_C(calcd) from eq 4. [c] $k_{meas} = \Delta H_{C meas} - \Delta H_B$ for a given adduct which according to ESP should be constant for all adducts of a given acid for a given pair of solvents. [d] $\Delta k = |k_{meas} - k_{av}|$ where k_{av} is determined for a given acid and transfer between a pair of solvents for different bases. The k_{av} values (in kcal mol^{-1}) for the systems studied are $CCl_4 \rightarrow C_6H_6$, $k_{av} = -0.84$; $CCl_4 \rightarrow o\text{-}Cl_2C_6H_4$, $k_{av} = -0.56$; $CCl_4 \rightarrow NO_2C_6H_5$, $k_{av} = -1.12$; $C_6H_6 \rightarrow C_6H_6$, $k_{av} = -1.09$; $C_6H_{14} \rightarrow o\text{-}Cl_2C_6H_4$, $k_{av} = -1.03$; $C_6H_{14} \rightarrow NO_2C_6H_5$, $k_{av} = -1.54$; $C_6H_6 \rightarrow o\text{-}Cl_2C_6H_4$, $k_{av} = 0.17$; $C_6H_6 \rightarrow NO_2C_6H_5$, $k_{av} = -0.33$; $o\text{-}Cl_2C_6H_4 \rightarrow NO_2C_6H_5$, $k_{av} = -0.48$. [e] Corrected for the specific interaction of free pyridine with the aromatic solvent of 0.9 kcal mol^{-1}. [f] Not corrected for the specific interaction of free pyridine with the aromatic solvents.

actions known to occur before α is determined. However, in view of the success of the ESP model, this does not seem worthwhile.

Because ESP has consistently met with success, we feel that the ESP model based on eq 1 and 7 should be employed for predicting enthalpies in polar solvents paying careful attention to the limitations specified. Two or more different solvents can be employed to check the assumptions of ESP. We do not advocate using the ESP model with free-energy data. In employing the ESP model, one must make no more experimental measurements than are required for the approach based on eq 4. The constant S (of eq 7) must be determined for every acid in every solvent, but then can be used for many different bases. The constant α (of eq 4) must be determined for each acid–base pair and then reportedly can be used in many solvents. It should be noted that we anticipate that the ESP model will not succeed if the adducts or donors are extensively associated in one solvent, but not in the other solvent involved in the transfer. Furthermore, one must use caution in employing the ESP model when the adduct is itself a Lewis acid or base that can undergo specific bonding interactions with the solvent being used.

Although in this study we held the acid constant, varied the base, and used weakly basic solvents, one could hold the base constant, vary the acid, and use acidic solvents.

Supplementary Material Available. Experimental data will appear following these pages in the microfilm edition of this volume of the journal. Photocopies of the supplementary material from this paper only or microfiche (105 × 148 mm, 24× reduction, negatives) containing all of the supplementary material for the papers in this issue may be obtained from the Journals Department, American Chemical Society, 1155 16th St., N.W., Washington, D. C. 20036. Remit check or money order for $3.00 for photocopy or $2.00 for microfiche, referring to code number JPC-74-454.

References and Notes

(1) Abstracted in part from the Ph.D. Thesis of R. Martin Guidry, University of Illinois, Urbana, Ill. 1974.
(2) R. S. Drago, M. S. Nozari, and G. C. Vogel, *J. Amer. Chem. Soc.*, **94**, 90 (1972).
(3) M. S. Nozari and R. S. Drago, *Inorg. Chem.*, **11**, 280 (1972).
(4) M. S. Nozari and R. S. Drago, *J. Amer. Chem. Soc.*, **94**, 6877 (1972).
(5) M. S. Nozari, C. Jensen, and R. S. Drago, *J. Amer. Chem. Soc.*, **95**, 3162 (1973).
(6) S. D. Christian, *J. Phys. Chem.*, **70**, 3376 (1966).
(7) J. Grundnes and S. D. Christian, *Acta Chem. Scand.*, **23**, 3583 (1969).
(8) S. D. Christian and E. E. Tucker, *J. Phys. Chem.*, **74**, 214 (1970).
(9) K. F. Purcell, J. A. Stikeleather, and S. D. Bunk, *J. Amer. Chem. Soc.*, **91**, 4019 (1969).
(10) R. M. Guidry and R. S. Drago, *J. Amer. Chem. Soc.*, **95**, 759 (1973).
(11) T. F. Bolles and R. S. Drago, *J. Amer. Chem. Soc.*, **88**, 3921 (1966).
(12) T. D. Epley and R. S. Drago, *J. Amer. Chem. Soc.*, **89**, 5770 (1967).
(13) M. S. Nozari and R. S. Drago, *J. Amer. Chem. Soc.*, **92**, 7086 (1970).
(14) R. M. Guidry and R. S. Drago, *J. Chem. Educ.*, submitted for publication.
(15) See paragraph at end of paper regarding supplementary material.

Difference Gel Chromatography of Kinetically Controlled Systems. Irreversible Polymerization

L. W. Nichol*

Department of Physical Biochemistry, John Curtin School of Medical Research, Australian National University, Canberra, A.C.T., 2601, Australia

and D. J. Winzor

Department of Biochemistry, University of Queensland, St. Lucia, Queensland, 4067, Australia (Received September 27, 1973)

A set of partial differential equations expressing mass conservation during migration of a system undergoing a kinetically controlled and irreversible association to form a single higher polymer has been solved to yield expressions for concentrations of species as a function of distance. These expressions have been adapted to describe elution profiles obtainable in difference gel chromatographic experiments. Characteristic features of these profiles are illustrated with numerical examples and are compared with those previously predicted for a kinetically controlled irreversible isomerization or dissociation.

The potential use of a difference chromatography experiment in which a solute in one solvent system (α) is introduced onto a gel column preequilibrated with another (β) has been explored in relation to the examination of rapidly polymerizing systems[1] and irreversibly isomerizing systems subject to kinetic control.[2] The latter treatment yielded equations which described elution profiles and provided analytical expressions for the evaluation of the relevant first-order rate constant from these profiles. In practice a change of solvent environment may also result in an irreversible and kinetically controlled polymerization as illustrated[3] by the time-dependent increase in weight-average molecular weight observed on the transfer of trypsin from pH 2 to 4.8. The purpose of this article is to present the theoretical expressions describing elution profiles pertaining to the difference chromatography of systems of the type

$$nA \xrightarrow{k} C \quad (n > 1)$$
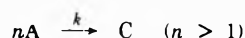
k being the nth-order rate constant.

The treatment is commenced by considering migration in a single-phase system with subsequent adaptation of the resulting expressions to the chromatographic situation. The statement of mass conservation during migration ignoring diffusional spreading[4] (for distance, $x > 0$ and time, $t > 0$) is

$$v_A'(\partial c_A{}^\beta/\partial x)_t + (\partial c_A{}^\beta/\partial t)_x = - k(c_A{}^\beta)^n \quad (1a)$$

$$v_C'(\partial c_C{}^\beta/\partial x)_t + (\partial c_C{}^\beta/\partial t)_x = k(c_A{}^\beta)^n \quad (1b)$$

where x is measured relative to an origin moving with the velocity of the solvent front ($\alpha\beta$ boundary), v_A' and v_C' are the respective velocities of monomer and polymer relative to the same frame of reference, and $c_j{}^\beta$ (j = A,C) is the weight concentration in the β region. In these terms and for a loading concentration $\bar{c}^\alpha$ the boundary conditions are

$$c_A{}^\beta = \bar{c}^\alpha \quad (x = 0, t > 0)$$
$$= 0 \quad (t = 0, x > 0)$$
$$\bar{c}^\beta = c_A{}^\beta + c_C{}^\beta = \bar{c}^\alpha \quad (x = 0, t > 0)$$
$$= 0 \quad (t = 0, x > 0)$$

Equations 1a and the sum of eq 1a and 1b (written in terms of the constituent concentration, $\bar{c}^\beta$) have been solved by integrating the corresponding Lagrange system of ordinary differential equations, the resulting general solution being examined as described previously.[2] Sets of solutions are obtainable for both cases $v_A' > v_C'$ and $v_A' < v_C'$, but as the latter is the realistic relative order of magnitude of species velocities in gel chromatography (polymers with larger Stokes radii than those of monomers being excluded more completely from the gel phase) only the following set is relevant in the present context. In the region $0 \leqslant x \leqslant v_A't$

$$c_A{}^\beta(x,t) = \bar{c}^\alpha \left\{ \frac{v_A'}{v_A'-k(1-n)(\bar{c}^\alpha)^{n-1}x} \right\}^{1/(n-1)} \quad (2a)$$

$$\bar{c}^\beta(x,t) = \frac{v_A'\bar{c}^\alpha}{v_C'} + \frac{(v_C'-v_A')\bar{c}^\alpha}{v_C'} \left\{ \frac{v_A'}{v_A'-k(1-n)(\bar{c}^\alpha)^{n-1}x} \right\}^{1/(n-1)} \quad (2b)$$

In the region $v_A't \leqslant x \leqslant v_C't$

$$c_A{}^\beta(x,t) = 0 \quad (3a)$$

$$\bar{c}^\beta(x,t) = \frac{v_A'\bar{c}^\alpha}{v_C'} \times$$

$$\left\{ 1 - \left[\frac{(v_A' - v_C')}{v_A' - v_C' - k(1 - n)(\bar{c}^\alpha)^{n-1}(x - v_C't)} \right]^{1/(n-1)} \right\} \quad (3b)$$

From eq 3b it follows that at $x = v_C't$, $\bar{c}^\beta(x,t) = 0$, the onset of the β-solvent plateau region ahead of all solute. When $x = v_A't$, eq 2b and 3b describe respectively the upper and lower limits of a step function of $\bar{c}^\beta$, behavior entirely analogous with the corresponding isomerization situation.[2] As required by mass conservation, the sum of the definite integrals of eq 2b and 3b between the limits indicated yields $\bar{c}^\alpha v_A't$. It is also clear from the form of these equations that the isomerization case ($n = 1$) required separate treatment.[2]

Equations 2 and 3 were adapted to describe elution profiles by the series of steps detailed previously[2] (including conversion to a fixed frame of reference) and with the ad-
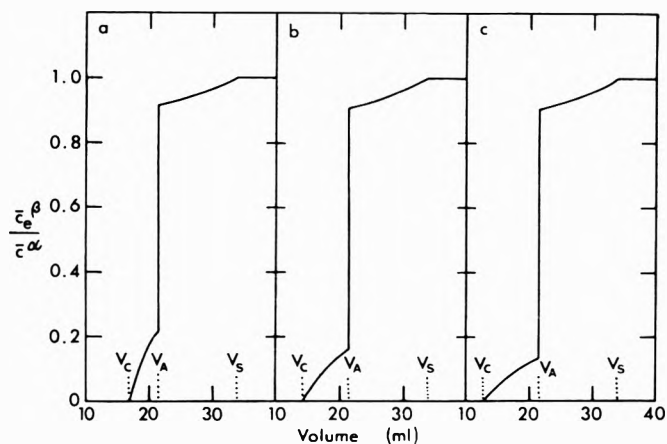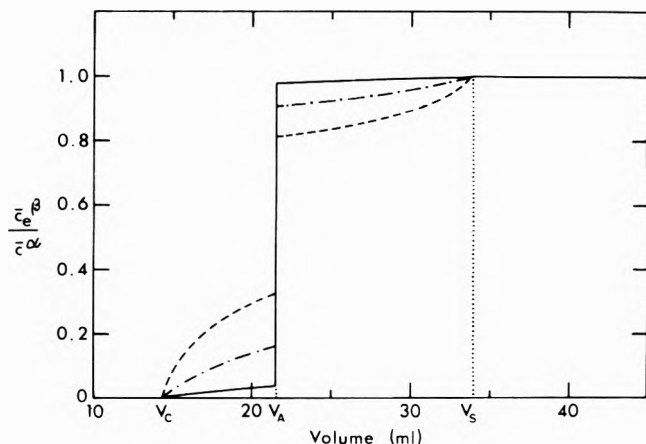
Figure 1. Computed elution profiles for solutes undergoing kinetically controlled polymerization. Patterns were calculated from eq 4 using the following common parameters: V_b = 35 ml, $\dot{V}$ = 0.5 ml/min, V_S = 33.8 ml, V_A = 21.5 ml, $\bar{c}^\alpha$ = 5 g/l. (a) n = 2, V_C = 16.9 ml, k = 0.0033 l. g^{-1} min^{-1}; (b) n = 3, V_C = 14.3 ml, k = 0.001 l.^{2} g^{-2} min^{-1}; (c) n = 4, V_C = 12.9 ml, k = 0.000031 l.^{3} g^{-3} min^{-1}.

Figure 2. Computed elution profiles for a solute undergoing kinetically controlled trimerization. Patterns were calculated from eq 4 using the following parameters: V_b = 35 ml, $\dot{V}$ = 0.5 m/min, V_S = 33.8 ml, V_A = 21.5 ml, V_C = 14.3 ml, k = 0.001 l.^{2} g^{-2} min^{-1} and values of 2 g/l. (—), 5 g/l. (-----), and 10 g/l. (---) for $\bar{c}^\alpha$.

ditional relationship $\hat{c}^\alpha = c^\alpha V_A/V_b$, where $\hat{c}^\alpha$ denotes the concentration of A averaged over the mobile and stationary phases, V_A is the elution volume of A, and V_b is the bed volume of the column; this relationship follows from eq 5 and 16 of ref 5. The expressions describing a chromatographic experiment are

$$\bar{c}_e^\beta = \bar{c}^\alpha \left\{ \frac{V_A - V_C}{V_S - V_C} \right\} \times$$
$$\left\{ \frac{\dot{V}(V_S - V_A)}{\dot{V}(V_S-V_A)+V_A k(n-1)(\bar{c}^\alpha V_A/V_b)^{n-1}(V_S-V)} \right\}^{1/(n-1)} +$$
$$\bar{c}^\alpha(V_S - V_A)/(V_S - V_C) \quad (V_A \leqslant V \leqslant V_S) \quad (4a)$$

$$\bar{c}_e^\beta = \bar{c}^\alpha \left\{ \frac{V_A - V_S}{V_S - V_C} \right\} \times$$
$$\left\{ \frac{\dot{V}(V_C - V_A)}{\dot{V}(V_C-V_A)+V_A k(n-1)(\bar{c}^\alpha V_A/V_b)^{n-1}(V_C-V)} \right\}^{1/(n-1)} +$$
$$\bar{c}^\alpha(V_S - V_A)/(V_S - V_C) \quad (V_C \leqslant V \leqslant V_A) \quad (4b)$$

in which $\bar{c}_e^\beta$ is the constituent concentration of A in the β region of the elution profile, V_A, V_C, and V_S are the respective elution volumes of A, C, and the solvent front, and $\dot{V}$ is the volume rate of flow of the column. In eq 4, $\bar{c}^\alpha$ is the applied concentration and also the plateau concentration in the α region of the elution profile. In the numerical examples of elution profiles that follow, V_A and V_C have been assigned magnitudes in keeping with the gel chromatographic behavior of a polymerizing protein with monomer molecular weight 25,000 on a 35-ml (V_b) column of Sephadex G-100. V_S was taken as the elution volume of sucrose, while $\dot{V}$ was set at 0.5 ml/min. Values of the nth order rate constants were selected such that half of the solute (on a weight basis) converted to polymer on exposure to β solvent for 60 min.

Theoretical elution profiles for monomer → dimer, monomer → trimer, and monomer → tetramer systems with $\bar{c}^\alpha$ = 5 g/l. are shown in Figure 1. Comparison with the corresponding isomerization case (Figure 2b of ref 2) reveals qualitative similarities with respect to (a) the terminating points of the reaction boundaries (V_C and V_S)

and (b) the existence of a distinct step in solute concentration at V_A. Since the profiles in Figure 1 all refer to systems with equivalent rates of polymer formation (on a weight basis), it is also evident that this step in concentration is relatively larger the larger the value of n. A feature that distinguishes monomer → polymer conversions from those involving isomerization is concentration dependence of the elution profile. This is illustrated for a monomer → trimer system in Figure 2, which shows that higher values of $\bar{c}^\alpha$ lead to decreased magnitudes of the discontinuity in $\bar{c}_e^\beta$ at V_A.

In the earlier treatment of kinetically controlled isomerization[2] it was suggested that integration of the elution profile between the limits V_A and V_C could provide a possible method of evaluating k. From eq 4b, the relevant expression for integration in the present study, it is evident that the same procedure could be adopted with systems undergoing monomer → polymer conversion, but that different expressions for the experimentally determined area Q pertain depending on the value of n (eq 5).

$$Q = \frac{(V_S - V_A)(V_A - V_C)\bar{c}^\alpha}{(V_S - V_C)} \times$$
$$\left\{ 1 - \frac{\dot{V}V_b \ln [1 + (k\bar{c}^\alpha V_A^2/\dot{V}V_b)]}{k\bar{c}^\alpha V_A^2} \right\} \quad (n = 2) \quad (5a)$$

$$Q = \frac{(V_S - V_A)(V_A - V_C)\dot{V}\bar{c}^\alpha}{(V_S - V_C)(n - 2)kV_A(\bar{c}^\alpha V_A/V_b)^{n-1}} \times$$
$$\left\{ 1 - \left[\frac{\dot{V} + kV_A(n - 1)(\bar{c}^\alpha V_A/V_b)^{n-1}}{\dot{V}} \right]^{(n-2)/(n-1)} \right\} +$$
$$\bar{c}^\alpha(V_S - V_A)(V_A - V_C)/(V_S - V_C) \quad (n > 2) \quad (5b)$$

Although these expressions may also be solved for k, diffusional spreading would render the experimental measurement of Q subject to overestimation in the event of there being a pronounced concentration step at V_A. However, it is evident from Figure 2 that this error may be diminished by suitable choice of the applied solute concentration $\bar{c}^\alpha$ in order to decrease the magnitude of the step. As in the case of kinetically controlled isomerization, a slower flow rate of the column ($\dot{V}$) would also lead to an improved experimental estimate of the required area.

In summary, the previous treatment of the difference gel chromatographic behavior of irreversibly isomerizing systems has been extended to include solutes undergoing a kinetically controlled association in the solvent system used to preequilibrate the column. It is clear from eq 1 that consideration has only been given to the formation of a single type of polymer (C), treatment of alternate reaction schemes involving appreciable amounts of polymers of size intermediate between A and C, each characterized by a different velocity, being exceedingly difficult. It is noteworthy, however, that the behavior of a system of the type A → nB, where dissociation occurs in the solvent system used to preequilibrate the column, has been implicitly described in the earlier work[2] since eq 1 of that reference expresses mass conservation during migration for either irreversibly isomerizing or dissociating systems. This ob-servation together with the expressions derived herein for associating systems suggests that the method should find wider experimental application than previously visualized for isomerizing systems because of greater differences between the elution volumes of monomer and polymer species compared with those likely to apply to isomeric solute forms.

References and Notes

(1) P. A. Baghurst, L. W. Nichol, R. J. Richards, and D. J. Winzor, *Nature (London)*. **234**, 299 (1971).
(2) S. M. A. Meggitt, L. W. Nichol, and D. J. Winzor, *J. Phys. Chem.*, **77**, 352 (1973).
(3) A. D'Albis, *Biochim. Biophys. Acta*, **200**, 40 (1970).
(4) G. A. Gilbert and R. C. Ll. Jenkins, *Proc. Roy. Soc., Ser. A*, **253**, 420 (1959).
(5) L. W. Nichol, A. G. Ogston, and D. J. Winzor, *J. Phys. Chem.*, **71**, 726 (1967).

COMMUNICATIONS TO THE EDITOR

Disproportionation and Recombination of Cyclopentyl Radicals

Sir: When annealed hydrocarbons are irradiated at low temperature, the radical concentration remains constant in the matrix as long as the sample is maintained below a temperature characteristic of the solid where the decay occurs. Recent results[1] have shown that these radicals can be quantitatively scavenged by dissolving the irradiated samples in a solvent that contains several specific scavengers, provided the dissolution takes place below the transition temperature. Previously reported works[2] are concerned with the measurement of the contribution of alkyl radical combinations to the formation of dimers in the case of solid undecane and solid n-pentane irradiated at low temperature.

This technique is now extended to the determination of the ratio of the rate constants for the disproportionation and the combination of cyclopentyl radicals in solid cyclopentane at 120°K.

The cyclopentyl radical is the only paramagnetic species observed by esr spectroscopy in solid cyclopentane samples irradiated with γ rays at 77°K.[3,4] In the case of annealed samples, the intensity of the esr signal remains constant when the temperature is raised from 77 to 120°K.[5] A rapid radical decay occurs near the transition point (122°K);[5] at this temperature, cyclopentyl radicals react to produce cyclopentane and dicyclopentyl. These compounds are found to be the main radiolysis products of cyclopentane.[6]

$$2c\text{-}C_5H_9\cdot \xrightarrow{k_d} c\text{-}C_5H_8 + c\text{-}C_5H_{10} \tag{1}$$

$$2c\text{-}C_5H_9\cdot \xrightarrow{k_c} C_{10}H_{18} \tag{2}$$
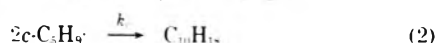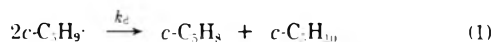
TABLE I: G Values of Cyclopentene and Dicyclopentyl for Molten and Dissolved Cyclopentane Samples

	$G(c\text{-}C_5H_{10})$	$G(C_{10}H_{18})$
Molten	2.25 ($\sigma = 0.24$)	0.69 ($\sigma = 0.05$)
Dissolved	1.09 ($\sigma = 0.25$)	0.31 ($\sigma = 0.05$)
ΔG	1.16 ($\sigma = 0.35$)	0.38 ($\sigma = 0.07$)

The yields of these products are measured for several annealed samples irradiated at a dose of 4 Mrads. All these samples are bleached with visible light. Some of them are melted, others are dissolved at 110°K in a solution of oxygen in propane following a procedure described in ref 1. In this case, cyclopentyl radicals are scavenged and reactions 1 and 2 do not occur. The results of these experiments are summarized in Table I.

The differences of the G factors between the two sets of experiments measure the contributions of reactions 1 and 2 to the production of cyclopentene and dicyclopentyl, respectively. They are related to the disproportionation-combination rate constants ratio in the following way

$$\frac{G_{c\text{-}C_5H_8}^{\text{molten}} - G_{c\text{-}C_5H_8}^{\text{diss}}}{G_{C_{10}H_{18}}^{\text{molten}} - G_{C_{10}H_{18}}^{\text{diss}}} = \frac{\int k_d(R\cdot)^2 \, dt}{\int k_c(R\cdot)^2 \, dt} = \frac{k_d}{k_c} =$$

$$\frac{1.16}{0.38} = 3.05 \quad (\sigma = 1.1)$$

It is worthwhile to note that these determinations do not need any assumption about the mechanism (the scavenger effect is specific) nor any approximation in the calculations.

References and Notes

(1) B. Tilquin, J. Allaert, A. Dautricourt, D. Mauer, and P. Claes, *Int. J. Radiat. Phys. Chem.*, **5**, 343 (1973).

(2) B. Tilquin, J. Allaert, and P. Claes. Symposium on the Mechanisms of Hydrocarbon Reactions, Hungarian Academy of Sciences Budapest, Siofok, June 6, 1973.

(3) C. Fauquenoit, J. P. Dodelet, and P. Claes, *Bull. Soc. Chim. Belg.*, **80**, 315 (1971).

(4) T. Ohmae, S. Ohnishi, K. Kuwata, H. Sakwai, and Z. Nitta, *Bull. Chem. Soc. Jap.*, **40**, 226 (1967).

(5) D. Mauer, B. Tilquin, and P. Claes, *Bull. Soc. Chim. Belg.*, **82**, 693, (1973).

(6) B. Tilquin and P. Claes, *Bull. Soc. Chim. Belg.*, **80**, 335 (1971).

Chemistry Department   **B. Tilquin**
University of Louvain   **J. Allaert**
B-1348 Louvain-la-Neuve, Belgium   **P. Claes***

A Dye Laser Flash Photolysis Kinetics Study of the Reaction of Ground-State Atomic Oxygen with Hydrogen Peroxide[1]

Sir: We would like to report on a recently completed study on the reaction of $O(^3P)$ with hydrogen peroxide over the temperature range 283–368°K. This reaction is of possible significance both in the atmosphere (where H_2O_2 is present as a trace constituent) and in combustion processes, especially H_2–O_2 flames.

A literature survey has shown that only one kinetics study has been reported[2] on this system and that set only an upper limit on the value of the rate constant at 300°K. The experimental difficulties involved with this reaction system are twofold: (1) the quantitative handling of hydrogen peroxide in a gas handling system; and (2) the generation of $O(^3P)$ in the absence of high concentrations of metastable O_2, OH, and HO_2. In the present study, the above problems were greatly minimized by (1) the use of an all-glass gas handling system and a glass reaction cell, and (2) the generation of $O(^3P)$ by the dye laser flash photolysis of ozone in the Chappius band at 6000 Å. The detection technique for atomic oxygen was that of resonance fluorescence and further details on this can be found in previous publications.[3,4] Also described in earlier work is the use of the tunable dye laser as a means of generating a clean source of ground-state atomic oxygen from photolysis of O_3.[5]

In this investigation, the limited temperature range of 283–368°K was defined by the thermal decomposition of H_2O_2 at high temperatures and the low vapor pressure of peroxide below 283°K. In the latter case, the small value of the bimolecular rate constant for reaction 1 at low temperatures was also a contributing factor. Throughout this study a major concern was the thermal decomposition of hydrogen peroxide both *via* homogeneous and heterogeneous processes. Accordingly, independent studies were carried out to determine the extent of this problem using a temperature-controlled recording Cary 14 uv spectrophotometer. At 298°K, it was found that H_2O_2 decomposed at a
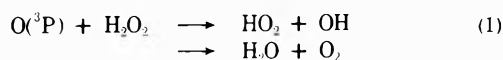
$$O(^3P) + H_2O_2 \longrightarrow HO_2 + OH \qquad (1)$$
$$\longrightarrow H_2O + O_2$$
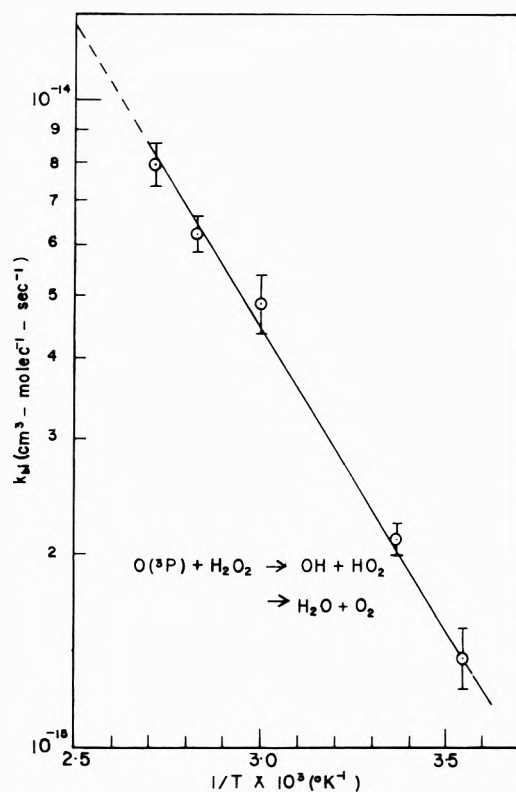
Figure 1. Arrhenius plot of the rate constant for reaction of ground-state atomic oxygen with hydrogen peroxide.

rate of 1%/min. Whereas, at 353°K, the decomposition of H_2O_2 was about 5%/min. In a typical experiment, the reaction mixture remained in the reaction cell for no more than 3 min. Pressure corrections due to decomposition of H_2O_2 were made accordingly.

The hydrogen peroxide used in this study was from Becco Chemical Division and had a purity level of 98%. Ozone was prepared using a ozonator and was stored in a trap filled with silica gel at Dry Ice-acetone temperatures. From uv absorption measurements, it was shown to have a purity of 94%. All pressure measurements of H_2O_2 and O_3 were made using a MKS Baraton pressure gauge.

The results from experiments performed over the temperature range 283–368°K are summarized in Table I. In all cases, the bimolecular rate constant was obtained from the slope of a plot of the pseudo-first-order rate constant, k_1, *vs.* the H_2O_2 concentration. The nonzero value for k_1 at zero H_2O_2 pressure is due to the loss of atomic oxygen by diffusion[3,4] and reaction with O_3.[5] At a fixed temperature this contribution to k_1 was always constant. The bimolecular rate constant for reaction 1 was determined to be $(2.12 \pm 0.33) \times 10^{-15}$ cm^3 molecule^{-1} sec^{-1} at 298°K. The reported rate constant is based on direct observations of the rate of decay of $O(^3P)$ and thus represents the total bimolecular rate constant for both reaction channels (HO_2 + OH and H_2O + O_2). Over the temperature range 283–368°K, a least-squares fit of the rate data to the Arrhenius equation (see Figure 1) gave the rate expression $k_1 = (2.75 \pm 0.41) \times 10^{-12} \exp\{2125 \pm 261/T\}$.

A consideration of several possible secondary reactions in this system involving O, OH, and HO_2 indicated that none of these processes would have influenced the $O(^3P)$ decay curves. This point was demonstrated experimentally by a variation in the flash intensity [hence $O(^3P)$ con-

TABLE I: Rate Measurements for Reaction of $O(^3P)$ with H_2O_2 over the Temperature Range 283-368°K

Temp, °K	Total pressure (He), Torr	O_2 pressure, mTorr	H_2O_2 pressure, mTorr	First-order decay constant, sec^{-1}	Bimolecular rate constant k_1, cm^3 molecule^{-1} sec^{-1} $\times 10^{15}$
283	50	150	0	46	
	50	150	500	70	
	50	150	800	84	1.39 ± 0.15
298	50	150	0	55	
	50	150	400	80	
	50	150	800	110	$2.12 + 0.12$
333	50	100	300	122	
	50	100	600	166	
	50	100	1200	250	4.89 ± 0.51
353	50	150	190	150	
	50	150	380	184	
	50	150	320	165	
	50	150	570	215	
	50	150	760	230	6.25 ± 0.41
368	50	150	180	161	
	50	150	450	220	
	50	150	900	312	7.97 ± 0.61

centration] by a factor of 5 without observing any significant change in the bimolecular rate constant.

As mentioned earlier, only one other measurement of reaction 1 has been reported, this being an investigation by Foner and Hudson[2] using a mass spectrometric technique. The reaction was studied at 298°K, and yielded only an upper limit for k_1 of $\leq 4 \times 10^{-15}$ cm^3 molecule^{-1} sec^{-1}. The two measurements, therefore, can be considered to be in good agreement within the assigned uncertainties.

Calculations based on available rate data[6] for reaction 2

$$OH + H_2O_2 \longrightarrow H_2O + HO_2 \tag{2}$$

and concentration data for O and OH in the troposphere and stratosphere indicate that reaction 2 is the dominate gas kinetic destruction mechanism for H_2O_2 in the atmo-

sphere. Only in the mid and upper stratosphere could reaction 1 account for possibly as much as 10% of the total loss of H_2O_2 via gas kinetic processes.

References and Notes

(1) This work was supported by the Climatic Impact Assessment Program, Office of the Secretary, Department of Transportation.
(2) S. N. Foner and R. L. Hudson, J. Chem. Phys., 36, 2681 (1962).
(3) D. D. Davis, R. E. Huie, J. T. Herron, M. J. Kurylo, and W. Braun, J. Chem. Phys., 56, 4868 (1972).
(4) R. E. Huie, J. T. Herron, and D. D. Davis, J. Phys. Chem., 76, 2653 (1972).
(5) D. D. Davis, W. Wong, and J. Lephardt, Chem. Phys. Lett., in press.
(6) N. R. Greiner, J. Phys. Chem., 72, 406 (1968).

Chemistry Department   **D. D. Davis***
University of Maryland   **W. Wong**
College Park, Maryland 20742   **R. Schiff**
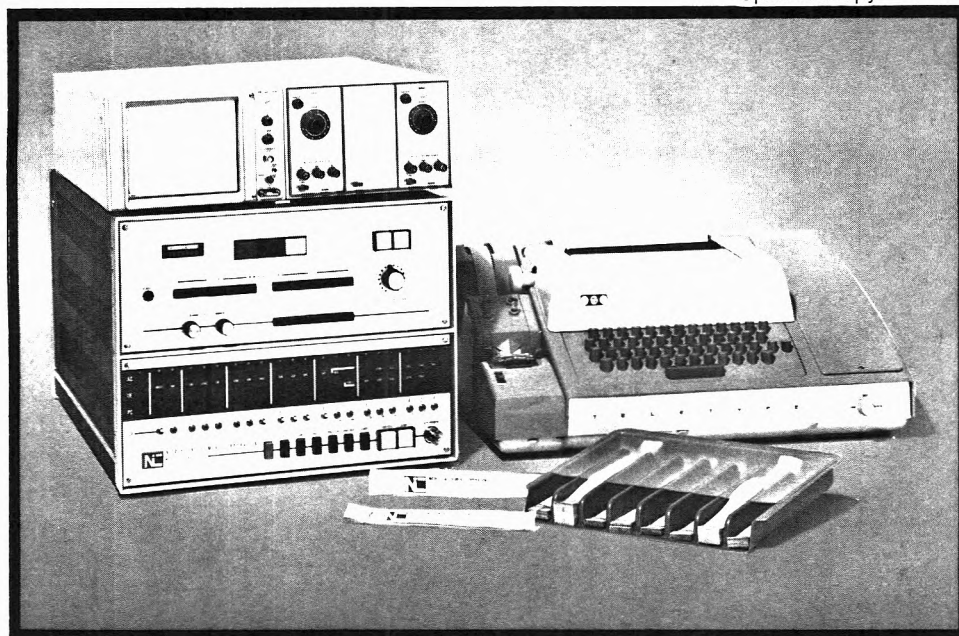
Laser Raman Spectroscopy
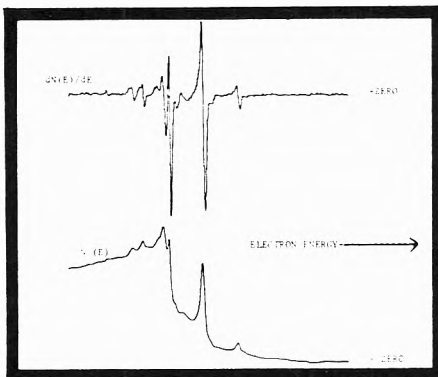
Auger Electron Spectroscopy
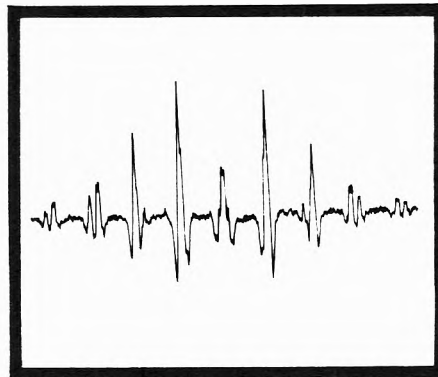
Electron Paramagnetic Resonance Spectroscopy

Here are just three Lab-80 analytical data system applications. What are your needs?

The LAB-80 is a general purpose data acquisition and processing system for analytical laboratory signal averaging applications. Software control, a wide choice of memory sizes and a wide range of options and accessories make it useful in a variety of laboratory experimental applications.

For maximum utility the LAB-80 memory features 20-bit words which offers maximum dynamic range and signal-to-noise enhancement through signal averaging. This word length permits the researcher to detect peaks differing in intensity by at least five orders of magnitude.

A powerful collection of software routines allows data acquisition at rates from one point per second to 100 kHz with display of either memory contents or input. For high speed applications data may be acquired through a transient recorder at sampling rates up to 100 MHz (10 nanoseconds between samples).

Once the data are acquired, easy-to-use commands allow nondestructive integration with compensation for offset and slope, differentiation, expansion and plotting of any part of the spectrum determined by a pair of cursors, or selected regions can be printed giving times and amplitudes of particular data points.

Further manipuation commands include three point smoothing, addition or subtraction of constants, and multiplication by selected factors, as well as the ability to add or subtract pairs of spectra.

For maximum versatility the data may be punched out on paper tape, transferred to magnetic tape or disk memory, or plotted on an X-Y or y-d plotter. An interpretive basic compiler is also available.

Phone or write for complete details or to discuss your application.

NICOLET INSTRUMENT CORPORATION

5225 Verona Road, Madison, Wisconsin 53711
Phone 608/271-3333 TWX: 910-286-2713

2 9 ГАВ. 2517